Lecture Notes in Physics

331

G. Winnewisser J.T. Armstrong (Eds.)

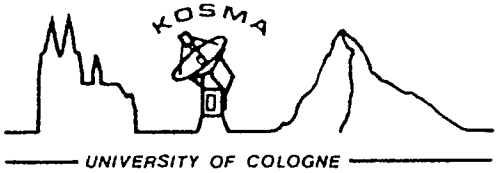

The Physics and Chemistry of Interstellar Molecular Clouds

mm and Sub-mm Observations in Astrophysics

Proceedings of a Symposium Held at Zermatt, Switzerland,
22–25 September 1988 to Commemorate the
600th Anniversary of the University of Cologne and
the 20th Anniversary of the Gornergrat Observatory

Springer-Verlag

Editors

G. Winnewisser
J. T. Armstrong
I. Physikalisches Institut, Universität zu Köln
Zülpicher Straße 77, D-5000 Köln 41, FRG

ISBN 3-540-51297-7 Springer-Verlag Berlin Heidelberg New York
ISBN 0-387-51297-7 Springer-Verlag New York Berlin Heidelberg

Printing: Druckhaus Beltz, Hemsbach/Bergstr.
Binding: J. Schäffer GmbH & Co. KG., Grünstadt

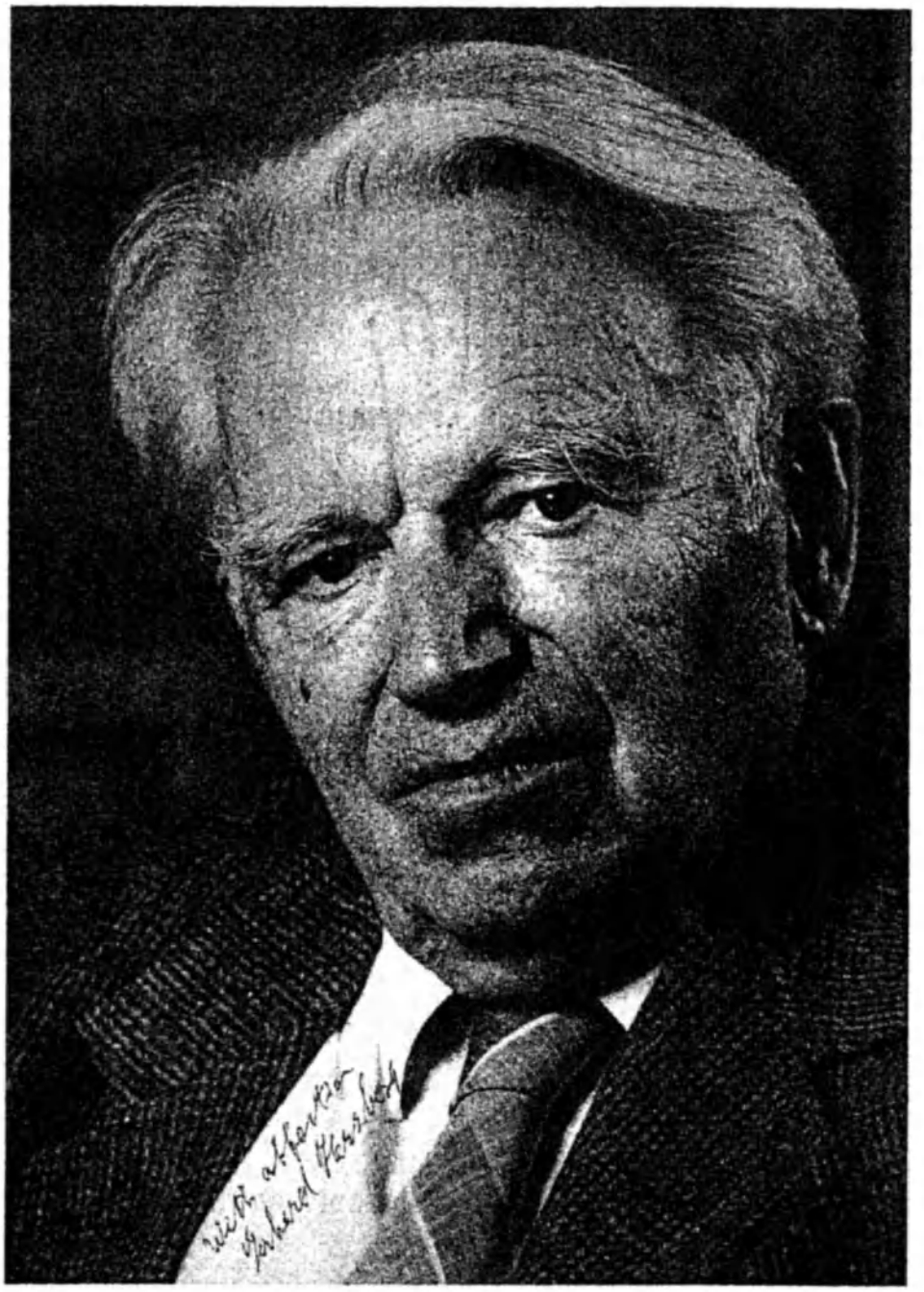

GERHARD HERZBERG

to whom this volume is dedicated.

FOUNDING AND FIRST BLOOMING OF THE UNIVERSITY

On May 21, 1388, in Perugia, Pope Urban VI issued the founding deed of the University of Cologne: "After careful consideration and review, we have, for the benefit and advantage not only of the city of Cologne, but also of the residents of the surrounding regions, in fatherly love, graciously granted the humble request of the councillors, assessors, citizens, and community of the city of Cologne, who for this in devotion have asked our favor, and decided, for the glory of God and the propagation of the Faith, and directed, through apostolic authority, that henceforth there shall be a University in the city of Cologne after the model of the University of Paris, which shall ever remain there."

GRÜNDUNG UND ERSTE BLÜTE DER UNIVERSITÄT

Am 21. Mai 1388 stellte Papst Urban VI. in Perugia die Stiftungsurkunde für die Universität zu Köln aus: „Nach sorgfältiger Überlegung und Prüfung haben wir nicht nur zum Nutzen und Vorteil der Stadt Köln, sondern auch der Einwohner der umliegenden Gebiete in väterlicher Liebe den demütigen Bitten der Räte, Schöffen, Bürger, und der Gemeinde der Stadt Köln, die in Ergebenheit um diese unsere Gunst gebeten haben, huldvoll entsprochen und zur Ehre Gottes und zur Förderung des rechten Glaubens beschlossen und kraft apostolischer Autorität angeordnet, daß in der Stadt Köln fortan eine Universität sein soll, nach dem Muster der Universität Paris, und für immer dort bleiben soll."

DER REKTOR DER UNIVERSITÄT ZU KÖLN

Grußwort

Es ist mir eine angenehme Pflicht, Sie hier in Zermatt anläßlich der internationalen Konferenz "The Physics and Chemistry of Interstellar Molecular Clouds" im Namen der Universität zu Köln herzlich willkommen zu heißen. Es ist ein besonderer Anlaß, das 600jährige Bestehen der Universität in diesem schönen Rahmen eines Köln-Zermatt Symposiums begehen zu können. Diese Konferenz ist eine von vielen Veranstaltungen, mit der die Universität ihren Geburtstag feiert.

Die Universität ist stolz, dieses schöne Observatorium auf dem Gornergrat zu betreiben. Zeigt es doch, daß der Blick der Universität wie vor 600 Jahren auch heute noch den Sternen und dem Weltraum zugewandt ist: Den Stern sehen Sie als höchsten Punkt im Wappen der Universität.

Prof. Dr. Peter Hanau

DER OBERBÜRGERMEISTER DER STADT KÖLN

Grußwort

Verehrte Damen, meine Herren,

sehr gerne folge ich dem Wunsch von Herrn Professor Dr. Winnewisser, Sie mit einigen Grußworten herzlich zum internationalen Symposium "The Physics and Chemistry of Interstellar Molecular Clouds" in Zermatt willkommen zu heißen. Ich gestehe, noch viel lieber wäre ich vom 25.–27. September 1988 unter Ihnen; denn wer fährt nicht gern nach Zermatt?

So wünsche ich Ihnen aus dem 2000-jährigen Köln in Namen von Rat und Verwaltung, aber auch persönlich, einen erfolgreichen Verlauf Ihrer zukunftsweisenden Konferenz. Wenn Sie das Observatorium auf dem Gornergrat besichtigen, werden Sie sich in der höchstgelegenen ständigen Forschungsstelle der Universität zu Köln befinden. Nur die "wissenschaftliche Konkurrenz" der Deutschen Forschungs- und Versuchsanstalt für Luft- und Raumfahrt aus Köln-Porz übertrifft anläßlich ihrer Weltraummissionen diesen Höhenrekord, aber eben nur kurzfristig.

Wenn Sie aus meinen Zeilen so etwas wie "Besitzerstolz" herauslesen, dann belegt diese Tatsache die freundschaftliche Verbundenheit der Kölner mit ihrer Universität, die vor 600 Jahren als Bürgeruniversität gegründet wurde. Daß die Universität zu Köln nicht in ihrer 600-jährigen Tradition erstarrt ist, beweist das Symposium des I. Physikalischen Instituts vom 22.–25. September 1988 in Zermatt.

Mit freundlichen Grüßen

Norbert Burger

Grüße des Burgerpräsidenten von Zermatt

Ladies and gentlemen,

it gives me great pleasure to welcome you here in Zermatt personally and on behalf of the Burgergemeinde. Although the history of Zermatt reaches back to the Middle Ages, the village and its surroundings became known long before the turn of the century for their beautiful location, scenery and climatic conditions. With the inauguration of the Gornergratbahn in 1898 and the construction of Hotel Belvedere on the summit, one of the most scenic spots in the Alps was opened to everyone, not only the devoted Alpinist, something which Mark Twain probably would have enjoyed on his journey to the Riffelberg. Now the Kulmhotel Gornergrat just below the summit houses the two observatories which are our windows to space. We, the people of Zermatt, take great pride that the Gornergrat has been discovered by astronomers and that astrophysicists from all over the world are participating at the Conference on "The Physics and Chemistry of Interstellar Molecular Clouds".

I wish all of you an enjoyable, informative, interesting and beautiful time here in Zermatt on the base of the Matterhorn.

Herzlich willkommen in Zermatt

E. Aufdenplatten
Burgerpräsident, Zermatt

Opening Remarks

Ladies and Gentlemen,

on behalf of the International Foundation "High-altitude Research Stations Jungfraujoch and Gornergrat" I welcome you to Zermatt, the famous tourist place, and I wish you a successful symposium on "The Physics and Chemistry of Interstellar Molecular Clouds". Our foundation recognized the climatically preferred location of Zermatt and its surroundings for astronomical observations more then 20 years ago. In collaboration with the Observatoire de Meudon, the Geneva Observatory and the Astronomical Institute of the University of Oxford in Great Britain, we therefore erected astronomical observatories on the two towers of the Kulmhotel of the Burgergemeinde Zermatt at Gornergrat. In 1984 the Gornergrat South observatory was taken over by the University of Köln. In the following years Professor Gisbert Winnewisser refurbished the observatory, enlarged the dome, and installed the new KOSMA 3m millimeter and submillimeter telescope. I have nothing to add to the beautiful results on interstellar molecular lines from Gornergrat. We are proud that the I. Physikalisches Institut of the Universität zu Köln is running its 3m radio telescope here in Switzerland. I thank Professor Winnewisser for his great scientific support of our foundation. I also thank him for having organized this conference at Zermatt. To you, ladies and gentlemen, I wish a successful symposium, more and deeper friendships among scientists from all over the world, and a pleasant stay at Zermatt.

H. Debrunner

Präsident Internationale Stiftung Hochalpine
Forschungsstationen Jungfraujoch und Gornergrat

Preface

This volume contains the lectures and posters presented at the Cologne-Zermatt Symposium on "The Physics and Chemistry of Interstellar Molecular Clouds" held in the Triftbachhalle in Zermatt from 22 to 26 September 1988. The objective of the meeting was twofold: to take stock of the recent scientific and technological developments in the field of millimeter, submillimeter, and far-infrared astrophysics, and to commemorate the 600^{th} anniversary of the University of Cologne and the 20^{th} year of astronomical observations from the Gornergrat, a nearby peak (alt. 3130 m) where the University has recently installed the KOSMA 3 m millimeter and submillimeter telescope. This year also marks the 20^{th} year of the detection of interstellar NH_3 and H_2O by C. H. Townes and his collaborators. The three and a half day meeting was attended by more than 150 participants from 13 countries, considerably more than originally anticipated. This large turnout made it necessary to move the lectures from the Grand Hotel Zermatterhof to the Triftbachhalle, which fortunately was made available by the town of Zermatt.

The conference covered topics from the early discoveries of interstellar molecular lines to the most recent contributions from large telescopes. The extended maps from the KOSMA 3 m Gornergrat telescope were presented, highlighting one focus of the conference: the utility of small telescopes for quick mapping of large regions – both galactic and extragalactic – and for selecting targets for more detailed study with larger telescopes, e.g. star-formation and outflow regions. Half a day each was devoted to the chemistry of interstellar molecular clouds and to status reports on new instrumentation and future projects.

Interstellar molecular spectroscopy would not have matured so quickly were it not for the tremendous pool of precise laboratory data for astronomers to fall back on. We were very fortunate to have with us "the father of modern spectroscopy", Gerhard Herzberg, as our Guest of Honour, to whom we dedicate this volume. We were thankful that C. H. Townes participated in the meeting and reminded us in his after-dinner speech how research so often leads to new and unexpected discoveries.

All who were present at the Cologne-Zermatt Symposium 1988 can testify to its success, owing to the enthusiasm for the subject matter by all participants, the excellent presentations from talks to posters, and the beautiful setting for the meeting at the foot of the Matterhorn. Our two secretaries, Frl. M. Alscher and Frau I. Klee, took care of all the organizational details with grace and efficiency. The Zermatt people were warm and generous hosts, especially the staff of the Grand Hotel Zermatterhof under the direction of Jean-Pierre Lanz.

It is a pleasure to express our thanks to the Deutsche Forschungsgemeinschaft, whose financial support made this conference possible. In addition, we have received generous contributions from the following institutions and companies: Office of Naval Research, U. S. Navy; Internationale Stiftung Hochalpine Forschungsstationen Jungfraujoch und Gornergrat; Burgergemeinde Zermatt; Gornergrat-Bahn; Brig-Visp-Zermatt Bahn; Firma Dornier, Friedrichshafen. The Observatoire de Genève supplied the poster walls.

G. Winnewisser and J. T. Armstrong, editors

Contents

Contributed Talks

Posters

Individual Regions

Invited Talks

Contributed Talks

Posters

External Galaxies

Invited Talks

Theory

PART II: The Chemistry of Interstellar Molecular Clouds

Invited Talks

Contributed Talk

Posters

Part III: Instrumentation

Status Reports

Posters

... and a Little Closer to Home

Indexes

Some Historical Remarks

G. Herzberg
National Research Council, Ottawa, Ontario, Canada

I feel deeply moved by the invitation of the organizers of this exciting meeting to participate in it as Guest of Honor. I am a relative newcomer to the field of sub-millimeter astronomy. I was certainly not there at the beginning of radio astronomy (although in 1947 my friend the late Gerard Kuiper took me to see the first radio telescope which Grote Reber had built in his back yard at Wheaton, Illinois, not too far from the Yerkes Observatory). I was however there in that prehistoric time at the very beginning of the study of molecules in the interstellar medium which occurred in 1937. Many years before that, molecules had been identified in comets and planetary atmospheres, and even some in stellar atmospheres. In 1937, Adams and Dunham had obtained the first high-resolution spectra of O and B stars with the then new Coudé spectrograph of the 100 inch telescope at Mt. Wilson. They observed a number of very sharp absorption lines in the violet, some of which they could identify as interstellar lines of a number of atoms and ions, while others they had to leave unidentified. It was Swings and Rosenfeld who very soon thereafter identified one of these lines as due to the CH molecule. Now of course every radio astronomer knows that you cannot be sure of an identification based on a single line. However, in this instance the line was found to be the only line from the very lowest rotational level (among perhaps 100 laboratory lines): that can hardly be an accident. In their identification of new interstellar atomic lines (just preceding the identification of CH), Adams and Dunham had found that in multiplets, only lines involving the lowest sublevel of the lower state occur because the time between collisions in the interstellar medium is long enough that even transitions of very low probability can take place and bring all atoms to the lowest state. Clearly this was also happening for molecules. I think therefore we must give credit to Swings and Rosenfeld for the discovery (identification) of the first interstellar molecule. I met Polydore Swings soon after this discovery. Swings made many other discoveries concerning stellar atmospheres (peculiar stars, *etc.*) and especially in cometary problems. Toward the end of his notable career (1964), he was elected president of the IAU. His work and life are well described in a short autobiography in the *Annual Reviews of Astronomy and Astrophysics*. But in it he does not mention what I consider his most important discovery, the first interstellar molecule. This discovery is clearly mentioned in the obituary written by Paul Ledoux for the Belgian Academy.

Soon after Swings and Rosenfeld, Andy McKellar at Victoria identified another electronic transition of CH and in addition the well-known CN lines near 3883 Å also on the basis of Adams and Dunham's spectra. There was left a series of four lines at 4232, 3938, 3745 and 3579 Å in Adams and Dunham's spectra which remained unidentified for another two years. In June 1941, Otto Struve (then director of the Yerkes Observatory)

invited a few of us including Swings, Beutler, Mulliken and Teller to an informal meeting at Yerkes Observatory to discuss this question. The structure of the observed spectrum made it certain that it was molecular in origin. Mulliken suggested $CH_2(^1B_1{-}^1A_1)$; Teller and I suggested CH^+ because of the similarity to BH. In Saskatoon, where I worked at the time, Alex Douglas and I had an apparatus available which could be used to test the assumption. Within a few days we observed a new band system whose 0–0, 1–0, 2–0 bands were approximately at the place of the first three unidentified interstellar lines. Indeed the latter agreed exactly with the R(0) lines of these bands; that is, the only lines coming from the lowest rotational level ($J = 0$). It took some time to make certain that the new spectrum was due to CH^+. The discovery of the next interstellar molecule, OH, accomplished by radio astronomical methods (Weinreb, Barrett, *et al.*) took place 22 years later. As you all know, five years after that the floodgates were opened with the discovery by Townes and his associates of NH_3 and H_2O.

Since that time, some 80 interstellar molecules have been identified and their distribution in interstellar clouds has been studied. The papers presented at this meeting have given a detailed and exciting view of the present status of this field. We must express our thanks to Gisbert Winnewisser and his colleagues for the very successful organization of this meeting and also our admiration for setting up the Gornergrat Observatory in record time. Much has already been accomplished and undoubtedly much more will come: there will be more interstellar molecules, more understanding of interstellar clouds, their physics and their chemistry.

Molecular Lines: Past, Present, Future

Wm. J. Welch
Radio Astronomy Laboratory
University of California
Berkeley, California

I. Introduction: Discovery of Interstellar Molecules

The study of interstellar molecules began with the discovery, in the early thirties, of narrow absorption features in the ultra-violet spectra of a few distant stars, features that were identified as interstellar absorption by CN, CH, and CH^+ (Swings and Rosenfeld, 1937; McKellar, 1941; Douglas and Herzberg, 1941). These absorptions arise from the lowest rotational levels of the molecules. Observation of these molecules revealed for the first time interesting chemical processes in the diffuse interstellar clouds. In addition, both these and later radio studies of interstellar molecules have provided important clues to more profound physical properites of the Galaxy and beyond. For example, the excitation of the two lowest levels of CN gave the first hint of the existence of the 2.7 K microwave background radiation.

The development of microwave spectroscopy following the second world war demonstrated the importance of high resolution long wavelength spectroscopic studies of gases in the elucidation of molecular structure. At the same time it also showed how the inherently high resolution of the heterodyne detectors used on radio telescopes could permit the reliable identification and study of many molecules that might exist in the interstellar medium. In an important IAU Symposium paper, Townes (1957) listed wavelengths for many simple molecules that could be observed in the microwave spectrum. Following the accurate laboratory measurement of the absorption frequency of the radical OH, Weinreb et al. (1963) succeeded in detecting this molecule in absorption toward Cas A at a wavelength of 18 cm. It was subsequently found that OH emits as a maser in many regions (Weaver et al., 1965).

Laboratory wavelengths for a number of polyatomic molecules at cm wavelengths were available with sufficient accuracy for their search at that time, but there was some reluctance to look for them based on the expectation that polyatomic molecules would have difficulty in forming in the interstellar medium. Nevertheless, Cheung et al. (1968, 1969) reported the detection of both interstellar water vapor and ammonia followed shortly by the detection of formaldehyde by Palmer et al. (1969). Figure 1 shows spectra of water vapor and formaldehyde from these detection papers. In addition to showing the presence of the species, these spectra reveal interesting physical information. The intensity of the water vapor emission implies maser emission, and the large velocity dispersion is the first hint of the explosive outflows that were subsequently identified in

star forming regions. The formaldehyde is seen in absorption agains the 2.7 K microwave background, since there is no radio continuum source in this direction. The spectrum verifies the existence of the background radiation and also shows that the excitation temperature of the upper level lies below the 2.7 K background, implying some sort of antimaser process.

The detection of the polyatomics made it clear that many other species should be present, and Penzias and Wilson at Bell Laboratories soon developed 3 mm receivers for the 36 foot antenna of the NRAO at Kitt Peak to search in the rich millimeter wavelength region of the spectrum. With a number of collaborators, they, and others using that telescope, discovered a great many interstellar molecules during the early seventies (e.g., Wilson et al., 1970; Snyder and Buhl, 1971; Turner, 1971; Solomon et al., 1971; Zuckerman et al., 1971).

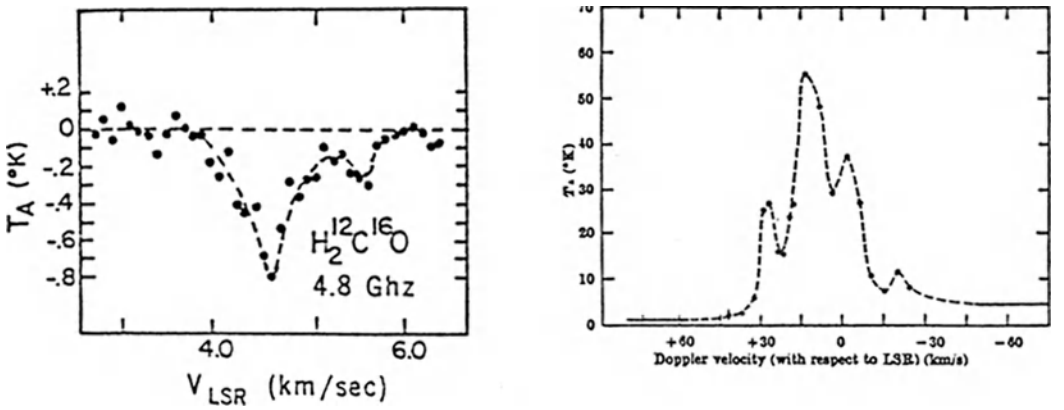

Fig. 1. Formaldehyde in absorption in the direction of Heiles Cloud 2 (Palmer et al., 1969); Water in emission in W 49 (Cheung et al., 1968)

More recently, there have been a few relatively complete spectral searches in the molecule-rich regions Orion/KL and Sgr B2. Cummins et al. (1986) surveyed Sgr B2 over 70–150 GHz with the 7 m BTL dish, Johansson et al. (1984) observed this source over 70–93 GHz with the Onsala 20 m telescope, and Sutton et al. (1985) surveyed Orion/KL over 208–263 GHz with a 10 m telescope at Owens Valley, finding over 800 lines. A summary of the molecules known as of June 1985 by Winnewisser and Herbst (1987) lists 70 identified species.

There is a continuous flow of further discoveries of molecules (e.g., CH_3C_5N [Snyder et al., 1985]) often enabled by laboratory spectroscopy (e.g., C_3H_2, the first interstellar ring molecule [Thaddeus et al., 1985]). In addition, the sensitivities of the Nobeyama 45 m and the IRAM 30 m telescopes have further accelerated detections of molecular lines. A recent paper of Cernicharo et al. (1987) reports the detection of some 50 lines of the linear radical C_6H at the 30 m which allows the determination of many of the molecular constants!

Theoretically, the initial discovery of polyatomic molecules was a surprise because it was difficult to understand how their formation could take place through normal gas phase chemical processes at the low densities of the interstellar medium. Subsequently,

Herbst and Klemperer (1973) showed that ion-molecule reactions could indeed produce polyatomics and were able to explain the observed abundance of many of the smaller molecules. These exothermic reactions have the necessary high cross sections at low temperatures and densities. For the larger more complex species, radiative association appears to be effective. In addition, important chemistry may be taking place on the surfaces of grains. It is easy to show that the time between collisions between grains and molecules is short compared to both the probable cloud lifetimes and the time required to reach steady state in the gas phase processes. This argues that molecules must stick and then be desorbed from grains in order that a gas phase exist at all. It seems likely that grains may play a catalytic role in all of interstellar chemistry. Note that ammonia, which is observed in many regions, is not well produced by the gas phase schemes and is probably catalyzed on grains. Finally, very great chemical enrichment is observed in the winds of massive protostars. Evidence is mounting that all stars, of nearly all masses, exhibit winds as they form, and it is possible that much of the molecular material in dust clouds may be the result of chemical processing in the high temperature winds and associated shocks of all the stars forming within the cloud.

II. Galactic Structure

Among the molecules, the discovery of CO by Wilson *et al.* (1970) has had the most profound impact in other areas of astronomy. This diatomic is sturdy, widely distributed throughout the Galaxy, and is collisionally excited into emission within clouds whose densities are only a few hundred hydrogen molecules/cm^3. It is widely observed throughout the Milky Way, and its study has significantly altered our view of the Galaxy. After the early studies of particular regions, a number of groups have carried out extensive maps of large regions of the Galaxy, particularly close to the plane (Dame *et al.*, 1986; Sanders *et al.*, 1986; Burton and Gordon, 1978).

Many new facts have emerged from these studies: Approximately half the hydrogen gas in the Galaxy is in molecular form. It is found in extensive complexes, called Giant Molecular Clouds, with masses up to 10^6 $M_\odot$ or more and densities between a few to more than 10^{10} H_2 molecules/cm^3. Young stellar associations are found within or near these complexes, indicating that star formation takes place within these clouds. The molecular clouds consist of clumps on all size scales down to the smallest observable (e.g., Solomon and Sanders, 1985). Most of this material exhibits power law relations between size, mass, and velocity dispersion and is in approximate virial equilibrium. There is another population, more easily observed at high latitudes, of lower mass clumps that are not in virial equilibrium (Blitz *et al.*, 1984). The H_2 gas is more highly concentrated toward the center of the Galaxy than is the atomic H, it is most dense in a ring between four and eight kpc radius, and its scale height is closer to that of the Pop I stars than is that of the atomic H. This latter fact suggests that the formation of stars is, on the average, simply proportional to the gas density.

III. Individual Regions

The observation of molecular emission and absorption in particular regions has produced important information, especially related to star formation. In the earliest stages of

formation, the stars are deeply imbedded in the clouds and can be studied only at infrared and radio wavelengths. In addition to providing information about density and temperature of the gas, the line emission also shows the radial velocity of the gas.

Figure 2 shows the classic study of the L1551 region in CO by Snell *et al.* (1980). From the asymmetries in the CO spectra shown in the lower left frame, they found that collimated gas is apparently flowing out from the central young star in a "bipolar" fashion. The momentum in the flow is too large to be directly driven by stellar luminosity. Subsequently, many such sources have been found with large momentum flows, too large to be directly radiatively driven, but nevertheless correlated with the central star luminosity. The most recent evidence suggests that virtually all stars exhibit outflows which may coexist with accretion. The winds may therefore be a simultaneous byproduct of the accretion that produces the stars (Shu and Lizano, 1987). Studies of molecules other than CO also reveal these winds. Many of the other species, which are as ubiquitous as CO but typically three or more orders of magnitude less abundant, require much higher densities of surrounding H_2 for them to be significantly excited into emission. These are useful for studies of the more dense regions.

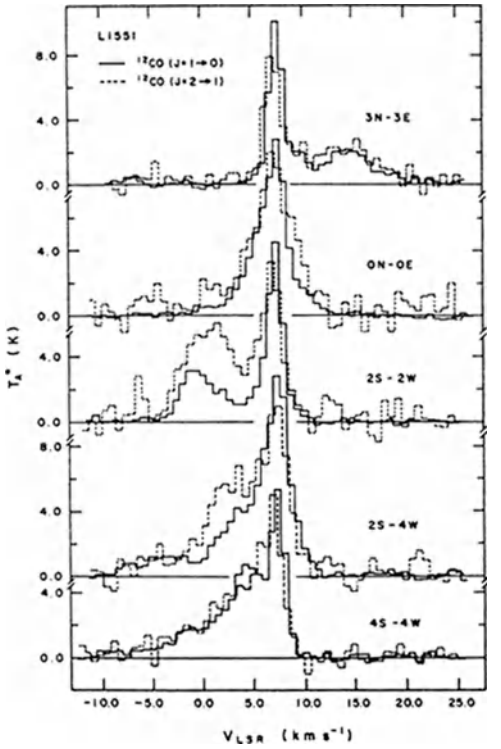

Fig. 2. CO in L1551 (Snell *et al.*, 1980)

Studies of different transitions of a given molecule often reveal processes at different temperatures which have different dynamics. Richardson *et al.* (1985) show CO spectra of the HH 7-11 region corresponding to transitions between the lowest three rotational states of the molecule. The spectra differ dramatically from one another, even though the energy

levels span only the range from 0 K up to about 33 K. Maps with adequate resolution show that the warmer gas is in a bipolar outflow (the two peaks in the spectrum) whereas the cooler gas is dominated by the quiescent cloud, which even shows self absorption. This is a good example of the potential power of multi-transition mapping.

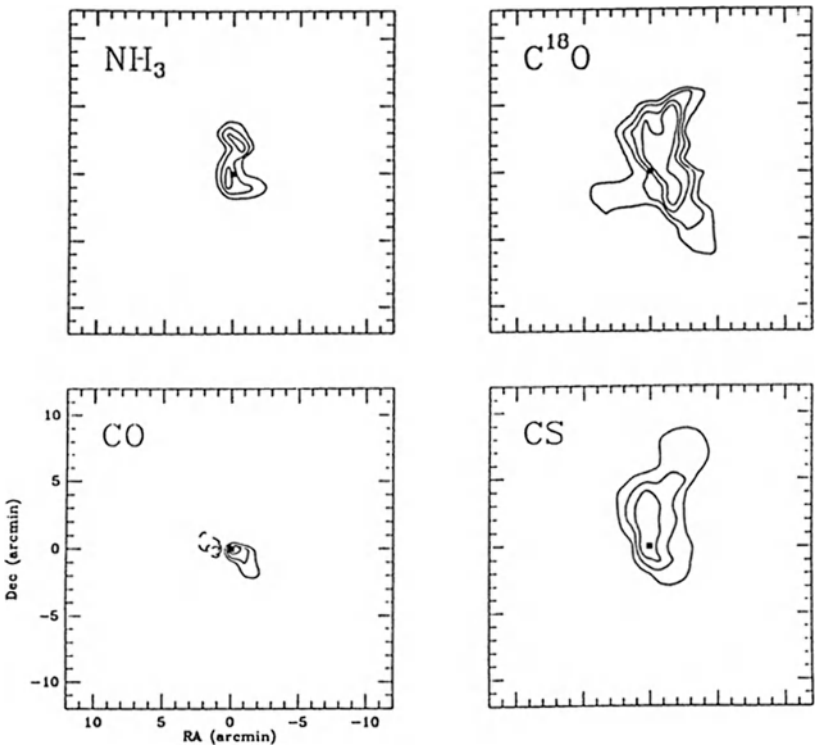

Fig. 3. Four molecular lines in B 5 (Fuller and Myers, private communication)

Maps of particular regions in different molecules show striking difference from one another. Figure 3, from Fuller and Myers (private communication), shows the low mass star formation region B 5 observed in four molecules. Some of the differences, e.g., CO vs $C^{18}O$, are due to optical depth effects, and some may be due to excitation, e.g., CS vs $C^{18}O$. The map of NH_3 may show real abundance differences. In regions of high mass star formation, where there are stronger winds and shocks, the differences are more dramatic and are almost certainly real abundance differences. Maps of many molecules at angular resolutions of about 3″ toward Orion/KL show some similarities but, on the whole, very large differences (Plambeck and Wright, private communication). The challenge is to understand the chemistry here.

IV. VLBI: The Highest Resolution

Maser emission from interstellar molecules, such as OH, H_2O, and SiO, provides the most spectacular evidence of non-LTE excitation of interstellar molecules. The first VLBI

observations of maser emission in OH (Moran *et al.*, 1968) showed clusters of tiny bright spots each as small as a few milliarcseconds. The brightest and most compact masers are those in H_2O, and the study of these sources has produced especially important astronomical results. Genzel *et al.* (1981) show the result of proper motion measurements of the water maser spots in the Orion/KL region. The masers are seen expanding from a central source near IRC2, the first unequivocal evidence of outflow and an explanation of the broad spectrum shown in Figure 1. From the proper motion, a first direct distance for the Orion region, 480 pc, is established. Following this success, the same group has obtained a proper motion distance to the Galactic Center source Sgr B2 by the same technique and thereby established the scale of the Galaxy. The distance from the sun to the center is 7.1 ± 1.5 kpc (Reid et al., in press).

The future will see proper motion distances to the nearest galaxies which exhibit maser emission. The work has already begun, but full exploitation of this technique awaits completion of the VLBA.

V. The Giant Stars

Wilson and Barrett (1968) discovered maser emission from a red giant star, showing the molecular richness of its envelope. Subsequent observations of late type giant envelopes show them to be rich in many molecules (Zuckerman, 1980). The study of the expanding envelopes in CO (Knapp and Morris, 1985) has enabled the estimation of mass loss and has shown, for example, that the red giants account for a substantial fraction of the return of stellar processed material to the interstellar medium. The carbon star IRC+10216 has an especially rich molecular spectrum. In addition to the enormous number of molecules, including long chains, there is now direct evidence of chemical evolution in its envelope (Bieging and Rieu, 1988). Molecules such as HNC and HC_3N are seen to increase in abundance in the envelope as it expands away from the star.

The future for studies in the chemistry of carbon star envelopes holds great promise. The physical structure is relatively simple and well understood as compared with molecular clouds, allowing for much more accurate modeling of observations. In addition, the time scales for expansion are comparable to the time scales of the late evolutionary stages of these stars. With care it may be possible to observe the isotopic evolution of the stellar interior metals in the distributions in the expanding envelope.

VI. The View Beyond, Molecules in Other Galaxies

Since the first detection of CO in other galaxies in the mid 1970's, there have been many studies of individual galaxies and extensive surveys, so that several hundred galaxies have now been detected (e.g., Stark *et al.*, 1986; Kenney and Young, 1986; Rickard and Blitz, 1985; Lo *et al.*, 1987; Casoli *et al.*, 1987; Israel, 1988). Most of this work is in CO, although a few other molecules have been detected in a few of the brightest galaxies. Most of these are spirals. The brightest are the so-called "starburst galaxies" (Rieke *et al.*, 1985). The sensitivity of CO observations compares very favorably with that of HI, and it is hoped that the CO work will delineate the distribution of the molecular

content of galaxies. The evidence is that the H_2/CO ratio varies greatly from one galaxy to the next (Israel, 1988), and considerable effort will be required to extract the H_2 distributions from the CO observations.

However, there are already interesting results. For example, surveys of the Virgo cluster galaxies (Stark *et al.*, 1986; Kenney and Young, 1986) show that those spirals nearer the cluster nucleus have a greater ratio of CO to H I than those in the outer parts, suggesting that the H I may be more readily stripped than the molecular gas by motions through the cluster medium. Another example is the recent high resolution study by Vogel *et al.* (1988) of M51 in CO shown in Figure 4. CO delineates the spiral arms and shows the streaming motions predicted by density wave theory that may trigger star formation. In the nearby galaxies M31 and M33, giant molecular clouds similar to those in our galaxy are seen.

The future promise of extragalactic studies is considerable. The CO work is already beginning to yield results with respect to galactic structure and evolution. Further progress will come from completely sampled observations at a large range of resolutions combined with studies at many other wavelengths. On the instrumental side, both the single dish focal plane arrays and the interferometers will play important roles.

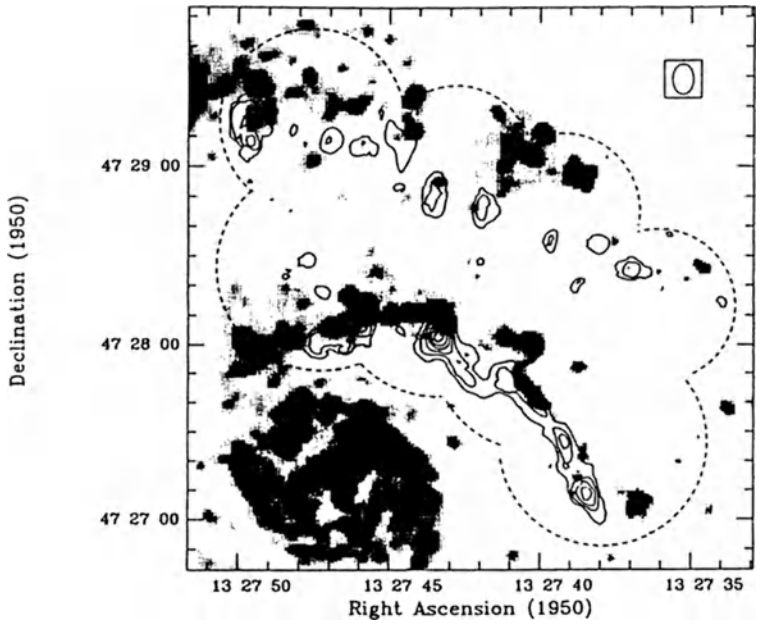

Fig. 4. M51 CO contours (Vogel *et al.*, 1988)

VII. The Instruments

The great interest in studying the molecular content of the interstellar medium has produced a remarkable increase in the number of telescopes that can operate at millimeter

and submillimeter wavelengths. There are, at present writing, 17 telescopes ranging in size from 1.5 m to 45 m operating at millimeter wavelengths. There are four new submillimeter telescopes, largely in the 10–15 m class. There are four arrays either in operation or soon to be operating at millimeter wavelengths, and there are plans for two new arrays for operation both at millimeter and at submillimeter wavelengths. Altogether, this activity exceeds all earlier numbers of telescopes at other radio wavelengths.

VII. The Future

Future developments in the various areas of molecular astronomy have been touched upon above. In terms of fundamental astronomy, the measurement of parallax distances in other galaxies stands out as an especially important future development. Perhaps the most important other exciting observation of the future which will be enabled by molecular line studies will be the detection of the formation of both stars and their associated solar systems. The basically thermal emissions that characterize these processes become stronger at the shorter submillimeter wavelengths, enabling the necessary high angular resolution. It will be the submillimeter arrays that will have the sensitivity and angular resolution to reveal these processes.

References

Bieging, J.H., and Rieu, N.Q. 1988, *Ap. J.*, in press.
Blitz, L., Magnani, L., and Mundy, L. 1984, *Ap. J. (Letters)*, **282**, L9.
Burton, W.B., and Gordon, M.A. 1978, *Astr. Ap.*, **63**, 7.
Casoli, F., Combes, F., and Stark, A.A. 1987, *Astr. Ap.*, **173**, 229.
Cheung, A.C., Rank, D.M., Townes, C.H., Thornton, D.D., and Welch, W.J. 1968, *Phys. Rev. Lett.*, **21**, 1701.
Cheung, A.C., Rank, D.M., Townes, C.H., and Welch, W.J. 1969, *Nature*, **221**, 917.
Cernicharo, J., Guélin, M., Menten, K. M., and Walsley, C. M. 1987, *Astr. Ap.*, **181**, L1.
Cummins, S.E., Linke, R.A., and Thaddeus, P. 1986, *Ap. J. Suppl.*, **60**, 819.
Douglas, A.E., and Herzberg, G. 1941, *Ap. J.*, **94**, 381.
Dame, T., Elmegreen, B.G., Cohen, R.S., and Thaddeus, P. 1986, *Ap. J.*, **305**, 892.
Genzel, R., Reid, M.J., Moran, J.M., and Downes, D. 1981, *Ap. J.*, **244**, 884.
Herbst, E., and Klemperer, W. 1973, *Ap. J.*, **185**, 505.
Israel, F. 1987, in *Millimetre and Submillimetre Astronomy*,, eds. R. D. Wolstencroft and W. B. Burton, Kluwer.
Johansson, L. E. B., et al. 1984, *Astr. Ap.*, **130**, 227.
Kenney, J. D., and Young, J. S. 1986, *Ap. J. (Letters)*, **301**, L13.
Knapp, G. R., and Morris, M. 1985, *Ap. J.*, **292**, 640.
Kutner, M., Thaddeus, P., Jefferts, K. B., Penzias, A. A., and Wilson, R. W. 1971, *Ap. J. (Letters)*, **164**, L49.
Lo, K. Y., Ball, R., Masson, C. R., Phillips, T. G., Scott, S., and Woody, D. P. 1987, *Ap. J. (Letters)*, **317**, L63.
McKellar, A. 1941, *Publ. Dominion Ap. Obs. Victoria, B. C.*, No. 15, **7**, 251.
Moran, J. M., et al. 1968, *Astron. J.*, **73**, S27.
Palmer, P., Zuckerman, B., Buhl, D., and Snyder, L. E. 1969, *Ap. J. (Letters)*, **156**, L147.
Richardson, K. J., White, G. J., Avery, L. W., Lesurf, J. C. G., and Harten, R. H. 1985, *Ap. J.*, **290**, 637.
Rickard, L. J, and Blitz, L. 1985, *Ap. J. (Letters)*, **292**, L57.
Sanders, D. B., Clemens, D. B., Scoville, N. Z., and Solomon, P. M. 1986, *Ap. J. Suppl.*, **60**, 1.
Shu, F., and Lizano, S. 1987, in *Interstellar Matter*, eds. P. Ho and J. M. Moran, Gordon and Breach.
Snell, R. L., Loren, R. B., and Plambeck, R. 1980, *Ap. J. (Letters)*, **239**, L17.
Snyder, L. E., and Buhl, D. 1971 *Ap. J. (Letters)*, **163**, L47.
Solomon, P. M., Jefferts, K. B., Penzias, A. A., and Wilson, R. W. 1971, *Ap. J. (Letters)*, **168**, L111.
Solomon, P. M., and Sander, D. B. 1985, in *Protostars and Planets II*, eds. D. Black and M. Mathews, Univ. of Arizona.

Stark, A. A., Knapp, G. R., Bally, J., Wilson, R. W., Penzias, A. A., and Rowe, H. E. 1986, *Ap. J.*, **310**, 660.
Sutton, E. C., Blake, G. A., Masson, C. R., and Phillips, T. G. 1985, *Ap. J. Suppl.*, **58**, 341.
Swings, P., and Rosenfeld, I. 1937, *Ap. J.*, **86**, 483.
Thaddeus, P., Vrtilek, J. M., and Gottleib, C. A. 1985, *Ap. J. (Letters)*, **299**, L63.
Townes, C. H. 1957, IAU Symposium No. 4, ed. H. C. van de Hulst, Cambridge Univ., p. 92.
Turner, B. E. 1971, *Ap. J. (Letters)*, **163**, L35.
Vogel, S. N., Kulkarni, S., and Scoville, N. Z. 1988, *Nature*, in press.
Weaver, H., Williams, D. R. W., Dieter, N. H., and Lum, W. T. 1965, *Nature*, **208**, 29.
Weinreb, S., Barrett, A. H., Meeks, M. L., and Henry, J. C. 1963, *Nature*, **200**, 829.
Wilson, R. W., Jefferts, K. B., and Penzias, A. A. 1970, *Ap. J. (Letters)*, **161**, L43.
Wilson, W. J., and Barrett, A. H. 1968, *Science*, **161**, 778.
Zuckerman, B., Ball, J. A., and Gottlieb, C. A. 1971, *Ap. J. (Letters)*, **163**, L41.
Zuckerman, B. 1980, *Ann. Rev. Astr. Ap.*, **18**, 263.

GALACTIC MOLECULAR SURVEYS: THE ROLE OF SMALL TELESCOPES

P. Thaddeus
Harvard-Smithsonan Center for Astrophysics
60 Garden Street, Cambridge, Massachusetts 02138

Stimulated by the discovery of interstellar molecules and the realization of the fundamental role of molecular clouds in star formation and galactic structure, an effort is underway in many countries to build new radio telescopes for spectral-line work. These instruments are designed to operate mainly at millimeter wavelengths, the band where most of the 85 molecules known to exist in space were identified and where molecules generally are most readily observed. Most of the effort and funding have been devoted to construction of large single-dish antennas and multielement interferometers, well suited for studying small sources but inefficient for extended objects. Some of the most interesting scientific issues raised by the discovery of cosmic molecules, however, such as the structure and evolution of molecular clouds and their role in the structure of the Galaxy, require surveys of large areas and large amounts of data, which are poorly addressed by high resolution instruments serving a long queue of users. Even for the detailed study of localized regions, large telescopes are often hobbled without preliminary survey work by small instruments, much as large optical reflectors would be crippled without preliminary wide-angle Schmidt surveys. The Gornergrat 3 m telescope, whose inauguration we are celebrating at this meeting, is the kind of instrument needed to establish a sound balance between large and small facilities in millimeter-wave astronomy.

Here I will summarize briefly the areas in molecular radio astronomy where small telescopes have proven effective, list the main surveys my students and colleagues and I have conducted in both hemispheres with two nearly identical 1.2 m instruments, and describe what I think are some promising opportunities for future work. By a small millimeter-wave telescope I mean one with an aperture of 1 to 3 meters, thus including both our two telescopes and the one on the Gornergrat. Although dwarfed in size by many new instruments, by the standards of early radio surveys of the sky such telescopes are not at all small in terms of wavelength and hence angular resolution. Table 1, for example, gives the resolution of several small telescopes at the most widely observed molecular line, the 1-0 transition of CO at 2.6 mm, and for comparison the aperture required at 21 cm to achieve the same resolution. Even our telescopes have the same resolution at CO as the 100 m Bonn antenna, the largest steerable paraboloid at 21 cm, and the Gornergrat telescope has nearly 3 times the Bonn resolution. All these small instruments have

surfaces accurate enough to work efficiently at the 2-1 and 3-2 CO lines, where their resolution is higher yet by factors, respectively, of 2 and 3. Since the landmark Australian-Dutch 21 cm surveys of the Galaxy were done with instruments with an aperture of less than 11 meters, by the standards of classical radio astronomy, all existing small millimeter-wave telescopes are remarkably large.

Telescope	Aperture	Beam (HPBW)	Equiv. 21 cm aperture
Cambridge-Cerro Tololo	1.2 m	8.8'	100 m
POM-2 (Plateau de Bure)	2.5	4.2	208
Gornergrat	3.0	3.6	250

Table 1. Small millimeter-wave telescopes

The kinds of work at which small telescopes excel include:

•The study of the large-scale distribution of molecular clouds in the Galaxy

•The mapping of individual nearby giant cloud complexes and dark nebulae

•The study of the relationship between molecular clouds and the diffuse component of Galactic gamma rays

•The study of the molecular component of the high-latitude infrared"cirrus"

•Preliminary molecular surveys of the nearest external galaxies, particularly the Magellanic Clouds.

Small telescopes, on the other hand, because of their limited angular resolution can not compete with large instruments in the study of

•Galaxies beyond the Local Group

•Molecules in circumstellar shells and bipolar outflows, and

•Maser point sources

and so far at least they have been little used for

•Molecular line surveys and the search for new molecules.

As examples of the range of problems that can be addressed with small telescopes, Table 2 lists the main molecular cloud studies undertaken with our two instruments. Nearly all are of the normal CO isotope at 115 GHz and, except for the surveys of the Magellanic Clouds (described by Dame and by Rubio elsewhere in this volume), all are of objects within our own Galaxy and were undertaken with three general objectives: 1) To produce a fairly complete unbiased inventory at low resolution of both nearby and distant

Survey	References
Molecular Clouds in Orion and Monoceros.	Kutner *et al.* 1977; Maddalena *et al.* 1986
Cygnus X Region of the Galactic Plane	Cong 1977
Deep Survey of the First Galactic Quadrant	Cohen *et al.* 1980, 1986; Dame *et al.* 1986
Molecular Clouds in the Vicinity of W3, W4, and W5	Lada *et al.* 1978
GMC's Associated with the Rosette Nebula, NGC 2264, and CMa OB-1	Blitz and Thaddeus 1980
Large Star-Free Cloud in Monoceros	Maddalena and Thaddeus 1985
Wide-Latitude Survey of the First Galactic Quadrant	Dame and Thaddeus 1985; Grenier 1989
Supernova Remnants in the Outer Galaxy	Huang and Thaddeus 1985, 1986
The Carina Arm	Cohen *et al.* 1985; Grabelsky *et al.* 1988
Dark Nebulae in Perseus, Taurus, and Auriga	Ungerechts and Thaddeus 1987
Entire Milky Way*	Dame *et al.* 1987
Region of the Galactic Center	Bitran 1987
IR Cirrus in Ursa Major	de Vries and Thaddeus 1987
Wide-Latitude Third and Fourth Galactic Quadrants	May *et al.* 1988; Nyman 1989
Deep Survey of the Fourth Galactic Quadrant	Bronfman *et al.* 1988
Large Magellanic Cloud	Cohen *et al.* 1988; Dame this vol.
Small Magellanic Cloud	Rubio this vol.
Dark Clouds in Ophiuchus	de Geus *et al.* 1989
Southern Coalsack	Nyman *et al.* 1989
Thirty-Four Galactic Clusters	Leisawitz *et al.* 1989

* A composite of a number of surveys, most at a resolution of 0.5°

Table 2. Major CO surveys undertaken with the telescopes in the U. S. and Chile

molecular clouds for comparison with other "global" surveys, especially the IRAS survey at 100 μ and the COS-B survey of the Galactic component of high- energy γ-rays; 2) To survey the distant clouds in the inner Galaxy at full resolution to determine their mass and distribution throughout the system; and 3) To study individual nearby clouds in detail, especially those associated with well-studied regions of star formation.

The culmination of our low resolution survey work is a composite map at a resolution of 0.5° of the molecular clouds in a thick band along the the entire Milky Way (Dame *et al.* 1987). With this it has been possible to partition most of the molecular gas within 1 kpc of the solar system into discrete clouds, to associate many of these with dark nebulae, stellar associations, and other Population I, and to determine the mean density and scale height of molecular gas in the local interstellar medium — parameters quite poorly known previously which are of considerable value in many areas of Galactic astronomy and may even be relevant to the evolution of the comet cloud of the solar system. Further, from an intercomparison of our low-resolution surveys, 21 cm surveys, and the high-energy γ-ray data obtained by COS-B, it has been possible to calibrate over much of the Galaxy the important CO-to-H_2 ratio [specifically, the ratio of velocity-integrated CO line emission W_{CO} to H_2 column density $N(H_2)$] required to derive the mass of molecular clouds. The result, $N(H_2)/W_{CO} = 2.3 \pm 0.3 \times 10^{20}$ cm^{-2}/ (K km s^{-1}) (Strong *et al.* 1988), is in fairly good agreement with that derived under quite different assumptions by two other methods, i.e., from star counts and from the virial theorem.

Although the surveys listed in Table 2 represent a fairly complete inventory of Population I in the Galaxy — except for the high latitude cirrus — they can nearly all be profitably extended in resolution and sensitivity with small telescopes, and the exploration of the Galaxy with the CO isotopic species and heavier molecules can hardly be said to have begun. The following are some of the projects that will keep small telescopes well occupied for the next generation.

Giant Molecular Clouds Fairly general agreement now exists among observers that the mass spectrum of molecular clouds over much of the Galaxy is fairly "flat", with most of the mass in the largest condensations. Evidence supporting this conclusion has been obtained from the "molecular ring" at R ~ 4 kpc to the Perseus Arm beyond the solar circle; in this large region the mass cutoff at the high end is apparently between 5×10^6 and 10×10^6 $M_\odot$, with 50–70 % of the total mass in objects more massive than 1×10^6 $M_\odot$. Bronfman *et al.* (1988) derived from a joint analysis of our Northern and Southern deep surveys a total molecular mass of 1.2×10^9 $M_\odot$ between R = 2 kpc and the solar circle, so the molecular gas there is sufficient for at most a few hundred such giant clouds. Near the

solar circle their characteristic separation is several kiloparsecs; one of those nearest to the Sun is associated with the SNR W44 in the Sagittarius Arm, and a second is associated with Cas A and NGC 7538 in the Perseus Arm, both at a distance of about 3 kpc.

Nearly 20 years after the discovery of interstellar CO, astonishingly *none* of the near giant clouds has been adequately surveyed in CO or any other molecule. Those like the Cas A object which are close enough to be visible optically are of particular interest from the standpoint of star formation, and as they typically cover areas of at least 10 deg^2 are ideal subjects for study with small telescopes. The general issues which can be addressed are among the most challenging in the fields of star formation, Galactic structure, and interstellar gas dynamics: How and why do these huge concentrations of dense gas form, and how do they evolve? How long do they last? What is the efficiency of star formation? How does star formation depend on density and other parameters, and how destructive is it to the structure and integrity of the clouds? If star formation in the giant clouds represents a self-propagating conflagration, as some observations suggest, on what scale does this process operate, and what is the relative contribution to it of the two most likely sources of disruption: supernovae and OB winds?

Other questions of a somewhat more specialized nature should also be addressed: How good, for example, is CO as a mass tracer vs. ^{13}CO and $C^{18}O$? As a general survey tool, are the higher rotational transitions of CO (e.g., 2-1 and 3-2) largely degenerate with the 1-0 transition, or are they a significant source of new information? How important and extensive are the atomic halos of the giant clouds, and do the clouds possess molecular halos deficient in CO? It would be foolish to suppose that observations with small telescopes alone will answer such questions, but by providing the mass and velocity structure they are the necessary first step. Since CO emission can almost be said to define a molecular cloud, the best way to begin the systematic investigation of the giant clouds is with complete, well-sampled surveys in CO and possibly ^{13}CO.

Dark Nebulae Nearby dark nebulae like the Taurus Dark Clouds and the Great Rift in the Milky Way are modest in mass relative to the giant clouds, but they are of great interest because they are so close that star formation, particularly that of late-type stars, can be studied in detail. Some of them cover solid angles an order of magnitude larger than that of the nearest giant clouds and are therefore particularly suitable for study with small telescopes. Nearly all our surveys of large dark nebulae have been at reduced angular resolution (e.g., Ungerechts and Thaddeus 1987), so even in CO there is a great deal more to be done. As with the giant clouds, a systematic study of heavier molecules has hardly begun.

Spiral Structure The structure of the Galaxy within the solar circle is still a largely unsolved problem requiring much further work best done with small telescopes. Our Northern and Southern CO surveys have shown that the Perseus and Carina Arms in the outer Galaxy are well defined in molecular clouds, and there now can be little doubt that molecular observations are *in principle* a very powerful tool with which to determine the distribution of matter in a spiral system such as ours. To determine the actual structure of the crowded inner arms of the Galaxy is not an easy matter, however, largely because of the twofold kinematic distance ambiquity within the solar circle. The giant clouds may be the key to the solution for two reasons: first, they are so luminous that they can be distinguished at large distances, and, second, from their Population I progeny it is often possible to determine approximate distances and so resolve the kinematic ambiguity. Because of the large areas to be covered, small telescopes are well qualified for investigations of this sort. We have made a start by showing that the Sagittarius Arm in the first Galactic quadrant is fairly well defined by large clouds, and that with the Carina Arm in the fourth quadrant it may represent a single feature at a pitch angle of about 10° extending nearly three-quarters of the way around the Galaxy (Grabelsky *et al.* 1988). We have as yet, however, no unambiguous model for the arrangement of clouds near the peak of the molecular distribution about halfway to the Galactic Center in the molecular ring, and whether we are observing spiral arms there, or a bar, or both, is quite unclear. To dissect the structure of the inner Galaxy will require observations at many wavelengths, but those with small telescopes of CO and other molecules will undoubtedly be an important part of the solution.

Line Surveys Spectral line surveys and the discovery of new molecules have until now been a virtual monopoly of large telescopes, but for reasons not fundamental. One is simply that until recently only large facilities have been equipped with the expensive wide band spectrometers and sensitive receivers tunable over a substantial part of the millimeter-wave spectrum required for such work; another is that the best molecular sources discovered to date (e.g., Sgr B2, Ori A, and IRC+10216) tend to be somewhat smaller than the beams of small telescopes. The Gornergrat telescope near the top of its range in the submillimeter band will begin to resolve some of these rich sources and so should be able to undertake line surveys nearly as sensitive as those done with larger instruments. The possibility always exists, too, that new close sources like TMC-1 will be found that are both rich in exotic molecules and fairly large in angular extent. Further, line surveys and the search for new molecules typically require large amounts of observing time and so are generally easier to schedule on small telescopes than large ones. For these reasons, a

growing fraction of the work in this area might be expected to be done by small telescopes during the next few years.

Infrared Cirrus The high-latitude far infrared "cirrus" observed by IRAS can often be detected in CO, but these objects have almost no associated star formation and de Vries in his thesis (1988) has calculated that they probably constitute *in toto* only a few percent of the mass of the molecular cloud population in the general vicinity of the Sun. The molecular component of the cirrus is apparently the chaff of the molecular cloud distribution — the small mass end of the spectrum — visible largely because of the absence of confusion with background or foreground objects at high latitude and of little importance relative to the large molecular clouds nearer the plane. The cirrus, however, is almost certainly close, with the usual claim in astronomy to attention of close objects , and it poses several interesting questions well addressed with small telescopes. Just how close in fact is it? Is it in the process of formation, or dissolution, perhaps the result of the breakup of much larger clouds under the lash of star formation? What is the energy source of the far-infrared emission? What relationship if any does the cirrus have to the large system of arcs observed at 21 cm? As with the giant clouds, what is mainly needed at this point are systematic low-flux surveys starting with CO, and since the cirrus covers a significant fraction of the sky at high latitudes, these can be done properly only with small instruments able to devote a substantial time to the project.

Nearby Galaxies The Large Magellanic Cloud has already been rather completely surveyed with our telescope in Chile (Cohen *et al.* 1988), and the Small Magellanic Cloud partially so, providing a starting point for detailed studies with the new SEST telescope at high resolution. In the LMC the molecular clouds are quite extensive, covering at least 10% of the inner 6° x 6° of the galaxy, but they are also faint in CO, probably owing to the low metallicity, and will require many years to study adequately with SEST. A large amount of work therefore remains to be done on the LMC with small telescopes such as ours. We may undertake a deeper survey of the 1-0 line around the main molecular condensations, particularly the huge complex extending south from 30 Dor for over 2000 pc.

The Magellanic Clouds are not the only galaxies in the Local Group which can be profitably studied with small telescopes, especially instruments like the Gornergrat which are somewhat larger than ours. For example, over the last decade only a small fraction (~ 15%) of M31 has been surveyed in CO with the 7 m Bell telescope, and a complete survey to guide the IRAM 30 m telescope and other large instruments is badly needed; a complete

survey at high sensitivity with the Gornergrat telescope would be of considerable value, as might a similar study of M33.

REFERENCES

Bitran, M. 1987, Ph. D. dissertation, Univ. Florida.
Blitz, L., and Thaddeus, P. 1980, *Ap. J.*, **241**, 676.
Bronfman, L., *et al.* 1988, *Ap. J.*, **324**, 248.
Cohen, R. S., Cong, H.-I., Dame, T. M., and Thaddeus, P. 1980, *Ap. J. Lett.*, **239**, L53.
Cohen, R. S., *et al.* 1985, *Ap. J. Lett.*, **290**, L15.
Cohen, R. S., Dame, T. M., and Thaddeus, P. 1986, *Ap. J. Suppl.*, **60**, 695.
Cohen, R. S. *et al.* 1988, *Ap. J. Lett.*, **331**, L95.
Cong, H.-I. 1977, Ph. D. dissertation, Columbia Univ.
Dame, T. M., and Thaddeus, P. 1985, *Ap. J.*, **297**, 751.
Dame, T. M. *et al.* 1986, *Ap. J.*, **305**, 892.
Dame, T. M., *et al.* 1987, *Ap. J.*, **322**, 706.
Georgelin, Y. M., and Georgelin, Y. P. 1976, *Astr. Ap.*, **49**, 57.
de Geus, E. J., Bronfman, L., and Thaddeus, P. 1989, *Astr. Ap.*, in press.
Grabelsky, D. A., *et al.* 1988, *Ap. J.*, **331**, 181.
Grenier, I. 1989, in preparation.
Huang, Y.-L., and Thaddeus, P. 1985, *Ap. J. Lett.*, **295**, L13.
Huang, Y.-L., and Thaddeus, P. 1986, *Ap. J.*, **309**, 804.
Kutner, M. L., Tucker, K. D., Chin, G., and Thaddeus, P. 1977, *Ap. J.*, **215**, 521.
Lada, C., Elmegreen, B., Cong, H.-I., and Thaddeus, P. 1978, *Ap. J. Lett.*, **226**, L39.
Leisawitz, D., Thaddeus, P., and Bash, F. 1989, *Ap. J. Suppl.*, in press.
Maddalena, R. J., and Thaddeus, P. 1985, *Ap. J.*, **294**, 231.
Maddalena, R. J., Morris, M., Moscowitz, J. and Thaddeus, P. 1986, *Ap. J.*, **303**, 375.
May, J., Murphy, D. C., and Thaddeus, P. 1988, *Astr. Ap. Suppl.*, **73**, 51.
Nyman, L. Å., Bronfman, L., and Thaddeus, P. 1989, *Astr. Ap.*, in press.
Nyman, L. Å. 1989, in preparation.
Strong, A. W., *et al.* 1988, *Astr. Ap.*, **207**, 1.
Ungerechts, H., and Thaddeus, P. 1987, *Ap. J. Suppl.*, **63**, 645.
de Vries, H. W., Heithausen, A., and Thaddeus, P. 1987, *Ap. J.*, **319**, 723.
de Vries, H. W. 1988, Ph. D. dissertation, Columbia Univ.

Mass Calibration of CO Surveys: New Insight from IRAS

J.B.G.M. Bloemen
Leiden Observatory, P.O. Box 9513, 2300 RA Leiden, The Netherlands

Summary

The relation between integrated CO line intensity W_{CO} and H_2 column density is discussed, with emphasis on new constraints set by the IRAS survey in the 100-μm band. For clouds predominantly heated by the ambient ISRF, N_{H_2}/W_{CO} appears to be anti-correlated with the FIR emissivity per nucleon inside the cloud relative to that in the surrounding medium. This suggests a correlation between N_{H_2}/W_{CO} and total extinction for clouds with $A_v > 1$ mag, in accordance with expectations, ranging from typically about $(0.5-1)\times10^{20}$ molecules cm^{-2} (K km s^{-1})$^{-1}$ for clouds with $A_v \simeq 1-3$ to $\sim 2\times10^{20}$ for giant molecular clouds.

1 Introduction

Molecular hydrogen plays an important role in studies of the structure and evolution of galaxies, but direct H_2 observations are unfortunately only feasible for selected small-scale regions. These direct detections are restricted to either far-ultraviolet wavelengths where cold H_2 appears in absorption, but the number of suitable background stars is small (e.g. Spitzer and Jenkins 1973; Savage et al. 1977), or near-infrared wavelengths where excited H_2 appears in emission, but this possibility is limited to regions where H_2 is heated by shocks or an intense ultraviolet radiation field (e.g. Shull and Beckwith 1982; Black and van Dishoeck 1987). The CO molecule, next most abundant after H_2, is relatively easy to observe (particularly the J = 1→0 transition of ^{12}CO at 2.6 mm, discussed here) and therefore frequently used as a probe of molecular gas. It is evidently essential to know how to convert from the observed CO integrated intensity (hereafter referred to as W_{CO}) to a column density of H_2, a subject of much discussion in several respects (see e.g. Lequeux 1981; Dickman, Snell, and Schloerb 1986; van Dishoeck and Black 1987; Maloney and Black 1988; Bloemen 1989). This N_{H_2}–W_{CO} conversion factor (hereafter referred to as $X \equiv N_{H_2}/W_{CO}$) can be expected to be sensitive to such cloud parameters as density, temperature, and abundances, as discussed in detail by Kutner and Leung (1985) and Maloney and Black (1988). Because the J = 1→0 transition is optically thick for most molecular clouds, it is in fact not evident that this transition can be used at all to obtain H_2 column densities. On a Galactic scale, when averaging over a large number of clouds, CO appears to be a useful tracer of N_{H_2}, although the underlying reason is not fully understood. Evidence has come particularly from studies of the COS-B γ-ray observations (Lebrun et al. 1983; Bloemen et al. 1986), which have also provided an estimate of the average Galactic X value (briefly discussed in the next section). This γ-ray calibration factor is probably the most reliable one for Galactic large-scale analyses.

Because of their limited sensitivity, available γ-ray observations are not suitable for the mass calibration of individual (local) clouds, except for a few massive complexes. Instead, extinction measurements are frequently used for clouds visible at medium and high latitudes; typical examples are the studies of Dickman (1978), Frerking, Langer, and Wilson (1982), and Magnani, Blitz, and Wouterloot (1988). New insight into the mass calibration of CO surveys can be obtained from the IRAS observations, on which this paper concentrates. The particular importance of the infrared calibration method is its coherence, in the sense that it is applicable, in principle, to large-scale CO surveys of the Galactic disk as well as to CO observations of individual local clouds. This paper describes in some detail new infrared calibration results for large-scale CO surveys of the Milky Way and compares the findings with studies of individual clouds.

2 Inferences from Gamma-Ray Observations

The diffuse Galactic γ-ray emission originates primarily from the interactions of cosmic-ray particles with interstellar gas. Basically, the observed γ-ray intensity in a certain direction traces the product of gas density and cosmic-ray density, integrated along the line of sight. Because the spatial distributions of the two dominant gas mass components, neutral atomic and molecular gas, are quite different, X can be estimated from a correlation study of γ-ray, CO, and HI surveys. Using the velocity information of the CO and HI observations as a distance indicator, large-scale variations in the cosmic-ray density can be determined simultaneously and thus be taken into account (Bloemen et al. 1986). From the most complete study of this type (Strong et al. 1988), using the final COS-B data base, the Columbia CO surveys (Dame et al. 1987), and several HI surveys, all covering the entire Galactic disk, the average X value was found to be $(2.3 \pm 0.3) \times 10^{20}$ molecules cm^{-2} (K km s^{-1})$^{-1}$. Strictly speaking this value should be regarded as an upper limit, but there are good reasons (from the γ-ray point of view) to believe that the real X value is not much lower (see review by Bloemen 1989). There is no indication from the γ-ray data for a large-scale variation of X throughout the Galaxy, but small-scale variations can certainly not be excluded. Particularly in the Galactic-centre region, X may be drastically different (Blitz et al. 1985; Stacy et al. 1987). On the other hand, γ-ray analyses of some individual molecular cloud complexes in the solar neighbourhood — the Orion-Monoceros and Cepheus clouds — lead to consistent results (Bloemen et al. 1984; Grenier and Lebrun 1989).

The reliability of the γ-ray calibration method has been disputed recently because of some differences between the above-mentioned results obtained by the COS-B group and those obtained by the Durham group from parallel analyses of the COS-B data (Bhat et al. 1986; Wolfendale 1988). They advocate an X value of 1.5×10^{20} in the solar vicinity and 1×10^{20} in the molecular ring at 4 – 7 kpc from the Galactic centre. The reason for the differing results appears to be twofold (see Bloemen 1989): *(a)* the radial γ-ray emissivity distribution adopted by the Durham group is steeper than the one derived by the COS-B group (a difference by a factor of ~ 1.8 between R = 10 and 5 kpc) and *(b)* the specific CO surface densities used by the Durham group [from Sanders, Solomon, and Scoville (1984)] are relatively high. The latter point is discussed in detail by Bronfman et al. (1988), who showed that the high CO surface densities presented by Sanders et al. can be attributed to two facts. Firstly, the W_{CO} values of the survey used by Sanders et al.

are simply $\sim$ 20% higher than those of the Columbia survey. Secondly, there is some debate among CO observers on the radial-unfolding procedure to be applied; using the procedure advocated by Bronfman et al. would lead to an average CO surface density in the inner Galaxy that is $\sim$ 40% lower than derived by Sanders et al. The method used by the COS-B group does not depend on such unfolding procedures. Altogether, these effects account for a correction factor of $1.8 \times 1.2 \times 1.4 \approx 3.0$ (although the factor of 1.4 may of course not be applicable). This renders the differences fully understandable.

3 Inferences from Infrared Observations

3.1 Decomposition of the FIR Milky Way

The IRAS surveys of the Galactic disk in the 60-μm and 100-μm bands can be unravelled by a procedure similar to that applied to the γ-ray data. Such an analysis was recently performed by Deul, Bloemen, and Thaddeus (1989; hereafter DBT). DBT made a detailed quantitative comparison of the IRAS surveys with HI and CO sky maps for selected Galactocentric distance intervals, R = 2 – 4, 4 – 8, 8 – 10, 10 – 12, 12 – 15, and > 15 kpc ($R_\odot \equiv 10$ kpc). These six wide intervals are dictated by the requirement that the gas distributions in the rings (projected on the sky) must be distinctly different in order to be able to ascertain the contribution of each ring to the observed infrared emission. The HI and CO data sets are the same as used in the γ-ray analysis of Strong et al. (1988). The selected rings are identical as well. It was assumed that the infrared intensity maps for the 60-μm and 100-μm IRAS passbands can be represented as a linear combination of the HI and CO maps of the selected radial intervals — with the exclusion of those regions that have a strong contribution from HII regions, as discussed below:

$$I_\lambda = \left(\sum_{i=1}^{6} \varepsilon_\lambda(R_i) \left(N_{HI,i} + 2Y_\lambda W_{CO,i} \right) \right) + I_{b,\lambda} \qquad [\mathrm{MJy\ sr^{-1}}], \tag{1}$$

where $\varepsilon_\lambda(R_i)$ ($i = 1, \cdots, 6$), Y_λ, and $I_{b,\lambda}$ are free parameters. $\varepsilon_\lambda(R_i)$ is the infrared emissivity [MJy sr^{-1} (H atom cm^{-2})$^{-1}$] of the dust mixed with the atomic gas in the i^{th} distance interval, $N_{HI,i}$ and $W_{CO,i}$ are the maps of the HI column density and the velocity–integrated CO brightness temperature for this interval, and $I_{b,\lambda}$ is an isotropic background. The parameter Y_λ [molecules cm^{-2} (K km s^{-1})$^{-1}$] is the product of the conversion factor X and the ratio of the emissivity of the dust associated with the molecular to that of the atomic gas, $\varepsilon_{\lambda,H_2}/\varepsilon_{\lambda,HI}$, so

$$Y_\lambda = \frac{\varepsilon_{\lambda,H_2}}{\varepsilon_{\lambda,HI}} \cdot X, \tag{2}$$

where $\varepsilon_{\lambda,HI} \equiv \varepsilon_\lambda$. In other words, Y_λ includes effects related to different conditions in the atomic and molecular gas, like different dust temperatures, dust-to-gas ratios, and dust properties. Note that using only one Y_λ parameter in Eq. 1 (although allowed to be different for the 60-μm and 100-μm passbands) implies that X and $\varepsilon_{\lambda,H_2}/\varepsilon_{\lambda,HI}$ — more precisely, their product — are constrained to be independent of Galactocentric radius. To see whether this assumption is reasonable a model with two Y_λ parameters for each passband was considered as well, one for R < 8 kpc, the other for R > 8 kpc.

A maximum-likelihood technique, as applied in the γ-ray work of the COS-B group, was used to determine the values of the fit parameters. The fit region was limited to the latitude range $|b| < 10°$. Two 20° longitude intervals, centered on the Galactic centre and anti-centre directions, were excluded because of the poor kinematic distance information there.

DBT made an effort to eliminate the contribution of warm dust in HII regions (which are clearly visible as strong peaks in the infrared sky maps, particularly in the 60-μm band) by excluding from the fit those pixels that have 60μm/100μm intensity ratios exceeding 0.35 (corresponding to dust temperatures $T_d \gtrsim 27$ K for a λ^{-2} opacity law). Owing to the line-of-sight integration of cold and warm dust, however, this criterion rejects only regions most affected by the presence of HII. DBT verified that the results do not depend sensitively on the criterion for the exclusion of HII regions. This point is taken up again below. Although the modelling of DBT is a significant improvement compared to other recent large-scale IRAS analyses (Pérault et al. 1989; Sodroski et al. 1989), it is still too simple. A clear over-simplification is the assumption of axial symmetry in the emissivity distribution, implying that parameters like the dust-to-gas ratio and the dust temperature in the HI and H_2 gas components are taken to be constant throughout each ring (although allowed to be different for the two gas components via the Y_λ parameter). This is evidently not a good approach if local heating sources play an important role. It seems, however, as will be seen below, that this problem is largely eliminated by the exclusion of regions with 60μm/100μm intensity ratios > 0.35.

3.2 Large-scale FIR Properties

DBT tested different versions of their model, using the likelihood-ratio technique, in order to investigate whether all free parameters are indeed required. Each of the model versions has different constraints on the fit parameters, such as $Y_{60} = Y_{100}$ [equivalent to $\varepsilon_{60,H_2}/\varepsilon_{100,H_2} = \varepsilon_{60,HI}/\varepsilon_{100,HI}$ — see Eq. 2] and $\varepsilon_{60}(R)/\varepsilon_{100}(R) =$ constant. DBT found that the latter constraint is indeed fully acceptable, i.e. a model in which the 60μm/100μm ratio of the emissivity (per nucleon) is independent of R fits the data not significantly worse than the most general model. In summary, the basic fit and test results of DBT are the following:

- The infrared emissivity per nucleon, $\varepsilon_\lambda(R)$, decreases significantly with increasing Galactocentric radius (Fig. 1).
- $Y_{60} = (0.65 \pm 0.11) \times 10^{20}$ and $Y_{100} = (0.84 \pm 0.20) \times 10^{20}$ mol. cm^{-2} (K km s^{-1})$^{-1}$.
- The 60/100μm emissivity ratio is constant as a function of R within uncertainties (Fig. 1), $\frac{\varepsilon_{60,HI}}{\varepsilon_{100,HI}} \equiv \frac{\varepsilon_{60}}{\varepsilon_{100}} = 0.27 \pm 0.03$ and $\frac{\varepsilon_{60,H_2}}{\varepsilon_{100,H_2}} \equiv \frac{Y_{60}}{Y_{100}} \cdot \frac{\varepsilon_{60,HI}}{\varepsilon_{100,HI}} = 0.20 \pm 0.06$, although the latter may have some radial dependence in view of the uncertainty.

Introducing an additional free parameter $r \equiv Y_\lambda(2\text{-}8 \text{ kpc})/Y_\lambda(>8 \text{ kpc})$, as discussed above, did not improve the fit; r was found to be consistent with unity.

Fig. 2 shows longitude profiles of the observed and modelled 100-μm intensities (for 60-μm profiles see DBT). The figures indicate that there is generally good agreement, but some strong peaks in the data are not fitted by the model (particularly at 60μm). These are probably mainly the HII regions that were not excluded by the criterion. The longitude profiles suggest that these remaining HII regions did not have a strong

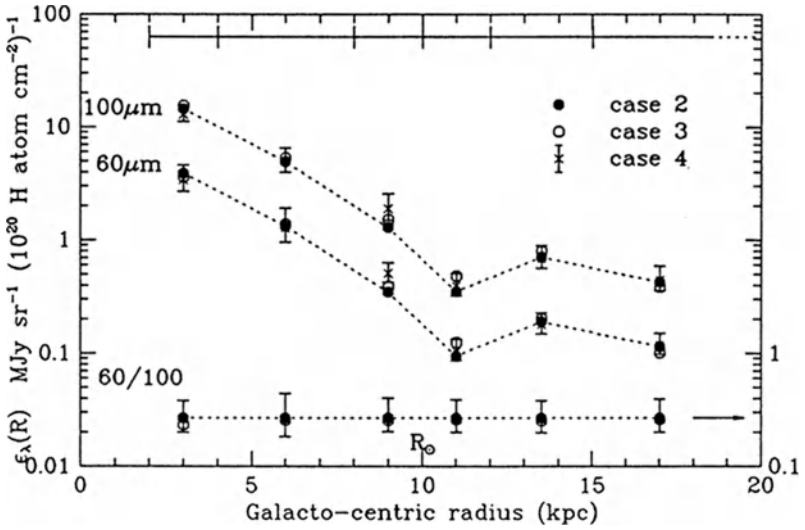

Fig. 1. Galactocentric distributions of the infrared emissivity of dust associated with atomic gas. Case 2 corresponds to the preferred model discussed in the text. Within uncertainties, the radial dependence of the emissivity distribution for dust mixed with molecular gas is identical, but the 60μm/100μm ratio is smaller (see text).

influence on the fitting process because most peaks appear to be excesses on top of the model predictions. This is gratifying and in fact not surprising because the peaks contribute to only a minor fraction of the total number of pixels fitted. DBT repeated some fits with none of the HII regions excluded and found that the parameter values are indeed not significantly different. This gives further assurance that the results do not depend sensitively on the criterion for exclusion of HII regions.

It seems plausible to attribute the increase of the emissivity towards the inner Galaxy to the increase of the mean intensity of the interstellar radiation field of the Galaxy (ISRF) (Mathis, Mezger, and Panagia 1983), i.e. an increase of the dust temperature. However, the finding that the emissivity gradient is not accompanied by a change in the 60μm/100μm emissivity ratio (indicating a constant color temperature), is hard to understand in this scenario, if the model of 'standard' grains (Mathis, Rumpl, Nordsieck 1977) is assumed to be applicable. In addition, the resulting color temperatures of 24 K and 22 K (adopting a λ^{-2} opacity law) for dust mixed with atomic gas and molecular gas, respectively, are higher than expected. A very similar result was obtained by Walterbos and Schwering (1987) for M31. These findings can be understood if the emission in the 60-μm band has a considerable contribution from particles not in thermal equilibrium, such as the small particles briefly heated by the absorption of a single stellar photon, as discussed by Draine and Anderson (1985) and Puget, Léger, and Boulanger (1985).

3.3 Derivation of X

In order to derive X from the obtained Y_λ estimates one has to know the ratio between the infrared emissivities per nucleon inside and outside the molecular clouds, i.e. $\varepsilon_{\lambda,H_2}/\varepsilon_{\lambda,HI}$ (see Eq. 2). This can be done in an elegant way if the infrared emission in both passbands would originate from dust particles in thermal equilibrium, making use of the 60μm/100μm colors to estimate the equilibrium temperatures. Owing to the

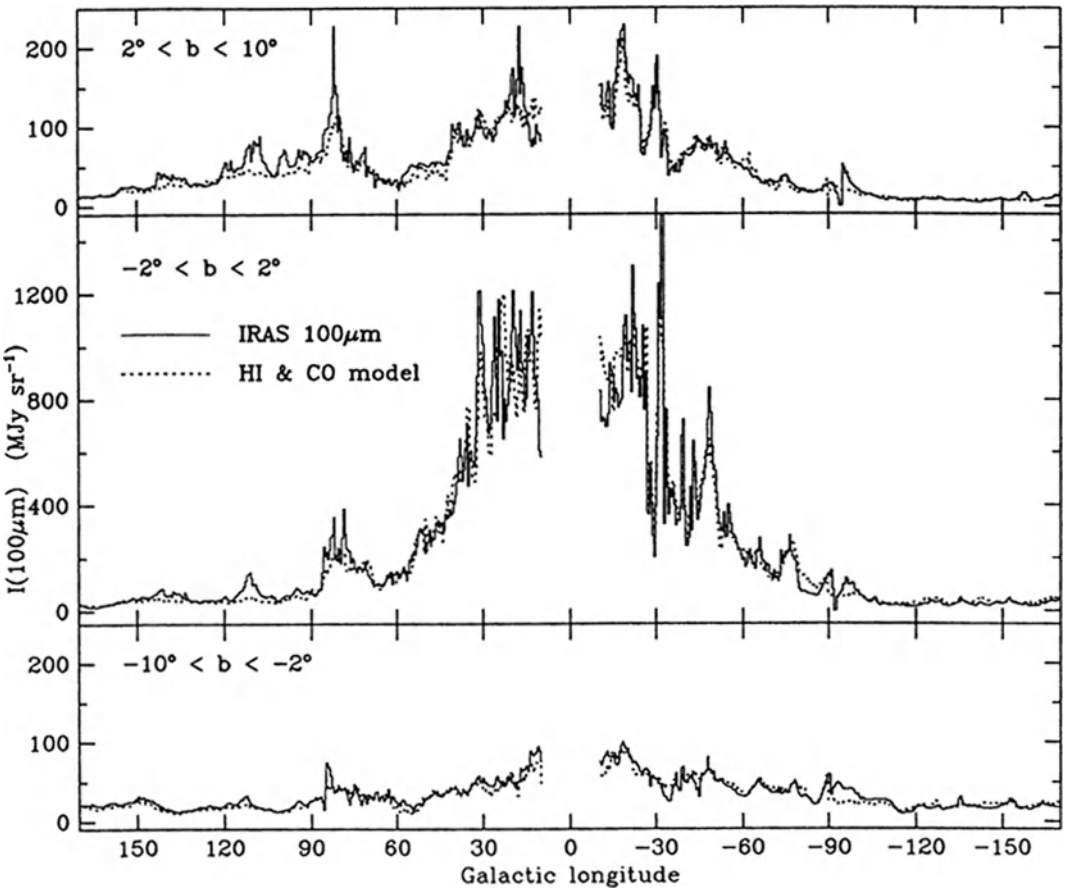

Fig. 2. Longitude distributions of the observed and expected infrared intensities in the 100-μm band. Sky pixels containing intense H II regions were excluded in the fitting procedure (see text) and are not included in these profiles.

probably significant contribution from small grains to the emission in the 60-μm band, however, this approach is not feasible. It would be further complicated by the contamination from possibly remaining HII regions. Because both the presence of small particles and the remaining HII regions affect mainly the parameter estimates for the 60-μm band, the most reliable constraint on X can probably be obtained from Y_{100}, on which the following discussion is concentrated.

Before discussing the ratio $\varepsilon_{100,H_2}/\varepsilon_{100,HI}$, it may be illustrative to review the Y_{100} values that have been obtained from correlation studies of CO, HI, and 100-μm observations of individual clouds at medium and high latitudes and from other studies of the Galactic disk. A compilation is presented in Table 1 — most authors do not give explicitely the Y_{100} value, but it can be easily derived from other quantities given, without assumptions (except for Weiland et al. 1986; footnote 2). Two interesting effects can be seen: (*a*) There is a remarkably small spread in the Y_{100} estimates, despite the differing approaches that were followed, the non-negligible uncertainties, and the diversity in cloud types. (*b*) There is a gratifying consistency among the Y_{100} values obtained from

Table 1. Values of Y_{100}, either given in the source or derived from quantities given there. These can be regarded as estimates of the N_{H_2}/W_{CO} ratio if the 100-μm emissivity (per nucleon) would be the same inside and outside the molecular cloud(s).

Source	Y_{100}[1]	Clouds
Weiland et al. (1986)	0.6[2]	HLC 16, 20, 30 of Magnani et al. (1985)
de Vries et al. (1987)	0.5	Ursa Major (Lynds 683)
de Geus (1988)	0.6	Ophiuchus
Heithausen & Mebold (1989)	0.6	Ursa Major (Lynds 629, 683, 691)
Boulanger et al. (1989)[3]	0.4-0.6	Auriga, Cepheus, Chamaeleon, Lupus, Mon R2, Taurus
	0.9	Orion
Pérault et al. (1989)	0.8	Galactic disk
Sodroski et al. (1989)	0.7	"
Deul et al. (1989) (DBT)	0.8	"

[1] Units: 10^{20} molecules cm^{-2} (K km s^{-1})$^{-1}$.

[2] From I_{100}/W_{CO}, assuming $\epsilon_{100,HI} = 1$ MJy sr^{-1} (10^{20} H atom cm^{-2})$^{-1}$.

[3] The authors excluded regions with clear evidence for star formation, mainly important for Orion.

studies of the Galactic disk, despite the facts that widely different methods of analysis were used, particularly in the treatment of HII regions, and that the parts of the disk included in the analyses are not identical (note that DBT found indeed no evidence for a large-scale variation of Y_λ throughout the Galactic disk).

The small spread in Y_{100} values implies a considerable spread in X values among different categories of molecular clouds, because $\epsilon_{100,H_2}/\epsilon_{100,HI}$ is expected to vary. This can be seen as follows. Dust in molecular clouds is expected to be predominantly heated by the external ISRF, unless the cloud is forming high-mass stars which develop an HII region (see e.g. Boulanger and Pérault 1988). Statistically speaking, the latter is only relevant for giant molecular clouds with masses larger than $\sim 10^5$ $M_\odot$, so particularly the Y_{100} estimates obtained for the Galactic disk and Orion can be expected to be influenced by star formation. Regions for which this is evident have been excluded, but the fact that for the disk and Orion the highest Y_{100} values are found may be a reminiscent effect. Let us proceed under the assumption that the external ISRF is the dominant heating source for the dust, and that the dust properties and gas-to-dust ratio inside and outside a cloud are not different. For the simple case of a uniform, spherical cloud heated from outside by a uniform radiation field, $\epsilon_{100,H_2}/\epsilon_{100,HI}$ is then only a function of total optical depth through the cloud centre (Flannery, Roberge, and Rybicki 1980; Mathis, Mezger, and Panagia 1983). Boulanger and Pérault (1988) derived explicit values: $\epsilon_{100,H_2}/\epsilon_{100,HI} = 0.54$, 0.37, and 0.25 for total visual extinctions $A_v = 2$, 5, and 10 mag, respectively. Hence, X ranges from about Y_{100} to $4Y_{100}$ for $A_v \simeq 1 - 10$ mag. The real situation is of course much more complicated because the cloud geometry plays an important role. Nevertheless, the above illustrates that X may range typically from about $(0.5-1)\times10^{20}$ molecules cm^{-2} (K km s^{-1})$^{-1}$ for clouds with $A_v = 1-3$ mag (such as most of the clouds studied by Boulanger et al. — Table 1) to roughly $\sim 2\times10^{20}$ for giant molecular clouds, and possibly even larger for dark dust clouds. For $A_v < 1$ mag, X should approximately be equal to Y_{100} in this scenario, but the CO emission from such diffuse, and mostly young clouds (e.g. the high-latitude clouds — Magnani, Blitz, and Mundy 1985) can be expected to be affected by various other effects (see Magnani, Blitz, Wouterloot 1988).

Another way of stating the above is that for a cloud predominantly heated by the ambient ISRF, X appears to be anti-correlated with the FIR emissivity per nucleon inside the cloud relative to that in the surrounding medium, and thus correlated with the total extinction of the cloud (for $A_v > 1$ mag). The underlying reason is probably the inverse proportionality between X and the gas temperature, predicted by models (Kutner and Leung 1985; van Dishoeck and Black 1987; Maloney and Black 1988). A coherent analysis of a larger sample of clouds of different categories is needed to substantiate the near constancy of Y_{100} suggested by Table 1.

Acknowledgements. I acknowledge partial support from the Laboratory for Space Research Leiden and receipt of a Fellowship from the Royal Netherlands Academy of Arts and Sciences (KNAW).

References

Bhat, C. L., Mayer, C. J., Wolfendale, A. W. 1986. Philos. Trans. R. Soc. Lond. A 319:249
Black, J. H., van Dishoeck, E.F. 1987. Ap. J. 322:412
Blitz, L., Bloemen, J. B. G. M., Hermsen, W., Bania, T. M. 1985. Astr. Ap. 143:267
Bloemen, J. B. G. M. 1989. Ann. Rev. Astr. Ap. 27, in press
Bloemen, J. B. G. M., Caraveo, P. A., Hermsen, W., Lebrun, F. et al. 1984. Astr. Ap. 139:37
Bloemen, J. B. G. M., Strong, A. W., Blitz, L., Cohen, R. S., Dame, T. et al. 1986. Astr. Ap. 154:25
Bronfman, L., Cohen, R. S., Alvarez, H., May, J., Thaddeus, P. 1988. Ap. J. 324:248
Boulanger, F., Cohen, R. S., Gaida, M., Grenier, I., Koprucu, M. et al. 1989. Ap. J., preprint
Boulanger, F., Pérault, M. 1988. Ap. J. 330:964
Cox, P., Krügel, E., Mezger, P. G. 1986. Astr. Ap. 380:396
Dame, T. M., Ungerechts, H., Cohen, R. S., de Geus, E., Grenier, I. et al. 1987. Ap. J. 322:706
Deul, E. R., Bloemen, J. B. G. M., Thaddeus, P. 1989. Astr. Ap., in press [DBT]
Dickman, R. L. 1978. Ap. J. Suppl. 37:407
Dickman, R. L., Snell, R. L., Schloerb, F. P. 1986. Ap. J. 309:326
van Dishoeck, E. F., Black, J. H. 1987. In 'Physical Processes in Interstellar Clouds', eds. G. E. Morfill & M. Scholer, Dordrecht: Reidel, p. 241
Draine, B. T., Anderson, N. 1985. Ap. J. 292:494
Flannery, B. P., Roberge, W., Rybicki, G. B. 1980. Ap. J. 236:598
Frerking, M. A., Langer, W. D., Wilson, R. W. 1982. Ap. J. 262:590
de Geus, E. J. 1988. PhD Thesis University of Leiden
Grenier, I., Lebrun, F. 1989. Astr. Ap., preprint
Heithausen, A., Mebold, U. 1989. Astr. Ap., in press
Kutner, M. L., Leung, C. M. 1985. Ap. J. 291:188
Lebrun, F., Bennett, K., Bignami, G. F., Bloemen, J. B. G. M. Buccheri, R. et al. 1983. Ap. J. 274:231
Lequeux, J. 1981. Comments on Astrophysics 9:117
Magnani, L., Blitz, L., Mundy, L. 1985. Ap. J. 295:402
Magnani, L., Blitz, L, Wouterloot, J. G. A. 1988. Ap. J. 326:909
Maloney, P., Black, J. H. 1988. Ap. J. 325:389
Mathis, J. S., Mezger, P. G., Panagia, N. 1983. Astr. Ap. 128:212
Mathis, J. S., Rumpl, W., Nordsieck, K. H. 1977. Ap. J. 217:425
Pérault, M., Boulanger, F., Puget, J. L., Falgarone, E. 1989. Ap. J., in press
Puget, J.L., Léger, A., Boulanger, F. 1985. Astr. Ap. 142:L19
Sanders, D. B., Solomon, P. M., Scoville, N. Z. 1984. Ap. J. 276:182
Savage, B.D., Bohlin, R.C., Drake, J.F., Budich, W. 1977. Ap. J. 216:291
Shull, J.M., Beckwith, S. 1982. Ann. Rev. Astr. Ap. 20:163
Sodroski, T. J., Dwek, E., Hauser, M. G., Kerr, F. J. 1989. Ap. J., in press
Spitzer, L., Jenkins, E.B., 1975. Ann. Rev. Astr. Ap. 13:133
Stacy, J. G., Dame, T. M., Thaddeus, P. 1987. Proc. Int. Cosmic Ray Conf., 20th, Moscow 1:117
Strong, A. W., Bloemen, J.B.G.M., Dame, T. M., Grenier, I., Hermsen, W. et al. 1988. Astr. Ap. 207:1
de Vries, H. W., Heithausen, A., Thaddeus, P. 1987. Ap. J. 319:723
Walterbos, R. A. M., Schwering, P. B. W. 1987. Astr. Ap. 180:27
Weiland, J. L., Blitz, L., Dwek, E., Hauser, M. G., Magnani, L., Rickard, L. 1986. Ap. J. Lett. 306:L101
Wolfendale, A. W. 1988. In 'Molecular Clouds in the Milky Way and External Galaxies', eds. R. Dickman, R. Snell, J. Young, Heidelberg: Springer-Verlag, p. 76

IRAS View at Nearby Molecular Clouds

F. Boulanger

Ecole Normale Supérieure, 24 rue Lhomond, 75005 Paris, France
and
IPAC, Caltech 100-22, Pasadena CA 91125, U.S.A.

The all-sky survey carried out by the Infrared Astronomy Satellite (IRAS) at 12, 25, 60, and $100\mu m$ provided the first complete set of observations of interstellar matter outside the galactic plane, an achievement which is far beyond the scope of existing millimetric radio telescopes . These infrared (IR) observations bear a wealth of informations about molecular clouds, in particular about star formation activity, the spatial distribution of dust and gas, the radiation field inside clouds, and dust properties which have just started to be explored. In this paper we review the first results of IRAS studies of nearby molecular clouds.

1. Heating of Dust in Molecular Clouds

Dust in molecular clouds is heated both by embedded stars and the interstellar radiation field of the Galaxy. The relative contribution of these two sources of heating to the IR emission of molecular clouds have been discussed by Boulanger and Pérault (1988, hereafter BP). The heating by the ISRF places a lower limit on the ratio between infrared luminosity and mass of gas which depends on the effective optical depth of the clouds to the stellar radiation. For homogenous spherical clouds radiation transfer calculations lead to L_{IR}/M_{H2} ratios of $0.3 - 0.8 L_\odot/M_\odot$ for clouds of total visible extinction between 2 and 10 magnitudes (BP). For the star formation rate and initial mass function of the solar neighborhood (see BP for references) the luminosity of embedded stars smaller than a few $M_\odot$ is negligible compared to the luminosity absorbed from the ISRF. Low-mass stars can locally create warm points in clouds but they have a negligible contribution to the infrared luminosity of the interstellar medium on the scale of a whole molecular complex. This implies that the IR luminosity of clouds forming only low- mass stars does not bear any information about their star formation efficiency which can be estimated only from statistics of embedded objects. The ISRF is the dominant heating source of dust over most of the volume of these clouds and over the parts where they are not optically thick to the stellar radiation the far-IR brightness may be used as a tracer of the distribution of interstellar matter (see section 2).

The luminosity of a single ionizing star ($M_* > 20 M_\odot$) is comparable to the luminosity a giant molecular cloud (GMC) of $10^5 M_\odot$ absorbs from the ISRF. Thus, for clouds forming high mass stars the dust heating comes from stars associated with the cloud and not from the ISRF. Then, the IR luminosity may be used to estimate the total luminosity of the stars formed by the cloud. However, studies of nearby clouds associated with H II regions (Leisawitz and Hauser 1989, BP) show that only a small fraction of the luminosity of an OB association is absorbed by the parent

molecular clouds. For Orion, BP find that the IR luminosity of the 300pc sphere centered on the Trapezium represents only 20% of the luminosity of the OB association. In the case of Orion only the radiation of stars younger than a few $10^6 yrs$ that still lie within a few parsecs from the Orion A and B clouds is locally converted into IR emission. The radiation from stars in the older sub-associations located several tens of parsecs from the dense cloud in regions of low gas density travels more than several hundreds parsecs before being absorbed. Generalizing the Orion results to other GMC-H II region associations we conclude that the IR luminosity of GMC's represents the energy output of the stars formed in the last few $10^6 yrs$. This short-term *memory* has to be taken into account when deriving star formation efficiencies from L_{IR}/M_{H2} ratios. If this result applies to star- forming regions in the molecular ring the average star formation efficiency of GMC's associated with H II regions, $\dot{M}/M_{gas}$, could be several times larger than the value of $4 10^{-10} yr^{-1}$ (for $M_* \geq 2M_\odot$) derived by Mooney and Solomon (1988).

2. Far-IR Emission as a Tracer of Gas Column Density

Away from local heating sources one expects the far-IR emission to correlate with the distribution of gas column density over regions of low or moderate opacity to the interstellar radiation. The validity of this statement can be established by comparing the spatial distribution of the far-IR emission with that of other tracers of gas column density. The correlation between the IR emission and the distribution of the nearby H I gas has been studied by numerous authors (see BP and references therein). A tight linear correlation is observed between the distribution of the IR and H I emission over fields of several tens of degrees outside the galactic plane. This correlation proves that the interstellar radiation field and the dust abundance are roughly uniform on scales of 1 to 100 pc. It also implies that the far-IR is a good tracer of gas column density over the regions of small opacity occupied by atomic gas. At high galactic latitude the average ratio $I_\nu(100\mu m)/N_H$ is $0.85 MJy/sr$ for $10^{20} Hcm^{-2}$ (BP) which is equivalent to a $I_\nu(100\mu m)/A_v$ ratio of $15.9(MJy/sr)/mag$. Recently, Lange et al. (1989) reported measurements of the sub-mm emission of dust associated with H I gas at high galactic latitude which show that the 100, 140, and 260 μm fluxes can be all fitted by a single modified black-body curve. This result suggests that in regions of moderate opacity to the ISRF the 100μ emission comes from the bulk of the dust. Probably, only in regions of high opacity large dust grains become too cold to be detected at $100\mu m$.

IRAS data have been compared to extinction measurements and molecular data to see to what extent the far-IR emission may be used to probe the spatial distribution of molecular matter. Comparisons between $100\mu m$, A_v and $W(^{13}CO)$ (^{13}CO emission integrated in velocity) have been published for a few dark clouds. References, names of clouds, and results of these comparisons are summarized in Table 1. For all clouds a good linear correlation is found between $100\mu m$ and A_v for $A_v < 3mag$. The values of $100\mu m/A_v$ derived from these analyses vary from 5 to 9 MJy/sr per magnitude, on average a factor 2 times smaller than the value for H I gas at high galactic latitude. This difference between the far-IR emissivity of molecular clouds and atomic gas is not surprising since we do expect the ISRF to be somewhat attenuated inside molecular clouds.

Simple models of the penetration of the interstellar radiation in clouds predict an attenuation factor comparable to what is observed (see BP). However, a detailed understanding of the relation between far-IR brightness and A_v depends on several characteristics of molecular clouds which are yet unknown, and which may vary from cloud to cloud. First, the penetration of the interstellar radiation depends on the degree of inhomogeneity of the clouds, and the effective extinction at which the molecular matter is. If clouds are inhomogenuous on very small scale as indicated by high resolution observations of nearby clouds (Falgarone and Pérault 1989) the extinction measured from star counts with a resolution of typically a few arcminutes (i.e. a few 0.1 pc for the nearest clouds) may not be representative of this effective extinction. Second, the effect of the attenuation of the ISRF on the far-IR emission depends on the optical properties of the dust grains which emit at $100\mu m$. The more these dust grains absorb in the UV and blue part of the ISRF spectrum the faster the $100\mu m - A_v$ saturates. Further, for grains in thermal equilibrium a weaker radiation field implies a smaller temperature which could reduce the fraction of the emission which falls in the IRAS band (see BP).

The $100\mu m$ and ^{13}CO emission are also well correlated. Results and references for these analyses are listed in Table 1. The straight comparison between $100\mu m$ and $W^{13}CO$ leads to good linear correlations. Langer et al. (1988) found for the B5 cloud an even tighter correlation by comparing the ^{13}CO emission with the $100\mu m$ optical depth. The latter is derived from the $100\mu m$ brightness using the color temperature between 60 and $100\mu m$ as the dust temperature. In B5, the $60\mu m/100\mu m$ color ratio decreases from the edge to the center of the cloud. However, as pointed out by Langer et al., the physical interpretation of this new correlation is unclear because the values of $\tau_{100\mu m}$ derived on the basis of the $60/100\mu m$ color temperature leads to a $\tau_{100\mu m}/A_V$ ratio an order of magnitude smaller than the ratios predicted by interstellar dust models (Draine and Lee 1984) and than the ratio one may derive from the sub-mm observations of dust at high galactic latitude by Lange et al. (1989). The most probable explanation of this discrepancy is that the color temperature is not the physical temperature of the dust grains emitting at $100\mu m$ because a fraction of the $60\mu m$ emission comes from a population of grains which does not emit at $100\mu m$ (Draine and Anderson 1985, Boulanger et al. 1988, Laureijs et al. 1989). The improvement in the correlation may then be fortuitous: the color temperature correction approximately compensating for the saturation of the $100\mu m - A_v$ relation at high A_v. From the numbers in Table 1 we derive an average ratio $100\mu m/W^{13}CO$ of $2(MJy/sr)/(Kkm/s)$. In dark clouds $W(^{13}CO) and A_V$ correlate for $A_v > 0.5 - 1 mag$ with slopes ranging from 1.0 to $2.7(Kkm/s)/mag$ (see review by Guélin and Cernicharo 1988). For the few clouds where $100\mu m$ has been compared with both $W^{13}CO$, and A_v the $100\mu m - W^{13}CO$ correlation leads to a slightly smaller $100\mu m/A_v$ ratio than the direct $100\mu m - A_v$ comparison. Since the slopes of the correlation are measured over a range of A_v higher for $100\mu m - W^{13}CO$ than for $100\mu m - A_V$ this difference probably results from a flattening of the $100\mu m - N_H$ relation with increasing column density.

The comparison of the IRAS data with A_v and ^{13}CO data shows that the $100\mu m$ brightness is a good tracer of dust and gas column density in nearby clouds not associated with high mass

star formation up to an A_v of about 3 magnitudes. These analyses, however, are presently limited to a few clouds because A_v and ^{13}CO measurements have only been obtained over limited areas of nearby molecular complexes. On the other hand the main nearby clouds have been almost completely mapped in ^{12}CO with the Harvard-Columbia 1.2 m telescope (Dame et al. 1987). These CO observations with an angular resolution of 8' or 30' depending on the cloud (see Dame et al.) were used to compare the extended structure of the CO and far-IR emission of nearby clouds. Away from star-forming regions a linear correlation is found between $100\mu m$ and WCO. The clouds for which this comparison was done are listed in Table 2. Examples of $100\mu m$-CO diagrams have been presented by BP and Boulanger(1988). The ratios between $100\mu m$ and CO brightness derived from this analysis are given in Table 2. They range between 0.7 and $2.5(MJy/sr)/(Kkm/s)$ with an average value of $1.4(MJy/sr)/(Kkm/s)$. For each of the clouds in Table 2 we studied the correlation between $100\mu m$ and H I emission in the close vicinity of the cloud. The slope of this correlation (Table 2) does change from cloud to cloud. These changes probably trace variations in the intensity of the ISRF and/or the dust-to-gas ratio. A straight comparison between the average $100\mu m/WCO$ and $100\mu m/N_{HI}$ ratios leads to an average N_{H2}/WCO ratio of $0.7/A\,10^{20}cm^{-2}/(Kkm/s)$ where A represents the ratio between the molecular and atomic value of the $100\mu m$ emissivity per nucleon. As explained earlier, A is smaller than one because the interstellar radiation is attenuated inside molecular clouds and possibly because the grains are colder and emit a smaller fraction of their emission in the $100\mu m$ band of IRAS. The results of the $100\mu m - A_v$ correlation (Table 1) gives values of A in the range 0.3 to 0.7. Assuming that these values obtained for a few clouds are representative we derive an average estimate of $X = N_{H2}/WCO$ in the range 1.1 to $2.1{\cdot}10^{20}cm^{-2}/(Kkm/s)$, smaller than the value of $2.6{\cdot}10^{20}cm^{-2}/(Kkm/s)$ derived from γ ray data for giant molecular clouds in the inner Galaxy by Bloemen et al. (1986), but comparable with the value of $1.5{\cdot}10^{20}cm^{-2}/(Kkm/s)$ advocated by MacLaren et al. (1988). Low values of X have also been obtained for high Galactic latitude clouds (de Vries et al. 1987, Weiland et al. 1986). For Orion, the only nearby cloud for which an estimate of X was derived from γ−ray data (Bloemen et al. 1984), the IR and γ−ray estimates of X are $0.9/A$ and $2.6{\cdot}10^{20}cm^{-2}/(Kkm/s)$. These two estimates agree if $A = 0.34$ which is within the range of values one may derive from the comparison of the $100\mu m/A_v$ ratios in Table 1 and the $100\mu m/N_{HI}$ ratios in Table 2. There is a significant scatter in the $100\mu m/WCO$ listed in Table 2. Since these differences are not reflected in the corresponding $100\mu m/N_{HI}$ they do not result from variations in the intensity of the ISRF or the dust abundance and could reflect changes in the X ratio from cloud to cloud.

3. Abundance of Small Particles

In this section we inter-compare the emission of molecular clouds at the four IRAS wavelengths 12, 25, 60, and $100\mu m$. The emission observed at these four wavelengths comes from different particles. While the $100\mu m$ probably comes from large dust grains in equilibrium with the radiation field, the 12 and $25\mu m$ emission, and possibly part of the $60\mu m$ emission come from

transiently excited particles (see review by Puget and Léger 1989). The IR colors of clouds bear information on the abundance and the optical properties of these particles.

The sensitivity of IRAS observations was sufficient to detect the emission of molecular clouds at the 4 wavelengths for a wide range of colors. After subtraction of the zodiacal light IRAS images show that the mid-IR (12 and 25μm) and the 100μm emission are distributed very differently. Some clouds or pieces of clouds have no mid-IR emission while other clouds in the same region show brightness ratios between the mid-IR and 100μm higher than the average colors measured on large scale in the Galaxy. For example upper limits of the color ratio $R(12,100) = I_\nu(12\mu m)/I_\nu(100\mu m)$ as low as 0.003 and values as high as 0.16 have been obtained for clouds in the Chamaeleon region (Boulanger et al. 1988). For comparison the average R(12,100) color ratio in the solar neighborhood is 0.042 (BP). Color measurements obtained for small areas (size $\sim 0.5pc$) of clouds in Taurus, Ophiuchus, Chamaeleon, Ursa Major have been reported by Boulanger et al. (1989). In all clouds large variations in the R(12,100), and R(25,100) color ratios are seen on scales as small as the resolution of the measurements, 0.5 pc. For dark clouds the R(60,100) colors also varies across the clouds and its variations are correlated with that of R(12,100). For high latitude clouds the R(60,100) is rather uniform.

Systematic color variations from the edge to the center of a cloud have been reported by Chlewicki et al. (1987) for a cloud in Chamaeleon and by Beichman et al. (1988) for B5 in Perseus. For these clouds R(12,100) decreases by a factor of about 3 to 4 from the edge to the center. Beichman et al. and Laureijs et al. (1988) have interpreted this limb-brightening of the 12μm emission as an excitation effect in the context of a model wherein small grains absorb mainly in the UV and consequently are excited only in a shell at the surface of the cloud. In many clouds, however, the color variation do not correlate with the opacity of the cloud, as traced by the 100μm brightness. Three cuts across filaments in Taurus are presented in figure 1 to illustrate this statement. These cuts were taken from IRAS images of Taurus after zodiacal subtraction. Their center lie within a few degrees from each other. For all three cuts the peak 100μm brightness is between 10 to $12 MJy/sr$ which for the $100\mu m/A_v$ values given in Table 1 correspond to a total A_v of about $1.5 mag$. Despite a similar peak 100μm brightness the three filaments have completely different colors and color morphology. The first filament shows no color variation. The second filament shows two components a low brightness envelope + a central peak, corresponding to a narrow filament in the images, with very different colors. In the third cut there is a continuous variation of the colors from one side to the other. Color values for these cut are summarized in Table 3. Both the large amplitude of the color variations and the varying morphology of the color variations cannot be explained by the excitation effect mentioned earlier. This leads us to the conclusion that there are large variations of the abundance of small particles in nearby clouds.

The physical origin of these abundance variations is unclear. A possible explanation for depletion is that the small particles coagulate or condense on large grains in the densest part of clouds. However, the time-scale for condensation on large grains is large compare to the mixing time scale of molecular matter: $\sim 5{\cdot}10^5$ yrs over 0.5 pc (Omont 1986). The small particles probably

play an important role in the heating and the chemistry of interstellar gas (d'Hendecourt and Léger 1987, Lepp and Dalgarno 1988a and b). Also, they probably account for a large fraction of the opacity of clouds in the UV. Therefore, variations in the abundance of small particles probably induce important changes in the physics and chemistry of clouds.

References

Beichman, C., Wilson, R.W., Langer, W., and Goldsmith, P. 1988, Ap. J., 332, L81.

Bloemen, J.B.G.M., et al. 1984, Astr. Ap. 139, 37.

Bloemen, J.B.G.M., et al. 1986, Astr. Ap. 154, 25.

Boulanger,F., 1987, Thèse d'Etat, Université Paris VI.

Boulanger, F., 1988, Molecular Clouds in the Milky Way and External Galaxies, Reidel, in press

Boulanger, F., and Pérault, M., 1988, Ap. J. 330, 964 (BP).

Boulanger, F., Falgarone, E., Helou, G., and Puget, J.L., 1989, Proceedings of the I.A.U. Symposium 135 on Interstellar Dust, eds. L. J. Allamandola and A.G.G.M. Tielens, in press.

Cernicharo, J., and Guélin, M. 1987, Astr. Ap. 176, 299.

Chlewicki, G., Laureijs, R.J., Clark, F.O., and Wesselius, P.R. 1987, Star Formation in Galaxies, ed. C.J. Lonsdale Persson (Washington: GPO).

Dame, T.M., et al. 1987, Ap. J. 322, 706.

Draine, B.T., and Lee, H.M., 1984, Ap. J., 285, 89.

Draine, B.T., and Anderson, N. 1985, Ap. J., 292, 494.

d'Hendecourt, L.B., and Léger, A. 1987, Astr. Ap. 180, L9.

de Vries, C.P., and Le Poole, R.S. 1985, Astr. Ap., 145, L7.

de Vries, H.W., Heithausen, A., and Thaddeus, P. 1987, Ap. J., 319, 723.

Falgarone, E., Pérault, M. 1988, Astr. Ap. 205, L1.

Guélin, M., and Cernicharo, J., 1988, Molecular Clouds in the Milky Way and External Galaxies, Reidel, in press.

Lange, A.E., et al., 1989, G., Proceedings of the I.A.U. Symposium 135 on Interstellar Dust, eds. L. J. Allamandola and A.G.G.M. Tielens, in press.

Langer, W.D., Wilson, R.W., Goldsmith, P.F., and Beichman, C. 1989, Ap. J in press

Laureijs, R.J., Mattila, K., and Schnur, G. 1987, Astr. Ap. 184, 269.

Laureijs, R.J., Chlewicki, G., and Clark, F.O. 1989, Astr. Ap. in press.

Leisawitz, D., and Hauser, M.G. 1989, Ap. J. in press.

Lepp, S., and Dalgarno, A. 1988a, Ap. J., 324, 553.

Lepp, S., and Dalgarno, A., 1988b, Ap. J., 335, 769.

MacLaren, I., Richardson, K.M., and Wolfendale, A.W., 1988, MNRAS, in press.

Mooney, T.J., and Solomon, P.M. 1988, Ap. J., 334, L51.

Omont, A. 1986, Astr. Ap., 169, 159.

Puget, J.L., and Léger, A., 1989, Ann. Rev. Astr. Ap., in press.

Snell, R.L., Heyer, M.H., and Schloerb, F.P. 1989, Ap. J. in press

Weiland, J.L., Blitz, L., Dwek, E., Hauser, M.G., Magnani, L., and Rickard, L.J. 1986, Ap. J., 306, L101.

TABLE 1. $I_\nu(100\mu m) - A_v$ and ^{13}CO Comparisons

Cloud	$I_\nu(100\mu m)/A_v$ (MJy/sr)/mag. (1)	$I_\nu(100\mu m)/W(^{13}CO)$ (MJy/sr)/(Kkm/s) (2)	References
B5	5.	1.8	Langer et al. (1989)
B18	...	1.3	Snell et al. (1989)
Chamaeleon	7.	2.8	Boulanger (1987)
High Latitude Cloud $l = 314°$, $b = -25°$	9.	...	de Vries and Le Poole (1985)
Heiles 2	5.	...	Cernicharo and Guélin (1986)
"	...	2.2	Snell et al. (1989)
L1642	8.3	...	Laureijs et al. (1987)

(1): slope of the $100\mu m - A_v$ correlation
(2): slope of the $100\mu m - W(^{13}CO)$ correlation

TABLE 2. $I_\nu(100\mu m) - WCO$ Comparisons

Clouds (1)	$I_\nu(100\mu m)/WCO$ (MJy/sr)/(Kkm/s) (2)	$I_\nu(100\mu m)/N_{H\ I}$ (MJy/sr)/($10^{20} Hcm^{-2}$) (3)
Auriga	0.8	1.0
Cepheus	0.7	0.75
Chamaelon I	1.3	1.3
Chamaeleon II	0.8	1.3
Lupus	1.2	1.9
Mon R2	1.2	1.0
Northern Orion Filament	1.9	1.0
Orion A	2.2	1.3
Orion B	2.5	1.3
Southern Orion Filament	1.6	1.0
Taurus	0.8	1.0

(1): see Dame et al. (1987) for references about CO observations
(2): slope of the $100\mu m - WCO$ correlation
(3): slope of the $100\mu m - N_{H\ I}$ correlation in the vicinity of the cloud

TABLE 3. IR Colors

Cut (1)	Color Morphology	Positions (2)	$\frac{I_\nu(12\mu m)}{I_\nu(100\mu m)}$	$\frac{I_\nu(25\mu m)}{I_\nu(100\mu m)}$	$\frac{I_\nu(60\mu m)}{I_\nu(100\mu m)}$
1	Constant Colors		0.037	0.05	0.18
2	Hot Envelope + Cold Central Peak	Envelope	0.10	0.11	0.22
		Peak	< 0.01	< 0.015	0.05
3	Variation from one side to the other	A	0.04	0.04	0.17
		B	0.02	0.02	0.13
		C	< 0.009	< 0.009	0.10
(3)			0.042	0.054	0.21

(1): cuts 1,2, and 3 are presented in Figure 1a,b, and c respectively
(2): Positions A, B, and C along cut 3 are indicated in figure 1c
(3): Average Colors of high galactic cirrus from BP listed for comparison.

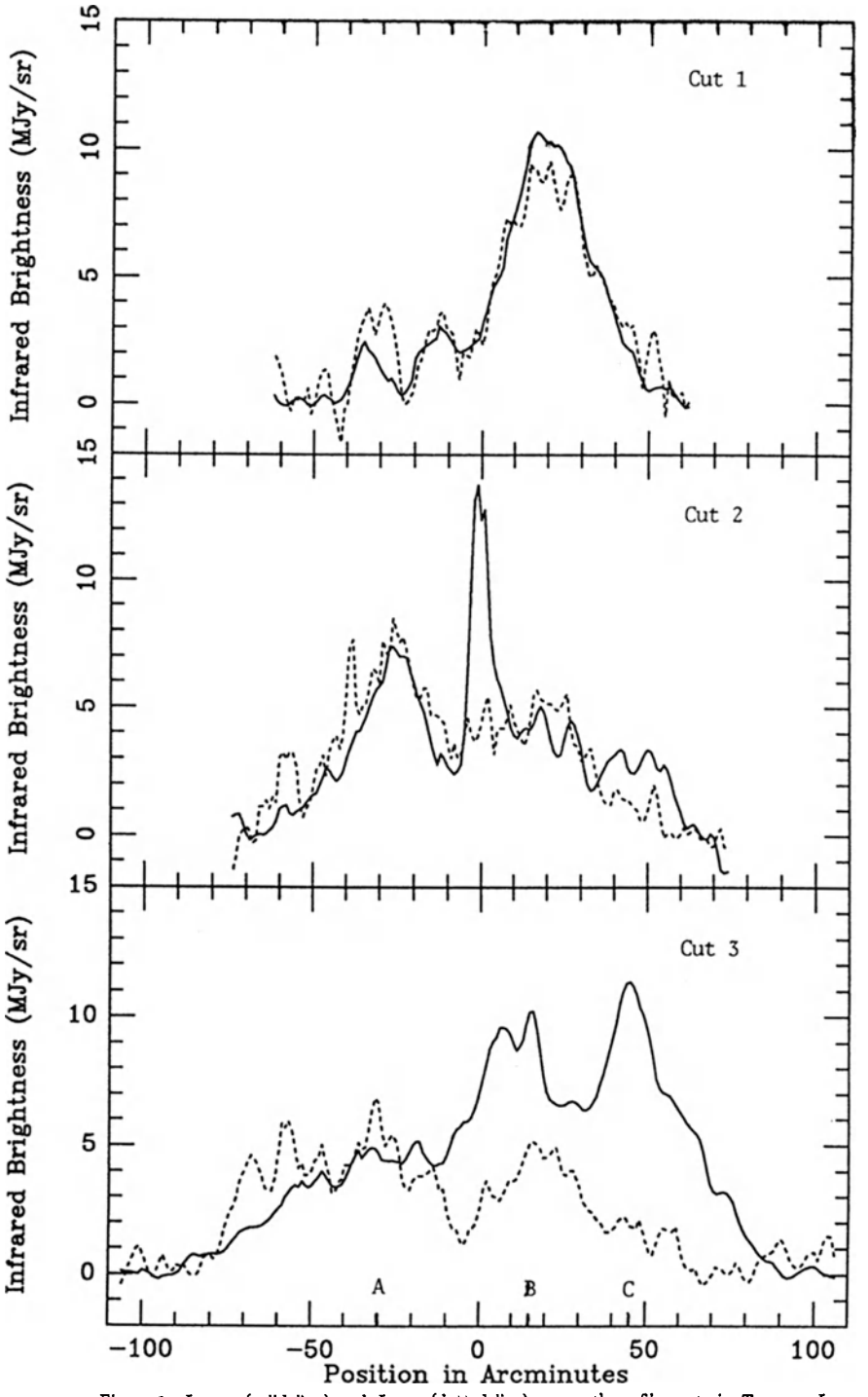

Figure 1: $I_{100\mu m}$ (solid line) and $I_{12\mu m}$ (dotted line) across three filaments in Taurus. $I_{12\mu m}$ is scaled by 20 in cut 1 and 3, and 10 in cut 2. The centers of the cuts 1, 2, and 3 are $\alpha = 4h48m50s\ \delta = 25°23'$, $\alpha = 4h34m07s\ \delta = 24°11'$, $\alpha = 4h15m44s\ \delta = 24°25'$, respectively. $I_{25\mu m}$ and $I_{60\mu m}$ are not plotted to keep the figure clear but all colors are given in Table 3.

PHYSICAL CONDITIONS IN DARK CLOUDS

Philip C. Myers
Harvard-Smithsonian Center for Astrophysics
Cambridge, Massachusetts, USA

SUMMARY

We discuss physical conditions in interstellar molecular clouds with visual extinction A_V ~ 1-10 magnitudes, based primarily on observations of spectral lines of CO and NH_3. *Diffuse clouds* with $A_V \sim 1$ mag have kinetic energy density which is primarily nonthermal, and is comparable to that of the "intercloud" gas; diffuse clouds have too little mass to bind their internal motions by gravity; their incidence of low-mass cores and low-mass stars is rare. *Dark clouds* with mean $A_V \sim 3$ mag have kinetic energy density which is primarily nonthermal, like diffuse clouds; but much greater than that of the intercloud gas, unlike diffuse clouds. Dark clouds are generally gravitationally bound. They are often surrounded by a number of diffuse clouds; in dark clouds low-mass cores and low-mass stars are common. *Low-mass cores* have mean $A_V \sim 10$ mag. Their kinetic energy density is mainly thermal, unlike their surrounding dark or diffuse clouds, and much higher than that of the intercloud gas. Cores are generally bound, and are frequently associated with low-mass stars. Several lines of evidence indicate that the nonthermal energy density in most molecular clouds is largely magnetic.

1. Introduction

Dark interstellar clouds are molecular clouds evident by their absorption and/or reflection of optical starlight. They are useful "laboratories" in which to study the physics of molecular clouds and star formation, because they are relatively numerous, near to the Sun, detectable in many molecular lines, and easily resolved by centimeter-and millimeter-wavelength telescopes. In this paper we summarize physical properties of three "types" of dark clouds distinguished by their mean visual extinction A_V: "diffuse" clouds with $A_V \sim 1$ mag, "dark" clouds with $A_V \sim 3$ mag, and "low-mass cores" with $A_V \sim 10$ mag. We discuss the clouds in terms of their ability to bind their internal motions by self-gravity; their relative energy densities in kinetic, magnetic, and gravitational form; and their stellar content.

Our knowledge of cloud properties is derived mainly from maps and spectra of molecular emission lines, made with radio telescopes operating at centimeter and millimeter wavelengths. At present, most available information comes from filled aperture ("single-dish") telescopes. Single-dish maps are made one pixel at a time, by serially stepping the telescope beam in a two-dimensional grid, with beam spacing usually equal to the FWHM beam width. The smallest visible angular scale is that of the diffraction-limited beam, or 0.2-2 arcminutes for most telescopes, depending on line frequency and diameter of the primary reflector. For a cloud at 500 pc, the smallest visible linear scale is then 0.03–0.3 pc. The largest visible angular scale is set by the step size and the number of times the telescope beam is stepped: this depends on many factors, including the signal-to-noise ratio of the spectral line, the available observing time, and the strategy adopted by the

observer. A "minimal" map strategy is to map the emission to define the half-maximum intensity contour, e.g., one beam beyond the half-maximum contour. This method can underestimate the extent of a cloud, especially if its emission consists of multiple peaks separated by deep valleys. Such a pattern of emission is often called a "complex" or "cloud complex." Most molecular cloud line maps are 3–30 beams in extent, or 0.1–10 pc for clouds at 500 pc.

We rely here on data from observations of the 2.6 mm J = 1 → 0 rotational line of ^{12}CO to define molecular clouds, and on data from observations of the 1.3 cm (J,K) = (1,1) rotation-inversion line of NH_3 to define "cores," or condensations within clouds. Use of these lines is convenient because they are extensively observed. However, other lines, such as the rotational lines of ^{13}CO, $C^{18}O$, and CS, also reveal molecular cloud properties. We emphasize that in a given cloud the density, column density, line width, size, temperature, and mass indicated by a line varies from one line to the next, primarily because each line traces a different mean density of collision partners (mainly H_2 molecules and He atoms) needed for excitation. In turn, this density defines a size scale, over which the quantities derived from the line observations are averages. The CO and NH_3 lines are useful because they trace size scales separated by a large factor - 10^{1-3} - and because these size scales reveal several aspects of cloud physics and star formation. For a discussion of "clumps" with an intermediate size of $\sim$ 1 pc traced by the ^{13}CO line, see Elmegreen (1985). For a discussion of cloud structure in terms of hierarchical organization, see Scalo (1988).

2. Physical Properties

Table 1 summarizes properties of diffuse and dark clouds as revealed by ^{12}CO line observations (e.g., Magnani, Blitz, and Mundy 1985; Keto and Myers 1986; de Geus, Bronfman and Thaddeus 1989), and of low-mass cores, as revealed by NH_3 line observations (e.g. Myers and Benson 1983, Benson and Myers 1989). We distinguish "low-mass" cores from "massive" cores such as the Kleinmann-Low nebula in Orion, which have significantly greater density, temperature, mass, and velocity dispersion than do low-mass cores, and more massive stars. The characteristic size R is the FWHM size of the emission line map. For diffuse and dark clouds, the mass M within R is obtained by integrating the column density in each beam over the map area within R. The mean number density within R is obtained from M, R, and a model of a uniform sphere. The FWHM line width Δv is due mainly to Doppler shifts in the molecular motions and is generally greater than the thermal width by a significant factor. The gas kinetic temperature T is derived from the brightness temperature of the line: the ^{12}CO J = 1→ 0 line is optically thick, so the line brightness is close to the transition excitation temperature, which in turn is a measure of the kinetic temperature. For diffuse clouds, T is much less certain than for dark clouds.

Table 1

Physical Properties of Diffuse Clouds, Dark Clouds, and Low-Mass Cores

Type	A_V (mag)	Tracer Line	R (pc)	n (cm^{-3})	M ($M_\odot$)	Δv (km s^{-1})	T (K)
Diffuse	1	^{12}CO 1-0	0.3–3	30-500	0.5-100	0.7–1.5	10?
Dark	3	^{12}CO 1-0	3–10	10^{2-3}	10^{3-4}	1–3	10
Low-Mass Core	10	NH_3 (1,1)	0.05–0.2	10^{4-5}	0.3–10	0.2–0.4	10

The diffuse clouds have mean visual extinction $\lesssim 1$ magnitude and can be seen on Palomar Sky Survey photographs by their faint reflection of starlight. They are most easily recognized at high galactic latitude, where they reflect the diffuse starlight from the plane. Diffuse clouds can vary appreciably in their molecular content; they have been classified as "CO-rich" and "CO-poor" by Lada & Blitz (1988). Those discussed here are known by their CO properties. Some diffuse clouds are much larger than the representative value ~ 1 pc given in Table 1. A few diffuse clouds are known to have low-mass cores from their NH_3 emission (L1489 and Bernes 48, Myers & Benson 1983; and MBM21, Stacy, Myers & de Vries 1988). A few are also known to have associated low-mass stars. Also, a larger number of diffuse clouds have small, opaque knots on optical photographs, indicating the probable presence of low-mass cores.

Dark clouds have mean extinction of several magnitudes and are therefore recognized more by their absorption of background starlight than by reflection. Like the diffuse clouds, dark clouds have a great range of size and visual appearance. The properties given in Table 1 refer to the well-studied complexes in Taurus and Ophiuchus. Many smaller and more isolated dark clouds ("globules") are also known (Leung 1985). Dark clouds also vary widely in the number and distribution of their cores and stars: the Taurus-Auriga complex has more than 100 visible T Tauri stars (Cohen & Kuhi 1979; Herbig & Bell 1988) and a comparable number of pre-main-sequence stars detectable via their x-ray emission (Walter *et al.* 1988). In contrast, the dark cloud complex in Aquila, whose most prominent member is Lynds 673, has only a few T Tauri stars (Herbig 1962) and NH_3 cores (Benson & Myers 1989). The proportion of massive (OB) stars in nearby dark clouds is low: a few examples are AB Aur in Taurus-Auriga; BD+30°549 in Perseus; HD 147889 in Ophiuchus; TY CrA in Corona Australis; and HD 200775 in Lynds 1172. It is unclear whether the general tendency for low-mass clouds to make low-mass stars reflects a difference in relevant physical conditions such as magnetic fields, temperature, density structure, and ionization between low-mass and massive clouds, or rather merely a difference in the mass available to make stars of all types.

For low-mass cores the properties in Table 1 are based on NH_3 line observations. Here R and Δv are determined from maps and spectra as before; while n and T are generally deduced from excitation analysis of the (J,K) = (1,1), (2,2), and higher-excitation lines; and M is obtained from n, R, and the model of a uniform sphere. Low-mass cores are known in dark and diffuse clouds within a few hundred pc from the Sun. They are remarkable in their narrow, nearly thermal line widths, and in their relationship to low-mass stars. In 12 low-mass cores without stars analyzed by Benson (1986), the mean kinetic temperature is $T = 10$ K, and the mean FWHM line width is $\Delta v = 0.27$ km s^{-1}. Hence, the ratio of nonthermal to thermal velocity dispersion for a molecule of mean molecular weight ($2.3 m_H$, allowing for 10% Helium) is only 0.5. In contrast, the same ratio is 14 for a massive core with $\Delta v = 2$ km s^{-1} and $T = 50$ K. Low-mass cores in dark clouds have associated low-luminosity ($L \lesssim 10\ L\odot$) *IRAS* sources in about half of the ~ 100 cases examined by Beichman *et al.* (1986). This propensity of low-mass cores to form low-mass stars, and the similarity of the mass within the typical NH_3 core line map to 1 $M_\odot$, suggest that the typical molecule in a starless core has a relatively high likelihood of adding its mass to that of a forming star. Thus molecules in low-mass cores are "destined for stardom," and low-mass core properties are often considered as initial conditions for models of low-mass star formation (e.g., Shu, Adams & Lizano 1988).

3. Cloud energetics

Table 2 presents a comparison of energy densities and equilibrium magnetic field strengths for the objects described in Table 1. These comparisons reveal that diffuse clouds have internal pressure comparable to that of the intercloud medium; that dark clouds and low-mass cores are gravitationally bound; that the kinetic energy density of diffuse and dark clouds is primarily

nonthermal; and that many clouds and cloud cores probably have nearly equal magnetic and nonthermal kinetic energy density. For each object in Table 1, representative values of the listed cloud parameters were used to calculate the "nonthermal kinetic energy" density

$$K_{NT} = 3mn\sigma_{NT}^2, \tag{1}$$

where m is the mean molecular mass, 2.3 m_H; the "thermal kinetic energy" density,

$$K_T = 3mn\sigma_T^2, \tag{2}$$

and the gravitational potential energy density

$$U_G = \frac{3GMmn}{5R}. \tag{3}$$

Here each "kinetic energy" density is twice the true kinetic energy density, as in the virial theorem, and all notation follows that of Myers & Goodman (1988a). Each energy density in Table 2 is expressed in terms of 10^4 cm^{-3}K times Boltzmann's constant, a measure of the energy density of the intercloud medium. This value lies within a factor ~ 3 of most estimates (Kulkarni & Heiles 1987). The equilibrium magnetic field strength

$$B = \sqrt{4\pi K_{NT}} \tag{4}$$

is calculated by equating the magnetic and nonthermal kinetic energy terms of the virial theorem.

Table 2

Observed Energy Densities and Equilibrium Magnetic Field Strengths of Diffuse Clouds, Dark Clouds, and Low-Mass Cores

Object	Energy Density			Equilibrium Magnetic Field Strength
	Nonthermal Kinetic	Thermal Kinetic	Gravitational	
	(1.38×10^{-12} erg cm^{-3})			(μG)
Diffuse Cloud	2	0.3	0.08	6
Dark Cloud	40	3	50	30
Low-Mass Core	20	60	70	20

Note – Each energy density is calculated from typical values of cloud and core properties in Table 1, according to equations (2)–(4) of Myers and Goodman (1988b). Each "kinetic energy" density is twice the three-dimensional kinetic energy density, as in the virial theorem. Each energy density is given in units of 1.38×10^{-12} erg cm^{-3}, or 10^4 times Boltzmann's constant, taken as a measure of the intercloud energy density. The equilibrium magnetic field strength is ($4\pi \times$ nonthermal kinetic energy density)$^{1/2}$.

The energy densities in Table 2 increase monotonically with increasing number density from those of diffuse clouds to those of low-mass cores. Among these, only the diffuse clouds have kinetic energy density comparable to the intercloud value. The diffuse clouds are also distinctive in that they are the only objects far from gravitational binding: their kinetic energy density exceeds their gravitational energy density by an order of magnitude. Thus, the typical diffuse cloud is not bound by self-gravity (Magnani, Blitz & Mundy 1985), but may be close to pressure balance with the intercloud gas (Keto & Myers 1986; Elmegreen 1988).

In contrast to the diffuse clouds, dark clouds and low-mass cores appear to be gravitationally bound, in that $K_{NT} + K_T$ lies within a factor 2 of U_G. But the relative values of K_{NT} and K_T indicate that dark clouds and low-mass cores have different means of support. Thus, the low-mass cores are supported against gravity primarily by thermal motions, while dark clouds are dominated by nonthermal motions.

The equilibrium field strengths in Table 2 are similar, within factors of 2-3, to available magnetic field strengths, suggesting an important role for magnetic energy in cloud dynamics and evolution. For diffuse clouds the equilibrium field strength is 6 μG, within a factor 2 of most estimates of the "background" field strength throughout the Galaxy (Heiles 1987). This similarity implies that diffuse clouds which are in "pressure balance" with the intercloud gas may be largely in magnetic pressure balance; and that diffuse clouds which are overpressured and expanding may not expand freely, but instead may be retarded or constrained by various magnetic interactions. The equilibrium field strengths in dark clouds, giant clouds, and low-mass cores, 20–30 μG, are also remarkably similar. A possible explanation for this similarity involves "photoionization-regulated star formation" (McKee & Lin 1988). Some five Zeeman effect measurements of field strength in these objects have been reported, and these lie within a factor 2 of the equilibrium values (Crutcher, Kazès & Troland 1987; Myers & Goodman 1988a; Goodman *et al.* 1989). Similarly, some five field strengths, typically $\sim$ 100 μG, are known for large massive cores, and more than ten, typically $\sim$ 3000 μG, are known from OH masers for small, massive cores. In each case the observed field strength appears within a factor 2 of the equilibrium value (Myers & Goodman 1988a).

If the available measured field strengths in dark clouds, giant clouds, and low-mass cores described above are representative, the empirical trends between nonthermal velocity dispersion σ_{NT}, cloud size R, and cloud density n first discussed by Larson (1981) have a simple explanation. The nonthermal kinetic energy density, the gravitational energy density, and the magnetic energy density are then essentially equal, so equations (1), (3), and (4) yield

$$\sigma_{NT} = \left(\frac{G}{45}\right)^{1/4} B^{1/2} R^{1/2} \tag{5}$$

and

$$n = \left(\frac{5}{G}\right)^{1/2} \frac{B}{4\pi m R}. \tag{6}$$

These equations can be expected to match the observed correlations, provided that the relative range of B is small compared to the relative range of R. Since the correlations are known for three decades in R, from 0.1 to 100 pc, even a factor of 30 scatter in B allows a discernible correlation (Myers & Goodman 1988b).

4. Discussion

The foregoing material suggests that in many molecular clouds the magnetic energy density is comparable to the nonthermal kinetic energy density; and those clouds with relatively high extinc-

tion and relatively frequent star formation are also gravitationally bound, i.e. their gravitational energy density is also comparable to their kinetic and magnetic energy densities.

Recently, an important new piece of evidence has arisen. Sensitive CO observations in Chamaeleon (Keto and Myers 1986), Taurus-Auriga (Ungerechts and Thaddeus 1987), and Ophiuchus (de Geus, Bronfman and Thaddeus 1989; Loren 1989) show that the bright, large, dense, star-rich, and bound parts of each complex are accompanied by numerous faint, small, rarefied, star-poor, and unbound regions. These diffuse clouds associated with dark clouds are similar in size, extinction, and velocity dispersion to the more isolated diffuse clouds discussed by Magnani, Blitz, and Mundy (1985).

This pattern of dense, bound gas surrounded by less dense, unbound gas is similar to the situation of dense low-mass cores inside diffuse clouds, discussed in Sections 1 and 2, except for a factor of $\sim$ 10 difference in size scale. Together, these examples suggest that we now have some evidence for a kind of a critical radius, which divides gravitationally bound gas from gravitationally unbound gas in a cloud or cloud complex. If so, the discussion above implies that a three-way equipartition (magnetic, kinetic, and gravitational) applies inside the critical radius while a two-way equipartition (magnetic and kinetic) applies outside.

How do these patterns of energy density develop and evolve? Since gravity is a central force, one may speculate that the self-gravitating regions develop from the "inside out" and enlarge as more mass accretes onto them. This process is then similar in some ways to the "inside-out collapse" discussed by Shu (1977), but with some interesting differences: (1) it cannot be a runaway collapse, since the self-gravitating dark cloud shows no kinematic evidence of global collapse, and contains stars much older than its free-fall time; (2) the magnetic field is energetically significant, and must therefore play an important role in the dynamical evolution; and (3) the geometry of the dark cloud is highly complex, with many local maxima of density; and nonspherical, with many filamentary elements. It will be valuable to study the prevalence of this bound-unbound structure in more dark cloud complexes.

I thank G. Winnewisser and the other members of the Organizing Committee for their invitation to speak, and for their kind hospitality.

REFERENCES

Beichman, C.A., Myers, P.C., Emerson, J.P., Harris, S., Mathieu, R., Benson, P.J. & Jennings, R.E. (1986). *Ap. J.*, **307**, 337.

Benson, P.J. (1986). In *Masers, Molecules, and Mass Outflows in Star Forming Regions*, ed. A. D. Hashchick, p. 55. Westford, MA: Haystack Observatory.

Benson, P.J. & Myers, P.C. (1989). *Ap. J., Suppl.*,in press.

Cohen, M. & Kuhi, L.V. (1979). *Ap. J. Suppl.*, **41**, 743.

Crutcher, R.M., Kazès, I. & Troland, T. H. (1987). *Astr. Ap.*, **181**, 119.

DeGeus, E. J., Bronfman, L., and Thaddeus, P. (1989). *Ap. J.*, submitted.

Elmegreen, B.G. (1985). In *Protostars and Planets II*, ed. D. C. Black & M. S. Mathews, p. 33. Tucson: University of Arizona.

Elmegreen, B.G. (1988). In *Interstellar Matter*, ed. J. M. Moran & P. T. P. Ho, p. 55. New York: Gordon & Breach.

Goodman, A. A., Crutcher, R.M., Heiles, C., Myers, P. C. & Troland, T. H. (1989). *Ap. J. (Letters)*, in press.

Heiles, C. (1987). In *Interstellar Processes*, ed. D. J. Hollenbach & H. A. Thronson, p. 171. Dordrecht: Reidel.

Herbig, G. H. (1962). *Advances in Astronomy & Astrophysics*, **1**, 47.

Herbig, G. H. & Bell, K. R. (1988). *Lick Observatory Bulletin* No. 1111.

Keto, E. R. & Myers, P. C. (1986). *Ap. J.*, **304**, 466.

Kulkarni, S. R. & Heiles, C. (1987). In *Interstellar Processes*, ed. D. J. Hollenbach & H. A. Thronson, p. 87. Dordrecht: Reidel.

Lada, E. A. & Blitz, L. (1988). *Ap. J. (Letters)*, **322**, 377.

Larson, R. B. (1981). *M. N. R. A. S.*, **194**, 809.

Leung, C. M. (1985). In *Protostars and Planets II*, ed. D. C. Black & M. S. Mathews, p. 104. Tucson: University of Arizona.

Loren, R. B. (1989). *Ap. J.*, in press.

Magnani, L., Blitz, L. & Mundy, L. (1985). *Ap. J.*, **295**, 402

McKee, C. F . & Lin, J.-Y. (1988). In *Origin, Structure, and Evolution of Galaxies*, ed. L. Z. Fang. Singapore: World Scientific. In Press.

Myers, P. C. & Benson, P.J. (1983). *Ap. J.*, **266**, 309

Myers, P. C. & Goodman, A. A. (1988a). *Ap. J. (Letters)*, **326**, L27.

Myers, P. C. & Goodman, A. A. (1988b). *Ap. J.*, **329**, 392.

Scalo, J. (1988). In *Molecular Clouds in the Milky Way and External Galaxies*. ed. R. Dickman, R. Snell & J. Young. Dordrecht: Reidel. In press.

Shu, F. H. (1977). *Ap. J.*, **214**, 488.

Shu, F. H., Adams, F. C. & Lizano, S. (1987). *Ann. Rev. Astr. Ap.*, **25**, 23.

Stacy, J. G., Myers, P. C. & de Vries, H. W. (1988). In *Molecular Clouds in the Milky Way and External Galaxies*, ed. R. Dickman, R. Snell & J. Young. Dordrecht: Reidel. In press.

Walter, F., Brown, A., Mathieu, R., Myers, P. C. & Vrba, F. (1988). *A. J.*, **96**, 297.

High Latitude Molecular Clouds and the IR Cirrus

U. Mebold
Radioastronomisches Institut der Universität Bonn
Auf dem Hügel 71,D-5300 Bonn 1, FRG

1.Introduction

This paper reviews interpretations of line observations of high latitude ($|b|\geq 25°$), diffuse ($A_V \leq 1.5$ mag) molecular clouds. These clouds are infrared emitters and are part of the so-called "IR cirrus" (cf. Low et al. 1984). The high latitude diffuse molecular clouds, which may also be called "diffuse cirrus molecular clouds", are to be distinguished from the classical diffuse clouds. The latter are CO-poor ($N(CO)/N(H) < 10^{-6}$) compared to the diffuse cirrus molecular clouds which have $N(CO)/N(H) > 10^{-5}$. This review will not be complete and the well known high latitude dark clouds ($A_V \geq 1.5$ mag) like L134, which are typical of low latitude dark clouds, will not be discussed at all.

The discussion of the galactic cirrus can be dated back as far as the publication of the "Catalog of Bright Nebulae" by Lynds (1965). The nebulae listed in that catalog (LBN hence foreward) are part of the IR cirrus and appear to be good tracers of molecular gas. Sandage (1976) interpreted these nebulae as dust clouds which scatter the light from the galactic plane back to the observer. He could reproduce the observed brightness by adopting dust grains with an albedo A = 0.5 and isotropical scattering properties (G = 0.0). The problem of their distance was raised e.g. by Minkowski et al. (1972) who noted a spatial association of some of these nebulae with "high velocity clouds", probable halo population objects. A spatial association of a large fraction of the high latitude LBNs with large scale HI- and radio continuum loops (cf. Heiles and Jenkins 1976, Wesselius and Fejes 1973) suggested that they are the tips of dusty "ice-bergs" in large-scale gaseous filaments. The first detection of molecules in high latitude diffuse nebulae (LBN406/412/415) was made by Goerigk et al. (1983). They used CO to trace molecular hydrogen because the HI observed in these nebulae fell short by a factor of 10 to explain the minimum extinction estimated from star counts.

The link between the dust in the LBNs and the dust to be expected in the large-scale HI filaments was established by the discovery with the IRAS satellite of the IR cirrus by Low et al. (1984). This discovery established the possibility of deriving distances of these large scale filaments by studying lines of sight to stars which do or do not show interstellar absorption lines or extinction. This allows to study the physics, chemistry, kinematics, and dynamics of these features and their interaction with the galactic disk far up into the halo of our galaxy.

2. Survey-type work

A survey of the CO molecule in a fairly complete sample of high latitude diffuse nebulae was published by Magnani, Blitz and Mundy (1985, MBM hence foreward). They observed 57 clouds at $|b|\geq 25°$ by sampling every fifth antenna beam within one cloud. The clouds cover

about 50 square degrees of sky and are distributed fairly regularly over the area selected. From the effect of differential galactic rotation on the clouds they estimate an average distance of D≈100 pc and an average displacement from the galactic plane of <z>≈60 pc. This small distance is a consequence of the selection criterion that the clouds have "a noticeable drop in star density". Therefore most of the clouds appear to be disk population objects. Mean diameters of the clouds are <s> ≈ 1.7 pc. Their masses, derived from the standard conversion factor $XWCO=2.5\cdot10^{20}$ $mol(cm^2Kkm/s)^{-1}$, range from 0.6 to 300 $M_\odot$ with a mean of 40 $M_\odot$. The so-called X-factor, denoted by XWCO here, is defined as the ratio of the molecular hydrogen column density, $N(H_2)(cm^2)$, and the ^{12}CO line integral, WCO(Kkm/s). The gravitational stability of the clouds was estimated by comparing the virial velocity dispersion, σ_{vir}, with the observed velocity dispersion, σ_{obs}. Ratios of $\sigma_{obs}/\sigma_{vir}$ = 1 - 20 indicate that most of these molecular clouds are gravitationally unbound systems, i.e. transient phenomena.

Similar conclusions are reached in a study of 15 high latitude, southern sky (225°≤l≤320°, b≤20°) CO clouds by Keto and Myers (1986). Their clouds are similar in most respects to those of MBM, but have simpler structures, smaller sizes, and lower masses, possibly because of differences in selection. They supplement their CO data by extinction estimates from star counts. A comparison of the total gas column densities - or the masses - of the clouds estimated from the ^{12}CO line integral and $XWCO = 3\cdot10^{20}$ $mol(cm^2Kkm/s)^{-1}$, from the extinction and the standard gas-to-dust ratio $N(H_2)(cm^{-2}) = 9.4\cdot10^{20}\cdot A_V(mag)$, and from the assumption of virial stability confirms the result of MBM that the clouds are gravitationally unbound systems. They argue, however, that the clouds may not be expanding systems but rather may be confined by the pressure of the surrounding intercloud medium. If the ^{12}CO line parameters in their Table 1 (note that the line integral, $I(^{12}CO)$, in that Table and in the subsequent discussion is low by a factor of ≈2.35) are used to calculate XWCO from their extinctions and the standard gas-to-dust ratio, a range of XWCO values of $4.3\cdot10^{20} \geq XWCO \geq 0.64\cdot10^{20}$ $mol(cm^2Kkm/s)^{-1}$ is found. Values as low as $0.3\cdot10^{20}$ $mol(cm^2Kkm/s)^{-1}$ are found (de Vries 1988), if that part of the extinction, which is due to the HI gas, is considered separately.

As transient objects, the high latitude diffuse clouds are physically and chemically in a non-steady state. So these clouds may be ideal objects to study formation and destruction processes for molecules and dust. We will therefore emphasize determinations of molecular abundances in these clouds, inparticular of the XWCO-ratio.

Using the extinctions, which Magnani and de Vries (1987) derived from starcounts for a subset of the sample of the MBM clouds, adopting the standard gas-to-dust ratio $N(H)(cm^{-2})=1.4\cdot10^{21}\cdot A_B$ (mag), and ignoring the true HI content of the clouds, i.e. assuming $N(H)\approx N(H_2)$, Magnani et al.(1988) deduce $XWCO=3.2(^{+3}_{-2})\cdot10^{20}$ $mol(cm^2Kkm/s)^{-1}$. Note that the scatter found here, as well as that found in the data of Keto and Myers (1986), is not caused by observational uncertainties, but is real. This indicates that large differences do exist in the astrophysical conditions - e.g. radiation field or chemical abundances - prevailing in these clouds. By calibrating the WCO values of MBM by ^{13}CO lines these authors derive a column density ratio $N(CO)/N(H_2)\approx1.2\cdot10^{-4}$. From OH and H_2CO line observations they find $N(OH)/N(H_2)=2\cdot10^{-6}$ and $N(H_2CO)/N(H_2)=3\cdot10^{-9}$, values which are clearly above normal and about normal, respectively, compared to dark clouds. Considering that we are discussing diffuse clouds, these column density ratios are surprisingly large. Lada and Blitz (1988) compare

them to the classical diffuse clouds ($N(CO)/N(H_2)<10^{-6}$) and call them "CO-rich".

Heithausen et al.(1987) discovered the 6-cm absorption line of H_2CO in 4 out of a sample of 15 CO clouds in the area $125° \leq l \leq 145°$, $35° \leq b \leq 45°$. Mebold et al.(1987) report the first detection of NH_3 in diffuse galactic cirrus clouds and derive column density ratios $N(NH_3)/N(H_2CO) = 1$ to 0.06, $\langle N(NH_3)/N(H_2)\rangle = 0.5 \cdot 10^{-8}$, and $\langle N(H_2CO)/N(H_2)\rangle = 7 \cdot 10^{-8}$. The latter two ratios are well below and well above, respectively, the typical ratios for dark clouds in the galactic disk. The difference between the $N(H_2CO)/H(H_2)$ ratios found by Magnani et al.(1988) and (the larger one) by Mebold et al. is caused by the difference in the estimates of $N(H_2)$. The H_2CO column densities ($N(H_2CO) \approx 3.1 \cdot 10^{12}$ cm^{-2}) are similar but Mebold et al. use an extinction estimated from star counts, the standard gas to dust ratio, and the 21-cm line observations of de Vries et al.(1987) while Magnani et al.(l.c.) used the CO observations of MBM and the standard X-factor.

In summary, the results discussed in the present section indicate that a) the true scatter found for the XWCO ratio in the high latitude diffuse molecular clouds is larger than a factor of six and b) the molecular abundances in a small fraction of these clouds are surprisingly large for diffuse clouds. They may even be larger than the molecular abundances in dark clouds.

3. Individual Clouds or Structures

Investigating individual clouds in high galactic latitudes one takes advantage of negligible confusion by superposition effects along the line of sight. In the plane one tends to derive global properties of a mixture of clouds and physical conditions along the line of sight, which are hard to rationalize. We will here reconsider the molecular abundance ratios of isolated high latitude clouds with the aim to check the averages discussed in the previous section.

Special efforts have been made to determine distances to some of the cirrus molecular clouds in order to get reliable estimates of their astrophysical properties. The method used is to find out whether stars, which are projected against the clouds, are in front of or behind the clouds. The presence or absence of interstellar extinction and/or absorption lines at the velocity of the CO emission and the analysis of these observations yields distances and column densities for the individual clouds discussed below. The results are collected in Table 1; WCO or XWCO values are included only when they are given in the quoted publication.

The two so far "nearest" molecular clouds, MBM12 and MBM16, have been studied in the interstellar NaI D, CaII K, and CH 4300 A lines by Hobbs et al.(1986) and Hobbs et al.(1988). They find that CH is overabundant by at most a factor of 10. Adopting the standard gas-to-dust ratio, assuming that $N(H)=N(H_2)$, and using the CO results from MBM and Magnani et al.(1988) and the extinction from Magnani and de Vries (1987) for MBM16, they derive the column density ratio $N(CO)/N(H_2) \geq N(CO)/N(H) \approx 10^{-4}$ and classify these clouds as "CO-rich" diffuse clouds. If a large fraction of the observed extinction is associated with HI-gas, $N(H_2)$ is over estimated and these clouds might be even more CO-rich than the dark clouds in the galactic disk.

The cloud L1569/MBM18 has been studied by Franco (1988). Using his extinction estimates, the standard gas-to-dust ratio, and the MBM CO-data, one finds $XWCO \geq 3 \cdot 10^{20}$ mol(cm^{2}Kkm/s)$^{-1}$ for that cloud.

The previously unknown high latitude molecular cloud MCLD(56,-44) has been studied by de Vries and van Dishoek (1988). From the data summarized in Table 1 they find an XWCO-ratio close to the standard value ($XWCO \approx 2.0 \cdot 10^{20}$ mol(cm^{2}Kkm/s)$^{-1}$), and classify this cloud as beeing similar to a classical diffuse cloud, but having slightly increased molecular abundances ($N(CO)/N(H_2) \approx 10^{-5}$) because of a reduced UV radiation field, slightly larger H_2 column densities, and possibly a smaller gas phase carbon abundance ($\delta_C = 0.1$).

The cloud LBN105/MBM40 has been studied by Lilienthal et al.(1988; 1989) in the interstellar NaI D lines. Since this cloud is associated with the North Polar Spur, the available 21-cm and ^{12}CO line data with the ≈9 arcmin resolution deserve further analysis.

The Ophiuchus dark clouds have been discussed by de Geus (1988) on the basis of a ^{12}CO line survey carried out with the 1.2-m Columbia University telescope in Chile, extinction derived from Walraven photometry towards the stellar members of the Sco-Cen OB association, 21-cm line data observed with the NRAO 43-m telescope, and IR 100μm and 60μm data observed with the IRAS satellite. The author derives $XWCO = 10^{19}$ mol(cm^2 Kkm/s)$^{-1}$ from WCO, τ_{100}, the dust optical depth at 100μm, and the assumption that $\tau_{100}/N(HI) = \tau_{100}/N(H_2)$. This is one of the smallest XWCO-values in the literature so far.

Table 1: Distances and Column Densities of High Latitude Clouds

name,pos. (l°,b°)	authors	distance, method	column density or column density ratio
MBM 12 (150,-34)	Hobbs et al.1986	65 pc Na D lines	$E(B-V) \approx 0.1$ mag at WCO ≈ ≈ 1 K km/s level $\langle N(NaI) \rangle = 22 \cdot 10^{11}$ cm^{-2} $\langle N(CaII) \rangle = 6 \cdot 10^{11}$ cm^{-2} $\langle N(CH) \rangle \leq 4.5 \cdot 10^{12}$ cm^{-2}
MBM 16 (172,-38)	Hobbs et al.1988	$60 \leq d \leq 95$ pc Na D lines	$\langle N(NaI) \rangle = 17 \cdot 10^{11}$ cm^{-2} $N(CaII) = 1.3 \cdot 10^{11}$ cm^{-2} $N(CH) \leq 6.9 \cdot 10^{12}$ cm^{-2}
L1569/MBM18 (189,-37)	Franco,1988	130 pc (uvbyβ)	$\langle E(B-V) \rangle = 0.2$ mag outside the WCO=0.5 K km/s level
MCLD (56,-44)	de Vries van Dishoeck 1988	$d \leq 210$ pc VBLUW phot., abs.lines towards HD 210121	$E(B-V) \approx 0.3$ mag $N(NaI) \geq 8 \cdot 10^{12} \cdot$ cm^{-2} $N(CaII) = 8 \cdot 10^{12}$ cm^{-2} $N(CH) = 3.5 \cdot 10^{13}$ cm^{-2} $N(CH^+) = 6.0 \cdot 10^{12}$ cm^{-2} $N(CO) = 1.0 \cdot 10^{16}$ cm^{-2} $N(HI) \approx 2 \cdot 10^{20}$ cm^{-2}
L105/MBM40 (48,+45)	Lilienthal 1988	80 pc NaI D lines	$N(NaI) = 1.5 \cdot 10^{12}$ cm^{-2}
Oph clouds (352,+17)	de Geus 1988	125 pc VBLUW phot	$XWCO = 10^{19}$ mol(cm^{2}Kkm/s)$^{-1}$

The discussion of the individual clouds in the present section confirms that the molecular abundances of the diffuse molecular clouds in the galactic cirrus are well below those of the classical diffuse clouds and compare better to the abundances of the dark clouds or cloud complexes in the galactic plane. It is evident again that XWCO spans a large range: $6 \cdot 10^{20} \geq XWCO \geq 10^{19}$ mol(cm^{2}K km/s)$^{-1}$. As the mean of these values of XWCO (see above) is close to the most recent value of the standard X-factor, $XWCO = 2.3 \cdot 10^{20}$ mol(cm^{2}Kkm/s)$^{-1}$, it is tempting to interpret the dark clouds for which this value applies (cf. the article of H. Bloemen in the present volume) as systems with a mixture of physical conditions that produce the observed range of molecular abundance ratios.

4. On the Origin of the Extreme Values of XWCO

A new method of deriving XWCO has been introduced by de Vries et al. (1987). If the IR emission per nucleon in atomic, a_{HI}, and in pure molecular clouds, a_{H2}, is known, I_{100} can be used to derive XWCO e.g. by correlating I_{100} and WCO. In the present section determinations of I_{100} per nucleon in HI clouds, $a_{HI} = I_{100}/N(HI)$, and per nucleon in molecular clouds, $a_{H2} = I_{100}/2 \cdot N(H_2)$, are reviewed. For a cloud consisting of a mixture of HI and H_2 gas I_{100} is then given by $I_{100} = a_{HI} \cdot N(HI) + a_{H2} \cdot N(H_2)$. Determinations of either a_{HI} or a_{H2} by the direct or indirect use of a gas-to-dust ratio will not be considered, because one of the aims of this exercise is to supply evidence for a different gas-to-dust ratio in the molecular and the atomic parts of at least some high latitude diffuse molecular clouds.

Determinations of a_{HI} for high latitude regions, which probably do not have molecular gas, are in the rather narrow range between 0.7 and $1.0 \cdot 10^{-20}$ MJy/sr cm^2 (Boulanger et al. 1985, McGee et al. 1986, Fong et al. 1987, de Vries et al. 1987, Heithausen and Mebold 1988). The two low latitude regions for which Tereby and Fich (1986) drive $a_{HI} = 0.64$ and $0.42 \cdot 10^{-20}$ MJy/sr cm^2 probably sample a mixture of atomic and molecular gas. Determinations of a_{H2} from extinction and the standard gas-to-dust ratio for dark clouds generally give values which are between 0.3 and $0.5 \cdot 10^{-20}$ MJy/sr cm^2 (cf. Cernicharo and Guelin 1987 etc). This indicates $a_{HI} > a_{H2}$, i.e. the IR emission per nucleon for atomic regions is larger than that for molecular clouds. Evidence for $a_{HI} < a_{H2}$ is, however, presented at the end of this section.

de Vries et al.(1987) derive a_{HI} and XWCO from an I_{100}-N(HI)-WCO data cube for a cirrus molecular cloud complex associated with a large, high latitude loop structure, called the Polar Loop. The complex subtends an area of about 50 square degree at the sky and is centered at $(l,b) \approx (140°,+38°)$. The authors assume that I_{100} is proportional to the total number of hydrogen nuclei along the line of sight $I_{100} = a \cdot (N(HI) + 2 \cdot N(H_2))$, i.e. they assume $a_{HI} = a_{H2} = a$. They calibrate a in regions where WCO=0, i.e. $a = a_{HI}$. Further, using $N(H_2) = XWCO \cdot WCO$, they derive XWCO from the two coefficients a and b in the equation $I_{100} = a \cdot N(HI) + b \cdot WCO$, i.e. from $b = 2 \cdot a \cdot XWCO$. They find $a = 1.0 \cdot 10^{-20}$ cm^{2}MJy/sr and the rather small value $XWCO = 0.6 \cdot 10^{20}$ mol(cm^{2}Kkm/s)$^{-1}$.

Using essentially the same data but supplementing them with extinctions derived from star counts, Heithausen (1987) and Heithausen and Mebold (1988) find that the standard gas-to-dust ratio $N(H) = N(HI) + 2 \cdot N(H_2) = 1.7 \cdot 10^{21} \cdot A_V$ is valid for these cirrus molecular clouds and that a linear relation exists between I_{100} and A_V or N(H). From an analysis of the 3-D data cube they find further that I_{100} per

HI atom in the CO-free regions, $a_{HI}(WCO=0)$, equals that per HI atom in the CO emitting regions, $a_{HI}(WCO=0) = a_{HI}(WCO>0)$. Since the HI and the H_2 gas are probably well mixed in these clouds, $a_{HI}(WCO>0) \approx a_{H_2}$ and the assumption $a_{HI} = a_{H_2}$ of de Vries et al.(1987) is justified. Heithausen and Mebold (1988) finally point out that the linear relations found between Av, N(H), and I_{100} imply directly $a = a_{HI} = a_{H_2}$. So the gas-to-dust ratio in the Polar Loop molecular clouds appears to be the same for the atomic and the molecular parts of the clouds and appears to be close to the value found by Bohlin et al. (1979).

A similar analysis has been performed for the Draco nebula, a high latitude molecular cloud that is located ≥500 pc above the galactic plane and is colliding with an HI high velocity cloud, (see the paper by Herbstmeier et al., this volume). It shows that $a_{HI} \neq a_{H_2}$, namely $a_{H_2} \approx 2.5 \cdot a_{HI}$. This is apparently opposite to the results quoted at the beginning of the present section. Anyhow, once a_{H_2} is known, XWCO can be derived from $I_{100} = a_{HI} \cdot N(HI) + a_{H_2} \cdot XWCO \cdot WCO$ and the observed quantities N(HI) and WCO. Herbstmeier et al. find for the Draco nebula $XWCO \approx 2 \cdot 10^{19}$ mol(cm^{2}Kkm/s)$^{-1}$. This X-factor is even lower than that found by de Vries et al. (1987) or Heithausen and Mebold (1988).

Tentative interpretations of the results for the Draco nebula are dicussed by Herbstmeier et al.(in the present volume). High resolution ^{12}CO and ^{13}CO line mapping (Rohlfs et al.1988, Heithausen and Mebold 1988) indicates that clumping, optical depth, or excitation effects are probably not responsible for the large a_{H_2} and the small XWCO values. However, saturation effects of the HI emission could possibly cause problems and are to be studied in the future. At present Herbstmeier et al. prefer to explain the large CO abundance by enhancement in slow shocks (Rohlfs et al., 1988) and the large value for a_{H_2} by a relatively large number of very small grains (<30 nm) with relatively large temperatures (Rohlfs 1988).

The Draco nebula is extreme with respect to its small X-ratio and is extreme with respect to its location in the Galaxy and possibly with respect to its most recent chemical history in a low velocity shock. Does it make sense to discuss this extreme case in the context of the more typical clouds found elsewhere? We regard this peculiarity as an apparent one only. This nebula is easily observable as an isolated object in high galactic latitudes. Its non-steady-state is probably one of vigorous molecule formation and is possibly the ideal case to exemplify what the physical conditions are close to shock fronts in actively starforming molecular clouds.e

The other extremes are nebulae which have very large X-ratios. The conditions for which an enhanced radiation field destroys CO but leaves H_2 or dust essentially unaffected are well understood (van Dishoeck and Black 1987). Examples are clouds like LBN1114 in the U Sco association (de Geus 1988, Wennmacher 1987). Here CO lines are detected only in parts of the cloud while in other parts no CO is found although an average extintion of about 1 mag is observed in this area.

It is not difficult to imagine how in a cloud with star formation activity the standard X-factor can be obtained as an average over regions with physical conditions inbetween these two extremes. Further observational effort is required to demonstrate in detail that the two extremes are coexsistent in star forming dark clouds.

5. Summary and Conclusion

The diffuse high latitude molecular clouds, also called diffuse cirrus molecular clouds, are, from the statistics of larger samples (see section 2) and from distance determination of individual clouds (see section 3), disk population objects (<z>=60 pc). So far only one cloud, the Draco nebula, is known to be well outside the z-range of disk clouds (z≥500pc). Their average size is about 1.7 pc and their masses are in the range of ≈1 to≈ 300 $M_\odot$, if the total gas column density is estimated from the standard X-ratio: XWCO≈$2.6 \cdot 10^{20}$ mol$(cm^2 Kkm/s)^{-1}$. For the molecular species detected in the diffuse cirrus molecular clouds the following column density ratios have been derived:

$N(CO)/N(H_2) \approx 1.2 \cdot 10^{-4}$ $\quad$ $N(OH)/N(H_2) \approx 2 \cdot 10^{-6}$
$N(H_2CO)/N(H_2) \approx (7-0.3) \cdot 10^{-7}$ $\quad$ $N(NH_3)/N(H_2) \approx 1 \cdot 10^{-8}$

These column density ratios are of the order of - or some times even larger than - those found for dark clouds or for giant molecular clouds. This is unexpected because the typical extinction in these clouds ($A_V \leq 1$ mag), which to some extent controls the radiation density, is significantly smaller than that in dark clouds. Comparing them to the classical diffuse clouds shows rather that their extinction is close to (or slightly larger than) that of the diffuse clouds but that their molecular abundances are about two orders of magnitude larger than in classical diffuse clouds.

The diffuse cirrus molecular clouds have two peculiarities that distinguish them from the dark clouds. These are the excess of a factor of 10-100 of their internal kinetic energy over their gravitational energy and the rather large scatter of XWCO=$N(H_2)$/WCO between $6 \cdot 10^{20}$ and $1 \cdot 10^{19}$ mol$(cm^2 Kkm/s)^{-1}$. The former result led MBM to conclude that these clouds are expanding systems while Keto and Myers suggest that they are in pressure balance with the surrounding intercloud medium.

We propose as a working hypothesis that the large scatter of the X-ratio is caused by the instability of the gravitationally unbound clouds: The lower extreme of XWCO indicates a state of growth of a molecular cloud e.g. in a low velocity shock which enhances molecular abundances. The other extreme of XWCO indicates a state of decline of a molecular cloud e.g. by the molecule dissociating radiation field of young bright stars or supernovae. The standard value of XWCO = $2.3 \cdot 10^{20}$ mol$(cm^2 Kkm/s)^{-1}$ may then be understood as an average of all possible values of XWCO between these extremes for a cloud which is in some kind of equilibrium of molecule formation and destruction.

It should be possible to reproduce the observed molecular abundances in the frame work of present day interstellar chemistry by non-steady-state models, for which the boundary conditions are adapted to the observations (e.g. $A_V \leq 1$ mag in a normal interstellar radiation field, shock enhancement of molecular abundances) and the equilibrium conditions for molecule formation and destruction are offset such that either formation or destruction dominates. Then the time dependence of the molecular abundances can be followed and compared to the properties of the sample of the diffuse cirrus molecular clouds that are known today. In this sense the galactic cirrus may hold the key tests to the validity of current chemical models of interstellar molecules.

References:

Bohlin, R.C., Savage, B.D., Drake,J.F., 1978, Astrophys. J., 224, 132

Boulanger, F., Baud, B., van Albada, G.D., 1985, Astron. Astrophys. 144, L9

Cernicharo, J.,Guelin M., 1987, Astron. Astrophys. 176, 299

de Geus, E.J.; 1988, Proefschrift, Sterrewacht Leiden

de Vries, H.W.; 1988, Ph.D. Thesis Columbia University, N.Y.

de Vries, C.P., van Dishoeck, E.F.; 1988, Astron. Astrophys. 203, L23

de Vries, H.W., Heithausen, A., Thaddeus, P.; 1987, Astrophys. J., 319, 723

Fong, R., et al., 1987, Monthly Notices Roy. Astron. Soc. 224,1059

Franco, G.A.P.; 1988, Astron. Astrophys., 202, 173

Goerigk, W., Mebold, U., Reif, K., Kalberla, P.M.W., Velden, L.; 1983, Astron. Astrophys. 120, 63

Heiles, C., Jenkins, E.B.; 1976, Astron. Astrophys. 46, 333

Heithausen, A., 1987, Ph.D. Thesis, Universität Bonn

Heithausen, A., Mebold, U., de Vries, H.W.; 1987, Astron. Astrophys. 179, 263

Heithausen, A., Mebold, U., 1988, Astron. Astrophys. in press

Hobbs, L.M., Blitz, L., Magnani, L.; 1986, Astrophys. J., 306, L109

Hobbs, L.M., Blitz, L., Penprase, B.E., Magnani, L., Welty, D.E; 1988, Astrophys. J.327, 356

Keto, E.R., Myers, P.C., 1986, Astrophys, J. 304, 466

Lada, E.A., Blitz, L.; 1988, Astrophys. J., 326, L69

Lilienthal, D., 1987 Diploma Thesis Universität Bonn

Lilienhtal, D., Black, J.H., Mebold, U., 1989 in prep.

Low, F.J., et al., 1984 Astrophys.J.(Letters) 278, L19

Lynds, B.T.; 1965, Astrophys.J. Suppl. 12, 163

Magnani, L., Blitz, L., Mundy, L.; 1985, Astrophys. J., 295, 402

Magnani, L., Blitz, L., Wouterloot, J.G.A.; 1988, Astrophys. J., 326, 909

Magnani,L., de Vries C.P., 1986, Astron. Astrophys. 168, 271

McGee, R.X., Haynes, R.F., Grognard, R.J.M., Malin, D., 1986, Monthly Notices Roy. Astron. Soc., 221, 543

Mebold, U., Heithausen, A., Reif, K.; 1987, Astron. Astrophys. 180, 213

Rohlfs, R.; 1988, Ph.D. Thesis, Universität Bonn

Rohlfs, R., Herbstmeier, U., Mebold, U., Winnberg, A.; 1988 Astron. Astrophys. in press

Minkowski, R., Silk, J., Siluk, R.S.; 1972, Astrophys..J. 175, L123

Sandage, A.; 1976, Astron.J. 81, 954

Tereby S., Fich, M., 1986, Astrophys. J., 309, L73

van Dishoeck, E.F., Black,J.H., 1987, in:"Physical Processes in Interstellar Clouds", Eds. G.E. Morfill and M. Scholer, Reidel Pub. Comp. Dordrecht, Holland

Wennmacher A., 1988 Diploma Thesis Universität Bonn

Wesselius, P.R., Fejes, I., 1973, Astron. Astrophys. 24, 15

Physical Conditions in Molecular Clouds: Sub-mm and far-IR CO Observations

J. Stutzki
Max Planck Institut für Physik und Astrophysik, Institut für Extraterrestrische Physik, D-8046 Garching b. München, F.R.G.

Sub-mm and far-IR spectroscopic observations probe a very different regime of temperature and density of molecular clouds compared to mm-wave observations. In addition, transitions of new species, e.g. rotational transitions of light hydrides (NH_3, Keene, Blake and Phillips 1983; HCl, Blake, Keene and Phillips 1986) or the fine structure lines of [CI] and [CII] become observable only at these higher frequencies.

This article concentrates on the excitation of the sub-mm and far-IR CO lines. The newly discovered heavy rotor transitions in the submm, tracing extremely high densities, are discussed briefly in the article by Harris et al. in this volume. Recent observations of the fine structure lines of [CI] and [CII] and their astrophysical interpretation are discussed in Stutzki et al. 1988b.

I. Submm and Far-IR Observations of Carbon Monoxide

Table 1 summarizes the present body of data on short-submm and far-IR CO observations. It shows that almost all sources are strong emitters in the mid- and higher-J CO transitions, with observed brightness temperatures often similar or even higher than in the low-J mm-wave transitions. The typical cold clouds (section I. in Table 1) are of course difficult to detect in mid-J CO transitions simply because the temperature is too low. The most striking result from Table 1 is the presence of bright submm CO emission with line widths comparable or even narrower than observed in the low-J mm-wave lines, but brightness temperatures which are often higher (section II. and III. in Table 1). In addition, many of the luminous outflow sources are very bright in the submm-and far-IR CO lines (section III. in Table 1.), implying that a large amount of very warm, dense material is in the outflow (Jaffe, Genzel, and Harris, 1987; Jaffe et al. 1988, Stacey et al. 1989).

In the following, I will discuss why these observations imply the presence of a very warm, dense component of molecular gas, whose existence is usually overlooked by mm-wave observations of CO.

II. Excitation of Submm and Far-IR Transitions of CO

All excitation calculations discussed in the following where made in escape probability approximation for a homogeneous, spherical cloud (see Stutzki and Winnewisser 1985). Though certainly a simple approximation, it serves well for a rough discussion of the important, basic characteristics of the excitation. Three parameters characterize a cloud in this model: the kinetic temperature T_{kin}, the H_2 volume density $n(H_2)$, and the quotient of column density and linewidth $N(CO)/\Delta v$. The CO column density below is given for the case of Δv = 10 km/s, but the results can easily be scaled to different linewidths by scaling the column density appropriately.

Fig. 1 shows the calculated main beam brightness temperature and the optical depth of the ^{12}CO transitions up to J=10→9 for physical conditions typical for the bulk of the molecular material in a dense, massive cloud core. At these high densities and column densities the CO transitions are thermalized (up to J≈9, where the critical density of the transitions becomes greater than the assumed density of $10^{4.5}$ cm^{-3}) and optically thick. The linear decrease in main beam brightness temperature with J is due to the Rayleigh-Jeans approximation, which results to first order in the subtraction of $h\nu/2k$ from the excitation temperature of the transitions (which in turn equals the kinetic temperature). At higher temperatures, however, the population is distributed over enough rotational states, that the emission in the lowest-J transitions starts to get optically thin, even for the high column density of 10^{19} cm^{-2} (compare Fig. 6).

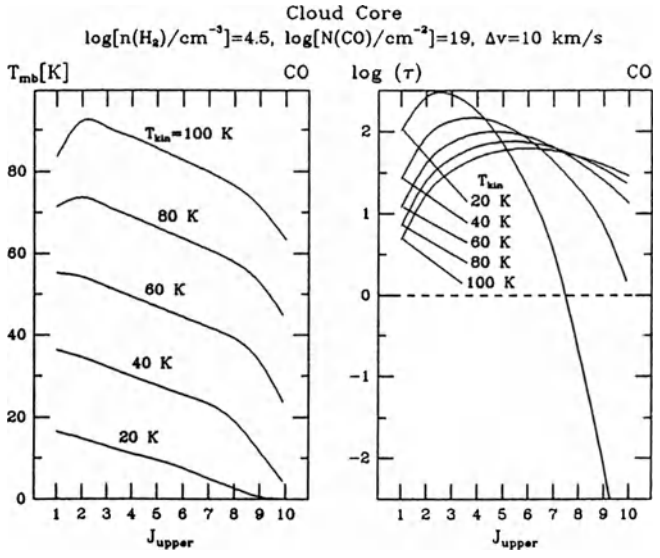

Fig. 1: ^{12}CO main beam brightness temperature T_{mb} and optical depth as calculated in escape probability approximation for a homogeneous spherical cloud. The parameters chosen are typical for the bulk of the material in giant molecular cloud cores. Note that even in the thermalized limit (T_{ex} =T_{kin}) the brightness temperature decreases with increasing J because of the Rayleigh-Jeans approximation.

The weak CO J=7→6 emission observed from some of the typical cold cloud cores (Table 1) may be explained in this way as thermalized, optically thick emission from cool gas ($T_{kin} \approx 20$ K) with a density high enough to still populate the J=7 state.

In many cases the narrow line width mid-J CO emission observed can not come from the bulk of the molecular cloud: the observed brightness temperatures of e.g. the CO J=7→6 line often imply a minimum kinetic temperature of the emission region of 80-100 K, substantially warmer than the material observed in the lines up to J=4→3. A possible explanation may seem to be that some of the material in the cloud core is warmed up slightly by embedded IR sources or some other mechanism.

However, any explanation that puts the warm material in the cloud core has the serious problem of how to avoid self-absorption in cooler outside layers of the cloud (which is not observed). Fig. 2 illustrates that even for the case of a rather low volume and column density cloud envelope, containing only a few percent of the total column density from Figure 1, the optical depth in the mid-J transitions is still substantial, and will not allow the radiation from the warm core to escape the cloud. Even small amounts of medium temperature and density material will completely obscure the CO emission from the warm core. The lack of self-absorption in the observed CO J=7→6 spectra of W49 and W51 thus indicates the presence of a pressure (n×T) discontinuity in these sources (Jaffe, Genzel and Harris, 1987). On the other hand, the deep self-absorption dip in the outflow spectrum towards DR21 (Fig. 3, Jaffe et al. 1989, White et al. 1986) demonstrates the

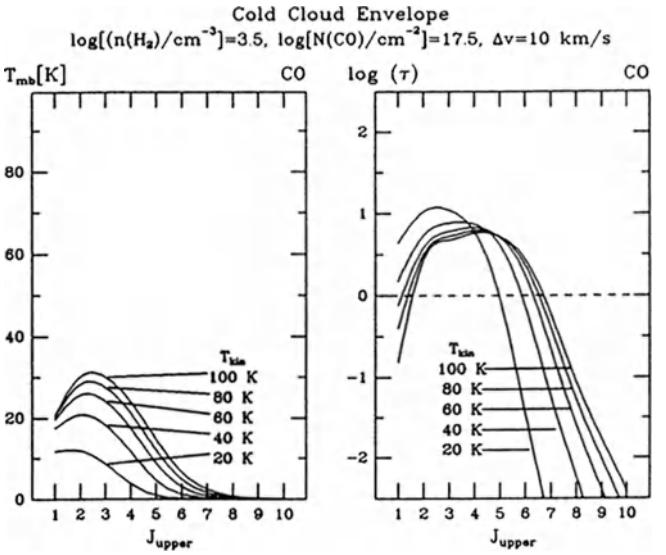

Fig. 2: Same as Fig. 1, but for a low density cloud envelope containing only 3 percent of the total column density of $N(CO)=10^{19}$ cm^{-2}. Note that the mid-J CO lines are still optically thick and will absorb out any warm emission from the cloud core.

importance of self-absorption effects in some sources, and actually yields very detailed information on the physical parameters of the absorbing layer.

The widespread presence of strong submm CO emission without self-absorbed profiles indicates that the warm molecular gas is often located in the outside layer of the clouds or on the surfaces of clumps. The narrow line width in many sources, the correlation with UV intensity and the overlap with [CI] and [CII] emission regions make photodissociation regions on clump surfaces in a clumpy molecular cloud core a likely candidate for the origin of the observed warm, quiescent CO emission (Harris et al. 1987, Stutzki et al. 1988a, Genzel et al. 1988). Fig. 4 shows as an example of this class of sources a typical CO J=7→6 spectrum from NGC 2024. In this source the narrow linewidth, which at some positions is only marginally wider than the thermal linewidth at the minimum kinetic temperature of about 80 K (derived from the observed brightness temperature in the case of thermalized emission filling the beam), definitely rules out any shock related heating mechanism.

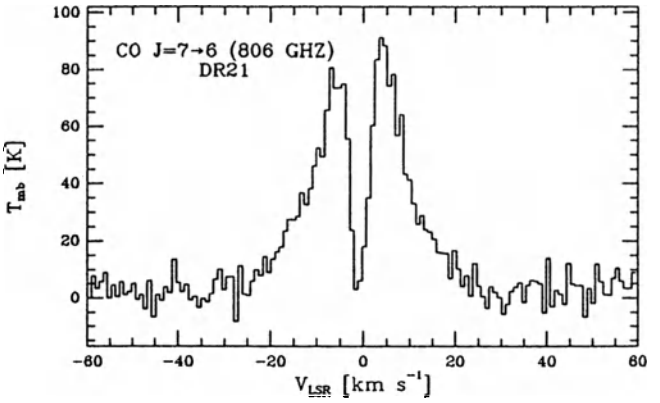

Fig. 3: CO J=7→6 emission from DR21 (Jaffe et al. 1989). Note the very wide emission out to velocities of ±30 km/s and the very deep, narrow self-absorption spike in the line center.

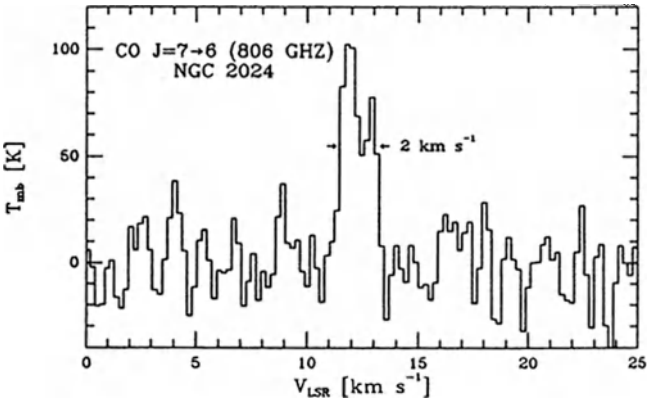

Fig. 4: CO J=7→6 emission from NGC 2024. Note the peak T_{mb} of 80 K implying a minimum kinetic temperature of 100 K in the emission region (in the case of thermalized emission filling the beam) and the narrow width (FWHM) of 2 km/s.

In all sources where far-IR CO lines are also detected, the comparison between the submm and far-IR line intensities indicates temperatures of a few hundred K, densities around $10^{4.5}$ cm^{-3}, and CO column densities around 10^{18} cm^{-2} (e.g. Harris et al. 1987). Fig. 5 illustrates the sensitive dependence of the relative line intensity between far-IR and submm CO lines on temperature and density. The relative intensity of only two lines determines roughly the product $n(H_2)\times T_{kin}$, i.e. the pressure in the emission region. Additional information from other lines then constrains the physical parameters in more detail.

At the high temperatures typically observed in the submm and far-IR CO emission regions the population is spread over that many states (and the population difference between subsequent states in the rotational ladder is that small) that even the mid-J submm transitions have an optical depth near unity, despite the rather high typical CO column density of about 10^{18} cm^{-2}. As shown in Fig. 6 the brightness temperatures observable are thus substantially lower than the kinetic temperature of the emission region. In addition, beam filling factors of typically 0.2 to 0.3 in a clumpy cloud have to be invoked to explain the observed, still lower, main beam brightness temperatures.

Due to the low optical depth in the low-J transitions the emission of this warm, dense component is very insignificant in the mm-wave CO transitions. This is true even in cases of extreme column density and density (Fig. 6b) and explains why CO observations up to J=3→2 fail to detect this warm, dense component.

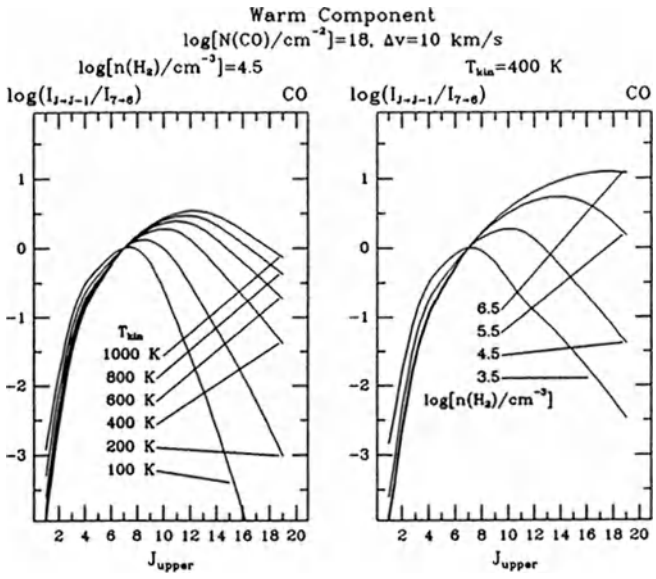

Fig. 5: The relative integrated intensity for submm and far-IR CO lines is a good indicator of $n(H_2)\times T_{kin}$ (or pressure) in the emission region, as shown here by variation of the relative line intensities with temperature and density. The mid-temperature cases on the left are representative for the warm, dense component in giant molecular cloud cores like M17 (Harris et al. 1987), the highest density cases on the right match the observations of the warm, quiescent gas in Orion (compare Stutzki et al. 1988b).

III. Heating Sources for the Warm, Dense Gas

Shocks are certainly important for heating the warm molecular material observed in luminous outflow sources. The narrow linewidth of the submm CO emission now found in many molecular cloud cores, however, requires either a very high efficiency of rather low velocity shocks for heating the material, or even excludes shocks as a possible heating source (Harris et al. 1987). UV radiation can directly heat molecular material in photodissociation regions (PDR's) to the observed high temperatures. The origin of the quiescent submm and far-IR CO emission in PDR's is also favoured by recent [CII] and [CI] observations, as discussed by Stutzki et al. 1988b. However, one should note that all theoretical PDR model up to now fail to explain the large amount of warm molecular material observed by about an order of magnitude.

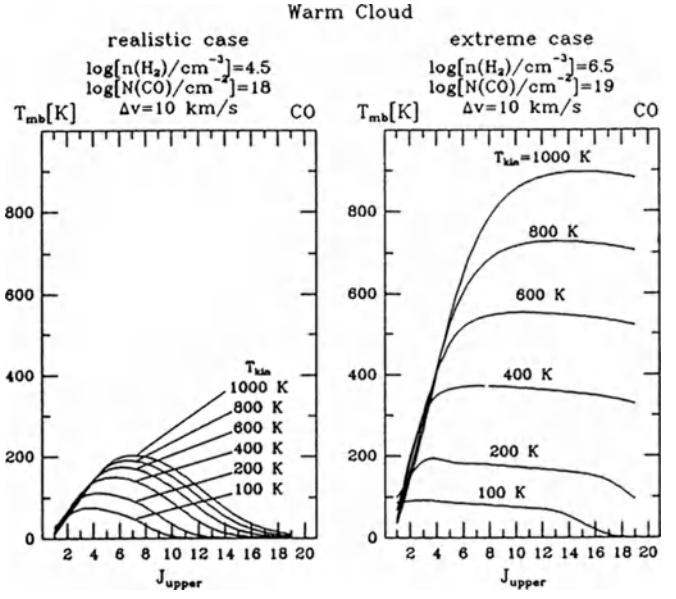

Fig. 6: T_{mb} versus J, left: for the physical parameters found to be typical for the submm and far-IR CO emission regions in giant molecular cloud cores, and right: for the unrealistic, extreme case of very high density and column density, showing that even there the low optical depth in the low-J lines makes the identification of this component very difficult from mm-wave CO observations.

References

Blake, G.A., Keene, J., and Phillips, T.G., 1986, Ap.J. 295, 501
Boreiko, R.T., Betz, A.L., and Zmuidzinas, J., 1989, Ap.J. submitted
Genzel, R., et al., 1988, Ap.J. 332, 1049
Harris, A.I., et al., 1987, Ap.J. (Letters) 322, L49
Jaffe, D.T., Harris, A.I., and Genzel, R., 1987, Ap.J. 316, 231
Jaffe, D.T., et al., 1988, Ap.J. submitted
Koepf, G.A., et al. 1982, Ap.J. 260, 584
Krügel, E., et al., 1988, Astr.Ap. submitted

Keene, J., Blake, G.A., and Phillips, T.G., 1983, Ap.J (Letters) 271, L27
Schmid-Burgk, J., et al., 1988, Astr.Ap. submitted
Stacey, G.J., et al., 1989, in prep.
Stutzki, J., and Winnewisser, G., 1985, Astr.Ap. 144, 13
Stutzki, J., et al., 1988a, Ap.J. 332, 379
Stutzki, J., et al., 1988b, in "Submillimetre and Millimetre Wave Astronomy", ed. A.S. Webster (Kluwer), in press
White, G.J., et al. 1986, Astr.Ap. 159, 309

Table 1: Summary of Short-Submm and Far-IR CO Observations

Source	6-5	J=7-6 Tmb[K]	J=7-6 Δv[km s-1]	14-13	16-15	17-16	>20
I. Cold Clouds							
HH9		7	9				
L1551		3	2.6				
B35		<5					
ρ Oph		<6					
		<6†					
IC 1396		<10					
V645		<5					
L134		<3†					
II. Quiescent Warm Gas							
W3	100§		7				
		26†	10†				
Ori e^1C		80	7.1	x	x	¶	
		65	6.8				
Ori Bar		67	4.8	x			
OMC1, S3		20	1.8				
OMC2	§	18	3.5				
NGC 2023	§	55	1.3				
NGC 2024	§	80	1.4				
NGC 2068		30†	1.4†				
Mon R2		40	2.3				
S255		16†	5.5†				
G12.41+0.50		20	7				
W43		15	11				
M17 SW		90	7	x	x		
M17 KW		45†	9†				
G34.3+0.1		50	9				
S140		14†	6†				
S106		50	9				
		16†	6†				
W75S		45	7				
III. Outflow Sources (plus Quiescent Warm Gas)							
Ori BN/KL	§	175	50	x	x		x
NGC 2071		7	25	x			
		7‡	20‡				
		(25	13)				
W33		(10	9)‡				
GL490		50	15				
		<6					
		<2‡					
W49	§	45	25	x			
W51		30	25		x		
		(45	8)				
G12591		4	15				
DR21	§	65	25	x	x		
		(25	8)				
		self absorbed					
W75 N		30	13				
Ceph A		12	30				
		6‡	30‡				
		(30	8)				
		(12	9)‡				
G333.6-0.7				x	x		x
NGC 7538		<2‡			x		
IV. Galactic Center							
20km/s cloud		15	30				
2 pc ring		8	100		x		
Sgr B2	§	20	45				
V. SN Remnants							
IC 443 core		25	20				
IC 443 shock		6	70				
VI. Late Type Stars							
IRC+10216	§	13	21				
		9†	20†				
CIT 6		<4					
R Leo		<4					

¶ Boreiko, Betz, and Zmuidzinas, 1989, Ap.J., submitted
§ Koepf et al., 1982 (IRTF, 35")
† Krügel et al., 1988 (KAO, 100")
‡ Krügel et al., 1988 (UH88", 45")
§ UCB/MPE receiver at JCMT, 7"
- other submm observations: UCB/MPE receiver at IRTF (30") and UKIRT (25")
- other far-IR observations: UCB Tandem Fabry-Perot, KAO (55")

The Physical Structure of Star Forming Regions

Glenn J. White

Department of Physics, Queen Mary College, University of London,
Mile End Road, London E1 4NS, England

Introduction

Molecular clouds are now known to be highly inhomogeneous structures, with density condensations on various length scales ranging from giant molecular cloud sizes (~100 pc) to protostellar envelopes (~0.001 pc). Our current understanding of these regions is of a process of hierarchical fragmentation, which may be linked to the mass function for stellar populations born from a particular molecular cloud. The determination of the mass function of individual gas clumps in a cloud is an important probe of the future star-forming history of a cloud, and has bearing on fragmentation and the whole star-formation process. Until recently, studies of these aspects have been limited as a consequence of the inadequate angular resolution of millimetre wave telescopes, and hence searches for evidence of clumping have been made using statistical methods which compare spatial and velocity information at a large number of positions within a cloud (Kleiner & Dickman 1984), or through the presence of multiple components present in spectra from individual positions (Martin et al 1985). More recently, it has become possible, using high angular resolution, well sampled maps with high dynamic range, to make direct images of star formation regions, allowing us to have a less biased view of the physical processes which operate.

Towards a number of high-mass star formation regions, there is a close association between the neutral gas in the star forming molecular cloud, and ionised gas resulting from the photo-dissociation caused by the UV emitted from massive early type stars. At the interface between such an HII region and a molecular cloud, is a neutral gas layer which is subject to both an intense radiation field, and to shocks arising from the expansion of the ionisation front of the HII region. The gas in these regions is highly excited, hot, and may be fairly dense, and as such we expect that the submm-λ transitions will be moderately strong. In order to study these interface regions, we have made studies of several edge-on ionisation fronts lying adjacent to dense molecular clouds.

Recent theoretical modelling which calculates the energy balance and chemical equilibrium of dense molecular clouds illuminated by high uv-fields (Tielens & Hollenbach 1985a,b) and shocks (Draine & Roberge 1984), has contributed considerably to our understanding of the physical environment in the interface regions between ionised and neutral gas lying at the edge of star formation regions. Similarly new observational studies have provided additional impetus to such modelling with the rather surprising detection of significant amounts of hot (T ~ 200-400 K) gas at the edges of clouds, and the anomalous excitation of several molecular species in these interface regions. In addition to the chemical models previously mentioned, the interaction of the ionisation shocks with the molecular cloud material can result in a strong enhancement of the molecular abundances of some specific species, and lead to dynamical effects which will affect the velocity field of the material close to the interface regions, which should be detectable with submm-λ spectroscopic techniques. These models have been moderately successful in their

general predictions, but not all of the predictions are supported by recent observational material (Rainey et al 1987).

Using new high angular resolution JCMT 15m observations, covering large areas with both good sampling and high dynamic range, it is possible to directly image star formation regions in a relatively unbiased way, to study the large scale effects of star formation on a molecular cloud.

Observations

The data shown in this paper were obtained with the James Clerk Maxwell Telescope at Mauna Kea, Hawaii. For the CO J=2-1 observations of S88, which were carried out as part of the scientific commissioning of the telescope, the rms accuracy of the surface was estimated to be ~ 75 μm. The beamsize was measured to be 22 arc seconds, and the value of η_{fss} estimated as 0.75. The later observations of M17 were carried out after improvements to the surface, for which the surface error had been reduced to ~ 38 μm rms. The tracking and pointing of the telescope, based on observations of planets, was believed to be better than 5 arc seconds. The observations were obtained using a 230 and 345 GHz cryogenic Schottky system (the so-called 'System A_{lower}' and 'System B' respectively), with either an autocorrelator or AOS backend. A more complete description of this, and other JCMT instrumentation has recently been given by White (1988).

CO J=3-2 Observations of M17

The observations of integrated J=3-2 ^{12}CO emission close to the interface with the HII region are shown in Figure 1.

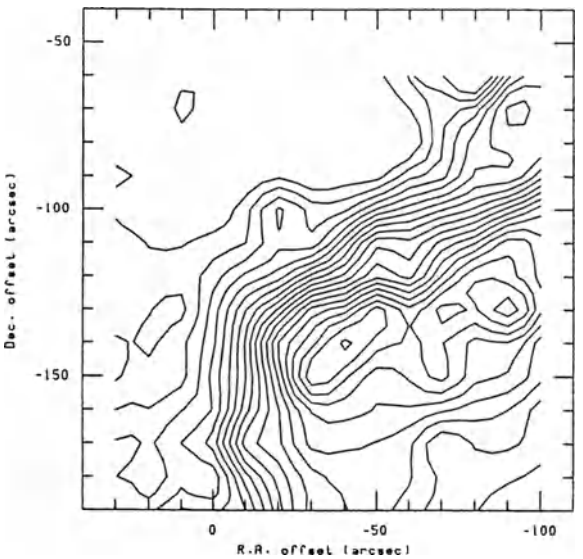

Fig. 1. Integrated CO $J = 3 - 2$ map of M17. The contour levels are spaced every 25 K km s^{-1}. The lowest level is 6 K km s^{-1}. The center position is $18^h17^m32^s.5$, $-16°10'15''$ (1950).

The ridge of CO emission seen in a more extensive J=1-0 map (White et al in preparation) extends approximately 6 arc minutes along a SE-NW direction. The CO J=3-2 map of integrated emission contains evidence for several clumps which lie close to a CO peak seen in the lower resolution data of Rainey et al (1987). The eastern edge of the complex is sharply bounded, with the CO emission falling from T_R^*= 30 - 40 K to less than 10 K over distances of 20-30 arc seconds (0.2 - 0.3 parsecs). To the east of this sharp boundary of the cloud lies the ionisation bar which is seen most clearly from radio wavelength studies (Felli et al 1984). The proximity of an ionisation bar to the neutral cloud material, and the rapid decline in CO emission going across the front, suggests that the neutral gas may be dissociated or depleted close to the interface region, and raises the possibility of external heating by the OB cluster which ionizes most of the M17 region.

^{13}CO J = 3-2 Observations of M17

The ^{13}CO observations show a rather different spatial distribution to that of the CO maps, in particular the emission is more concentrated into a smaller number of resolved clumps, and the eastern edge of the cloud is considerably more sharply bounded, lying about 40 arcseconds (~ 0.5 pc) further into the main molecular cloud than is indicated by the CO observations. The map of integrated ^{13}CO emission is shown in Figure 2.

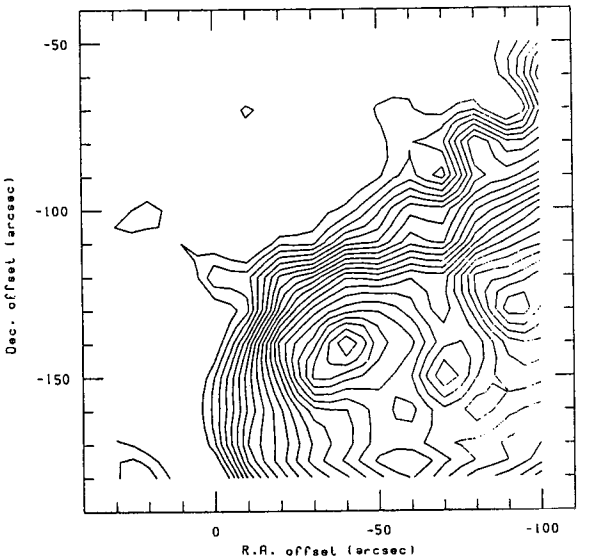

Fig. 2. Integrated ^{13}CO $J = 3 - 2$ map of M17. The contour levels are spaced every 12.5 K km s^{-1}. The lowest level is 37.5 K km s^{-1}.

CS J=7-6 observations of M17

Mapping in the CS J=7-6 line, which is a tracer of dense gas (White et al 1983, Snell et al 1984), shows only a ***single*** intensity maximum, which lies ***between*** the two CO hot-spots seen in the CO J=1-0 data (White et al, in preparation). The high critical density and compact nature of the emission suggest that we are seeing the dense core of the cloud. The CS J=7-6 map is shown in Figure 3

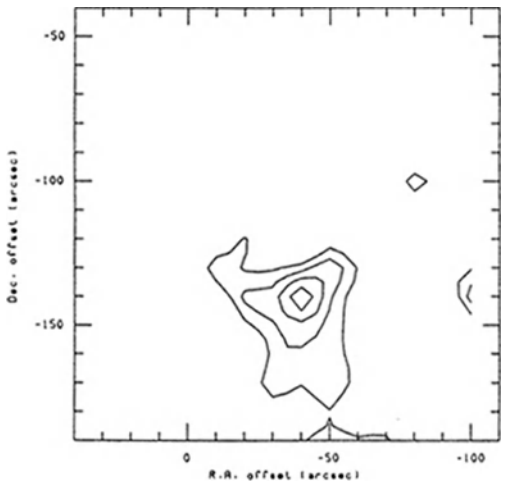

Fig. 3. Integrated CS $J = 7 - 6$ map of M17. The contour levels are spaced every $30\,\mathrm{K\,km\,s^{-1}}$. The lowest level is $10\,\mathrm{K\,km\,s^{-1}}$.

The fragmentary nature of the M17 Molecular Cloud

The fragmentary (or clumpy) structure of molecular clouds has long been recognised from theoretical studies of the collapse of a gas cloud, and has been inferred from observations of many groups of molecular line astronomers in the interpretation of data (particularly that of high excitation lines) (see for example Wilson 1985 and references therein, Snell et al 1983, Martin, Sanders & Hills 1982, Richardson et al 1986 a,b). The effects of such fragmentation provide an efficient path for the transfer of angular momentum from the overall rotation of the cloud into orbital motions of the remaining fragments, throughout the isothermal collapse phase of the star-formation process. The size scales of the fragmentation have been too small to observe directly in most molecular line studies conducted to date, apart from those in which interferometric measurements have been made of a few lines such as NH_3 and H_2CO, with the VLA towards sources such as Orion. The present observations coupled with the more extensive observations of White et al (*in preparation*) have been successful at resolving the M17 cloud into up to 22 separate fragments, with typical size scales of 0.25 pc. For molecular cloud material with a

mean temperature of 50 K and $n(H_2)$ of 10^5 cm^{-3}, the Jeans length for collapse, l_j, is given by

$$l_j = \left\{ \frac{T}{10\,K} \right\}^{0.5} \left\{ \frac{n(H_2)}{10^4\,cm^{-3}} \right\}^{-0.5} pc$$

which for gas of density 10^5 cm^{-3}, and temperature 50 K, corresponds to $l_j \sim 0.2$ pc, similar to that which is actually observed for the characteristic size scale the fragments in the M17 complex.

The temperature structure of the M17 Molecular Cloud

The CO data can be used to map the temperature structure of the cloud. The excitation temperature is determined from the relationship (in this case for the J=1-0 transition);

$$T_{ex} = \frac{h\nu}{k} \frac{1}{\ln\left\{ 1 + \frac{h\nu}{k} \left\{ \frac{T_R^*}{\eta\,(1-\exp(-\tau))} + 0.82 \right\} \right\}}$$

The temperature structure of the M17 cloud shows considerable inhomogeneity. The bulk of the gas in the main molecular ridge has an excitation temperature > 30K, and in places approaches 70K. The temperature maxima are associated with the fragments lying close to the maser group, where $T_{ex} \sim 70$K at (50, -120) in the velocity range 19-20 km s^{-1}, and towards the southern CO source originally detected by Thronson & Lada 1986, close to (-30, -260).

We have made a series of cross-cuts across the edge of the cloud, moving perpendicular to the ionisation bar, which trace the variation of T_{ex}, τ (^{13}CO) and $N(H_2)$, as determined from the CO J=3-2 data. In the centre of the M17 cloud, the excitation temperature is typically 60 -70K. Some of the individual cross-cuts resolve the edge of the cloud where the antenna temperature changes by a factor of two over a distance of ~ 40 arcseconds (~ 0.4 pc). However the scans which cross the cloud edge close to the position of the maser sources (where the H_2 emission is strongest), do not resolve the edge of the cloud, the most rapid variability occurring close to (-40, -110). The peak of the distribution of the 2μm molecular hydrogen line lies **exactly positioned at the edge of the CO ridge**, where the excitation temperature of the gas is changing most rapidly. This strongly suggests that the shock plays a direct role in the compression, excitation and heating of the gas along the front face of the molecular cloud. The edge of the cloud, seen as the point at which the CO antenna temperature drops to half of the on-cloud temperature lies at an average of 25 arcseconds into the molecular cloud from the ionisation ridge.

Relationship to other objects in the cloud

Comparing the present observations with the B_γ and H_2 emission observed in the near infrared (Gatley et al 1986), we find that the B_γ (tracing the distribution of ionized hydrogen) lies well to the east of the edge of the M17 molecular cloud, whereas the H_2 peaks lie ***exactly*** on the sharp rim of the neutral molecular cloud seen in CO. This strongly suggests that the B_γ traces the distribution of ionised gas that has already passed through the shock, the position of which is now shown in the H_2 data. This indicates

that the shock is strongly interacting with, and modifying the structure of the face of the cloud. Most of the fragmentary structure in the cloud as seen in the lower CO J=1-0 studies lies close to the position of the two main H_2 peaks. The region of ***dense*** ($n(H_2) \sim 2 \times 10^6$ cm^{-3}) gas lies directly adjacent to the H_2 peak along a line to the centre of the neutral cloud core. It is at exactly this position close to the H_2 peak that the CO J= 3-2 transition is strongest (as opposed to the J= 1-0 transition, which does not have such high excitation requirements, which peaks further in to the neutral cloud core).

CO Observations of S88

The HII region S88 is a low emission-measure nebula, located at a distance of ~ 2.8 kpc. About 20 arc minutes to the SE of the main nebulosity, are situated two bright optical knots. These have been studied at radio wavelengths by Felli & Harten (1981), who show that there is emission from a multi-component compact HII region. The radio emission comes from two regions, S88-A, and S88-B. The more easterly component, S88-B, has a high electron density and emission measure, and lies behind up to 40 magnitudes of visual extinction. About 40 arc seconds (equivalent to 0.21 pc) southwest of the radio knots, a small region of extended H_α emission is seen, having a diameter of ~ 50 arc seconds. The neutral cloud associated with S88 has been studied in a variety of molecular lines, including OH (Turner 1970), CO (Evans et al 1981, Phillips et al 1988), H_2O (White 1978, Blair et al 1978), and the ionised gas from recombination line studies of H_α and $C_{176\alpha}$ (Silvergate & Terzian 1978). From observations of the velocity structure found in these molecular line and optical observations, there is evidence for outflow of the ionised gas relative to the molecular cloud.

A total of 162 CO J=2-1 spectra were obtained during the present observations. The map of peak T_R^* for the CO J=2-1 data shown in Figure 4.

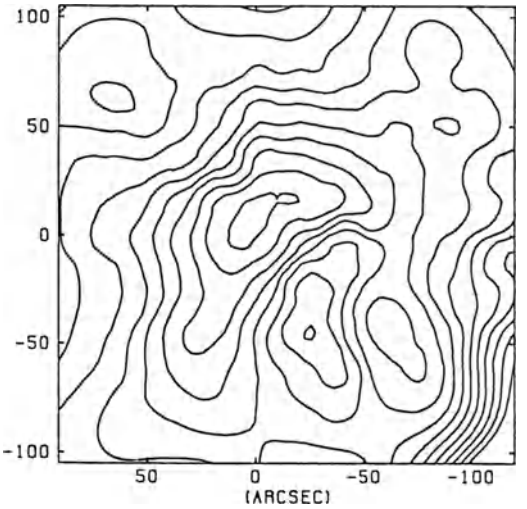

Fig. 4. Peak T_R^*(CO $J = 2 - 1$) map of S88. The highest contour, close to the (0,0) position, is 63 K, and the individual levels are spaced every 5 K. The center position is $19^h44^m42^s.5$, $+25°05'30''$ (1950).

The CO J=2-1 emission shows a horseshoe-like distribution, with the CO temperature peak lying at (+10,+10), close to the position of S88B. Towards this peak, the CO line temperature, T_R^* ~ 62 K, which is ~ 30 percent hotter than the dust temperature estimated by Evans et al (1981) from far-infrared data measured with a 37 arc second beam. The two 'legs' of the horseshoe extend up to 2 arcminutes southwards, a secondary peak in the western 'leg' having T_R^* ~ 47 K. This latter peak is coincident with IRS-5, another apparently embedded and intense near-infrared point source (Evans et al 1981). The CO J=2-1 emission wraps around the area showing optical H_α emission, which is coincident with a marked depression in the CO contours. The rapid fall off in emission at the boundary between the 'legs' and the ionised gas is barely resolved with the present angular resolution. There is good general agreement between the positions of the 50 and 100 μm continuum peaks shown by Evans et al (1981) and the present observations, although the peak of the dust temperature distribution lies about 30 arc seconds S of the position where we see the highest CO gas temperatures, and where the J=1-0 ^{13}CO line peaks (White & Fridlund 1988, unpublished Onsala data).

The map of integrated CO J = 2-1 emission shows a similar horseshoe-like structure to that seen previously, although the integrated emission is more concentrated close to the S88B region, the western 'leg' of the horseshoe is substantially less prominent. The structure of the region is dominated by the horseshoe-like distribution of material. From the individual velocity maps, it appears that the material along the bar is fragmented into a number of clumps. The dynamical structure is complicated. The main blue-shifted clump of gas lies to the northeast, in the highly obscured part of the cloud close to the radio knots. Associated with the optical H_α emitting region to the southwest of S88B, one small clump, G, of blue-shifted emission is also seen, although this comes from an optically opaque region lying at the edge of the H_α region. At all other places in the horseshoe and to the southwest, the gas is predominantly redshifted relative to the ionised flow.

A possible geometry for S88 would be to consider that the source is highly fragmented, with some of the clumps moving away from the cloud core, as sketched in Figure 5.

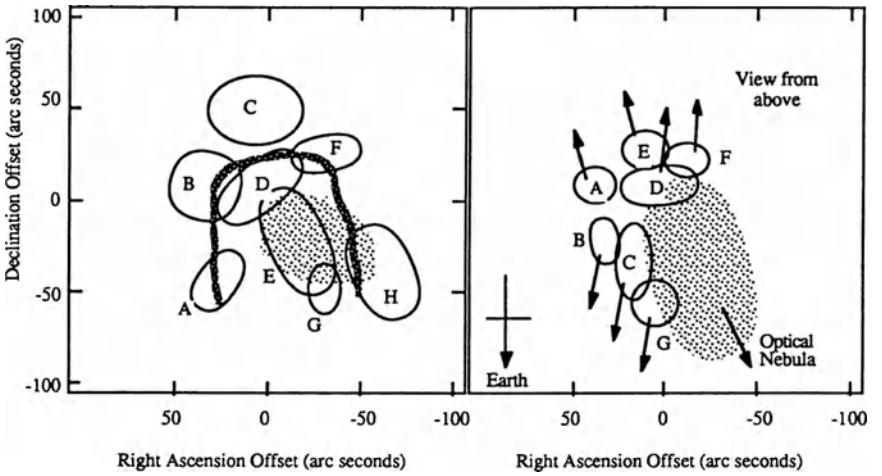

Fig. 5. Schematic diagram of clumps in the S88 region.

In this scenario, the fragment D, lies close to the core of the molecular cloud (at the position of the ^{13}CO peak), fragments B and C are fragments coming towards the Earth, and fragments A, E and F, moving away. The existence of clumpy structure such as this can also be seen in the observations of other disrupted sources such as L1551 (Rainey et al 1987) and NGC 2024 (White et al *in press*). This would suggest that clump G be associated not with the main flow containing the other clumps, but that it be separately excited at the edge of the H_α flow. In this scenario, the H_α region is a cavity on the front face of the cloud, in which inhomogeneities in the local density gradients have resulted in a low density region, which allows the optical flow to break out of the edge of the cloud. An interesting test of this model would be to map the distribution of the 2 μm H_2 and Br_α lines, which would be expected to trace the relative distributions of neutral and ionised gas.

An alternative, although perhaps less plausible model, is that the horseshoe morphology is due to material excited along the periphery of an outflow cavity, inside of which the H_α region fits. Although there are embedded sources which may be able to heat clumps D and H, the other clumps do not appear to have embedded heat sources. Additional energy, such as that available from photoelectric heating or shocks could be required to explain the temperature distribution which is seen. Studies of other regions (Harris et al 1988) have indicated the presence of significant amounts of warm quiescent material lying close to neutral-ionised gas interfaces, which appear to have gas temperatures significantly in excess of the temperature of the majority of the local dust. A discussion of the various heating processes is given by Hollenbach (1988). The rather limited available body of data on S88 is insufficient to critically and quantitatively allow discrimination between the alternative models at the present time.

The CO J=2-1 and ^{13}CO spectra can be used to form a first order estimate of the local gas density and mass of material in the ridge. We have used a Large Velocity Gradient (LVG) model to calculate the ratio of antenna temperatures for the CO J=2-1 and ^{13}CO J=1-0 lines (White & Fridlund 1988), assuming that the kinetic temperature of the gas is 60 K, as suggested by the CO observations. Further, a value for $\log(X/(dv/dr)) = -4.3$ (Phillips et al 1988) is adopted for S88. We find that the total mass of material in the main part of the horseshoe (see the map of integrated CO emission) is ~ 400 $M_\odot$, and that assuming its depth back into the cloud is similar to the width, the particle density, $n_{H_2} \sim 3.5 \times 10^4$ cm^{-3}. This value is consistent with that derived from our previous CO J=2-1 and 3-2 observations, the upper limits set by Evans et al (1981), and similar to that estimated for the electron density ($> 2 \times 10^4$ cm^{-3}) by Felli & Harten (1981). This then confirms that this molecular cloud core in which a high mass star has formed, has no evidence for the presence of a high density (n_{H_2} > a few x 10^5 cm^{-3}) region, similar to that seen towards many other high mass star forming molecular cloud cores. If this density is uniform throughout the core region, then the masses of the individual fragments shown in Figure 5 range from a few up to a few hundred solar masses. Rotational motion of the cloud surrounding the core, is sufficiently small (the velocity gradient is ~ 1.4 km s^{-1} pc^{-1}), that the material is almost certainly gravitationally bound to the core.

Acknowledgements

The observations of S88 reported in this paper form a preliminary report of data which were collected during the Scientific Commissioning phase of the James Clerk Maxwell Telescope. The data will be fully described in a more extensive paper at a later time. The commissioning data are co-owned by, and form a tribute to the many people who have collaborated over the last decade to construct this very fine

telescope. Although it is impossible to acknowledge the role of everybody here, I would like to mention the dedicated work and efforts of people at ROE, RAL, and the Universities of Cambridge, Kent, London (QMC), Manchester (Jodrell Bank), Utrecht and Groningen, as well as the Dwingeloo Laboratories of the Netherlands Foundation for Radio Astronomy. In particular, the roles of Dr. Richard Hills, the Project Scientist, and Dr. Ron Newport, the Project Manager, were crucial to the success of the project. The James Clerk Maxwell Telescope is operated by The Royal Observatory, Edinburgh on behalf of the partner countries Holland, Canada and the United Kingdom. Mm and Submm Astronomy at QMC and elsewhere in the UK is supported by The Science & Engineering Research Council.

References

Blair, G.N., Davis, J.H., & Dickinson, D.F., 1978, *Astrophys. J.*, **226**, 435.

Draine, B.T. & Roberge, W.G., 1984,*Astrophys J*, **282**, 491.

Evans, N.J.E., Blair, G.N., Harvey, P., Israel, F., Peters, W.L., Scholtes, M., de Graauw, Th. & Vanden Bout, P., 1981, *Astrophys. J.*, **250**, 200.

Keene, J., Blake, G., Phillips, T.G., Huggins, P.J. & Beichman, C., 1985, *Astrophys J.* **299**, 967.

Kleiner, S. & Dickman, R. 1984, *Astrophys.J.*, **286**, 255.

Martin, H.M. et al, 1985, *Mon. Not. Roy. Astr. Soc.*, **208**, 35.

Phillips, J. P., White, G.J., Rainey, R., Avery, L.W., Richardson, K.J., Griffin, M., Cronin, N.J., Monteiro, T. & Hilton, J. 1988, *Astr. Astrophys.*, **190**, 289.

Rainey, R., White, G.J., Richardson, K.J., Griffin, M.J., Cronin, N.J., Monteiro, T and Hilton, J. 1987, *Astr.Astrophys.*, **179**, 237.

Silvergate, P.R. & Terzian, Y. 1978, *Astrophys. J.*, **224**, 437.

Tielens A. & Hollenbach, D. 1985a, *Astrophys J.* **291**, 722.

Tielens A. & Hollenbach, D 1985b, *Astrophys.J.* **291**, 747.

Turner, B.E. 1970, *Astrophys. Lett.*, **6**, 99.

White, G.J., 1978, *Ph.D. Thesis*, University of Kent, Canterbury.

White, G.J. Rainey, R., Hayashi, S. & Kaifu, N., 1987, *Astr.Astrophys*, **173**, 337.

White, G.J., 1988, p 27, *Mm & Submm Astronomy*, eds R.Wolstencroft & W.Burton, Kluwer Publishers.

Circumstellar Envelopes

H. Habing
Sterrewacht Leiden

1. Introduction

Stars become old when hydrogen burning, their source of energy while on the main sequence, becomes less efficient. This constitutes an energy crisis, and the star switches to helium burning. All stars swell in this process and radiate now through a much larger suface area; consequently they become red. In most stars, namely those of not very large mass, helium burning increases the energy output by large factors: the stars become giants, red giants. The outer layers of the star are less strongly bound: the stellar mass has remained the same, but the stellar radius has often increased by a factor of a hundred and the gravitational attraction at the surface thus decreased by a factor of ten thousand! Although we do no know the precise reasons, it is no surprise that some red giants lose matter, or rather, easily eject matter back into interstellar space. A few stars are so good at throwing away outer layers that they are completely hidden in a circumstellar envelope of very large size (up to say a third of a parsec) and are detectable only through their infrared emission.

I think it to be historically correct to say that our insight into what happens after the red giant phase has come from an interplay of observations and theory; infrared and radio observations on the one hand and elaborate computer modelling of stellar interiors on the other. Here I will discuss only observations of circumstellar envelopes, a subject that started in the sixties with the discovery that red giants, and especially the small fraction of long period variables, emit more (sometimes much more) infrared emission than an extrapolation of the visual spectrum predicted. This was called the infrared excess. The first systematic compilation of such objects is found in the Infrared Catalogue (usually referred to as "IRC") by Neugebauer and Leighton (1969). A great surprise was the discovery of maser line emission from some of the stars by Wilson and Barrett in 1968. This discovery created an interest that was of very long duration, although it may never have been considered very fashionable. A good summing up of what had been achieved at the eve of IRAS can be read in the review paper by Kleinmann *et al.* (1981). Then IRAS came and produced a catalogue containing tens of thousands of stars with circumstellar shells–see Habing (1987) for a duscussion of the content of the IRAS catalog in this respect. In combination with the new millimeter and submillimeter telescopes that come into operation at about the same time (IRAM, SEST, JCMT), the new reservoir of infrared active stars has created a flood of articles, revealing one interesting object after another. In this review I will not give details, but will refer to two excellent review papers by Oafsson (1988, 1989). Instead I want to summarize briefly a few fundamental

reasons why I think that the study of circumstellar envelopes is of importance and why it will remain so for a few more years. I will also argue that probably we know by now examples of all the important types–although undoubtedly some extreme and very interesting individual objects are still waiting to be discovered.

2. Four Lasting Reasons to Study Circumstellar Envelopes

The first reason to study stars with circumstellar shells is a very subjective one: they are intriguing because so much about them can be learned. A main reason is that they are so large: I mentioned already that the largest objects have the size of the better part of a parsec (and that often means of the order of an arcminute) and they are not optically thick at all wavelengths; thus we are enticed to study their internal structure. Interferometry is certainly one of the technique to lay bare how the envelopes are built up; radio interferometry in the OH maser lines is a prime example but there are good prospects for interferometry at other wavelengths, e.g., in the infrared, such as is being developed these days by Townes and his collaborators. OH interferometry has revealed that most ($> 95\%$) of the objects are by and large spherical, but recently several bipolar objects have been detected; the best known case is OH 231.8+4.2 (Morris *et al.*, 1987). It is thought that the stars develop into planetary nebulae, and those, we know, are often not spherical, but bipolar, so when does the change occur? In any case, circumstellar envelopes are just ripe for detailed investigations with different, new and developing techniques, that by themselves will make these objects important for quite a few years to come.

The second reason has to do with the first. Because the objects are so large (up to a few arcminutes), we can measure the structure and thus obtain a good quantitative description of the physical conditions. This then will allow us to use circumstellar envelopes as a laboratory for molecular research, intermediate between a true laboratory on Earth and the dense molecular cloud, where the structure is very irregular and will always remain poorly known. I would therefore like to make a plea for stars with circumstellar envelopes as guinea pigs to test out our laboratory insights before we attack interstellar clouds and regions of star formation. Especially the large fraction of circumstellar envelopes with more or less spherical outlines are geometrically simple, and one can hope that it will be possible to give an accurate description of the physical conditions. For example good spherical models already exist of the distribution of dust, and of its temperature, models that are based on the analysis of the overall infrared spectrum. The favourite papers of most authors appear to be those by Rowan-Robinson and Harris (1983), but I want to draw your attention also to the nice, deep paper by Bedijn (1987)–and not only because he is one of my former graduate students. Do not get the impression that from these models we know all that is worth knowing; we are still far away from a satisfying description: the dynamics of the gas-dust mixture, the formation and the properties of the dust, the presence of inhomogeneity (large blobs ejected by the star) and the extent by which external photons, notably UV photons, can penetrate inward, all these points need much elucidation.

The third reason to study circumstellar envelopes is the role they play in stellar and galactic evolution. In the basic cycle in which stars form out of the interstellar medium and finally return a fraction of their material back into that same interstellar medium,

the phase of the circumstellar envelopes is critical. How much matter is returned? Is it enriched e.g. by carbon or is it almost equal in composition to what went in? What grains are ejected, and how many atoms heavier than helium are locked up in the grains? And how does the white dwarf emerge, the hard core of the red giant and the only part that will not be destroyed during the late evolution? It is becoming clear that models of galactic populations, used e.g. to understand the colours of other galaxies, are inadequate without the incorporation of red luminous stars, such as are about to produce circumstellar envelopes, and that to calculate the further evolution of such a population one needs insight into when and how the circumstellar envelope phase occurs.

My final argument to support the studies of circumstellar envelopes is my own favourite. The stars are in a very luminous phase of their existence and are thus strong emitters. The energy they radiate away emerges mainly in the infrared and thus is not affected at all (or in a very minor way) by interstellar extinction. For probing the conditions in the inner part of the Galaxy, these stars are the only ones available, and they are close to ideal. I will admit that Baade found several windows that allow us some glimpses into the inner parts of our Galaxy, but I often feel that relying on Baade's Windows is like driving your car when the windows are frosted over and you have just managed to make a few small areas frost free: too small for save driving, but enough to get you started when you are in need of time! To support my opinion I refer to two papers–I apologize for blowing my own trumpet, for I was quite involved in both: the discovery that OH/IR stars very close to the Galactic Center form a system in fast rotation with a large velocity dispersion (Lindquist *et al.*, 1988) and the demonstration that one can obtain a very well defined synoptic view of our Galaxy, complete with a galactic bulge, by selecting stars with strong circumstellar shells (thus selecting intrinsically strong infrared emitters) from the IRAS catalogue (Habing *et al.*, 1985). The accurate measurement of the radial velocity for many of these stars via the 1612 MHz maser line of OH now enables us to get, for the first time, a detailed insight into the dynamics of a flattened elliptical system (Dejonghe and te Lintel Hekkert, in preparation).

3. Do We Know All Types of Stars with Circumstellar Envelopes?

The statement that one knows everything cannot be proven to be right; one can only show it to be wrong by turning up examples of an unknown kind. I realize the danger of my boast and yet I think that we may well have categorized and recognized all the major types of objects with circumstellar envelopes in the IRAS catalogue. IRAS surveyed the sky in four photometric channels centered at 12, 25, 60 and 100 μm. The smallest number of point sources were found in the last channel, and most of these appear to be galaxies; for stellar purposes the important channels are the first three. Three photometric measurements invite you to make a colour-colour diagram, and many people have made such diagrams (in the margin I notice that it is remarkable in how many ways one can do this; although each diagram can be transformed by a linear transformation into any other, the number of scales used in the vertical and in the horizontal direction is very large and almost always it takes some effort, and quite a few mistakes coupled with frustration, to compare the results of one author with the other). Now in making this diagram several people have noticed that certain types of objects have preferences for certain areas. van

der Veen has checked this point in quite some detail and finds that he can understand the full diagram, or rather that he can explain why each area is populated by the objects one appears to find there (van der Veen and Habing, 1988). Admittedly van der Veen's explanation is largely qualitative, but it suggests that by and large we understand what there is in the IRAS point source catalogue. One has to remain careful. As an example, take the location of carbon stars in the diagram: most of them are found in a well defined area, but there are interlopers in areas reserved for other objects.

Let me finish with a brief summary of one of the most beautiful surprises, the story of which is a true detective story, worthy of old Conan Doyle: the case of the Frosty Lion, IRAS 09371+1212. This object at high galactic latitude (in the sign of Leo, hence its nickname) is a strong source with very unusual colours. There had been speculation that it might be a galaxy, but it was firmly placed inside our own when $1-0$ CO line emission was discovered at a low radial velocity. The major puzzle it posed to authors (Forveille *et al.*, 1987) was the strength of the 60 μm detections. After some consideration they argued that such a spectral shape could not be produced by a continuum spectrum; whatever emitted the radiation must contain a strong spectral feature. Hence they postulated that we might see here emission from a band at 45 μm from water ice–a band long known in the laboratory and only inconclusively detected in the Orion Nebula. First evidence supporting the hypothesis came from the detection by several groups of a very strong ice band at 3.05 μm; one of the discoverers (Geballe) is reported to have said: I never saw such a strong one in my life. And finally in the spring of this year the decisive direct observation of the spectral band was made from the Kuiper Airborne Observatory. At this meeting Omont is going to show you this spectrum. Returning to my argument: IRAS 0937+1212 is an extraordinary example of a star losing matter. In one sense it is of a known kind; yet the conditions are so exceptional that it deserves special attention. Our insight in the contents of the IRAS point source catalogue may be almost complete, but more surprises like the Frosty Lion will turn up.

References

Bedijn, P. J. 1987, *Astr. Ap.*, **186**, 136.

Dejonghe, H., and te Lintel Hekkart, P. 1988, in preparation.

Forveille, T., Morris, M., Omont, A., and Likkel, L. 1987, *Astr. Ap.*, **176**, L13.

Habing, H. J. 1987, in *Circumstellar Matter*, eds. I. Appenzeller and C. Jordan (Reidel), p. 197.

Habing, H. J., Olnon, F. M., Chester, T., Gillet, F., Rowan-Robinson, M., and Neugebauer, G. 1985, *Astr. Ap.*, **152**, L1.

Kleinmann, S. G., Gillett, F. C., and Joyce, R. R., *Ann. Rev. Astron. Astrophys.*, **19**, 411.

Lindquist, M., Winnberg, A., Habing, H. J., Matthews, H. E., Olnon, F. M. 1988, in IAU Symposium No. 136, *The Galactic Center*, ed. M. Morris, in press.

Morris, M., Guilloteau, S., Lucas, R., and Omont, A., 1987 *Ap. J.*, **321**, 888.

Neugebauer, G., and Leighton, R. B. 1969, "Two Micron Survey", NASA Sp-3047.

Olofsson, H. 1988, *Space Science Reviews*, **47**, 145.

Olofsson, H. 1989, in IAU Coll. No. 106, *Evolution of Peculiar Red Giant Stars*, eds. H. R. Johnson and B. Zuckerman (Cambridge Univ. Press), in press.

Rowan-Robinson, M., Harris, S., 1983, *Mon. Not. Roy. Astr. Soc.*, **202**, 767.

van der Veen, W. E. C. J., and Habing, H. J. 1988, *Astr. Ap.*, **194**, 1987.

Wilson, W. J., and Barrett, A. H. 1968, *Science*, **161**, 778.

MOLECULAR LINE SURVEYS

Åke Hjalmarson
Onsala Space Observatory, S–439 00 Onsala, Sweden

In the conference program this review has been placed in between the physics and the chemistry of interstellar molecular clouds. My duty must be to answer questions like: "Are molecular line surveys at all useful?" and "What new has resulted from this extensive consumption of telescope time?". I do hope to convince you that the line surveys have been productive not only in terms of thousands of new lines but rather because of the rich harvest of new molecules, much improved molecular abundances, new molecular physics and much improved molecular cloud physics.

Introduction

Today some 80 molecules have been identified in interstellar/circumstellar clouds (see Table 1), mainly via observation of more than 2000 lines in the frequency range 0.7 to 3800 GHz. A few asymmetric top rotors contribute with a very large number of lines, e.g. $HCOOCH_3$ (>200), CH_3OH (>150), $(CH_3)_20$(>70), CH_3CH_2CN(>100) and SO_2(>100). Some 100 lines are due to CH_3CN. The number of U–lines (U = unidentified) tabulated is several 100. To remind ourselves about the richness of some molecular spectra it is useful to note that e.g. $HCOOCH_3$ has some 10000 transitions in the band 1–600 GHz.

Identification of new molecules

In Table 1 molecules discovered *accidentally* (since their signatures appeared in broad band spectra during otherwise aiming observations) *or via spectral line surveys* have been *underlined*. About 30% of the interstellar molecules have been identified in this way, rather than via dedicated searches at laboratory measured frequencies of species selected for one reason or another. The compounds discovered in this unbiased way to a large extent are "non–terrestrial" ones. The earliest examples were the *molecular ions* HCO^+ and N_2H^+, the *isomer* HNC, the *radical* C_2H and also the strong SiO (v=1, J=2–1) *maser from a vibrationally excited state* – subsequently verified by terrestrial laboratory spectroscopy, where the required sensitivity could be achieved only by means of integration at the approximately known transition frequency of the interstellar molecular candidate.

For many of the more recent discoveries due to spectral scans "*high resolution* (10^7:1) *spectroscopy in space*" – together with terrestrial spectroscopy – has been cruxial for the identification and determination of molecular parameters, e.g., C_3H, C_4H, C_5H, C_6H, C_3N, C_2S, C_3S and CH_2CN. Here the high frequency resolution is achieved by means of the very narrow spectral lines from the quiescent dark cloud TMC–1 – our remarkable interstellar carbon chain source.

Table 1. INTERSTELLAR MOLECULES

Simple molecules:

H_2	CO	NH_3	CS
HCℓ	SiO	SiH_4 *	SiS
C_2	HNO ?	CH_4 *	OCS
PN	SO_2	H_2O	H_2S
NaCℓ *	AlCℓ *	KCℓ *	AlF *

Nitriles, acetylene derivatives, and related molecules:

HCN	HC≡C–CN	$H_3C–C≡C–CN$	$H_3C–CH_2–CN$
H_3CCN	$H(C≡C)_2–CN$	$H_3C–C≡C–H$	$H_2C=CH–CN$
CCCO	$H(C≡C)_3–CN$	$H_3C–(C≡C)_2–H$	HNC
CCCS	$H(C≡C)_4–CN$	$H_3C–(C≡C)_2–CN$	HNCO
HC≡CH *	$H(C≡C)_5–CN$	H_3CNC ?	HNCS
$H_2C=CH_2$ *			

Aldehydes, alcoholes, ethers, ketones, amides, and related molecules:

$H_2C=O$	H_3COH	HO–CH=O	H_2CNH
$H_2C=S$	H_3CCH_2OH	$H_3C–O–CH$ O	H_3CNH_2
$H_3C–CH=O$	H_3CSH	$H_3C–O–CH_3$	H_2NCN
$NH_2–CH=O$	$H_2C=C=O$		
HC_2CHO	$(CH_3)_2C=O$?		

Ions:

CH^+	HCS^+	H_2D^+ ?	$HCNH^+$
HN_2^+	SO^+	$HOCO^+$	HOC^+ ?
H_3O^+ ?	HCO^+		

Cyclic molecules:

C_3H_2	SiC_2 *	c–C_3H

Radicals:

CH	C_2H	CN	HCO
OH	ℓ–C_3H	C_3N	NO
	C_4H	NS	SO
	C_5H	C_2S	H_2CCN
	C_6H	$HSiC_2$ or HSC_2 *	

* Detected only in envelopes around evolved stars.
Molecules discovered accidentally or via spectral line surveys are underlined.

The identifications of the *cyclic molecules* C_3H_2 (abundant in interstellar as well as in circumstellar sources) and SiC_2 (only detected in circumstellar envelopes) and of the *metal halids* NaCℓ, AℓCℓ, KCℓ and AℓF (in the IRC+10216 envelope) are other notable achievements based upon spectral line surveys.

The increasing sensitivity resulting from cryogenic receivers and larger telescopes, access to new frequency bands and some focusing on other sources than Sgr B2 and Orion A has kept the detection rate of new molecules at the average level of about 4 per year. In this context it may be appropriate to stress that nowadays also dedicated searches for specific molecules (with known frequencies) normally require multi–line detection and match–up to expected line patterns to really prove an identification. Although this is somewhat similar to a spectral line survey it is also clear that in such dedicated searches one is allowed to spend considerably more integration time per frequency band than is ever possible in a spectral scan. Therefore the molecular abundance levels reached in searches for specific molelcules often are lower than is achievable in line surveys. Here the advantage of a broad band survey rather is to allow pattern recognition among remaining U–lines – after the "cleaning up" of all transitions from already known species.

Some 30 new molecules have been identified since 1980 – half of them are results from spectral scans. Of these latter species 12 are due to line surveys in the circumstellar envelope of the carbon star IRC+10216 and in the dark cloud TMC–1. Deep dedicated searches at known transition frequencies in TMC–1 also have lead to the discovery of a number of carbon chain species as get unique to this source – C_3O, CH_3C_3N, CH_3C_4H, CH_3C_5N, and HC_2CHO.

Of the 80 species known today some 55 have been seen in the Sgr B2 molecular cloud complex, 40 in the Orion A molecular cloud, 45 in TMC–1 and 35 in IRC+10216. It may be interesting to note that TMC–1 contains 14 carbon chain species not (yet) observed in Orion A and Sgr B2. TMC–1 and IRC+10216 have 24 species in common, 15 of which are carbon chains (CO, and perhaps HCO^+, are the only common O–species).

High frequency spectral scans – towards the confusion limit

I will here briefly comment on existing spectral line surveys. Line densities and estimates of confusion limits are compiled in Table 2.

The OSO spectral scan (Johansson et al. 1984, 1985) covered the frequency range 72–91 GHz towards Orion A and IRC+10216. The result for Orion A was some 200 lines from 24 already known interstellar molecules + Hα, β, γ, δ and Heα. About 100 lines were astronomically new transitions. The existence in Orion A of $HCOOCH_3$, HNCO, CH_2CHCN and H_2CCO was proved. The fraction of *U–lines* was *below 10%*. In IRC+10216 our result was 45 lines from 12 known species, including the detection of the first (and as yet only) molecule containing the methyl group in this source, CH_3CN. In addition 14 U–lines were reported. We tentatively assigned 4 of the U–lines as close doublets of the radical C_3H – later on verified by a match–up of many doublets due to this species observed in

IRC+10216 and in TMC–1 ("high resolution spectroscopy in space" resulting in well–resolved hyperfine splitting) in combination with laboratory spectroscopy (Thaddeus et al. 1985a, Gottlieb et al. 1985).

The OVRO molecular line survey (215–263 GHz) of Orion A (Sutton et al. 1985, Blake et al. 1986) resulted in some 800 lines from 29 known molecules. 80% of the lines were assigned to SO_2, CH_3OH, $HCOOCH_3$, $(CH_3)_2O$, CH_3CN, CH_2CHCN, and CH_3CH_2CN – a result very much relying on supporting laboratory spectroscopy. The existence of HCOOH and (probably) CH_3CHO in Orion A was proved. The remaining number of *U–lines* is low – *only* 4%.

The AT & T Bell Laboratories survey of some 60% of the spectrum between 70 and 150 GHz towards the Sgr B2 molecular cloud (Cummins et al. 1986) contains some 450 lines from 40 molecules, including *30 U–lines (about 7%)*. The identifications of the new interstellar species CH_3SH, HNCS, HCS^+ and $HOCO^+$ were results published much earlier, but relying upon the large spectral coverage. A number of molecules have so far only been detected in Sgr B2. One reason certainly is that compared to Orion A a much larger volume is sampled. For the same telescope and observing frequency the area sampled in Sgr B2 is $(8.5 \text{ kpc}/0.5 \text{ kpc})^2 \approx 250$ times larger. This also means that large variations of physical and chemical conditions may be expected. Such source structure has indeed been observed by means of the Nobeyama 45 m telescope and by the VLA (Goldsmith et al. 1987, Vogel et al. 1987). It appears that a multi–position spectral line survey at sufficiently high angular resolution could be very rewarding both in terms of new molecules and for our understanding of cloud chemistry/physics.

A rather sensitive *NRAO line survey* of Sgr B2 and Orion A from 70–115 GHz has become available only very recently (Turner 1988). For Sgr B2 some 800 lines have been catalogued *some 20%* of which are *U–lines*. The Orion A spectrum contains 900 lines of which *25%* are *U–lines*. Although some of the many lines may result from a "more optimistic attitude" it is convincingly clear that this line (and U–line) density is much higher that found with the Bell Laboratories 7 m telescope towards Sgr B2 and with the Onsala 20 m telescope towards Orion A. In case of Sgr B2 the $(11/7)^2 \sim 2.5$ times *higher sensitivity to spatially unresolved sources* of the NRAO Kitt Peak 11 m telescope could contribute. In case of Orion the *higher sensitivity to extend molecular cloud emission* of the NRAO telescope may be a reason. A comparison of the OSO and NRAO survey results reveals that for emissions from compact cloud components the intensities scale roughly as $(20/11)^2 \sim 3$. In fact quite a few of the OSO $HCOOCH_3$ & $(CH_3)_2O$ lines are not (clearly) seen in the NRAO scan. This also applies to most of few the OSO U–lines (from compact sources?). On the other hand very few of the NRAO U–lines are visible in the OSO spectra and may therefore emanate in the extended ridge clouds. A clue in this direction may be that in the OSO data U85339 (now known to be due to C_3H_2) has a factor of 3 *lower* intensity, while the pointlike emissions are a factor of 3 *stronger*, compared to the NRAO data.

An *NRAO submillimeter survey* of Orion A emission lines in the range 330–360 GHz (Jewell et al. 1988) appeared while this review was written. Some 180 lines from 19 molecules were detected, 30 of

which *(17%)* were denoted *U–lines*. Here SO_2, CH_3OH and CH_3CN account for 45% of the lines while in the OSO and OVRO scans this fraction is only 20 and 25%.

The very sensitive *IRAM* (30 m telescope) *spectral scan* of the carbon star IRC+10216 still is unpublished, although pieces have appeared in papers on identifications of new molecules. A brief report (including relevant references) was given at the recent meeting in Kona, Hawaii (Lucas and Guélin 1988). The survey covers over 90 GHz of frequency space (80–116 GHz, 130–174 GHz and also some bands below 80 and around 230 GHz). About 500 lines were detected, most of which for the first time. Some 220 arise from new molecules (C_5H, C_6H, c–C_3H, C_2S, C_3S, NaCℓ, KCℓ, AlCℓ, AlF) or new isotopic variants. About 100 U–lines remain. A large number of lines from vibrationally excited (known) molecules have appeard, among them 40 from C_4H. The average line density is about 5 per GHz, considerably higher at low frequencies (>10 per GHz, as estimated from published spectra) and decreasing with increasing frequency.

Table 2. Observed line density vs confusion limit

Observatory Source	Frequency range (GHz)	Line[a] width (MHz)	Observed line density (per GHz)	Confusion[b] line density (per GHz)
OSO/ORI	72–91	8	11	125
NRAO/ORI	70–115		20	
OVRO/ORI	215–263	25	17	40
NRAO/ORI	330–360	40	6	25
BELL/SGR	72–115	20	10	50
	125–144		8	
NRAO/SGR	70–115		18	
OSO/IRC	72–91	9	3	110
IRAM/IRC	80–116	11	>10?	90
	130–174			

a) Estimated mean full line width

b) 1000/Line width (a)

From Table 2 it appears that we are already approaching the spectral confusion limit in the OVRO 215–263 GHz survey of Orion A. In fact Sutton et al. (1984) estimate that 40% of the observed broad band flux at 1.3 mm is due to line emission. In the NRAO 70–115 GHz survey of Sgr B2 the observed line density is only a factor of 3 lower than the confusion limit. In the other surveys tabulated there is still spectral space to accomodate a fivefold increase of the line density.

However, at increasing sensitivity we also may envisage – from our present experience – *difficult enemies* in our hunting for new molecules, which can only be defeated by extensive support from

laboratory spectroscopy – isotopic variants and high energy ground, vibrational and torsional states of already known molecules, e.g. CH_3OH, $HCOOCH_3$, $(CH_3)_2O$, CH_3CH_2CN and CH_2CHCN. In this spirit some 40 U–lines in the IRAM line survey of IRC+10216 recently have been assigned to transitions in the lowest bending state (v_7) and the overtone state ($2v_7$) of C_4H (Guelin et al. 1987, Yamamoto et al. 1987a).

Lower frequency spectral surveys of TMC–1

The very large AOS (acousto – optical spectrometer) system installed in the Nobeyama 45 meter telescope has made possible a spectral scan of the 22–24 GHz and 36–50 GHz bands in TMC–1. The difficulty here is the very narrow width of the molecular lines (~ 0.5 km s^{-1}). A number of strong U–lines have been reported (Kaifu et al. 1987). They have all been identified by laboratory spectroscopy with transitions from the new carbon chain species C_2S and C_3S (Saito et al. 1987, Yamamoto et al. 1987b)

A rather high sensitivity survey of the spectral region 18.5 to 21.5 GHz in TMC–1 is performed with the NRAO 43 m telescope by Irvine and collaborators. In the region surveyed some 10 new (weak) lines were detected in a very narrow interval around 20.12 GHz, while the U–line density was very low in surrounding frequency bands. Collaborative efforts at Nobeyama now have lead to the detection of another 10 (weak) lines near 40.24 GHz. These lines bunches fit in with other U–lines at 80.48 and 100.60 GHz observed in TMC–1 and Sgr B2 (Irvine et al. 1988). Laboratory work at Nagoya University has lead to the identification of the CH_2CN radical (Saito et al. 1988). The non–existence of strong U–lines in the surveyed spectral band may seem discouraging, but is "compensated" by the appearance of the very strong line U18343 just outside the surveyed region. This line was accidently discovered during a search for NH_2C_2H and was subsequently assigned to the small hydrocarbon ring C_3H_2 (Matthews and Irvine 1985, Thaddeus et al. 1985b).

Cloud physics and chemistry

The uniformly calibrated spectra and multi–transition data resulting from spectral line surveys have lead to *much improved knowledge of molecular abundances*, especially so since molecular population distributions often can be determined (rather than assumed). Since the population distributions depend upon the excitation we also get improved estimates of *cloud temperatures and densities*. In Orion A the rather unique spectral signatures (velocity and linewidth) of the different emission regions (ambient cloud, warm clump, hot core, outflow) has allowed analysis of each component separately. The *chemical selectivity* between the physically different Orion A cloud components is very pronounced.

Here some relevant references are Johansson et al. (1984), Cummins et al. (1986), Blake et al. (1987), Irvine et al. (1987), and Turner and Ziurys (1988). A comparison of IRC+10216 abundances with interstellar ones is provided by Irvine et al. (1985).

Concluding remarks

It is important to stress that for complex species abundance limits often are not very good although intensity limits may seem low. The reason is population partition among many available energy states. Since our searches are still limited by sensitivity and not yet by spectral confusion we should remember that *absence of evidence does not mean evidence of absence.*

References

Blake, G.A., Sutton, E.C., Masson, C.R. and Phillips, T.G. 1986, Astrophys.J. Suppl. 60, 357.

Blake, G.A., Sutton, E.C., Masson, C.R. and Phillips, T.G. 1987, Astrophys.J. 315, 621.

Cummins, S.E., Linke, R.A. and Thaddeus, P. 1986, Astrophys.J. Suppl. 60, 819.

Goldsmith, P.F., Snell, R.L., Hasegawa, T. and Ukita, N. 1987, Astrophys.J. 314, 525.

Gottlieb, C.A., Vrtilek, J.M., Gottlieb, E.W., Thaddeus, P. and Hjalmarson, Å. 1985, Astrophys.J. 294, L55.

Guélin, M., Cernicharo, J., Navarro, S., Woodward, D.R., Gottlieb, C.A. and Thaddeus, P. 1987, Astron.Astrophys. 182, L37.

Irvine, W.M., Schloerb, F.P., Hjalmarson, Å. and Herbst, E. 1985, in Protostars and Planets II, eds. D. Black and M. Matthews, U. Arizona Press, p. 579.

Irvine, W.M., Goldsmith, P.F. and Hjalmarson, Å. 1987, in Interstellar Processes, eds. D.J. Hollenbach and H.A. Thronson, Jr, Reidel, p. 561.

Irvine, W.M., Friberg, P., Hjalmarson, Å., Ishikawa, S., Kaifu, N., Kawaguchi, K., Madden, S.C., Matthews, H.E., Ohishi, M., Saito, S., Suzuki, H., Thaddeus, P., Turner, B.E., Yamamoto, S. and Ziurys, L.M. 1988, Astrophys,J. 334, L107.

Jewell, P.R., Hollis, J.M., Lovas, F.J. and Snyder, L.E. 1988, NRAO Preprint.

Johansson, L.E.B., Andersson, C., Elldér, J., Friberg, P., Hjalmarson, Å., Höglund, B., Irvine, W.M., Olofsson, H. and Rydbeck, G. 1984, Astron.Astrophys. 130, 227 (also 1985, Astron.Astrophys.Suppl. 60, 135).

Kaifu, N., Suzuki, H., Ohishi, M.., Miyajai, T., Ishikawa, s., Kasuga, T., Morimoto, M. and Saito, S. 1987, Astrophys.J. 317, L111.

Lucas, R. and Guélin, M. 1988, IRAM Preprint No 138, invited review at the symposium Submillimeter and Millimeter Astronomy, Kona, Hawaii, Oct. 1988.

Matthews, H.E. and Irvine, W.M. 1985, Astrophys.J. 298, L61.

Saito, S., Kawaguchi, K. Yamamoto, S., Ohishi, M., Suzuki, H. and Kaifu, N. 1987, Astrophys.J. 317, L115.

Saito, S., Yamamoto, S., Irvine, W.M., Ziurys, L.M., Suzuki. H., Ohishi, M. and Kaifu, N. 1988, Astrophys.J. 334, L113.

Sutton, E.C., Blake, G.A., Masson, C.R. and Phillips, T.G. 1984, Astrophys.J. 283, L41.

Sutton, E.C., Blake, G.A., Masson, C.R. and Phillips, T.G. 1985, Astrophys.J.Suppl. 58, 341.

Thaddeus, P., Gottlieb, C.A., Hjalmarson, Å., Johansson, L.E.B., Irvine, W.M., Friberg, P. and Linke, R.A., 1985a, Astrophys.J. 294, L49.

Thaddeus, P., Vrtilek, J.M. and Gottlieb, C.A. 1985b, Astrophys.J. 299, L63.

Turner, B.E. 1988, NRAO Preprint.

Turner, B.E. and Ziurys, L.M. 1988, in Galactic and Extragalactic Radio Astronomy, eds. G.L. Verschuur and K.I. Kellerman, Springer, p. 200.

Vogel, S.N., Genzel, R. and Palmer, P. 1987, Astrophys.J. 316, 243.

Yamamoto, S., Saito, S., Guélin, M., Cernicharo, J., Suzuki, H. and Ohishi, M. 1987a, Astrophys.J.. 323, L149.

Yamamoto, S., Saito, S., Kawaguchi, K., Kaifu, N. Suzuki, H. and Ohishi, M. 1987b, Astrophys.J. 317, L119.

THE STRUCTURE AND KINEMATICS OF MOLECULAR CLOUDS FROM LARGE SCALE MAPPING OF MILLIMETER LINES

John Bally, Antony A. Stark, and Robert W. Wilson
AT&T Bell Laboratories, Holmdel, N. J. 07733
and
William D. Langer
Princeton University, Princeton, N. J.

INTRODUCTION

We have used the AT&T Bell Laboratories 7-meter diameter offset Cassegrain mm-wave antenna (100″ diameter beam size) to map the structure and kinematics of molecular clouds in the ^{12}CO and ^{13}CO $J = 1 - 0$ and CS $J = 2 - 1$ lines. By using a sensitive SIS receiver (T_{SSB} = 60 to 190 K) and a strategy of dedicated observing, we have accumulated a data base containing about 300,000 spectra with a typical (rms) noise level of order 0.3 K in 0.25 MHz resolution channels. About 85% of this data is in the ^{13}CO line, about 10% is in the CS line, and the remaining 5% is in the ^{12}CO line. The largest data cubes are images of the Orion B molecular cloud (80,000 ^{13}CO [Fig. 1] and 15,000 CS spectra), a 3′ grid of the Galactic Plane from $\ell = 5°$ to 116° (Stark *et al.* 1987) containing about 80,000 ^{13}CO and 10,000 ^{12}CO spectra, the Orion A cloud (33,000 ^{13}CO; 4,000 ^{12}CO; 4,000 CS spectra; Bally et al. 1987a), the NGC 1333 region (33,000 ^{13}CO and 5,000 CS spectra), Mon R2 (30,000 ^{13}CO spectra) and the Galactic Center region (15,000 CS and 10,000 ^{13}CO spectra; Bally *et al.* 1987b, 1988). A variety of smaller regions, including S255, LkHα 208, the Pleiades, L723, ON-1, M16, and others have been mapped. This data represents work utilizing about 70% of the available observing time on the 7-meter antenna during the last five years.

Since the spectra contain more than 64 independent velocity channels of information, the cubes with over 15,000 spectra have over 1 million pixels of data. The analysis and visualization of such large amounts of three-dimensional data present a major challenge. The conventional contour map cannot display all the available information, and the data are best shown as images in which color is used to represent the velocity structure. These images can be used to analyze the structure and kinematics of molecular clouds, to investigate the relationship between the gas, dust, and the stellar objects associated with the clouds, and to look for systematic behavior in the cloud properties as a function of cloud environment. These studies were undertaken with the hope that eventually they will lead to a better understanding of cloud formation, evolution, and destruction, of

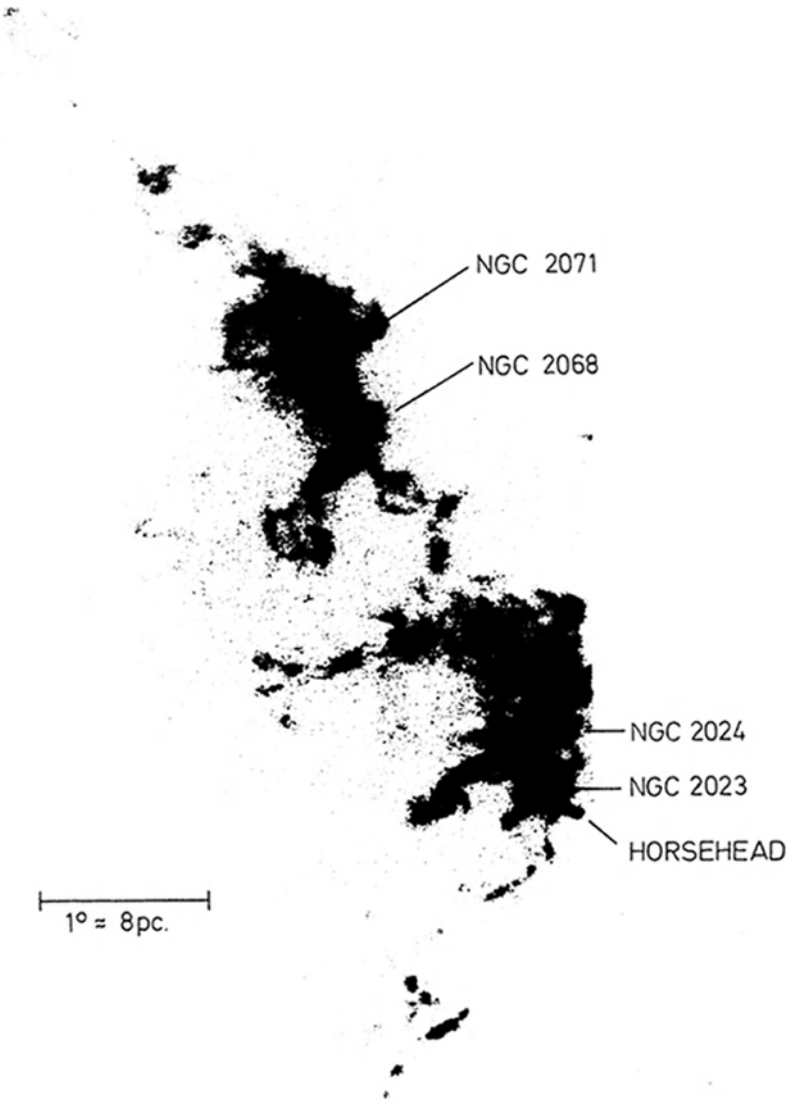

Fig. 1. A ^{13}CO $(1-0)$ image showing the Orion B molecular cloud from $V_{LSR} = 7$ to 9 km s^{-1}. The NGC2024, NGC2023, and Horsehead Nebula regions are at the lower right, while NGC2068 and NGC2071 are at the upper left. About 77,000 frequency-switched spectra, obtained on a $1'$ grid, were used to construct this image. Note the "tongue" of gas extending east from the region between NGC2023 and NGC2024 and the one degree diameter limb-brightened bubble to the south-east of NGC2068.

the star formation process, and finally, a better understanding of how to use molecular studies to probe the evolution and structure of the Galaxy.

In this discussion, we present only an overview of the main results and defer detailed discussion until the maps are published in detail elsewhere. The three main points we wish to make are: (1) Molecular clouds consist mainly of filaments, sheets, bubbles, and cavities, suggesting that shock waves play an important role in controlling the cloud dynamics and morphology. (2) In one cloud, (Orion A) where multi-transition studies have been made, the ^{13}CO lines appear to be optically thick. (3) The molecular clouds lying within the inner 1 kpc region of our Galaxy containing the Galactic Center are very different from the clouds lying in the disk of the Galaxy.

FILAMENTS, SHEETS, BUBBLES, AND CAVITIES

The ^{13}CO isotopic variant of carbon monoxide is about 90 times less abundant than the common ^{12}CO species. We expected that the opacity of the ^{13}CO lines would be relatively low, allowing observation of emission from most of the radiating volume of a molecular cloud. To the extent that the excitation temperature of ^{13}CO is constant throughout a cloud and that the $(1-0)$ line is optically thin, our images are a measure of column density of hydrogen having a volume density above about 1,000 cm^{-3}.

The images provide an approximate view of the internal structure and velocity field of molecular clouds. A striking feature is the high degree of filamentation and the presence of cavities and bubbles. Molecular clouds do not have a "relaxed" structure which might be expected of an object whose components have survived many dynamic time-scales (cloud crossing times). Clouds can not be modeled as a "gas" consisting of individual particles, in this case cloud cores, whose motion is responding to the overall gravitational potential of the entire cloud.

The bubbles and filaments cover a large range of size scales, from the resolution limit (0.2 pc in Orion) to sizes comparable to the extent of the clouds themselves (about 30 pc). Some of the filaments are 50 to 100 times as long as they are wide, are very straight, and probably have a string-like topology. Other structures are curved and may be sheets of matter which appear filamentary due to the effects of limb brightening. This topology can be easily generated by shock waves propagating through the cloud; the existence of sheets is an indication that shocks play a dominant role in the dynamics of molecular clouds and determine the cloud morphology. The most likely source of shocks are the stars which are born from the molecular clouds themselves. On a small scale, the energetic outflows frequently found to be associated with star-formation (*e.g.*, Armstrong 1988) may energize the bubbles and cavities and may disrupt individual star-forming cloud cores. On larger scales, ionization, interaction with main-sequence stellar winds, and the eventual demise of massive stars in supernova explosions can supply enough kinetic energy to modify cloud structure.

A third process that may be important is the dynamical effect of the heating produced by non-ionizing UV radiation in the surface layers of clouds. Stars of spectral type between B3 and late A radiate copious amounts of energy at longer UV wavelengths which heat gas in dissociation regions to hundreds or even thousands of degrees by photo-electrons ejected from dust grains and by molecular dissociation heating. The thermal expansion of gas away from the cloud boundary layer effectively converts the

energy in the radiation field to kinetic energy of motion. The 10 pc scale bubbles in Orion, and the large scale bubble seen in the IRAS images of the region surrounding the Pleiades star cluster, may have their origins in this mechanism since there are no known stars capable of producing winds or ionization and none of the properties of supernova remnants are observed.

In the Orion region, most of the non-sheet-like filaments, as well as the cometary shape of the Orion A cloud, are aimed towards the center of the Ori I OB association. This 2×10^7 year old group is located near the center of the Orion super-bubble, whose eastern edge coincides with Barnard's Loop. The large scale distribution, morphology, and kinematics suggest that the molecular gas in Orion may have been extensively shaped by the interaction with the super-bubble. This interaction may be responsible for the compression of the northern part of the Orion A cloud and the western edge of the Orion B cloud, which are now experiencing OB star formation.

The main Orion A filaments are aligned with the major axes of about a dozen optical outflows identified in this region by Reipurth (1988). Uchida (private communication) has suggested that magnetic fields may be responsible for both the existence and support of the filaments and for the co-alignment of outflows produced by stars forming out of cores condensing from the filaments. In this model, the filaments are cylindrical tubes of gas containing an axial magnetic field whose strength is sufficient to control the gravitational collapse.

^{13}CO IS OPTICALLY THICK OVER 95% OF THE SURFACE OF THE ORION A CLOUD

A poster by Castets *et al.* at this meeting illustrates a surprising result of a four-transition study of the Orion A cloud: the ^{13}CO lines are optically thick over most of the cloud area. This conclusion comes from the observation that at most positions (a notable exception is the Orion A core near the BN-KL region), the ^{13}CO $J = 2-1$ line profiles and intensities are identical to the $J = 1-0$ line profiles and intensities. Nevertheless, the ^{12}CO lines are typically three times stronger than the ^{13}CO lines; this is the observation that has lead to the "standard" picture in which the ^{13}CO lines are optically thin under the assumption that the excitation temperatures of ^{12}CO and ^{13}CO are equal and uniform throughout the cloud.

One possible explanation of our observations is that the ^{13}CO lines are subthermally excited. Our CS $J = 2 - 1$ observations, however, indicate that the gas in most of the region studied has sufficient density to thermalize the ^{13}CO lines. This leaves two alternatives: either the excitation temperature at the depth into the cloud where $\tau(^{13}\mathrm{CO}) = 1$ is about three times lower than the excitation temperature where $\tau(^{12}\mathrm{CO}) = 1$, or the beam filling factor of the ^{13}CO-emitting region is much less than that of the ^{12}CO-emitting region. The first alternative is reasonable for externally heated clouds. Since the interstellar UV radiation penetrates about as far as $\tau(^{12}\mathrm{CO}) = 1$ (for a line width of 3 to 5 km s^{-1} at 30 K), the ^{12}CO lines are formed in the warm outer parts of the cloud, while the ^{13}CO lines, which penetrate deeper into a typical cloud probe a zone having a much lower gas temperature. The observation that ^{13}CO is thick implies that the "standard" picture of the excitation conditions in CO-emitting gas must be revised, with potentially important implications for the interpretation of all CO data.

GALACTIC CENTER CLOUDS ARE DIFFERENT

Extensive CS and ^{13}CO mapping of the inner 10 degrees of the Galaxy (Bally *et al.* 1987b and 1988) have shown that the molecular clouds in this region of the sky differ from those in the Galactic disk. The clouds are found to be much denser in the inner Galaxy since $J = 2 - 1$ CS emission is much brighter and more widespread than anywhere else in the Galaxy. In addition, the clouds have intrinsic linewidths of around 20 to 40 km s^{-1}, about an order of magnitude larger than for typical clouds near the Sun. These two properties may be a consequence of the strong shear produced by the differential rotation of the Galaxy (Stark *et al.* 1988; see Gusten 1988). For a cloud to remain gravitationally bound against the Galactic shear, it must be much denser than a typical cloud near the Sun. In order for such a cloud not to collapse rapidly under its own self gravity, it must be in rough virial equilibrium, which for the high mean densities implies a large linewidth. What supports these clouds against collapse? A milligauss magnetic field would do; such a field has been inferred in this region from observations of the non-thermal radio filaments seen in this part of the sky.

The overall distribution of the molecular gas is very asymmetric in both Galactic longitude and in velocity. The only other known population of objects having this distribution in the sky are the radio filaments, which suggests that the filaments and the molecular cloud populations may be closely coupled in some way. The so called "arched filaments," located north of Sgr A, exhibit radio recombination line emission at the same velocity as the -30 km s^{-1} molecular cloud. Further evidence for a close association between a particular filament and a particular cloud is given in Bally and Yusef-Zadeh (1989). The distribution of the clouds on the sky and in velocity, when combined with the presence of large "forbidden" velocities not permitted by purely circular motion about the center, suggests that much of the molecular gas may be located in a pair of dust lanes, similar in nature to the dust lanes associated with the nuclear regions of galaxies with a stellar bar. The dust lane model can explain both the asymmetric distribution of the gas in velocity and the presence of forbidden velocities, since in such a lane, most of the individual particles (molecular clouds) move about the center on elongated orbits. A consequence of this scenario is that in the inner 500 pc to 1 kpc region of our Galaxy, the stellar distribution may be tri-axial. This possibility provides the most natural and compelling explanation of the gas properties and can be eventually tested by detailed studies of the stellar distribution and dynamics of the inner Galactic bulge.

REFERENCES

Armstrong, J. T. 1988, this volume.

Bally, J., Langer, W. D., Stark, A. A., and Wilson, R. W. 1987a *Ap. J. (Letters),* **312**. L45.

Bally, J., Stark, A. A., Wilson, R. W., and Henkel, C. 1987b *Ap. J. (Suppl.),* **65**, 13.

Bally, J. and Yusef-Zadeh, F. 1989 *Ap. J.,* in press.

Bally, J., Stark, A. A., Wilson, R. W., and Henkel, C. 1988 *Ap. J.,* **324**, 223.

Castets, A., Duvert, G., Bally, J., Wilson, R. W., and Langer, W. D. 1988, this volume.

Gusten, R. 1988, this volume.

Stark, A. A., Bally, J., Knapp, G. R., Krahnert, A., Penzias, A. A., and Wilson, R. W. 1987 IAU Symposium #115, "Star Forming Regions," ed. M. Piembert and J. Jugaku, p. 495.

Stark, A. A., Bally, J., and Wilson, R. W. 1988 IAU Symposioum #136, "The Galactic Center," ed. M. Morris and E. Serabyn, in press.

Reipurth, B. 1988 *Astr. Ap.*, in press.

THE POPULATION AND DISTRIBUTION OF MASSIVE STARS EMBEDDED IN GALACTIC MOLECULAR CLOUDS

Ed Churchwell[1], D.O.S. Wood[2]

[1] Univ. of Wisconsin, currently MPIfR, Bonn, F.R.G.
[2] Univ. of Wisconsin, currently Center for Astrophysics, Boston, U.S.A.

1. Summary

We describe a new technique to select and count the number of O stars in the Galaxy that are still embedded in their natal molecular clouds. The sample of ultracompact HII regions mapped by Wood and Churchwell (1989) are used to calibrate the FIR colors of embedded O stars and to show that they are the only galactic objects with these colors that can be detected with IRAS throughout the entire galaxy. We estimate that the present number of embedded O stars (or O star clusters) in the Galaxy is in the range 1650 to 3300; and the fraction of embedded O stars is $\geq$0.1 but <0.2 of all O stars. The current rate of massive star formation in the galactic disk is estimated to be $\geq 3\times10^{-3}$ O stars/yr.

2. Introduction

Ultracompact (UC) HII regions are formed by O and early B stars that are still embedded in their natal molecular cloud. All UC HII regions have 100μm flux densities 10^3–10^4 times greater than that of the maximum radio continuum (see Wood and Churchwell 1989, hereafter WC) and they are point sources for IRAS. This implies that the stellar luminosity is converted to far infrared (FIR) radiation close to the star, which requires that the star be embedded in a dense, dusty medium. They also display sharp ionization fronts in radio continuum images which implies a dense, neutral, confining medium.

UC HII regions, therefore, represent recently formed O and early B stars that are still embedded in their natal molecular cloud. If one could count all of them, it would provide a direct estimate of the present rate of massive star formation in the Galaxy as well as an estimate of their contribution to the global energetics of the galaxy. Here, we describe a technique to select and count embedded O stars.

3. Selection Criteria

The spectra shown in WC illustrate that the IR flux distributions of UC HII regions are very similar from one object to another independent of the morphologies of the ionized gas. This implies that the FIR colors of UC HII regions (i.e. embedded O and B stars) should be confined to small areas in FIR color–color plots. To test this hypothesis, we have plotted the FIR colors of those UC HII regions mapped by WC that have measured FIR flux densities at all four bands in the IRAS Point Source Catalog (PSC). Not only are they tightly confined in FIR color–color plots, but, more importantly, few other types of objects share the same FIR colors. This is illustrated

in Figures 1 and 2 where the FIR colors of the known UC HII regions mapped by WC (solid dots) are compared with those of sources in the PSC lying in a narrow strip from RA=13^h00^m to 13^h10^m over all declinations (crosses, 527 objects) and those in a 2°x2° box centered on the Galactic plane at longitude 40° (open squares, 209 sources).

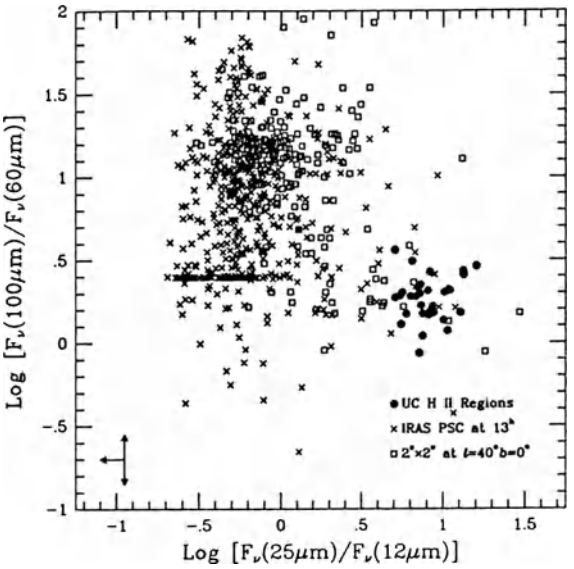

Fig.1. The colors of IRAS PSC sources associated with the known UC HII regions (filled circles) are compared with a selection of IRAS sources taken from a 2°x2° box in the Galactic plane at 40° longitude (squares) and a group of IRAS sources that lie between 13^h00^m and 13^h10^m in Right Ascension (crosses).

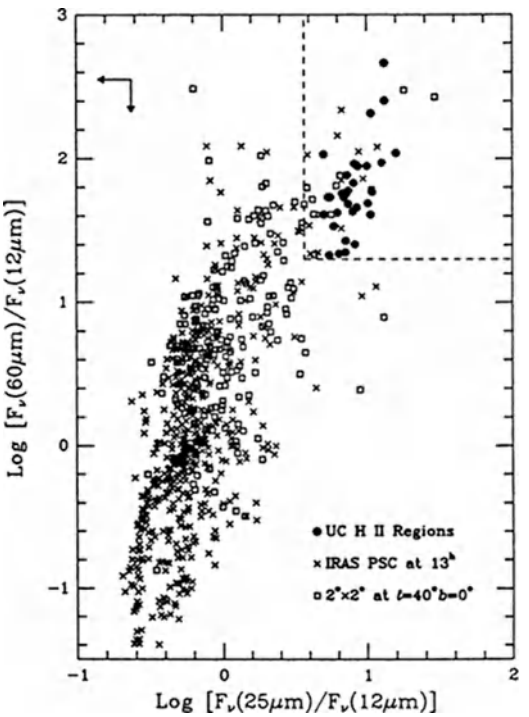

Fig.2. Same as for Figure 1 except the 60/12μm vs. the 25/12μm colors (flux densities ratios) are plotted.

In both figures, it is obvious that very few of the randomly selected objects lie in the same region as the sample of known UC HII regions. The largest differences between the sample of known UC HII regions and the randomly selected samples occur for flux density ratios at wavelengths 60/12 and 25/12μm.

Guided by these results, we have searched the entire PSC for all sources with the same FIR colors as the known sample of UC HII regions. The search criteria were: F(60)/F(12)$\geq$19.91, F(25)/F(12)$\geq$3.70, flux quality at 25 and 60μm$\geq$2 (i.e. no upper limits at these wavelengths allowed), and objects found in catalogs of stars and galaxies were not included. These criteria select objects with FIR colors lying to the right of the vertical dashed line and above the horizontal dashed line in Figure 2. An upper limit at 12μm can only shift a point further to the upper right (i.e. to redder colors). The final number of objects selected using this two color criterion is probably incomplete because: 1) some of the sources rejected for having an upper limit at 60μm or 25μm might have appropriate colors; 2) the PSC is incomplete for the most distant early B stars at 12μm and to a lesser extent at 25μm; and, 3) heavily confused portions of the Galactic plane are not included in the PSC. Based on the number of sources found when we relaxed our upper limit rejection criteria and by the fact that even in the Galactic plane, the PSC is probably 86% complete for sources with flux densities $\geq$10Jy (IRAS Explanatory Supplement, p. VIII-10), it is doubtful that the actual number of embedded OB stars is underestimated by more than a factoe of two. The FIR colors of some embedded low-mass stars are similar to those of embedded massive stars, but they have much lower luminosities and can only be detected by IRAS out to fairly small distances from the Sun. We, therefore, believe that our sample of FIR color selected sources are dominated by embedded O and early B stars, although there is some contamination by a small number of nearby, embedded, low mass stars.

4. The Sample

A total of 1708 objects (~0.7% of the entries in the PSC) satisfy the above criteria.

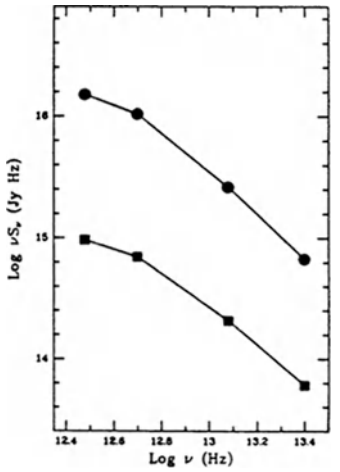

Fig.3 The FIR flux density distribution (median flux density in each IRAS band) of the IRAS sources known to contain UC HII regions is compared with that for embedded OB star candidates selected by FIR colors. The solid dots are for the UC HII region mapped by WC. The solid squares are for the FIR color selected embedded OB star candidates.

In Figure 3, we plot the median flux density in each of the IRAS bands for the color selected sample of embedded massive star candidates (filled squares) and for the known UC HII regions mapped with the VLA (filled circles). This figure demonstrates two important points: 1) the two color criteria have successfully identified sources with spectra similar to those associated with known UC HII regions; and, 2) the color selected candidates have IR fluxes that are about an order of magnitude less than those of the radio sample of UC HII regions. The PSC is more sensitive than the VLA survey of WC which was biased toward more luminous objects.

4.1 Galactic Distribution

The distribution in galactic coordinates of the color selected sample of embedded O star candidates is shown in Figure 4. As expected, the sources are tightly confined to the Galactic plane and are found primarily in the first and fourth quadrants.

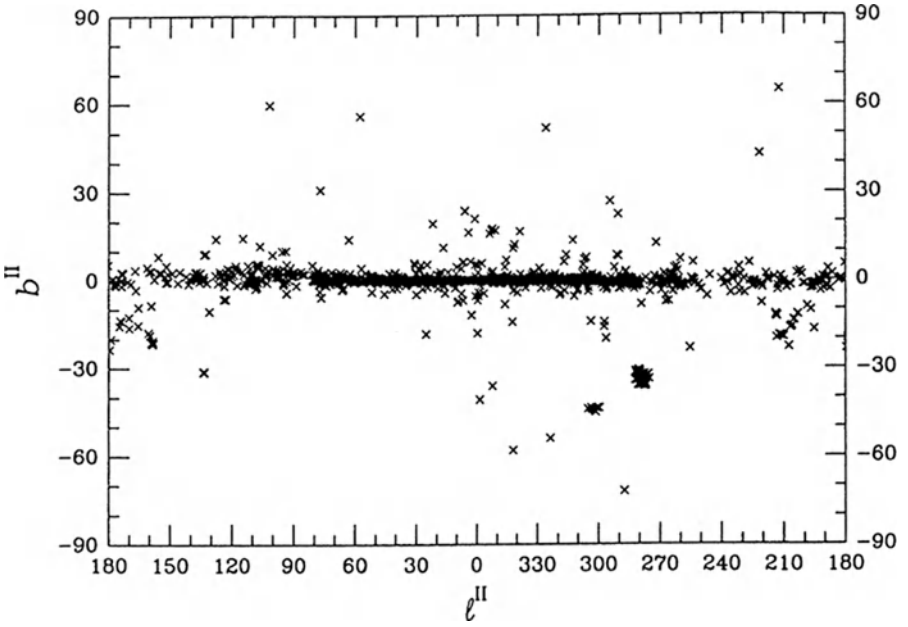

Fig.4 The galactic distribution of the 1708 embedded OB star candidates selected by color from the PSC.

A histogram of the distribution with galactic latitude is plotted in Figure 5.
The distribution is centered at latitude 0° to within a single bin (less than 0.2°) and it falls off exponentially away from the plane with an angular scale height of 0.6°±0.05° (the dashed curve in Fig.5). At a distance of 8.5kpc, this angular scale height corresponds to a z distance of ~90pc, in good agreement with the scale heights of OB stars and molecular clouds.

The distribution of sources shown in Fig.4 is very similar to that of the molecular clouds mapped by Dame et al. (1987). Essentially every major molecular cloud complex

identified in their composite galactic plane map is also identifiable in Fig.4.

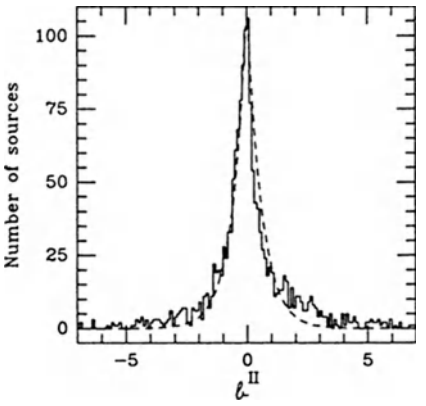

Fig.5 A histogram of the galactic latitudes of the embedded OB star candidates. The dashed line is the function $112e^{|b|/0.6°}$.

This illustrates that the selected objects are both a galactic plane population and associated with molecular clouds, as expected. Both the gaps and the concentrations of the CO emission in the galactic plane also appear as gaps and concentrations in Fig.4. The LMC and SMC (l,b≈280°,−35° and ≈300°, −45°) are also apparent in Fig.4. We find 58 objects in the LMC and 13 in the SMC; excluding these, the high galactic latitude sources (|b|>15°) constitute a very small fraction of the total sample. There are only 18 objects with b>15° and 37 with b<−15° (i.e. ~3% of the sources associated with the galactic plane.

4.2 The Fraction of Massive Stars Embedded in Molecular Clouds

We can roughly estimate the fraction of O stars that are still embedded in their natal molecular clouds by comparing the number of visible O stars in the solar neighboorhood with the color selected sample if we assume that: 1) most of the OB star candidates are O stars because the IRAS sample is sensitivity limited; 2) they are uniformly distributed over the galactic disk; and, 3) the disk has a radius of 15kpc. Monte Carlo simulations were calculated for several possible distributions of 1640 sources and compared with the observed distribution in the (l,b) plane; a uniform distribution in the galactic plane with a vertical scale height of ~100pc produced the best results of any of the models tested. According to Conti et al. (1983), there are 436 O stars within 2.5kpc of the Sun that are not embedded in or hidden behind molecular clouds. We find about 1640 embedded OB star candidates in the Galaxy from the IRAS color selected sample (excluding those in the SMC and LMC). Under the above assumptions, one would expect to find about 45 O stars embedded in molecular clouds (and uncounted by Conti et al.) within 2.5kpc of the Sun. Thus, within 2.5kpc of the Sun, about 10% of all O stars are embedded in molecular clouds. Due to the probable incompleteness of our sample, this fraction could be as high as 20% but probably not higher. This implies that an O star typically spends between 10 and 20% of its main sequence lifetime embedded in its natal molecular cloud; we will assume 15% in the following.

4.3 The Current Rate of O Star Formation

The rate of O star formation in the galactic disk can be estimated from the ratio of the total number of O stars in the disk to the average time they spend embedded in their natal molecular cloud. Since the main sequence lifetime depends on spectral type, we must estimate the typical spectral type of the stars in our sample. using the WC sample as a guide, the average luminosity is equivalent to a single O5 ZAMS star, however, if the luminosity is produced by a cluster of stars, then the most massive star would be about an O7.5 ZAMS star (Miller and Scalo 1979). Adopting the cluster model, we find a current O star formation rate $>3x10^{-3}$ O stars/year. If an O5 ZAMS star were used, the rate would be $\sim 7x10^{-3}$ O stars/yr. These are lower limits because our sample is incomplete, perhaps by as much as a factor of two.

A typical cluster of stars with a Miller-Scalo inital mass function and an upper mass of $25M_{\odot}$ (O7.5 ZAMS) will have ~6 O stars and a total of ~37 stars with mass $>8M_{\odot}$. Assuming that all stars $>8M_{\odot}$ eventually explode as supernovae, and taking into account the different lifetimes of the stars in the cluster, the expected supernovae rate would be about one every 25yr.

References

Conti, P.S., Garmany, C.D., de Loore, C., Vanbeveren, D.: 1983, Ap.J. bf 274, 302

Dame et al.: 1987, Ap.J. 322, 706

Miller, G.E., Scalo, J.M.: 1979, Ap.J. Suppl. bf 41, 513

Wood, D.O.S., Churchwell, E.: 1989, Ap.J. Suppl. in press (WC)

Magnetic Fields in Interstellar Water Masers

D. Fiebig and R. Güsten

Summary

We report the first detection of Zeeman splitting in the $(6_{16}-5_{23})$ rotational transition of interstellar H_2O masers. The measurements of Stokes parameter V and I spectra (circular polarization) have been performed at the MPIfR 100-m telescope. Depending on the hyperfine transition that is actually masing, we derive typical magnetic field strengths of $B_{\|}\sim 40\,\mathrm{mG}$ (F=7–6) and $\sim 60\,\mathrm{mG}$ (F=6–5). The relation between magnetic field strength and gas density is discussed.

Introduction

Interstellar magnetic fields have been searched for by various techniques. In order to derive the *strength* of the magnetic field, only via the Zeeman splitting of atomic (HI) and molecular (OH, SiO) lines the field strength in higher density neutral gas phases can be derived *directly* (though often only the field component along the line of sight is inferred).

Magnetic field measurements in the diffuse interstellar phase ($n<100\,\mathrm{cm^{-3}}$) revealed field strengths of the order of some μG (e.g. Troland and Heiles 1982). Recent observations of dark clouds ($n\sim 10^3\,\mathrm{cm^{-3}}$) detected fields of some $10\,\mu$G (Goodman et al., 1988, this conference) and measurements of dense cloud cores ($n\sim 10^5\,\mathrm{cm^{-3}}$) yielded upper limits of $<70\,\mu$G (Fiebig and Güsten, 1988b). The highest magnetic field strengths reported so far, which are on the order of some mG (e.g. Gaume and Mutel, 1987), have been found in OH maser regions ($n\sim 10^{7-8}\,\mathrm{cm^{-3}}$).

Provided a correlation between the magnetic field strength and the local gas density holds, field strengths on the order of some 10 mG are expected in the high density H_2O maser clumps ($n\sim 10^{9-11}\,\mathrm{cm^{-3}}$). However, the Zeeman line splitting of the non-paramagnetic H_2O molecule is extremely small (a few 10 Hz at most) and no successful H_2O Zeeman experiment has been reported up to now.

Theoretical Background

Maser emission arises from one (or several) of the six hyperfine components of the H_2O $(6_{16}-5_{23})$ rotational transition (Fig. 1a). For the non-paramagnetic H_2O molecule, the Zeeman splitting of the energy hyperfine levels is mainly due to the interaction of the molecule's *nuclear* magnetic moment with the external magnetic field (B) and hence is weaker by $\sim 10^3$ than that for radicals like OH or CCS. In the weak field limit, the splitting energy is given by (Gordy and Cook, 1970):

$$\Delta E_Z = -(\alpha_J g_J + \alpha_I g_I)\mu_N M_F B \tag{1}$$

with

$$\alpha_J = \frac{J(J+1)+F(F+1)-I(I+1)}{2F(F+1)} \tag{2}$$

$$\alpha_I = \frac{F(F+1)+I(I+1)-J(J+1)}{2F(F+1)} \tag{3}$$

I(=1) is the nuclear spin, μ_N the nuclear magneton and M_F the magnetic quantum number; $g_I = 5.585$ and the g_J factors $g_6 = 0.6565$ and $g_5 = 0.6959$ are from Kukolich (1969). For magnetic field strengths of the order of 100 mG, the application of the weak field limit is justified, because the Zeeman splitting energy $\Delta E_Z\,(\sim 10^{-24}\,\mathrm{erg})$ is small compared to the hyperfine interaction energy $(\sim 10^{-21}\,\mathrm{erg})$.

Due to the selection rules for allowed dipole transitions ($\Delta F = 0,\pm1$; $\Delta M_F = 0,\pm1$) each hyperfine line is split into three groups of lines, each having definite polarization characteristics. For a typical maser line ($\Delta v_L \sim 0.5\,\mathrm{kms}^{-1} \hat{=} 37\,\mathrm{kHz}$) the observed right(RHC)- and left(LHC)-handed circularly polarized spectra, corresponding to the $\sigma^{\pm}$ line components, will therefore be only slightly shifted against each other, $\Delta\nu_Z \sim 10^{-3}...10^{-4}\,\Delta\nu_L$.

The difference spectrum $T_B(\mathrm{LHC}) - T_B(\mathrm{RHC})$, which is a Stokes parameter V spectrum, will show up as a sine shaped residue, representing the first derivative of the total power spectrum (Stokes parameter I). The peak temperature of the V spectrum $T_B(\mathrm{V})$ is a sensitive measure of the magnetic field strength. In order to quantify this dependence we constructed synthetic V spectra by convolving the basic Zeeman pattern of Fig. 1b with Gaussian profiles of different half power widths. The results of these calculations are shown in Fig. 2. The field direction is assumed to be parallel to the line of sight.

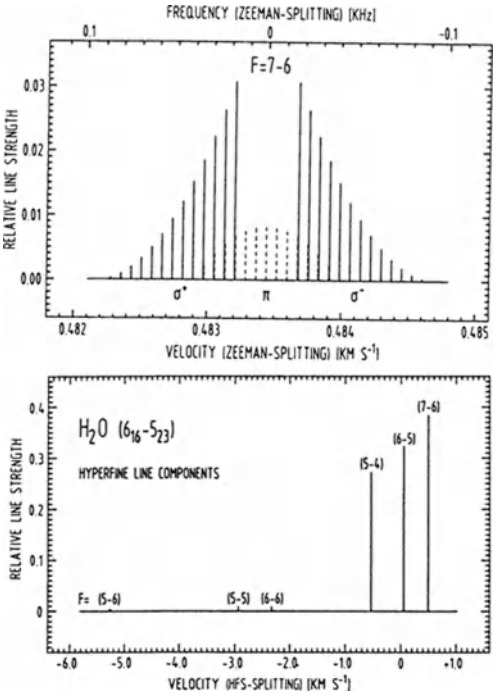

Fig. 1a (lower panel) Hyperfine pattern of the H_2O ($6_{16} - 5_{23}$) rotational transition. 1b (upper panel) Zeeman pattern of the F=7-6 hyperfine component for an external field of 50 mG.

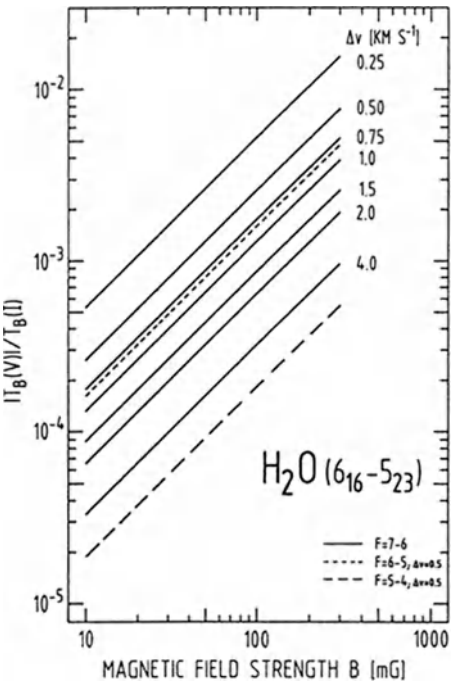

Fig. 2 Peak Amplitude of normalized V spectra ($T_B(\mathrm{V})/T_B(\mathrm{I})$), versus magnetic field strength $B = B_{\parallel}$, for different maser line widths. For reference, results for other major hyperfines ($\Delta v = 0.5\,\mathrm{kms}^{-1}$) are given.

Instrumentation and Observations

The observations were carried out with the MPIfR 100-m-telescope. Its beam width was 41″ at 22.235 GHz. The K-band receiver was equipped with a stepping septum polarizer to allow for circular polarization measurements (Davis et al., 1967; Chen and Tsandoulas, 1973). Careful alignment of the feed horn to the optical axis of the telescope reduced beam squint to $\sim 1''$. Because of the properties of the polarizer it was not possible to measure also the Stokes parameters Q and U. However, in order to verify the purity of the incoming radiation, the receiver box was

rotated in steps of 90° during subsequent measurements. Spurious, linearly polarized signals in the V spectra showed up by reversing the typical V spectrum profile.

Results

We surveyed 34 galactic interstellar H_2O masers and selected those 10 sources that revealed strong (> 200 Jy) and narrow ($< 1\,\mathrm{kms}^{-1}$) line emission with least possible blending between adjacent velocity components. Fig. 3 shows the I and V spectra for W3(2), Orion-KL and S140; the derived magnetic field strengths are -43 mG, -38 mG and $+17$ mG, respectively.

Due to the wide velocity coverage and high luminosity of the W49N masers, good quality V spectra for in total 9 individual velocity features were obtained for this source (4 upper limits). Fig. 4 shows the full I spectrum of W49N and the field strengths derived for the velocity features indicated.

Note, that the numbers quoted depend on the choice of the hyperfine component assumed to be masing. All results mentioned refer to the F=7–6 transition.

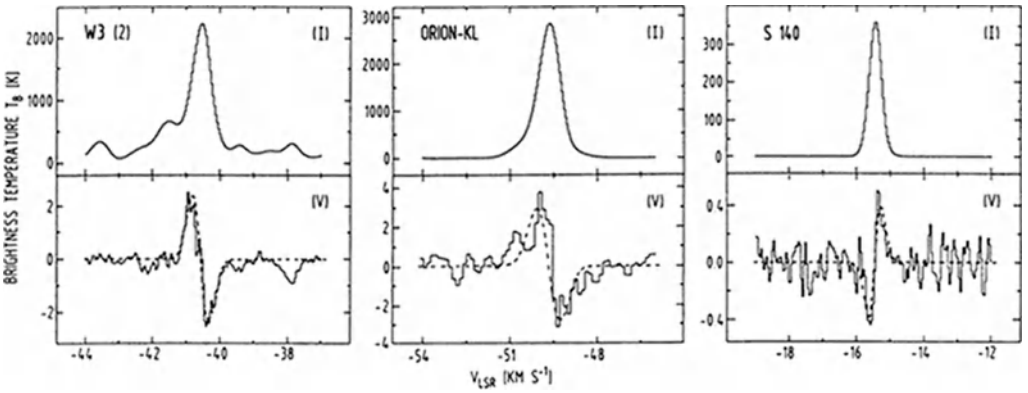

Fig. 3 Total power (I) and difference (V) spectra of three maser sources. Fits of synthetic V spectra to the main (Gaussian) velocity component are superimposed.

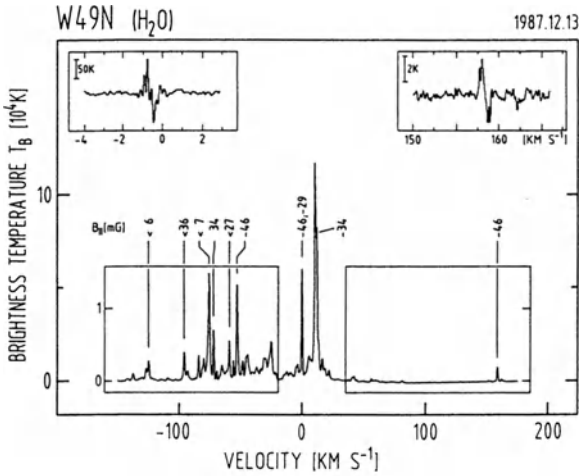

Fig. 4 Composite diagram of the W49N H_2O maser source, showing the magnetic field strengths inferred for individual velocity features. For two of the maser clumps, (at $v_{LSR} \sim -0.6\,\mathrm{kms}^{-1}$ and $+158.3\,\mathrm{kms}^{-1}$) difference spectra are inserted.

Discussion

The relation between magnetic field strength and gas density for different types of interstellar sources as found by observations is summarized in Fig. 5. At first glance this seems to be in nice agreement with theoretical calculations, yielding $B \sim n^{\kappa}$, $\kappa = 0.5$. This might suggest that the field remains coupled to the gas even at (exotic) densities of $\sim 10^{10}\,\mathrm{cm}^{-3}$. But some points of caution are to be considered.

First, while during the rather short lived maser phenomenon ($\tau_m \sim 10^{7-8}\,\mathrm{s}$) the field seems frozen to the gas, this need not be the case for similar high density phases during the late star formation process. At densities $n \sim 10^{10}\,\mathrm{cm}^{-3}$, τ_m is shorter than the adiabatic diffusion time scale $\tau_{ad} \sim 10^{9}\,\mathrm{s}$, but during cloud core contraction, ambipolar diffusion may become important at much lower densities (Mouschovias et al., 1985; Nakano, 1985).

Second, the sample of Fig. 5 is inhomogeneous, probing different and not obviously evolutionary related phases of the interstellar medium. Theoretical predictions on the other hand refer to self-gravitating clouds only - a condition that is definitely not satisfied in H_2O maser clumps.

In order to strengthen our conclusions, a more complete sample of H_2O maser sources and complementary interferometric observations need to be obtained.

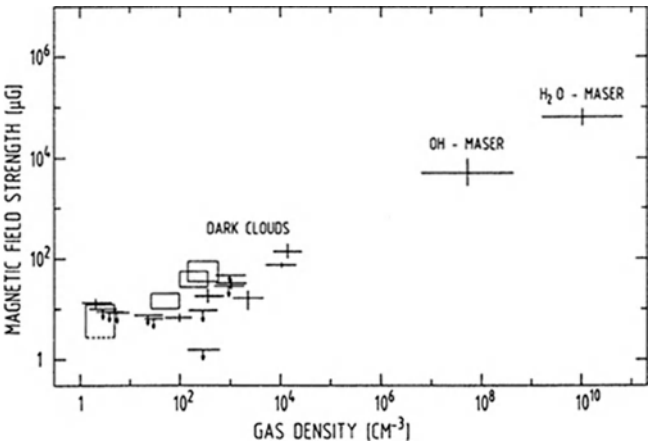

Fig. 5 Magnetic field strength versus gas density, as compiled by Troland and Heiles (1986) for diffuse and dark clouds and Myers and Goodman (1987) for OH masers. The cross indicating H_2O masers refers to B_{max} from Fiebig and Güsten (1988a).

References

Chen, M.H., Tsandoulas, G.N.: 1973, IEEE *Trans. Ant. Prop.*, **21**, 389

Davis, D., Digiondomenico, O.J., Kempic, J.A.: 1967, G-AP Symp. *Dig.*, p.26

Fiebig, D., Güsten, R.: 1988a, *Astron. Astrophys.*, in press

Fiebig, D., Güsten, R.: 1988b, *Astron. Astrophys.*, in preparation

Gaume, R.A., Mutel, R.L.: 1987, *Astrophys. J. Suppl.*, **65**, 193

Goodman, A.A., Crutcher, R.M., Heiles, C., Myers, P.C., Troland, T.H.,: 1988, *Astrophys. J.*, Preprint

Gordy, W., Cook, R.L.: 1970, in *Microwave Molecular Spectra*, Interscience Publ.

Kukolich, S.G.: 1969, *J. Chem. Phys.*, **50**, 3751

Mouschovias, T.Ch., Paleologou, E.V., Fiedler, R.A.: 1985, *Astrophys. J.* **291**, 772

Myers, P.C., Goodman, A.A.: 1988, *Astrophys. J.*, **326**, L27

Nakano, T.: 1985, *Publ. Astron. Soc. Japan*, **37**, 69

Troland, T.H., Heiles, C.: 1982, *Astrophys. J.* **252**, 179

Troland, T.H., Heiles, C.: 1986, *Astrophys. J.* **301**, 339

IRAS Sources beyond the Solar Circle[1]

J. G. A. Wouterloot and J. Brand
Max-Planck-Institut für Radioastronomie, Bonn

At large galactocentric distances (R), CO surveys are very incomplete due to the small number of clouds and their small angular sizes. IRAS sources with colours of star forming regions, selected according to criteria by Wouterloot and Walmsley (1986), can be used as a tracer of molecular clouds. Because the star forming activity per unit mass of H_2 is similar at all locations in the outer Galaxy ($R > 8.5$ kpc) (Wouterloot *et al.*, 1988; Kutner, 1988), the distribution of these sources will be that of H_2. Using the 30 m IRAM telescope and the 15 m SEST, we searched for CO $(1-0)$ emission in the direction of 1224 sources located in the interval $85° < \ell < 280°$ and $-10° < b < 10°$ and detected 1004 (82%) of them. A velocity coverage of 208 km/s (IRAM) or 220 km/s (SEST) was used, with resolutions of 0.20 km/s and 0.11 km/s respectively. Typical T_A^*(rms) values were 0.7 K (IRAM) and 0.3 K (SEST). The distribution in ℓ and b of the non-detections is smooth, suggesting that these IRAS sources are predominantly extra-galactic. Forty-nine IRAS sources in our sample are actually identified as galaxies in the point source catalogue. Twenty-three IRAS sources are identified as planetary nebulae, about half of which were detected. Some of these may actually be compact HII regions if only because of their high CO temperatures, which are atypical for planetary nebulae.

To associate CO emission at a particular velocity with the IRAS source, we made use of the line parameters: For the IRAS sources with only one emission line, we always assumed it was associated. In the case of multiple lines, we assumed the one with the highest T_A^* to be associated, unless there was emission at a very large absolute velocity, because in the outer Galaxy (especially at locations well away from the plane) the chance superposition of a background cloud is very unlikely.

We calculated a kinematic distance for each CO emission component using the rotation curve derived by Brand (1986) in slightly adjusted form: $\Theta/220 = (R/8.5)^{0.0302}$. This curve results in $\Theta(20\text{ kpc}) = 227.3$ km/s. The distances of the emission components associated with the IRAS sources in combination with the IRAS fluxes give L_{IR}. From the distribution of luminosities over distances of all sources, we conclude that sources with $L_{IR} > 2300\ L_\odot$ form a complete sample.

Figure 1 shows the distribution of the CO clouds projected on the Galactic plane. Excluding the objects inside the cone around the anticenter direction where kinematic distances are uncertain, we see that: (1) there are no clouds further away than $R = 20$ kpc, and (2) because each cross is associated with an IRAS source, this implies there is no star formation beyond that distance either. If there were any more distant bright IRAS sources, we would have detected them.

[1] Partly based on observations collected at ESO, La Silla, Chile

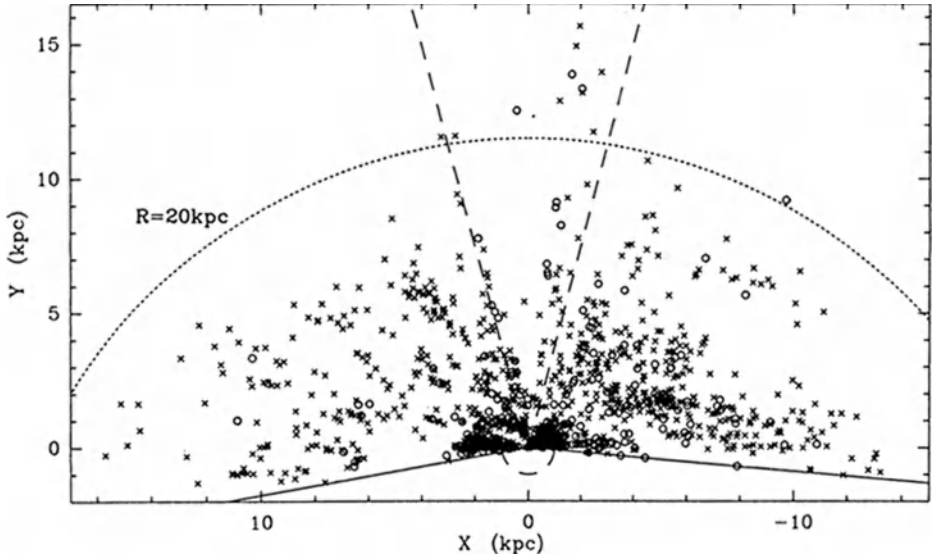

Fig. 1. Distribution of CO emission associated with the IRAS sources in our sample (×) and other spectral components (o) projected on the Galactic plane. The Sun is at (0, 0), the Galactic center at (0, 8.5). The longitude limits of our sample are indicated by the drawn lines; the dashed lines mark a $\pm 15°$ cone around $\ell = 180°$ where kinematic distances are very uncertain and our data are incomplete. Objects inside the dashed circle with a radius of 1 kpc around the Sun have small radial velocities and therefore uncertain kinematic distances.

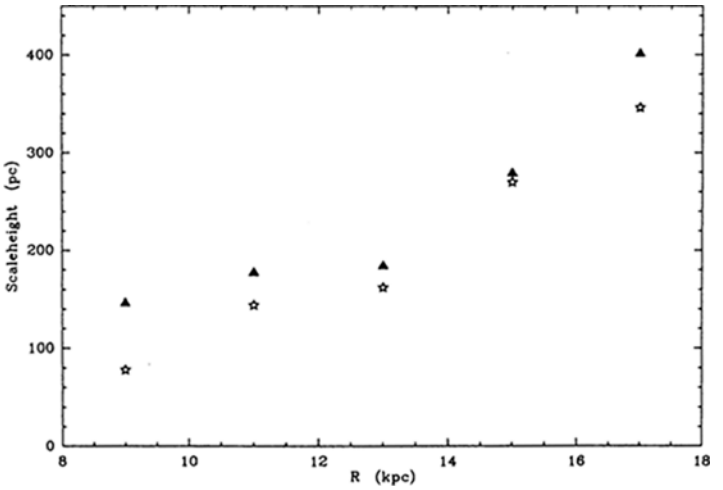

Fig. 2. Comparison of the scale heights of CO (stars) and HI (triangles) as a function of R. HI data were derived from Burton and te Lintel Hekkert (pers. comm.).

There is a higher density of points in the second quadrant (around (−4, 2)) than in the third. These are objects in the Perseus arm, for which there is no clear equivalent in the south. There is a remarkable lack of sources just behind the Perseus arm, while several clouds lie further beyond it. This area cannot be studied by optical methods. Similarly, the "fingers" (areas of low foreground extinction that allow one to see HII regions out to large distances) are not present in this plot: there are distant objects at all longitudes.

We have compared the z distribution of IRAS sources/CO clouds in intervals in R, as a function of galactocentric azimuth with HI data by Burton and te Lintel Hekkart (pers. communication). The warp of the Galactic plane is confirmed by the tilt of the molecular layer, which increases with R by the same amount as that of the HI plane. From the scatter of the z values of all CO components around their mean, we derived the scale height as a function of R shown in Fig. 2. The flaring of the gas layer (both atomic and molecular) is clearly visible. The CO scale height increases from 80 pc at $R = 9$ kpc to 350 pc at $R = 17$ kpc; while at $R = 9$ kpc the HI disk is about twice as thick as the CO layer, the two are almost of equal thickness at $R = 13$ kpc and beyond.

For $R < 10.5$ kpc and $R > 13.5$ kpc, the surface density of IRAS sources with $L_{IR} > 2300\ L_\odot$ as a function of R is equal for $85° < \ell < 165°$ (North) and $195° < \ell < 280°$ (South) (see Fig. 3). In the interval 10.5 kpc $< R <$ 13.5 kpc, the Perseus arm objects cause a peak in the distribution of the northern sources. Both North and South have a relative lack of sources around 10 kpc, which in the north may be attributed to the inter-arm region (between the local and the Perseus arms). For $R > 13.5$ kpc the surface density of sources in both hemispheres decreases, but much slower than that derived by Sanders *et al.* (1984) because their CO survey is incomplete.

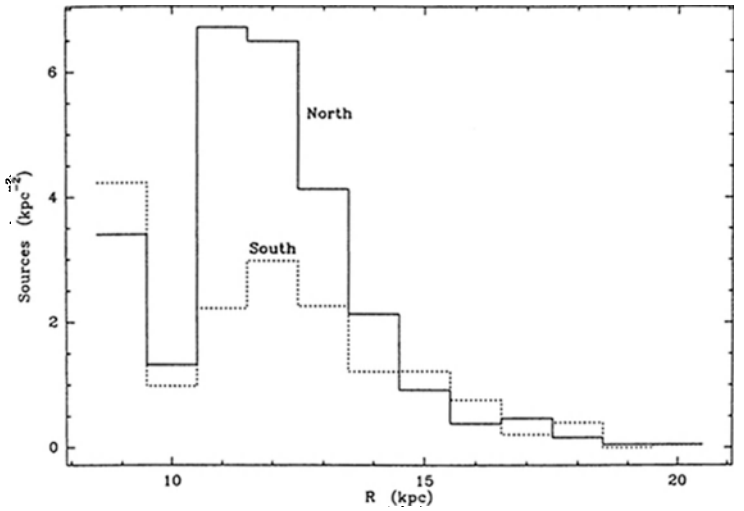

Fig. 3. Surface density of IRAS sources with $L_{IR} > 2300\ L_\odot$ for $85° < \ell < 165°$ (North), and $195° < \ell < 280°$ (South).

Using the HI data by Burton and te Lintel Hekkert, we find that between $R = 10$ kpc and 15 kpc there is no strong decrease in the ratio $\sigma(H_2)/\sigma(HI)$ if the distribution of IRAS sources is taken to be that of the molecular material.

References Brand, J.: 1986, Ph. D. thesis, University of Leiden
Kutner, M. L,: 1988, in: *The Outer Galaxy,* (eds. L. Blitz, J. Lockman; Springer-Verlag), p. 198
Sanders, D. B., Solomon, P. M., Scoville, N. Z.: 1984, *Astrophys. J.,* **276**, 182
Wouterloot, J. G. A., Brand, J., Henkel, C.: 1988, *Astron. Astrophys.,* **191**, 323
Wouterloot, J. G. A., Walmsley, C. M.: 1986, *Astron. Astrophys.,* **168**, 237

The Prevalence of Neutral Gas in Massive Post-Main-Sequence Nebulae

J.P. Phillips
Physics Department, Queen Mary College,
Mile End Road, London E1 4NS, England

A. Mampaso
Instituto de Astrofisica de Canarias
La Laguna, Tenerife, Spain

1. Introduction

Of the large number of planetary nebulae so far investigated in the rotational transitions CO, the maser transitions of OH, the quadrupole components of H_2, and the 21cm hyperfine transition of HI, only a relatively small fraction appear to be to be associated with neutral gas (cf. Schneider et al, 1987; Knapp, 1987; Payne, Phillips, and Terzian, 1988; and Zuckerman and Gatley, 1988). Of those that *have* been detected in CO, a total of some 10 sources to date, a very large proportion appear to be characterised by extremely high central star temperatures, anamolous He, N, and C abundances, and bipolar morphologies; features which also define the sub-category of type I post-main-sequence (PMS) nebulae (cf. Peimbert and Torres-Peimbert, 1982).

Such sources are believed to derive from stellar progenitors having a broad range of masses $M_*/M_\odot < 10$, and concomitantly large shell ejection masses of order $< 9\ M_\odot$. Similarly, it is also apparant that many of these sources are in possession of high velocity, and high mass-loss rate stellar winds. Superficially therefore, one might imagine such nebulae to represent prime candidates for the detection of neutral (and shocked) material in post-main-sequence sources.

We report, in the following, the results of a CO J=2→1 survey of nine type I nebulae with the 12 metre NRAO antenna at Kitt Peak:

TABLE 1

Source	$T_r^*(K)$ †3	V_{lsr}(km.sec^{-1})
NGC 2346	.41±.03	3.5
M 2-9	<.12	102.7
NGC 6302	.75±.24	-46.0 †2
HB 5	†1	-17.9
NGC 6537	<.20	-4.1
NGC 6629	<.36	26.6
NGC 6751	<.22	-24.8
NGC 6853	<.21	-32.7
NGC 7008	<.10	-60.9

†1 Peak temperature ambiguous - see discussion; †2 The central velocity of the HII region is $V_{lsr} \sim -31.4$ km sec^{-1}; †3 Upper limits correspond to $2\sigma_{rms}$.

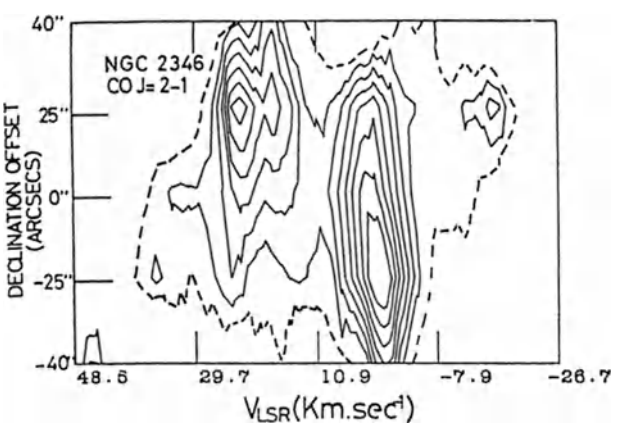

Figure 1 Spatial-velocity map of NGC 2346 in CO J=2→1. Contours intervals set at .05K, lowest contour at T_r^* ~ 0.05K.

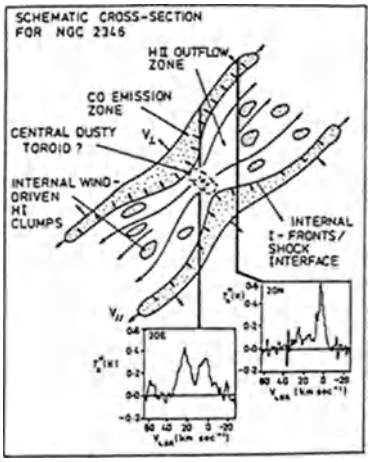

Figure 2 Schematic cross-section of NGC 2346, together with representative CO J=2→1 spectra.

2. Results

The results of our survey may be briefly summarised as follows:

i) The larger proportion of our sources (~ 77 %) are found to contain no emission with $T_r^* > 0.1$ K (table 1), whilst the complete sample of type I nebulae measured to date, some 14 sources in total, are found to be associated with emission in no more than ~ 20 % of cases. Whilst this proportion appears overall to be extremely low - and less perhaps than might have been expected - it appears neverthless to be considerably greater than for the broader swathe of PMS sources.

ii) At least two, and possibly three of the nebulae are associated with CO J=2→1 emission:

a) NGC 2346 displays well defined core splitting of the CO profile, implying an overall expansion velocity ~ 23 km sec^{-1}, with evidence for a much broader plateau feature extending over a range ~ 57 km sec^{-1} (fig 1); features which appear to closely mimic the low excitation optical line properties measured by Walsh (1983). Spatial-velocity mapping through the core reveals that the higher velocity component predominates to the north, whilst the lower velocity component is preferentially enhanced to the south; an apparant reverse of the trend displayed by the higher velocity plateau feature.

The results for the primary expansion component are readily explained if we are observing a tilted collar of neutral gas (see fig 2), and appreciable levels of emission close to the central star, where the optical structure also displays a sharply defined waist; although the apparantly differing behaviour of the plateau feature is less readily explicable. An LVG analysis of our J=2→1 results, together with CO J=1→0 spectroscopy taken with a similar beamsize (Bachiller et al, 1988), also

suggests that the outflow components are associated with a range of densities $10^{3.5} \rightarrow >10^4$ cm^{-3}, and concomitantly large velocity gradients $dv/dr > 500$ km $sec^{-1} pc^{-1}$. Under these circumstances, it is tempting to believe that much of the CO emission may derive from a similar shock zone to that occupied by H_2 quadrupole emission (Zuckerman and Gatley, 1988).

b) Our observations of NGC 6302 sugeest a line strength of ~ 2.7 K, some three times greater than for J=1→0 spectroscopy with a larger beam (Zuckerman and Dyck, 1986). We believe much of this disparity is explainable if the core emission source is of a size comparable or less than that of the present beam (B = 30 arcsecs). Although the velocity of this emission is of order V_{lsr} ~ -46 km sec^{-1}, some 15 km sec^{-1} different from that of the central HII region, there is clear evidence from recent OH measures that it must be directly associated with the source (Payne, Phillips, and Terzian, 1988).

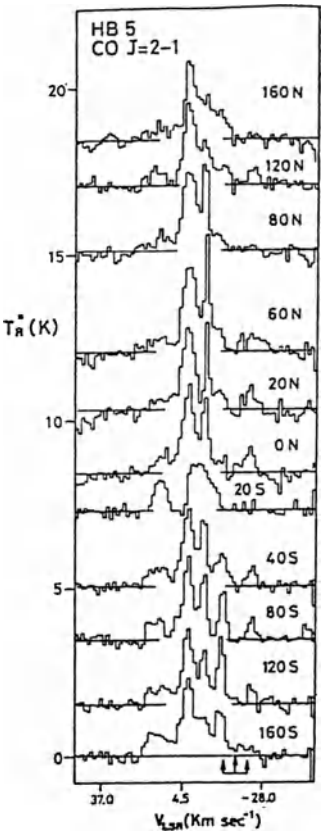

Fig 3 N-S CO J=2→1 traverse through HB 5.

c) The spectroscopy of HB 5 reveals a broadly distributed regime of complex kinematic activity, with evidence for at least five seperate kinematic components, and rapid variability over small projected distances. Whist the extent of this emission (see fig 3) suggests that it may not directly derive from the central star, we believe there is a prima facie case for supposing the high velocity HII region to be interacting with enveloping ambient gas.

3. Discussion

It appears from the above discussion that two, and possibly three of the nebulae investigated here are associated with significant levels of CO J=2→1 emission. Given however the large envelope masses that these sources are presumed to possess, it is pertinent to ask why all such nebulae are not detected. We review below the various possibilities:

1) The molecular envelopes are dissociated. Where this arises because of the central star radiation field, then we find dissociation periods to be substantially in excess of 10^3 years; greater, in most of our cases, than the probable evolutionary lifetime. Alternatively, Glassgold and Huggins (1983) have noted that for progenitor temperatures $T_* > 2500$ K, the outflow envelope will again be largely dissociated. Under these circumstances, however, we might expect to observe correspondingly large amounts of 21 cm HI emission or absorption; a feature which Schneider et al (1987) have recently demonstrated to be absent down to extremely low mass limits.

2) The nebulae are completely ionised by the central star radiation field. Given the presumed envelope masses of these sources, and probable evolutionary lifetimes, it would be rather surprising to encounter such a singular absence of neutral material. Spergel et al (1983), for instance, find that the progression of ionisation fronts is strongly determined by the ~ t^{-1} decline in central star ionising flux; an analysis which yields ionisation periods in excess of 2.10^4 yrs for a progenitor mass-loss rate > 10^{-4} $M_\odot$ yr^{-1}.

3) The neutral zone is extremely heterogeneous and clumped, leading to high levels of beam dilution and correspondingly reduced values of antenna temperature. This possibility cannot be entirely dismissed, although we note that given optically thick CO emission from clumps with temperature ~ 50 K, then an extraordinarily low value of dilution W < 10^{-3} would be required to explain the upper limit temperatures in table 1, implying corresponding densities $n(H_2) > 10^7$ cm^{-3} (for an assumed a nebular radius R_o = 0.1pc, mass $M(H_2)$ = 0.3 $M_\odot$, and clump size < $0.1R_o$).

Under these circumstances, therefore, we are inclined to believe that whilst all of these mechanisms may play at least some role in quenching the observed CO temperatures, a more important contribution may arise from the large HI velocity gradients expected for these sources (> 10^2 km $sec^{-1}pc^{-1}$) - gradients that would lead to an appreciable reduction in τ(CO), and correspondingly reduced values of T_r^*. Similarly, such high gradients, when combined with large (post-shock) densities will be expected to lead to appreciably enhanced gas cooling rates, and low gas kinetic (and CO excitation) temperatures. It follows from this, therefore, that whilst the present J=2→1 CO survey has been relatively unsuccessful, further investigations to higher sensitivities may result in many more detections.

References

Bachiller, R., Gomez-Gonzalez, J., Bujarrabal, V., and Martin-Pintado, J., 1988. Astron. Astrophys. (submitted)

Knapp, G.R., 1987. in Late Stages of Stellar Evolution, ed. S. Kwok and S.R. Pottasch, D. Reidel Publishing Co., Dordrecht, Holland

Payne, H.E., Phillips, J.A., and Terzian, Y., 1988. Astrophys. J. 326, 368

Peimbert, M., and Torres-Peimbert, S., 1982. I.A.U. Symposium No 103, ed D.R. Flower, D. Reidel Publishing Co., Dordrecht, Holland

Schneider, S.E., Silvergate, P.R., Altschuler, D.R., and Giovanardi, C., 1987. Astrophys. J. 314, 572

Spergel, D.N., Giuliani, J.L., and Knapp, G.R., 1983. Astrophys. J. 275, 330

Walsh, J.R., 1983. Mon. Not. Roy. Astr. Soc. 202, 303

Zuckerman, B., and Dyck, H.M., 1986. Astrophys. J. 311, 345

Zuckerman, B., and Gatley, I., 1988. Astrophys. J. 324, 501

DETECTION OF FAR-INFRARED ^{13}CO LINE EMISSION

A. Poglitsch[1], R. Genzel[1], G.Stacey[2]
[1]Max-Planck-Institut für Physik und Astrophysik, D8046 Garching
[2]University of California, Berkeley CA 94720

SUMMARY. The first detection of far-infrared ^{13}CO line emission toward the core of Orion-KL is reported. About 10 to 30 $M_\odot$ of dense and warm ($T \geq 200K$) gas are required for the 151μm J=18->17 ^{13}CO line flux.

OBSERVATIONS AND RESULTS

The data were taken on the NASA Kuiper Airborne Observatory in January 1988 with the UCB tandem Fabry-Perot spectrometer. A 3-element linear array of stressed Ge:Ga detectors with a spatial resolution of 55" was employed. The spectral resolution was 32 km s^{-1} FWHM for the central detector. In addition to the ^{13}CO J=18->17 transition at 151.4315 μm, we also observed the nearby ^{12}CO J=17->16 line at 153.2669 μm.

The results for the central detector are shown in Figure 1. The J=18->17 ^{13}CO line flux is $2.3\pm0.7 \times 10^{-18}$ W cm^{-2}. The ratio of J=17->16 ^{12}CO to J=18->17 ^{13}CO line fluxes is 37±8. The ^{13}CO flux can be used directly for an estimate of the mass of warm molecular gas at the core of Orion-KL. For optically thin emission and a $^{13}CO/H_2$ abundance ratio

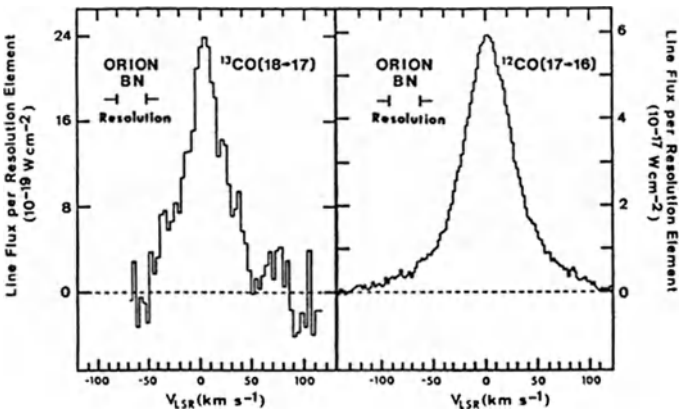

Fig.1. Spectra of the 151 μm J=18-17 transition of ^{13}CO (left) and the 153 μm J=17-16 transition of ^{12}CO (right) towards the position of the BN-object in Orion. Both observations employed the same spatial (55" FWHM) and spectral (32 km/s FWHM) resolutions. Instrumental lineshape: modified Lorentzian.

of 10^{-6}, total gas masses of 5 $M_\odot$ at a gas temperature of 500K and 50 $M_\odot$ at 200K are required to account for the ^{13}CO flux. Significant ^{13}CO emission was also detected in the 55" north-west off-center detector.

The ^{13}CO profile is narrower than the ^{12}CO profile. The intrinsic width of the ^{13}CO line is $\leq$ 17km s^{-1}, while the ^{12}CO line has a width near 27km s^{-1} (FWHM) as determined by MEM deconvolution.

DISCUSSION

Our measurements show that the ^{13}CO and ^{12}CO far-infrared lines have different line profiles and that the ^{13}CO line flux is significantly larger than expected for a single, optically thin ^{12}CO far-infrared emission component assuming the standard abundance ratio.

For quantitative evaluation of possible interpretations we computed level populations and line intensities as function of density, temperature, and column density in an escape probability radiative transfer formalism. We assumed a CO/H_2 abundance ratio of 10^{-4} (Watson et al. 1985) and a $^{12}CO/^{13}CO$ abundance ratio of 90 (Scoville et al. 1982).

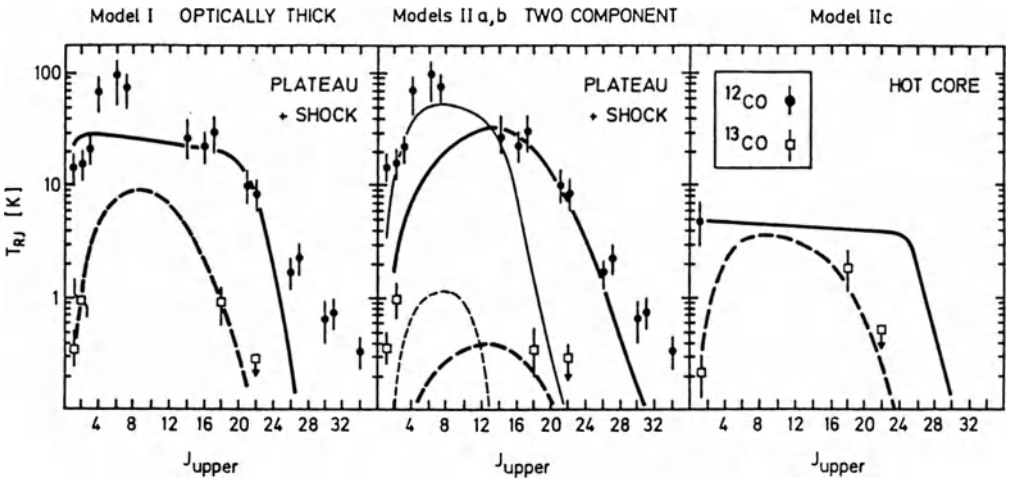

Fig.2. Representative models of the mm, submm, and far-infrared high-velocity CO emission in Orion-KL. All measurements are expressed in terms of Rayleigh-Jeans brightness temperatures at line center and are converted to a common beam size (1' FWHM). ^{12}CO data are given as filled circles, ^{13}CO data as open squares. The model calculations are represented by continuous curves for ^{12}CO and by dashed curves for ^{13}CO, respectively. The left panel shows the "optically thick" model (I). The center panel shows the models for plateau (IIa: thin lines) and for shock (IIb: heavy lines). The right panel shows the model for the hot core (IIc).

The first model we considered assumes a single emission component with optically thick ^{12}CO far-infrared lines; it is plotted in Fig.2 as model I together with the CO data points . A Temperature of $\approx$ 200 K and a hydrogen density of $\approx 10^7 cm^{-3}$ in combination with an area filling factor of $\approx$ 0.3 describe the far-infrared measurements adequately. With a CO column density near $5x10^{19} cm^{-2}$ the ^{12}CO lines also have enough optical depth to account for the difference in ^{12}CO and ^{13}CO line width. The model fails, however, to predict the observed submm brightness temperatures.

Model II in Fig.2 is based on three emission components: the high velocity plateau emission (IIa) accounts for the mm and submm ^{12}CO lines; it represents warm gas (T $\approx$ 300K) in the outflow from the infrared cluster. The shock region (IIb) is hot (T $\approx$ 700K) and optically thin gas which accounts for the far-infrared ^{12}CO lines and the high-velocity components of the ^{13}CO line. The hot core (IIc) is a region of high column density but low velocity dispersion which is exhibited by the narrow peak in the ^{13}CO line profile. The ^{12}CO far-infrared emission from this region is optically thick. From the decomposition of the ^{13}CO line in a narrow component (hot core) and a wide component (shock) we infer a hydrogen mass of $\approx$ 10 $M_\odot$ in the hot core and a $^{12}CO/^{13}CO$ abundance ratio of 85 $\pm$ 20, in agreement with the standard value. For the 55" NW position, however, we find a $^{12}CO/^{13}CO$ flux ratio of 50 $\pm$ 20 which is either not consistent with the small size (10") of the hot core, or requires a lower $^{12}CO/^{13}CO$ ratio (cf. Blake et al. 1986). A decomposition of the center position line based on a lower abundance ratio would still be consistent with our data.

We therefore have to check wether the observed flux ratio could be explained by a very low $^{12}CO/^{13}CO$ abundance ratio alone. This, however, seems rather unlikely due to the clear difference in line shape between the two isotopic lines: the narrow peak assigned to the hot core contributes at least 20% of the total line flux; the corresponding hydrogen mass in the hot core should not be less than 25% of the value for the standard abundance ratio.

REFERENCES

Blake, G.A., Sutton, E.C., Masson, C.R., and Phillips, T.G. 1986, Ap.J. Suppl. 60, 357.

Scoville, N.Z., Hall, D.N.B., Kleinmann, S.G., and Ridgway, S.T. 1982, Ap.J. 253, 136.

Watson, D.M., Genzel, R., Townes, C.H., and Storey, J.W.V. 1985, Ap.J. 298, 316.

DEUTERATED WATER IN HOT CORES

C.M. Walmsley, C. Henkel, T. Jacq
Max-Planck-Institut für Radioastronomie, 5300 Bonn 1, F.R.G.

A. Baudry
Observatoire de l'Université de Bordeaux, 33270 Floirac, France

Abstract

We have used the IRAM 30-m and the Effelsberg 100-m telescopes to observe HDO and $H_2{}^{18}O$ in the Orion-KL region and in other hot molecular cores ($T \geq 100$ K). We find that deuterium is enriched by factors of 100-1000 over the interstellar D/H abundance ratio of 10^{-5}. Since the temperature in such sources is too high to explain our results in terms of equilibrium ion-molecule chemistry, we conclude that the chemistry is far from steady-state. One interpretation is that we are observing the constituents of steady-state recently evaporated grain mantles. The deuterium enrichment then reflects the gas temperature in a previous phase of the cloud evolution where the mantles were laid down.

1. HDO is a substitute for Water?

Water is notoriously difficult to observe under normal interstellar medium conditions. The well known water masers form in clumps whose density is orders of magnitude larger than that of normal molecular clouds. The water vapour in our atmosphere prevents us from observing the transitions which one can expect to be excited at the temperatures and densities of the molecular gas. As a consequence, our only direct knowledge of interstellar water is under the highly untypical conditions which prevail in the maser regions. While interesting in themselves, their observation yields no information concerning the molecular cloud water abundance.

On the other hand, theoretical models (see e.g. Brown et al. (1988)) predict that water may have an abundance comparable to that of CO. It is likely to be produced in large quantities in shocked gas and in many circumstances is an important coolant. However, the chemical models are very uncertain and a direct observation of the water abundance is very desirable. Even if the atmosphere were not present, it would be difficult to deduce the water abundance from observations of the water lines themselves since they for the most part should be highly optically thick. One approach to this problem is to observe $H_2{}^{18}O$ (see Jacq et al. 1988) but in this case, one is in practise restricted to a single transition 200 K above ground and the derived water

column densities are consequently very uncertain. It is therefore of great interest to study the deuterated substitution HDO.

Our program using HDO as a tracer for hot water in hot cores has brought some useful results. In the first place, we believe that we have found HDO in Sgr B2, G34.3+0.2, W3(OH) and W51d as well as confirming the result of Olofsson (1984) for W51 main. In all of these except W3(OH), we have been able to observe at least three transitions giving confidence in the identifications. Towards Orion-KL, we have made small maps of the HDO emission with angular resolutions of 12-15 arc sec. and conclude that the HDO emitting region is extremely compact and coincident with the hot core region seen in NH_3 maps. An interesting feature of our results is that in most sources (again the exception is W3(OH)) where we have found HDO with the 30-m, we have also found a feature (see Jacq et al. 1988) in the 203 GHz $H_2{}^{18}O$ line at Kitt Peak. The derived HDO/H_2O ratio (assuming a terrestrial abundance ratio for $H_2{}^{18}O$) is of order 10^{-3} and we conclude that HDO is highly fractionated in the hot molecular clumps where massive star formation is taking place. Moreover, we can assume that the HDO rotation temperature is applicable also to $H_2{}^{18}O$ and hence improve the estimate of water column density and abundance. A more detailed account of these results is being prepared for publication in Astronomy and Astrophysics.

References

Brown, P.D. et al. 1988, Mon. Not. R. Astr. Soc. 231, 409
Jacq, T. et al. 1988, Astr. Ap. 199, L5
Olofsson, H. 1984, Astr. Ap. 134, 36

METSÄHOVI MM - WAVE OBSERVATIONS OF INTERSTELLAR CLOUDS AND SIO MASERS

J. Harju, P. Harjunpää, T. Liljeström, K. Mattila, J. Solasaari and M. Toriseva

Helsinki University Observatory
Tähtitorninmäki, SF-00130 Helsinki, Finland

ABSTRACT. The 13.7 meter radio telescope (see Urpo, 1975) at the Metsähovi Radio Research Station near Helsinki has been used since 1980 for spectral line observations. The first programs were devoted to time variability studies of the interstellar and stellar water masers at 22.2 GHz (Mattila et al. 1983, 1984, 1985, 1988). In 1985 a new spectral line receiver was put into operation for the 75-115 GHz band (Malkamäki et al. 1985). Results of some CO, HCO^+, HCN, HNC and SiO projects with the Metsähovi radio telescope are presented.

1. A DENSE CORE AND AN OUTFLOW SOURCE ASSOCIATED WITH S 76

Observations of HCO^+, ^{12}CO and ^{13}CO J=1-0 emission have been made towards S76 with the Metsähovi radio telescope (beam width ~1'). The HCO^+ mapping revealed a dense core centered ~1' (0.5 pc) SW of the H_2O maser/IRAS point source S76E ($\alpha = 18^h53^m47^s$, $\delta = 7^o49'26''$). The FWHM extension of the HCO^+ core is ~3' (1.4 pc). The ^{13}CO map shows a maximum ~1' north of the HCO^+ maximum and has a FWHM diameter ~5'.

The CO and ^{13}CO lines show a strong and broad (~8 km s^{-1}) blue-shifted wing component centered ~1' west of the S76E H_2O-maser/IRAS position (Fig.1). A weaker red-shifted wing-component is centered at the same position as the blue wing component. The extension (FWHM) of the blue-shifted and red-shifted ^{13}CO wing are ~5' and 3', respectively.

2. HCN AND HNC OBSERVATIONS OF DENSE CORES

We have studied the variation of the abundance ratio [HNC]/[HCN] in a sample of dark clouds as well as the spatial variation of the intensity ratios of HCN hyperfine components in L810, L1174 and L1551. We found that the observed HNC/HCN intensity ratios are consistent with the earlier result according to which the respective abundance ratio is of the order of 1 in cold dark clouds. However, HCN and HNC distributions are not identical. In L1551, only the HNC map resembles the ammonia distribution (Menten and Walmsley, 1985). The observed HCN hyperfine ratios (Fig. 2) can be understood in terms of scattering of radiation from the core in the foreground gas.

3. HCO^+ CLUMPS IN L1155

The central area of L1155 ($l = 102^o.54$, $b = 15^o.32$) has been mapped in the HCO^+ (J=1-0) line using the Metsähovi radio telescope. The observations reveal two cloud clumps (Fig. 3). The roundish NE clump has an almost constant radial velocity $V_{LSR} \sim 2.5$ km/s while the elongated western cloud component has a velocity gradient ranging from 0.7 km/s in the north to 1.6 km/s in the south. In the clump centers we observed and detected also $H^{13}CO^+$ emission (Fig. 4). These HCO^+ maxima coincide with the maxima of the NH_3 (1,1) line area contour map, which we have observed with the Effelsberg 100-m telescope. The clump centers indicate thus a density enhanced HCO^+ emission. The third HCO^+ maximum in Fig. 3 is located in the front between these two dense clumps. It may arise from a third dense cloud clump or one can also speculate that the enhanced HCO^+ emission in this front region is due to a collision of the two dense clumps.

4. SiO MASER PROJECTS AT METSÄHOVI

We have chosen 12 late-type oxygen-rich long period variables (mostly Miras) for our 86 GHz SiO (J=2-1, v=1) line monitoring list, most of which are so bright that optical light curves are available of them: o Cet, IK Tau, TX Cam, Ori KL, R LMi, R Leo, RT Vir, U Her, GY Aql, χ Cyg, R Aqr, R Cas. The SiO maser associated with Ori KL is included as a unique object, and because it is a strong source suitable for checking system performance. All of these stars are monitored simultaneously in the 43 GHz (J=1, v=1) line with the Yebes 14-m telescope in Spain.

We have used the catalogued optical data of Miras for a search for new SiO (J=2, v=1) masers in Miras. The SiO maximum is expected 0...0.3 P after the optical maximum. The newly detected sources are:

name	spectral type	date	phase
S Cas	Se	18. 8.85	0.96
T Cas	M7.5	18.12.85	0.08
Z Cas	M7e	17.12.85	0.15
U UMi	M6e	19.12.85	0.19

REFERENCES

Malkamäki,L., Mattila,K., Räisänen,A., Peltonen,J., Lehto,a.: 1985, ESO Conf. Proc. No. 22

Mattila,K., Malkamäki,L., Holsti,N., Toriseva,M., Anttila,R.: 1983, Mitteilungen d. Astron. Ges. 60, 446

Mattila,K.: 1984, in Proc. of Nordic Astron. Meeting, Obs. & Astrophys. Lab. Report 6/84

Mattila,K., Holsti,N., Toriseva,M., Malkamäki,L.: 1985, Astron. Astrophys. 145, 192

Mattila,K., Toriseva,M., Liljeström,T., Anttila,R., Malkamäki,L.: 1988, Astron. Astrophys. Suppl. Ser. 73, 209

Menten,K.M., Walmsley,C.M.: 1985, Astron. Astrophys. 146, 369

Urpo,S.: 1975, Helsinki University of Technology, Radio Laboratory Report S73

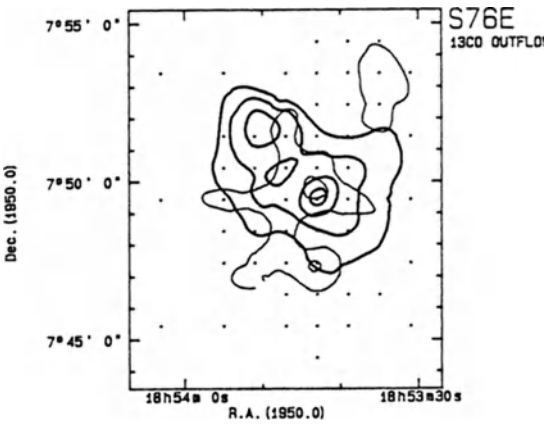

Fig. 1

Contour map of the integrated ^{13}CO wing emission in S76E. The blue wing contours (thick lines) are at intervals of 2 K km/s with the lowest contour at 8 K km/s. The red wing contours (thin lines) are 1 and 2 K km/s. The velocity interval of the blue and red wing is 25-32 km/s and 35.5 - 38 km/s, respectively.

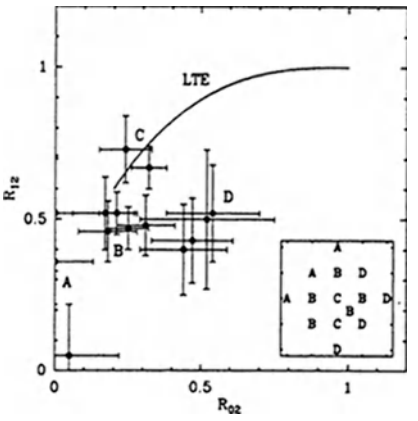

Fig. 2

HCN hyperfine ratio R_{12} vs. R_{02} in L810. LTE ratios would lie on the solid curve. The ratios are similar to those observed in giant molecular clouds. The small box present the variation of these ratios over the source (spacing 40").

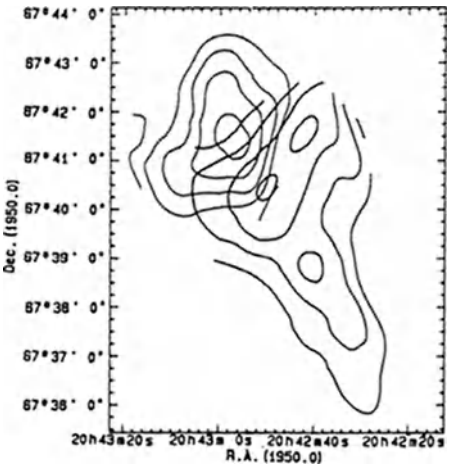

Fig. 3

Contour map of $T_R^*(HCO^+)$ in L1155. The contours are at intervals of 0.2 K with the lowest contour at 0.5 K

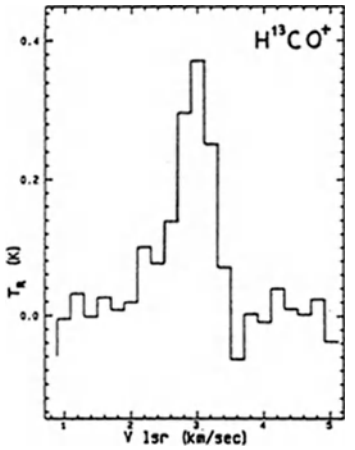

Fig. 4

$H^{13}CO^+$ spectrum towards the center of the NE cloud component of L1155.

Star Formation in Bright-rimmed Globules: Evidence for Radiation-driven Implosion

K. Sugitani
College of General Education, Nagoya City University
Mizuho-ku, Nagoya 467, Japan

Three molecular outflows in three bright-rimmed globules, Ori-I-2, L1206, and rim E (Pottasch 1956) in IC1396, have been discovered (Fig. 1). These outflows are associated with cold IRAS point sources without optical counterparts, good candidates for recently formed stars. The IRAS sources are located just at the peaks of ^{13}CO emission, and are separated only by 0.1 – 0.2 pc from the bright rims. The shock waves preceding the ionization fronts, i.e., bright rims, can propagate to the positions of the IRAS sources in considerably short time scales, i.e., several times 10^4 yr. This suggests that star formation was triggered by the ionization/shock fronts in these bright-rimmed globules. The data well match the radiation-driven implosion model for star formation proposed by Klein et al. (1980), and Sandford et al. (1982). Therefore, I consider that these are the first direct evidence for star formation induced by the radiation-driven implosions.

Densities and star formation efficiencies of the bright-rimmed globules were examined in order to reveal the influences of the radiation-driven implosions, compared with isolated dark globules and dense cores in dark clouds with similar mass range. The densities derived from the ^{13}CO data are all higher than 10^4 cm^{-3}. The ratios of globule mass to luminosity of the associated IRAS sources $M_{\rm cloud}/L_{\rm IR}$, 0.1 – 0.3 $M_\odot/L_\odot$, are much lower than those of the isolated dark globules and the dense cores, 3.3 – 16 $M_\odot/L_\odot$. On the $M_{\rm cloud}/L_{\rm IR}$ versus density diagram of Fig. 2, the bright-rimmed globules are located toward the lower right corner. This suggests that the radiation-driven implosions cause the globules to have higher densities, and consequently higher efficiency of star formation, than the isolated dark globules or the dense cores in dark clouds. That is, more luminous, and perhaps more massive, stars were formed in the bright-rimmed globules.

REFERENCES

Klein, R.I., Sandford, M.T. II, and Whitaker, R.W. 1980, Space Sci. Rev., 27, 275.
Myers, P.C., Linke, R.A., and Benson, P.J. 1983, Ap. J., 264, 517.
Pottasch, S. 1956, Bulletin of the Astronomical Institute of the Netherlands, Vol. XIII, No. 471, 77.
Sandford, M.T. II, Whitaker, R.W., and Klein, R.I. 1982, Ap. J. 260, 183.

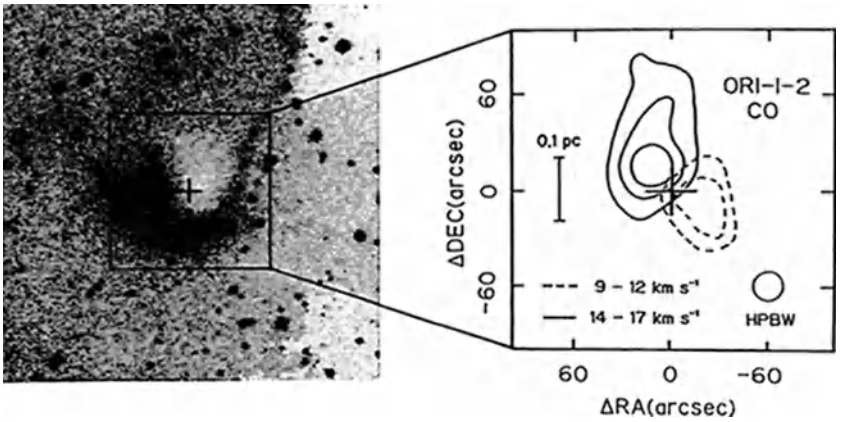

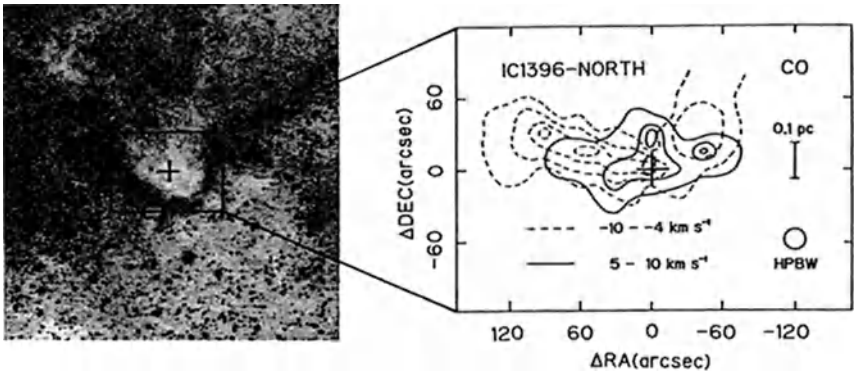

Fig. 1. Outflow maps of CO (1–0) from the NRO 45 m telescope. Photos are from the red POSS plates. The lowest contours and intervals, respectively, are ORI-I-2: $1\,\mathrm{K\,km\,s^{-1}}$ and $0.5\,\mathrm{K\,km\,s^{-1}}$ and IC1396-north: $2\,\mathrm{K\,km\,s^{-1}}$ and $1\,\mathrm{K\,km\,s^{-1}}$. Center positions (1950) are Ori-I-2: $5^{\mathrm{h}}35^{\mathrm{m}}33\overset{\mathrm{s}}{.}2$, $-1°46'50''$ and IC1396-north: $21^{\mathrm{h}}39^{\mathrm{m}}10\overset{\mathrm{s}}{.}3$, $+58°02'29''$. Crosses show IRAS05355 − 0146 and IRAS21391+5802.

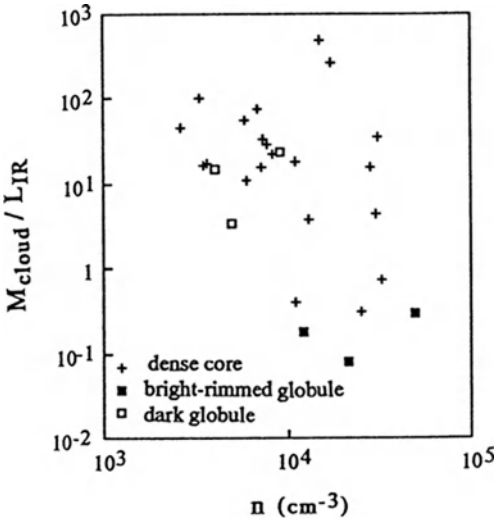

Fig. 2. $M_{\mathrm{cloud}}/L_{\mathrm{IR}}$ vs. density diagram. Filled squares denote bright-rimmed globules, open squares denote isolated dark globules, and crosses denote dense cores of Myers et al. (1983).

CO OBSERVATIONS IN THE DIRECTION OF SUPERNOVA REMNANTS

N. Junkes[1], E. Fürst[1], W. Reich[1], Y. Fukui[2], K. Tatematsu[2]

[1]Max-Planck-Institut für Radioastronomie
Auf dem Hügel 69, D-5300 Bonn 1
Federal Republic of Germany

[2]Department of Astrophysics, Faculty of Science
Nagoya University, Chikusa-ku, Nagoya 464,
Japan

Summary

We have mapped selected Supernova remnants in the 115 GHz line of $^{12}CO(1-0)$ with the KOSMA-3m-telescope. At this frequency the beamsize of 3.6 arcmin allows mapping large-scale CO structures across the remnants and to study the interaction of SNR's with ambient molecular gas. ^{13}CO observations at selected positions have been made to derive column density and mass of the molecular clouds.

We present preliminary results for the two SNR's G18.95-1.1 and G54.4-0.3. They are extended SNR's in the first quadrant of the Galactic plane. In spite of distance ambiguity and confusion due to unrelated molecular clouds in the line-of-sight there is evidence for a correlation of radio continuum (λ11cm), infrared (IRAS 60μ) and ^{12}CO emission for these supernova remnants.

G54.4-0.3 shows a striking alignment of the radio continuum shell and CO emission at 40 $km \cdot s^{-1}$.

1. Introduction

Up to now only a few Supernova remnants are known, which are interacting with molecular clouds. Earlier observations were severely undersampled. Large-scale CO surveys of SNR's have been restricted to the second and third quadrant to avoid the confusion in the first quadrant caused by the large number of unrelated molecular clouds along the line-of-sight as well as the distance ambiguity.

There are some convincing examples for SNR - cloud interaction: Broad molecular line emission (linewidth $\leq$ 100 $km \cdot s^{-1}$) was detected in IC443 and is interpreted as postshock molecular gas caused by the SNR shock wave [1]. A similar feature has not been found for any other supernova remnant. Another remnant which possibly shows SNR - cloud interaction is the Cygnus loop. Radio and optical intensities of the shell are enhanced near the position of two small molecular clouds [2]. Small samples of probably interacting supernova remnants were analyzed in HI- [3] and CO- [4] line emission.

By comparing observations made in HI, molecular lines, radio continuum and infrared emission, we have found more evidence for SNR - cloud interaction and propose two more candidates.

2. Observations

We observed supernova remnants in the J=1-0 transition of ^{12}CO with the KOSMA-3m-telescope [5] in July 1987 and July/August 1988. The HPBW of the telescope at a frequency of 115 GHz is 3'.6. We used a cooled Schottky mixer receiver with 200K DSB noise temperature and a high-resolution acousto-optical spectrometer with 32 kHz channel spacing and 64 MHz bandwidth yielding a resolution of 0.08 $km \cdot s^{-1}$.

The sources were mapped in a raster-scan mode with 3' grid spacing and about 4 minutes integration time per position. We used the position switching mode with one to two ON's per OFF depending on weather conditions. The spectra have been corrected for atmospheric attenuation. Calibration was checked by regular observations of Orion A and DR21 giving an error of less than 12%. We subtracted linear baselines and convolved the spectra to a resolution of 0.7 $km \cdot s^{-1}$ to improve the signal-to-noise ratio (RMS < 0.4K).

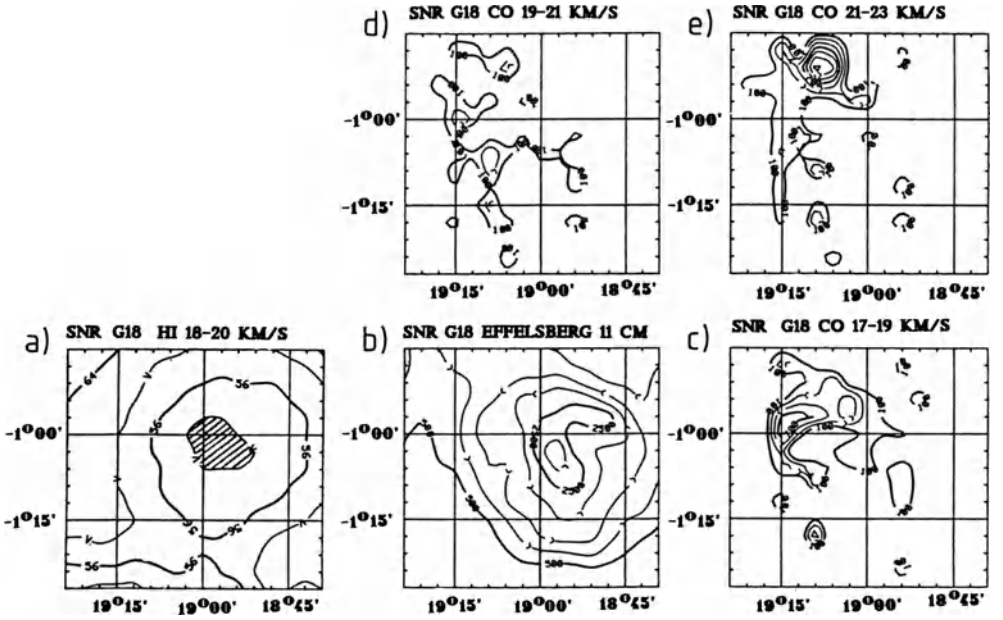

Fig. 1: SNR G18.95-1.1. a) Channel map showing a minimum in HI emission for 18-20 km·s^{-1}. b) 11cm radio continuum map (4.3' beam). c) - e) CO channel maps 17-23 km·s^{-1}.

3. The Sources

G18.95-1.1 is an unusual composite-type supernova remnant with filamentary structure and varying spectral index [6]. At the position of the remnant there is a distinct depression in HI emission (Fig. 1a) at a radial velocity of ~18 km·s^{-1}. At the eastern side of the remnant HI emission as well as IRAS 60μ emission is enhanced in an arc-like structure. Our CO observations confirm this feature in the same velocity interval (Fig. 1c-e). Mapping the complete remnant is necessary to determine the CO structure associated with this remnant (cf. Fig. 1b).

G54.4-0.3 (HC40) is an extended shell-type supernova remnant [7]. This source was selected after analysing infrared data in the direction of the remnant. We found several IRAS point sources (colour temperature ≈30 K) on the shell of the remnant. High resolution ^{12}CO observations with the 30m IRAM telescope detected small CO clouds (≈2' diameter) at these positions in a velocity range of 34-40 km·s^{-1}.

We observed a large area across the remnant with the KOSMA-3m-telescope. The resulting channel maps with velocities between 36 and 44 km·s^{-1} are shown in Fig. 2b-d. There is a striking alignment between the CO feature at this velocity and the structure of the remnant in radio continuum (Fig. 2a). The CO emission is enhanced at the outer border of the remnant and shows a shell-like structure. Assuming a physical relation between the SNR and the CO emission we can derive a kinematic distance of 3.5 or 8 kpc (according to distance ambiguity). A rough estimate for the column density gives $N_H \approx 10^{22}$ cm^{-2} [8]. The molecular cloud has therefore a mass of $3 \cdot 10^4$ $M_\odot$ (3.5 kpc) or $1.5 \cdot 10^5$ $M_\odot$ (8 kpc). Model calculations suggest that the formation of the CO shell results from a stellar wind. The Supernova remnant expands into the bubble inside the shell. To derive a model of SNR-cloud interaction for G54.4-0.3 we will combine our CO results with observations of other molecules (OH) and radio continuum as well as IR data at different wavelengths.

A detailed analysis is in preparation.

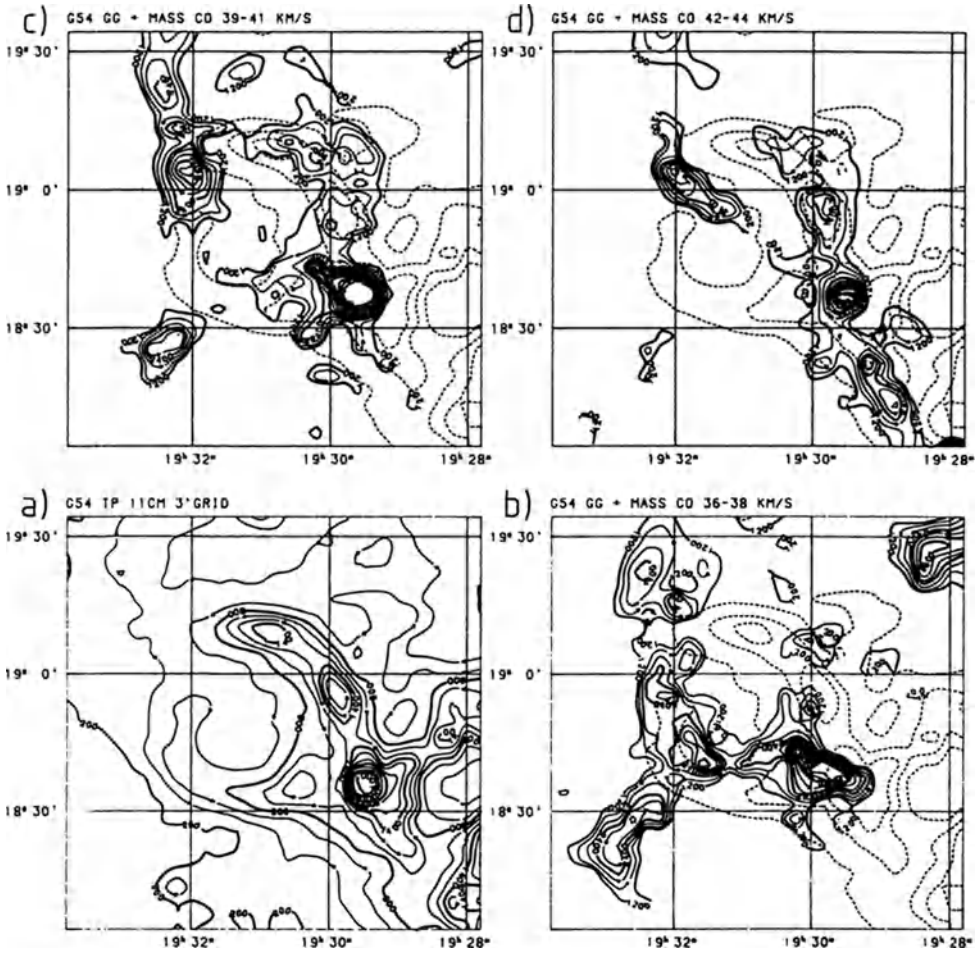

Fig. 2: SNR G54.4−0.3. a) 11cm radio continuum map. b) Channel maps in CO between 36 and 44 km·s^{-1}. The maps show a combination of KOSMA CO data in the central part and data from the FCRAO CO Survey [9]. Radio continuum contours are superposed as dotted lines.

References

1. DeNoyer, L.K.: 1979, Astrophys. J. 232, L165
2. Scoville, N.; Irvine, W.M.; Wannier, P.G.; Predmore, C.R.: 1977, Astrophys. J. 216, 320
3. Braun, R.: 1986, Astron. Astrophys. Suppl. 63, 345
4. Fukui, Y.; Tatematsu, K.: 1988, in *Supernova Remnants and the Interstellar Medium*, IAU Coll. 101, eds. R.S. Roger and T.L. Landecker, Cambridge University Press.
5. Winnewisser, G. et al.: 1986, Astron. Astrophys. 167, 207
6. Fürst, E.; Hummel, E.; Reich, W.; Sofue, Y.; Sieber, W.; Relf, K.; Dettmar, R.-J.: 1989, Astron. Astrophys. (in press)
7. Caswell, J.L.: 1985, Astron. J. 90, 1224
8. Liszt, H.S.: 1982, Astrophys. J. 262, 1989.
9. Sanders, D.B.; Clemens, D.P.; Scoville, N.Z.; Solomon, P.M.: 1986, Astrophys. J. Suppl. 60, 1

DENSE CORES ASSOCIATED WITH DIFFUSE, HIGH-LATITUDE MOLECULAR CLOUDS

J. G. Stacy, P. C. Myers, and H. W. de Vries
Harvard-Smithsonian Center for Astrophysics, Cambridge, Massachusetts USA

Summary

We have identified an unusual class of diffuse, high-latitude molecular clouds (HLC's) which contain dense ammonia cores. We present preliminary ^{12}CO and NH_3 observations of two diffuse, high-latitude clouds, Bernes 48 and MBM 21, which contain dense cores and, in at least one case, an associated IRAS source. These results raise fundamental questions regarding core and star formation in molecular clouds.

1. Observing Program

We have surveyed an extensive catalog of positions toward high-latitude molecular clouds (HLC's) for evidence of ammonia emission indicative of dense molecular cores and potential star-forming regions. Our preliminary results (Stacy, Myers, and de Vries 1988) indicate that two apparently distinct types of HLC contain dense ammonia cores. The first type appears to be related to the well-known opaque dark clouds, with which they share similar properties. The second, however, represents a highly unusual, "CO-rich" class of diffuse molecular cloud. To date we have detected ammonia emission in five HLC's of the latter type. We report here on complementary ^{12}CO and NH_3 mapping observations of two diffuse clouds which contain dense cores, one associated with the reflection nebulosity Bernes 48 (Bernes 1977), the other with cloud number 21 in the catalog of Magnani, Blitz, and Mundy 1985 (=MBM). All observations of the NH_3 (1,1) line at 1.3 cm wavelength were conducted with the 37-meter radio telescope of the Haystack Observatory (1.'5 HPBW at 23.7 GHz), while ^{12}CO (J=1→0) observations at 2.6 mm were conducted with the CfA (formerly Columbia) 1.2-meter telescope (8.'7 HPBW at 115 GHz). Ammonia and CO maps were obtained at grid spacings of 1.'0 and 7.'5, respectively. Typical observing parameters for the Haystack and CfA telescopes can be found in Myers and Benson 1983, and Dame *et al.* 1987.

2. Diffuse Clouds with Dense Cores

The optical reflection nebulosity Bernes 48 (l,b=111.°7,20.°1) is located on the northern periphery of the Lynds 1228 dark cloud. A young stellar object, IRAS point source 21004+7811, is coincident with the position of an ammonia core previously mapped by Benson 1983, and Benson and Myers 1988. L1228 is listed as a point detection (cloud number 161) in the ^{12}CO "intermediate-latitude" catalog of MBM. The Bernes 48 cloud is part of an extended complex of opaque and diffuse clouds, which may be a local "spur" of interstellar material extending from the

Table 1. Estimates of Core/Cloud Virial Mass Fractions

Object	l	b	d	R	T_a^*	V_{LSR}	ΔV_{obs}(FWHM)	M/M_{virial}
	(degrees)		(pc)		(K)		(km s^{-1})	
BERNES 48	111.7	20.1	200					
core				0.1	0.29	-7.5	0.75	0.5
cloud				0.3	1.2	-7.6	2.3	0.015
MBM 21	208.4	-28.4	200					
core				0.08	0.11	4.80	0.70	0.9
cloud				0.36	4.6	4.75	1.2	0.07

Columns: 1: Object name; 2,3: Galactic longitude and latitude of peak position; 4: Assumed distance in parsecs; 5: Mean radius to half-maximum intensity contour; 6: Antenna temperature at map peak position (CO for cloud, NH_3 for core); 7: Mean center velocity with respect to the LSR; 8: *Observed* velocity width, used to derive total *intrinsic* line widths for virial mass estimates; 9: Ratio of derived mass to estimated virial mass (assuming a homogeneous sphere).

Galactic plane in Cepheus toward the north celestial pole. CO mapping of the L1228 complex is currently in progress with the CfA 1.2 m telescope. Strong ammonia detections have been recorded in nearby opaque regions of the L1228 complex, as well as in another diffuse cloud to the north of the Bernes 48 nebulosity.

The MBM 21 diffuse cloud (l,b=208°.4,-28°.4), originally listed as a point detection in the CO catalog of MBM, has been fully mapped in ^{12}CO with the CfA telescope. A weak ammonia core is coincident with the CO peak position, and has been mapped in NH_3 $(1,1)$. This cloud may also contain a young stellar object, as IRAS point source 04591-0857 is located within the half-maximum CO intensity contour of the MBM 21 cloud, approximately 4'.5 west of the ammonia core; its exact relationship to the ammonia core, however, remains to be established. The MBM 21 cloud is a member of a long, filamentary complex of diffuse and opaque clouds, which can be clearly seen in reflection, possibly due to the presence of the nearby supergiant star Rigel (d~200 pc), located approximately 5° to the east. Two other diffuse clouds in this complex have also been detected in ammonia.

3. Implications for Star Formation

The unambiguous detection of NH_3 emission from diffuse HLC's demonstrates that even these apparently tenuous, "low-extinction" objects can harbor small, dense cores. As summarized in **Table 1**, the estimated masses of these cores are within a factor of two of the virial masses indicated by their observed line widths, implying that the cores are likely to be self-gravitating objects. This is in marked contrast, however, to the masses estimated for the "parent" diffuse clouds, which are only a few percent of the value needed to maintain the clouds in gravitational equilibrium. *These results indicate that dense cores, and potentially stars, can exist as discrete substructures within clouds that are* not *gravitationally-bound.* The dilemma posed for molecular cloud physics is obvious: How do such tenuous and low-mass objects form self-gravitating concentrations of molecular gas with densities of order $\sim 10^4$ particles cm^{-3}, comprising a significant fraction of the total cloud mass? Further, what mechanisms or instabilities are likely to trigger core/star formation in such objects? Note that the time scales usually assumed for core collapse and star formation are at least an order of magnitude greater than the free expansion times deduced for HLC's ($t_{exp} \sim 10^{6-7}$ yrs), suggesting that other "external" confinement mechanisms, possibly magnetic fields, play a dominant role in such objects.

Both the Bernes 48 and MBM 21 diffuse clouds are small, relatively isolated members of much larger, more extended cloud complexes containing large populations of both diffuse and opaque clouds. It is highly desirable to compare the properties of dense cores found in diffuse clouds with those found in the more well-studied dark clouds. The Bernes 48 and MBM 21 complexes, therefore, are ideally suited for such a comparative study. Numerous candidate regions have been identified for further investigation, several of which have already yielded postitive detections. Finally, we note that the transparent nature of the diffuse class of HLC, combined with their large angular extent in some cases, poses particular difficulties in selecting appropriate regions for ammonia observations. Observations of molecular tracers sensitive to intermediate-density gas (e.g., ^{13}CO) would greatly facilitate the search for dense cores by more precisely identifying promising target regions.

References

Benson, P. J. 1983, Ph.D. Thesis, Massachusetts Institute of Technology.

Benson, P. J. and Myers, P. C. 1988, *Ap. J.*, submitted.

Bernes, C. 1977, *Astron. Astrophys. Suppl.*, **29**, 65.

Dame, T. M. *et al.* 1987, *Ap. J.*, **322**, 706.

Magnani, L., Blitz, L., and Mundy, L. 1985, *Ap. J.*, **295**, 402.

Myers, P. C. and Benson, P. J. 1983, *Ap. J.*, **266**, 309.

Stacy, J. G., Myers, P. C., and de Vries, H. W. 1988, in *Proceedings of the FCRAO Meeting on Molecular Clouds in the Milky Way and External Galaxies*, ed. R. L. Dickman (New York: Springer-Verlag), in press.

First Results from Observations of Southern Star Forming Regions with the Swedish ESO Submillimetre Telescope

M. Olberg[1], B. Reipurth[1] and R.S.Booth[2]
[1]European Southern Observatory, La Silla, Chile
[2]Onsala Space Observatory, Sweden

ABSTRACT

During the first observing period with SEST we have looked for molecular outflows around a number of prominent southern Herbig Haro objects. We present here preliminary observational results for three of them, HH46/47, HH56/57 and HH120. A more detailed analysis will be presented in forthcoming papers. High spatial resolution radio data at millimetre wavelengths are essential to complete our picture of the physical conditions in the observed regions which so far has been based exclusively on optical and infrared data obtained at ESO and elsewhere.

Introduction

Herbig Haro objects are shock excited emission nebulae intimately connected with the energetic outflow phenomena occuring during the formation phase of stars.

Whereas there is ample observational material on southern HH objects from optical and infrared observations, the examination of their vicinities at millimetre and submillimetre wavelengths with high enough spatial resolution to resolve the structures of their associated molecular outflows has only recently been made possible with the commissioning of the new 15m Swedish ESO submillimetre telescope (SEST) located at ESO's site on Cerro La Silla, Chile. The telescope has been desrcribed in detail by Booth et al. (1988).

We present first results from radio observations of the J=1−0 transition of the ^{12}CO and ^{13}CO molecule of three prominent groups of southern Herbig Haro objects, namely HH46/47, HH120 and HH56/57. The first two are both situated in small, isolated dark cometary globules in the Gum nebula, whereas the latter is found in a molecular cloud in Norma and has drawn particular attention after a flare up of a FU Orionis type star at its NE edge had been reported (Graham and Frogel, 1985) at the position of an earlier detected infrared source (Reipurth and Wamsteker 1983).

From our data we are able to calculate outflow masses and energetics, which should add to our understanding of these remarkable objects.

Results

In the case of HH46/47 we were able to detect red wing emission emanating from the position of the infrared source towards HH46C, i.e. into the globule. The blue lobe of the outflow is weak compared to the red. This is what we would expect if the outflows are mainly material sliding down the inside of a wind blown cavity, as the blue side of the flow clearly has burst through the surface of the globule, and little of a cavity is remaining. In Fig. 1 the wing emission is plotted on top of the integrated ^{13}CO emission.

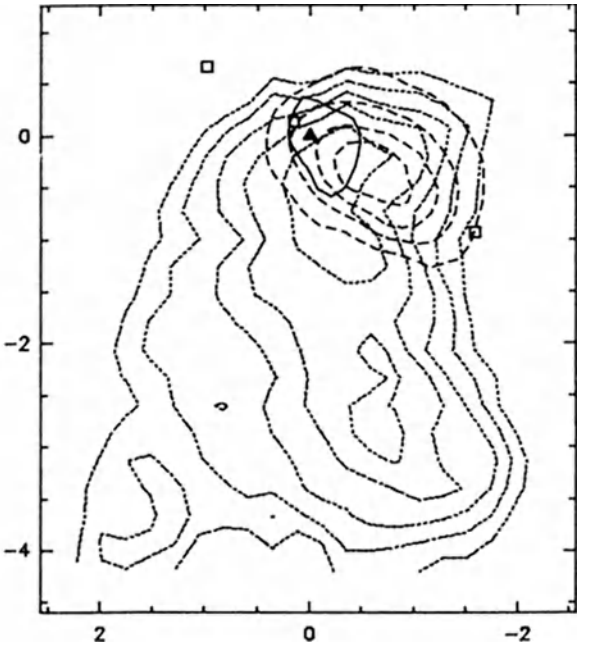

Fig. 1. HH46/47 ^{12}CO red (short dash) and blue (solid line) wing emission plotted on top of contours of integrated ^{13}CO intensity (dotted line). Offsets are given in arcminutes. The position of the infrared source is marked by a filled triangle and the open squares from NE to SW mark HH47A, HH46 and HH46C, respectively.

For HH120 (Fig. 2), the blueshifted emission is smeared out over a big area and does not reveal the typical appearance of a clearly defined lobe. Still, the amount of blueshifted gas is comparable to the mass contained in the well outlined red lobe. Our ^{13}CO spectra show a well defined cloud core at the location of the infrared source, with $v_{LSR} = 6.0$ km/s.

Finally, our map of the region around HH57/56 (Fig. 3) displays the clearest case of a bipolar molecular outflow. Both lobes are well defined. However there are two closely separated energy sources in the region, HH57 IRS and Re 13, and it is difficult at our resolution to determine the relative importance of the two sources. The well defined southwestern blue lobe appears to emerge from Re 13, and it is flowing along the line defined by HH56 and Re 13. A less massive blue lobe is south of HH57 IRS and lies on the line between HH57 and the infrared source. The red lobes from these two flows blend northeast of the sources.

In all three cases the velocity of the outflows reach only modest values and the resulting mechanical luminosities are correspondingly low. It should be noted, however, that we have used mass-weighted velocity averages in our calculations. If one used the

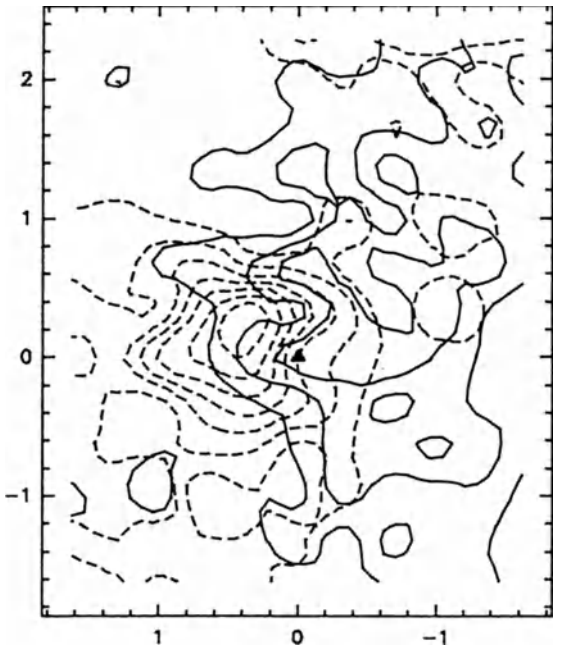

Fig. 2. Contour plot of ^{12}CO red (short dash) and blue (solid line) wing emission for HH120, the position of which is marked by a filled triangle. Offsets are given in arcminutes.

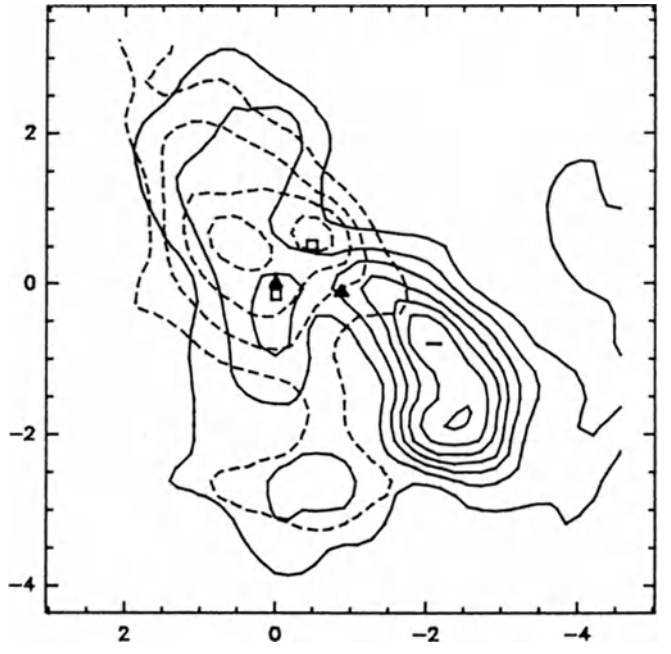

Fig. 3. Same as Fig. 2, but for HH56/57. The positions of the HH57 infrared source at (0,0) and of Re 13 are marked by filled triangles. The open squares mark HH57 and HH56, respectively.

maximum detected velocities and took into account projection effects, which are certainly present but unknown, the luminosities could easily be greater by an order of magnitude, as the velocity enters quadratically. We also neglected low-velocity material hidden in the line cores. This will presumably affect the energetics less, but could increase the outflow masses by 40% to 70% (Bally and Lada, 1983).

In all of the three regions we are probably witnessing low-mass star formation: only low-mass stars are expected to form within cometary globules of dimensions as small as ESO 210-6A or CG30, whereas in the case of HH57/56 the fact that the exciting star is of FU Orionis type indicates that it is probably an object of no more than one to two solar masses.

Table 1: Outflow Characteristics

Outflow	α_{1950}	δ_{1950}	T_{ex} (K)	Δv (km/s)	τ_d (years)	M ($M_\odot$)	L ($L_\odot$)
HH46/47	$08^h24^m16.4^s$	$-50°50'43''$	15.7	3.0	$7 \cdot 10^4$	0.16	$0.2 \cdot 10^{-2}$
HH120	$08^h07^m40.0^s$	$-35°56'02''$	13.2	3.5	$2 \cdot 10^5$	4.51	$1.5 \cdot 10^{-2}$
HH56/57	$16^h28^m56.8^s$	$-44°49'08''$	9.5	4.0	$1.1 \cdot 10^5$	5.2	$5.9 \cdot 10^{-2}$

References

Bally, J. and Lada, C.J. 1983, *Ap. J.*, **265**, 824.

Booth, R.S., Delgado, G., Hagström, M., Johansson, L.E.B., Murphy, D.C., Olberg, M., Whyborn, N.D., Greve, A., Hansson, B. and Lindström, C.O. 1988, *Astr. Ap., in preparation.*

Graham, J.A. and Frogel, J.A. 1985, *Ap. J.*, **289**, 331.

Reipurth, B. and Wamsteker, W. 1983, *Astr. Ap.*, **119**, 14.

Methyl cyanide (CH_3CN) in molecular cloud cores

Per Bergman and Åke Hjalmarson
Onsala Space Observatory, S-439 00 Sweden

We have been investigating the physical and chemical conditions in the molecular cloud cores of W51, G34.3+0.2, and NGC 7538 by using the symmetric top molecule methyl cyanide (CH_3CN). All observations have been made with the Onsala 20 metre telescope and the observed transitions were CH_3CN(J=6-5, K=0-5) at 110 GHz.

CH_3CN is a prolate symmetric top molecule and its rotational energy is a function of two principal quantum numbers, J and K. Due to centrifugal distortion the energy difference between adjacent J-levels decreases as K increases. Hence, it is possible to cover several transitions with different excitation energies within one spectrum. It is this fact that makes CH_3CN a good temperature probe.

Figure 1 shows the spectra of the sources and we see, in the case of W51M, that all six K-components are clearly visible. We can directly tell, by the appearance of the K=5 component, that the kinetic temperature must be fairly high (since J=6-5, K=5 is almost 200 K above the ground state). Note that the K=5 component is blended with the K=0 and K=1 components of the isotopic species $CH_3{}^{13}CN$ J=6-5.

The population of each level is determined by the statistical equilibrium (SE) equations coupled with the radiative transfer equation. Here we have used the large-velocity-gradient (LVG) approximation wich considerably simplifies the solution of the radiative transfer equation. The LVG-approximation assumes that the radiative trapping can be treated locally in terms of a photon escape probability. This criterion is fulfilled if we have a large velocity gradient present in a cloud or a clumpy medium with a large velocity dispersion.

Spherical homogeneous models have been computed for a three parameter grid of T_{kin}, n_{H_2}, and $X[CH_3CN]/(dv/dr)$ using a method described by Goldreich and Kwan (1974). The parameters are estimated by comparing the models to the observation. In order to ensure that the determination will be independent of the source size and the beam efficiency we compare the line ratios of the models to those of the observation. The best-fit parameter set are found by minimising the statistic χ^2. If χ^2 is close to 1, we have a three parameter set that describes the observation well. A confidence region can also be obtained from the χ^2-values.

Let us compare the spectra of the sources W51M and NGC 7538, see Figure 1, since their shapes are quite different, by looking at the contour plots of the χ^2-values at the best-fit kinetic temperature, Figures 2a and 2b. A cross indicates the best-fit point and the hatched area is the 90 % confidence region. Along a straight line with slope -1 we have a constant CH_3CN column density and it is this parameter that can be estimated with the

highest accuracy for both these sources. In the case of W51M the density n_{H_2} is rather well-defined (because the transitions below 100 K are optically thick, τ is approximately 2) while for NGC 7538, which has a lower optical depth, the density confidence interval is very broad. Of course, when the density determination is uncertain the parameters: CH_3CN abundance (X[CH_3CN]), H_2 column density (N_{H_2}), and the mass (M_{H_2}) show the same large uncertainties (see Table 1).

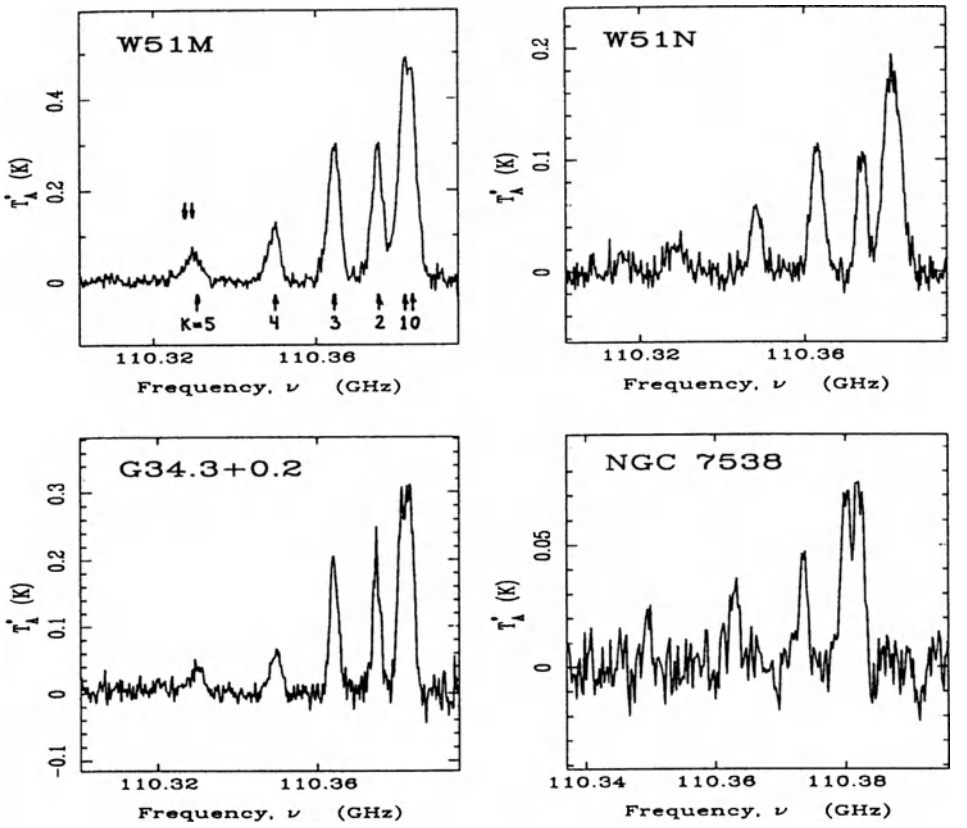

Figure 1

The rather high optical depths obtained from the LVG-analysis of W51M, W51N, and G34.3+0.2 makes it impossible to use a simple rotation diagram to estimate the kinetic temperature (and H_2 column density). Observations of the isotopic species $CH_3{}^{13}CN$ have confirmed that transitions below 100 K in these cores have an optical depth of the order 2-3. The ratio $T_A(CH_3CN)/T_A(CH_3{}^{13}CN)$ is ≈20. Together with the gaussian shape of the lines and the small beam filling factors this implies that the CH_3CN originates from many small clumps within the beam. Furthermore, the obtained CH_3CN abundances are a factor of 10-100 higher than earlier estimates in this type of source (cf. Irvine *et al.*, 1987). This enhancement of CH_3CN toward the core may be explained by evaporation of grain mantles due to higher temperatures close to regions with massive star formation.

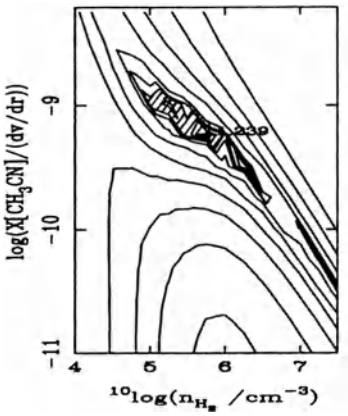

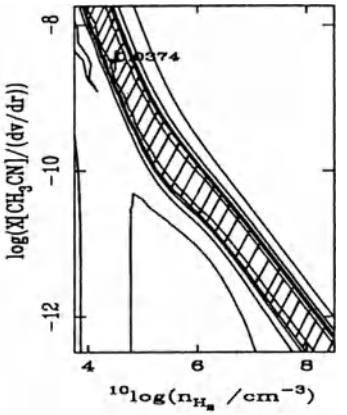

Figures 2a and 2b

	W51M	W51N	G34.3+0.2	NGC 7538
T_{kin} (K)	100^{+40}_{-20}	105^{+75}_{-30}	75^{+20}_{-10}	40^{+40}_{-15}
$\log(n_{H_2}/cm^{-3})$	$5.75^{+0.75}_{-0.75}$	$5.25^{+1.0}_{-1.0}$	$4.25^{+0.75}_{-0.25}$	4.5
Angle (arcsec)	$5.2^{+3.3}_{-0.8}$	$3.5^{+2.3}_{-1.3}$	11^{+6}_{-3}	
$\log(X[CH_3CN])$	$-7.55^{+0.36}_{-0.44}$	$-6.9^{+1.0}_{-0.35}$	$-6.5^{+0.36}_{-1.35}$	
$\log(N_{H_2}/cm^{-2})$	$23.53^{+0.69}_{-0.61}$	$22.85^{+0.85}_{-0.80}$	$22.0^{+0.7}_{-0.2}$	
$\log(N_{CH_3CN}/cm^{-2})$	$16.0^{+0.25}_{-0.50}$	$15.9^{+0.50}_{-0.25}$	$15.6^{+0.25}_{-0.75}$	$15.2^{+0.7}_{-1.0}$
Mass ($M_\odot$)	110^{+300}_{-60}	10^{+25}_{-7}	3	

Table 1: Physical parameters obtained by the LVG-analysis.
The errors correspond to 90 % confidence.

REFERENCES

Andersson, M.: 1985, in (Sub)millimeter Astronomy, eds. P.A. Shaver and K. Kjar, ESO Conf. Workshop Proc. No. 22, pp 353-364

Goldreich, P. and Kwan, J.: 1974, *Astrophys. J.*, **189**, 441

Goldsmith, P.F., Krotkov, R., Snell, R.L., Brown, R.D., and Godfrey, P.: 1983, *Astrophys. J.*, **300**, 737

Green, S.: 1986, *Astrophys. J.*, **309**, 331

Irvine, W.M., Goldsmith, P.F. , and Hjalmarson, Å.: 1987, in Interstellar Processes, eds. D.J. Hollenbach and H.A. Thronson Jr., Reidel, pp 561-609

Sutton, E.C., Blake, G.A., Genzel, R., Masson, C.R., and Phillips, T.G.: 1986, *Astrophys. J.*, **311**, 921

CO Observations of 2nd Quadrant IRAS Sources

J. Braine[1], C. Dupraz[2], F. Casoli[2], F. Combes[1,2], M. Gérin[2]

(1) DEMIRM, Observatoire de Paris, Section de Meudon, F-92195 Meudon cedex
(2) Radioastronomie Millimétrique, ENS, 24 Rue Lhomond, F75231 Paris cedex 05

Summary:

Systematic observation of strong second quadrant IRAS sources at low resolution has revealed a surprising number of broad wings frequently associated with other clouds along the same line of sight as the IRAS source but undetected by IRAS.

Observations:

We have carried out a survey with the Gornergrat millimeter-wave telescope (^{12}CO J=1-0 HPBW = 4' at 115GHz) of 54 of the stronger IRAS point sources in the second galactic quadrant with a color temperature below 75 K. In almost all cases there was no other IRAS source located nearby and S(100m) > S(60m).

The major surprises were (a) the number of spectra with several, frequently separate, emission line peaks; and (b) the very large zero-intensity velocity widths compared to gaussian fits with the upper parts of the spectra. In many cases distinct peaks in the same spectrum were associated with broad wings when no other IRAS source could be found in the region. This leads us to think that flows are not the only source of broad-winged molecular (CO) emission.

60% of the 54 spectra show two or more distinct emission lines while in 29 out of the 54 cases /b/ > 2°. As the signals are fairly weak in general, the sources are either outer regions of large molecular clouds or small clouds. While emision was generally confined to the plane, more than 20% of the lines of sight showed molecular emission at heights above 200pc above the plane.

Perhaps the most interesting feature of the observations is the frequency of broad wings in the absence of observed IR sources (see also Blitz et al. 1988). Superpositioning of clouds at similar velocities in such a way that wings are seen without being part of the cloud believed to be observed could be used to explain isolated cases, especially in the galactic plane and most effectively towards the interior of the Galaxy. The number of examples and the low noise level of the spectra (rms noise < 50mK) make another type of explanation necessary.

Five sources where only one line was present were reobserved with the NRAO telescope at Kitt Peak (^{12}CO J=1-0 HPBW = 1'). At the higher resolution the lines had smaller wings with the half power width remaining the same or increasing. Distinct velocity structure also appeared which was unobserved at the Gornergrat resolution indicating quite small clumps with high excitation temperatures. The Kitt Peak spectra were relatively flat-topped compared to the approximately gaussian upper halves of the corresponding Gornergrat spectra (see figures 1 and 2).

Interpretation:

While this behavior is not completely incompatible with the presence of a bipolar flow, it would be surprising given that in all cases the velocity width at the base was larger in the low resolution spectra than in the Kitt Peak data. An alternative explanation is that the medium is very **inhomogeneous** (clumpy) even on a very small scale and that these clumps are individually very diluted in the 4' beam but many more are present. This, along with the increasing influence of the envelope, gives a much more even velocity coverage and creates the rather smooth appearance of these line profiles. The base is wider simply because a wider range of velocities is found in the larger area covered. In a flow one often finds the highest velocities near the center, although there are many factors involved. It is quite possible that these inhomogeneities are spawned by flows but have lifetimes 10 to 100 times longer than the flow lifetime.

An additional reason for expecting a non-flow explanation for the frequency of wings is that most bipolar flows are smaller than 1 pc and have wing temperatures of 1 to 2 K. Such flows appearing in the Perseus arm would not show wings when viewed at 4' resolution. Once again one is led towards an explanation whereby more high velocity material is found in a large beam, thus yielding detectable wings.

A series of simulations of molecular clouds as an ensemble of optically thick clumps with individually gaussian spectra and mass varying from about $0.02M_O$ to $2M_O$ most closely ressembled the data when the clump to clump velocity dispersion was slightly inversely correlated with the mass (see figures 3 and 4). The spectrum of mass was chosen such that $N(m) \alpha m^{-1.5}$ as is often taken for larger clouds. The bulk of the emission comes from the larger clumps but the wings are created by the smaller higher velocity clumps, which seems reasonable if one assumes something close to equipartition of energy.

We see these clouds as very inhomogeneous or clumpy objects where the inhomogeneities come either from past stellar flows or from low-velocity shock fronts. This is supported by the fact that simulations of cloud emission using smooth variations of density and temperature give lines that are generally much more self-reversed than what is actually seen. In the cases where the small cloud is part of a Giant Molecular Cloud as opposed to being isolated the clumps need not be bound to the small cloud but to the surrouding GMC, thus allowing a considerably wider range of velocities and broader wings. Modelization of these emitting clumps indicates that the low temperature high velocity wings where no flow is currently present probably result from the **cumulated emission of the small masses** which, through an approximate equipartition of energy, have higher velocities than the larger clumps. The mean free path of the clumps is less than 1 pc which makes the equipartition hypothesis more plausible, given the relatively short times involved.

References:

Blitz, L., Magnani, L. Wandel, A. 1988 Ap. J. **331**, L127.

* Kitt Peak (NRAO) is operated by Associated Universities, Inc., under contract with the National Science Foundation.

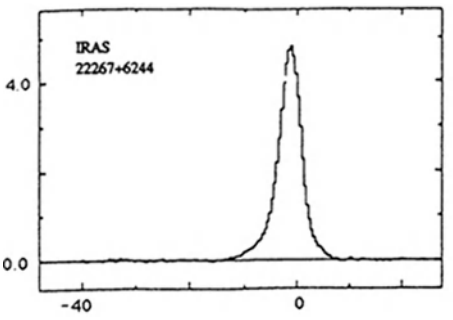

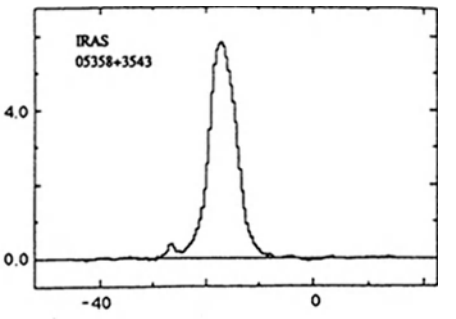

Figures 1a and b. Gomergrat observations of IRAS sources 22267+6244 and 05358+3543. Δv=19 and 18km/s.

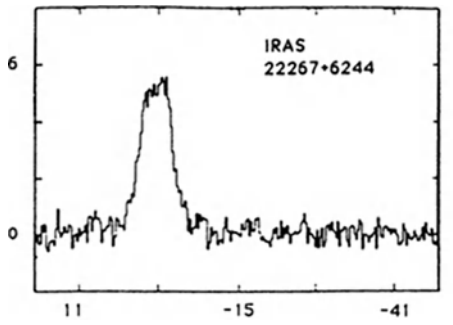

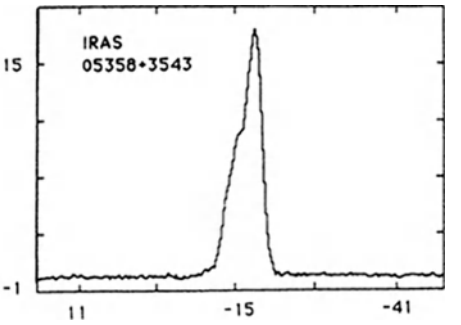

Figures 2 a and b. Kitt Peak observations of the same sources. Δv=15 and 13 km/s respectively.

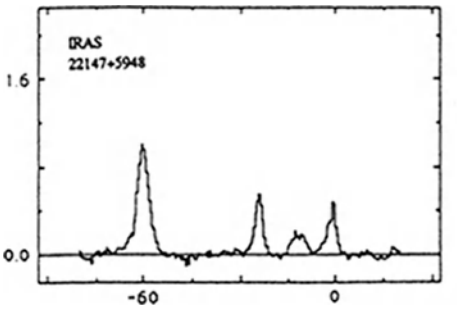

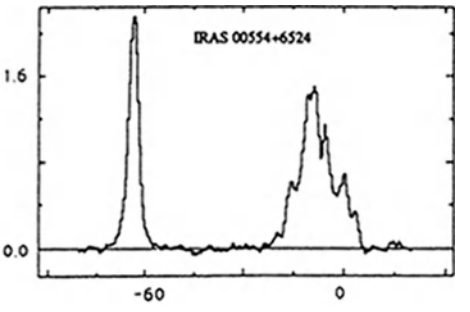

Figures 3 a and b. Gomergrat observations of IRAS sources 22147+5948 and 00554+6524. Two examples out of the majority of spectra showing more than one line. These spectra cannot be considered "representative" because of the wide variety of lines recorded. CO mesospheric emission is present.

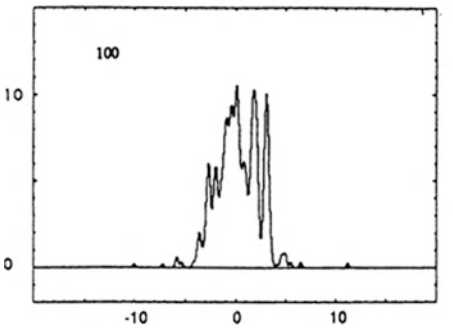

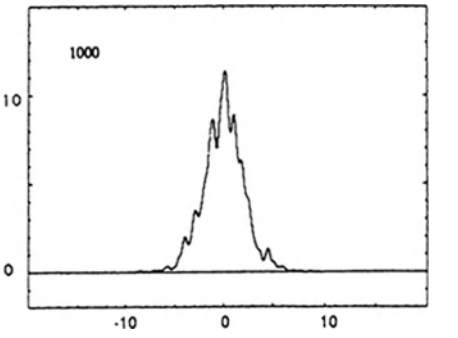

Figures 4 a and b. Simulations of emission of 100 and 1000 clumps as described above. No envelope emission is added, which contributes to the "roughness" of the spectra. Figure 4c is 4b smoothed by combining 5 channels to indicate the dependence on frequency resolution.

Dust Temperature Estimations for Dark Clouds in the Taurus Region Deduced from Correlations between ^{13}CO Line and 100 μm Infrared Emission

H. Weikard [1,2] and G. Duvert [1]

[1] Groupe d'Astrophysique de l'Observatoire de Grenoble, CERMO, B.P. 53 X, 38041 Grenoble CEDEX, France

[2] I. Physikalisches Institut der Universität zu Köln, Zülpicher Straße 77, 5000 Köln, FRG

Abstract

^{13}CO column density maps are compared pixel by pixel with the IRAS 100 μm Sky Brightness Images for which no background correction was applied. The combination of an expression for the flux density of a dusty object with the relationship between ^{13}CO column density and molecular hydrogen density leads to a linear correlation between ^{13}CO column density and infrared brightness at 100 μm . The proportionality factor depends only on the dust temperature. The data often show this strong linear correlation. We derive estimations for dust temperatures. We obtain "infrared offsets" which can differ a lot even for neighbouring fields in the sky.

Data

Using the Bordeaux 2.5 m telescope POM-1 more than 2800 spectra had been obtained from 1980 to 1985 in the ^{13}CO ($1 \rightarrow 0$) line (see Table 1). The half power beamwidth was 4.'4, spectra were taken with a 5' spacing.

Region	Reference	Number of spectra
L1489	1	41
L1495	1	811
L1506 - L1535 - L1521 (partially)	3	774
L1534 (Heiles' Cloud 2)	2	452
L1543 - L1551		257
L1505 - L1513 - L1517	1	301
B30		224

Table 1 : The regions observed with POM-1 and the number of spectra resp. pixels examined for this work

References:
(1) Duvert et al. 1986
(2) Cernicharo and Guélin 1987
(3) Nercessian et al. 1988

We use IRAS 100 μm Sky Brightness Images from the third coverage (HCON3). The resolution is about 5'. No background removal was tried for these data.

Assumptions on Dust and Gas Properties

The flux density of a dusty molecular cloud of mass M is given by (Hildebrand 1983)

$$F_\nu = \frac{3}{4}\frac{M_d}{D^2 \rho_d}\frac{Q_{abs}(a,\lambda)}{a} B_\nu(T_d),$$

where D is the distance, $M_d = Z \cdot M$ the dust mass, ρ_d the grain volumic density, a the grain radius, $Q_{abs}(a,\lambda)$ the absorption efficiency for the grains, and T_d the dust temperature.
Assuming a mixture of silicate and graphite grains ($Q_{abs}/a = 150/\mathrm{cm}$ for $a = 0.1$ μm (cf. Draine 1987), $\rho_d = 2.5$ g/cm^3) and a dust-to-gas mass ratio $Z = 0.01$, we get (now in terms of brightness)

$$\frac{S_\nu(\lambda = 100\,\mu\mathrm{m})}{\mathrm{MJy/sr}} = 3700 \frac{M}{M_\odot}\left(\frac{\mathrm{pc}}{D}\right)^2 \exp\left(-\frac{144\,\mathrm{K}}{T_d}\right). \quad (1)$$

Using $N(H_2) = 5 \cdot 10^5\, N(^{13}CO)$ (Dickman 1978) we have

$$\frac{M}{M_\odot} = 8.0 \frac{N(^{13}CO)}{10^{15}/\mathrm{cm}^2}\left(\frac{D}{\mathrm{pc}}\right)^2. \quad (2)$$

Finally we combine expressions (1) and (2) to get

$$\frac{N(^{13}CO)}{10^{15}/cm^2} = 3.4 \cdot 10^{-5} \exp\left(\frac{144\,K}{T_d}\right) \frac{S_\nu(\lambda = 100\,\mu m)}{MJy/sr} \,. \qquad (3)$$

Furthermore, we assume that ^{13}CO is thermalized at a gas kinetic temperature of 10 K to convert integrated intensities to column densities:

$$\frac{N(^{13}CO)}{10^{15}/cm^2} = 0.435 \frac{\int T_A \, dv}{K \cdot km/sec} \,.$$

Procedure and Results

The (integrated intensity resp. column density) radio maps are compared pixel by pixel with the IRAS images (equal weighted least square regression analysis). In some cases pixels with an infrared excess due to point sources are discarded.

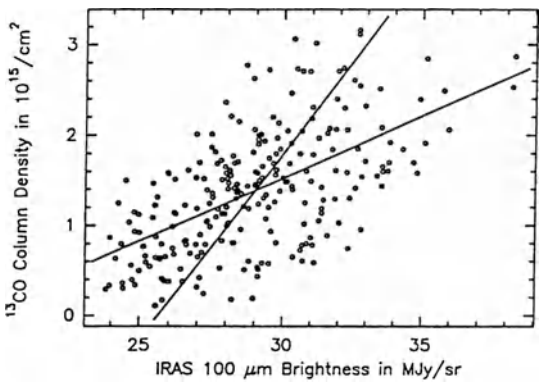

The entire regions (Table 1) show correlation coefficients between r = 0.58 (B30) and r = 0.79 (L1489) (cf. also Fig. 1). However, in every region we find smaller fields where the data are strongly correlated (r > 0.85, see Table 2): Fig. 2 presents L1543S as an example.

The correlations in more extended regions seem to be disarranged by an unknown background within the IRAS images.

Fig. 1: The correlation for the region L1524 – L1529 (243 pixels): The correlation coefficient is r = 0.58. This result is to compare with those for six smaller fields in Table 2.

Field	Number of pixels	Correlation coefficient	Slope in $(10^{15}/cm^2)/(MJy/sr)$	Infrared offset in MJy/sr
L1489	34	0.85	0.27	16.0
B209	135	0.90	0.23	17.5
B10	130	0.91	0.34	22.5
L1495E	33	0.88	0.31	24.0
B213SW	38	0.95	0.39	18.5
B210N	33	0.90	0.20	19.5
L1506	91	0.89	0.27	22.0
L1524NE	43	0.93	0.28	23.5
L1524SE	23	0.90	0.41	26.5
L1524NW	36	0.90	0.34	22.5
L1524SW	24	0.91	0.41	24.0
L1529	44	0.91	0.37	25.0
L1529S	47	0.90	0.28	27.5
L1535	55	0.92	0.19	28.5
L1521S	51	0.95	0.21	21.0
L1534N	92	0.95	0.21	27.0
L1534E	67	0.93	0.16	29.0
L1534SW	79	0.93	0.23	34.0
L1543NW	35	0.91	0.32	32.0
L1543S	41	0.93	0.19	27.5
L1551NW	33	0.91	0.30	27.5
L1513	32	0.85	0.23	28.5
L1517N	38	0.90	0.29	28.0
L1573SE	35	0.85	0.14	46.5
B30SE	16	0.92	0.08	43.0

Table 2 : Preliminary results on some selected fields
The slopes and the offsets are determined from the mean of the two regression lines.
The six fields between the two spacings represent approximately the pixels used in Fig. 1.
Note the difference in the infrared offsets for neighbouring fields (see for example L1534E and L1534SW)!

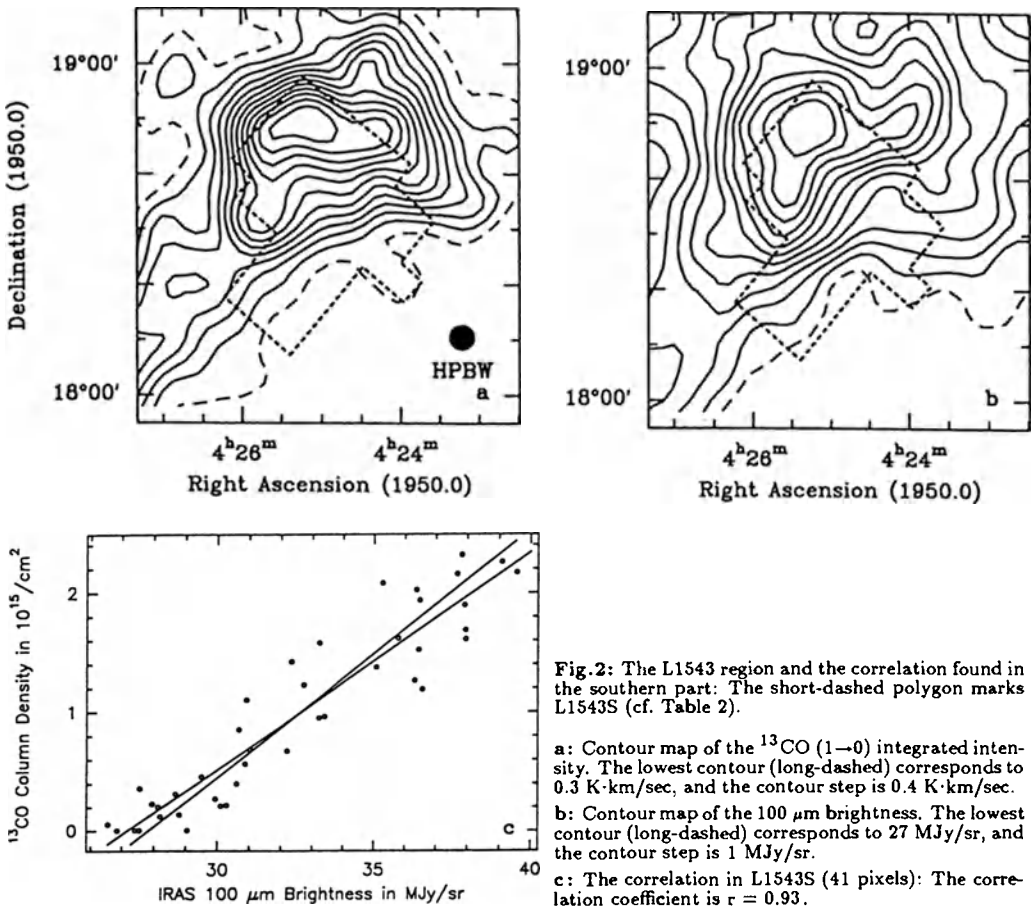

Fig.2: The L1543 region and the correlation found in the southern part: The short-dashed polygon marks L1543S (cf. Table 2).

a: Contour map of the ^{13}CO (1→0) integrated intensity. The lowest contour (long-dashed) corresponds to 0.3 K·km/sec, and the contour step is 0.4 K·km/sec.

b: Contour map of the 100 μm brightness. The lowest contour (long-dashed) corresponds to 27 MJy/sr, and the contour step is 1 MJy/sr.

c: The correlation in L1543S (41 pixels): The correlation coefficient is $r = 0.93$.

The slopes given in Table 2 vary by a factor of at least 2. This leads to dust temperatures between 15 and 17 K (cf. expression (3)).

Acknowledgement: This work is supported by the European Economic Community under contract number ST2-0305.

References

J. Cernicharo and M. Guélin: Astron. Astrophys. **176**, 299 (1987)
R.L. Dickman: Astrophys. J. Suppl. Ser. **37**, 407 (1978)
B.T. Draine: Princeton Observatory Preprint 213, Princeton University Observatory, Princeton 1987
G. Duvert, J. Cernicharo, and A. Baudry: Astron. Astrophys. **164**, 349 (1986)
R.H. Hildebrand: Q. Jl. R. astr. Soc. **24**, 267 (1983)
E. Nercessian, A. Castets, J. Cernicharo, and J.J. Benayoun: Astron. Astrophys. **189**, 207 (1988)

Optically Thick ^{13}CO Emission from the Orion GMC

A. Castets[1], G. Duvert[1], J. Bally[2], R. W. Wilson[2] and W. D. Langer[3]
[1]Groupe d'Astrophysique de Grenoble, BP 53X, F-38041 Grenoble, France
[2]HOH L#241, AT&T Bell Laboratories, Holmdel, NJ 07733, USA
[3]Plasma Physics Department, Princeton University, Princeton, NJ 08544, USA

Abstract

Moderate resolution (2.'5) obsevations of the ^{13}CO $J=1\rightarrow 0$ and $J=2\rightarrow 1$ lines in the Orion A molecular cloud reveal that ^{13}CO is optically thick over all the main filament. We present a ^{13}CO column density map of this region as deduced from both lines using an LVG code. This map reveals several peaks in the main filament with column densities greater than $4\cdot 10^{16}$ cm^{-2}.

We present the first multi-transition analysis of the CO emission from an entire molecular cloud using $J=1\rightarrow 0$ ^{12}CO and ^{13}CO data obtained with the AT&T Bell Laboratories 7 m antenna and observations of the $J=2\rightarrow 1$ ^{12}CO and ^{13}CO lines taken with the POM2 2.5 m telescope located on the Plateau de Bure.

The $J=1\rightarrow 0$ data were obtained with a 100″ beam and sampled every 1′. The $J=2\rightarrow 1$ data were obtained with a 2.'2 beam and were sampled every 2.'5. We have convolved the Bell Laboratories spectra to match the POM2 beam, and resampled it on the POM2 map. This four-transition analysis covers a one square degree region centered on the BN/KL region of the Orion A molecular cloud.

Although the observed ^{12}CO $J=2\rightarrow 1$ and $J=1\rightarrow 0$ profiles are nearly identical (with $[T_A\,^{12}CO(2\rightarrow 1)]/[T_A\,^{12}CO(1\rightarrow 0)]\simeq 1.0$ for all velocities) as expected for optically thick and thermalized emission lines, the observed ^{13}CO line ratios deviate from the expected optically thin values suggested by the $[T_A\,^{12}CO(1\rightarrow 0)]/[T_A\,^{13}CO(1\rightarrow 0)]\simeq 3$ ratio seen towards most lines of sight.

We find that the ratio $[T_A\,^{13}CO(2\rightarrow 1)]/[T_A\,^{13}CO(1\rightarrow 0)]\simeq 1.0$ (Table 1), indicating that ^{13}CO is also optically thick *if* it is thermalized! Since ^{12}CO is thermalized, it is reasonable to expect ^{13}CO to be also, since the optically thinner isotopic species probes deeper into what is expected to be the denser interior of clouds. In Orion A, the $J=2\rightarrow 1$ CS line is brighter than 0.5 K over most of the mapped region (Bally et al., 1987) and $I(^{13}CO)/I(CS)\simeq 3$ to 5 over the "S-shaped" filament, so the gas density is sufficient to thermalize even the ^{13}CO $J=2\rightarrow 1$ line. An opacity of order unity implies that the excitation temperature of the ^{13}CO emitting region is two to three times lower than the excitation temperature of the ^{12}CO emitting region.

Only toward the well-studied, dense Orion A core containing the BN/KL region do we find a ratio $[T_A\,^{13}CO(2\rightarrow 1)]/[T_A\,^{13}CO(1\rightarrow 0)]\simeq 2$, suggesting thin ^{13}CO emission!

Table 1. ^{13}CO line parameters at selected offsets in the "S-shaped" filament. The reference position for offsets is $5^h32^m47^s, -5°24'30''$. $\tau(1 \rightarrow 0)$ and $\tau(2 \rightarrow 1)$ are deduced from an LVG code.

$\Delta\alpha$ (')	$\Delta\delta$ (')	ΔV km/s	Ta1-0 °K	Ta2-1 °K	Tk °K	τ 1-0	τ 2-1	N(^{13}CO) cm^{-2}
-7.50	-22.5	2.25	8.9	6.80	17.5	1.9	4.8	4.06E16
-5.00	-22.5	2.75	10.	8.50	20.0	1.46	4.20	5.03E16
-2.50	-17.5	2.75	9.4	9.10	25.5	0.72	2.68	3.54E16
-2.50	-15.0	2.75	11.	9.10	28.0	1.28	4.11	5.15E16
-2.50	-10.0	3.25	5.1	6.50	26.0	0.21	1.16	1.73E16
0.00	-5.00	3.75	10.	13.5	56.0	0.13	1.53	4.56E16
0.00	0.00	3.75	9.1	16.5	62.0	0.04	1.00	4.78E16
0.00	2.50	2.75	11.	16.3	53.5	0.14	1.48	4.09E16
0.00	10.0	2.50	10.	11.2	34.0	0.43	2.15	3.19E16
2.50	15.0	2.00	13.	13.6	32.5	0.74	3.04	4.09E16
2.50	20.0	2.00	11.	12.7	26.5	0.7	2.54	3.38E16

The ^{13}CO line probes deeper into a cloud than the ^{12}CO line. The penetration depth, expressed as a column density lying in front of the $\tau \simeq 1$ surface, is given by

$$N_p(\mathrm{cm}^{-2}) = \frac{2.4 \cdot 10^{14}\, T_{rot}\, \Delta V(\mathrm{km\,s}^{-1})}{1 - \exp(-h\nu/kT)},$$

which gives (for both ^{12}CO and ^{13}CO being optically thick with $\Delta V = 3$ km s^{-1}, and assuming $[H_2]/[^{13}CO] = 7 \cdot 10^5$ and $[H_2]/[^{12}CO] = 1.0 \cdot 10^4$): $N_p = 1.2 \cdot 10^{22}$ cm^{-2} for ^{13}CO and $N_p = 1.3 \cdot 10^{21}$ cm^{-2} for ^{12}CO. (We assume that $T_{rot} = T = 30$ K for ^{12}CO and 10 K for ^{13}CO.) Thus the ^{13}CO emission region is effectively shielded from external heating by the radiation field while the ^{12}CO layer is readily heated, making a large temperature difference between the regions probed by the two isotopic species reasonable in the absence of internal heating sources.

Since the column density deduced from an LVG code is, to a large extent, quite insensitive to the assumed kinetic temperature, we use ^{12}CO $J = 2 \rightarrow 1$ as a temperature probe to determine the ^{13}CO column density map of Fig. 1. This map reveals several clumps in the main filament with column densities higher than $4 \cdot 10^{16}$ cm^{-2}.

A more complete analysis of these observations, including a determination of the H_2 density in Orion, will be published in the coming year.

Reference

Bally, J., Langer, W. D., Stark, A. A., Wilson, R. W.: 1987, *Ap. J (Letters)*, **312**, L45

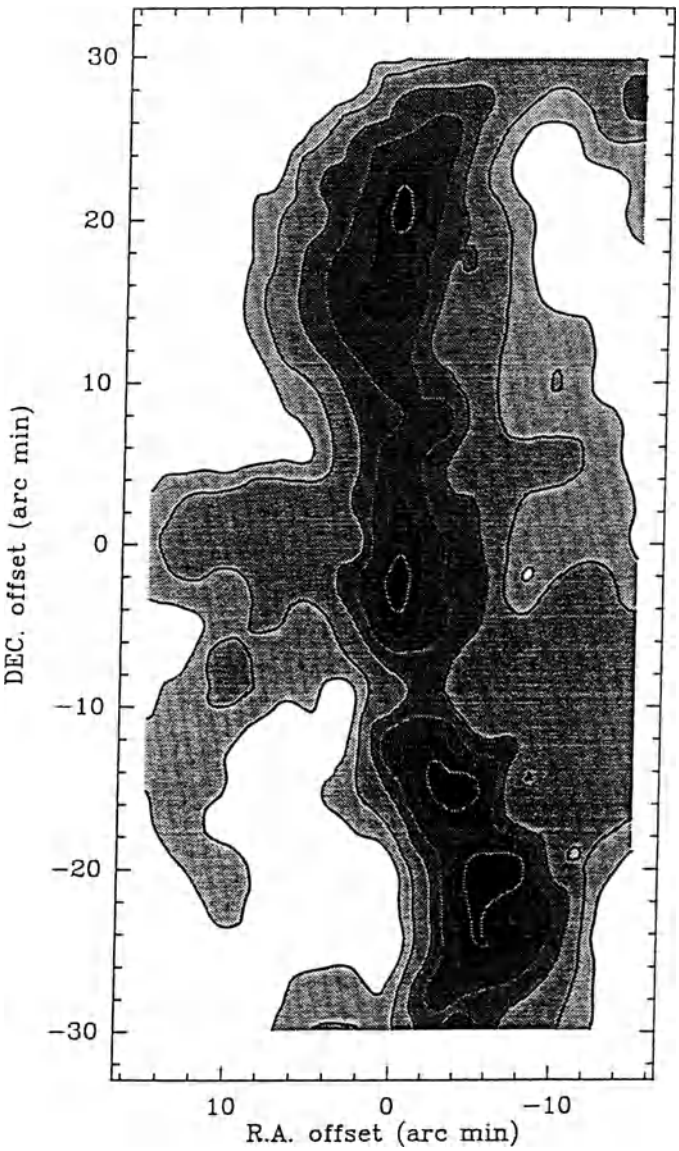

Fig. 1. Preliminary ^{13}CO column density map of the Orion Molecular Cloud, deduced from an LVG model. Levels are $5 \cdot 10^{15}$, 10^{16}, $2 \cdot 10^{16}$, $3 \cdot 10^{16}$, $4 \cdot 10^{16}$, $5 \cdot 10^{16}$ cm^{-2}.

Detection of 53 new 86 GHz SiO masers associated with IRAS point sources

L. Haikala
I. Physikalisches Institut, University of Cologne
and
Observatory and Astrophysics Laboratory, Helsinki

Abstract

The detection of 53 new SiO v=1, J=2→1 masers in a survey of IRAS point sources is reported. The detection rate was 46%. It is argued that a major portion of the IRAS point sources with IR properties similar to those of known SiO masers are also SiO emitters.

Introduction

Maser emission (OH, H_2O, SiO) associated with stars has been known for about twenty years. The maser emission takes place in the circumstellar gas/dust envelopes (CSEs) around late type stars. These envelopes are strong emitters in the IR region. IRAS Point Source Catalogue (IPSC) provides therefore a unique tool for finding new masering stars. The position of known SiO maser stars in IRAS colour-colour plots was used as a guideline in choosing SiO maser candidates, which were then observed with the SEST 15 m telescope.

All the IRAS point sources which have been identified as stars and have good quality fluxes at 12 and 25 μm and at least medium quality flux at 60 μm in IPSC are plotted in Figure 1a. A selection of SiO masering stars (Engels 1979) is plotted in Figure 1b. The box shows the criteria used in choosing the maser candidates. In the selection, a detection at 100 μm was required to increase the probability of the object's being nearby.

Observations

A total of 114 southern IRAS point sources were observed in May 1988 at the SEST 15 m telescope at SiO v=1, J=2–1 (86.242 GHz) frequency in dual beam switching mode. The spectral resolution of the KOSMA high resolution AOS used in the observations was 43.3 kHz (0.15 km s^{-1} at 86 GHz). The observations covered a velocity range of $\pm$150 km/s in the Local Standard of Rest. The noise RMS reached in the survey was 2.5 Jy or less.

Results

Fifty-three new 86 GHz SiO masers were found. Of these, 45 had stellar identifications, three were previously known non-IRAS IR objects and six had no identification in the Point Source Catalog. Two were previously known as 43 GHz SiO masers. The positions of the new SiO masers and the nondetections on the IR colour-colour diagram are shown in Figures 2 a and b, respectively. Sample spectra of the detected masers are shown in Figure 3. No baseline correction has been done.

Discussion

The IR properties of the detected and nondetected objects are not different from each other. The high detection rate and the known strong variability of SiO masers make it probable that a large fraction of the objects that were not detected are also SiO emitters at times. This implies that most of the objects in Figure 1 a around the position of the known and new SiO masers are in fact SiO masering stars.

van der Veen and Habing (1988) divided the IRAS colour-colour diagram into different regions according to the optical and IR properties of the objects in these regions. Excep for U Mic, all the new SiO masering objects lie in the regions occupied by thin, O-rich and moderately thick, O-rich CSEs in the division of van der Veen and Habing (1988). Only the star U Mic lies clearly in the region of C-rich CSEs. Fifteen SiO candidates observed in the survey reported here have IRAS 12μ fluxes larger than 500 Jy. SiO was detected in eight of these objects. Of the nondetections, five lie in the region of C-rich CSEs, even though these objects occupy only a small part of the colour-colour region where SiO emission was sought. U Mic could be a C-rich object showing SiO maser emission. Curiously, the 12μ flux of U Mic is only 33 Jy.

References

van der Veen, W. E. C. J. and Habing, H. J.: 1988, Astron. and Astrophys. **194** 125

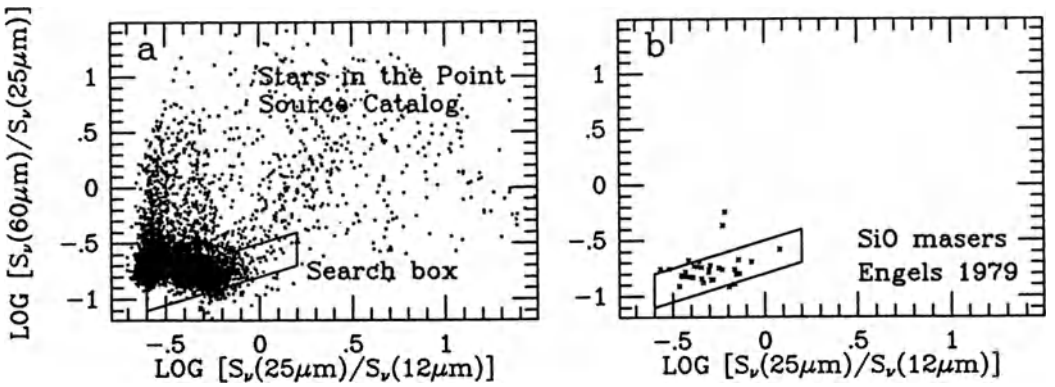

Fig. 1a. Colour-colour plot of all objects classified as stars in the IRAS Point Source Catalog with good quality fluxes at 12 and 25μ and at least medium quality flux at 60μ. The search box shows the region from which the SiO maser candidates were chosen. **b.** As a but for SiO masers in Engels (1979)

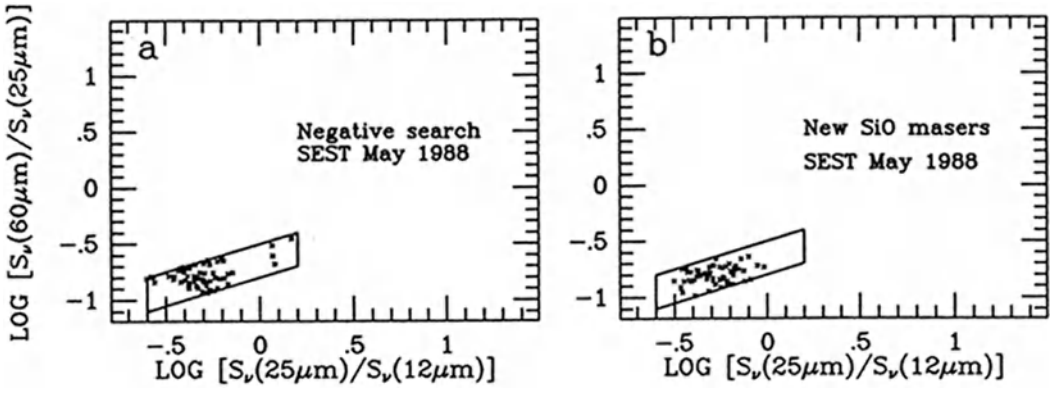

Fig. 2. Observed SiO candidate point sources: **a.** No SiO emission detected, **b.** SiO detected.

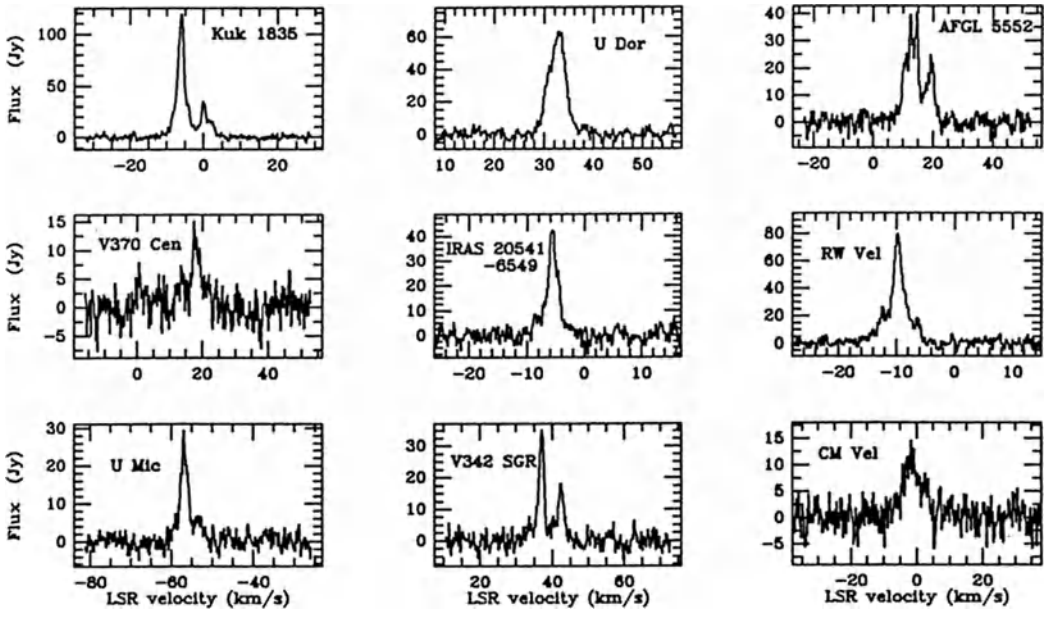

Fig. 3. Sample spectra of new SiO masers. No baseline correction has been made.

The Largest Molecular Cloud Complexes in the Southern Milky Way

L. Bronfman[1], L. Nyman[2] and P. Thaddeus[3]
[1]Universidad de Chile
[2]Onsala Space Observatory
[3]Harvard-Smithsonian Center for Astrophysics

With our completion of the Columbia Deep CO Survey of the fourth Galactic quadrant, covering from $\ell = 300°$ to 348° within 2° of the plane, at a resolution of 0.°125, it has become possible to establish the gross distribution of molecular gas in the inner Galaxy over a large fraction of the area within the solar circle (Bronfman *et al.*, 1988). According to our analysis, at least half of the interstellar gas in this region of the disk is in molecular form. Most of the molecular gas is concentrated in cold and compressed clouds which, particularly in the vicinity of spiral arms, are often arranged into large cloud complexes; these complexes are confined to and fill about 1% of a thin (120 pc FWHM) layer about the plane.

We have now identified from our new CO survey of the fourth Galactic quadrant, following the same method used by Dame *et al.* (1986) to analyze their first quadrant CO survey, the 50 largest molecular complexes in the southern Milky Way, in a region roughly limited by the 3 kpc expanding arm and the solar circle (Table 1). The majority of these complexes have masses exceeding $5 \times 10^5\, M_\odot$; some of them, with $5 \times 10^6\, M_\odot$, are among the largest in the Galaxy. Most if not all have intense infrared counterparts; many seem to be sites of active star formation, as suggested by their close association with HII regions and IRAS point sources (Bronfman, 1989).

Molecular complexes in the fourth Galactic quadrant seem to be organized, in addition to the Carina arm (Grabelsky *et al.*, 1988) and to the 3 kpc arm (Bronfman, 1986), into two large scale features roughly coincident with major spiral arms proposed by Georgelin and Georgelin (1976) based on the distribution of HII regions: the Centaurus arm, radius $R \sim 0.8\, R_\odot$, and the Norma arm, tangent to the line of sight at $\ell \sim 328°$ and at a mean Galactocentric radius $R \sim 0.55\, R_\odot$. Since perturbations in the velocity field caused by the action of energetic events may introduce large uncertainties in the derived kinematic distances, particularly for the Centaurus arm (Nyman *et al.*, 1987), further studies of CO spiral structure must be preceded by a careful examination of peculiar velocities associated with the major molecular cloud complexes catalogued here.

References

Bronfman, L. 1986, Ph.D. Thesis, Columbia University.
Bronfman, L., Cohen, R., Alvarez, H., May, J., and Thaddeus, P. 1988, *Ap. J.*, **324**, 248.
Bronfman, L. 1989, in preparation.
Dame, T. M., Elmegreen, B. G., Cohen, R. S., and Thaddeus, P. 1986, *Ap. J.*, **305**, 892.
Georgelin, Y. M., and Georgelin, Y. P. 1976, *Astr. Ap.*, **49**, 57.
Grabelsky, D., Cohen, R. S., Bronfman, L., and Thaddeus, P. 1988, submitted to *Ap. J.*
Nyman, L., Bronfman, L., Cohen, R. S., and Thaddeus, P. 1987, *Ap. J.*, **314**, 374.

Table 1. The brightest CO sources in the fourth quadrant of the Galactic plane within the solar circle. The twofold ambiguity in the kinematic distances has been tentatively solved with the help of associated HII regions, H_2CO absorption, and the examination of the latitude position and extent of the clouds. Radii were calculated as $R = (A/\pi)^{1/2}$, where A is the area of cloud with emission larger than 3σ. We used $R_\odot = 8.5$ kpc, $V_\odot = 220\,\mathrm{km\,s^{-1}}$, and a conversion factor $N(H_2)/W(CO) = 2.2\times10^{20}\,\mathrm{K\,km\,s^{-1}/kpc}$ (Dame *et al.*, 1986) throughout the analysis.

Longitude	Latitude	V_{LSR} (km/s)	ΔV_{FWHM} (km/s)	D (kpc)	R (pc)	$\log M/M_\odot$
302°0	0°8	−40	11	2.8	91	6.06
305.3	0.9	−41	21	4.4	139	6.27
308.0	−0.4	−14	5	9.4	41	5.51
308.4	−0.2	−61	8	3.0	55	5.61
309.0	−0.3	−11	11	9.9	87	5.67
309.4	0.0	−45	12	4.0	110	5.63
311.7	0.0	−50	18	4.2	118	6.08
311.7	−0.1	−10	19	10.6	94	5.16
312.5	0.0	−14	16	10.4	108	5.54
313.8	0.0	− 7	9	11.3	82	4.87
314.2	0.1	−47	16	3.5	101	5.84
316.4	−0.4	− 7	5	11.8	51	5.58
316.4	0.1	−45	13	3.2	72	5.44
316.6	0.0	−21	8	10.9	93	5.65
318.3	−0.2	−18	10	11.4	139	5.85
318.4	0.0	−42	14	3.0	88	5.72
319.6	−0.3	−10	24	12.3	117	6.10
320.3	−0.1	− 8	16	12.8	101	6.07
320.8	−0.2	−59	12	4.0	88	5.31
322.6	0.5	−53	9	3.6	56	5.09
323.0	0.6	−33	8	2.3	89	5.44
323.7	−0.4	−65	5	4.2	48	4.75
324.0	0.3	−52	9	3.5	62	5.29
326.5	0.5	−43	10	2.9	67	5.83
327.0	−0.4	−60	9	3.9	60	5.53
328.2	0.7	−92	16	5.7	112	6.10
328.4	0.0	−73	11	4.6	134	6.10
328.5	0.3	−44	11	3.0	79	5.50
329.5	0.6	−91	18	5.5	87	5.77
331.1	0.3	−45	8	3.1	65	5.54
331.4	−0.1	−92	14	5.5	82	6.18
331.5	0.1	−65	12	4.1	96	6.06
332.6	0.2	−47	12	3.3	56	5.82
333.7	−0.1	−48	14	3.3	77	6.15
333.9	−0.1	−89	12	5.2	111	6.06
334.5	0.5	−66	12	4.3	90	6.00
337.1	−0.1	−117	14	6.4	70	5.71
337.1	−0.1	−74	13	11.0	162	6.64
337.8	0.0	−56	13	11.8	141	6.60
338.9	−0.2	−117	10	5.7	66	5.57
339.0	0.7	−60	10	4.2	38	5.38
340.0	−0.3	−90	10	5.4	95	5.35
340.7	−0.1	−123	10	5.7	92	5.78
341.1	−0.3	−44	13	3.6	114	6.17
342.4	0.1	−79	12	5.2	88	6.07
342.6	−0.4	−27	10	2.7	80	5.90
342.8	0.1	−124	14	5.6	87	5.85
344.1	0.2	−69	10	4.9	96	5.86
344.8	0.1	−43	10	3.9	69	5.34
345.6	1.1	−15	10	1.9	39	5.59

Molecular Outflows

J. T. Armstrong
I. Physikalisches Institut, Universität zu Köln, FRG

SUMMARY

I describe recent outflow results from the Gornergrat 3 m telescope and discuss them in the context of the support of molecular clouds. Recent results in modeling clump-clump interactions and in finding outflows in unbiased surveys lend support to the idea that outflow energy is the major source of support for some clouds. I devise a "turbulent luminosity" for discussing the energetics of cloud support.

I. Introduction

Since the realization early in this decade that many star-formation regions contain high-velocity gas, often in the form of bipolar outflows, a great many outflow sources have been identified, sometimes several to a cloud, and often extended on scales of a parsec or more. Meanwhile, one of the long-standing puzzles in molecular-line astronomy has remained a puzzle: why are the linewidths in most molecular gas so much greater than the thermal velocities of the molecules? Something is maintaining the "turbulence" of the gas for times that are long compared to a free-fall time: either a dissipation rate that is slower than expected, or continuing energy input into the gas, or some of both. The work of Scalo and Pumphrey (1982) suggests that dissipation rates may be as much as an order of magnitude longer than a free-fall time. In addition to stellar winds and HII regions, several other sources of energy input have been suggested, including "star-cloud turbulence" (Henricksen and Turner 1984), Alfvén waves (*e.g.*, Shu, Lizano, and Adams 1986), Galactic rotation (Fleck 1981), and, of course, outflows (*e.g.*, Margulis and Lada 1985; Margulis, Lada, and Snell 1988).

In this paper, I discuss the importance of outflows to the energetics of bulk motion in molecular gas. I show some recent mapping results from the Gornergrat 3 m telescope, including some newly-discovered flows and some observations of previously known flows. I then discuss these results, along with some survey results of Fukui *et al.* (1986) and of Margulis and Lada (1985) in the light of the possibility that a significant fraction of the support of turbulence in molecular clouds comes from outflows.

II. KOSMA Results

We have been pursuing two types of outflow observation with the KOSMA 3 m telescope on the Gornergrat. We have searched for new outflows in promising objects such as

red nebulous objects (RNOs) (Cohen 1980) and IRAS point sources selected for colors characteristic of embedded stars. Our 3.'9 beam at 115 GHz will miss compact outflows due to beam dilution, but will find detached outflows that may be missed by larger telescopes. We have mapped extended outflows near RNO109 (Armstrong and Winnewisser 1989) and three IRAS point sources (L1228, L1221, and IRAS 22336+6855; Haikala and Laureijs 1988; Haikala and Dietrich 1988a).

We have also been mapping known outflows. A few extended outflows – L1551 especially – have previously been mapped to low surface brightness levels with high angular resolution, but the cost in observation time with large telescopes is high; thus, many other extended flows are not as sensitively mapped. With a small telescope, mapping to low surface brightness levels over a large area is quicker, making it easier for us find out how extended these outflows are. We have mapped the outflow in NGC2071, and have a partial maps of an outflow near ρ Oph and of the L1551 outflow.

Red Nebulous Objects

Of 13 sources observed from Cohen's catalog (1980), 11 show CO emission, and four to seven show high-velocity wings (Fig. 1). Except for L673, near RNO109, we have no mapping data for these sources, but the presence of the RNOs makes it more likely that the high-velocity gas is indeed due to star formation rather than some other process.

The distance to L673 is not well determined; a reasonable estimate is 300 pc (Herbig

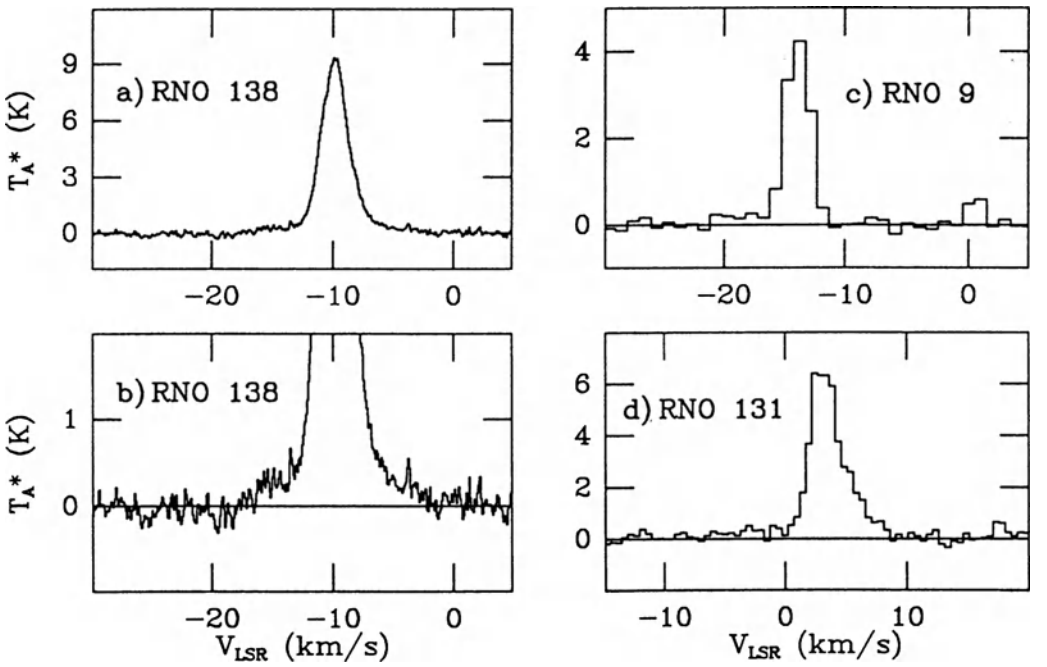

Fig. 1. ^{12}CO (1–0) spectra. **a, b:** RNO138, showing low-intensity red and blue wings. **c:** RNO9, showing a possible faint blue wing. **d:** RNO131, with a clear red wing and also a possible faint blue wing. Velocity resolution in **a** and **b**: 0.082 km s^{-1}; in **c** and **d**, 0.49 km s^{-1}

and Jones 1983). It contains two, and perhaps three, outflows. The first one discovered, by Edwards and Snell (1982) with the FCRAO 14 m telescope, is near AS353A, a T Tauri star, and HH32. The size that Edwards and Snell measured was $\sim 5'$. Knapp and Padgett (1984) observed the outflow region with the Bell Labs 7 m telescope and found a somewhat larger size, $\sim 7'$, and also found some hint of an outflow $5'$ to $10'$ further north. We observed the whole cloud with the 3 m telescope, and found another outflow in the northern part of the cloud, more or less centered on RNO109 (Fig. 1; Armstrong and Winnewisser 1989). The observed major axis of this northern outflow is $18'$. The outflow near HH32 is barely visible in our data; evidently it is beam diluted. The total mechanical luminosity of the RNO109 and HH32 outflows, scaled to a distance of 300 pc, is $0.024\,L_\odot$. The third outflow, if it is real, contributes less than $0.004\,L_\odot$ (Knapp and Padgett 1984).

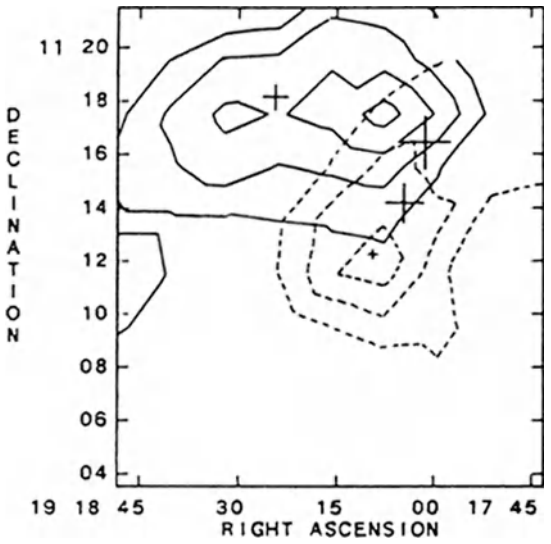

Fig. 2. Contours of total CO column density in the northern part of L673 for the red (solid line; 9.0 to 15.2 km s^{-1}) and blue (dashed line; -0.8 to 5.4 km s^{-1}) lobes of the northern L673 outflow. Contour levels are 3, 4, 5, and 6 times 1.4×10^{15} cm^{-2}. The crosses represent IRAS 25 μm point sources; the largest is RNO109.

IRAS Sources

Haikala and Dietrich (1988a) have been surveying IRAS point sources selected for colors characteristic of embedded stars and for intermediate luminosity with both the Gornergrat telescope and the SEST telescope. One of them is L1228, a high latitude dark cloud ($\ell = 20°$) that contains an outflow of $20'$ size found by Haikala and Laureijs (1988) (Fig. 3). Its distance is poorly known; Haikala and Laureijs scale their derived parameters to 100 pc, which places it at one scale height above the plane. Its mechanical luminosity is $0.04\,(D/100\,\mathrm{pc})\,L_\odot$. Haikala and Dietrich (1988a) show an outflow of $\sim 10'$ size in L1221, another high-latitude dark cloud, and another outflow, also $\sim 10'$ in size, near IRAS 22336+6855.

Mapping of Known Outflows

Haikala and Dietrich (1988b) have made some preliminary observations of CO (1–0) near the outflow in NGC2071. A comparison of the high-velocity gas observed in the

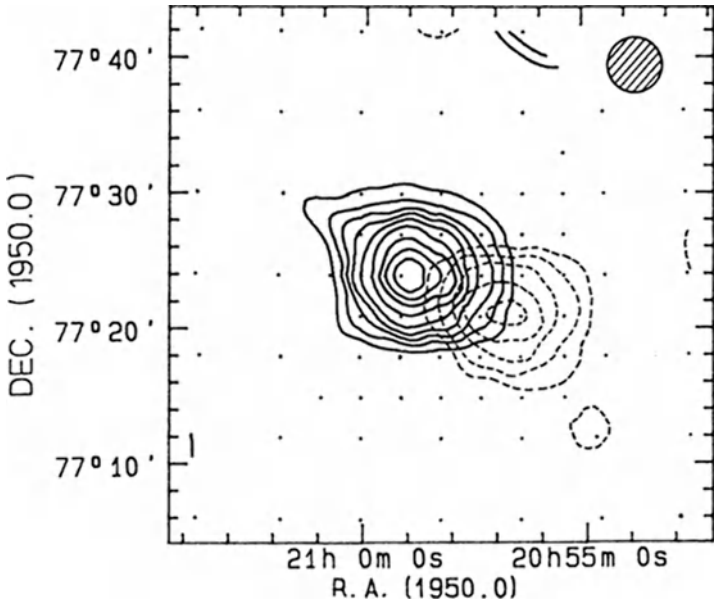

Fig. 3. Contours of CO (1−0) line intensity in L1228, integrated over the red (dashed line; −5.5 to 0 km s^{-1}) and blue (solid line; −15 to −9.5 km s^{-1}) wings. Contour levels start at 2.1 K km s^{-1} and continue in steps of 0.3 K km s^{-1}; dots show observed positions; and the 3.'9 beamsize is indicated with a circle.

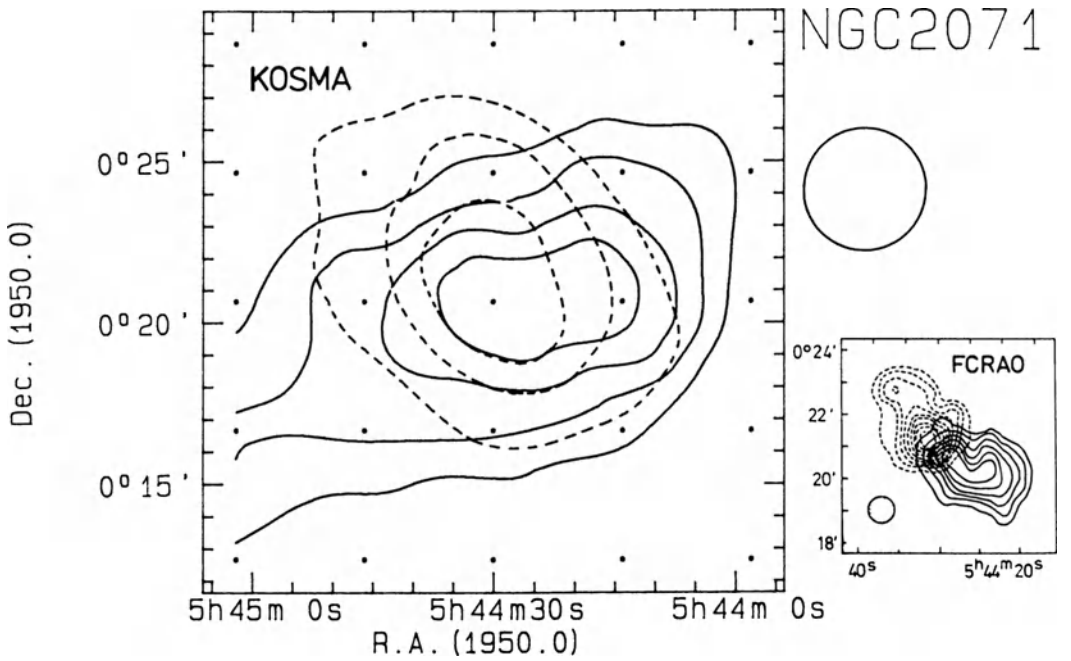

Fig. 4. Red- and blue-shifted CO (1−0) emission in NGC2071. To the left is a map made with the Gornergrat telescope. Contour levels are 1.5, 2.5, ... K km s^{-1}. Integration intervals, limited by the frequency-switching range in these observations, are 0 to 5 km s^{-1} and 15 to 20 km s^{-1}. To the right is the map presented by Snell *et al.* (1984). Contour levels are the same as in the Gornergrat map. The integration intervals, however, are wider: −20 to 5 km s^{-1} and 15 to 30 km s^{-1}.

Gornergrat spectra with the high-velocity gas observed by Snell *et al.* (1984) shows a somewhat more extended outflow in the 3 m data (Fig. 4). This is similar to the situation in L673, where the size observed by Knapp and Padgett (1984) is somewhat larger than that observed by Edwards and Snell (1982). Haikala and Dietrich (1988b) have also observed an outflow in the ρ Ophiuchi cloud, shown in Fig. 5.

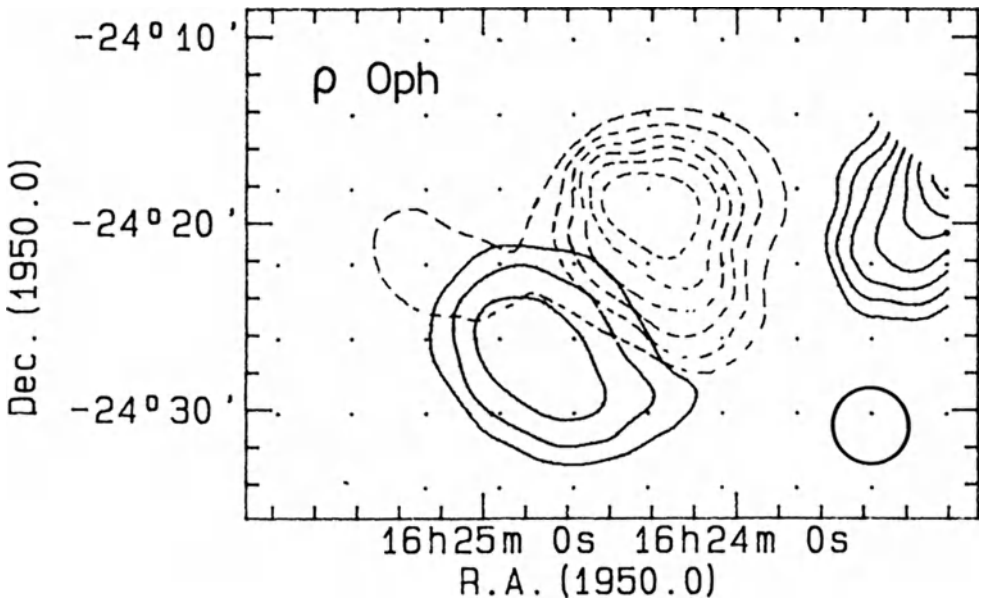

Fig. 5. Red- and blue-shifted CO (1−0) emission in the ρ Ophiuchi cloud; the red wing is shown with solid contour lines. Contour levels are 2.5, 3.0, 3.5, ... K km s^{-1}. Integration intervals are −5 to 1 km s^{-1} and 6 to 12 km s^{-1}.

Gierens (1988) has observed part of the L1551 outflow to determine whether the outflow is filled or hollow, but the data can also be used to compare the extent of the outflow as measured by the 3 m and 14 m telescopes. L1551 has been very completely mapped with the 14 m, and in this case, the width of the outflow (the only direction in which Gierens mapped) in the 3 m data agrees well with that in the 14 m data.

III. Are outflows the source of cloud turbulence?

What does all this mean for the energetics of molecular clouds? First, it is more confirmation that there is a large number of outflows and that most, if not all, stars undergo an outflow episode early in their lives. Second, there is now some indication that there are many *extended* outflows, where "extended" is a vague term indicating typical sizes of the order of half a parsec or more. If outflows are somewhat bigger than we have thought, they are more energetic and older than previously believed.

As to the outflow sizes, first consider the Gornergrat results I have been discussing. The L673 outflow is 1.3 × 0.9 pc in size; the L1228 outflow (if its distance $D = 100$ pc)

is 1.2 × 0.6 pc; the L1221 outflow is 0.3 pc (also for $D = 100$ pc), and the outflow in NGC2071 is ~ 2 pc in the Gornergrat map (with $D = 500$ pc [Strom *et al.*, 1975]), about twice the size shown by Snell *et al.* (1984). Some mechanical luminosities and dynamical timescales are shown in Table 1.

Table 1. Outflow timescales and mechanical luminosities

Source	Size	t_{dyn}	L_{mech}
L673			
AS 353A[a]	0.2 pc	3×10^4 yr	$0.012\,L_\odot$
Middle[b]	0.26	7×10^4	< 0.004
RNO 109[c]	1.3	9×10^4	0.012
L1228[d]	$0.5\,(D/100\,\mathrm{pc})$	$2 \times 10^4\,(D/100$ pc)	$0.04\,(D/100\,\mathrm{pc})$
Orion A[e]			
L1641N	0.3	1×10^4	2.0
L1641S	1.2	4×10^4	
Orion A East			
Orion A West			
Mon OB1[f]			
D	1.2	3×10^4	13
E	0.7		
G	0.9		
H	0.3		
I	0.6		

a. Edwards and Snell (1982) b. Knapp and Padgett (1984)
c. Armstrong and Winnewisser (1989) d. Haikala and Laureijs (1988) e. Fukui *et al.* (1986)
f. Margulis and Lada (1985); Margulis, Lada, and Snell (1988)

Consider as well two other recent studies. Fukui *et al.* (1986) have done an unbiased survey of the Orion A cloud and a few others. They have found four new outflows in Orion; two of them are quite extended (L1641N and S with maximum extents of 0.3 pc and 1.2 pc, respectively). Margulis and Lada (1985) and Margulis, Lada, and Snell (1988) have done an unbiased survey of the Mon OB1 cloud and find five to eight outflows with sizes ranging from 0.3 pc to 1.2 pc. The sizes and dynamical timescales, when given, are also shown in Table 1, as well as the total mechanical luminosities for these sets of outflows.

Now we can proceed to do some comparison of the energy in the turbulent motions themselves with the mechanical luminosity of the outflows. The approach I will take is to calculate how many outflows are necessary, in terms of energy, to sustain the observed turbulence.

First, I devise a "turbulent luminosity," the rate at which turbulent energy is lost via dissipation:

$$L_{\rm turb} = \frac{E_{\rm kin}}{t_{\rm diss}}. \tag{1}$$

The kinetic energy $E_{\rm kin}$ and dissipation time $t_{\rm diss}$ of the turbulence are given by

$$E_{\rm kin} = \frac{3}{16 \ln 2} M \Delta V^2, \tag{2}$$

$$t_{\rm diss} = X t_{\rm cross}, \tag{3}$$

$$\text{with} \quad t_{\rm cross} = \frac{d}{\Delta V / \sqrt{\pi \ln 2}}, \tag{4}$$

where d is the linear size of the cloud, ΔV is the FWHM linewidth, M is the mass, and X lies somewhere between unity and 10. This works out to

$$L_{\rm turb} \simeq 0.03 \left(\frac{M}{10^4 M_\odot}\right) \left(\frac{\Delta V}{1 \text{ km s}^{-1}}\right)^3 \left(\frac{d}{1 \text{ pc}}\right)^{-1} \left(\frac{X}{10}\right)^{-1} L_\odot. \tag{5}$$

Then the number of outflows needed to sustain the loss of turbulent energy through dissipation is

$$N = \frac{L_{\rm turb}}{\epsilon L_{\rm mech}}, \tag{6}$$

where ϵ is the efficiency of transferring outflow energy to turbulent motions.

I have already mentioned the results of Scalo and Pumphrey (1982), which correspond to $X = 7$. I have used this value in Table 2, which shows the number of outflows necessary to sustain the turbulence under the assumption that $\epsilon = 1$ using data for the observed outflows in the L673 (Armstrong and Winnewisser 1989), Orion A (Fukui *et al.* 1986), and Mon OB1 (Margulis and Lada 1985; Margulis, Lada, and Snell 1988) clouds. Comparison of the $N_{\rm needed}$ and $N_{\rm obs}$ columns shows that efficiencies ϵ of 5% to 30% are needed for energy injection from outflows to balance dissipative loss of turbulent energy.

Table 2. Number of outflows necessary to sustain turbulence

Source	$M_{\rm cloud}$	$d_{\rm cloud}$	ΔV	$L_{\rm turb}$	$N^a_{\rm needed}$	$N_{\rm obs}$
L673[b]	$300\,M_\odot$	2.4 pc	2.7 km s^{-1}	$0.011\,L_\odot$	0.8	2-3
Orion A[c]	20000	20	3	0.12	0.5	9
Mon OB1[d]	30000	15	6	1.9	0.9	5-8

a. Calculated with $X = 7$ and $\epsilon = 1$ (see text) b. Armstrong and Winnewisser (1989)
c. Fukui *et al.* (1986) d. Margulis and Lada (1985); Margulis, Lada, and Snell (1988)

One possible objection to this picture concerns clouds with supersonic linewidths but no embedded IRAS sources. If outflows are the source of support for these clouds, there should be some sign that star formation has taken place.

One way out of this difficulty is provided by the Scalo and Pumphrey result that the timescale for dissipation of turbulence may be several crossing times. In L673, $t_{\rm diss}$ is 10^7 yr for $X = 7$. That is enough time for a star with a peculiar velocity within the cloud of 1.8 km s^{-1} to move 18 pc, or enough time for a star to drift entirely out of the cloud before the turbulence dissipates. It is also enough time for some stars to evolve onto the main sequence, when they will cease to be conspicuous IR objects; if they are not massive stars, we may not know that they are there. RNO109 may be an example of the first process. The fact that it is optically visible suggests that it is near the front surface of the cloud. It may have drifted nearly out of the cloud since it started making the outflow that seems to be associated with it.

Another possible objection concerns the morphology of clouds and cloud complexes. The image of Orion B shown by Bally (1988) shows many loops and filaments, structures that do not look "relaxed," and that indicate that the structure of the complex is dominated by shocks. One possibility is that some of this structure is due to "fossil" outflows. Another, perhaps more likely, possibility, is that support due to outflows is more important on small scales; the difference in scale between L673 and Orion B is about an order of magnitude.

V. Conclusions

My conclusions, roughly in order of decreasing certainty, are:

1. There are many outflows. The numbers of known outflows from the work of several groups has strengthened the conclusion that nearly all, if not all, stars go through an outflow-producing phase at the beginning of their lives.
2. Many of them are extended outflows. These results also suggest that the number of "extended" outflows is large, and that the measured sizes of outflows are to some degree influenced by the size of the telescope with which they are observed. This is not just a matter of poorer resolution with smaller telescopes; it also seems to be a selection effect.
3. Outflows can be a major source of support for turbulence in clouds. The efficiency of transfering kinetic energy from the outflow to the turbulent velocity field need not be higher than 5% to 30%. The Scalo and Pumphrey (1982) results also give us a possible way out of the problem of clouds with supersonic linewidths but no IR sources: there may be enough time for a star to form, create an outflow, and either drift out of its parent cloud or evolve onto the main sequence before the resulting turbulence dissipates.

Acknowledgements. The written version of this talk benefitted from discussions with J. Bally. L. Haikala, O. Dietrich, and K. Gierens kindly supplied data in advance of publication. The KOSMA 3 m radio telescope at Gornergrat-Süd Observatory is operated by the University of Cologne and supported by the Deutsche Forschungsgemeinschaft (DFG) through grant SFB-301, as well as special funding from the Land Nordrhein-Westfalen. The Observatory is administered by the Hochalpine Forschungsstationen Jungfraujoch und Gornergrat, Bern.

References

Armstrong, J. T., and Winnewisser, G. 1989, *Astr. Ap.*, in press.
Bally, J. 1988, this volume.
Cohen, M. 1980, *A. J.*, **85**, 29.
Edwards, S., and Snell, R. L. 1982, *Ap. J.*, **261**, 151.
Fleck, R. C. 1981, *Ap. J. (Letters)*, **246**, L151.
Fukui, Y., Sugitani, K., Takaba, H., Iwata, T., Mizuno, A., Ogawa, H., and Kawabata, K. 1986, *Ap. J. (Letters)*, **311**, L85.
Gierens, K., 1988, this volume.
Haikala, L., 1988, this volume.
Haikala, L., and Dietrich, O. 1988a, this volume.
Haikala, L., and Dietrich, O. 1988b, in preparation.
Haikala, L., and Laureijs, R. 1988, *Astr. Ap.*, submitted.
Henriksen, R. N., and Turner, B. E. 1984, *Ap. J.*, **287**, 200.
Herbig, G. H., and Jones, B. F. 1983, *A. J.*, **88**, 1040.
Knapp, G. R., and Padgett, D. L. 1984 preprint; unpublished.
Margulis, M., and Lada. C. J. 1985, *Ap. J.*, **299**, 925.
Margulis, M., Lada, C. J., and Snell, R. L. 1988, preprint.
Scalo, J. M., and Pumphrey,W. A. 1982, *Ap. J. (Letters)*, **258**, L29.
Snell, R. L., Scoville, N. Z., Sanders, D. B., and Erickson, N. R. 1984, *Ap. J.*, **284**, 176.
Shu, F., Lizano, S., and Adams, F. 1986, in *Star Forming Regions*, (IAU Symposium No. 115), M. Peimbert and J. Jugaku eds., Reidel, Dordrecht.
Strom, K. M., Strom, S. E., Carrasco, L., and Vrba, F. J. 1975, *Ap. J.*, **196**, 489.

OPTICAL EMISSION-LINE JETS IN STAR FORMATION REGIONS

Reinhard Mundt

Max-Planck-Institut für Astronomie, Königstuhl 17
6900 Heidelberg, Fed. Rep. of Germany

SUMMARY. The morphological and kinematical properties of optical emission-line jets and related collimated "optical" flows from young stellar objects are reviewed. Some recently obtained high-quality CCD images are displayed to illustrate the morphological properties of these flows and their associated bow-shock like structures. The available data on the driving sources of these flows are also reviewed.

1. INTRODUCTION

It it now generally accepted that energetic, and often bipolar, mass outflows are an important phase in early stellar evolution for all types of young stars. Evidence for such outflows is provided by a variety of phenomena (see e.g. Lada 1985, Mundt 1985a, Strom and Strom 1987, Staude 1988). Many of these phenomena result from the interaction of the outflowing matter with the surrounding molecular cloud.

The two most detailed studied phenomena are: (1) high-velocity molecular gas (HVMG) and bipolar molecular flows, (2) Herbig-Haro (HH) objects and optical jets. In the former case one studies the molecular gas components near young stellar objects (YSOs) with significantly higher velocities than the typical turbulent velocities of molecular clouds (~ 1 km/s). In the vicinity of stars of low to moderate luminosity (1-100 $L_{\odot}$) the characteristic velocity of the molecular flows is 5-20 km/s. The HVMG itself is probably molecular cloud material which has been somehow accelerated by the stellar wind. For example, it could be located in the shell of a wind-blown cavity. The properties of molecular outflows has extensively been discussed in a number of recent reviews (e.g. Lada 1985, Snell 1987) and will not be further discussed here.

Optical emission-line jets and HH objects associated with young stars trace flow components with a much higher degree of collimation and velocity than the HVMG. The measured radial velocities can reach values of up to 450 km/s and for some jets the opening angle is less than 1 degree. A discussion of some of the observational properties of the jets and those of their sources will be given below. For a more extensive discussion the reader is referred to Mundt, Brugel, and Bührke 1987 (hereafter MBB87).

HH objects and jets are intimately related phenomena. Both show the same emission line spectrum, which is formed behind radiative shock waves with velocities of 40-100 km/s. Furthermore, several long known HH objects form the brightest knots of a jet. On the basis of such observations it has been suggested (e.g. Mundt 1985b) that many HH objects simply represent the locations of the most brightest radiative shocks in a jet from a young star. This does not imply a unique model for all HH objects, since there is a large variety of ways to excite shocks in a collimated outflow (e.g. MBB87). For example, one expects strong shocks in the working surface of the jet, but it also possible to excite shocks along the jet (e.g. through fluid dynamical instabilities).

The currently available data on jets, HH objects, and collimated optical flows have been discussed extensively in several recently published review articles (Schwartz 1983; Mundt 1985a, 1985b 1987, 1988, Cantó 1986, Dyson 1987, Strom and Strom 1987). Since so many recent reviews are available, only few topics will be discussed here.

2. OBSERVATIONAL PROPERTIES

2.1 Morphology

Most jets and collimated optical flows have been discovered within the past 6 years through deep CCD imaging of HH objects and YSOs in the strongest emission lines of HH objects (e.g. Hα, [SII] $\lambda\lambda$6716, 6731). In order to be sure that the observed structures are indeed due to in situ formed line emission (and not due to scattered light) a continuum frame has to be taken as well.

Definitions of a jet or collimated flow from a young star were recently discussed by Mundt (1988). He suggested to define a jet as a

knotty, elongated structure with an HH-like spectrum and a length-to-diameter ratio L/D ≥ 5. In the case of a collimated flow the spectrum and morphology is the same, but the length-to-diameter ratio is smaller (2 ≤ L/D < 5).

By far the best example of a jet is the one emanating from HH34-IRS (see Fig. 1). An example of a collimated flow is DG Tau (e.g. Mundt 1988), HH43 (e.g. Strom et al. 1986), or HH57 (e.g. Reipurth 1985a). So far more than about 25 jets and more than about 15 collimated optical flows have been discovered. The most extensive lists of such objects have been published by MBB87 and by Strom et al. (1986). Additional recent examples are discussed by Reipurth (1985b, 1988), Reipurth and Graham (1988), Ray (1987), Solf (1987), Hartigan and Graham 1987, Mundt (1988), and by Mundt, Ray and Bührke (1988).

On the following pages several examples of jets associated with YSOs are shown. All these CCD images have been taken in January 1987 at the prime focus of the 3.5 m telescope on Calar Alto, Spain. For

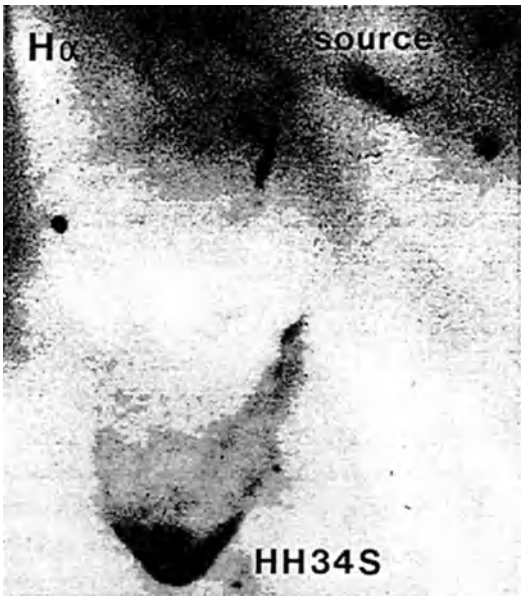

Fig. 1a: Hα image of the HH34S region. A knotty jet is pointing towards HH34S (see Fig. 1b). Note that HH34S has the shape of a bow shock. On all figures north is up and east to the left. Image size 75x85 arcsec.

Fig. 1b: Isointensity contour plot of a [SII] CCD frame of the jet associated with HH34S. Twelve knots are visible in the section shown in a typical separation of 2 arcsec. Image size 15x31 arcsec.

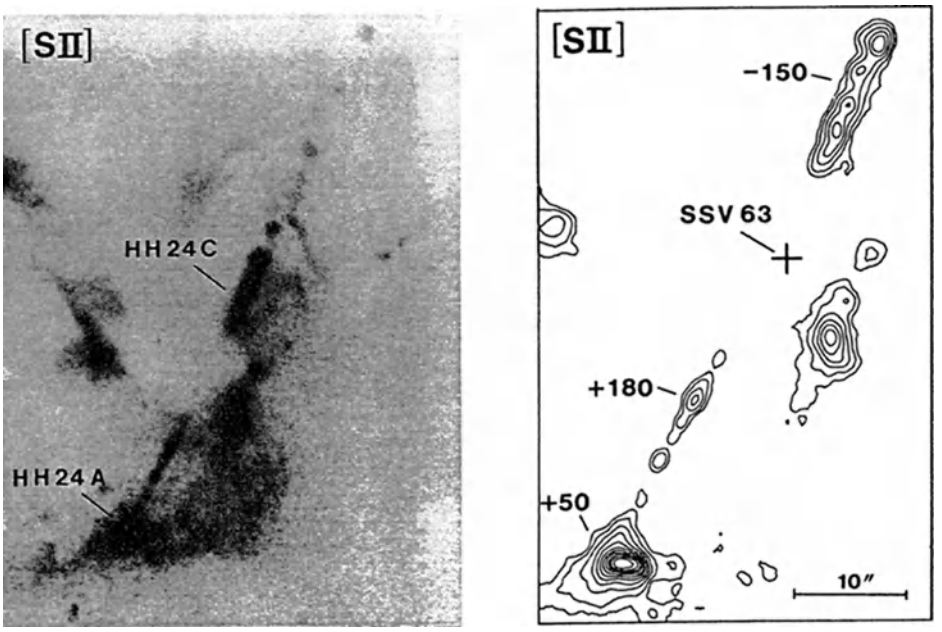

Fig. 2: HH24 region. The [SII] image and the corresponding contour plot show the knotty bipolar jets emanating from SSV63 (Solf 1987). The indicated numbers in this and the following figures are km/s. Image size of the left hand part 175x250 arcsec.

most images displayed here a [SII] λλ6716, 6731 interference filter was used ($\Delta\lambda$ = 70 Å).

Among the presently known jets the following morphological features seem to be common in a significant number of them:

- knots along the jet
- bow shocks or bright knots at the jet's end
- wiggles

(i) Knots Along the Jet

The best examples of knotty stellar jets shown here are associated with the following sources: HH34-IRS (Fig. 1), HH24-SSV63 (Fig. 2), and HH30-star (Fig. 3). The HH34 jet is of course the most striking example. 13 knots have been discovered by Bührke, Mundt, and Ray (1988) over a distance of 30 arcsec from the source. It should be pointed that all jets show knots on high dynamic range images; i.e

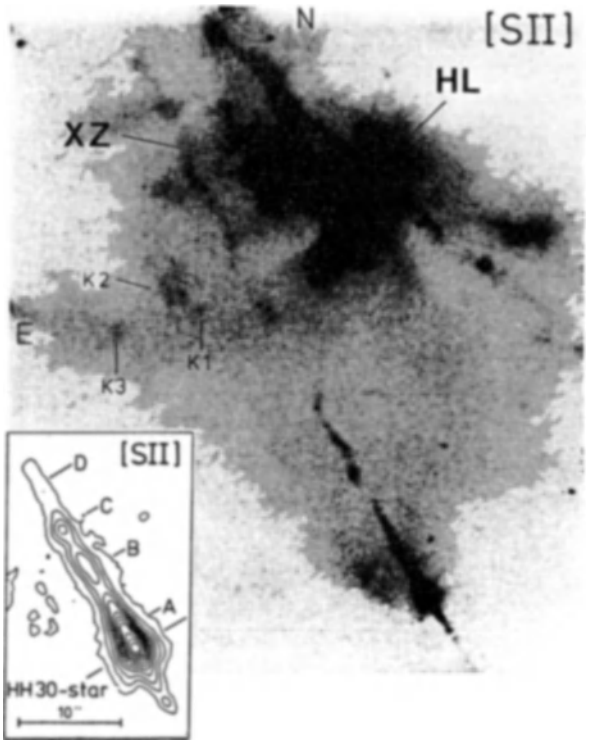

Fig. 3a: HH30-HL/XZ Tau region. High contrast [SII] image, showing the 2 arcmin (0.1 pc) long jet emanating from the HH30-star. A corresponding contour plot of this jet near the source is also shown. The "over-exposed" region near XZ/HL Tau is shown more clearly in Fig. 3b.

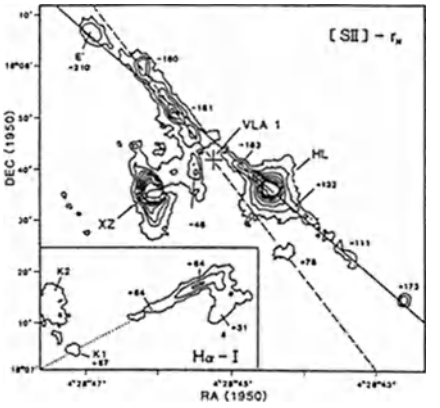

Figure 3b: Composite "pure" emission line contour plot of the HL/XZ Tau region. The majority of this plot shows the difference between [SII] and a red continuum frame (r_N). It has been shown by Mundt, Ray and Bührke (1988) that in this small region 4 sources generate jets or other "optical" flows, namely HL Tau, VLA1, XZ Tau and the not yet discovered Hα-jet source.

knots are very probably a morphological property common to all jets.

ii) Bow Shocks and Bright Knots at the Jet's End

These morphological features are described here together, since they are physically closely related (i.e. part of the jet's working surface). One of the best examples of an association between a jet and a bow shock like structure is HH34S (see Fig. 1). Other good examples are HH1, RNO 43N (see Fig. 4) or RNO 43S. Bright knots are observed at the end of several flows. Examples are the HH46/47 jet (e.g. Graham and Elias 1983) or the jet associated with AS 353A (Hartigan, Mundt and Stocke 1986). Wheather a bright knot or an extended

Fig. 4: RNO 43N; this is a further example of an extended HH object of which the outer edge (at least at the western side) has the shape of a bow shock. The associated jet is relatively diffuse and patchy. Image size about 70 x 120 arcsec.

bow shock appears at the jet's end depends on various factors which have been discussed elsewhere (e.g. Mundt 1988).

iii) Wiggles

Nearly all jets are not perfectly straight, but show at least small changes in direction. Among the examples shown here, wiggles are most prominent in the case of HH30.

2.2 Kinematic and Spectroscopic Properties

In Table 1 the typical observational properties of the jets and their sources are summarized.

As mentioned in section 1 the jets show the same spectrum as HH objects. In several cases of knotty jets and knotty collimated flows a spectrum of rather low excitation is observed (e.g. I([SII] $\lambda\lambda$6716, 6731)/I(Hα) $\approx$ 3). The best examples are the flows from HH34-IRS (Reipurth et al. 1986), SSV13 (Brugel, Böhm, and Mannery 1981), SSV63 (Solf 1987), HH1-VLA1 (Strom et al. 1985), and DG Tau B (MBB87). Their excitation can be explained by very oblique internal shocks.

Table 1: Typical properties of jets from young stars

projected length:	0.02 - 0.5 pc
length-to-width ratio:	10 - 20
opening angle:	1 - 10°
radial velocity:	0 - 400 km/s
velocity dispersion (FWHM):	< 30 km/s (6 cases), ~100 km/s (5 cases)
$v_{tangential}$ of bright knots:	50 - 350 km/s
electron density:	400 - 2000 cm^{-3}
spectrum:	shock-excited emission line spectrum (HH spectrum), v_{shock} = 40-100 km/s
sources:	low luminosity IR sources (1-10 $L_{\odot}$) or highly extincted T Tauri like stars with reflection nebulae.

Radial velocity data are available for nearly all flows. The mean radial velocities are of the order of 100-150 km s^{-1}, with a maximum observed velocity of about 400 km s^{-1} (for details see MBB87).

The relatively high radial velocities are accompanied by moderate velocity dispersions of typically 30-100 km s^{-1} (FWHM). Recent observations with the Coudé spectrograph of the 2.2 m telescope on Calar Alto (T. Bührke, priv. comm.) showed that the jets of HH30, HL Tau, Haro 6-5B, DG Tau B have very small velocity dispersions in the [SII] lines (FWHM ≤ 30 km/s). Such small velocity dispersions are expected on theoretical grounds, if the emitting material is excited by oblique internal shocks (Falle, Innes and Wilson 1987).

Both blue and redshifted jets are observed. About 50% of the know flows are optically bipolar on the basis of radial velocity or proper motion data (see e.g. Fig. 2 and 3). In about half of these, there are strong differences in the morphology (e.g. opening angle) and spectroscopic properties between the two sides of the outflow (MBB87). Proper motion data using photographic plates are available for 40% of the flows. However, mainly measurements of the brightest knots were possible, which are located normally at the end of the flow. The measured tangential velocities range from 50-350 km s^{-1}. Recently Neckel and Staude (1987) were able to measure the proper motions of the knots of the L1551-IRS5 jet with the help of CCD images. For all 4 knots in the jet they derived a tangential velocity of about 200 km/s. Similar data were obtained by Mundt et al. (1989)

for the jets from HL Tau and VLA1-HL Tau with tangential velocities of up to 380 km/s.

For more than 15 of the currently known jets and collimated flows the radial velocities are high enough (> 50 km/s) to study radial velocity variations along the flow axis (for details see MBB87). In general a complex velocity field is observed and sometimes several flow components are present. The only correlation in the kinematic data is the following: when a bright knot is present at the end of the jet a radial velocity decrease is observed within or near the knot (or the data are at least consistent with a decrease). This has been interpreted by flow deceleration in the jet's working surface (e.g. MBB87). Known examples are the flows associated with T Tau, DG Tau, HH24, HH33/40, HH46/47, and AS 353A. The corresponding kinematic data in the case of HH24-SSV63 are indicated in Figure 2. However, there is no indication that the flow velocity gradually decreases along the jet (before the bright knot at the jet's end), which means that the kinetic energy is transported rather efficiently along the jet (MBB87; Bührke, Mundt, and Ray 1988).

The electron density N_e in the jets, based upon the [SII] 6716/6731 line ratio, has typically values of 400-2000 cm^{-3}. In 9 of the 12 flows with reasonable [SII] data N_e is decreasing along the flow direction, or at larger distances from the source the average electron density is smaller. This correlation is not surprising, since for a diverging flow with constant mass flux and velocity the density should decrease with increasing distance from the source.

3. PROPERTIES OF THE JET SOURCES

In all cases, where the jet source is detectable on a CCD frame (e.g. an I frame) a reflection nebula can be detected on deep exposures. In a few cases only a reflection nebula is detectable, since the source itself is so highly extincted; probably by a circumstellar disk (e.g. VLA1-HH1/2, Strom et al. 1985). About 70% of these nebula can be described as conical or cometary in nature, and perhaps most interestingly in at least 8 cases the nebular axis and jet axis is approximately aligned. One of the best examples are the jets associated with L1551-IRS5 (e.g. Mundt and Fried 1983) and 1548C27 (Mundt et al. 1984).

For the nebula associated with Haro 6-5B, L1551-IRS5 and R Mon detailed polarization maps have been obtained (see respectively Gledhill, Warren-Smith, and Scarott 1986; Lenzen 1987; Aspin, McLean, and Coyne 1985). These and other observations (e.g. Hodapp 1984 and references therein) show that SSV13, Haro 6-5B, DG Tau, L1551-IRS5, R Mon, and 1548C27 are highly polarized objects with polarization ranging from 5-22%. A interesting fact is that for all these highly polarized objects (except 1548C27; see Craine, Boeshaar, and Byard 1981) the electric polarization vector is approximately perpendicular to the jet (measured angles 72-89°). These observations are attributed to the presence of a circumstellar disk) the axis of which defines the outflow axis. In such a situation the high polarization can in principle be explained by scattering within the polar lobes of the disk (Elsässer and Staude 1978). For a detailed discussion of the available polarization data of outflow sources and YSOs the reader is referred to Bastien (1988).

Most sources are (or appear) highly reddened ($A_v \gtrsim 3$-5). The high A_v values and the associated reflection nebula argue for a considerably smaller average age compared to typical T Tauri stars. Very probably the jet sources belong to the youngest optically selected YSOs. The flows from the sources with large optical brightnesses have all high radial velocities of > 150 km s^{-1}. This suggests that their low A_v-values result from a relatively large angle (greater than say 30°) between the line of sight and the plane of the presumed circumstellar disk.

Nearly all published jet sources have luminosities of 0.5-60 $L_\odot$. Only R Mon has a much higher luminosity (~ 740 $L_\odot$). This does not mean that highly collimated flows are predominantly associated with low luminonsity stars, since the published data are heavily biased towards these YSOs. Indeed, in a recent CCD survey of high luminosity (10^3-3×10^4 $L_\odot$) CO outflow sources Poetzel, Ray, and Mundt (1989) found about 10 sources associated with HH emission; three of these sources have jets.

References

Aspin, C., McLean, I.S., and Coyne, G.V. 1985, Astr.Ap. **149**, 158

Bastien, P. 1988, in "Polarized Radiation of Circumstellar Origin", ed. G.V. Coyne (Vatican Obs.), in press

Brugel, E.W., Böhm, K.-H., Mannery, E., 1981, Ap.J.Suppl. **47**, 117

Bührke, T., Mundt, R., and Ray, T. 1988, Astr.Ap., submitted

Cantó, J. 1986, in "Cosmical Gas Dynamics", ed. F.D. Kahn, VNU Science Press (Utrecht)

Craine, E.R., Boeshaar, G.O., and Byard, P.L. 1981, A.J. **86**, 751

Dyson, J.E. 1987, in "Circumstellar Matter", eds. I. Appenzeller and C. Jordan, Reidel (Dordrecht), p. 159

Elsässer, H., and Staude, H.J. 1978, Astr.Ap. **70**, L3

Falle, S.A.E.G., Innes, D., and Wilson, M.J. 1987, M.N.R.A.S. **225**, 741

Gledhill, T.M., Warren-Smith, R.F., and Scarott, S.M. 1986, M.N.R.A.S. **223**, 867

Graham, J.A., and Elias, J.H. 1983, Ap.J. **272**, 615

Hartigan, P., and Graham, J.A. 1987, A.J. **93**, 913

Hartigan, P., Mundt, R., Stocke, J. 1986, A.J., **91**, 1357

Hodapp, K.-W. 1984, Astr.Ap. **141**, 255

Lada, C.J. 1985, Ann. Rev. Astron. Astrophys. **23**, 267

Lenzen, R. 1987, Astr.Ap. **173**, 124

Mundt, R. 1985a in "Nearby Molecular Clouds", ed. G. Serra, Lecture Notes in Physics, **217**, Springer Verlag (Heidelberg), p. 160

Mundt, R. 1985b in "Protostars and Planets II", eds. D. Black and M. Matthews, University of Arizona Press (Tucson), p. 414

Mundt, R. 1987, in "Circumstellar Matter", eds. I. Appenzeller and C. Jordan, Reidel (Dordrecht), p. 147

Mundt, R. 1988, in "Formation and Evolution of Low Mass Stars", eds. A.K. Dupree, M.T.V.T. Lago (Kluwer Academic Publ., Dordrecht), p. 257

Mundt, R., Brugel, E.W., and Bührke, T. 1987, Ap.J. **319**, 275 (MBB87)

Mundt, R., Bührke, T., Fried, J.W., Neckel, T. Sarcander, M., and Stocke, J. 1984, Astr.Ap. **140**, 17

Mundt, R., and Fried, J.W. 1983, Ap.J. (Letters) **274**, L83

Mundt, R., Ray, T., and Bührke, T. 1988, Ap.J. (Letters) **333**, L69

Mundt, R., Ray, T., Bührke, T., and Raga, A. 1989, in prep.

Neckel, T., and Staude, J. 1987, Ap.J. (Letters), **322**, L27

Poetzel, R., Ray, T., and Mundt, R. 1989, in prep.

Ray, T. 1987, Ast.Ap. **171**, 145

Reipurth, B. 1985a, Astr.Ap. **143**, 435

Reipurth, B. 1985b, in "(Sub)-Millimeter Astronomy", ESO-IRAM-Onsala Workshop, eds. P. Shaver and K. Kjar, p. 459

Reipurth, B. 1988, Astr.Ap., in press

Reipurth, B., Bally, J., Graham, J.A., Lane, A., and Zealey, W.J. 1986, Astr.Ap. **164**, 51

Reipurth, B., and Graham, J.A. 1988, Astr.Ap., in press

Schwartz, R.D. 1983, Ann. Rev. Astron. Astrophys. **21**, 209

Snell, R.L. 1987, in "Stars Forming Regions", eds. M. Peimbert and J. Jugaku, Reidel (Dordrecht), p. 213

Solf, J. 1987, Astr.Ap. **184**, 322

Staude, J. 1988, in "Structure of Galaxies and Star Formation", proceedings of the 10th Europ. Reg. Astr. Meeting of the IAU

Strom, S.E., and Strom, K.M. 1987, in "Star Forming Regions", eds. M. Peimbert and J. Jugaku, Reidel (Dordrecht), p. 255

Strom, S.E., Strom, K.M., Grasdalen, G.L., Sellgren, K., Wolff, S., Morgan, J., Stocke, J. and Mundt, R. 1985, A.J. **90**, 2281

Strom, K.M., Strom, S.E., Wolff, S.C., Morgan, J., and Wenz, M. 1986, Ap.J. Suppl. **62**, 39

THE GALACTIC CENTER - A Larger Scale View

Rolf Güsten
Max-Planck-Institut für Radioastronomie
Auf dem Hügel 69, 5300 Bonn 1, Federal Republic of Germany

ABSTRACT. The large scale kinematics and physical characteristics of the interstellar gas within the innermost few 100 pc of the galactic center is discussed. A major fraction of the total of $\sim 10^8$ $M_\odot$ of dense gas, representing ~10 % of the Galaxy's neutral mass, resides in a number of giant (~100 pc sized) molecular cloud complexes. In comparison with the galactic disk, these clouds reveal outstanding physical and chemical characteristics. Pervasive high temperatures ($\langle T_k \rangle \sim 70$ K), linewidths ($\geq$10-20 kms^{-1}) and densities ($\langle n \rangle \sim 10^4$ cm^{-3}) seem related to the clouds' location (tidal stresses) in the steep gravitational potential of the central stellar cluster.

1. INTRODUCTION

The galactic center is the only galactic nucleus which it is possible to study at sub parsec scale, and hence it has received continuing attention during the last two decades. In this review, I will concentrate on the morphology of the central mass distribution, and on the heavily perturbed kinematics and exceptional physical characteristics of the interstellar gas within the innermost few hundred pc of the galactic nucleus. The galactic center cloud population differs significantly from giant molecular clouds found in the more quiescent galactic disk, and understanding the excitation conditions of the galactic center gas, seems a necessary condition in order to properly analyze molecular line data measured towards extragalactic nuclei. More comprehensive reviews can be found in Genzel & Townes (1987; emphasizing the central 10 pc of the Galaxy), and in particular, in the proceedings of the recent IAU Symposium No.136 on 'The Galactic Center' (ed. M. Morris, Los Angeles, July 1988). The following, rather condensed discussion follows closely my review on the distribution of gas and dust within the innermost few degrees, presented at that conference.

2. LARGE-SCALE KINEMATICS

As defined by the spatial fall-off of the far-infrared dust and radio continuum emission (and of the stellar and interstellar mass surface densities), the galactic center stands out from the inner disk component with a characteristic size of 3 x 2 degrees (Fig.1; 1° = 150 pc for R_o=8.5 kpc). [On larger scales however, the lower density gas inside the so-called '3-kpc arm' is kinematically distinct from the more quiescent galactic disk in its highly perturbed motions, with non-circular (outward directed) velocities of the same order as the rotational velocities.] Between a few 100 pc and ~2 kpc from the nucleus, much of the interstellar gas, traced best in the HI 21 cm line, resides in a tilted disk whose plane of symmetry is inclined by ~20° relative to the galactic plane, and which major characteristics can be modelled by motions along closed, non-self-intersecting elliptical streamlines (Burton & Liszt, 1978; Liszt & Burton, 1980).

Embedded within this tilted (HI) ellipsoid, resides a massive (~10^8 M_o), ~450 pc sized layer of dense molecular clouds (composed of huge cloud complexes such as Sgr A, Sgr B2, and 'Clump 2'; sketched in Fig.1). The gas distribution is azimuthally asymmetric with ~2/3 of the mass displaced to positive longitudes (e.g., Bally et al., 1988, for the most complete data coverage), and bulk velocities of the main ridge (Fig.2) are significantly lower than expected for a smooth gas distribution in equilibrium rotation about the nucleus. According to Cohen & Dent (1983) most clouds are located in a narrow bar-like structure, inclined to the l-o-s by ~50°. A physically and kinematically distinct feature is the so-called 'expanding molecular ring', whose near side is prominently absorbing the Sgr A continuum at v_r ~ -135 kms^{-1} (Fig.2). The ring is tilted relative to the galactic plane by ~10°, with an orientation similar to that of the larger-scale HI ellipsoid.

The dynamics behind these features is not yet understood. In view of the short timescales involved - differential galactic rotation tends to wipe out these asymmetries within a few 10^6 yr -, the perturbed kinematics might be due to a recent explosive event some 10^6 yr ago (e.g., Oort 1982). But the energetic requirements are prohibitive (~10^{55} erg), and because of the lack of any direct evidence for violent activity on these timescales, it is more likely that the observed non-circular velocities and the transient morphology represent the dynamical response of the gas to an (oval or bar-like) perturbation of the central gravitational potential. On larger scales, e.g. for the galactic 3-kpc arm (Sanders, 1979), numerical simulations have been successful in showing that rotating stellar bars may force the gas into elliptical ringlike orbits (outside the bar). Whether there exists any rapidly rotating, non-axisymmetric perturbation associated with the innermost stellar cluster, that might result in the strong dynamical response required for the 'expanding molecular ring', needs to be explored both observationally and theoretically (see discussion in Sanders, 1988).

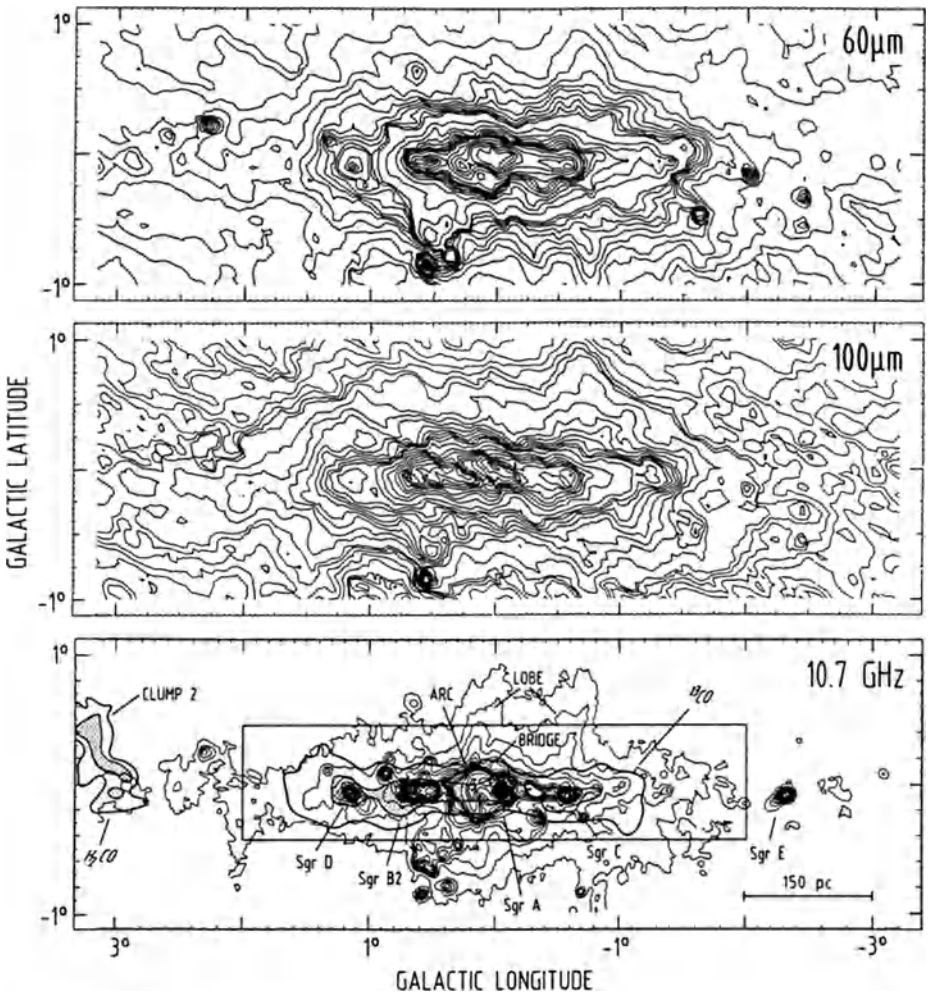

Fig.1. Guide to the inner few 100 pc of the galactic center, showing the molecular gas layer (Heiligman, 1987; Zylka et al., 1988) superimposed on the 10 GHz radio continuum emission (Handa et al., 1987). Prominent radio features are labelled. Top panels display the 60 and 100 μm surface brightness distribution, as inferred from the IRAS data by Cox & Laureijs (1988).

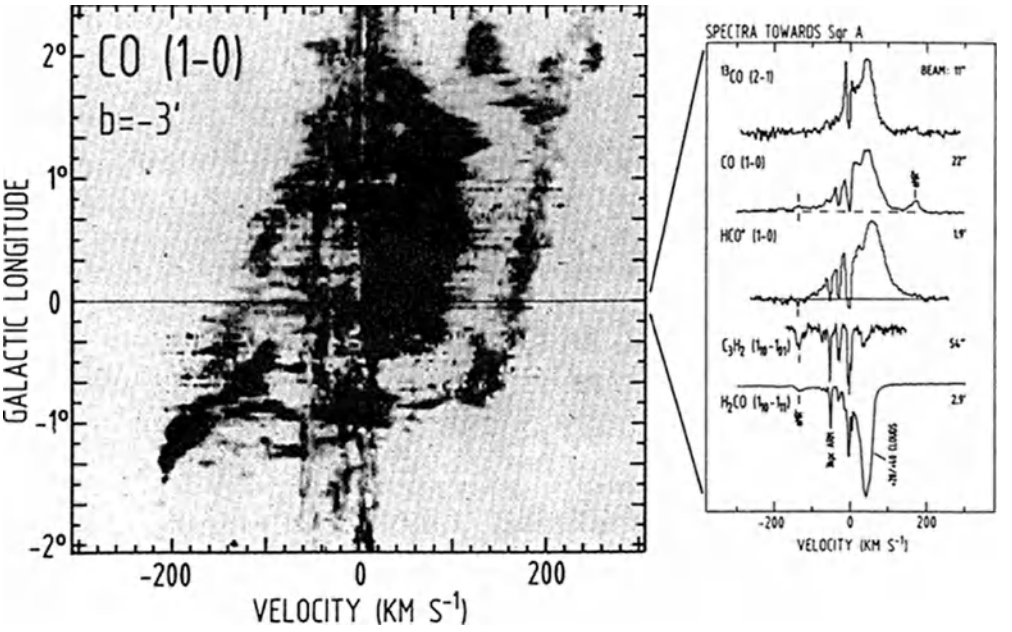

Fig.2. Grey-scale representation of the CO(1-0) longitude-velocity diagram along the galactic plane (b=-3'; Liszt & Burton, 1978). To the right, selected emission and absorption line spectra towards the galactic nucleus are compared. Major velocity features arise from the '+20/+40 kms^{-1} clouds' close to the galactic center, the 'expanding molecular ring' at v~-135 and +165 kms^{-1} (front and rear part, respectively), and from several larger scale line-of-sight structures (gas at v=-54 kms^{-1} resides in the so-called '3 kpc-arm'). [From Güsten, 1988]

3. GLOBAL CHARACTERISTICS OF THE CENTRAL 500 pc

A total of ~10^8 $M_\odot$ of dense (dominantly molecular) gas, representing 5-10% of the Galaxy's neutral mass content, has settled in this thin (~40 pc FWHM) central gas layer. Volume averaged gas densities, <n> ~100 cm^{-3}, exceed typical mean densities anywhere else in the Galaxy by ~2 orders of magnitude (see Table I for a compilation). But comparison with the <u>total</u> mass of stars (and gas), as inferred from the HI rotation curve and the 2 μm IR radiation of the stellar cluster, shows that only a small fraction of matter, μ ~0.01, is left in the interstellar phase. The bulk of matter, $M_* \sim 7\ 10^9$ $M_\odot$ inside 500 pc galactocentric radius, is locked-up in long-lived low-mass stars. The advanced state of evolution of the galactic center (for comparison, μ_D ~0.05-0.10, in the galactic disk) is consistent with the enhanced chemical enrichment of the interstellar medium with ejecta from evolved stars (e.g., Güsten &

Table I. Characteristics of the Central Gas Layer [from Güsten (1988)]

	Central 500 pc	Galactic Disk
Masses and Densities		
Stars M_*	$10^{9.8}$ $M_\odot$	--
Gas, atomic	$10^{6.4}$ $M_\odot$	$\sim 10^9$ $M_\odot$
.., molecular	$10^{7.9}$ $M_\odot$	$\sim 10^9$ $M_\odot$
Gas fraction $\mu = M_g/M_*$	~0.01	~0.05-0.10
Abundance [HI]/[H_2]	~0.05	~2
Gas density $\langle n \rangle_v$	100 cm^{-3}	1-2 cm^{-3}
.. surface density σ	$\geq$100 $M_\odot pc^{-2}$	~5 $M_\odot pc^{-2}$
Star Formation		
Rate Φ	0.3-0.6 $M_\odot yr^{-1}$	~5.5 $M_\odot yr^{-1}$
Efficiency Φ/M_g	5 10^{-9} yr^{-1}	10^{-9}-10^{-8} yr^{-1}
	Center Clouds	**Disk Clouds**
Cloud Characteristics		
Mass [$M_\odot$]	10^{5-6}	
Size [pc]	20-30	
Density [cm^{-3}] $\langle n \rangle$	~10^4	~$10^{2.5}$
Temperature [K] $\langle T \rangle$	~70	~15
hot phase	~200	--
Vel.dispersion [kms^{-1}]	10-20	$\leq$5
Magnetic field [mG]	(~0.5)	$\leq$0.1
Isotopic Abundances		
$[^{12}C]/[^{13}C]$	~25	~75
$[^{16}O]/[^{18}O]$	~200	~400
$[^{14}N]/[^{15}N]$	~1000	~400

Ungerechts, 1985). While due to the 30 mag of l-o-s extinction towards the nucleus, absolute (interstellar) abundances are difficult to determine, studies of C-N-O isotope substituted molecules (at cm/mm wavelengths) have revealed enrichment in 'secondary' nuclei by a factor of 2-3 as compared with solar system abundances (Table I; so-called secondary nuclei are synthesized in second-generation stars on seed-nuclei from earlier stellar processing, and to first order, their fractional isotopic abundance is proportional to $\ln(1/\mu)$).

Despite its evolved (gas-depleted) state of evolution, in the central bulge large scale star formation is taking place at an efficiency, $\Phi/M_g \sim 5\ 10^{-9}\ yr^{-1}$, similar to that in the local and inner galactic disk. According to (thermal) radio continuum studies, probing the number N_{Lyc} of hydrogen ionizing stellar photons, about 10% of the Galaxy's present OB star formation is associated with the central CO layer (Mezger & Pauls, 1979). Assuming a standard initial mass function (which however may not apply to the unique physical boundary conditions in galactic center clouds), a total star formation rate of $\Phi \sim 0.3\text{-}0.6\ M_\odot yr^{-1}$ is estimated (R <500 pc). Comparison with the infrared luminosity of the extended emission associated with the galactic center, $L_{IR} \sim 10^9\ L_\odot$ from the innermost $3^\circ x2^\circ$ (acc. to FIR data from IRAS; Cox & Laureijs, 1988), yields an exceptionally high infrared excess, IRE >30 ($IRE = L_{IR}/N_{Lyc}$). This may either imply a sharply declining IMF beyond m ~10 $M_\odot$ (Odenwald & Fazio, 1984; only stars more massive than ~10 $M_\odot$ contribute significantly to the IMF-integrated Lyc-photon production, while intermediate mass stars dominate the integrated luminosity), or more likely, is suggestive of a major contribution to the dust heating from old bulge K and M giants (Cox & Laureijs, 1988).

4. PHYSICAL CONDITIONS OF GALACTIC CENTER CLOUDS

Recent large-scale surveys in density-tracing molecules (CS: Bally et al., 1987, and this meeting; H_2CO cm transitions: Zylka et al., 1988) have shown that mean H_2 densities $\langle n \rangle \geq 10^4\ cm^{-3}$ are representative of the bulk of molecular gas inside a few hundred pc galactocentric radius. Excitation studies of symmetric top molecules (NH_3, and CH_3CCH; Morris et al., 1983; Güsten et al., 1985) revealed uniformly high gas temperatures, $T_{kin} \sim 70$ K - irrespective of the local environment of the cloud and its (projected) distance to the nucleus. Highly supersonic turbulent motions (linewidth ~15-30 kms^{-1}) are characteristic of individual clouds, although, if several clumps superpose in the beam a total velocity coverage of >100 kms^{-1} may be observed.

Hence, on average, galactic center clouds are denser, warmer and more turbulent than clouds in the outer galactic disk (see Table I, for comparison), and in part these differences can be explained as due to the clouds' unique location in the gravitational potential of the galactic nucleus. Within the inner few 100 pc, a high gas density $n(cm^{-3}) \geq \langle n \rangle_T \sim 10^4 \cdot [75/R_{gc}]^{1.8}$, seems a necessary condition to survive tidal stresses in the steep gravitational potential of the central bulge (to first-order approximation, $V_{rot} \sim R^{0.1}$; see e.g., Fig.13 of Genzel & Townes, 1987). If assuming virialization, the turbulent pressure is adjusted to match these densities, the predicted linewidth, $dv \sim 17\ kms^{-1} \cdot [R_{cl}/10pc] \cdot [150pc/R_{gc}]^{.9}$ is close to the values typically observed. Dissipation of this supersonic turbulence on small scales then may provide the heating mechanism which accounts for the uniformly high gas tem-

peratures. As these are well in excess of the temperature of the dust, $\langle T_d \rangle \sim 30$ K, collisions with radiatively heated warm dust are excluded as a major heating source, and instead, a process is required that acts directly upon the gas. From a comparison with possible alternative scenarios such as UV-photoelectric, cosmic ray and magnetic viscous heating (the latter being difficult to evaluate), turbulent energy dissipation seems the most attractive mechanism [see Güsten (1988) for details]. But as the dissipation timescale is rather short ($\tau_d \sim 10^6$yr), turbulence is to be replenished continuously. Probably, due to strong differential rotation (tidal stresses), orbital energy of the clouds around the galactic center is transferred efficiently into small-scale (local) turbulence (Fleck, 1980).

REFERENCES

Bally,J., Stark,A.A., Wilson,R.W., Henkel,C.: 1987, Astrophys.J.Suppl. 65,13
Bally,J., Stark,A.A., Wilson,R.W., Henkel,C.: 1988, Astrophys.J. 324,223
Burton,W.B., Liszt,H.S.: 1978, Astrophys.J. 225,815
Cohen,R.J., Dent,W.R.F.: 1983, in 'Surveys of the Southern Galaxy', p.159, ed.W.B.Burton & F.P.Israel, Reidel Publ.Comp.
Cox,P., Laureijs,R.: in IAU Symp.136, 'The Galactic Center', in press, ed. M.Morris
Fleck,R.C.: 1980, Astrophys.J. 242,1019
Genzel,R., Townes,C.H.: 1987, Ann. Rev. Astron. Astrophys. 25,377
Güsten,R.: 1988, in IAU Symp.136, 'The Galactic Center', in press, ed. M.Morris
Güsten,R., Ungerechts,H.: 1985, Astron.Astrophys. 145,241
Güsten,R., Walmsley,C.M., Ungerechts,H., Churchwell,E.: 1985, Astron.Astrophys.142,381
Handa,T., Sofue,Y., Nakai,N., Hirabayashi,H., Inoue,M.: 1987, P.A.S.Japan 39,709
Heiligman,G.M.: 1987, Astrophys.J. 314,747
Liszt,H.S., Burton,W.B.: 1978, Astrophys.J. 226,790
Liszt,H.S., Burton,W.B.: 1980, Astrophys.J. 236,779
Morris,M., Polish,N., Zuckerman,B., Kaifu,N.: 1983, Astron.J. 88,1228
Odenwald, S.F., Fazio,G.G.: 1984, Astrophys.J. 283,601
Oort,J.H.: 1982, in 'The Galactic Center', p.180, ed. G.Riegler, AIP Conf.Proc. 83
Sanders,R.H.: 1979, in IAU Symp.84, 'Large-Scale Characteristics of the Galaxy', p.383, ed. W.B.Burton, Reidel Publ. Comp.
Sanders,R.H.: 1988, in IAU Symp.136, 'The Galactic Center', in press, ed. M.Morris
Zylka,R., Güsten,R., Henkel,C., Batrla,W.: 1988, Astron.Astrophys. submitted

THE NEARBY CASSIOPEIA AND CEPHEUS MOLECULAR CLOUDS AND THE EXISTENCE OF A CLOSE SUPERNOVA REMNANT

Isabelle A. GRENIER
Service d'Astrophysique, C.E.N. Saclay, 91191 Gif/Yvette Cedex, France
Centre d'Etude Spatiale des Rayonnements, Toulouse, France

ABSTRACT:

The study of the recent ^{12}CO observations by the Columbia millimeter-wave telescope in the 2nd Quadrant ($100^0 \leq l \leq 140^0$), at medium latitude towards Cepheus (b up to 22^0) and near the plane towards Cassiopeia, has revealed a vast nearby molecular complex. It comprises two main concentrations resting at a distance of about 300 pc and containing 0.6 and 1.0 10^5 M_0 respectively. The clouds seem to be shaped by a large bubble (12^0 in diameter), the presence of which is strongly suggested by soft X-ray and radio observations. This bubble is interpreted as a 4 10^4 year old supernova remnant lying at about 300 pc.

THE CASSIOPEIA AND CEPHEUS MOLECULAR CLOUDS:

In 1967, Heiles first explored the content of the interstellar medium in the Cepheus direction ($100^0 \leq l \leq 140^0$, $13^0 \leq b \leq 17^0$) by observing the 21 cm line emission. He found two HI accumulations (on both sides of $l=120^0$) with double-peaked lines indicating further that two sheets of gas are lying on the line of sight somewhere around 500 pc. In 1986, exploiting the HI deficiency noticed with respect to absorption measurements, Lebrun mapped in ^{12}CO the low longitude part of the region, where he found a large molecular cloud. This result and the presence of other areas of relative HI deficiency prompted a new sensitive CO survey of the entire Cepheus region ($100^0 \leq l \leq 140^0$, $8^0 \leq b \leq 22^0$).

The observations have been carried out at an angular resolution of 0.5^0 using the Columbia University Telescope (Grenier et al. 1989, alias G89). Next to the first detected cloud, the data reveal another vast CO concentration at $l>120^0$. The good correlation between the spatial and velocity distributions of the CO and HI emissions manifests the physical relationship between the molecular gas and the known HI clouds. Whereas a certain confusion exists in the spatial and velocity distribution of the diffuse HI clouds, especially below 120^0, the "clumpiness" of the molecular gas allows to further describe the distribution of the local interstellar medium in this direction. The velocity partition of the CO emission is well defined throughout the region. And from kinematical arguments as well as various optical indicators (see G89 and Dame et al. 1987), distance estimates of 800 and 300 pc can be adopted for the two velocity components, centered on -12 and

0 kms^{-1} respectively. The farthest clouds therefore most probably belong to the Local Arm.

The closest material accounts for the large majority of the surveyed CO emission. As the same velocity partition exists near the galactic plane, the Cepheus observations have been merged to the 2nd Quadrant CO survey ($b \leq 10^0$, Dame et al. 1987) and a [-8, +8 km/s] selection has been applied to reveal the extended structure of the nearby clouds (figure 1). The gas obviously gathers within two broad complexes, named Cassiopeia ($l>120^0$) and Cepheus ($l<120^0$) after the constellations they largely cover. Their wide angular extent (Cassiopeia for instance stretches along a 30^0 arc) indeed supports the proximity just mentioned (≈300 pc). Then, the use of a $N(H_2)/WCO$ conversion factor of 2.3 10^{20} mol. cm^{-2} K^{-1} km^{-1} s, as derived from the gamma-ray galactic survey (Strong et al. 1989), yields mass estimates of 1.0 and 0.6 10^5 M_0 for Cassiopeia and Cepheus respectively. Such values imply that these clouds represent prominent features of our vicinity. But it is not yet known whether they are isolated entities or they form a unique, gravitationally bound complex.

A CLOSE SUPERNOVA REMNANT BETWEEN CASSIOPEIA AND CEPHEUS?

Various facts have induced further investigations: particularly, the ring-like disposition of the clouds, the very steep front of the Cepheus cloud at high longitude, where unusually wide CO lines are observed, and the pronounced lack of CO emission outside this edge. The "hole" in CO also corresponds to an HI depleted area. Nevertheless, it appears as a region of enhanced X-ray emission in the soft energy range (130 to 930 eV, McCammon et al. 1983). The zone of highest X-ray flux is outlined on figure 1 to show its correlation with the clouds structure. Then, the radio map at 408 MHz (Haslam et al. 1981) shows a brightness temperature enhancement which delineates the rims of the X-ray emitting region (figure 2). Below 10^0, the radio loop structure disappears in the highly contrasted emission from the galactic disc and from famous bright sources. At higher frequency (820 MHz, Berkhuijsen et al. 1973), despite the low resolution, a faint loop is visible. A crude estimate of the spectral ratio would favor a non-thermal nature of the radio emission. Finally, no Hα line emission has been detected from the whole area (Sivan, 1974).

The comprehensive view of this region at various wavelengths and the striking correlation observed between the different radiations, especially along the steep front at low longitude, strongly suggest the presence of a nearby bubble filled with a hot plasma, with a temperature of at least a few 10^5K. From the apparent possible interaction between the bubble and the Cepheus cloud, we rely on the cloud distance to evaluate the size of the bubble. At 300 pc, its approximate diameter of 12^0 corresponds to a reasonable radius of the order of 30 pc.

As no catalogued massive star has been found inside the bubble, the explanation

Figure 1: Map of the nearby CO emission (integrated over [-8, +8 km s^{-1}]) with a lowest contour and steps of 2 K km s^{-1}. The solid and dashed lines represent the highest flux contours of the soft X-ray emission in the B and M1 bands respectively (after McCammon et al.).

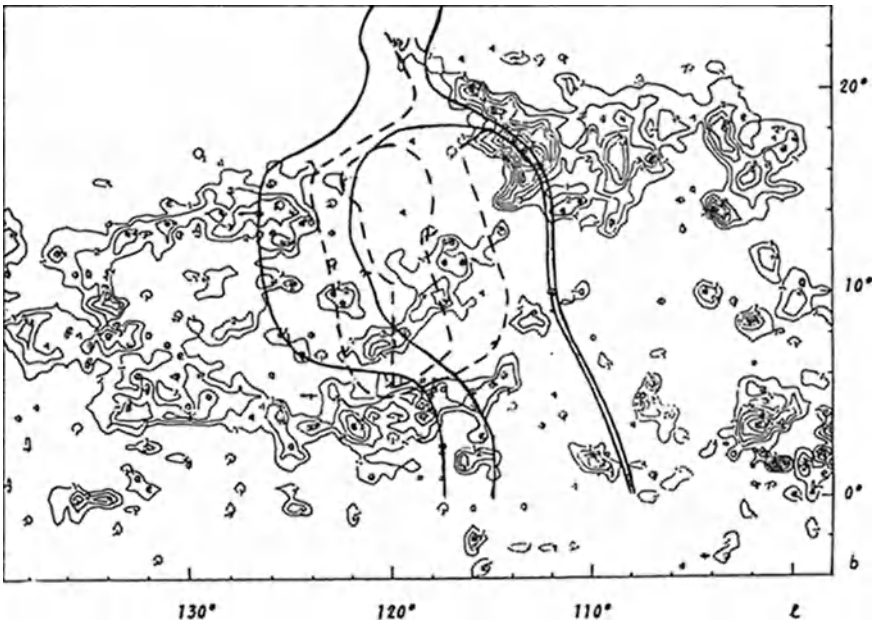

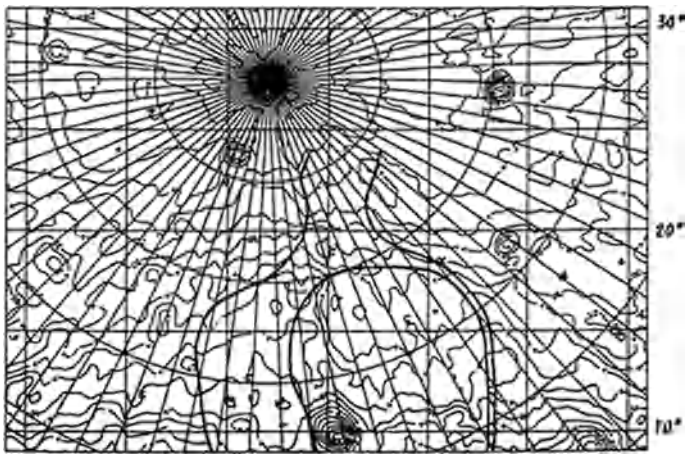

Figure 2: Map of the 408 MHz radiation (after Haslam et al.) where the two highest X-ray flux contours in the B band have been reproduced.

of a wind-driven shell has been dismissed and a supernova origin tested by determining the overall characteristics of the supposed remnant. A classical Sedov model has been used as a first approximation to describe the adiabatic expansion of the remnant. The quoted distance and radius, and the soft thermal X-ray fluxes

have led to estimates of the bubble temperature and ambient hydrogen density. Since McCammon et al. suspected a high background contamination of their data in this region, only fluxes from the "structured" enhancement have been considered by subtracting the surrounding emission. A critical discussion of the X-ray data and details on the model equations applied can be found in G89. Because of the uncertainties in the X-ray measurements, extreme cases of temperature have been derived using the fluxes obtained in different energy ranges. The resulting characteristics of the supposed remnant, which are listed in table 1, should of course be considered as orders of magnitude. They show, however, that a supernova origin of the bubble is quite plausible. The present observation set is indeed consistent with a type I supernova explosion happening 300 pc away from the Sun, $4\ 10^4$ years ago.

To confirm this scenario, more accurate X-ray measurements are essential, as well as radio surveys at different frequencies in order to remove the thermal background. Other typical manifestations such as filaments can be looked for. Because of its closeness, the confirmed supernova remnant would provide an interesting target to study the evolution of such objects near their radiative phase. The interaction between the remnant and Cepheus would also give an excellent illustration of the behaviour of a shocked dense molecular cloud.

Temperature (K)	$0.5\ 10^6$	$1.5\ 10^6$	$2.2\ 10^6$
Ambient ISM density (cm^{-3})	0.2	0.2	0.1
Expansion velocity (km s^{-1})	190	320	390
Conserved energy (erg)	$0.5\ 10^{51}$	$1.2\ 10^{51}$	$1.0\ 10^{51}$
Present age (years)	$6.2\ 10^4$	$3.6\ 10^4$	$3.0\ 10^4$

Table I: Characteristics of the supposed nearby supernova remnant.

REFERENCES:

Berkhuijsen E.M., 1973, Astr. Ap. 24, 143.
Dame T.M., Ungerechts H., Cohen R.S., de Geus E.J., Grenier I.A., May J., Murphy D.C., Nyman L.-A., Thaddeus P., 1987, Ap. J. 322, 706.
Grenier I., Lebrun F., Arnaud M., Dame T., Thaddeus P., 1989, submitted to Ap. J.
Haslam C.G.T., Salter C.J., Stoffel H., Wilson W.E., 1981, Astr. Ap. Suppl. 41, 1.
Heiles C., 1967, Ap. J. 149, 97.
Lebrun F., 1986, Ap. J. 306, 16.
McCammon D., Burrows D.N., Sanders W.T., Kraushaar W.L., 1983, Ap. J. 269, 107.
Sivan J.-P., 1974, Astr. Ap. Suppl. 16, 163.
Strong A.W., Bloemen J.B.G.M., Dame T.M., Grenier I.A., Hermsen W., Lebrun F., Nyman L.-A., Pollock A., Thaddeus P., 1989, Astr. Ap. in press.

H_2 2.12 μm spectroscopy and imaging of HH objects

H. Zinnecker[1]
R. Mundt[2]
A. Moneti[3]
T.R. Geballe[4]
W.J. Zealey[5]

Summary

We have obtained high spectral resolution observations of a number of Herbig-Haro (HH) objects in the H_2 v=1-0 S(1) line at 2.12 μm. Objects observed included HH1/2, HH7-11, HH19, HH32A, HH40, and HH43, all associated with jet-like features or collimated optical outflows. Here we present velocity-resolved 2.12 μm spectroscopy for HH40 (an HH-object moving close to the line of sight) and for HH43B (an HH-object moving close to the plane of the sky). The full set of observations including interpretation is given in Zinnecker *et al.* (1989). We also present high spatial resolution H_2 2.12 μm images of HH40 and HH43.

Observations

The 2.12 μm H_2 line profiles were obtained with the UKIRT infrared Fabry-Perot system (effective resolution 30-35 km/s) using a diaphragm of diameter 11″ for both HH40 and HH43. The H_2 images were obtained with the IR-array imager at the CTIO 1.5m telescope through a narrowband filter centred on the v=1-0 S(1) line. The IR-camera used had 58x62 pixels and a resolution of 0.9″ /pixel. The exposure time was 2x120sec and 5x60sec for HH40 and HH43, respectively. The images are sky subtracted, but not flat fielded, and should be viewed as preliminary test images.

Results

1) HH40

In the optical, HH40 is a bright knot within the HH33/40 jet, i.e. not associated with the end of the flow which is probably marked by HH33 (Mundt *et al.* 1987). The fact that HH40 and its associated jet have a rather high radial velocity of about 100 km/s in Hα (Mundt *et al.* 1984, Mundt *et al.* 1987), together with the fact that at the same time HH40 is rather bright in the H_2 S(1) line (Elias 1980), makes this object an ideal target for a comparison of velocity-resolved spectra in the Hα and the H_2 S(1) line. Fig. 1 shows that the shocked H_2 emission is redshifted; the line shape is asymmetric with an unresolved core at + 15 km/s and a wing extending up to +80 km/s, i.e. almost up to about half the maximum velocity of the Hα line. The most attractive interpretation

[1]MPE Garching
[2]MPIA Heidelberg
[3]ESO Garching
[4]JAC Hilo
[5]Univ. Wollongong

of these findings is that external molecular gas gets entrained in the collimated flow and heated by internal shocks occurring in the jet itself and/or in its shear layer. The H_2 image of HH40 (Fig. 3a) is quite low signal-to-noise but because of the reference star in the bottom part of the image the location of the peak emission is well defined and can be compared to optical CCD images in Hα or [SII] whose emission is spread over a similar area (FWHM of order 3"). An H_2 image with a longer exposure is needed to probe the existence of a more extended low-level H_2 emission in HH40.

2) HH43

High-spatial resolution Hα and 2.12 μm H_2 images of HH43 have recently been published by Schwartz *et al.* (1988) demonstrating a very close spatial correlation between the optical and infrared line emission. In the optical, HH 43 is a very low excitation HH object; in the infrared, it has the strongest H_2 S(1) line emission among the known HH objects with H_2 emission. Hα profiles were observed by Böhm and Solf (1989) who find a peak velocity at -20 km/s and a symmetric line shape with a FWHM = 60 km/s. The small peak velocity indicates that the associated flow moves close to the plane of the sky. Our 2.12 μm H_2 line profile (Fig. 2) is also nearly symmetric with a FWHM = 45 km/s which corresponds to a true width of 10-20 km/s after deconvolution with the instrumental profile. The peak velocity of the 2.12 μm emission occurs at -4 km/s, i.e. redshifted by 16 ($\pm$ 5) km/s w.r.t. the Hα emission. According to Schwartz *et al.* the excitation structure can be explained by a clump embedded in a collimated outflow which gives rise to a bow shock around that obstacle.

Our nearly symmetric H_2 line profile is consistent with such a view. However, low velocity shocks excited by the collimated outflow and moving into the external molecular gas (Zinnecker *et al.* 1989) or reformation of H_2 in the gas phase downstream in a dissociative shock (Schwartz *et al.* 1988) might also explain the H_2 data. Our H_2 image (Fig. 3b) agrees very well with that published by Schwartz *et al.* including the foreground star seen a few arcsec towards the west of the H_2 emission. We note the double structure in the H_2 image which could well be due to the two wings of a bow shock, although the observed H_2 geometry is difficult to reconcile with an exciting source in the NW (where it is suspected, Schwartz *et al.*).

Apologies

This paper failed to be presented as an oral contribution at the conference due to the late arrival of the speaker (HZ). Apologies!

References

Böhm, K.H. and Solf, J. (1989). in preparation
Elias, J.H. (1980). Ap.J. 241, 728
Mundt, R., *et al.* (1984). Astron. Astrophys. 140, 17
Mundt, R., Brugel, E.W., and Bührke, T. (1987). Ap.J. 319, 275
Schwartz, R.D., Williams, P.M., Cohen, M., and Jennings, D.G. (1988). Ap.J. 334, L99
Zinnecker, H., Mundt, R., Geballe, T.R., and Zealey, W.J. (1989). Ap.J. (in press)

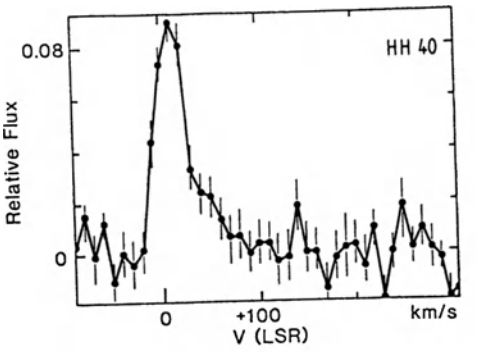

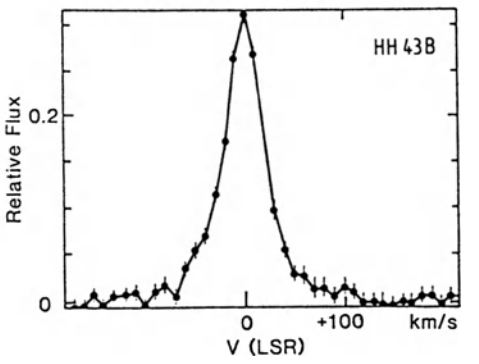

Fig.1
Velocity-resolved 2.12 μm H_2 spectrum of HH40.

Fig.2
Velocity-resolved 2.12 μm H_2 spectrum of HH43B. Notice the nearly symmetric line profile (the blue wing is slightly stronger).

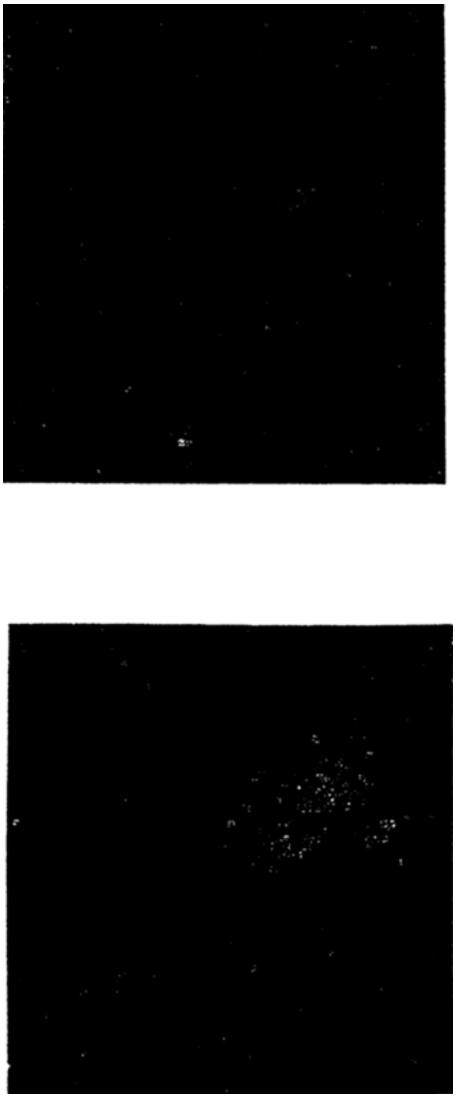

Fig.3(ab)
Infrared images of HH40 and HH43 in the H_2 v=1-0 S(1) line. Notice the presence of a star in each image which is helpful to line up the distribution of the H_2 emission with the optical data. The size of each frame is approximately 1′x1′.

SULFUR OXIDES IN ρ OPHIUCHI CLOUD CORES: SYMPTOMS OF STAR FORMATION?

Alwyn Wootten
NRAO, Edgemont Road, Charlottesville, VA 22903-2475
Robert B. Loren
Millimeter Wave Observatory, Department of Astronomy, The University of Texas, Austin TX 78712

The ρ Oph molecular cloud contains many dense cores in which it maintains a robust level of star-forming activity. During the first phases of star formation, gravitational energy is released which may warm the surrounding cloud and alter its chemistry. We have sought such chemical changes in a few cores, changes which might signal the onset of star formation. In several regions, peaks of DCO^+ column density are displaced from peaks of $H^{13}CO^+$ column density and embedded infrared sources, signalling destruction of temperature-sensitive DCO^+ molecules as the core is warmed. Since endoergic reactions initiate the sulfur chemistry in molecular clouds, we have mapped emission from sulfur oxides to complement the DCO^+ maps. In this paper we present evidence that the abundance of SO_2 is enhanced near the infrared source GSS30, which lies near the ρ Oph A molecular core.

Comprehensive SO_2 maps of the A and B1 cores of the ρ Ophiuchi molecular cloud were made in both the 3_{13}-2_{02} (104 GHz) and 3_2-2_{11} (208 GHz) lines of SO_2 using the 12 m telescope of the NRAO. For comparison, observations were also made of the $J = 2$–1 line of $C^{34}S$, a scarce isotope of a ubiquitous molecule whose abundance we expected to be little affected by thermal effects. Details of the receiver and observational technique can be found in Wootten and Loren (1987).

Toward ρ Oph A, both SO_2 lines peak quite strongly 1′ west of the cloud core as located by Loren and Wootten (1986). In ρ Oph A, the 104 GHz SO_2 emission appears as an unresolved $\leq 1'$ peak in a more extensive low intensity structure which extends SE-NW while shifting gradually in velocity. Higher resolution (30″) maps in the 208 GHz transition (Fig. 1) show that the peak, still unresolved, lies just north of GSS30, an infrared asymmetric bi-lobed reflection nebula in which an edge-on accretion disk obscures the central star (Castelaz *et al.* 1985). In contrast, the $C^{34}S$ $J = 2-1$ emission, which we were unable to map as fully, shows no clearly defined peak at GSS30, instead having a local minimum there. Furthermore, the SO_2 lines have only half the width of $C^{34}S$ (Fig. 1 inset), suggesting that they sample only a portion of the velocity field along the line of sight. Possibly, SO_2 emission arises only in a chemically differentiated core which contributes only a portion of the linewidth through the entire cloud, while $C^{34}S$ emission arises over a more extended path length.

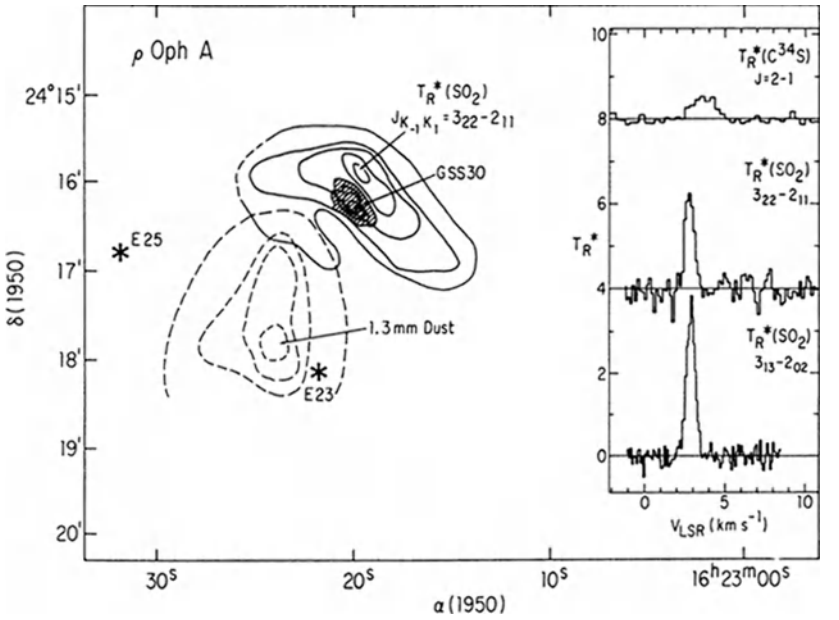

Fig. 1. Map of peak emission intensity, T_R^*, in the 3_{22}-2_{11} (208 GHz) line of SO_2 (solid lines). Dashed contours delineate the region of continuum emission at 1.3 mm from dust grains (Schwarz *et al.* 1988), and crosses locate IR sources. The stippled region outlines the 2 μm map of GSS30 (Castelaz *et al.* 1985). Spectra taken at the SO_2 emission peak of the $J = 2-1$ line of $C^{34}S$ (top), and the 3_{22}-2_{11} (208 GHz) and 3_{13}-2_{02} (104 GHz) (bottom) lines of SO_2 are shown in the inset.

Peak emission in the B1 core in the 3_{13}-2_{02} line occurs quite close to the elongated rotating clumps (called B1W hereafter) mapped in 2 cm H_2CO at the VLA by Wadiak *et al.* (1985). However, the $C^{34}S$ emission defines a broad region generally peaking southeast of the objects found by Wadiak *et al.*. The SO_2 emission again peaks very sharply in an unresolved region, surrounded by a weakly emitting extension. No embedded objects are known in the B1 core. Weaker emission in the 3_{22}-2_{11} line displays no strong peak.

In a few other regions, notably the L1689N core around the 'protostar' IRAS 16293−2422, SO_2 emission was detected but time did not permit us to map its extent. About several lower luminosity objects, including WL16, we detected nothing.

The SO_2 emission in ρ Oph B1 shows a very similar distribution to the maps of other molecules, except, perhaps, for a slight tendency to peak closer to B1W. In ρ Oph A, however, the distribution of SO_2 quite remarkably favors the region near the recently formed star GSS30. What causes this difference in the morphology of sources mapped in these two molecules? Which physical parameter of the cloud controls its appearance in these lines: density, temperature, molecular abundance, or an unidentified trait?

ρ Oph A is the warmest of the known cores in the cloud. The peak of the self-reversed CO profile reaches 30 K (Loren 1989) in a 2′ beam and a dust temperature of 37–41 K was measured by Harvey, Campbell and Hoffman (1979) using a 30″ beam. At the position of GSS30, the peak CO $J = 2-1$ temperature reaches 14 K in a 1′ beam, a lower limit to the temperature owing to the striking self-reversal of the profile. A region of high velocity gas also occurs in this region, traced by weak wings on CO (Loren *et al.* 1980)

and HCO^+ (Loren and Wootten 1982) profiles, but its origin cannot be unambiguously assigned to GSS30, as several infrared sources crowd the region. Emission from the (1,1) and (2,2) lines of ammonia at 1′ resolution (Wootten 1989) can also be used to estimate the temperature. Although at GSS30 the lines are only a third of their peak intensity, reached at the core position, they indicate the same temperature prevails at both locations. Weak emission from the temperature-sensitive DCO^+ molecule arises from the southern part of the core and may signal generally cooler temperatures in that region. The weakness of the emission, however, suggests either that the cool region is quite small, or that the temperature remains near 25–30 K there. We conclude that a fairly constant temperature obtains over the general molecular emission region near ρ Oph A, and is not a likely cause of the differing emission distributions.

The density in this region was measured using formaldehyde emission by Loren, Sandqvist and Wootten (1983). Peak density was $n(H_2) \sim 4 \times 10^5\,cm^{-3}$ found in the ρ Oph A core, rapidly declining at offset positions. Unfortunately the 2′ resolution of this analysis is too coarse to be satisfactory. Loren and Wootten (1986) observed a number of high density tracers near ρ Oph A with 1′ resolution. In the $J = 1-0$ HCO^+ line, strong self-reversed profiles are found in the core, so the $J = 1-0$ $H^{13}CO^+$ line was mapped with 1′ resolution. The intensity of this line drops by a factor of two between the core and GSS30 positions. At the core, a $J = 3–2$ $H^{13}CO^+$ profile (Loren, Wootten, Mundy and Peters 1989), also taken with 1′ resolution, indicates a density of 3×10^5 cm^{-3}, in agreement with other measures. We conclude that density does appear to peak at the ρ Oph A core positon, and that the column density, at least, of such hopefully thin tracers as $H^{13}CO^+$ and ammonia declines toward GSS30. As no mechanism occurs to us by which a column density decline can produce the striking enhancement observed in SO_2 emission, we conclude that density variation alone cannot explain the morphology of the SO_2 distribution.

From the two lines which were measured, an estimate may be made of the rotational temperature, if the emission is optically thin. The strength of the line raises doubts about this assumption, particularly in ρ Oph A, but little firm evidence exists to suggest the optical depth of the line yet. The complex structure revealed by the 1.3 mm map suggests that the 3 mm peak may be substantially beam-diluted. Assuming the source size to be that measured at 1.3 mm, the rotational temperature is 5 K; if we use measured intensities we estimate $T_{rot} = 8.5$ K. The optically thin LTE column density in ρ Oph A is then $N(SO_2) = (1 \pm 0.3) \times 10^{14}\,cm^{-2}$.

The weakness of the high frequency line at ρ Oph B1 makes estimation of source size difficult. A reasonable limit on rotation temperature, however, is 6 K, which indicates an optically thin LTE column density of $N(SO_2) = (2.5 \pm 1.0) \times 10^{13}\,cm^{-2}$.

Both lines are weak at IRAS 16293, and no map provides guidance on the size of the source. Assuming the source fills the beam, the strength of the high frequency line suggests $T_{rot} = 60$ K and $N(SO_2) = 7 \times 10^{13}\,cm^{-2}$. If, however, the source is diluted at 3 mm, $T_{rot} = 6$ K could obtain, for $N(SO_2) = 3 \times 10^{13} cm^{-2}$. Further data is needed for this source.

To see whether a case can be made for an abundance variation of SO_2 near GSS30, we must finger a foil. We choose $C^{34}S$ $J = 2-1$ emission owing to its scarcity, hence likely low optical depth. Additionally, however, it has lines near both target SO_2 lines, hence beam-filling and efficiency factors tend to cancel out in the analysis. Furthermore,

CS is a well-investigated molecule, for which abundances in a wide range of clouds have been estimated.

Using a dipole moment of $\mu = 1.96\,\mathrm{D}$, we find the column density of $C^{34}S$ to be given by

$$N(C^{34}S\ J{=}2{-}1) = \frac{9.1 \times 10^{14}\, T_R\, \Delta V(\mathrm{km\,s^{-1}})}{(1 - e^{-4.6/T_x})(e^{-2.3/T_x})}\ \mathrm{cm^{-2}}$$

Here we have assumed the emission to be optically thin, and that the molecular levels are populated according to a uniform rotational temperature T_x. This temperature has not been measured for $C^{34}S$, but probably lies between that measured for SO_2 and the kinetic temperature of the cloud.

In ρ Oph A, the column density of $C^{34}S$ is $4 \times 10^{15}\mathrm{cm^{-2}}$, for an abundance ratio of $[SO_2]/[C^{34}S] \sim 0.025$. In contrast, at B1 a ratio of $[SO_2]/[C^{34}S] \sim 0.003$ is obtained from the larger $N(C^{34}S) = 7.7 \times 10^{15}$ cm^{-2} column density there. The IRAS 16293 cloud core lies somewhat above this value at $[SO_2]/[C^{34}S] \sim 0.007$. These ratios provide strong evidence that the morphologically distinct SO_2 distribution in ρ Oph A arises in a chemical abundance enhancement, of about an order of magnitude, near the young star GSS30. In fact, if we really wanted to go out on a limb, we might claim that the three sources form an evolutionary sequence, with the younger star-forming region at IRAS 16293 intermediate in SO_2 enhancement.

Acknowledgements. The National Radio Astronomy Observatory (NRAO) is operated by Associated Universities, Inc., under contract with the National Science Foundation.

References

Castelaz, M. W., Hackwell, J. A., Grasdalen, G., Gehrz, R. D. and Gullixson, C. 1985 Ap. J., 290, 261.
Harvey, P. M., Campbell, M. F. and Hoffman, W. F. 1979 Ap. J., 228, 445.
Loren, R. 1989 Ap. J., in press.
Loren, R. and Wootten, A. 1982, ESA SP-192 Galactic and Extragalactic Infrared Spectroscopy , p. 93.
Loren, R. and Wootten, A. 1986 Ap. J., 306, 142.
Loren, R., Sandqvist, A. and Wootten, A. 1983, Ap. J., 270, 620.
Loren, R., Wootten, A., Sandqvist, A., and Bernes, C. 1980, Ap. J. (Letters), 240, L65.
Loren, R., Wootten, A., Mundy, L. and Peters, W. 1989, Ap. J., in limbo.
Wadiak, E. J., Wilson, T. L., Rood, R. T. and Johnston, K. J. 1985, Ap. J. (Letters), 295, L43.
Wootten, A. and Loren, R. 1987 Ap. J., 317, 220.

MEASUREMENT OF THE MAGNETIC FIELD IN THE MOLECULAR CLOUD B1

A.A. Goodman and P.C. Myers
Harvard-Smithsonian Center for Astrophysics, Cambridge, Massachusetts

R.M. Crutcher
University of Illinois, Urbana

C. Heiles
University of California, Berkeley

I. Kazès
Observatoire de Paris-Meudon, Meudon, France

T.H. Troland
University of Kentucky, Lexington

SUMMARY

By measuring the Zeeman effect in OH emission lines, we have determined the line-of-sight component of the magnetic field strength in the molecular cloud Barnard 1 (B1) to be -27±4 μG as measured with the 3′ beam of the Arecibo 305-m telescope, and -19±3 μG as measured with the 15′ beam of the Green Bank 43-m telescope.

Theoretical evidence for the importance of magnetic fields in molecular clouds is abundant (e.g. Mouschovias 1987a,b or Myers and Goodman 1988a,b [hereafter MGa,b] and references therein). Observational evidence, however, is far more scarce (e.g. Heiles 1987).

The range of densities $10^3 \lesssim n \lesssim 10^5$ cm^{-3} represents the least dense regime in a molecular cloud where self-gravitating gas is observed to be associated with one distinct molecular cloud core, and often with a very young star. The 1665 and 1667 MHz lines of OH, as observed in dark molecular clouds, are thought to trace densities $n \gtrsim 10^3$ cm^{-3} (Graedel, Langer, and Frerking 1982). Therefore, if one both maps a cloud and measures the Zeeman effect in these OH transitions, one has enough information to assess the magnetic field's role in the support and dynamics of the cloud.

In the past, attempts to measure magnetic fields via detection of the Zeeman effect in (non-masing) OH emission have resulted in upper limits (Lang and Wilson 1979) and one 3σ detection of 10 ± 3 μG in the Ophiuchus dark cloud (Crutcher *et al.* 1988). To maximize the likelihood of detecting the Zeeman effect in a dark cloud, we chose the Arecibo 305-m telescope for our experiment, where the 3′ FWHM beamsize at 1665 MHz is well matched to the average size of a dense clump in a relatively nearby (140-400 pc) cloud, minimizing beam dilution.

To choose sources, we attempted to predict what Zeeman signal would be observed in a given cloud, based on measured line width and antenna temperature, and on a predicted magnetic field strength (cf. Goodman *et al.* 1989). The field strength predictions were based on a model of equilibrium between magnetic, kinetic, and gravitational energy (MGa,b).

At Arecibo, after evaluation of 40 candidate clouds, three were chosen for long integration Zeeman observations. One, B1, gave a detection of -27 ± 4 μG after 50 hours of integration. The other two clouds, after similar integration times, gave 3σ upper limits of $\sim 15 - 20$ μG (Goodman *et al.* 1989). Figure 1 shows the 1665 and 1667 MHz maps and Zeeman profiles for B1, as measured at Arecibo in February of 1988.

In July of 1988, B1 was observed in OH emission at the Green Bank 43-m telescope, with a 15′ FWHM beam; and a Zeeman signal corresponding to -19 ± 3 μG was detected after about 60 hours of integration. (See Figure 2). Approximately 10 other positions have been observed in OH emission at Green Bank, and all have yielded upper limits (Crutcher *et al.* 1988). The

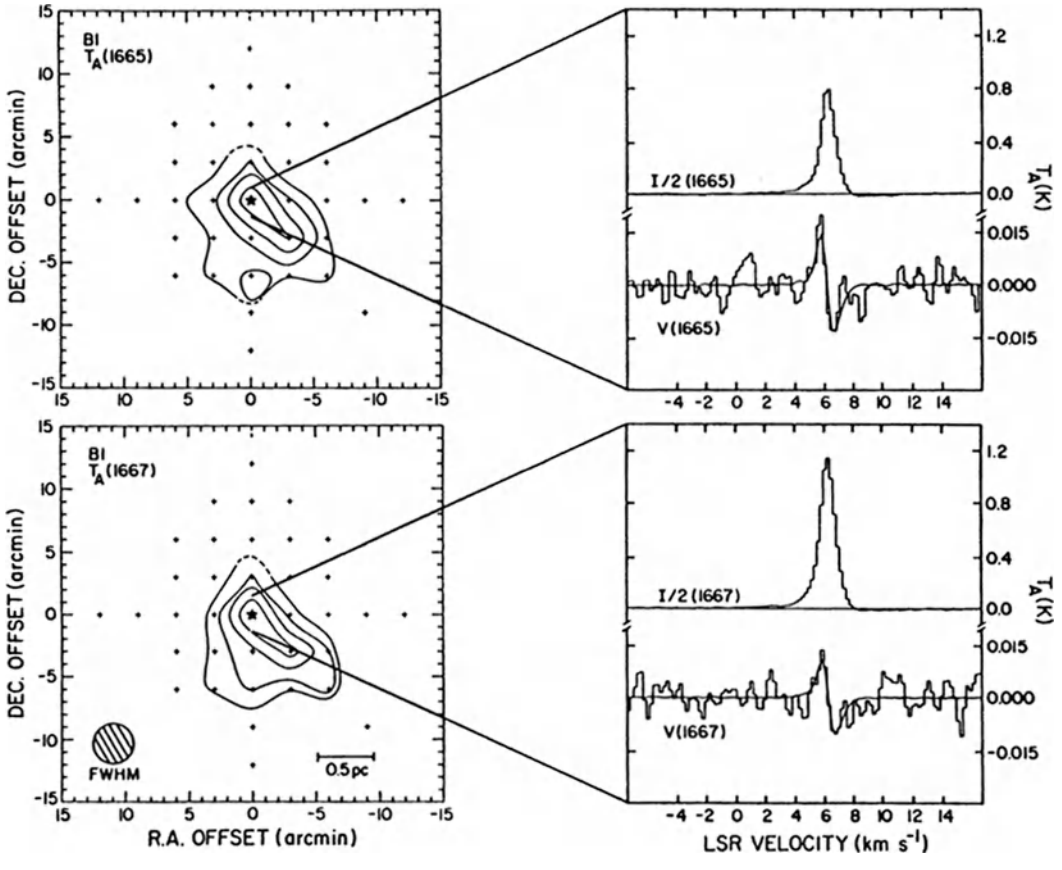

Figure 1: Summary of OH observations of B1 at Arecibo. Panels at left show maps of 1665 and 1667 MHz OH emission in B1. Contours of antenna temperature, T_A: 1665 map 0.40, 0.50, 0.60, 0.70 K; 1667 map 0.70, 0.85, 1.00, 1.15 K. Crosses indicate positions observed; additional emission (not shown) is present in the direction of the dashed contours. The filled star represents *IRAS* 03301+3057 ($\alpha(1950) = 3^h30^m10^s.5$; $\delta(1950) = 30°57'47''$). Panels at right show the Stokes I/2 and Stokes V spectra for long-integration Zeeman observations of both transitions at the (0,0) map position ($\alpha(1950) = 3^h30^m12^s.0$; $\delta(1950) = 30°57'26''$). Superimposed on the V-spectra are theoretical Zeeman patterns corresponding to a line-of-sight magnetic field strength of -27 μG for 1665 MHz and -25 μG for 1667 MHz.

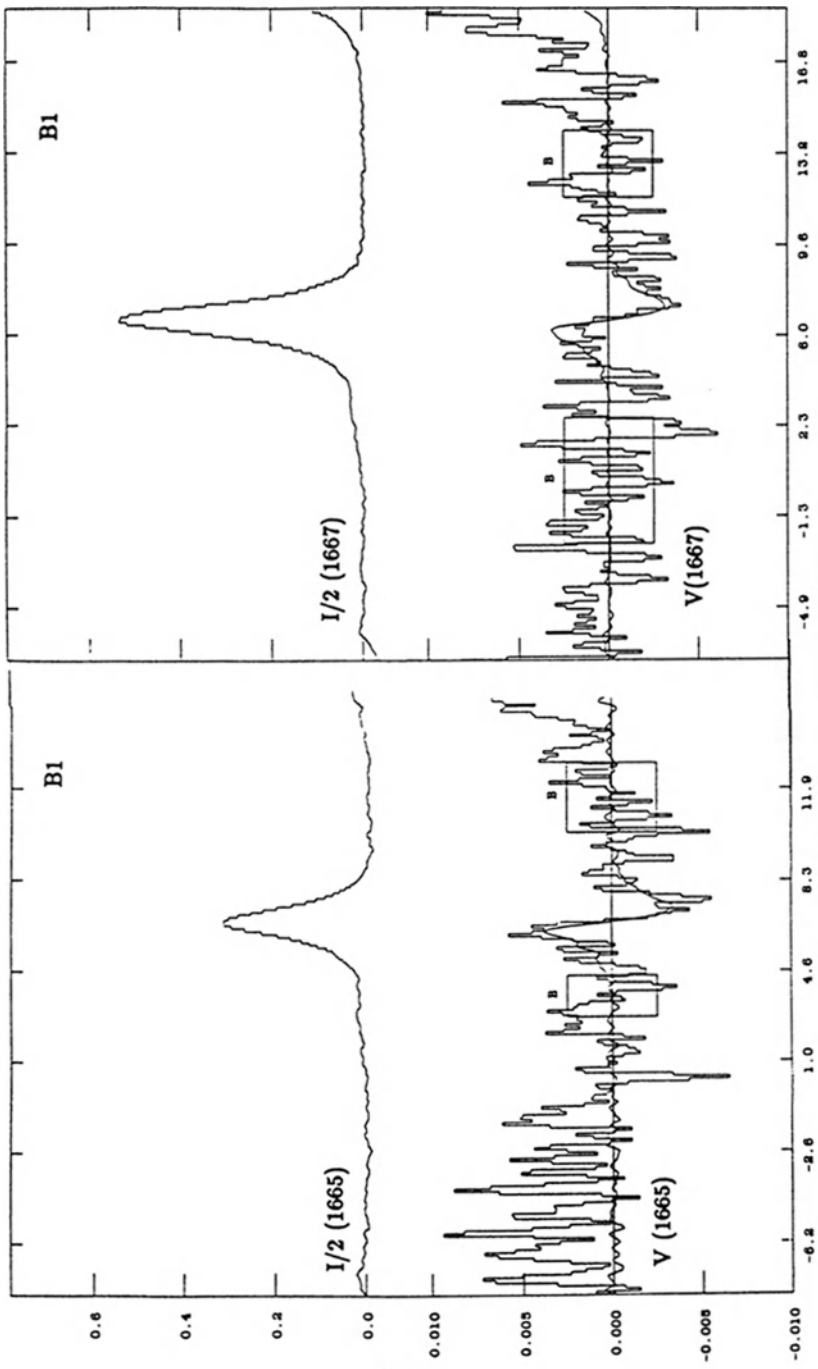

Figure 2: OH observations of B1 at the Green Bank 43-m telescope. The observed position is the same as in Figure 1. Panels at top show the Stokes I/2 spectra for long-integration observations of the 1665 and 1667 MHz transitions of OH. The panels directly below show the Stokes V spectra for each transition. Superimposed on each V-spectrum is the theoretical Zeeman pattern corresponding to a line-of-sight magnetic field strength of -20 μG. (Boxes labelled "B" mark the sections of data used in baseline removal.)

exceptionally widespread extent of strong OH emission around B1, as mapped at Green Bank, may diminish the effects of beam dilution, which may be responsible for its being the only position detected.

Results from both observatories agree well with field strength predictions based on MGa,b, as well as other models (e.g. Mouschovias 1987a,b; see Goodman *et al.* 1989 for further discussion.)

The technique employed to derive field strength values from the Stokes-V spectra shown in Figures 1 and 2 is only sensitive to the line-of-sight component of the magnetic field. On average, in a statistical sample, the field strengths derived in this way need to be multiplied by two to esitimate total field strength, although this factor may not apply to a small, sensitivity-limited, sample where only the strongest fields will be detected.

B1 is part of a complex of dark clouds in Perseus, located 350 pc from the sun (Herbig and Jones 1983). Some ten condensations, including B1, each with mean density $n \gtrsim 10^3$ cm^{-3}, are distributed within lower density molecular gas ($n \sim 10^2$ cm^{-3}) which extends for 30 pc in projection (Bachiller and Cernicharo 1984, 1986). The *IRAS* point source 03301+3057 is located near the peak of an NH_3 core ($n \gtrsim 10^4$ cm^{-3}) located at the projected center of the Arecibo OH maps shown in Figure 1 (Bachiller and Cernicharo 1984), and it has a spectrum typical of an embedded low-mass protostar (Beichman *et al.* 1986). Indeed, many Perseus consensations are associated with protstellar *IRAS* point sources.

It is now desireable to make OH Zeeman observations at Arecibo of additional Perseus condensations that are similar to B1, to determine the field strength thoughout the complex; to examine the extent to which virial and magnetic equilibrium apply; and to pursue the relation of magnetic fields to the process of low-mass star formation.

REFERENCES

Bachiller, R. and Cernicharo, J. 1984, *Astron. and Astrophys.*, **140**, 414.

Bachiller, R. and Cernicharo, J. 1986, *Astron. and Astrophys.*, **166**, 283.

Beichman, C.A., Myers, P.C., Emerson, J.P., Harris, S. , Mathieu, R.D., Benson, P.J., and Jennings, R.E. 1986, *Ap. J.*, **307**, 337.

Crutcher, R.M., Troland, T.H., Kazès, I., Heiles, C., Goodman, A.A., and Myers, P.C. 1988, in preparation.

Goodman, A.A., Crutcher, R.M., Heiles, C., Myers, P.C., and Troland, T.H. 1989, *Ap. J. (Letters)*, submitted.

Graedel, T.E., Langer, W.D., and Frerking, M.A. 1982, *Ap. J. Supp.*, **48**, 321.

Heiles, C. 1987, in *Interstellar Processes*, eds. D. Hollenbach and H.A. Thronson (Dordrecht: Reidel), p. 171.

Lang, K.R. and Willson, R.F. 1979, *Ap. J.*, **227**, 163.

Mouschovias, T. Ch. 1987a, in *Physical Processes in Interstellar Clouds* eds. G. Morfill and M. Scholer (Dordrecht: Reidel), p. 453.

_____1987b, in *Physical Processes in Interstellar Clouds* eds. G. Morfill and M. Scholer (Dordrecht: Reidel), p. 491.

Myers, P.C. and Goodman, A.A. 1988a, *Ap. J. (Letters)*, **326**, L27.

Myers, P.C. and Goodman, A.A. 1988b, *Ap. J.*, **329**, 392.

IRAS06277+7125: AN ATOMIC AND MOLECULAR OUTFLOW SOURCE IN THE GALACTIC CIRRUS?

Andreas Heithausen
Radioastron. Institut der Universität Bonn
Auf dem Hügel 71, D-5300 Bonn 1

During the investigation of atomic and molecular gas in high galactic latitude cirrus clouds the circular IRAS cloud centred at l=143°.3423, b=24°.2074 was observed in HI and CO. These observations show that it is a bipolar outflow source possibly associated with a small bow shock object.

Figure 1 shows the almost circular cloud at 100μm taken from the HCON-1 survey centred at an unidentified 100μm IRAS point source. The diameter (full width at half maximum) of the I(100μm)-cloud is about 14' on the sky, which corresponds to a linear size of about 0.4pc at an assumed distance of 100pc. The constant ratio of the 60μm to 100μm intensities reveals a dust colour temperature of T_D=21±2K. The dust cloud was completely mapped in the ^{12}CO (J=1→0) line with the KOSMA 3m telescope on the Gornergrat and in the 21cm line with the Effelsberg 100m telescope. While the CO and IRAS clouds are nearly circular the HI cloud is elongated, the extent is 0.4pc·0.7pc.

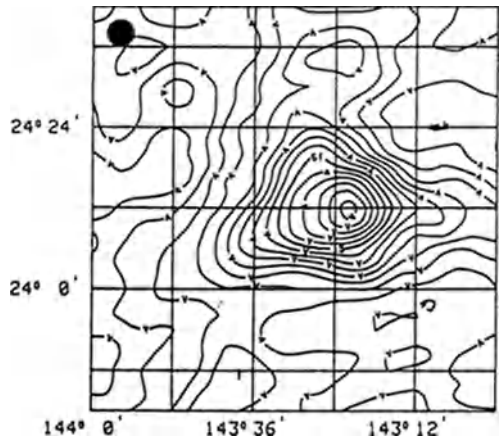

Figure 1 shows the 100μm IRAS HCON1 map in galactic coordinates. No background has been removed. Numbers are in MJy·sr^{-1}, the step between two contours is 0.5 MJy·sr^{-1}.

Using the method described by de Vries et al. (1987) we find that the ratio of the 100μm intensity, I(100μm) to the column density of hydrogen, N(H), is $I(100\mu m)/N(H)=(0.67\pm0.10)\cdot10^{-20}$ [$cm^2\cdot(MJy\cdot sr^{-1})$]. The factor $X(^{12}CO)$ that converts the integrated CO line, $W(^{12}CO)$, into column densities of molecular hydrogen is $X(^{12}CO)=(0.53\pm0.11)\cdot10^{20}$ [$molecules\cdot cm^{-2}\cdot(K\cdot km\cdot s^{-1})^{-1}$], this is similar to the value found by de Vries et al. (1987) but a factor 5 less than the value for the galactic plane. Here it was assumed that the infrared emission per nucleon was the same for the molecular as for atomic part of the cloud which was in detail shown for other cirrus clouds by Heithausen and Mebold (1988).

The CO lines of the nebula show two distinct velocity components, one component centred at lsr-velocity of about $-2.0km\cdot s^{-1}$, the other one at $+1.4km\cdot s^{-1}$ (see Figure 2). The HI line at the same velocity as the red and blue shifted CO components shows a similar bipolar shape.

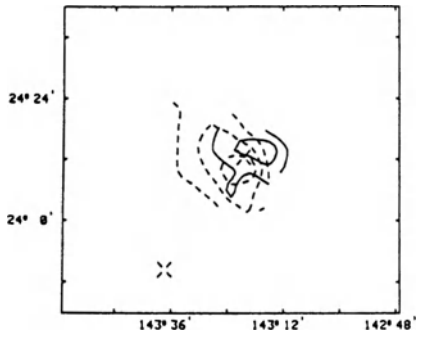

Figure 2: The bipolar CO nebula. The X sign indicates the unidentified point source IRAS06277+7125 at the centre of the cloud. The two CO components are centred at $v=-2.0km\cdot s^{-1}$ (hashed line) and $+1.4km\cdot s^{-1}$ (solid line). The direction of the outflow points directly to the U-shaped object near the second unidentified IRAS point source which is located at $l=143^{\circ}.6235$, $b=23^{\circ}.8409$.

The comparison of the virial mass of the molecular cloud ($\approx40\ M_{\odot}$) with its hydrogen mass ($0.5\ M_{\odot}$) shows that this cloud is far from being gravitationally bound; thus the cloud is probably expanding. The two distinct velocity components seen at ^{12}CO and the velocity distribution seen in the HI line could then be explained as atomic and molecular gas flowing out from the centre of the cloud. Unlike in other cirrus clouds (Mebold et al. 1987) or near other outflow objects in star forming regions (c.f. Myers et al. 1988) a dense core near the centre of the bipolar nebula could not be found. The centre of the cloud is not be visible as an absorption feature on the POSS. Using a 'normal' gas-to-dust ratio and the column density derived from HI and CO a peak blue visual extinction of $0^{m}.4$ is found on a 4' beam. Observations at the centre position

with the 100m telescope showed no significant NH_3 lines. Whether or not a starlike object of about 16^m visual magnitudes seen at the same position is physically connected to IRAS06277+7125 and is the driving force of the outflow nebula must be shown by sensitive optical CCD observations. From the distance of the two intensity maxima of the blue and red shifted components (0.24pc) and the expansion velocity (1.7 $km \cdot s^{-1}$) the age of this cloud is found to be about 70000 years. The masses in the red and blue shifted components corresponds to 0.2 $M_\odot$ each resulting in a mass loss rate of $3 \cdot 10^{-6}$ $M_\odot \cdot year^{-1}$ which is similar to other outflow objects seen in known regions of star formation.

A small U-shaped object seen on the red and blue POSS plate is located close to the second unidentified IRAS point source near the dust cloud at galactic longitude l=143°.6235 and galactic latitude b=23°.8409. Its open side points directly to the centre of the cloud which is the same direction as the movement of the outflow. Spectroscopic observations of this 'bow shock object' (Ellis et al. 1984) by Krautter et al. (1987) showed strong Hα and [OIII] emission lines. A unique classification as belonging to a cataclysmic variable which is placed on the border of this object, as nova like or as planetary nebula failed (Krautter et al. 1987). If this object is really associated with the bipolar nebula around IRAS06277+7125 the shape and the emission lines of the bow shock can be explained as similar to Herbig-Haro objects found in regions of known star formation.

Conclusions:

The dust and molecular cloud around IRAS06277+7125 is probably the first detected bipolar outflow nebula in the galactic cirrus seen in CO as well as in neutral hydrogen. Kinematic age and kinetic energy of this nebula are similar to the respective values for other outflow objects.

The nature of the driving source for this outflow is yet unclear. Optical CCD observations of the central source should help to find out whether or not this source is connected to a star-like object seen at the same position.

If the bipolar nebula is connected to a nearby emission line object the shape and the Hα lines could be explained as similar to Herbig-Haro objects.

References:

de Vries, H.W., Heithausen, A., Thaddeus, P. 1987, *Astrophys. J.* **319**, 723,
Ellis, G.L., Grayson, E.T., Bond, H.E. 1984, *Publ. Astron. Soc. Pacific* **96**, 283
Heithausen, A., Mebold, U. 1988, *Astron. Astrophys.* (in press)
Krautter, J., Klaas, U., Radons, G. 1987, *Astron. Astrophys.* **181**, 373
Mebold, U., Heithausen, A., Reif, K. 1987, *Astron. Astrophys.* **180**, 213
Myers, P.C., Heyer, M., Snell, R.L., Goldsmith, P.F. 1988, *Astrophys. J.* **324**, 907

The Morphology of the Bipolar Outflow in L1551

K. M. Gierens
I. Physikalisches Institut, Universität zu Köln

SUMMARY

A method to analyse the morphology of molecular outflows is proposed. The different center-to-limb variation of high velocity wings for the two kinds of outflow models (hollow shell and "flow in a pipe") is used to determine the flow morphology of the outflow in L1551. It is shown that all published spectra are consistent with the "flow in a pipe" model.

Introduction

In their famous article on the bipolar outflow in L1551, Snell, Loren and Plambeck [1] proposed an illustrative model which explained the high velocity wings of CO lines and their spatial variation. The model consists of a jet of ionized gas which sweeps the molecules up on its way through the molecular environment. This leads to a thin expanding shell of molecules surrounding a cavity containing essentially no molecules. The observed high velocity wings are then produced by the expanding shell.

In his thesis [2], Levreault proposed another model for the outflow, the "flow in a pipe" model. In this model, the streaming molecular gas which produces the high velocity wings fills the entire outflow region. It flows fast near the outflow axis and slowly at the edges.

Obviously, both kinds of models are consistent with the observed velocity distribution, and the position-velocity diagrams published by Moriarty-Schieven *et al.*[3] and Uchida *et al.*[4] can be produced by either flow. Analyses of velocity distributions and position-velocity diagrams therefore cannot be used for the determination of the true flow morphology.

In this article, I propose a method capable of differentiating between the two kinds of flow. The distinction is based on the center-to-limb variations of the high velocity wings. The method is applied to ^{12}CO and ^{13}CO spectra of L1551 taken with the Cologne 3 m telescope on the Gornergrat and to spectra of higher spatial resolution ([3] and [5]). The results support the "flow in a pipe" model for L1551. Further details can be found in [6].

Theoretical High Velocity wings

For the calculation of high velocity wings, a simple cylindrically symmetric flow is used, which can be formed to be hollow or filled. The following velocity law is employed:

$$V_z(\varrho) = V_0 \cdot [1 - (\varrho/R)^\alpha],$$

where (z, ϱ) are the usual cylindrical coordinates, V_0 is the flow velocity on the outflow axis, and R is the radius of the cylinder. We neglect helical rotation [4], expansion and acceleration in the z-direction [7].

The cylindrical flow is observed with a circular telescope beam of radius $R_B = R/4$ on the source. The telescope response is 1 inside R_B and 0 outside.

The exponent α has a strong influence on the shape of a single line profile. But the differentiation between the two flow models is based on the appearence of the center-to-limb variation in the high velocity wings and is not affected by the actual value of α. A strong density gradient towards the edges of the outflow does not destroy the possibility of the distinction between the two kinds of flows.

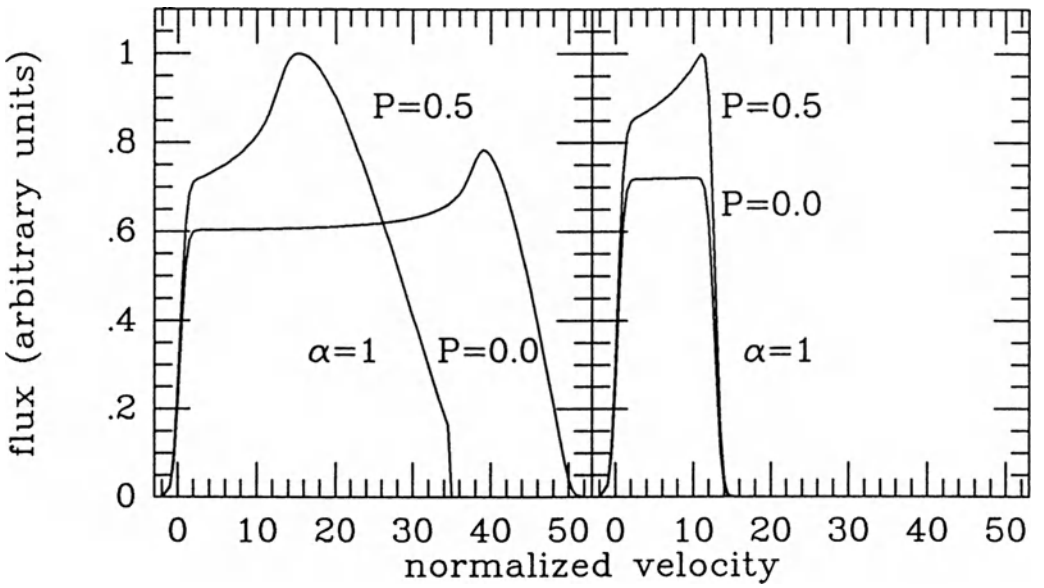

Fig. 1. High velocity wings for full (left) and hollow (right) cylindrical outflows. α is the exponent of the velocity law. $P = 0.0$ means a telescope beam centered on the outflow axis; for $P = 0.5$, the beam points midway between the axis and the edge of the outflow. Emission from the parent molecular cloud is not shown.

Different telescope positions across the cylindrical outflow clearly reveal the different features in the two types of flows (see Figure). The characteristics of the center-to-limb variation are summarized in three points:

1. The line shapes for filled flows show a strong center-to-limb variation, whereas the shapes of lines from a hollow flow do not.
2. The maximum normalized velocity (*i.e.* velocity along the line of sight in units of the thermal velocity of the molecules) in the line wings decreases from the axis towards the edge for a filled flow, but remains constant for a hollow one.

3. Profiles of a hollow flow reveal limb brightening in the entire wing. In the case of the filled flow, the low normalized velocities show limb brightening, the high ones limb darkening. The limb brightened part of the wing may be hidden by the emission from the parent molecular cloud. In this case, the entire observed wing will show limb darkening.

These findings are valid for all values of α and also in the presence of a density gradient.

Application to L1551

L1551 is the ideal testing ground for this method because of its large angular size, its small inclination to the plane of the sky, the clear separation between the blue and the red lobes, and its nearly cylindrical shape at some distance from the central source, IRS-5. High signal-to-noise CO observations were made with the Cologne 3 m telescope in the northeastern lobe where the velocity field is smooth. The spectra show a strong decrease of the maximum wing velocity for positions closer to the outflow edges. Indications for helical rotation are also found, which is consistent with the results of Uchida *et al.* (1987). As a consequence of the large telescope beam (3.'9 at 115 GHz), a general limb darkening for all velocities in the line wings is found. It is caused by the strong decrease of the beam filling factor of the high velocity gas when the telescope points toward the edges of the lobe.

The spectra in [3] and [5], with spatial resolutions of about 45″ and 83″, respectively, follow exactly the predictions of model for a filled outflow with a steep velocity decrease with ϱ near the outflow axis and a flatter velocity law near the edges. All the effects mentioned in the above section can be seen. But the most important feature is that these high resolution spectra show also limb darkening in the entire wing in the immediate neighborhood of the outflow edge. According to point 3) in the above section, this implies a filled flow. It should be noted that a general limb darkening cannot be produced by a hollow shell, nor by a hollow conical one. (For more details see [6].)

All observations of the bipolar outflow in L1551 can be explained with Levreault's "flow in a pipe" model. The exponent of the velocity law should be small, *i.e.* $0.5 \lesssim \alpha \lesssim 1$. The rotational and expansion velocity components in L1551 are small relative to the main V_z component, since our simple model, which neglects these components, is able to produce the main features of the spectra, in particular their center-to-limb variation.

References

1. Snell, R.L., Loren, R.B., Plambeck, R.L.: Ap. J. Letters 239, L17 (1980).
2. Levreault, R.M.: Ph. D. thesis, University of Texas Technical Report No. 85-1 (1985).
3. Moriarty-Schieven, G.H., Snell, R.L., Strom, S.E., Schloerb, F.P., Strom, K.M., Grasdalen, G.L.: Ap. J. 319, 742 (1987).
4. Uchida, Y., Kaifu, N., Shibata, K., Hayashi, S.S., Hasegawa, T.: in M. Peimbert, J. Jugaku (eds.) Star Forming Regions, IAU Symp. 115, Reidel, Dordrecht (1987).
5. Rainey, R., White, G.J., Richardson, K.J., Griffin, M.J., Cronin, N.J., Monteiro, T.S., Hilton, J.: Astron. Astrophys. 179, 237 (1987).
6. Gierens, K.M., Winnewisser, G.: Astron. Astrophys. (submitted).
7. Fridlund, C.V.M., Sandqvist, A., Nordh, H.L., Olofsson, G.: Astron. Astroph. 137, L17 (1984).

CO OUTFLOW AND GLOBAL PROPERTIES OF THE HIGH LATITUDE CLOUD L1642

T. Liljeström and K. Mattila
Helsinki University Observatory
Tähtitorninmäki, SF-00130 Helsinki, Finland

Abstract. We have mapped the high latitude dark cloud L1642 ($l=210\overset{\circ}{.}8$, $b=-36\overset{\circ}{.}7$) in the J=1-0 transition of ^{12}CO and ^{13}CO using the 11-m NRAO and 14-m FCRAO radio telescopes, and in the 21-cm HI line using the 100-m radio telescope at Effelsberg. Results are presented for the CO outflow detected around IRAS 04325-1419, and on the effects of the asymmetrical UV radiation field of OB stars on the HI gas associated with L1642.

RESULTS AND DISCUSSION

1. CO outflow around IRAS 04325-1419

Weak red- and blueshifted bipolar pedestal CO emission has been detected around IRAS 04325-1419. The mass in each wing is in the range $4\ 10^{-4}$ - $0.01\ M_\odot$. The estimated dynamical time scale of the outflow is in the range 0.4 - $16\ 10^4$ yr. The force , $F < 3\ 10^{-6}\ M_\odot km\ s^{-1} yr^{-1}$, and the stellar mass loss rate $dM_*/dt < 6\ 10^{-8}\ M_\odot\ yr^{-1}$, are comparable with those derived from optical observations of T Tauri winds.

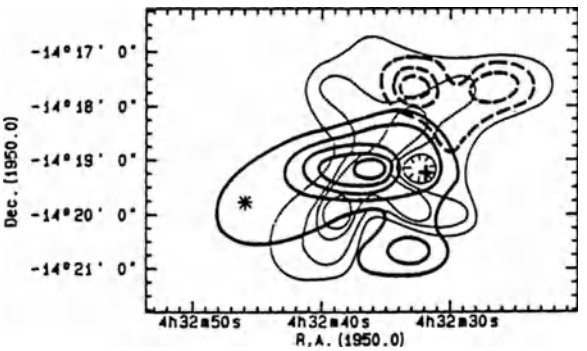

Fig. 1 Contour map of the integrated line area of the redshifted (thick solid lines) and blueshifted (dashed lines) CO emission around IRAS 04325-1419 (cross) superimposed on the $T_{ex}(^{12}CO)$ contours (thin lines). The contour levels for the outflow are at intervals of 0.2 K km/s with the lowest contour at 0.4 K km/s. The contour levels of $T_{ex}(^{12}CO)$ are at intervals of 0.5 K with the outermost contour at 14K

Fig. 1 shows that the emission in the redshifted wing ($1.14 < V_{LSR} < 2.44$ km s^{-1}) is stronger, and more extended than in the blueshifted wing ($-1.46 < V_{LSR} < -0.42$ kms^{-1}). This redshift-blueshift asymmetry of the outflow is best explained with the existence of a temperature gradient in the outflow area, and it may also indicate that the outflowing gas has a moderate opacity with $\tau_{12} \approx 1$-3 (see Bally and Lada, 1983). From Fig. 1 it is also seen that IRAS 04325-1419 is somewhat displaced from the outflow axis, a situation which can be explained if the tangential velocity of the star is 1 to 2 km s^{-1}, compatible with the one-dimensional velocity dispersion of T Tauri stars. The CO outflow is confined roughly within the border of a region of enhanced temperature (see Fig. 1) with $T_{ex}(^{12}CO)$ = 14 to 16 K (as compared to the cloud core temperature of $\sim$ 13 K). It is suggested that this temperature enhancement results from a collision at the interface between stellar wind and the ambient cloud (see Liljeström et al., 1988).

2. Global properties of L1642

The line width map of HI (Fig. 2) shows an increase from 2.5 to 2.9 km s^{-1} near the centre of the L1642 molecular cloud peaking on the "bright side" of L1642, i.e. the side facing the galactic plane. The spectra are narrow and do not reveal any sign of a second velocity component which could explain the line broadening as a blend effect. Although an explanation in terms of increased turbulence cannot be excluded, the fact that the IRAS 12 μm surface brightness map of Laureijs et al. (1987) shows a maximum (see Fig. 2) at the same position as the HI line broadening maximum supports the thermal line broadening model where the heating of the gas is due to the photoelectric emission from very small grains and/or PAHs.

Assuming that the turbulent and large scale motions are the same in the broadened HI line region and immediately outside this area a temperature enhancement of 47 K is obtained for the HI gas. Adopting for the L1642 HI cloud the temperature T_k = 81 K, an average value for diffuse clouds (Spitzer and Cochran, 1981), the increase of the HI line width corresponds to an increase of T_k from $\sim$ 80 to 130 K.

A simplified thermal balance model where the photoelectric heating rate of very small grains (Spitzer, 1978) is balanced by the cooling rates of C^+, CO and C (Langer, 1976) can explain a $\sim$ 50 K temperature enhancement if the mean projected surface area of grains/cm^3 per H atom is 2.0 10^{-21} cm^2. This value is consistent with the value of dust surface area as given by Spitzer (1978) if the extinction efficiency for these small grains is $Q_e \approx 1$. The requirement for additional grain area can be fullfilled by introducing the very small grains.

A ridge of excess HI emission has been detected at the outer edge of the dark cloud on its "bright side". From Fig. 3 it is seen that the column density ratio N_{HI}/N_H(tot) vs. A_V tends to be higher for the "bright side" than for the "shadow side" of L1642. Fig. 3 shows a general agreement between the H + H $\rightleftarrows$ H_2 equilibrium

model of Hollenbach et al. (1971) and the observations for $A_V > 1.4$ mag which corresponds to the projected distance $\rho < 0.85$ R (R=cloud radius) from the cloud centre. Based on the observations of Opal and Weller (1984) we estimate that the background UV radiation field in the vicinity of L1642 is about two times stronger on the "bright side" as compared to the "shadow side" of the cloud. Adopting for the model calculations a radiation field value half of that used by Hollenbach et al. (1971) we obtain the result shown by the dashed curve in Fig. 3. For a more detailed discussion see Liljeström and Mattila (1988).

REFERENCES

Bally, J., Lada, C.J.: 1983, Astrophys. J. 265, 824
Hollenbach, D., Werner, M., Salpeter, E.: 1971, Astrophys. J. 163, 165
Langer, W.: 1976, Astrophys. J. 206, 699
Laureijs, R., Mattila, K., Schnur, G.: 1987, Astron. Astrophys. 184, 269
Liljeström, T., Mattila, K.: 1988, Astron. Astrophys. 196, 243
Liljeström, T., Mattila, K., Friberg, P.: 1988, Astron. Astrophys., in press
Opal, C.B., Weller, C.S.: 1984, Astrophys. J. 282, 445
Spitzer, L.: 1978, Physical Processes in the Interstellar Medium, Wiley, New York
Spitzer, L., Cochran, W.D.: 1973, Astrophys. J. Letters 186, L23

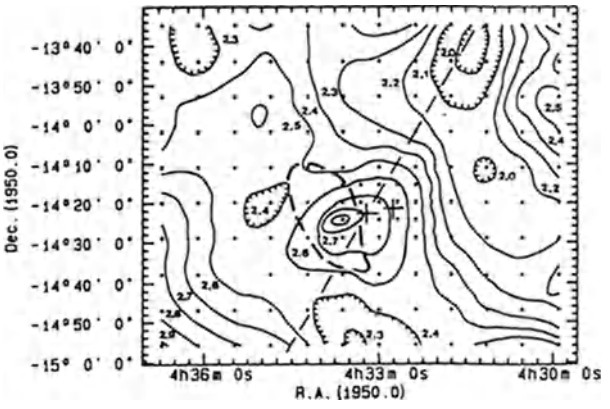

Fig. 2

The line width (FWHM) contour map of HI in L1642. Unit is km/s. The right hand cross is the centre of the molecular cloud. The dashed oval shows a maximum in the 12 μm map of Laureijs et al. (1987), and the thin dashed line the direction of the galactic equator

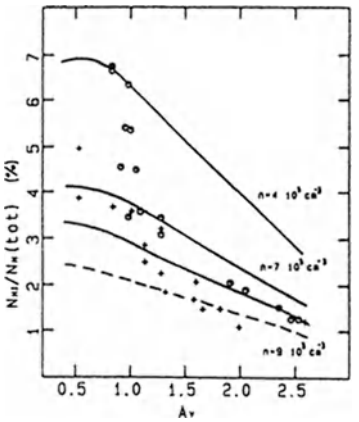

Fig. 3

The ratio $N_{HI}/N_H(tot)$ vs. A_V. The results for the "bright side" of L1642 are marked with open circles and the results for the "shadow side" with crosses. The three continuous curves correspond to the Hollenbach et al. (1971) $H+H \rightleftarrows H_2$ equilibrium model with the different gas densities n as indicated. The dashed line corresponds to $n=9 \cdot 10^3$ cm^{-3} and to a UV-field value = half of the bright side value

DUST AND GAS IN A HIGH LATITUDE CLOUD INTERACTING WITH HIGH VELOCITY CLOUDS

Uwe Herbstmeier, Reiner Rohlfs, Ulrich Mebold
Radioastronomisches Institut der Universität Bonn
Auf dem Hügel 71, D-5300 Bonn 1, FRG

The Draco Nebula is a diffuse cirrus molecular cloud which is located in the lower galactic halo (l,b,z) = (91°,+38°,500pc) (Goerigk et al. 1983, Johnson 1986, Rohlfs 1986, Goerigk and Mebold 1986). It is spatially associated and probably in collisional interaction with a group of HI clouds at high negative velocities (v = -100 km/s), so-called high velocity clouds or HVCs (Kalberla et al. 1984, Herbstmeier 1985, Mebold et al. 1985). There is good evidence that this collision has caused an enhancement of the CO abundance close to the interface region (Rohlfs et al. 1988). The aim of the present paper is to derive $XWCO = N(H_2)/WCO$, the ratio of the molecular hydrogen column density and the ^{12}CO line integral, and the CO abundance by using the 100μm emission (I_{100}) as a measure of the total gas content of the Draco Nebula.

The nebula has been observed in the 21 cm line with the 100 m telescope at Effelsberg (Goerigk et al. 1983, Herbstmeier et al. 1984) and in the ^{12}CO and the ^{13}CO (J=1→0) lines with the Bordeaux 2.5 m and Gornergrat 3 m telescopes (Mebold et al. 1985, Herbstmeier and Rohlfs 1988). Together with the IRAS 100μm emission the HI column density (N(HI)) and the ^{12}CO line integral form a 3-D data cube.

A data cube of this kind was analysed by Heithausen (1987) and Heithausen and Mebold (1988) to yield the IR emission per nucleon in the HI gas ($a_{HI} = I_{100}/N(HI)$), the H_2 gas ($a_{H2} = I_{100}/(2 \cdot N(H_2))$), and the XWCO ratio. Analogous to a procedure introduced by de Vries et al. (1987) these authors adopt a relationship of the kind

$$I_{100} = I_{100}(N(HI),WCO) = a_{HI} \cdot N(HI) + 2 \cdot a_{H2} \cdot XWCO \cdot WCO \qquad (1),$$

between the 100μm emission and the total gas content of the nebula and find that $a_{HI} = a_{H2} = 1 \cdot 10^{-20}$ cm^{2}MJy/sr and $XWCO = 0.5 \cdot 10^{20}$ mol(cm^{2}Kkm/s)$^{-1}$. Writing equation (1) in the form $I_{100}(N(HI),WCO) = a_{HI} \cdot N(HI) + b \cdot WCO$, with $b = 2 \cdot a_{H2} \cdot XWCO$, we see that their data are well represented by a plane in the I_{100}-N(HI)-WCO data cube (see Figure 1)

In the case of the Draco nebula we find that the data do not always fit to a plane. The data points with WCO=0, i.e. the lines of sight penetrating the periphery of the nebula, do have I_{100} values, which are clearly lower than what is to be expected from a fit of a plane to all data, i.e. including those lines of sight with WCO>0. Therefore we allow here for a more complex structure of the observed $I_{100}(N(HI),WCO)$-surface. As a_{H2} cannot be derived independently of XWCO, we argue that a_{H2} can be derived indirectly by assuming that - in the region where CO, H_2 and HI coexist - the IR emission per nucleon, a_{H2}, is identical to that per HI atom, $a_{HI}(WCO>0)$: $a_{H2} = a_{HI}(WCO>0)$. This seems plausible, if the HI and the H_2 gas are well mixed in our nebula.

As the uncertainties of the data do not allow to fit e.g. a more general surface we restrict ourselves to derive (see Figure 1)

- the value of the mean partial derivative,

$$\left\langle \frac{\partial I100(N(HI),WCO)}{\partial N(HI)} \right\rangle_{WCO=0} = a_{HI}(WCO=0),$$

which amounts to linear regression in the I_{100}-N(HI) plane, and

- the value of the mean partial derivative,

$$\left\langle \frac{\partial I_{100}(N(HI),WCO)}{\partial N(HI)} \right\rangle_{WCO>0} = a_{HI}(WCO>0),$$

which amounts to fitting a plane with the coefficients a_{HI} and b to those data only, which have WCO>0.

We find the values of $a_{HI}(WCO=0)$ and $a_{HI}(WCO>0)$ given in Table 1 and see that $a_{HI}(WCO>0) \approx 2 \cdot a_{HI}(WCO=0)$ for the most prominent feature within the Draco Nebula. This means that for lines of sight with WCO=constant>0 the increase of I_{100} with increasing N(HI) is steeper than for ones with WCO=0. Note that the values of $a_{HI}(WCO>0)$ are lower limits to a_{H2} only, $a_{H2} \geq a_{HI}(WCO>0)$, because those parts of the line of sight which pass through the front- and back-layer of the cloud do have the lower value of $a_{HI}(WCO=0)$. For the discussion below we adopt $a_{H2} = a_{HI}(WCO>0)$, because the true value of a_{H2} is not known.

Once a_{H2} is known, from the fit parameter $b = 2 \cdot a_{H2} \cdot XWCO$ we derive values for the ratio XWCO (see Table 1 for results). They are low even compared to the values of de Vries et al. 1987.

The interpretation of these results is not clear. High resolution ^{12}CO and ^{13}CO line mapping (cf. Rohlfs et al. 1988, Rohlfs 1988, Heithausen and Mebold 1988) indicates that clumping, optical depth or excitation effects of the CO lines cannot fully account for the large a_{H2} and low XWCO values. Preliminary results for the ratio of the line integrals of the ^{12}CO and ^{13}CO lines, $W^{12}CO/W^{13}CO \approx 10$ shows that optical depth effects can account for a deviation of the XWCO ratio of a factor between 2 and 3. The remaining factor of 10 has to be explained in a different way. The large values of $a_{HI}(WCO>0)$ could be explained by saturation effects of the HI spectral line. This saturation tends to decrease N(HI) while I_{100} remains unchanged so that $I_{100}/N(HI)$ is too large. This point will be investigated further. Although these excitation and radiation transfer effects need further attention, we propose an interpretation which considers peculiar dust grain properties as the origin. The rather large a_{H2} value may be the combined effect of a comparatively large number of very small grains and their comparatively larger temperatures. This is supported by results which Rohlfs (1988) obtained from model calcuations of the grain properties of the Draco Nebula. Rohlfs finds that only grains with sizes of about 30 nm have the back-scattering properties required to reproduce the observed brightness in the optical B and R bands. The reason for a peculiar grain size distribution and the low XWCO values found may then tentatively be identified with the abnormally large CO abundance, which in turn has been explained (Rohlfs et al. 1988) by the enhancement of molecular abundances by a shock of moderate velocity ($v \approx 20$ km/s). So the speculation is that the shock that has enhanced the CO abundance may also have produced relatively large numbers of very large molecules or very small grains.

References:

Bloemen, J.B.G.M., Strong, A.W., Blitz, L., Cohen, R.S., Dame, T.M., Grabelsky, D.A., Hermsen, W.,Lebrun, F., Mayer-Hasselwander, H.A., Thaddeus, P.: 1986, Astron. Astrophys. 154, 25

Goerigk, W., Mebold, U.: 1986, Astron. Astrophys. 162, 279

Goerigk, W., Mebold, U., Reif, K., Kalberla, P.M.W., Velden, L.: 1983, Astron. Astrophys. 120, 63

Heithausen, A.: 1987, Dissertation, University of Bonn

Heithausen, A., Mebold, U.: 1988, Astron. Astrophys. in press

Herbstmeier, U.: 1985, Diploma Thesis, University of Bonn

Herbstmeier, U., Rohlfs, R.: 1988, Astr. Ges. Abstr. Ser. 1, 28
Herbstmeier, U., Kalberla, P.M.W., Mebold, U.: 1984, Mitt. Astr. Ges. 62, 322
Johnson, H.M.: 1986, Astophys. J. 309, 321
Kalberla, P.M.W., Herbstmeier, U., Mebold, U.: 1984, IAU Coll. 81, p.243
Mebold, U., Cernicharo, J., Velden, L., Reif, K., Crezelius, C., Goerigk, W.: 1985, Astron. Astrophys. 151, 427
Rohlfs, R.: 1986, Diploma Thesis, University of Bonn
Rohlfs, R.: 1988, Dissertation, University of Bonn
Rohlfs, R., Herbstmeier, U., Winnberg, A., Mebold, U.: 1988, Astron. Astrophys. submitted
Tereby, S., Fich, M.: 1986, Astrophys. J. Letters 309, L73
de Vries, H.W., Heithausen, A., Thaddeus, P.: 1987, Astrophys. J. 319, 723

Table 1: Fit parameters for different regions of the Draco Nebula

No	(l ,b ,Δl,Δb)	a_{HI}(WCO=0)	Δ (1)	a_{HI}(WCO>0)	Δ (1)	XWCO	Δ (2)
1	92.5,40.5,7,3	1.5	0.1	2.7	0.5	0.9	0.2
2	94.5,37.5,1,1	0.2	0.03	2.5	0.3	1.2	0.2
3	91.0,37.5,1,2	1.5	0.2	1.3	0.2	0.7	0.2
4	92.5,36.5,1,1	2.4	0.2	1.6	0.3	2.5	0.6
5	92.0,38.5,1,1	-	-	2.6	0.8	6.0	0.2
6	R1, R2			0.6		27	
8	R3 (145,38)	1.0	0.4	1.0	0.1	5.0	0.3

Units: (1) 10^{20}MJy·ster^{-1}cm^{2} (2) 10^{19}cm^{-2}K^{-1}km^{-1}s
R1: Tereby et al. 1986, R2: Bloemen et al. 1986, R3: de Vries et al. 1987

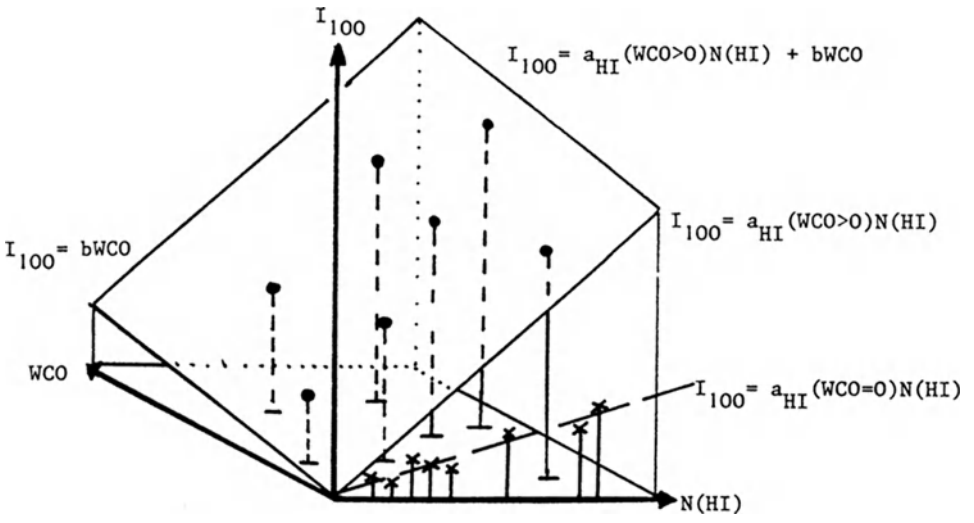

Figure 1: Sketch of the 3-D data cube and the plane fitted to the points with WCO>0 (points). Data points with WCO=0 are marked by crosses.

Recent Observations of the Molecular Outflow Source L1551 IRS5

C. V. M. Fridlund
Astrophysics Division, ESTEC, 2200 AG, Noordwijk, The Netherlands

G. J. White
Physics Dept., Queen Mary College, University of London, U.K.

Abstract

CO and ^{13}CO observations of the molecular outflow source L1551 IRS5 are reported. Lower limits to the mass and energetics are calculated, and these are found to be too high for the outflow to be radiatively driven by the central object. However, the values are found to be in quantitative agreement with recent far infrared results reported in the literature.

Introduction

In the last 10 years, it has come to be realised that the so-called bipolar molecular outflows are a common phenomenon, associated with the early evolution of both low- and high-mass stars.

One outflow source has become prototypical of low-mass star forming regions. This is the bipolar centered on the low luminosity infrared source L1551 IRS5. Situated in the Taurus Molecular Complex at a distance of roughly 150 pc, the molecular cloud L1551 shows multiple indications of ongoing star formation such as Herbig-Haro objects, optically visible jets and several T-Tauri stars. The infrared source itself has a luminosity of $25 - 40\,L_{\odot}$ (Fridlund *et al.*, 1980; Emerson *et al.*, 1984). This molecular outflow has been extensively observed, particularly in CO, since the discovery of its bipolarity by Snell *et al.* (1980). Due to the relative proximity of the cloud, and the orientation of the outflow at an inclination of $15°-30°$ to the plane of the sky, very small spatial elements can be resolved. The outflow has been shown to possess a shell-like structure (*e.g.*, Snell and Schloerb, 1985; Fridlund, 1987; Rainey *et al.*, 1987; Moriarty-Schieven and Snell, 1988). The ouflow in the blue-shifted lobe also is found to be accelerated as we progress further out from IRS5, and to possess velocity discontinuities, particularly close to one of the HH objects (Fridlund *et al.*, 1984). Observations of CS (Kaifu *et al.*, 1984) have shown the presence of a possible large (scales of 10^{17} cm) rotating molecular disk around

IRS5, and ^{13}CO data seem to confirm this as well as being indicative of the outflow being ejected from the surface of this disk (Fridlund, 1987; Fridlund *et al.*, 1988).

The present understanding of the physics behind the structure of the outflow is very sketchy, but involves either a hot narrow jet, ejected from IRS5 or its immediate vicinity (*e.g.*, at an accretion shock), or a massive wind, magnetohydrodynamically ejected from the surface of a large molecular disk, or a combination of both.

In order to gather data for testing of the theoretical models, we have, together with other collaborators, collected a large number of CO spectra in the 1–0, 2–1, and 3–2 transitions, as well as ^{13}CO 1–0 data. some results are already published, including a CO $J = 1$–0 map covering 60% of the blueshifted outflow (Fridlund *et al.*, 1984; Fridlund, 1987; Rainey *et al.*, 1987; Fridlund *et al.*, 1988). Here we report the result of high signal/noise ^{13}CO observations and their implicatons for the mass and energetics of the blue-shifted outflow lobe.

Mass and Energetics

A total of 271 CO $J = 1$–0 spectra separated by 20″ and integrated to reach an rms noise level of 0.3 K, and 55 ^{13}CO $J = 1$–0 spectra have been obtained at Onsala, using the 20 m telescope. The ^{13}CO spectra were integrated for 45–60 minutes, reaching a rms noise level of 0.1 K or less. Since the ^{13}CO are coincident with the CO spectra, we can calculate the column densities (N_{13}), assuming a common excitation temperature (T_x) and beam filling factors of 1. Going from N_{13} to the total mass is straightforward, but the assumptions made mean that the mass determined from the values of N_{13} will be lower limits only. The low values of T_x found from our data (5–15 K), as compared to 25–30 K as derived from observations at higher transitions (*e.g.*, Rainey *et al.*, 1987), indicates that the gas is clumpy. If we plot the CO temperature integrated over velocity against the values on N_{13}, we get Fig. 1. If CO were optically thin, and the beam filling factors actually were equal to 1, the data points would fall along a straight line. CO is actually thick in the center of the wing emission, but most of the wing profile consists either of thin emission or almost thin emission. The integration of the wing profile therefore probably does not miss much of the gas present. The scatter in the diagram can then be removed if we know the beam filling factors. Since we also have CO $J = 2$–1 and $J = 3$–2 observations of these positions, work is in progress to model each spectrum position radiatively. This will provide a better determination of T_x, and this will give us the filling factors and so a better value for the mass.

By assuming a relation between the N_{13} and the integrated intensity and velocity of CO such as those represented by the lines in Fig. 1, presently we arrive at a lower limit to the mass of the part of the outflow mapped by us in CO of $1\,M_\odot < M_{flow} < 2\,M_\odot$. In order to determine the energetics of the outflow gas, we need to analyse the kinematics of the gas and also take into account the geometrical orientation of the outflow, since we only observe the radial component. For a first estimate we can use the median value of the radial velocity component of the gas, that is 8 km s^{-1}. If the "blue" outflow is tilted 15° towards us out of the plane of the sky and the opening angle of the cone is roughly 30° (Liseau and Sandell, 1986), we can calculate the kinetic energy to be $10^{45}\,\mathrm{erg} < E_{kin} < 10^{46}\,\mathrm{erg}$. The mechanical power of the part of the outflow can be

estimated to be between 0.5 $L_\odot$ and 5 $L_\odot$. These values will be refined when the complete analysis is ready.

Our results fully confirm earlier conclusions that the flow can neither be radiatively driven, nor energetically sustained by IRS5 through radiation, since the luminosity of this object is too low. However, comparing the outflow energy derived above with the IRAS-determined FIR luminosity of the outflow of 10 $L_\odot$ (Clark *et al.*, 1986), we find that the observed flow could maintain the observed dust luminosity over the dynamical lifetime of the outflow (of order 10^4 years).

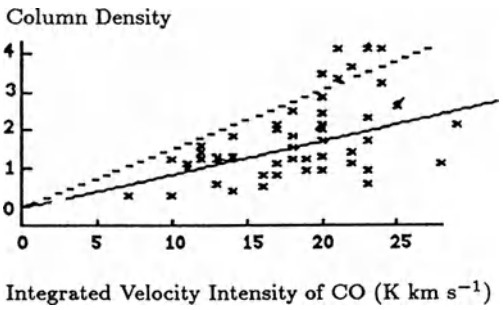

Fig. 1. The values of $N_{13}/1 \times 10^{15}$ have been plotted against the CO temperatures integrated over velocity. The dotted line represents the theoretical relation for thin CO emission and a beam filling factor of 1. The solid line is the rms average relation.

References

Clark, F.O., Laureijs, R.J., Chliwicki, G., Zhang, C.Y., van Oosterom, W., and Kestor, D. 1986, *Astr. Ap.*, **168**, L1.

Emerson, J.P., *et al.* 1984, *Ap. J.*, **278**, L49.

Fridlund, C.V.M., *et al.* 1980, *Astr. Ap.*, **91**, L1.

Fridlund, C.V.M., Sandqvist, Aa., Nordh, H.L., and Olofsson, G. 1984, *Astr. Ap.*, **137**, L17.

Fridlund, C.V.M. 1987, Ph.D. thesis, Univ. of Stockholm.

Fridlund, C.V.M., Sandqvist, Aa., Nordh, H.L., and Olofsson, G. 1988, *Astr. Ap.*, accepted.

Kaifu, N., *et al.* 1984, *Astr. Ap.*, **134**, 7.

Liseau, R., and Sandell, G. 1986, *Ap. J.*, **304**, 459.

Moriarty-Schieven, G.H., and Snell, R.L. 1988, *Ap. J.*, **332**, 364.

Rainey, R., *et al.* 1987, *Astr. Ap.*, **179**, 237.

Snell, R.L., Loren, R.B., and Plambeck, R.L. 1980, *Ap. J. (Letters)*, **239**, L17.

Snell, R.L., and Schloerb, F.P. 1985, *Ap. J.*, **295**, 490.

Strom, K.M., Strom, S.E., and Vrba, F.J. 1976, *A. J.*, **81**, 308.

THE STRUCTURE OF THE MOLECULAR OUTFLOW ASSOCIATED WITH HH7-11

Lewis B.G. Knee
Onsala Space Observatory, S-43900 Onsala, Sweden

We are conducting a program of CO(J=1-0) observations of the NGC1333 low-mass star formation region, using the Onsala 20 metre millimetre wavelength telescope (FWHM beam width 33" at 115 GHz). The objectives are to obtain a complete survey for molecular outflows driven by embedded pre-Main Sequence stars and to map at high resolution the bipolar outflow associated with the low mass object SSV13 and the HH7-11 nebulosity. These observations are a continuation of those originally reported by Liseau *et al.* (1988).

As reported by Liseau *et al.*, bipolar outflows appear to be associated with 5 of the 6 embedded IRAS far-infrared objects (see also Jennings *et al.*, 1987). The sixth embedded infrared object, NGC1333/IRAS1, has been found to have no CO outflow. Millimetre spectral line observations indicate it is coincident with an isolated, low mass, compact molecular cloud core. IRAS1 appears to be a very young, possibly protostellar object, which has yet to enter its molecular outflow phase (Knee *et al.*, 1988). The mapping project (on a full beam spacing grid, 30") is continuing at Onsala, and will be reported upon in full in a forthcoming publication (Knee, 1988a).

The high resolution CO observations (half beam spacing, 15") of the SSV13 blue-shifted outflow lobe have been discussed by Liseau *et al.*, who proposed a model of the outflow which disagrees in a number of aspects with that proposed for the L1551 outflow (*cf.* Moriarty-Schieven and Snell, 1988, Fridlund *et al.*, 1988). The observed distribution of radial velocity and integrated intensity of the CO high velocity wings did not lend support to the "wind evacuated shell" model proposed for L1551.

We have reanalyzed the high resolution data by means of a MEM algorithm (Bergman and Knee, 1988). Figure 1 shows the structure of the blue-shifted CO emission as "deconvolved" by the MEM. The result suggests that the outflow lobe does exhibit the "limb-brightened" spatial structure characteristic of L1551, and that this outflow may be an at least partially evacuated shell. The MEM result agrees in its general morphology with the interferometric observations of Grossman *et al.* (1988), but our result shows the shell-like structure more clearly. Further MEM experiments will be necessary to determine whether or not the SSV13 outflow also has a radial velocity field similar to that of L1551.

Also planned are observations of the SSV13/HH7-11 outflow in the ^{13}CO(J=1-0) transition. Such observations are necessary in order to obtain any improvement on the determination of excitation temperatures and column densities within the outflow.

We have confirmed the existence of extremely high velocity wings in the

HCO^+(J=1-0) emission from the position of SSV13, first reported by Lizano *et al.* (1988). Figure 2 shows the result of a very long integration observation made with the Onsala telescope (FWHM beam width 40" at 98 GHz). The blue-shifted wing is markedly different from the red-shifted wing at the very highest radial velocities (greater than 30 km/s from the cloud LSR radial velocity), as it has a roughly flat-topped profile which extends to more than 70 km/s from the ambient cloud line component at 8 km/s. Recent observations of L1551/IRS5 (Knee, 1988b) show that its high velocity HCO^+(J=1-0) emission is weaker, does not extend over such a wide range of radial velocity, and has very similar profiles in both the red- and blue-shifted wings.

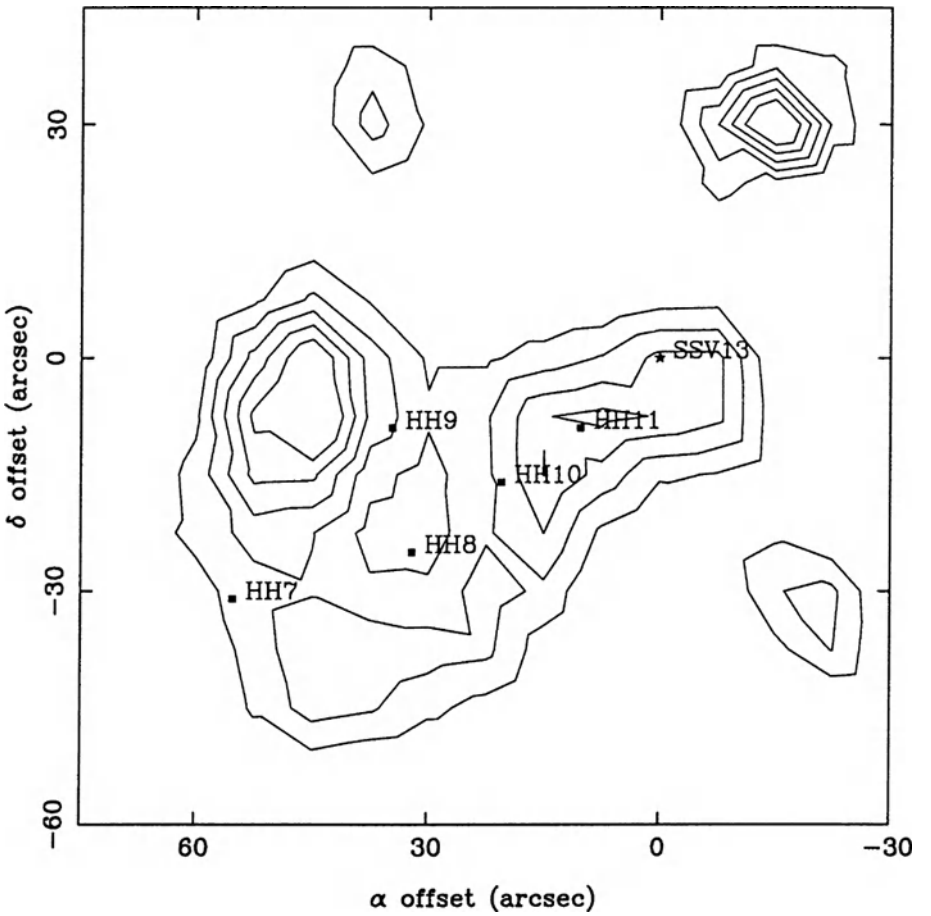

Figure 1. MEMed map of blue-shifted high velocity CO(J=1-0) emission near SSV13/HH7-11. Contours are of integrated antenna temperature (Kkm/s). Radial velocity integration range is -6.95 km/s to +3.45 km/s. Contour level 1 corresponds to 15 Kkm/s, and the contour increment is 10 Kkm/s. The origin of α and δ is the epoch 1950 position of SSV13 ($\alpha=3^h\ 25^m\ 58.2^s$ $\delta=+31°\ 05'\ 44.0''$).

We plan to observe additional positions in the SSV13/HH7-11 and the L1551 outflows in the HCO^+(J=1-0) transition in order to study the variation of the line profiles of the dense outflowing molecular gas, and to attempt to develop a simple geometrical model to explain the velocity structure of the line wings.

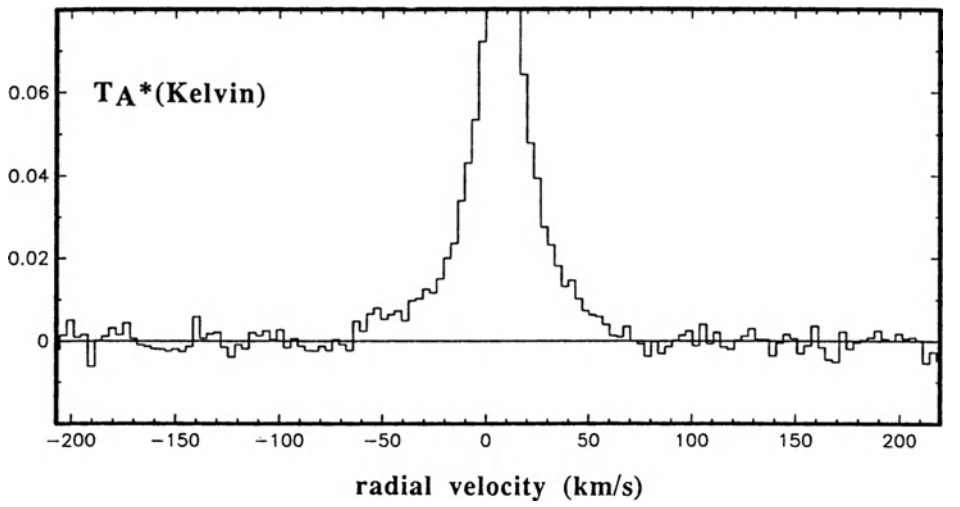

Figure 2. High sensitivity HCO^+(J=1-0) spectrum obtained towards SSV13. Temperature scale is chopper calibrated antenna temperature (T_A^*).

References

Bergman, P., and Knee, L.B.G., 1988. In preparation.

Fridlund, C.V.M., Sandqvist, Aa., Nordh, H.L., and Olofsson, G., 1988. *Astron. Astrophys.*, in press.

Grossman, E.N., Masson, C.R., Sargent, A.I., Scoville, N.Z., Scott, S., and Woody, D.P., 1987. *Astrophys. J.* **320**, 356.

Jennings, R.E., Cameron, D.H.M., Cudlip, W., and Hirst, C.J., 1987. *Mon. Not. R. Astron. Soc.* **226**, 461.

Knee, L.B.G., 1988a. In preparation.

Knee, L.B.G., 1988b. In preparation.

Knee, L.B.G., Cameron, D.H.M., and Liseau, R., 1988. In preparation.

Liseau, R., Sandell, G., and Knee, L.B.G., 1988. *Astron. Astrophys.* **192**, 153.

Lizano, S., Heiles, C., Rodríguez, L.F., Koo, B.-C., Shu, F.H., Hasegawa, T., Hayashi, S., and Mirabel, I.F., 1988. *Astrophys. J.* **328**, 763.

Moriarty-Schieven, G.H., and Snell, R.L., 1988. *Astrophys. J.* **332**, 364.

THE STARFORMING DARK CLOUD ε CHA I: SEST* CO OBSERVATIONS

K. Mattila
Helsinki University Observatory, Tähtitorninmäki, SF-00130 Helsinki, Finland

Introduction

The complex of several dark clouds and two T-associations near the star ε Chamaeleonis was first described in detail by Hoffmeister (1962). Cloud I is located at l = 297°, b = -16° and is thus sufficiently far off the galactic plane to minimize the confusion by background gas and dust clouds. Because of its short distance of 140 pc (Whittet et al., 1987) and the large number of associated young low-mass stars, the Cha I cloud is well suited for the study of the star formation process in dark clouds.

The population of associated stars and young objects comprises (for references, see Mattila and Toriseva, 1985): 21 RW Aur type stars, 45 Hα emission line stars, 3 visible reflexion nebulae, Ced 110-112, the Infrared Nebula, IRN, 4 Herbig Haro objects, HH48-51, embedded highly reddened stars detected from 2 μm surveys, warm far-IR sources detected by IRAS, young stars detected by their (chromospheric) X-ray emission.

The first extensive radio line mapping of the Chamaeleon I dark cloud has been reported by Toriseva, Höglund and Mattila (1985). The Parkes 64-m radio telescope was used to map the 6-cm formaldehyde absorption and the 18-cm OH emission. The integrated formaldehyde line intensity was found to agree quite well with the optical boundaries of the cloud.

CO outflow and dense core near HD 97300

The area close to the B9V star HD 97300 at the northern end of the Chamaeleon I dark cloud contains a small grouping of 5 low-mass PMS stars. Four further stars are located within a few arc minutes (see Fig. 1). An estimated mass of 12 $M_\odot$ for the stars in this cluster (including HD 97300) and 35 $M_\odot$ for the cloud gives a star-formation efficiency of ~25 %. This approaches the very high values found in the core of the ρ Oph cloud by Wilking and Lada (Ap.J. 274, 698, 1983). The proximity of the B9 type star HD 97300 suggests that its stellar wind may have triggered the formation of the low-mass star cluster.

This area has previously been investigated both in the near and far infrared (Jones et al., 1985, Baud et al., 1984) so that the distributions of dust and the embedded stars are fairly well known. It is apparent that this area is a very promising one for the study of low-mass star formation

* Swedish-ESO Submillimetre Telescope

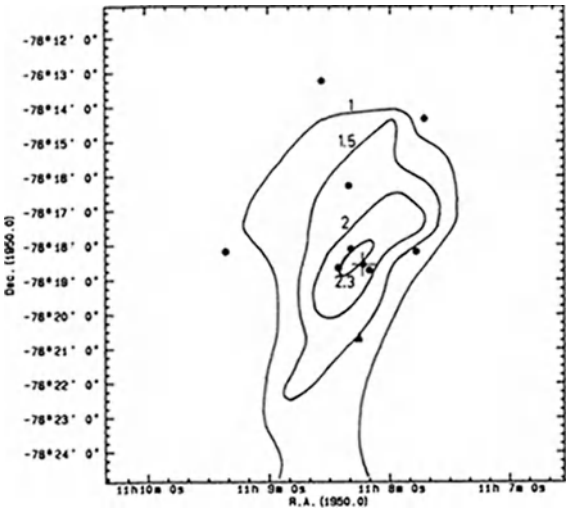

Fig. 1. $C^{18}O$ line area [K·km s^{-1}] map of the Cha I North dense core. Associated stars (dots) according to Jones et al. (1985). The center of the map at $11^{h}08^{m}14^{s}.8$, -76°, 18'37" is indicated with a cross, and HD97300 with a triangle.

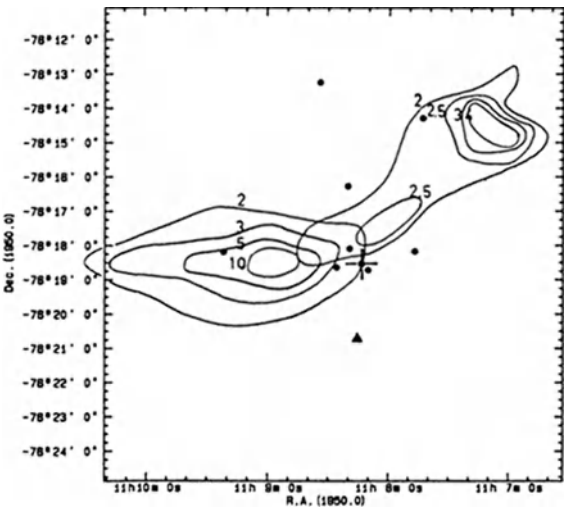

Fig. 2. CO outflow associated with the Cha I North dark core. The contours give the line area in K·km s^{-1} in the intervals:
-1.25 ... 3 km s^{-1} blue wing (thick lines)
6 ... 10 km s^{-1} red wing (thin lines)
Associated stars as in Fig. 1.

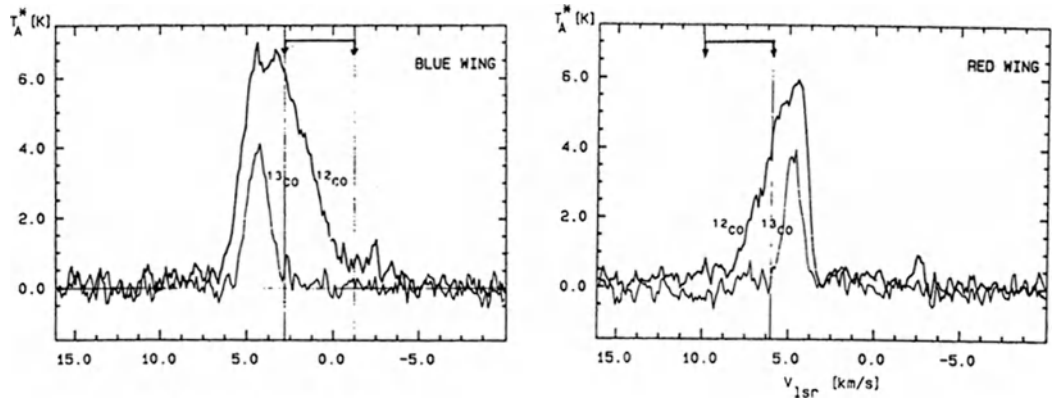

Fig. 3. CO and ^{13}CO spectra as observed in the blue lobe at (+2',0) and in the red lobe at (-5',+4') of the Cha I North outflow source.

and its connections with the ambient cloud material. It is thus important to investigate the properties of the molecular gas in this area.

We have surveyed the Cha I North area in the J=1-0 CO, ^{13}CO and $C^{18}O$ lines in April 2-9 1988 using the SEST. The mapping grid was 1 . Frequency switching within the band was used throughout and the signals from receivers A and B were added.

We have discovered a dense molecular core and a large outflow source, both of which are markedly well centered on the grouping of the 5 PMS stars. Our $C^{18}O$ line area map of the region is shown in Fig. 1. The CO outflow map is shown in Fig. 2. The area has also been observed in the ^{13}CO line which appears to be optically thick over most of the area. At position (0, -1') relative to the map centre the ^{13}CO profile is almost as strong as the ^{12}CO profile, but nevertheless the line widths are almost equal.

The outflow has an angular extent of ~8' from the centre corresponding to 0.3pc (for r = 140 pc). The velocity extension of the outflow is from -4 to +10 km s^{-1} (see Fig. 3). The outflow is clearly not associated with the bright star HD 97300 illuminating Ced 112 but with the grouping of five PMS stars ~2' North of it.

Searches for CO outflows at other positions

Less extensive ^{12}CO, ^{13}CO and $C^{18}O$ maps were made around the following positions :
HH 49/50 and IRAS 11054-7706C, the proposed central star of HH 49/50,
Ced 111 (HD 97048),
HH 51 and VZ Cha , the central star of HH 51.

In each of these cases weak outflows were indicated.

References

Baud, B., Young, E., Beichman, C.A., Beintema, D.A., Emerson, J.P., Habing, H.J., Harris, S., Jennings, R.E., Marsden, P.L. and Wesselius, P.R. 1984, Astrophys. J. 278, L53

Feigelson, E.D. 1984, in Lecture notes in physics No. 193: Cool stars, stellar systems and the Sun, p. 27. Springer-Verlag

Hoffmeister, C. 1962, Zs. f. Astrophys. 55, 290

Jones, T.J., Hyland, A.R., Harvey, P.M., Wilking, B.A. and Joy, M. 1985, Astron. J. 90, 1191

Mattila, K., Toriseva, M. 1985, Proc. ESO-IRAM-Onsala Workshop on "(Sub)Millimeter Astronomy", 421

Schwartz, R.D. 1977, Astrophys. J. Suppl. 35, 161

Toriseva, M., Höglund, B. and Mattila, K. 1985, Rev. Mexicana Astron. Astrof. 10, 135

Whittet, D.C.B., Kirrane, T.M., Kilkenny, D., Oates, A.P., Watson, F.G.,King, D.J. 1987, M.N.R.A.S. 224, 497

ON FRAGMENTATION OF DARK CLOUDS

H.J. Wendker, C. Feldt, T. Günter
Hamburg Observatory, FRG

L.A. Higgs, T.L. Landecker
DRAO Penticton, B.C., Canada

SUMMARY

By combining 100 m-RT and DRAO-SRT observations of the 21 cm HI line we have found a large number of small cloudlets showing self-absorption. They probably belong to the Cygnus Rift and may be a hitherto observationally unknown component of the fragmentation process. The molecular cloud of W80 breaks apart into a complicated substructure when seen in the H_2CO absorption line.

1. Introduction

It is usually agreed upon that dark clouds tend to show increasing density with decreasing size. Details of this fragmentation process are hardly known, however, because there is a substantial lack of observational evidence on the fragmentation status of individual clouds and how to distinguish between a genuine cloud and its substructure. For a review see e.g. Scalo (1985). We have tried to test the usefulness of probing the internal structure of dark clouds via mapping of HI and H_2CO absorption lines.

2. HI self-absorption

For the 21 cm HI absorption line study we combined a fully sampled map with high frequency resolution obtained with the Effelsberg 100 m-RT with a high angular resolution data set obtained with the DRAO synthesis interferometer. The field chosen is the centre of the Cygnus X region and thus covers a north-western portion of the Cygnus Rift. Surprisingly, a large number of small scale, faint self-absorption components appears when both data sets are inspected together. A sample map in the local radial velocity range from -10 to +10 km/s is shown in Fig.1. Components down to -5 K T_b absorption and down to the angular resolution limit of the interferometer (1' x 1.5') can clearly be

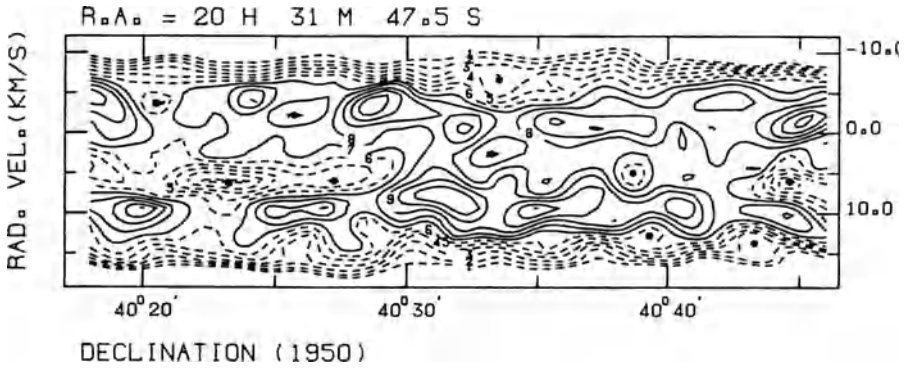

Figure 1: Sample radial velocity vs. declination map. Interferometer map with zero-spacings from 100 m-RT added. The resolution in this map is 1.5' x 2.6 km/s. The lowest contour is 85 K T_b, step is 4 K T_b. Local minima e.g. small self-absorption components are indicated by dots.

dealt with. If they belong to the Rift, these numbers correspond to a linear size of 0.2 pc and a column density of few times 10^{19} atoms cm^{-2} (spin temperature set to 50 K). The histograms in Fig.2 show that the number of components rapidly increases towards the instrumental limits so that many of them must be even smaller in size. Their projected density in the field centre is about 100 per square degree. Although the construction of the emission line background is not in all cases straight forward, the existence of these cloudlets is beyond doubt. Unfortunately, in the Cygnus X region our view tangentially along the local spiral arm results in a severe projection effect so that an individual assignment of the cloudlets either to the Rift or to dark clouds further away can not be made. A separation via radial velocity is also not possible (Piepenbrink and Wendker, 1988).

Under plausible assumptions these cloudlets have volume densities of a few tens atoms cm^{-3}. Such densities of neutral gas are usually not derived from HI emission where typically around 1 cm^{-3} is found. On the other side they are clearly less than those found from CO emission ($\gtrsim$ 100 particles cm^{-3}). The mass of the cloudlets is certainly well below the Jean's mass. Thus we speculate that they must represent parts of a dark cloud which were driven towards higher densities by turbulence and cooled. Their large abundance could mean that they are an important transition step in the fragmentation process.

3. H_2CO in W80

Another part of the density-size-relation of the fragmentation process which is not yet covered by many observations is the one beyond

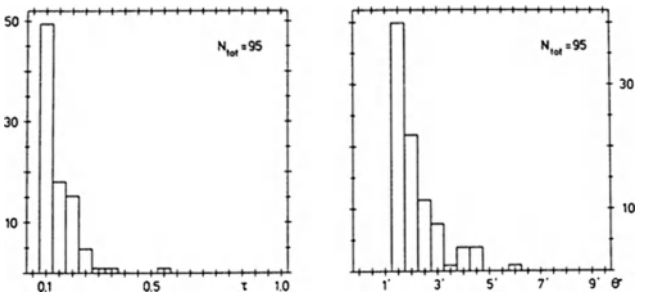

Figure 2: Histograms of the number of self-absorption components N vs. their optical depth τ and vs. their total extent θ .

the reach of CO emission e.g. roughly beyond 1000 particles cm^{-3}. A molecular line probe which is particularly suited for the range 10^3 to 10^4 cm^{-3} is the 6 cm H_2CO absorption line. To our knowledge no large dark cloud was yet mapped in H_2CO so that a size vs. density relation of substructure could be studied. We thus have mapped the dark cloud of W80 in this line with the 100 m-RT. From the profiles we deduced the existence of 26 components inside of the cloud with sizes between one third of the total diameter (20 pc) down to the grid size (0.8 pc) and particle densities between 1000 and 5000 cm^{-3}, all in the radial velocity range +10 and -10 km/s. A general trend is visible, namely increasing density with decreasing size. The observational uncertainties due to the fact that the grid size of the mapping was about twice the beam width (2.6') or larger prevent a more quantitative treatment. We intend to properly supplement the data. This molecular cloud (for a discussion of its known properties and surroundings, see e.g. Wendker et al. 1983) thus exhibits a complex substructure with a large range of scale sizes and densities.

Acknowledgement: Part of the work of CF and HJW was supported by DFG (grant We 741/7).

References:

Piepenbrink,A., Wendker,H.J.: 1988, Astron.Astrophys. 191, 313
Scalo,J.M.: 1985, in Protostars and Planets II p.201ff, University of Arizona Press
Wendker,H.J., Benz,D., Baars,J.W.M.: 1983, Astron.Astrophys. 124, 116

CO in the dark clouds north of the California nebula NGC 1499

R. Herbertz, H. Ungerechts, and G. Winnewisser
KOSMA – I. Physikalisches Institut der Universität zu Köln

We surveyed the CO emission from the dark clouds north of NGC 1499 with the KOSMA 3 m telescope on the Gornergrat near Zermatt, Switzerland. In the Columbia Survey of Perseus, Taurus, and Auriga [1] they stand out as particularly turbulent with linewidths of up to 10 km/s over angular scales of several degrees. Located at a distance of about 350 pc, the clouds have characteristics very different from those of the Taurus dark clouds. To date no signs of embedded star formation have been reported. We mapped the $J = 1 \rightarrow 0$ line of ^{12}CO on 3600 positions in a region of 20 deg^2 on a regular $4' \times 4'$ grid in right ascension and declination (Fig. 1), observed ^{13}CO at 20 positions with high ^{12}CO intensity and mapped ^{13}CO near the three strongest ^{12}CO peaks. At some positions the lines are narrow and almost Gaussian, but generally we find double and triple lines or broad, flat top lines (Fig. 2). Small fragments in the velocity range from -11 km/s to $+5$ km/s are found much farther north of the border of the California nebula than previously shown [2]. The profiles of the ^{13}CO spectra are fairly similar to those of ^{12}CO; the intensity ratio is typically in the range 1/3 to 1/10. The integrated intensities of the two CO isotopes show a reasonably good correlation, so that to first order the integrated ^{12}CO intensity seems to trace the column density. The total mass estimated from the integrated ^{12}CO intensity is 20 000 $M_\odot$. In our ^{12}CO data cube we can distinguish 10 components that are well separated and have average velocities around -7, -3 and $+3$ km/s, and typical linewidths of 2 to 4 km/s. Most of the more massive components with $\approx$ 1000 to 6000 $M_\odot$ are fragmented into smaller clumps with masses between 50 and 4000 $M_\odot$. The velocity dispersion of the large cloud components estimated from the width of the averaged ^{12}CO and ^{13}CO lines is in the range consistent with virialization.

References

1. Ungerechts, H., and Thaddeus, P. 1987, Ap. J. Suppl., 63, 645.
2. Elmegreen, D. M., and Elmegreen, B. G. 1978, Ap. J., 219, 105.

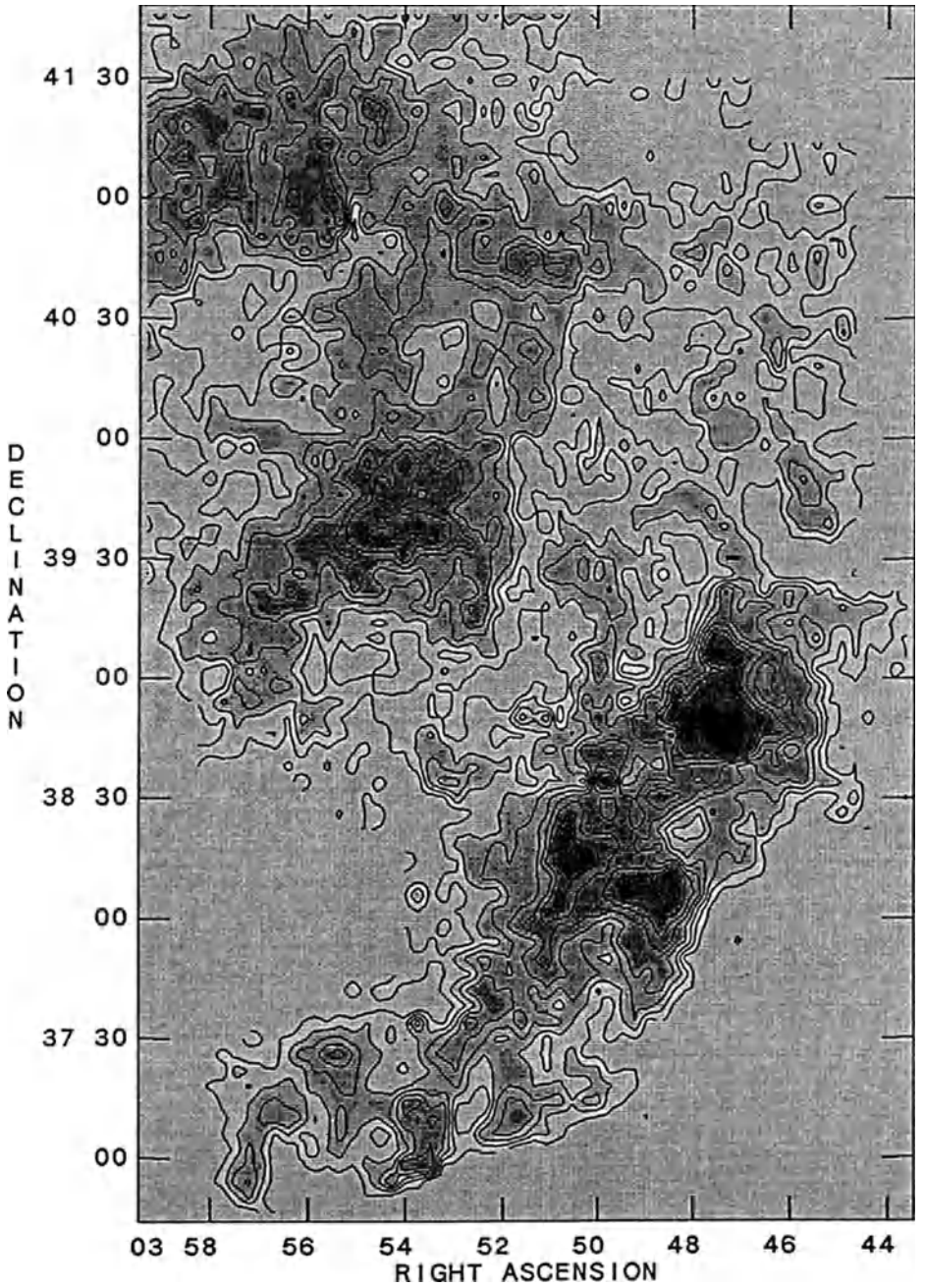

Fig. 1. Molecular clouds north of NGC 1499. The CO intensity was integrated over the velocity range −15 to +10 km/s; the contour levels are 4, 8, 12, ..., 44 K km/s.

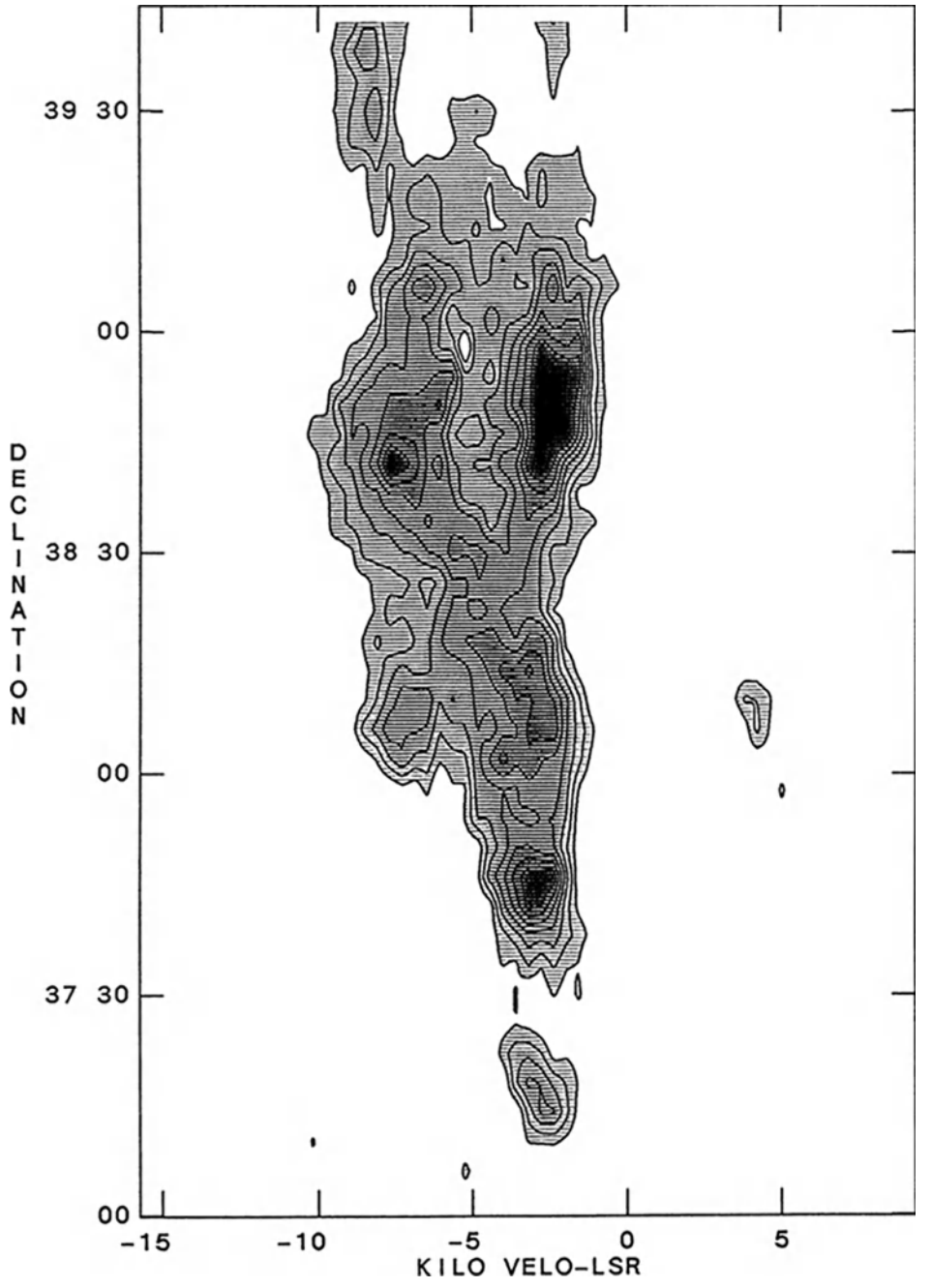

Fig. 2. Molecular clouds north of NGC 1499. Declination-velocity cut obtained by averaging the main beam brightness temperature over the range R.A. = 3^h46^m to 3^h50^m. The contour levels are 1, 1.5, 2.0, ..., 5.0 K.

A CO survey of the giant molecular cloud complex toward Cas A

H. Ungerechts[1] and P. Thaddeus[2]
[1] KOSMA – I. Physikalisches Institut der Universität zu Köln
[2] Harvard-Smithsonian Center for Astrophysics

With the 1.2 m telescope at the Center for Astrophysics we have undertaken a complete, well sampled survey of the 1→0 CO line toward the very large complex of molecular clouds in the Perseus Arm in the region of Cas A and NGC 7538. With a mass in the vicinity of $3 \times 10^6\,M_\odot$, this complex at a distance of roughly 3 kpc ranks as one of the very few objects near the top of the molecular cloud mass spectrum which is sufficiently close and unobscured to be visible optically, but it has not been intensively studied, and no general survey on the scale of the $8'$ resolution of our telescope has yet been reported. Our survey, done at a spectral resolution of 250 kHz (0.65 km/s), on a uniform grid of points spaced every 1/8 deg in latitude and longitude, covers over one-half of the region of the Galactic plane between $l = 107°$ and 114° and $b = -4°$ and $+2°$; the rms noise per spectral resolution element of the survey is about 0.12 K in antenna temperature corrected for beam efficiency (0.82).

Three major complexes, which for brevity we call A, B, and C, and several smaller clouds are easily identified in the map of velocity integrated intensity (Fig. 1). Complex A in the south includes the region toward Cas A located at $l = 111.7°$, $b = -2.1°$. The largest linewidths, up to 20 km/s, are found in the B1 segment of complex B in the center of our map; from our spectra it seems likely that two or more velocity components are severely blended. Complex C is the large molecular cloud associated with NGC 7538 at $l = 111.5°$, $b = 0.75°$. The velocity of the major clouds changes systematically from −37 km/s in complex A to −56 km/s in complex C. A large part (≈40 %) of the survey region is overlapped by CO emission at local arm velocities, $v_{LSR} \approx -15$ to +10 km/s.

We have calculated the masses for the three major complexes as well as 8 smaller clouds using a standard W_{CO} to $N(H_2)$ conversion factor, $2.6 \times 10^{20}\mathrm{cm}^{-2}[\mathrm{K\,km/s}]^{-1}$ (Table 1). Regions A, B, and C each contain about $5 \times 10^5\,M_\odot$; the masses of the smaller clouds are in the range 0.3 to $1 \times 10^5\,M_\odot$. Virial masses estimated from the total linewidth and angular extent of the clouds agree rather well with the mass from W_{CO} for A, B2, and C; the larger discrepancy found for B1, $M_{vir}/M_{CO} \approx 6$, is probably caused by the velocity blending described above.

Our goal over the next two years is to complement the present survey with a similar ^{13}CO survey with the 1.2 m telescope, and studies of selected regions of high activity in CO, ^{13}CO, and $C^{18}O$ with the KOSMA 3 m telescope, to obtain a much more complete and detailed description of a giant molecular cloud complex and its relation to its stellar offspring than any which we now possess.

Table 1. Derived Cloud Parameters

Peak	l	b	S_{CO} K km/s deg^2	Area deg^2	T_R^* K	v_{LSR} km/s	Δv km/s	M_{CO} $10^6 M_\odot$	M_{vir} $10^6 M_\odot$	
A1	111.25	−3.0	27.1	1.88	3.8	−38	10.2	0.42	0.88	Cas A
A2	112.5	−2.25	9.6	1.41	3.3	−36	7.9	0.15	0.46	
A'	112.125	−1.75	1.8	0.23	2.0	−46	11.6	0.028	0.40	
a	111.25	−1.5	5.9	0.70	3.0	−39	9.7	0.092	0.49	
b1	111.25	−0.625	3.2	0.56	3.0	−45	6.9	0.050	0.22	
B1	110.5	−0.375	22.2	1.56	4.7	−47	16.7	0.35	2.16	
B2	110.125	0.0	14.6	0.98	8.8	−52	7.0	0.23	0.30	
b2	109.375	0.25	2.9	0.40	3.0	−55	6.0	0.045	0.14	
b3	108.75	0.25	6.7	1.00	3.7	−53	5.1	0.10	0.16	
C1	111.5	0.75	27.1	1.75	8.2	−55	9.3	0.42	0.71	NGC 7538
C2	110.625	1.125	5.0	1.02	2.9	−57	8.3	0.078	0.43	
1	108.75	−1.0	5.6	0.75	6.7	−51	6.9	0.087	0.26	
2	109.0	−0.25	2.0	0.25	3.8	−47	6.5	0.031	0.13	
3	111.75	0.0	1.7	0.20	1.7	−30	3.7	0.026	0.04	
4	111.5	1.25	2.3	0.38	3.7	−46	5.5	0.036	0.12	

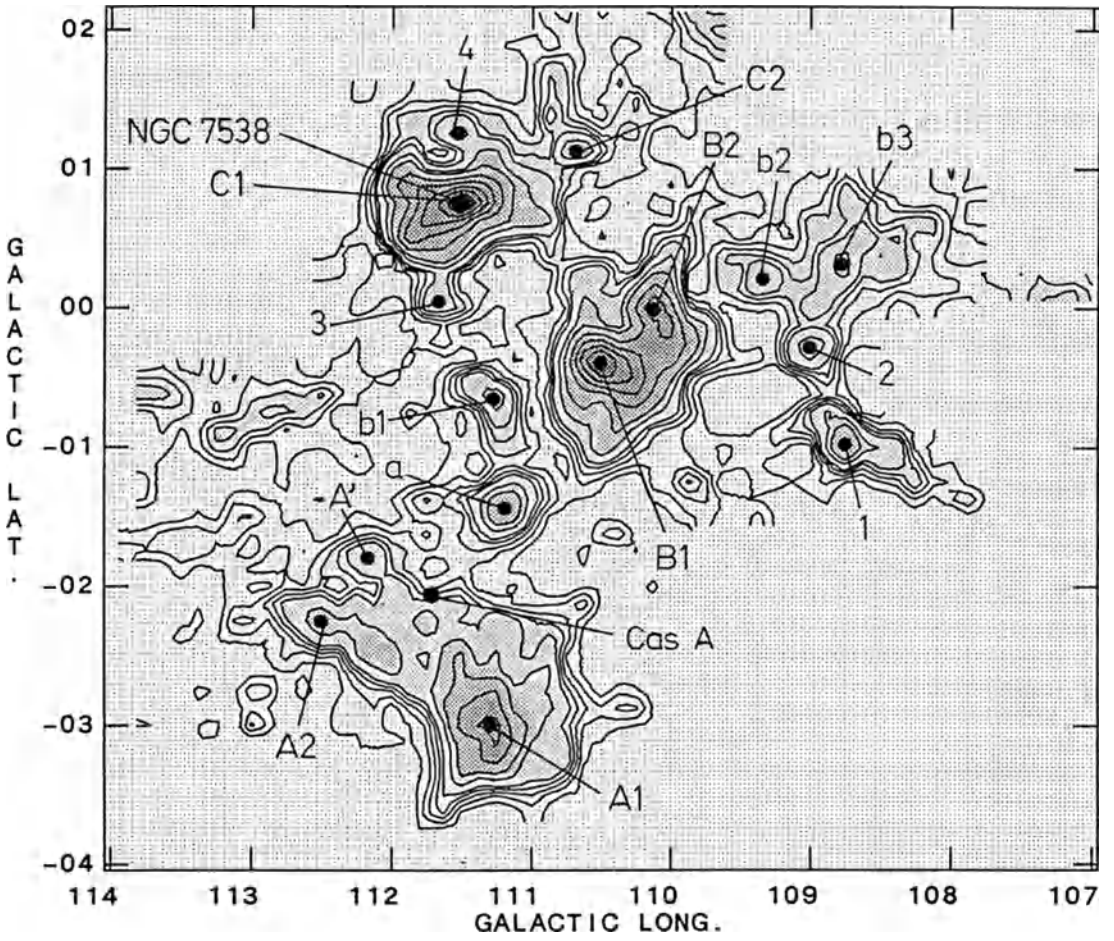

Fig. 1. The giant molecular cloud complex toward Cas A. The CO intensity was integrated over the velocity range −80 to −20 km/s (Perseus arm velocities). The positions of the CO peaks (Table 1) are indicated. The contour levels are 2, 4, 6, 8, 10, 15, 20, 30, 40, 50, 60, and 70 K km/s.

A Complete CO Map of the Nearest Molecular Cloud, L1457

T. Zimmermann and H. Ungerechts
KOSMA – I. Physikalisches Institut der Universität zu Köln

With the KOSMA 3 m telescope on the Gornergrat near Zermatt, Switzerland, we surveyed the $J = 1 \rightarrow 0$ line of ^{12}CO and ^{13}CO in the region of the dark clouds L1457, L1453, L1454, and L1458 where molecular gas is found at a distance of only 65 pc [1]. Halpern and Patterson [2] suggested that a hard X-ray source seen towards L1457 represents a very young protostellar object. CO maps published in the past [1,3] suffer from incomplete coverage or poor spatial resolution.

For our observations we used the KOSMA 3 m telescope with a high resolution AOS in frequency switching mode to obtain complete maps on a regular $4' \times 4'$ grid in right ascension and declination. The rms noise is about 0.5 K for ^{12}CO and 0.15 K for ^{13}CO after smoothing to 0.33 km/s resolution. So far we have mapped L1457 almost completely in ^{12}CO (Fig. 1) and ^{13}CO and moreover observed $C^{18}O$ at 25 selected positions.

The spectra show a complex velocity structure in L1457: at many positions the lines have two or three peaks within a total range of $\approx$15 km/s suggesting fragmentation and turbulence (Fig. 2). The velocity components fall into five ranges, four of which are disjunct, while the fifth partly overlaps two of the others: range I is -8.0 to -3.4 km/s; at declinations lower than $20°12'$ range II is -3.4 to -0.8 km/s, at higher declination range II is -5.4 to -0.8 km/s; range III is -0.8 to $+3.8$ km/s; range IV is $+3.8$ to $+6.7$ km/s. An exception to this straightforward distinction of velocity ranges is component V which occurs in the southwest of L1457, where lines of ranges II and III merge into a single line in the range -3.4 to $+3.8$ km/s. Within the velocity ranges I, II, and III the cloud structures are spatially connected; we therefore call them main components. On a smaller scale we identify a total of 15 clumps with sizes 0.05 to 1.06 deg^2; some of them are fragments of the main components, while others are separate. The masses estimated from the integrated CO intensities are 197 $M_\odot$ for the whole cloud; 50 $M_\odot$, 57 $M_\odot$, and 71 $M_\odot$ for the three main components; and 1 to 48 $M_\odot$ for the clumps.

References

1. Hobbs, L. M., Blitz, L., and Magnani, L. 1986, Ap. J. (Letters), 306, L109
2. Halpern, J. P., and Patterson, J. 1987, Ap. J. (Letters), 312, L31
3. Ungerechts, H., and Thaddeus, P. 1987, Ap. J. Suppl., 63, 645

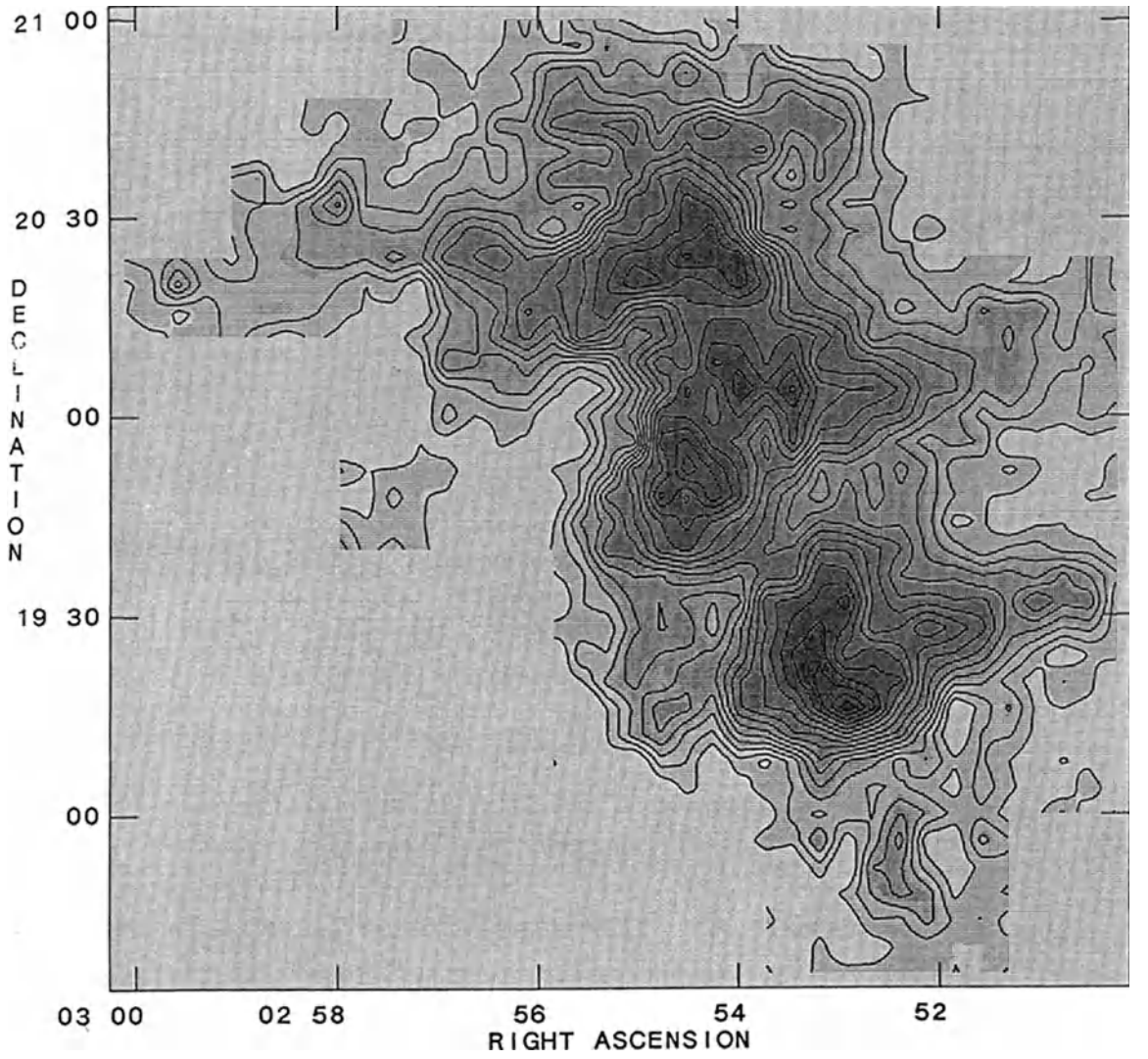

Fig. 1. The L1457 molecular cloud. The CO intensity was integrated over the velocity range −8 to +7 km/s; the contour levels are 2, 4, 6, ... , 30 K km/s.

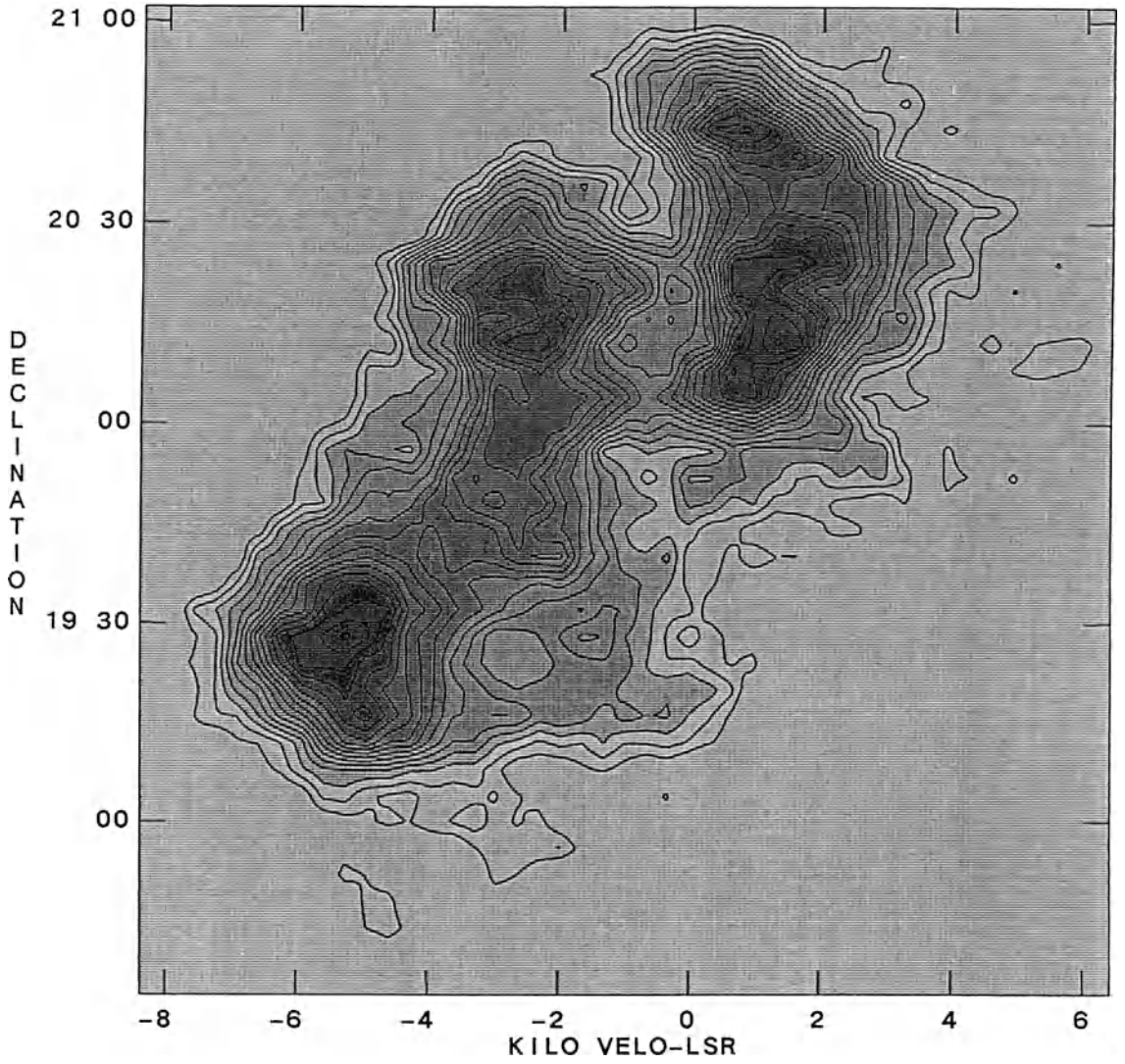

Fig. 2. The L1457 molecular cloud. Declination-velocity map obtained by averaging the CO intensity over the full range in right ascension; the contour levels are 0.2, 0.3, ... , 1.7 K.

A Survey of Dark Clouds near L1495

C. Kramer, J.T. Armstrong, and G. Winnewisser
KOSMA – I. Physikalisches Institut der Universität zu Köln

We surveyed a region of dark clouds near L1495 in the Taurus complex with the KOSMA 3 m telescope on the Gornergrat near Zermatt, Switzerland at the frequencies of the first rotational transition of CO and its isotopes.

The central part of the Taurus complex is characterized by a series of striking features. It has a rather filamentary and fragmentary appearance and a complicated kinematic structure. The presence of T Tauri stars, Herbig Haro objects, reflection nebulae and embedded IR sources suggests that star formation is an ongoing process in this region.

We made measurements of the ^{12}CO ($J = 1-0$) line over a region of 3 deg^2 on a regular 4′ by 4′ (0.16 pc by 0.16 pc) grid with the 4′ beam of the KOSMA telescope. ^{13}CO observations were done at 247 positions with high ^{12}CO intensity and C^{18}O observations were done at 57 positions in the southern part of the 3 deg^2 region. The ^{12}CO spectra show linewidths of 3 km/s and velocities between 2 and 12 km/s. At most positions we find triple lines, presumably corresponding to three main fragments covering the whole observed region. The ^{13}CO spectra and C^{18}O spectra show linewidths of 2 km/s; their optical depths are smaller than 0.5 for ^{13}CO spectra and smaller than 0.1 for C^{18}O spectra. The ^{13}CO and C^{18}O spectra confirm the division into three main fragments.

Depending on the calculation method used the mass of the observed 18 pc^2 region ranges between 1500 and 2700 $M_\odot$. Besides the three main fragments with masses between 400 and 1000 $M_\odot$, four sub-fragments have been found, the smallest with an extension of 0.9 pc^2 and a calculated mass between 10 and 60 $M_\odot$.

The number density of this smallest fragment is 750 cm^{-3}, whereas the average number density of the whole region is 550 cm^{-3}.

A comparison with the virial masses calculated from ^{13}CO and C^{18}O linewidths shows that the whole cloud, the main fragments, and the subfragments are near virial equilibrium.

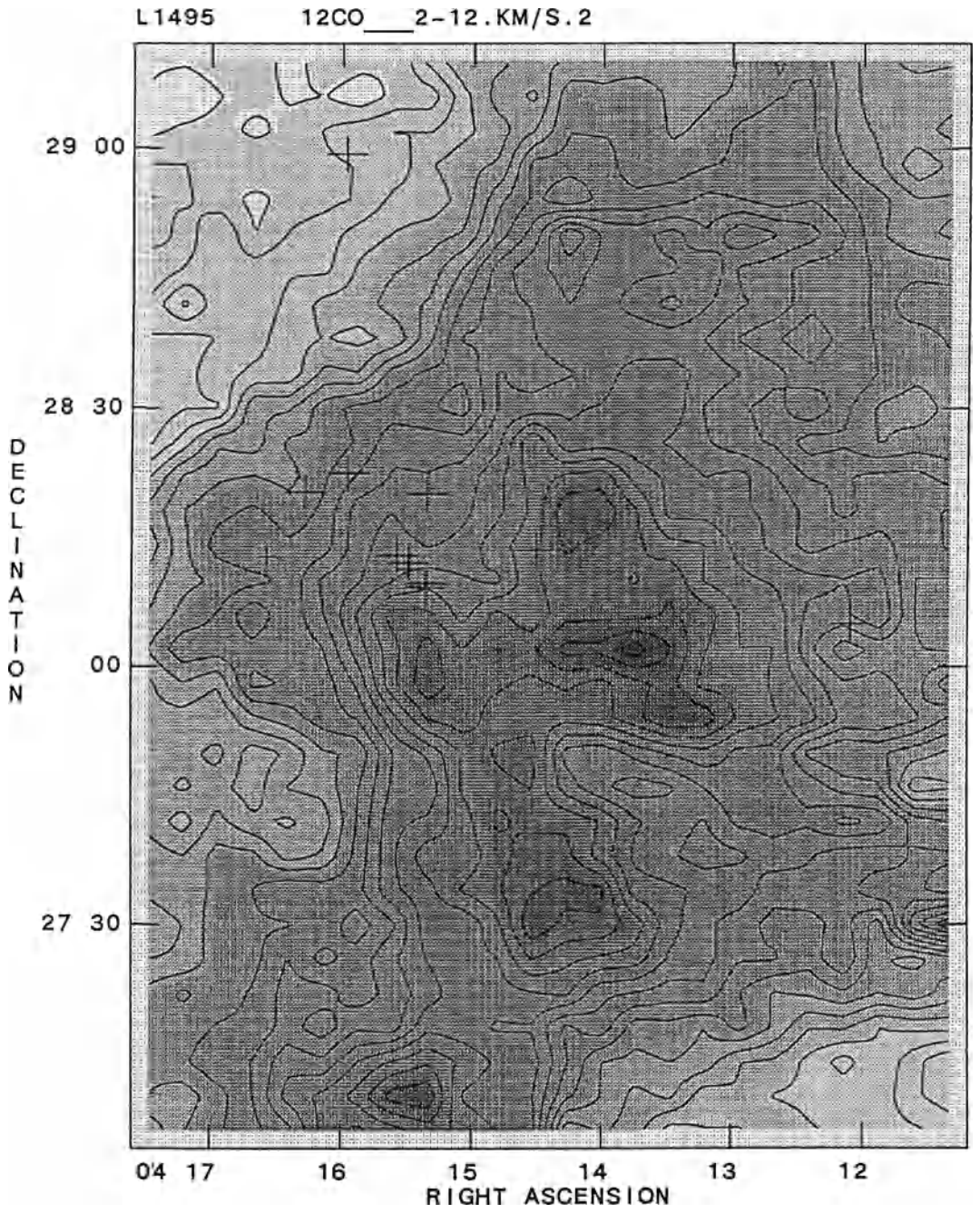

Fig. 1. The ^{12}CO intensity was integrated over the velocity-range 2–12 km/s; the contour levels are 6, 8, ... 38 K km/s; the big crosses represent the positions of T Tauri stars while the smaller crosses indicate the positions of reflection nebulae.

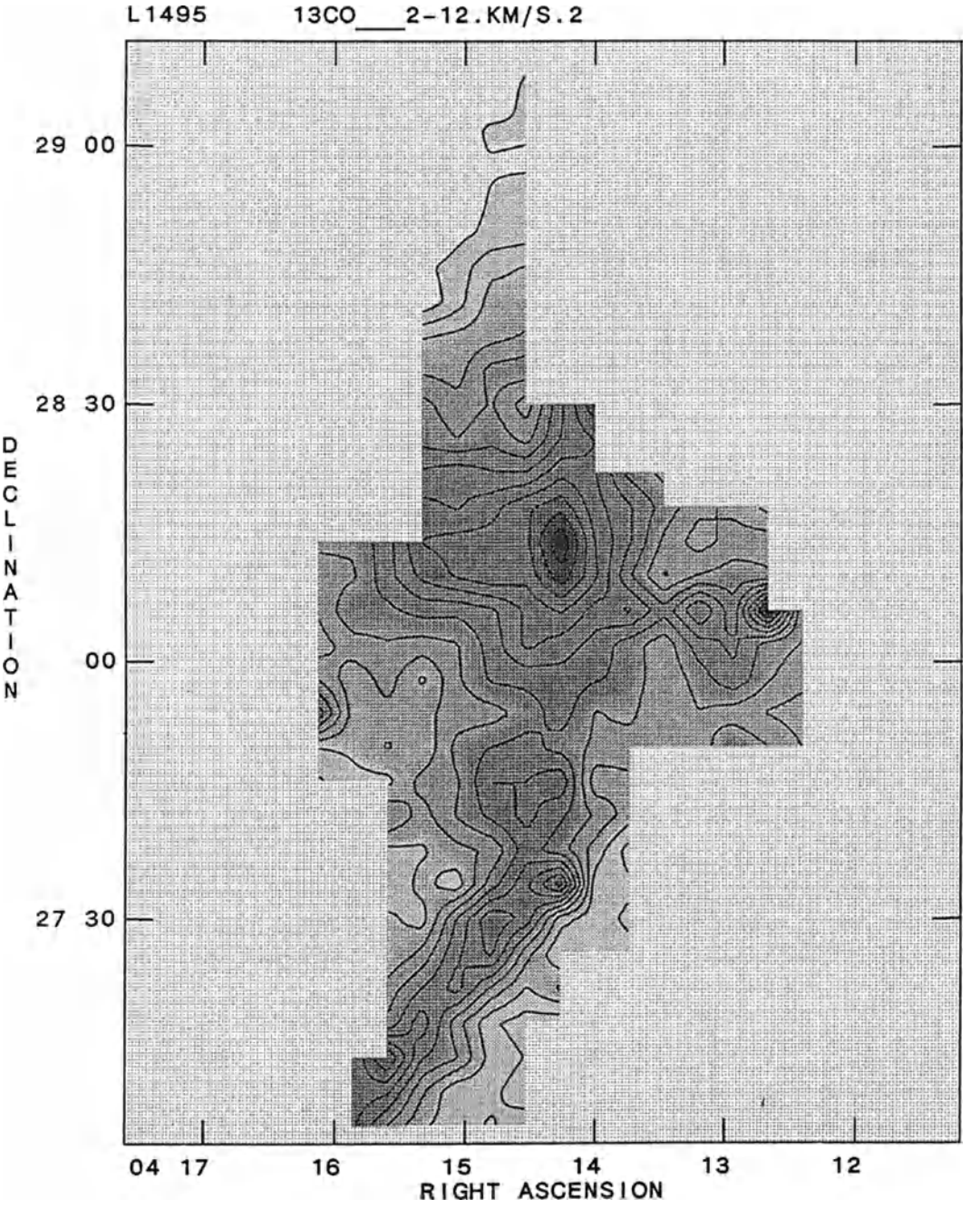

Fig. 2. Map of the integrated intensity of the ^{13}CO line; the velocity-range of the integration is 2–12 km/s; the contour levels are 2, 3, ... 13 K km/s.

Observations of $H_2{}^{18}O$ at 547 GHz with the Kuiper Airborne Observatory

P.G. Wannier[1], L. Pagani[2], P.J. Encrenaz[2], M.A. Frerking[1], S. Gulkis[1], T.B.H. Kuiper[1], A.Lecacheux[2], H.M. Pickett[1], W.J. Wilson[1].

1 : Jet Propulsion Laboratory, 4800 Oak Grove Drive, 91109, Pasadena, Cal., USA.
2 : Observatoire de Meudon, 92 195 Meudon Cedex, France.

Summary

The 1_{10}-1_{01} transition of $H_2{}^{18}O$ has been searched for in several sources without positive detection. However, in NGC 2264 and NGC 7538, possible emission features are suspected. Implications of these features, if confirmed, are discussed. Our best upper limit obtained in Orion (0.9 K) indicates that in that cloud, the water abundance should not be more than 1% that of CO.

Introduction

H_2O is a well-known feature of star-forming regions and of circumstellar enveloppes but no accurate determination of its abundance has yet been made. At present, the only detected lines of water are from highly excited states with non-thermal excitation (22, 183 [Waters et al.,1980] and 380 GHz [Phillips et al., 1980]) or lines of water isotopes (HDO, Henkel et al., 1987 and $H_2{}^{18}O$, Jacq et al., 1988, for recent observations). The abundance of HDO is critically dependant on the Deuterium fractionation while the the observed $H_2{}^{18}O$ line probably arises from a non-thermally excited state, and is difficult to interpret in terms of a water abundance.

We present in this paper our search for the fundamental rotation line 1_{10}-1_{01} of the ortho ^{18}O isotopic species of water at 547.676 GHz (λ = 0.548 mm) using the Kuiper Airborne Observatory (KAO, NASA).

No positive detection is reported with a best 1 σ limit of $\approx$ 0.9 K (in terms of main beam temperature, T_{MB}). However, for NGC 2264 and NGC 7538, there are some hints of a line : it is important to observe them again for confirmation.

Using a large-scale velocity gradient (LVG) model of radiative transfer and most recent He-H_2O collisional cross-sections (S. Green, private communication), an upper limit of 0.01 for the $[H_2O]/[CO]$ Ratio (**R**) is found for Orion, while no clear-cut explanation to the possible lines in NGC 2264 and NGC 7538 can be found. Medium density and high water abundance could explain these features as well as dense clumps with normal water abundance.

Observations and Results

Observations were done during two sets of flights in February and December 1987 from the NASA KAO. An uncooled Schottky Mixer was used with a Single Side Band noise temperature of 14,000 K at the chopper wheel location. The 91.5 cm telescope provided a beam-width of 2.7'. During the december flights, pointing position was checked and telescope efficiencies were evaluated by observations of Jupiter and the Moon. A 256 channel filter bank of 1 MHz resolution (0.548 km/s) was used and calibrations were done using hot and cold loads. Sky opacity and brightness were estimated by comparison with a cold load. All spectra presented here are correctly calibrated but no baseline has been removed.

The atmospheric line has been observed for the first time (fig.1) to our knowledge confirming the correct operation of the receiver. The observed intensity fits in well with predictions made from our atmospheric model. Atmospheric opacity is running from $\tau \approx 0.2$ in the wings to 0.5 at the center of the line at 45° elevation while flying at 12 km altitude.

A few clouds and evolved stars have been observed : Orion (BN-KL), NGC 2264, NGC 7538, W3 (IRS 5), DR 21, NGC 2024 and R Mon, Y UMa and R UMa. No positive detection to the 5 σ level has been made but for NGC 2264 and NGC 7538, there are possible hints of emission : NGC 2264 (fig. 2) shows two lines at 5 and 9 km/s at a 2 σ level which could also be a single line with strong absorption and NGC 7538 (fig. 3) shows a 3 σ line which after Hanning smoothing is close to 4 σ. The best upper limit has been obtained on Orion (fig. 4) with an r.m.s. noise of 0.91 K for an extended source and 1.2 K for a point source (here, we take into account a gain correction for a slight pointing error during one of the flights).

Discussion and Conclusion

In Orion, the Hot Core, Compact Ridge and Plateau, though both hot and dense (and there fore strong emitters, about 120 K) are too diluted to be detected (1 K line is expected) due to their small size (5" to 15" compared to the 160" beam). The Extended Ridge at a somewhat lower temperature (70 K $\pm$ 10 K) and lower density should have been detected if the water abundance is greater than 1% of the CO abundance.

In NGC 7538, there are a few hot sources similar to the Orion objects which are even more diluted and thus undetectable. Otherwise, this source shows, like NGC 2264 a rather extended region (3' in diameter) of mean density $10^{4\text{-}5}$ cm^{-3} with dust temperature around 35 to 40 K. Here, the LVG model indicates that with a density of 10^5 cm^{-3}, $T_{kin} = 30 - 40$ K and $R \geq 0.2$ a line of a few K can be observed. This density is in the upper end of the range of estimated densities in these two sources and R is very high. Another possibility is to invoke high density clumps ($\geq 10^6$ cm^{-3}) with R $\approx$ 0.01 to 0.1 which would provide lines of brightness temperature 9 K or more and which would be in limited number to get the appropriate filling factor to match the observed features. It can be shown that this is easily obtained without modifying the average estimated density of $10^{4\text{-}5}$ cm^{-3}. Thus, at the moment we cannot give a unique likely explanation to the features we might have detected in these two sources.

References

Henkel, C., Mauersberger, R., Wilson, T.L., Snyder, L.E., Menten, K.M., Wouterloot, J.G.A., Astron. Astrophys., 1987, 182, 299.

Jacq, T., Jewell, P.R., Henkel, C., Walmsley, C.M., Baudry, A., Astron. Astrophys., 1988, 199, L5.

Phillips, T.G., Kwan, J. and Huggins, P.J., 1980, in *Interstellar Molecules*, I.A.U. Symposium #87, p.21.

Waters, J.W., Gustincic, J.J., Kakar, R.K., Kuiper, T.B.H., Roscoe, H.K., Swanson, P.N., Rodriguez-Kuiper, E.N., Kerr, A.R. and Thaddeus, P., AstrophysJ., 1980, 235, 57.

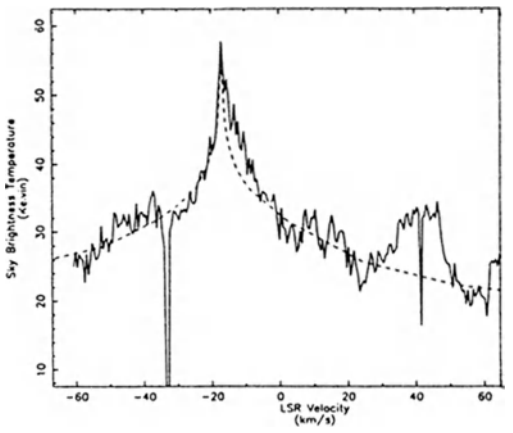

Fig. 1 : Telluric water emission (dashed line represents the model)

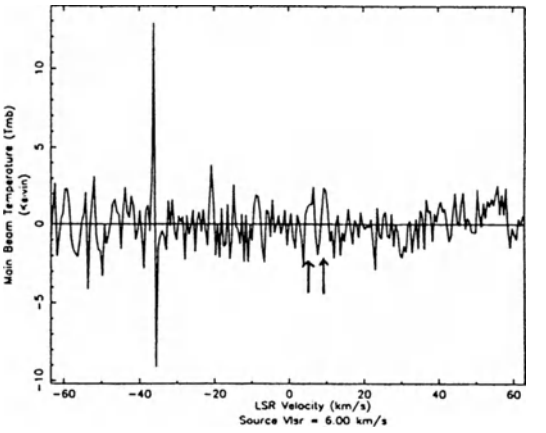

Fig. 2 : NGC 2264 (σ = 1.3 K)

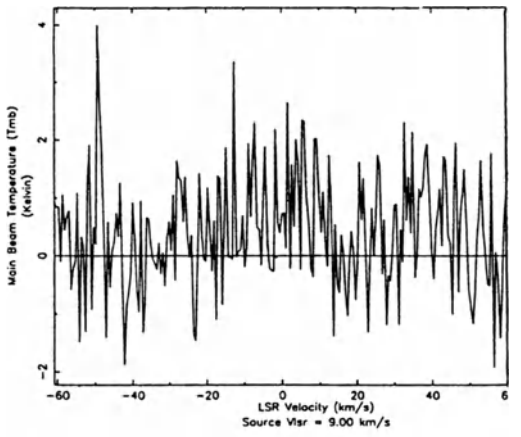

Fig. 4 : Orion A / BN-KL (σ = 0.91 K)

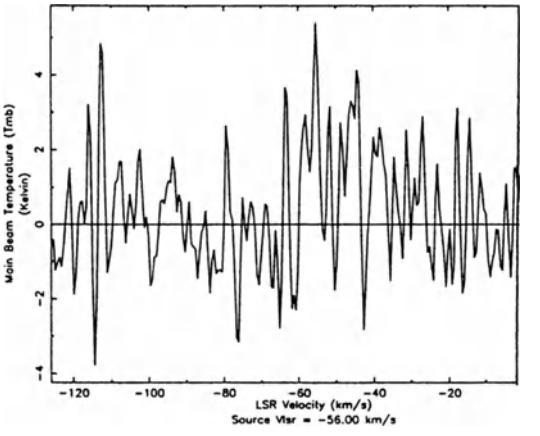

Fig. 3 : NGC 7538 (Hanning smooth, σ = 1.3 K)

G159.6-18.5: A POSSIBLE HIGH GALACTIC LATITUDE SUPERNOVA REMNANT

T. Pauls and P. R. Schwartz
E. O. Hulbert Center for Space Research
U. S. Naval Research Laboratory
Washington, DC 20375-5000

We report infrared and CO observations of the B4/L1470 region in Perseus, which we suggest may be a supernova remnant. The grey-scale image in Figure 1 was obtained from the IRAS 100 μm database, and shows a remarkable ring of emission just west of IC348. The ring, which has a diameter of about 75′, is centered at $\alpha_{1950} = 3^h 36.8^m$, and $\delta_{1950} = 31°39.4'$, or $l = 159.6°$, $b = -18.5°$. We have mapped a $2° \times 2°$ area centered on the ring in the J = 1→0 line of ^{12}CO with 4′ resolution using the KOSMA 3m radio telescope. These observations are plotted in Fig. 1 as contours of total integrated CO intensity superimposed on the IRAS grey-scale map. Our CO data are in good agreement with those of Bachiller and Cernicharo (1986), but have higher spatial and spectral resolution. There is very little correlation between the CO and 100 μm emission, as would be the case in a dark dust cloud, and based on the morphology we suggest that the ring may be a shell-type supernova remnant (SNR). In this case, our CO data may indicate some interaction between the shell and a molecular cloud in the southwest, because in this region the CO line profiles are much broader and show complex velocity structure. Additional evidence supporting our hypothesis comes from the all-sky radio continuum surveys of Haslam *et al.* (1982) at 408 MHz and Reich (1982) at 1420 MHz, both of which show a low surface-brightness source at the approximate position of the shell. We estimate a flux-density spectral index after background correction of about -1 from these data, which confirms that the radio emission is non-thermal.

Thus, we feel that the infrared dust shell, G159.6-18.5, is a supernova remnant with strong far infrared emission. G159.6-18.5 may be similar to IC443 which also shows strong infrared emission (cf. Mufson *et al.* 1986 and Dwek 1988).

Finally, we note that if our hypothesis is correct, G159.6-18.5 has the highest galactic latitude of any known supernova remnant.

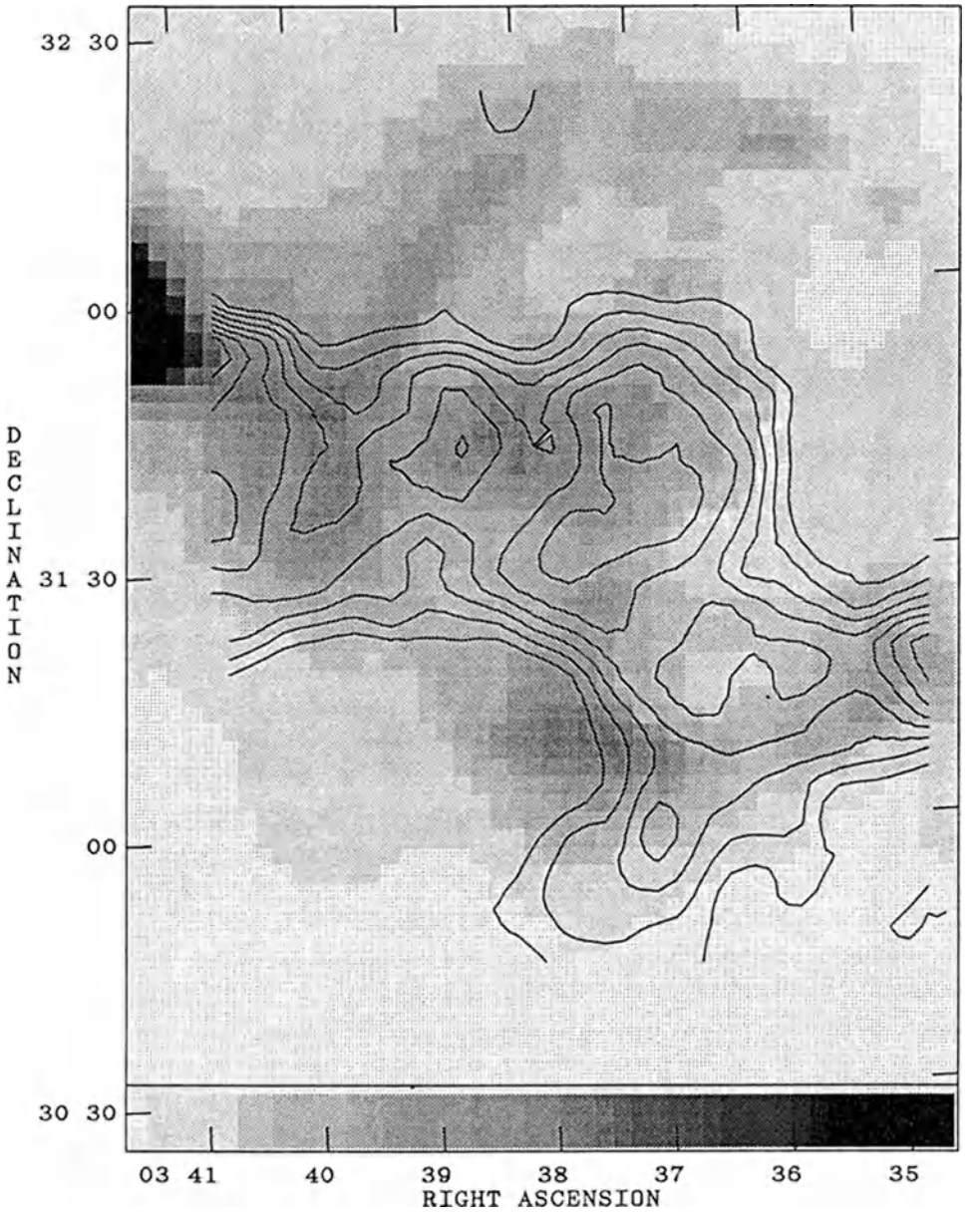

Figure 1: A combined infrared and CO image of the Perseus region near B4/L1470. The grey-scale image is 100 μm emission from the IRAS database on a linear scale between 6×10^{7} and 3×10^{8} Jy/Sr. The contours are total integrated ^{12}CO intensity in uniform steps between 19.5 and 58.5 K kms^{-1}. The strong infrared source on the left-hand edge near declination 32° is IC348.

References

Dwek, E.: 1988, in *Supernova Remnants and the Interstellar Medium*, R. S. Roger, T. L. Landecker,eds., Cambridge University Press.

Bachiller, R., Cernicharo, J.: 1986, *Astron. Astrophys.* 166, 283-290.

Haslam, C. G. T., Salter, C. J., Stoffel, H., Wilson, W. E.: 1982, *Astron. Astrophys. Supp. Ser.* 47, 1-143.

Mufson, S. L., McCollough, M. L., Dickel, J. R., Petre, R., White, R., Chevalier, R.: 1986, *Astron. J.* 92, 1349-1357.

Reich, W.: 1982, *Astron. Astrophys. Supp. Ser.* 48, 219-297.

PROPER MOTIONS OF THE OH MASERS IN W3(OH)

E. E. Bloemhof, M. J. Reid, and J. M. Moran
Harvard-Smithsonian Center for Astrophysics, Cambridge, Massachusetts, USA

SUMMARY

Using data from a seven-telescope VLBI experiment, we have remapped the 1665-MHz OH maser emission from W3(OH), a site of current star formation roughly 2.2 kpc distant. Both circular polarizations were observed with excellent UV coverage, and the resolution of the synthesized maps is about 5 milli-arc seconds. By comparing our new maps (epoch 1986) with maps made at an earlier epoch (1978), we can measure proper motions of individual maser features. Since the maser features are distributed in projection against the ultra-compact HII region, a study of their proper motions can probe the kinematics in the immediate vicinity of this very young object. Our preliminary results indicate a significant ordered divergent motion.

1. Introduction

Several striking facts about the OH masers in W3(OH) have been known since the first VLBI synthesis maps were made. The masers are distributed only over the western half of the ultra-compact HII region seen in continuum emission, although the HII region itself is a roughly symmetrical structure $\sim$1.5" in diameter. The maser features are closely clustered in radial velocity around a value that is red-shifted with respect to the apparent velocity of the HII region, which is optically thick at the frequency of the maser transition. These facts led Reid *et al.* (1980) to postulate that the masers are collapsing with the gravitational infall of remnant protostellar material. A competing interpretation had the masers located in the expanding high-density postshock region between the compact HII region and the ambient molecular cloud (Elitzur and de Jong 1978). To obtain a direct determination of the kinematics in the immediate environment of W3(OH), we undertook a VLBI experiment to remap the OH masers and measure their proper motions.

2. Experimental Technique

Data from epoch 1978 (Garcia-Barreto *et al.* 1987) were available in the form of calibrated visibilities, allowing them to be mapped with identical software and procedures used with our new data from epoch 1986. The maser feature used as a phase reference in 1978 was still strong and nearly unresolved in 1986.

We found that most maser features mapped in 1978 were still present in 1986, as expected from the persistence seen in single-dish spectra of W3(OH) over decade time scales. Further, the morphologies of individual features and larger-scale associations are also remarkably persistent (see Figure 1 for an example). Since features are well-separated in comparison to their characteristic sizes, the identification of features from one epoch to the next is straightforward.

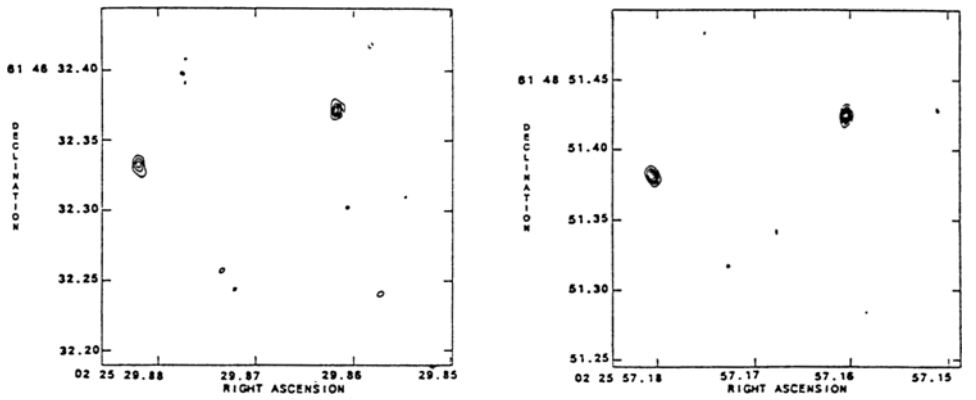

FIG. 1. Maps of individual maser features at epochs 1978 (left) and 1986 (right).

The sensitivity of each experiment was sufficient to allow position fitting of the 5 milli-arc second beam to a few tenths of a milli-arc second, typically. For comparison, a transverse velocity of 10 km s^{-1} (the expected sound speed in the ionized medium) at the distance of W3(OH) (2.2 kpc) would result in a proper motion of $\sim$ 8 milli-arc seconds over our time baseline of 8 years. Hence proper motions resulting from a shock-driven expansion would be easily detectable.

3. Preliminary Conclusions

A very simple analytic technique is to compute the change in separation from one epoch to the next of all pairwise combinations of maser features. The result, plotted as a histogram in Figure 2 for a subset of the data, is a non-parametric test for expansion or contraction of the ensemble of maser features. The data used in this Figure represent perhaps 1/3 of the total maser features to be found.

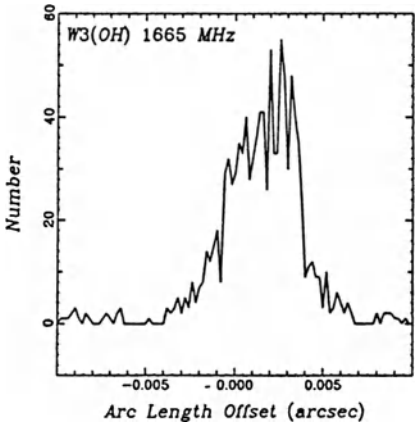

FIG. 2. Histogram of shifts (from 1978 to 1986) in separation of all possible pairwise combinations of maser spots found in preliminary scans of a subset of maps.

The bias toward positive shifts indicates, without any model assumptions, that maser spot positions are predominantly diverging. The apparent transverse velocity of this motion is a few kilometers per second, clearly less than the HII region sound speed of 10 km s^{-1}.

A more sophisticated analysis can be made by examining the distribution of motions over the field containing maser features (Figure 3). Motions are determined only up to an arbitrary additive vector constant, because positions are measured with respect to a single "reference" maser spot that may itself be moving. The motions as plotted have had a velocity of $(v_x,v_y) = (2,1)$ km s^{-1} added to them, as a first guess of the reference feature's motion. The general divergent motion is clear, and there is some indication that the apparent center of divergence is roughly coincident with the center of the compact HII region in W3(OH), which lies near (0,-1) in these relative coordinates.

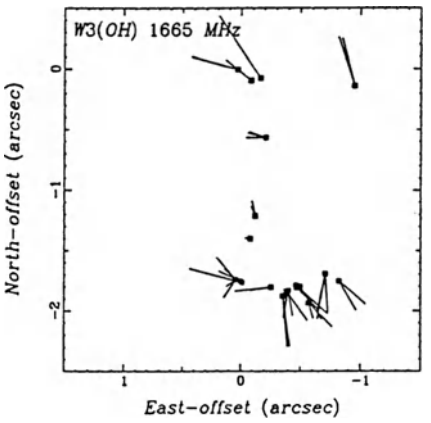

FIG. 3. Spatial map showing relative positions of maser spots (boxes) and their relative motions (solid lines, with lengths proportional to maser velocity: a line 1" long implies a velocity of 10 km s^{-1}).

The divergent motion is inconsistent with expectations based on the infall model, and is at first glance suggestive of an outflowing shock. However, it is still difficult to reconcile an outflow model with the fact that the maser radial velocities are redshifted with respect to ammonia emission and hydrogen recombination lines. It is also surprising that the range of radial velocities observed is so narrow ($\sim$ 1 km s^{-1} when Zeeman effects are accounted for) compared to transverse proper motions that are many times greater. A more sophisticated model involving an asymmetric flow of molecular material around the HII region may be required.

REFERENCES

Elitzur, M., and de Jong, T. (1978), *Astr. Ap.*, **67**, 323.

Garcia-Barreto, J. A., Burke, B. F., Reid, M. J., Moran, J. M., Haschick, A. D., and Schilizzi, R. T. (1987), *Ap. J.*, **326**, 954.

Reid, M. J., Haschick, A. D., Burke, B. F., Moran, J. M., Johnston, K. J., and Swenson, G. W. (1980), *Ap. J.*, **239**, 89.

The Embedded Objects in ε Cha I Cloud[1]

T. Prusti[2] R. Assendorp P. Wesselius

Laboratory for Space Research, Groningen

We are constructing the initial luminosity function for the pre-main sequence objects in the ε Cha I cloud. In order to obtain the spectral energy distributions, we carried out L and M photometry for associated sources. JHK fluxes are adapted from Glass (1979), Hyland et al. (1982), or Jones et al. (1985). Far-IR measurements are obtained from IRAS Serendipitous Survey Catalog, IRAS Point Source Catalog, and co-added IRAS pointed observations (Wesselius and Assendorp, 1987).

[1]Partly based on observations collected at the European Southern Observatory, La Silla, Chile

[2]On leave from Observatory, University of Helsinki, Finland

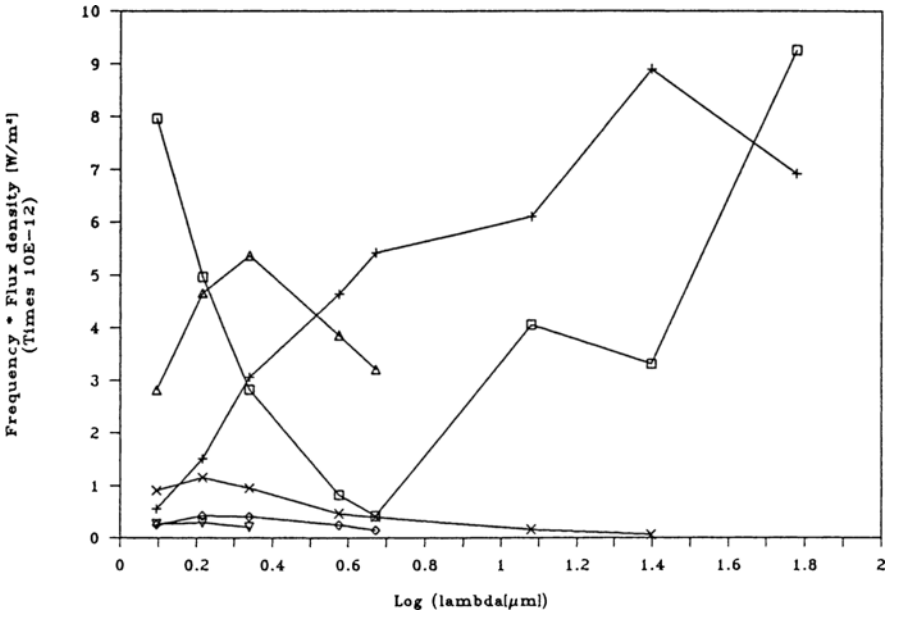

Figure 1: Visible sources have their energies peaking typically at the H band. Considerable amount of total energy is shortwards of 1 μm and occasionally longwards of 100 μm.

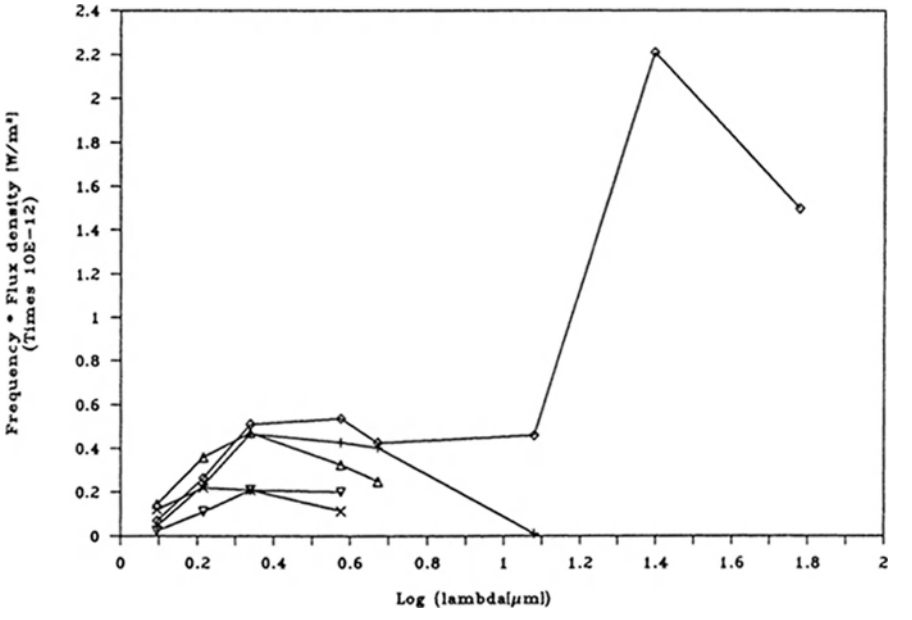

Figure 2: Non-visible stars have their energies peaking typically at the K band.

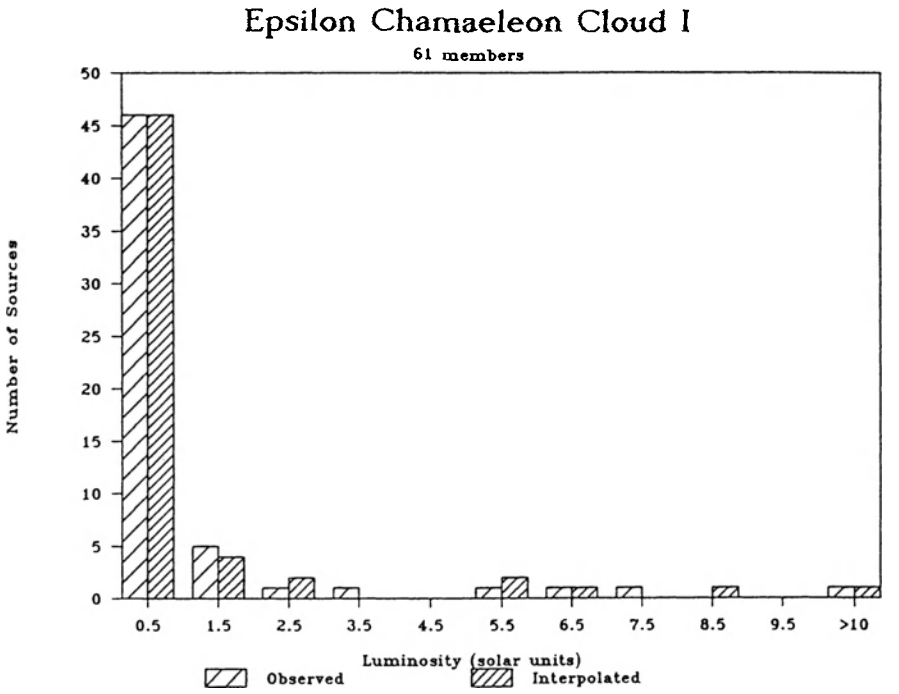

Figure 3: Total infrared luminosities between 1.25 and 100 μm. The *observed* bars contain only the actually observed fluxes giving zero flux to missing data. The *interpolated* bars contain the estimated flux of missing measurements — typically L and/or M band(s) — when detections exist at both sides of the unobserved value; no extrapolations were performed.

References

[1] Glass, I.S.: 1979, *Monthly Notices Roy. Astron. Soc.* **187**, 305

[2] Hyland, A.R., Jones, T.J., Mitchell, R.M.: 1982, *Monthly Notices Roy. Astron. Soc.* **201**, 1095

[3] Jones, T.J., Hyland, A.R., Harvey, P.M., Bruce, A., Wilking, A., Joy, M.: 1985 *Astron. J.* **90**, 1191

[4] Wesselius, P.R., Assendorp, R.: 1987: in Proceedings of 10th European Regional Astronomy Meeting of the IAU ed. J. Palouš 4, 63

Submillimeter Spectroscopy of the Very Dense Gas in Star Formation Regions

A.I. Harris, R. Genzel, U.U. Graf, and J. Stutzki
Max-Planck-Institut für Physik und Astrophysik
Institut für extraterrestrische Physik, Garching, FRG

D.T. Jaffe
Astronomy Department, University of Texas, Austin

Submillimeter and far-infrared molecular lines are excellent new tools for investigation of components of the interstellar medium and circumstellar matter with very high particle densities, $n(H_2) > 10^8$ cm^{-3}. One of their most useful applications is in deriving accurate information about the physical conditions and dynamics of star formation regions, including pre-protostellar condensations and the dense nebulae around newly-formed stars.

Submillimeter and far-infrared line emission from rotational levels of abundant interstellar molecules (e.g. HCN, HCO^+) are discriminating probes of the conditions in warm and dense gas. Warm, because the sub-mm and far-IR levels are generally 50 to 500 K above ground state in these molecules; and dense, because collisions must be frequent enough to excite the levels, which radiatively decay rapidly with the ν^3 dependence of the Einstein A-coefficient. Molecules with different dipole moments can be used as specific probes "tuned" to a wide range of densities in this component of the ISM. Submillimeter line emission traces warm and very dense gas ($T_{kin} > 100$ K, $n(H_2) > 10^7$ cm^{-3}, without radiative trapping). Other traditional density tracers, such as non-metastable NH_3 and lower-J HCN and CS lines, fall below this density regime by at least one to two orders of magnitude.

In the course of our preliminary submillimeter spectroscopy of large-dipole, heavy-top molecules, we have found six previously undetected lines toward the core of the Orion/KL star formation region (Fig. 1). The simple detection of these lines is unambiguous evidence for extremely dense gas ($n > 10^8$ cm^{-3}) in the "Hot Core" and outflows in the Orion/KL star formation region. Detailed studies of the HCN J=9-8 emission (Stutzki et al. 1988, Harris et al. 1989) shows that these sources are very clumpy, with gravitationally unstable gas condensations in the vicinity of the Orion/KL cluster. Earlier millimeter and centimeter wave observations were able to set lower limits to the density in this region, but it is now certain that these limits are several orders of magnitude lower than the actual densities of the cloud cores. Similarly dense gas is almost certainly a common component of the interstellar medium in other regions of star formation.

References:

Stutzki, J., Genzel, R., Harris, A.I., Herman, J., and Jaffe, D.T. 1988, Ap. J. (Lett.) 330, L125.
Harris, A.I., Genzel, R., Graf, U.U., and Stutzki, J. 1989 (in prep.)

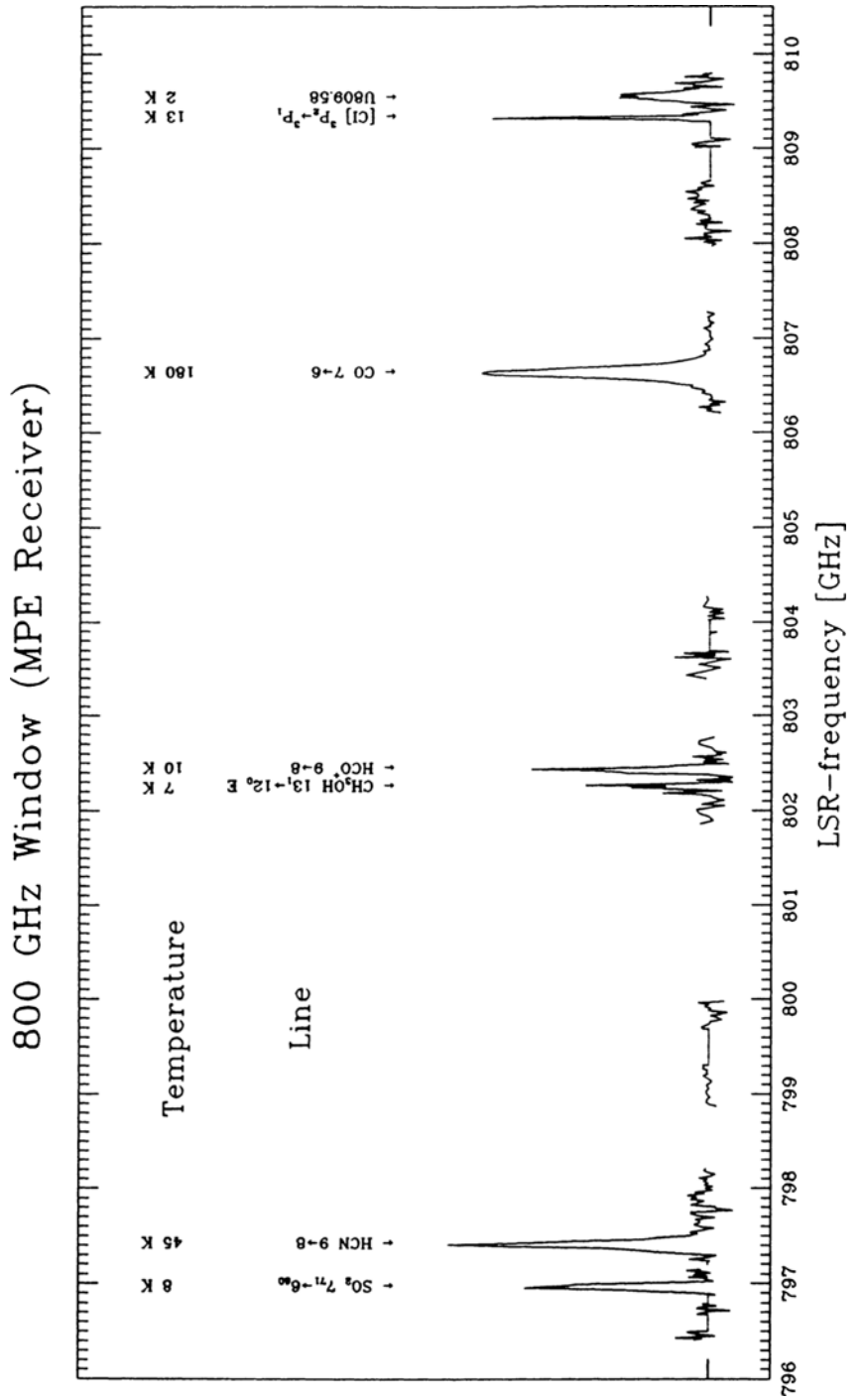

Figure 1
Spectrum of six lines from the the Orion Core near 800 GHz.
Note the large range of line temperatures.

CO survey of faint IRAS point sources

L. Haikala[1,2], O. Dietrich[1]
1. I. Physikalisches Institut, University of Cologne, FRG
2. Observatory and Astrophysics Laboratory, University of Helsinki, Finland

Abstract

A sample of faint IRAS point sources having IR spectra typical of sources imbedded in molecular clouds and their surroundings were observed with the Cologne 3 m telescope in the CO J=1→0 line. Three extended molecular outflows detected in the survey are presented in this paper.

Introduction

The observed large number of high velocity molecular outflows associated with young stellar objects suggests that star formation and high velocity outflows are closely connected. Outflows are probably an important phase of early stellar evolution. The turbulence created by outflows in the parent clouds may play an exceedingly important role in supporting these clouds against collapse. This possibility highligths the importance of observing not only the outflow but also the parent cloud.

A CO survey of IRAS point sources having a spectra rising towards 100 μm and their surroundings was started using the University of Cologne 3 m telescope. The half power beam width of the telescope is 3'.9 at 115 GHz. This allows a direct comparison with the IRAS survey maps (angular resolution of about 4' to 6'). We selected only relatively faint point sources ($F_{100\mu m} < 100$ Jy). This criterion selects either intrinsically strong distant sources or faint nearby sources. Beam dilution in the 3'.9 beam will select in favor of outflows around nearby and intrinsically faint IR sources.

Results

Forty point sources were observed in ^{12}CO using frequency switching mode and 167 kHz spectral resolution (0.44 km s^{-1} at 115 GHz). CO emission was detected at every position. The general characteristics of the observed CO lines are:

- Antenna temperatures are typical to those observed in dark clouds (2 K to 5 K).
- Line widths 2 km s^{-1} to 5 km s^{-1}
- Often asymmetric outflow like wings which are at most 12 km s^{-1} broad

A sample of the objects lying in unconfused regions of the sky were mapped in ^{12}CO and ^{13}CO. The CO spectra in the direction of three point sources (20582+7724 in L1228, IRAS 22266+6845 in L1221 and IRAS 22336+6855) and contour plots of the associated molecular outflows are shown in Figures 1 and 2. A CO and IR study of the outflow associated with L1228 and its surroundings is given in Haikala and Laureijs (1989). The

IRAS properties (flux and IR luminosity) and the geometrical parameters of the outflows are given in Tables 1 and 2, respectively. The archetype molecular outflow in L1551 is included in the tables as a comparison. Because only the kinematical distance to the new outflows is known, the parameters (including those of L1551) are scaled to the distance of 100 pc. Even though the angular sizes of the new outflows are relatively large, the calculated parameters are quite moderate. This is true even if the distances are a factor of four larger. Especially the IR luminosities of the outflow central sources are very small. This leads one to conclude that we are observing outflows associated with low-mass stars.

Discussion

The selection of faint IR candidates for outflow central sources from the IRAS point source catalogue has proved to be succesful. This approach has the advantage that it is not biased towards clouds where optical signposts of star formation activity are observed or towards conspicuous cores of extended dark clouds. In general, telescopes tend to probe structures which are about the size of their beams. A small telescope has therefore the advantage of being sensitive to structures larger than few arcminutes and is ideal for searching for such structures (Fukui et al., 1986; Armstrong and Winnewisser, 1988).

References

Armstrong, J. T. and Winnewisser G.: 1988, Astron. and Astrophys, accepted
Fukui Y., Sugitani K., Takaba H., Iwata T., Mizuno A., Ogawa H. and Kawataba K.: 1986, Astrophys. J. (Lett.) 311 L85
Haikala L. K. and Laureijs R.: 1989, Astron. and Astrophys, submitted

Table 1. IRAS properties of the outflow central sources. Luminosity is scaled to a distance of 100 pc

Source	F_{12}[Jy]	F_{25}[Jy]	F_{60}[Jy]	F_{100}[Jy]	$L_{IRAS}[L_\odot]$
L1551	10.1	106	373	456	21
L1228	1.2	3.2	11.6	17.6	0.4
L1221	1.0	3.6	12.2	25.4	0.4
22336+6855	1.6	2.0	17.4	55	0.6

Table 2. Outflow parameters. The diameter and the dyanamical age are scaled to a distance of 100 pc

Source	Diam. [pc]	v_{max} [km s^{-1}]	T_{dyn}	d_{kin}[pc]
L1551	0.6	15	2.3×10^4	-
L1228	0.5	12	2.4×10^4	600
L1221	0.3	10	1.5×10^4	370
22336+6855	0.3	6	2.5×10^4	580

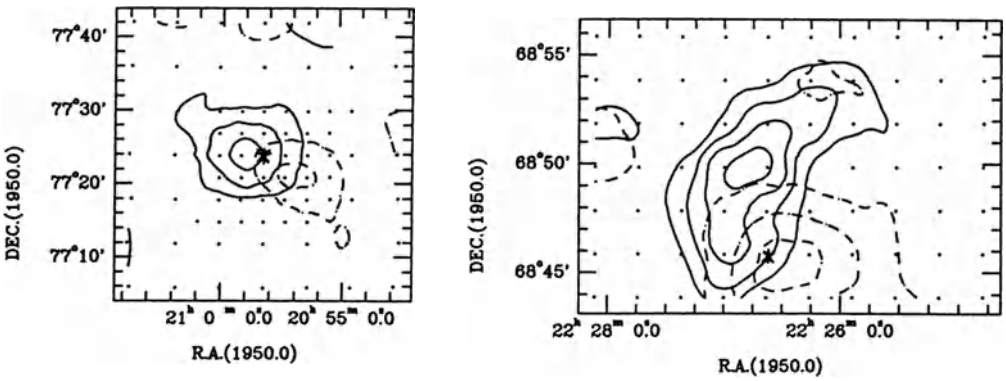

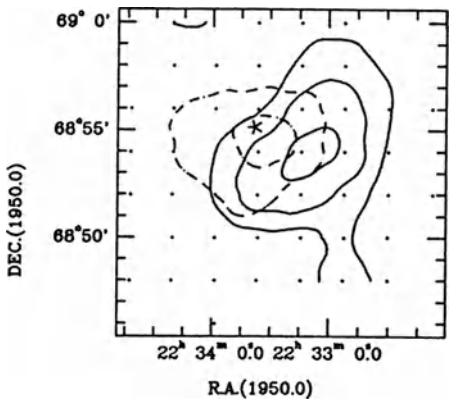

Figure 1a. CO "red" ($-5.5\,\mathrm{km\,s^{-1}} < v < 0\,\mathrm{km\,s^{-1}}$, dashed contour) and "blue" ($-15\,\mathrm{km\,s^{-1}} < v < -9.5\,\mathrm{km\,s^{-1}}$) wing integrated intensity in L1228. The contour levels are from 1.0 K $\mathrm{km\,s^{-1}}$ in steps of 1.0 K $\mathrm{km\,s^{-1}}$. IRAS 20582+7724 is marked with an asterisk. **b** CO "red" ($-3.2\,\mathrm{km\,s^{-1}} < v < 2.0\,\mathrm{km\ s^{-1}}$, dashed) and "blue" ($-10\,\mathrm{km\ s^{-1}} < v < -6.0\,\mathrm{km\ s^{-1}}$) wing integrated intensity in L1221. The contour levels are from 1.5 K $\mathrm{km\,s^{-1}}$ in steps of 0.8 K $\mathrm{km\,s^{-1}}$.IRAS 22266+6845 is marked with an asterisk.
c CO "red" ($-6.0\,\mathrm{km\ s^{-1}} < v < 0\,\mathrm{km\ s^{-1}}$, dashed) and "blue" ($-12\,\mathrm{km\ s^{-1}} < v < -8.2\,\mathrm{km\ s^{-1}}$) wing integrated intensity near IRAS 22336+6855. The contour levels are like in Figure 1 a. IRAS 22336+6855 is marked with an asterisk.

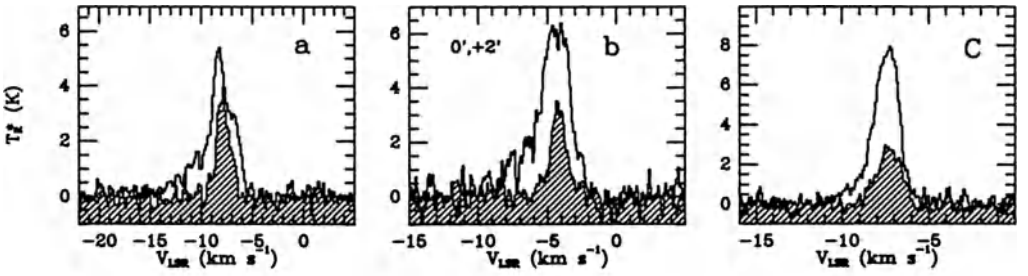

Figure 2. ^{12}CO and ^{13}CO (hatched) spectra in the directions of IRAS point sources **a.** 20582+7724, **b.** 22266+6845 (2' North of the point source), and **c.** 22336+6855

Far-Infrared Spectroscopy of Bipolar Flows

Adair P. Lane
Astronomy Department, Boston University
725 Commonwealth Avenue, Boston, Massachusetts 02215
and
M. R. Haas, D. J. Hollenbach, and E. F. Erickson
NASA Ames Research Center, Mail Stop 245-6
Moffett Field, California 94035

ABSTRACT

We report observations of the far-infrared fine-structure emission lines of [O I] at 63 μm, [Si II] at 35 μm, and [C II] at 158 μm, and of the $J = 22 - 21$ rotational line of CO at 119 μm from the region of massive star formation associated with the DR 21 H II region/molecular cloud core. We conclude that most, and possibly all, of the fine-structure line emission from DR 21 is produced in warm, dense, photoelectrically-heated atomic gas associated with a clumpy molecular medium.

INTRODUCTION

The DR 21 H II region/molecular cloud core contains one of the most energetic and spatially extended bipolar outflow sources yet discovered. At a distance of roughly 3 kpc, the high velocity molecular gas which defines the outflow source covers a region over 5 arcmin in extent, resulting in a *linear* size of $\sim$5 pc – nearly 30 times that of the well-studied Orion A/IRc2 outflow. A map of the 2.1 μm vibration-rotation line of molecular hydrogen published by Garden *et al.* (1986) reveals a highly collimated, double-lobed structure similar to that seen in the NGC 2071 outflow source (Lane and Bally 1986), but of far greater luminosity and linear extent. Between the two lobes of H_2 emission is a "gap" precisely coincident with the diffuse component of the DR 21 H II region, which extends eastward from the cluster of OB stars which ionize the gas. Based on H_2 line ratios, the excitation of the H_2 emission has been determined to be collisional excitation in nondissociative "molecular" shocks. We undertook far-infrared spectroscopic observations of the DR 21 region with the aim of determining whether these shocks or accompanying fast, dissociative "wind" shocks radiate strongly in [O I] at 63 μm, or whether the ultraviolet radiation field from the early-type stars in the region produces intense [O I] (63 μm), [C II] (158 μm), and [Si II] (35 μm) emission from photodissociated gas lying just outside the H II region.

OBSERVATIONS AND RESULTS

The data were obtained in August 1986 and June 1987 using the facility cooled grating spectrometer (Erickson *et al.* 1984, 1985) aboard NASA's Kuiper Airborne Observatory.

We detected the $^3P_1 \rightarrow ^3P_2$ line of [O I] at 63.1837 μm at 75 positions over a region of similar extent to that producing the 2 μm H_2 emission. A contour map showing the spatial distribution of the [O I] line emission is shown in Figure 1, superposed on the molecular hydrogen v = 1 − 0 S(1) line map from Garden *et al.* The H II region is indicated by the shaded area, from the 14.7 GHz continuum observations of Roelfsema, Goss, and Geballe (1988).

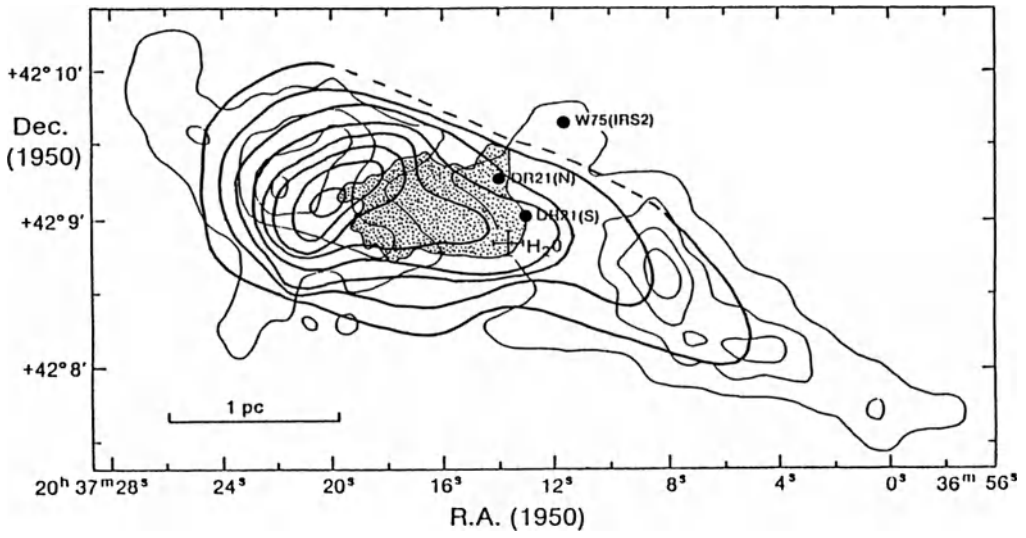

Fig. 1. Map of the DR 21 63 μm [O I] line emission (heavy lines). Contour levels are 1.90, 1.65, 1.39, 1.14, 0.89, 0.63, 0.38, and 0.13 × 10^{-2} erg s^{-1} cm^{-2} sr^{-1}. Light lines show selected contours from the map of the v = 1 − 0 S(1) line of H_2 from Garden et al. (1986). The shaded area shows the extent of the 14.7 GHz radio continuum emission from Roelfsema, Goss, and Geballe (1988). Positions of three 20 μm sources are shown as dots (Wynn-Williams, Becklin, and Neugebauer 1974) and the H_2O maser as a cross (Genzel and Downes 1977).

The [O I] emission is strikingly asymmetric with respect to the H_2 emission. At our spatial resolution (35″), a single strong [O I] peak with flux (4.9 ± 0.2) × 10^{-17} W cm^{-2} is seen at the eastern edge of the H II region. The total [O I] line luminosity is 600 ± 100 $L_\odot$, ∼0.1% of the total far-infrared luminosity of DR 21.

We also mapped the $^2P_{3/2} \rightarrow ^2P_{1/2}$ ground-state transition of [Si II] at 34.816 μm and the $^2P_{3/2} \rightarrow ^2P_{1/2}$ transition of [C II] at 157.741 μm on a strip along the axis of the molecular flow. Nine positions were observed in the [Si II] line with a 33.9″ beam and six positions were observed in [C II] with a 41.3″ beam. The distribution of these line fluxes also appears to be asymmetric with respect to the H_2 emission. The [O I]/[C II] line intensity ratio ranges from 2 to 8 (at the [O I] peak).

We searched for $J = 22-21$ CO emission at 118.6 μm at three positions, obtaining upper limits (3σ) of 0.06 to 0.2 × 10^{-3} erg s^{-1} cm^{-2} sr^{-1}.

INTERPRETATION

There are several possible mechanisms for collisionally exciting the far-infrared fine-structure lines in massive star formation regions. The far-ultraviolet (912–2000Å) radiation field of young, early-type stars (O4–B9) is capable of producing a photoelectrically heated region of predominantly neutral atomic gas at the H II/molecular cloud interface which cools primarily through the [O I] 63 μm and 145 μm lines, the 158 μm [C II] line, the 35 μm [Si II] line, and high-J rotational transitions of CO, as well as by far-infrared continuum emission from UV-heated dust (Tielens and Hollenbach 1985). In addition, shocks may be present in the vicinity of newly-formed stars, produced by the impact of high velocity gas outflows on ambient molecular cloud material. Molecular shocks cool primarily by line radiation of molecular and atomic species in the near- and far-infrared, particularly the quadrupole vibration-rotation lines of H_2, rotational lines of H_2O and CO, and the 63 μm [O I] line (Draine, Roberge, and Dalgarno 1983; McKee, Chernoff, and Hollenbach 1984).

By comparing our results with predicted line intensities and line ratios of shock models (e.g., Draine, Roberge, and Dalgarno 1983; Hollenbach and McKee 1989), we find that neither "molecular" shocks nor "wind" shocks (nor a combination) can account for the FIR line emission. We conclude that the [C II], the [Si II], and probably most (if not all) of the [O I] emission is produced in dense ($n = 1 - 5 \times 10^4\,\mathrm{cm}^{-3}$), warm ($T = 250 - 500\,\mathrm{K}$) photodissociated atomic gas on the surfaces of molecular clumps. These photodissociation regions are illuminated by FUV fluxes $\geq 10^4$ times the ambient interstellar field. The gas phase silicon abundance relative to hydrogen appears to be enhanced by a factor of ~6 over that observed toward ζ Oph. The morphology of the [O I] emission region, combined with other available data, suggests that a cavity filled with low-density ionized gas has formed in the molecular cloud, to the east of a cluster of newly-formed OB stars, with the [O I] peak marking the H II/molecular boundary layer. A more complete presentation of this work is given by Lane *et al.* (1989).

REFERENCES

Draine, B. T., Roberge, W. G., and Dalgarno, A. 1983, *Ap. J.*, **264**, 485.

Erickson, E. F., Houck, J. R., Harwit, M. O., Rank, D. M., Haas, M. R., Hollenbach, D. J., Simpson, J. P., and Augason, G. C. 1985, *Infrared Physics*, **25**, 513.

Erickson, E. F., Matthews, S., Augason, G. C., Houck, J. R., Rank, D. M., and Haas, M. R. 1984, *Proc. Soc. Photo-Opt. Instr. Eng.*, **509**, 129.

Garden, R., Geballe, T. R., Gatley, I., and Nadeau, D. 1986, *M.N.R.A.S.*, **220**, 203.

Genzel, R., and Downes, D. 1977, *Astr. Ap. Suppl.*, **30**, 145.

Hollenbach, D. J., and McKee, C. F. 1989, *Ap. J.*, (in press).

Lane, A. P., and Bally, J. 1986, *Ap. J.*, **310**, 820.

Lane, A. P., Haas, M. R., Hollenbach, D. J., and Erickson, E. F. 1989, in preparation.

McKee, C. F., Chernoff, D., and Hollenbach, D. J. 1984, in *16th ESLAB Symposium, Galactic and Extragalactic Infrared Spectroscopy*, eds. M. Kessler and J. Phillips, (Dordrecht: Reidel), p. 103.

Roelfsema, P. R., Goss, W. M., and Geballe, T. R. 1988, preprint.

Tielens, A. G. G. M., and Hollenbach, D. J. 1985, *Ap. J.*, **291**, 722.

Wynn-Williams, C. G., Becklin, E. E., and Neugebauer, G. 1974, *Ap. J.*, **187**, 473.

A COMPLETE CO SURVEY OF THE LARGE MAGELLANIC CLOUD

T. M. Dame
Harvard-Smithsonian Center for Astrophysics
60 Garden St., Cambridge, MA 02138

I'm going to describe a complete CO survey of the LMC which was carried out during 1983–84 with our 1.2 meter telescope at Cerro Tololo in Chile (Cohen 1983). The inner 6° x 6° of the LMC, the region containing nearly all the Population I material, was observed every 7.5', slightly better than every beamwidth, to an rms of 0.06 K. The telescope, essentially a copy of the Columbia instrument (Cohen *et al.* 1986) now at the CfA, has a beamwidth of 8.8' at the J=1→0 rotational transition of CO, and its 256 channel filter bank spectrometer provides a velocity resolution of 1.3 km s^{-1} and a range of 333 km s^{-1}. The survey and some of the work presented here result from a collaboration between our laboratory and the University of Chile (Cohen *et al.* 1988); the people involved were R. S. Cohen, G. Garay, J. Montani, M. Rubio, P. Thaddeus, and me.

A map of CO emission integrated over velocity, W_{CO}, is shown in Figure 1. The intensity in this map is roughly proportional to the column density of molecular hydrogen, although, as I will show below, the conversion from CO intensity to H_2 column density is probably different in the LMC from in the Galaxy. As expected from the abundance of active star formation, there is a great deal of molecular gas in the LMC: CO emission was detected over nearly 10% of the 38 deg^2 surveyed, and because the emission is very weak, with peak line temperatures of order 0.15 K, it is quite possible that a good deal more molecular gas lies just below the limit of our sensitivity.

The most striking object in Figure 1 is the gigantic molecular complex extending south from 30 Doradus. Since one degree in the LMC corresponds to nearly 1 kpc, this object is at least 2500 pc long, an order of magnitude larger than "giant" molecular complexes in our Galaxy. Even at this resolution the object is clearly composed of smaller clumps, and at higher resolution it would undoubtedly resolve into many clouds, complexes, and filaments. Nevertheless, it is evidently a fairly isolated and well defined object in its own right, certainly not a chance collection of clouds like those seen elsewhere in the LMC.

Because the LMC is so close, is favorably orientated to the line of sight, and contains an abundance of Population I, it is uniquely well suited to a study of the relation of molecular clouds to the process and immediate products of star formation. As Figure 1 shows, nearly all the known supernova remnants of the LMC — including SN 1987A — and most of the H II regions lie toward molecular clouds. The correlation of the molecular clouds with the

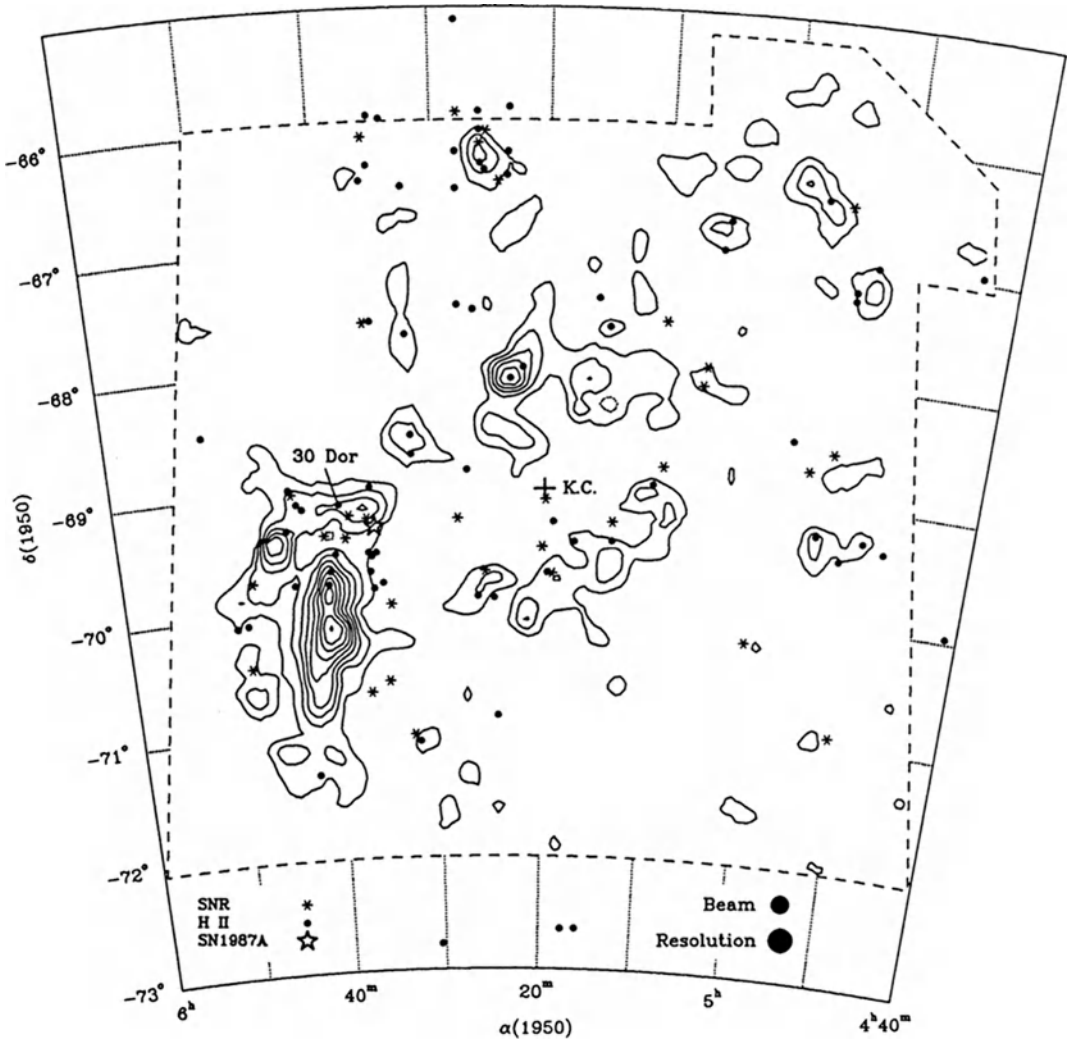

Figure 1. Map of velocity-integrated CO intensity in the LMC. The window of velocity integration is 30 km s-1 wide, centered at each position on the velocity of the strongest 21 cm component from Rohlfs *et al.* (1984), except toward three clouds in the 30 Dor complex where the window was widened by 10–20 km s-1 to include all emission. The contour interval is 0.38 K km s-1, about the 1.6 σ noise level. SNRs (Mathewson *et al.* 1983; 1984; 1985), supernova 1987A, and H II regions (6 cm continuum sources not identified as SNRs; McGee, Brooks, and Batchelor 1972) are shown for comparison. K.C. marks the kinematic center of the LMC (de Vaucouleurs and Freeman 1973).

H II regions is not unexpected, but that with the SNRs is surprisingly good because only the short-lived progenitors of type II SNs should be found near their parental molecular clouds at the time of detonation; this correlation may be evidence that type II SNs predominate in the LMC.

We have identified 40 individual molecular clouds in the LMC and cataloged positions, radial velocities, velocity dispersions, radii, and masses, computed both from the virial theorem and from their CO integrated intensities (W_{CO}). Although in our Galaxy the virial masses of molecular clouds are typically within a factor of 2 of their CO masses, in the LMC the virial masses are about an order of magnitude larger. It is likely that the N_{H_2}/W_{CO} ratio in the LMC is different from the Galactic value, since the metallicity there is several times lower than in the Galaxy (Dufour 1984). We were therefore faced with the problem of calibrating the N_{H_2}/W_{CO} ratio in the LMC.

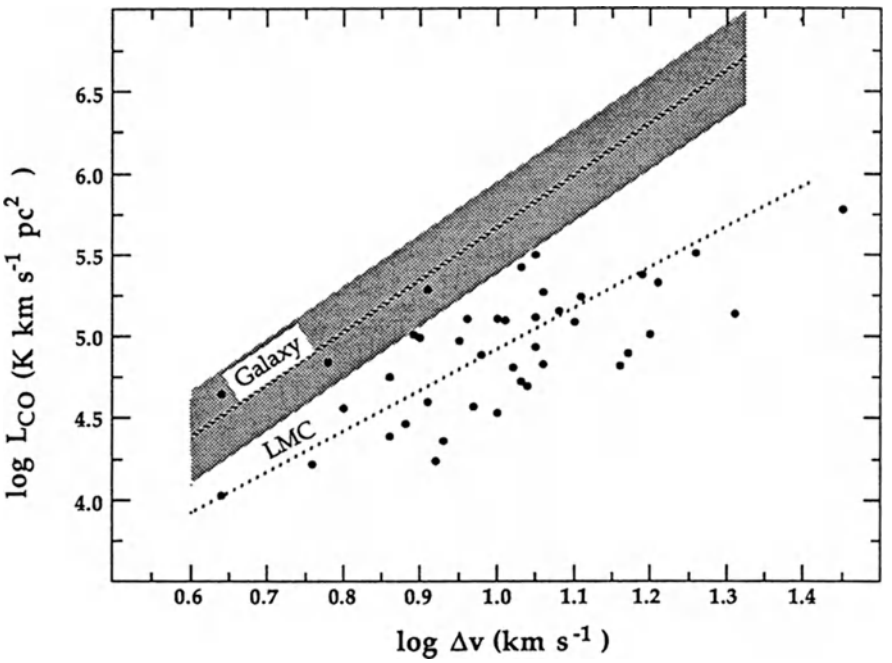

Figure 2. CO intensity integrated over velocity and projected area, L_{CO}, versus FWHM average line width, Δv, for molecular clouds in the LMC. L_{CO} is directly proportional to cloud mass. The line labeled LMC is a least-squares fit to the LMC clouds (plotted points). The line labeled Galaxy is a fit to the 34 large Galactic molecular clouds analyzed by Dame *et al.* (1986); L_{CO} values for these clouds were determined from Table 2 of Dame *et al.*, with a calibration correction of 1.29 applied (see Bronfman *et al.* 1988). The Galactic clouds are not plotted, but the shading indicates their ±1 σ spread about the linear fit.

Since the calibration of X_{LMC} with the virial theorem requires both the uncertain assumption of virial equilibrium and the measurement of cloud radii often at the limit of our resolution, we chose instead not to calibrate X_{LMC} directly but to determine only the ratio X_{LMC}/X_{Galaxy}. As Figure 2 shows, the LMC clouds follow a luminosity-line width relation very similar to that of Galactic clouds, except that the LMC clouds are about six times fainter. On the assumption that these two relations reflect an underlying *mass*-line width relation that is the same in both the LMC and the Galaxy, the offset of the luminosity-line width relation implies a six times larger N_{H_2}/W_{CO} ratio in the LMC, i.e., $X_{LMC} = 6\ X_{Galaxy}$. It thus appears that X scales roughly with the inverse first power of the metallicity, or perhaps slightly more steeply. The visibility of many of the clouds as dark nebulae (Hodge 1988), despite the four times higher gas-to-dust ratio in the LMC (Koornneef 1982), suggests that there is a large amount of gas in these objects. If we assume that all of the gas is molecular, a conversion factor at least six times the Galactic value is required to account for the optical opacity.

Using an N_{H_2}/W_{CO} ratio six times the Galactic value, the individual complexes we see have masses ranging from 300,000 to 17 million $M_\odot$, comparable to the masses of the largest complexes in our Galaxy, and the total mass of the huge 30 Dor complex is 60 million $M_\odot$, comparable to a segment of one of the inner spiral arms of our Galaxy 3 kpc long. The total mass of the molecular clouds observed in the LMC, 142 million $M_\odot$, is about one-fifth of the total H I mass (McGee and Milton 1966), and over the inner 3° of the disk where most of the molecular clouds are found, the molecular clouds are about one-third of the interstellar mass. It is quite possible that the space density of molecular gas in the plane of the disk is comparable or even larger than the atomic density, since the molecular gas is probably more confined to the plane, and more molecular gas may lie just below our sensitivity limit.

Although most of the motions of molecular clouds in the LMC can be attributed to the orderly rotation of the galaxy, toward 30 Doradus there is clear evidence of a lot of molecular mass accelerated by local processes. In Figure 3*a-d* the major H II regions in the vicinity of that complex, including 30 Doradus itself, are represented by the shaded regions. A section of the velocity-integrated map from Figure 1 is reproduced in Figure 3*a*, while 3*b-d* show the emission integrated over three contiguous velocity bins each 21 km s^{-1} wide. Figure 3*b* is centered on the velocity expected from galactic rotation in this region, which is also the velocity of the main body of the 30 Dor complex. The picture in Figure 3*b* is a familiar one, an H II region "blister" on the edge of a molecular cloud, but the linear scale here is much larger than for similar objects in the Galaxy. Figure 3*c*, integrated over a window centered 20 km s^{-1} higher, shows evidence of a ring of material roughly centered on the star-

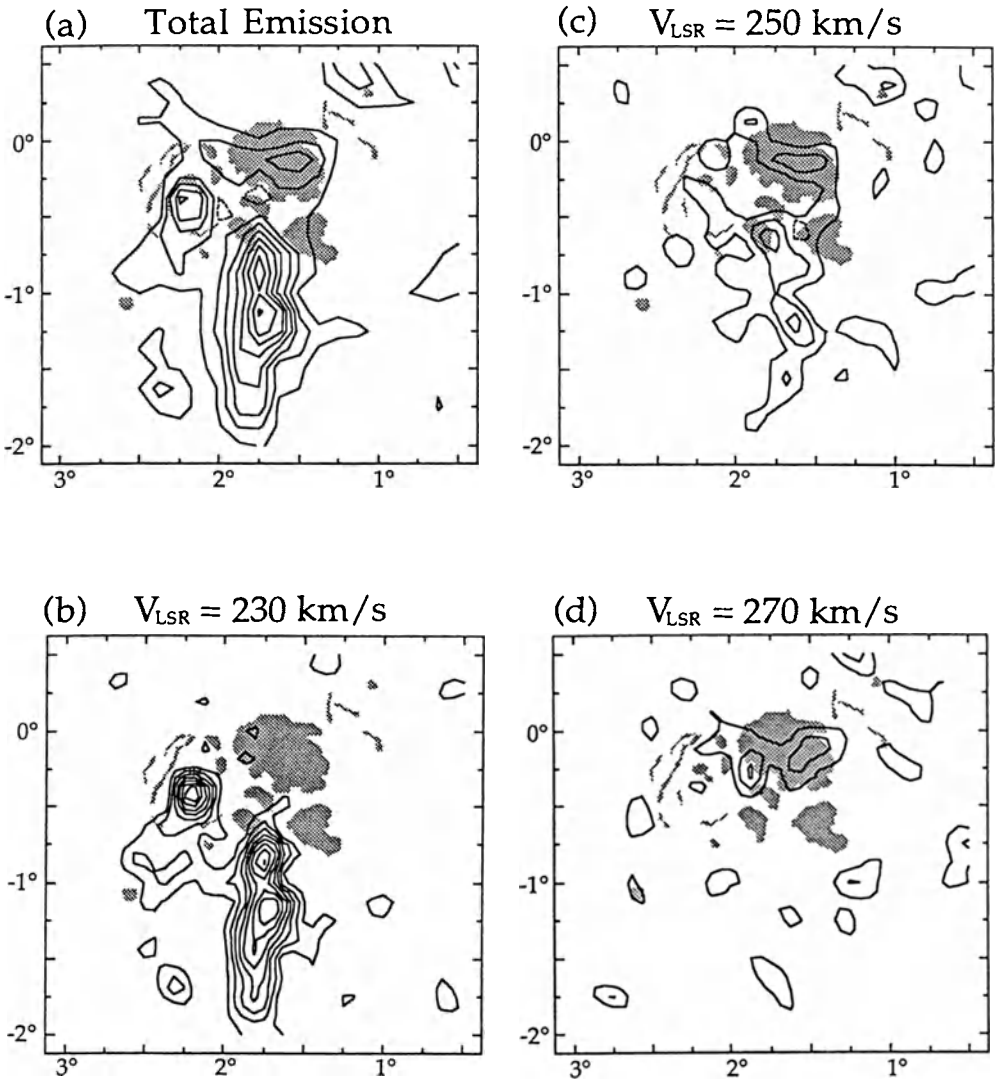

Figure 3. A comparison of velocity-integrated CO emission with the major H II complexes in the 30 Doradus region. The shading roughly outlines the positions of the large H II regions obvious in Plate 1 of Davies, Elliott, and Meaburn (1976), a 5-hour Hα+[N II] photograph through a 100 Å filter. The total velocity-integrated emission, produced as in Figure 1, is shown in *a*, while in *b-d* the emission is integrated over three contiguous velocity bins each 21 km s^{-1} wide, approximately centered on the velocities indicated above the maps: (*b*) 219 – 240 km s^{-1}, (*c*) 240 – 261 km s^{-1}, and (*d*) 261 – 282 km s^{-1}. The maps have been smoothed to a spatial resolution of 0°.25 to improve the signal-to-noise. The contour interval in all the maps is 0.44 K km s^{-1}. The axes are angular offsets from $\alpha = 5^h\ 20^m$, $\delta = -69°$.

formation activity, and 20 km s^{-1} higher still, in Figure 3*d*, emission appears near the center of the ring. Although the signal-to-noise ratios in Figure 3*b-d* are not high, we estimate that ~9 x 10^6 $M_\odot$ is contained in this apparent shell of expanding molecular material. With a radius for the shell of ~250 pc and an expansion velocity of order 20 km s^{-1}, the timescale of the expansion is ~10 million years and the kinetic energy of expansion ~3 x 10^{52} ergs — equivalent to the total energy ejected by about 30 supernovas. Since the efficiency of energy transfer to the clouds is probably quite low, that factor might have to be multiplied by 100 or more to account for the motions we see.

Evidence suggests that such an explosion of star formation has occurred previously in the LMC, in the region of Shapley's Constellation III (centered near 4^h 30^m, –66°), the only region in Figure 1 where the correlation of molecular gas with other Population I is not particularly good. A large H I shell with a diameter of 800 pc and an associated velocity perturbation of order 15 km s^{-1} is known to exist in the Constellation III region (Goudis and Meaburn 1978). The kinetic energy of expansion is ~7 x 10^{51} ergs, and the expansion timescale ~25 million years. It is plausible that what we are seeing is an evolutionary sequence, the 30 Dor complex and Constellation III being two snapshots separated by 10 million years or more.

It has often been suggested that the past rate of star formation in the LMC has been highly variable. For example, Hodge (1973), in a study of stars clusters, found that 60 % of the LMC clusters occur in groups isolated in space and time. The typical size of a group was about 1500 pc, and he found that groups apparently form very rapidly, in less than a million years, and that about one group was formed in the LMC every million years. Hodge noted that "this pattern of formation of stars in cells of approximately 1 kpc size is ... consistent with the idea that star formation occurs in locations and at times when the gas density is unusually large in areas of this scale." The existence of extremely large molecular complexes in the LMC, such as the one currently associated with 30 Doradus, and their rapid destruction by star formation, provides a ready explanation for Hodge's large groups of clusters, for the Shapley Constellations, and, more generally, for the episodic, highly variable rate of star formation in the LMC.

How and why do such huge objects, much larger than the molecular complexes in our Galaxy, form in the LMC? As is well known, much of the inner disk of the LMC rotates as a rigid body. Such a low-shear environment may be conducive to the formation of such large objects; Oort (1971) has cited the absence of differential rotation over the inner disk as a possible explanation for the fact that globular clusters apparently still form in the LMC, while in the differentially rotating Milky Way they do not. It may also be significant that the 30 Dor complex sits at the tip of the stellar bar. The essential difference between here

and the LMC may be the existence of the bar, which constitutes about 15% of the mass of the LMC, displaced about 1° from the kinematic center (de Vaucouleurs and Freeman 1973).

The wealth of information our survey provides on the kinematics of the LMC can only be summarized briefly here. We have fit the cloud velocities to the standard kinematic model of the LMC (e.g., de Vaucouleurs 1960), a thin, inclined, rotating disk which we characterized by four free parameters: the position angle of the line of nodes, the systemic velocity, and two parameters for the rotation curve. Since our data are insensitive to the position of the kinematic center of the disk and to its inclination, we have taken these parameters as fixed; they have been fairly well determined by others (see, e.g., de Vaucouleurs and Freeman 1973), and our results vary negligibly over their ranges of uncertainty. As Figure 4 shows, our best-fit rotation curve agrees extremely well with that

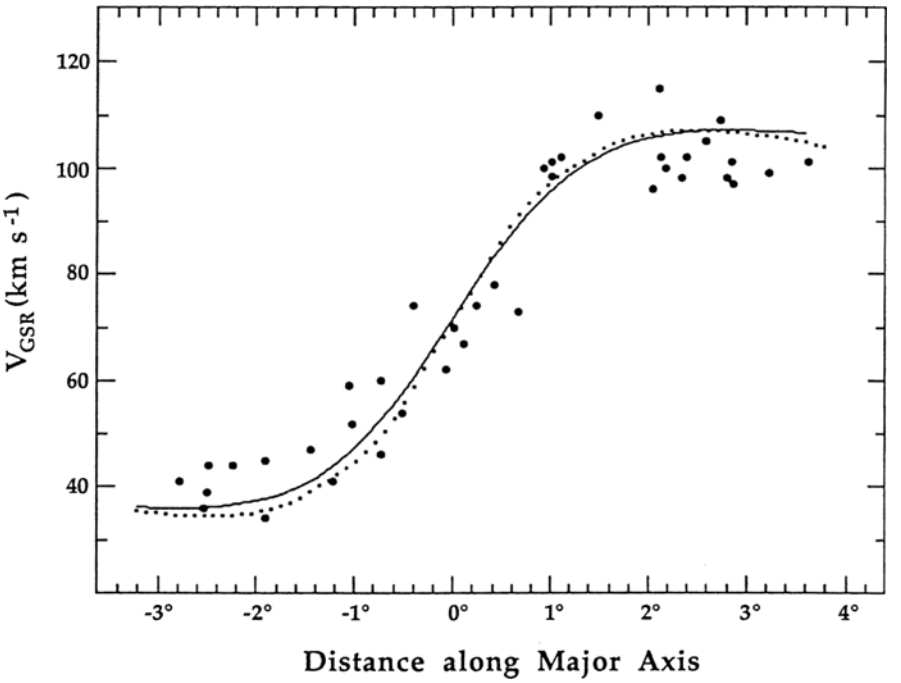

Figure 4. Galactocentric radial velocities for LMC molecular clouds (LSR velocities corrected for a solar motion of 220 km s^{-1} around the Galactic center) plotted versus projected angular distance along the kinematic line of nodes (p.a.=172°). The solid curve is the best-fit rotation curve (i.e., radial velocity versus angular distance along the kinematic line of nodes), given by equation A1 of Miyamoto and Nagai (1975) for the case of one spheroid, with $M = 7.1 \times 10^9$ M_θ and (a + b) = 2°.0; an inclination of 27° has been assumed and the fit systemic velocity, 72 km s^{-1}, has been added. The dotted curve is from Feitzinger (1980; adapted from his Fig. 15, with i = 32°.5 and V_{sys} = 71 km s^{-1}), determined from a variety of kinematic tracers. The scatter of points about the rotation curve is not representative of the true dispersion of the fit: owing to the differential rotation, only clouds lying precisely along the line of nodes are expected to fall on this line; the rest will have velocities somewhat less in absolute value.

derived by Feitzinger (1980) from a variety of other Population I species. Our position for the kinematic line of nodes, 172°, coincides more closely with the position of the geometrical major axis (~170°; de Vaucouleurs and Freeman 1973) than previous kinematic determinations using various objects (188°; Feitzinger *et al.* 1977), H I gas (208°; Rohlfs *et al.* 1984), or globular clusters (181° – 221°, increasing with cluster age; Freeman, Illingworth, and Oemler 1983). The line-of-sight velocity dispersion of molecular clouds determined from our model, 7.7 km s^{-1}, is less than that of both H I clouds (11.5 km s^{-1}; McGee and Milton 1966) and the mean of other Population I objects (10.5 km s^{-1}; Feitzinger 1980), suggesting that molecular clouds form a highly flattened system in the LMC and, thus, may be the best tracer of the disk kinematics.

REFERENCES

Bronfman, L., Cohen, R. S., Alvarez, H., May, J., and Thaddeus, P. 1988, Ap. J., **324**, 248.
Cohen, R. S. 1983, in *Surveys of the Southern Galaxy*, eds. W. B. Burton and F. P. Israel (Dordrecht: Reidel), p. 265.
Cohen, R. S., Dame, T. M., Garay, G., Montani, J., Rubio, M., and Thaddeus, P. 1988, *Ap. J. Lett.*, **331**, L95.
Cohen, R. S., Dame, T. M., and Thaddeus, P. 1986, *Ap. J. Suppl.*, **60**, 695.
Dame, T. M., Elmegreen, B. G., Cohen, R. S., and Thaddeus, P. 1986, Ap. J., **305**, 892.
Davies, R. D., Elliott, K. H., and Meaburn, J. 1976, *Mem. R. astr. Soc.*, **81**, 89.
de Vaucouleurs, G. 1960, *Ap. J.*, **131**, 265.
de Vaucouleurs, G., and Freeman, K. C., 1973, Vistas Astron., **14**, 163.
Dufour, R. J. 1984, in IAU Symposium 108: *Structure and Evolution of the Magellanic Clouds*, ed. S. van den Bergh and K. S. de Boer (Dordrecht: Reidel), p. 353.
Feitzinger, J. V. 1980, *Space Sci. Rev.*, **27**, 35.
Feitzinger, J. V., Isserstedt, J., and Schmidt-Kaler, Th. 1977, *Astr. Ap.*, **57**, 265.
Freeman, K. C., Illingworth, G., and Oemler, A. Jr. 1983, *Ap. J.*, **272**, 488.
Goudis, C., and Meaburn, J. 1978, Astr. Ap., **68**, 189.
Hodge, P. W. 1973, *A. J.*, **78**, 807.
Hodge, P. W. 1988, *Pub. A.S.P.*, *100*, *346*.
Koornneef, J. 1982, *Astr. and Ap.*, **107**, 247.
Mathewson, D. S. *et al.* 1983, Ap. J. Suppl., **51**, 345.
Mathewson, D. S. *et al.* 1984, Ap. J. Suppl., **55**, 189.
Mathewson, D. S. *et al.* 1985, Ap. J. Suppl., **58**, 197.
McGee, R. X., Brooks, J. W., and Batchelor, R. A. 1972. Austr. J. Phys., **25**, 581.
McGee, R. X., and Milton, J. A. 1966, Austr. J. Phys., **19**, 343.
Miyamoto, M. and Nagai, R. 1975, *Publ. Astron. Soc. Japan*, **27**, 533.
Oort, J. H. 1971, in *The Magellanic Clouds*, ed. A. B. Muller (Dordrecht:Reidel), p. 184.
Rohlfs, K., Kreitschmann, J., Siegman, B. C. and Feitzinger, J. V. 1984, Astr. Ap., **137**, 343.

The Molecular Content of Galaxies

Judith S. Young
Department of Physics and Astronomy and
Five College Radio Astronomy Observatory
University of Massachusetts, Amherst, MA 01003

ABSTRACT

H_2 and HI masses are compared with the optical luminosities, IR luminosities, colors, and dust masses for 124 galaxies whose molecular content have been measured as part of the FCRAO Extragalactic CO Survey. The observations indicate the range of star formation efficiencies observed as a function of galaxy type, luminosity, and environment. For a subset of these galaxies in which the distributions of ionized, atomic, and molecular gas are known, variations in the SFE as a function of radius are investigated.

I. INTRODUCTION

Because stars form in molecular clouds, the distribution and abundance of dense interstellar matter determine the morphology and evolution of the disk. Using the 14 m telescope of the Five College Radio Astronomy Observatory, CO observations have been made in more than 200 galaxies as part of the FCRAO Extragalactic CO Survey (HPBW=45"). These observations have been used to determine the H_2 distributions in galaxies, and the yield of young stars per unit mass of available gas $[L_*/M_{gas}]$ from galaxy to galaxy and as a function of radius in individual galaxies. Because many of the galaxies being studied are $\gtrsim$20 Mpc away, the properties we are determining are averages over regions at least a few kpc across.

II. THE H_2 CONTENT AND STAR FORMATION EFFICIENCY FROM GALAXY TO GALAXY

A. COMPARISON OF GLOBAL H_2 AND HI MASSES WITH IR LUMINOSITIES

Ever since the demonstration that CO and optical luminosities are correlated both within individual galaxies (Young and Scoville 1982a; Scoville and Young 1983; Solomon *et al.* 1983; DeGioia-Eastwood *et al.* 1984) and from galaxy to galaxy (Young and Scoville 1982b), substantial effort has been made to determine the yield of young stars in a galaxy per unit mass molecular gas available to form stars. With the success of the *IRAS* satellite, IR flux densities and color temperatures have now been

measured for galaxies across the sky. These observations provide a measure of the star formation occurring within a galaxy since studies of nearby galaxies indicate that the IR emission arises from dust heated by young stars in molecular clouds (*cf.* Rieke *et al.* 1980; Telesco and Harper 1980).

In this section, I compare the IR luminosities from coadded *IRAS* survey data (Young *et al.* 1988a) with the H_2 masses derived from published CO observations for 124 galaxies observed at FCRAO. These galaxies are part of the FCRAO Extragalactic CO Survey, which consists of observations at 2.6 mm of a complete, magnitude-limited sample of spiral and irregular galaxies selected on the basis of their declination and optical or infrared properties ($\delta > -20°$, $B_T° < 12$ or $S_{100} > 10$ Jy or $S_{60} > 5$ Jy). The derivation of H_2 masses employed here, discussed in Kenney and Young (1988), involves determining the CO flux of the model distribution which best matches the observed CO integrated intensities when sampled with a 45" gaussian beam. The CO fluxes are therefore corrected for source-beam coupling, and the H_2 masses are determined adopting a constant ratio of $N(H_2)/I_{CO} = 2.8 \times 10^{20}$ H_2 cm^{-2}/[K(T_R) km s^{-1}] (Bloemen *et al.* 1986). IR luminosities for the sample galaxies have been computed from 1 to 500 μm using both the 60 and 100 μm flux densities by following the method described in the Appendix of the IRAS Extragalactic Catalog (Lonsdale *et al.* 1985). The IR and CO fluxes described here are reported in Young *et al.* (1988a).

Figure 1 illustrates the comparison of the IR luminosities with H_2 masses for the sample galaxies, where the points are coded by dust temperature. The data in Figure 1 are best fit by

$$L_{IR} \propto M(H_2)^{1.0 \pm 0.03} \qquad (1)$$

It is apparent from Figure 1 that some of the scatter in the L_{IR}-$M(H_2)$ comparison arises due to the observed spread in dust temperature from galaxy to galaxy and the strong dependence of the IR luminosity on dust temperature; for galaxies of a given H_2 mass, those with higher T_{dust} have higher luminosities. Such a temperature dependence is not seen for the comparison of the IR luminosities and HI masses (Young *et al.* 1988a), from which we argue that *the IR emission is more closely tied to the molecular gas than to the total atomic gas content for this sample of galaxies.*

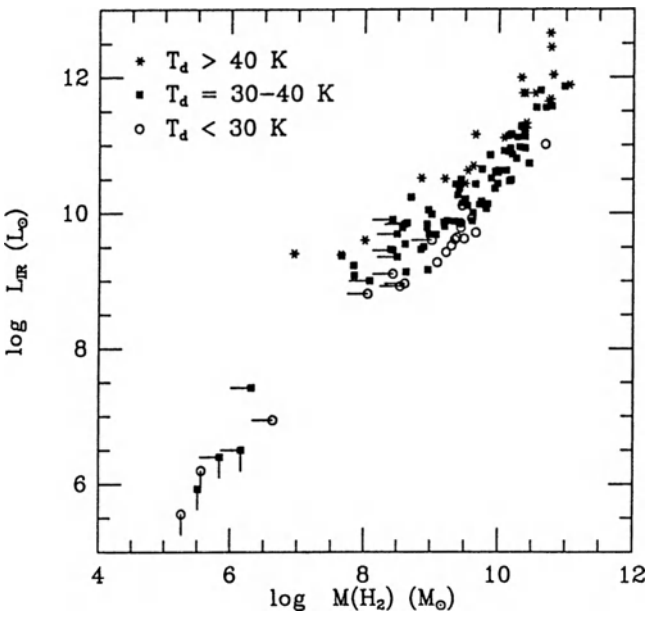

Figure 1. Comparison of IR luminosities with H_2 masses for 124 galaxies. Data points are coded by dust temperature as indicated to illustrate that some of the scatter observed is correlated with T_{dust}.

B. ORIGIN OF THE IR LUMINOSITY

If the energy source for the IR emission in galaxies is star formation, then comparisons of the IR luminosities with Hα luminosities should show a correlation. For 49 of the galaxies in the FCRAO Survey sample for which Hα fluxes are available in the literature (Kennicutt and Kent 1983; Bushouse 1986; Kennicutt *et al.* 1987), we find

$$L_{IR} \propto L(H\alpha)^{1.0\pm0.1} \qquad (2)$$

where the correlation coefficient is 0.78. Some of the scatter observed must certainly be related to extinction of the Hα since the fluxes have not been corrected for extinction. The fact that the slope of the L_{IR}-L(Hα) comparison is unity is consistent with the hypothesis that star formation powers the IR luminosity. Furthermore, Hα fluxes which have been corrected for extinction (Young, Klenimann, and Allen 1988) confirm this hypothesis. We therefore adopt the approach that the IR luminosity indicates the star formation rate (SFR) and that the ratio $L_{IR}/M(H_2)$ measures the SFR per unit mass of molecular gas, or the star formation efficiency (SFE).

Another measure of the present star formation rate is provided by the equivalent width of Hα (EWHα). The EWHα measures the Hα flux normalized by the underlying red continuum flux, and indicates the ratio of the present massive star formation rate to the star formation rate integrated over the lifetime of the galaxy. In Figure 2 we show a comparison of EWHα with the ratio $L_{IR}/M(H_2)$ in 40 galaxies for which Hα equivalent widths were available in the literature. The galaxies are coded as either early type (≤Sb) or late-type (≥Sbc) because of the known dependence of EWHα on type which arises from the large bulge contribution to the underlying red continuum in early-type galaxies. Figure 2 shows a good correlation between $L_{IR}/M(H_2)$ and EWHα for the 26 galaxies of type later than Sbc (correlation coefficient=0.86). Since a high EWHα indicates a high current rate of massive star formation relative to the star formation rate averaged over the lifetime of the galaxy, and assuming that $L_{IR}/M(H_2)$ indicates the efficiency of star formation, *the correlation between EWHα and $L_{IR}/M(H_2)$ suggests that galaxies which are forming many high mass stars at the present time are doing so through efficient conversion of gas into stars.*

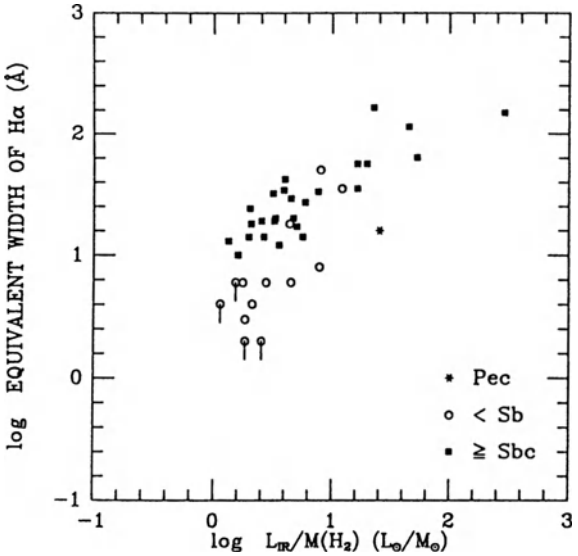

Figure 2. Comparison of the Hα equivalent width (EWHα) with $L_{IR}/M(H_2)$. Galaxy types are indicated as follows: open circles for early types (≤Sb), filled squares for late types (≥Sbc), and (*) for peculiars.

C. THE STAR FORMATION EFFICIENCY

As discussed in §II.B, we conclude that the ratio $L_{IR}/M(H_2)$ measures the efficiency of star formation in luminous galaxies of all dust temperatures. Figure 3 shows a plot of the ratio $L_{IR}/M(H_2)$ versus the 60/100 μm flux density ratio for 124 galaxies. We find that high dust temperatures and high star formation efficiencies are found both in galaxies with high luminosities and in galaxies with low luminosities. We suggest that *efficient star formation is responsible for the high dust temperatures observed, independent of the size of the galaxy, through the formation of more stars per unit molecular mass.* It is clear from studies of selected samples of galaxies that isolated galaxies have a low mean value of $L_{IR}/M(H_2)$, while merging/interacting galaxies have the highest values (Young *et al.* 1986b; Sanders *et al.* 1986; Solomon and Sage 1988). To illustrate this, the data points in Figure 3 are coded by environment.

One physical mechanism which may cause the SFE to be higher in merging/interacting galaxies than in isolated galaxies is cloud-cloud collisions. From numerical simulations, Noguchi and Ishibashi (1986) have shown that the rate of cloud-cloud collisions can increase substantially as a result of a galaxy-galaxy interaction. If, in addition, high mass stars form as a result of cloud-cloud collisions, the merging/interacting galaxies would be expected to have higher luminosities in young stars per unit molecular cloud mass, or higher SFE's, than isolated galaxies.

We note that environment can account for only part of the scatter in $L_{IR}/M(H_2)$ found among galaxies. Other parameters must also be important in causing variation in the SFE since even among isolated or interacting galaxies of a given dust temperature, there is a factor of 6-10 variation in the ratio $L_{IR}/M(H_2)$. Part of the scatter may arise from variations in the gas-to-dust ratio, the dust grain properties, the CO-H_2 proportionality, or the IMF from galaxy to galaxy.

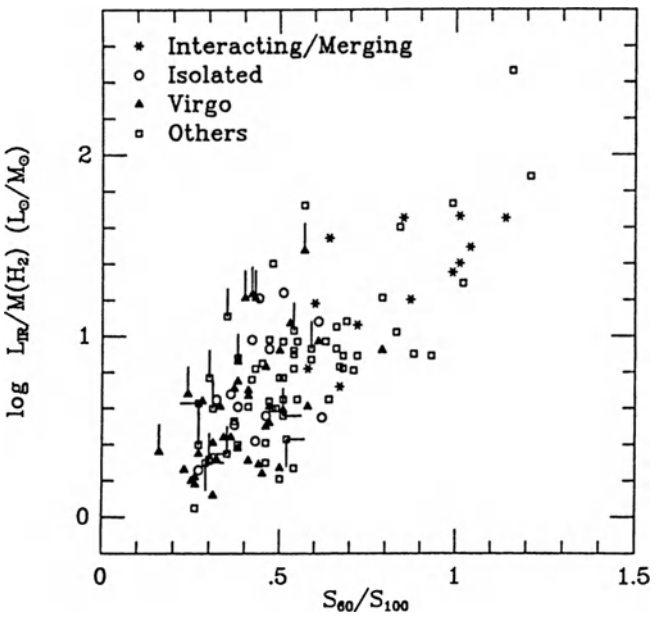

Figure 3. Comparison of the ratio $L_{IR}/M(H_2)$ with S_{60}/S_{100} for 124 galaxies. Points are coded by environment as indicated.

D. COMPARISON OF H_2 AND HI MASSES WITH DUST MASSES

Figures 4a and 4b show the comparison of H_2 and HI masses with dust masses derived from *IRAS* data. The best correlation found is for the $M(H_2)$-M_{dust} comparison, with a correlation coefficient of 0.97, compared with 0.79 for the comparison of M(HI) with M_{dust}. The fit to the data in Figure 4a indicates

$$M(H_2) \propto M_{dust}^{1.0\pm0.02} \qquad (3)$$

The mean value for the observed $M(H_2)/M_{dust}$ ratio is 570±50, a value which is significantly different from the values of ~100 for the Milky Way (Spitzer 1978; Hildebrand 1983) without including any of the atomic gas. As we have suggested previously (Young et al. 1986a; see also Stark et al. 1986a), IRAS is sensitive to warm dust, so that for galaxies containing a large fraction of dust colder than 30 K, the dust mass we calculate is an underestimate. The remarkably tight correlation between H_2 mass and dust mass (Figure 4a) is independent of galaxy type and of the temperature of the dust.

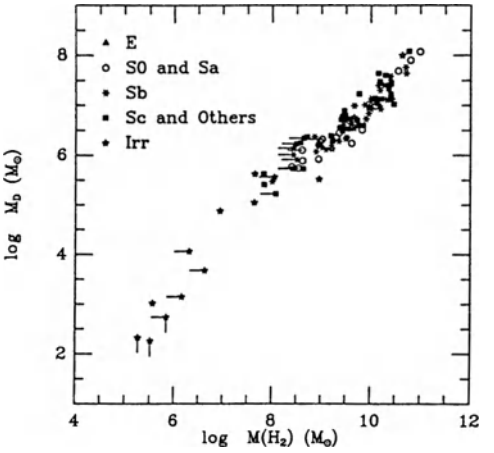

Figure 4a. Comparison of dust masses with global H_2 masses. Data points are coded by galaxy type as indicated.

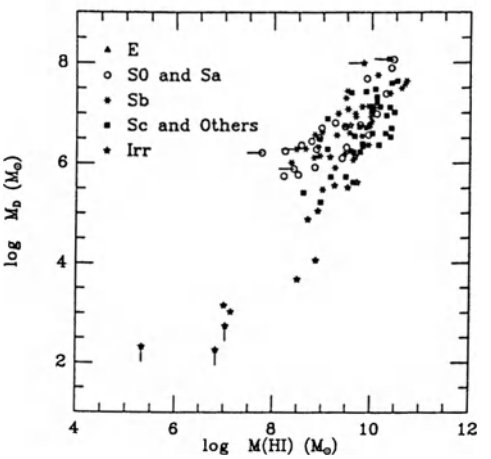

Figure 4b. Comparison of dust masses with global HI masses. Data points are coded by galaxy type as indicated.

III. THE H_2 CONTENT AND STAR FORMATION EFFICIENCY WITHIN GALAXIES

A. THE DISKS AND SPIRAL ARMS OF NGC 6946 AND M51

A complimentary approach to understanding galaxy evolution is to study individual galaxies in detail and to compare the radial distributions of various tracers within the disk of each one. NGC 6946 and M51 are two nearby well-studied relatively face-on late-type spiral galaxies which are ideal for comparing the distributions of young stars and gas within both the disk and the spiral arms. In both galaxies we find the remarkable result that all of the azimuthally averaged distributions -- blue light, FIR, Hα, radio continuum, and CO -- show similar radial behavior *except* that of the atomic gas (Young and Scoville 1982a; Scoville and Young 1983; Tacconi and Young 1986; Lord and Young 1988). We note that other luminous late-type spirals show these same characteristics in the azimuthally averaged radial distributions (Solomon *et al.* 1983; Kenney 1987).

The fact that the CO, blue light, Hα, FIR, and radio continuum distributions all show similar radial behavior when sampled at 2 kpc resolution is significant in terms of galaxy evolution. If the blue light measures the star formation rate integrated over the last $\sim 2 \times 10^9$ years (*cf.* Searle, Sargent, and Bagnuolo 1973), and the Hα flux measures the rate of formation of high mass stars, the fact that the blue/CO and Hα/CO ratios are constant as a function of radius indicates that *both the star formation rate for high mass stars and the integrated star formation rate for intermediate mass stars are proportional to the available supply of molecular gas,* or *the star formation efficiency is constant.* Because the atomic gas contributes such as small fraction of the total mass in the ISM in the inner disk of this and other luminous spirals, the data are also consistent with the star formation rate proportional to the gas surface density (H_2+HI) as a function of radius.

While azimuthally averaged radial distributions of CO, blue light, and Hα within the disks of NGC 6946 and M51 decrease smoothly as a function of radius when sampled at $\gtrsim$2 kpc resolution, any variations which occur at a particular radius are averaged out. In order to investigate the star formation efficiency on and off spiral arms, it is essential to study this azimuthal structure. Lord and Young (1988) and Tacconi and Young (1988) have compared fully sampled CO maps of M51 and NGC 6946 with Hα fluxes determined at 45" resolution. These studies do not address the arm/interarm contrast in the molecular cloud distribution, but do address the SFE on and off arms at a resolution of 2 kpc. Figure 5 shows the distributions of I-band light, Hα, H_2, and Hα/H_2 as a function of azimuth in NGC 6946 at a radius of 1.5' (Tacconi and Young 1988). At this radius, the Hα arms in NGC 6946 at 45" resolution stand out as factor of $\sim$4 enhancements relative to interarm locations; in CO at 45" resolution, the spiral arms appear as factor of $\sim$2 enhancements. Thus, at 45" resolution, the Hα/H_2 ratio in NGC 6946 is a factor of 2 higher on the arms than in interarm regions; Lord and Young (1988) find a similar result for M51. We conclude that *the efficiency of forming high mass stars in spiral arms of luminous galaxies is enhanced.* At larger radii in NGC 6946, we find the arm-interarm contrast in the Hα/H_2 ratio to be even greater.

Elevated Hα/CO ratios at particular locations in a galaxy indicate that there is a non-linear dependence of the star formation rate on the gas surface density. One possible mechanism which can explain the enhanced star formation efficiency is that of cloud-cloud collisions (Noguchi and Ishibashi 1986; Scoville *et al.* 1986), which should depend on the square of the cloud number density. The collection of clouds in a spiral potential could lead to star formation through an increase in the rate of cloud-cloud collisions.

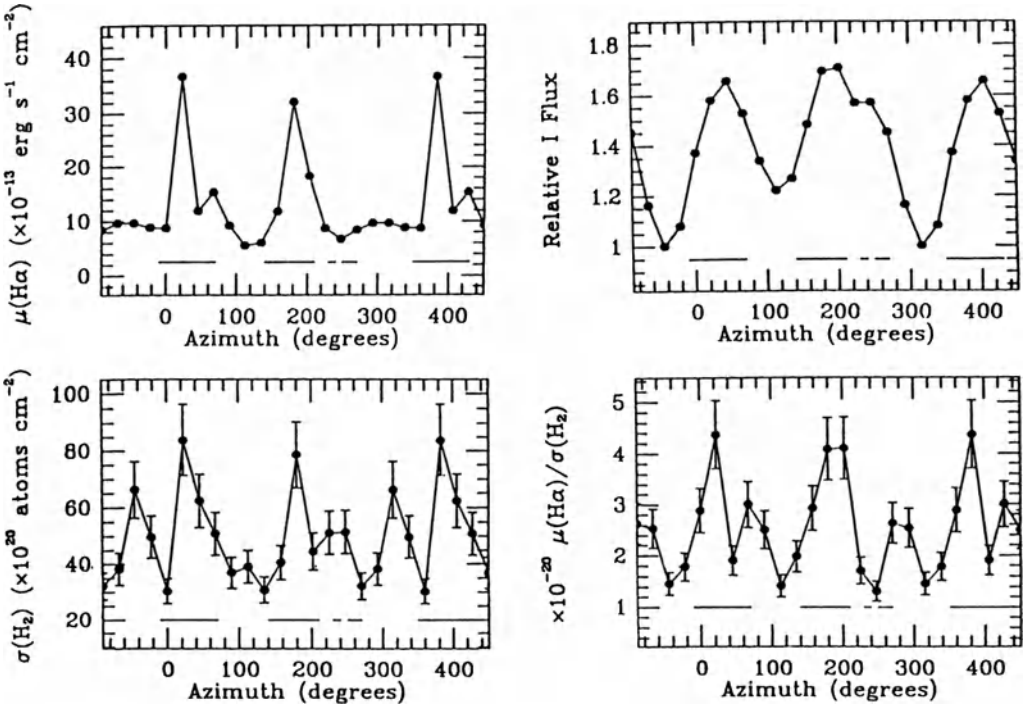

Figure 5. The azimuthal distributions of I-band, Hα, H_2, and Hα/H_2 surface brightness at a radius of 1.5' in the disk of NGC 6946 sampled at 45" resolution. Azimuths are defined from north through east, with north at 0°. The solid horizontal lines in the lower portion of each panel indicate the locations of the I-band spiral arms before smoothing the data to 45" resolution.

B. THE CENTERS AND DISKS OF M82 AND NGC 2146

The next question naturally arises is what locations in galaxies other than spiral arms are locations of elevated star formation efficiency. Two galaxies which we have found to exhibit unusually high SFE's in the centers are M82 and NGC 2146.

The Hα morphology of M82 is well-known, with emission extending primarily along the minor axis (*cf.* McCarthy *et al.* 1987). In contrast, the CO distribution is more extended along the major axis (Stark and Carlson 1984; Young and Scoville 1984). While the CO integrated itensities drop by a factor of 50 between the center and a radius of 3', the Hα flux in the same aperture drops by a factor of 2000. Thus, *the observed ratio of Hα/CO decreases by a factor of 400 with radius!* This result is in sharp contrast with the constant Hα/CO ratio as a function of radius in NGC 6946 and M51 described above. Because the intense radiation field in the center of M82 will heat the gas, the CO luminosity there may provide an overestimate of the H_2 mass, and thus an underestimate of the Hα/H_2 gradient.

NGC 2146 is a peculiar galaxy with an ultra-high IR surface brightness, rivaled only by NGC 1068. The Hα morphology of NGC 2146 is peculiar, with strong emission from the central 5 kpc and a string of HII regions extending along an arc 8' (50 kpc) long (Young *et al.* 1988b). The Hα distribution along the major axis sampled at 45" resolution shows a decrease in flux by a factor of 1000 over the central 90", while the CO distribution shows a decrease over the same region of a factor of 60. This galaxy, too, shows a marked drop in the observed Hα/CO ratio with radius.

The high central ratios of ionized to molecular gas in M82 and NGC 2146 suggest a high efficiency of high mass star formation in the centers of these galaxies. The gas depletion times there are several times 10^8 years. It is noteworthy that the mass of H_2 in the central 45" of these galaxies is ~20% of the dynamical mass in the same region. Given such large central gas concentrations, one expects a high rate of cloud-cloud collisions. If cloud-cloud collisions lead to the formation of high mass stars, one expects a high star formation efficiency in regions of high gas concentration. The mechanisms for producing such high central gas mass fractions include gas flow along bars in barred spiral galaxies, and galaxy-galaxy interactions which cause the gas clouds to lose angular momentum and fall to the center. Either or both mechanisms may be operating in M82 and NGC 2146.

IV. CONCLUSIONS

1) There is a good correlation between global IR luminosities and H_2 masses for 124 galaxies observed as part of the FCRAO Extragalactic CO Survey, such that $L_{IR} \propto M(H_2)^{1.0\pm0.03}$. We find that the IR emission in galaxies with $L_{IR} \gtrsim 10^{10}$ $L_\odot$ is from dust associated with molecular clouds.

2) We find a good correlation between IR and Hα luminosities, supporting the suggestion that the IR luminosity measures the star formation rate and the ratio $L_{IR}/M(H_2)$ measures the star formation efficiency. The correlation between Hα equivalent width and $L_{IR}/M(H_2)$ indicates that galaxies which are forming unusually large numbers of high mass stars are doing so through efficient conversion of gas into stars.

3) We find an excellent correlation between the warm dust and H_2 masses for 124 galaxies. The mean value of the ratio $M(H_2)/M_{dust} = 570\pm50$ for this sample.

4) The efficiency of star formation [from $L_{IR}/M(H_2)$] is higher in merging/interacting galaxies and lower in isolated galaxies.

5) Within the disks of the face-on spirals NGC 6946 and M51, we find that the azimuthally averaged star formation efficiency is constant with radius. On the spiral arms in these galaxies, we find Hα/CO enhanced by factors of 2-25 relative to the interarm regions, indicating that spiral arms are regions of enhanced efficiency in forming high-mass stars.

6) The peculiar galaxies M82 and NGC 2146 have azimuthally averaged Hα/CO ratios which decrease by factors of 400 and 15 as a function of radius, respectively. The centers of these galaxies have high molecular mass concentrations, with $M(H_2)$ comprising approximately 20% of the dynamical mass.

7) The elevated star formation efficiencies in interacting galaxies, on spiral arms, and in the centers of the peculiar galaxies M82 and NGC 2146 may result from the high gas concentrations in these regions which cause an increased rate of cloud-cloud collisions and subsequent high mass star formation.

REFERENCES

Bloemen, J.B.G.L., *et al.* 1986, Astr.Ap., **154**, 25.

Bushouse, H. 1986, Ph.D. Thesis, Univ. of Illinois.

De Gioia-Eastwood, K., Grasdalen, G.L., Strom, S.E., and Strom, K.M. 1984, Ap.J., **278**, 564.

Kenney, J. 1987, Ph.D. thesis, University of Mass., Amherst.

Kenney, J. and Young, J. 1988, Ap.J., in press (March 15, 1988).

Kennicutt, R.C. Jr. and Kent, S.M. 1983, A.J., **88**, 1094.

Kennicutt, R.C. Jr., Keel, W., van der Hulst, J.M., Hummel, E., and Roettiger, K.A. 1987, A.J., **93**, 1011.

Lonsdale, C.J., Helou, G., Good, J.C., and Rice, W.L. 1985, "Catalogued Galaxies and Quasars Observed in the IRAS Survey" (Washington, D.C.: U.S. Government Printing Office).

Lord, S., and Young, J.S. 1988, submitted.

McCarthy, P., Heckman, T.M., and van Breugel, W.J.M. 1987, A.J., **93**, 264.

Noguchi, M., and Ishibashi, S. 1986, M.N.R.A.S., **219**, 305.

Rieke, G.H., Lebofsky, M.J., Thompson, R., Low, F., and Tokunaga, A. 1980, Ap.J., **238**, 24.

Sanders, D.B., et al. 1986, Ap.J(Letters), **305**, L45.

Scoville, N., Yun, M., Clemens, D., Sanders, D., Waller, W. 1987, Ap.J.(Suppl.), **63**, 821.

Scoville, N.Z., and Young, J.S. 1983, Ap.J., **265**, 148.

Searle, L., Sargent, W.L.W., and Bagnuolo, W. 1973, Ap.J., **179**, 427.

Solomon, P., Barrett, J., Sanders, D.B., and de Zafra, R. 1983, Ap.J.(Letters), **266**, L103.

Solomon, P.M. and Sage, L. 1988, Ap.J., **334**, 613.

Stark, A.A., and Carlson, E. 1984, Ap.J., **279**, 122.

Tacconi, L., and Young, J.S. 1986, Ap.J., **308**, 600.

----- 1988, Ap.J., submitted.

Telesco, C.M., and Harper, D.A. 1980, Ap.J., **235**, 392.

Young, J.S., Claussen, M., Kleinmann, S., Rubin, V., and Scoville, N. 1988b, Ap.J.Letters, in press.

Young, J.S., Kleinmann, S.G., and Allen, L. 1988, Ap.J.(Letters), **334**, L63.

Young, J.S., Schloerb, F.P., Kenney, J, and Lord, S. 1986a, Ap.J., **304**, 443.

Young, J.S., et al. 1986b, Ap.J.(Letters), **311**, L17.

Young, J.S., and Scoville, N.Z. 1982a, Ap.J., **258**, 467.

----- 1982b, Ap.J.(Letters), **260**, L11.

----- 1982c, Ap.J.(Letters), **260**, L41.

----- 1984, Ap.J., **287**, 153.

Young, J.S., Xie, S., Kenney, J., and Rice, W. 1988a, Ap.J.Suppl., in press.

ON THE FAR-IR AND SUB-MM SPECTRA OF SPIRAL GALAXIES

A. A. Stark
AT&T Bell Laboratories; Holmdel, NJ 07733

J. A. Davidson
NASA Ames Research Center MS245-6; Moffett Field, CA 94035

D. A. Harper, R. Pernic, R. Loewenstein, S. Platt, G. Engargiola, S. Casey
University of Chicago, Yerkes Observatory; Williams Bay, WI 53191

ABSTRACT. We compare 160μm and 360μm photometric measurements of three normal spiral galaxies with theoretical models and observations at other wavelengths. Our observations indicate that on average spirals have few large, cold grains, in apparent discrepancy with the 1.3 mm measurements of Chini *et al.* (1986).

We have mapped three Virgo cluster spirals, NGC4254, NGC4501, and NGC4654, at 160μm (far-infrared) and 360μm (submillimeter) wavelengths with arrays of ^{3}He-cooled bolometers (Harper *et al.* 1989) using the NASA Kuiper Airborne Observatory and the NASA Infrared Telescope Facility (Stark *et al.* 1989). Almost all the power emitted from normal spiral galaxies appears at visible wavelengths or in the far-infrared; very little of the total power appears at radio wavelengths. The shape of the broad-band spectrum as it falls off towards radio wavelengths is not well known, because it is difficult to do photometry in the far-infrared and submillimeter. This paper briefly compares our observational results with predicted spectra.

Figure 1 is a composite far-infrared spectrum for "normal" spiral galaxies. Much of this figure is re-drawn from Figure 1 of Chini *et al.* (1986). It shows measured data points with error bars, and some theoretical curves. The points measured by us are plotted as triangles.

Far-infrared emission from spiral galaxies results from re-radiation of starlight energy absorbed at visual wavelengths by interstellar dust grains. The shape of the spectrum depends on the far-infrared emissivity of the grains and their temperature distribution (e.g. Puget 1985). The emissivity is a function of grain size and composition, quantities about which there is still considerable uncertainty; grain temperatures depend on the ambient starlight and visual opacity of the grains, quantities which are somewhat more certain.

Draine and Anderson (1985) and Rowan-Robinson (1986) have different grain models, but both use the radiation field of Mathis, Mezger and Panagia (1983) to compute the expected flux from the interstellar medium, so their assumptions about filling factors at various temperatures are similar. Draine and Anderson (1985) used a composite graphite and silicate model, as proposed by Mathis, Rumpl and Nordsieck (1977). The predictions of this model are shown as the lower dashed curve in Figure 1. Rowan-Robinson (1986) proposed an appreciable population of large grains in the diffuse interstellar medium, by analogy with the grain populations observed in dense regions. One of Rowan-Robinson's models for large, cold grains is shown as the upper dashed curve in Figure 1. The middle, sold curve in Figure 1 is a model fit by Chini *et al.* (1986) to their 1.3 mm data and the IRAS points. This model contains an appreciable population of large grains with a temperature of 16 K.

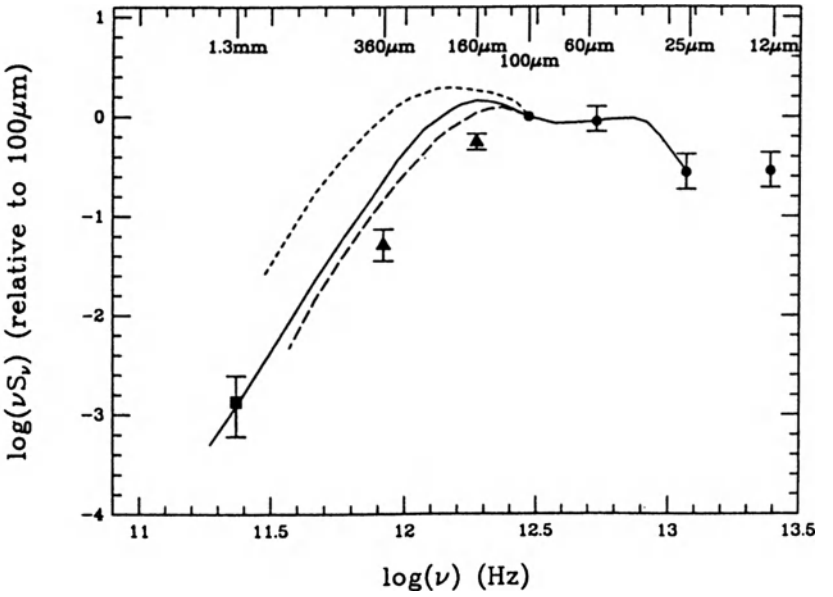

Fig. 1. A composite far-infrared spectrum of the total flux density from normal spiral galaxies. All data has been normalized so that $\nu S_\nu = 1$ at 100μm. The square point, the solid curve, and the four round points are redrawn from Figure 1 of Chini *et al.* (1986). The square data point at 1.3 mm is an average of galaxies measured by Chini *et al.*. The round points are averages of IRAS total flux densities for the same galaxies. The triangles are averages of our three (different) galaxies, normalized to their IRAS 100μm flux densities. The upper dashed curve is a model of Rowan-Robinson (1986); the lower dashed curve is a model of Draine and Anderson (1985).

It is immediately clear that the data at 360μm and 160μm data do not fit any of the models very well, although a Draine and Anderson (1985) model with a slightly higher mean grain temperature would fit our points but not the 1.3 mm data of Chini *et al.* (1986). There seem to be four possibilities: (1) The 360μm and 160μm points are incorrect. The point at 360μm has a large uncertainty, because the atmospheric opacity over Mauna Kea varied from about 40% to about 90% during the night these observations were made. We calibrated frequently and have attempted to include the uncertainties caused by atmospheric fluctuations in the error estimates, but it is possible that there is some uncorrected systematic error. We are considerably more confident of the 160μm point because of the low atmospheric noise at the KAO and because the 32F far-infrared camera has a 100μm filter which gives results consistent with IRAS measurements. Measurements in these two bands are independent, but both fall below the model predictions. (2) The 1.3 mm data of Chini are systematically high by a factor of about 3, and the appropriate grain emissivity model for galaxies as a whole is that of Draine and Anderson (1985), but with a slightly higher average grain temperature. (3) Both our data and the Chini *et al.* data are correct, indicating that the theoretical models are all inappropriate or incomplete. There might, for example, be a significant population of large grains with a temperature of 8 K. This could be checked by photometric observations at 600μm. (4) The premis of Figure 1 is incorrect — a composite far-infrared spectrum of normal spiral galaxies is meaningless, because normal spiral galaxies vary considerably in their far-infrared properties. The galaxies we observed at 360μm should be observed at 1.3 mm as well.

Our data in the far-infrared and submillimeter are inconsistent with models having large, cold grains. We argue that there are few very large or cold grains contributing to the far infrared and submillimeter flux from these galaxies. There is, however, an apparent discrepancy between our observations and those of Chini *et al.* (1986) which can only be resolved by further observations.

This work was supported in part by NASA grant NGR14-001-227 and NSF grant AST-8513974 to the University of Chicago.

REFERENCES

Chini, R., Kreysa, E., Krügel, E., and Mezger, P. G. 1986 *Astr. Ap.*, **166**, L8.

Draine, B. T., and Anderson, N. 1985 *Ap. J.*, **292**, 494.

Harper, D. A., Pernic, R., Davidson, J. A., and Loewenstein, R. 1989 (in preparation).

Mathis, J. S., Mezger, P. G., and Panagia, N. 1983 *Astr. Ap.*, **128**, 212.

Mathis, J. S., Rumpl, W., and Nordsieck, K. H. 1977, *Ap. J.*, **217**, 425.

Puget, J-L., 1985 in *Birth and Infancy of Stars* ed. R. Lucas, A. Omont, and R. Stora (North-Holland: Amsterdam) p. 77.

Rowan-Robinson, M. 1986 *M.N.R.A.S.*, **219**, 737.

Stark, A. A., Davidson, J. A., Harper, D. A., Pernic, R., Loewenstein, R., Platt, S., Engargiola, G., and Casey, S. 1989 *Ap. J.*, 15 April in press.

[CII] Line Emission from Spiral Galaxies

G. J. Stacey[1], R. Genzel[2], J. B. Lugten[3], and C. H. Townes[1]

[1]Dept. of Physics,University of California, Berkeley, CA USA
[2]Max-Planck-Inst. for Extraterrestrial Physics, Garching, FRG
[3]Inst. for Astronomy, Univ. of Hawaii, Honolulu, HI USA

SUMMARY. We have measured 158 μm [CII] line emission from a sample of thirteen gas rich galaxies. The new data are combined with the previous sample of six infrared bright galaxies of Crawford et al. 1985. The [CII] line is bright in all of the galaxies detected amounting to between .1 and 2% of the total nuclear far-infrared (FIR) luminosity, and is therefore one of the primary gas coolants in these regions. The [CII] emission arises from warm (T - 300 K), dense (N_H ~ 10^3→10^4cm^{-3}) photodissociated gas at the interface regions between giant molecular clouds and ionized gas regions, and is a very sensitive indicator of starformation activity. The integrated [CII] to the ^{12}CO line intensity ratio is constant for starburst galaxies and star formation regions in our own galaxy. This suggests that much of the observed ^{12}CO line radiation from starburst galaxies arises in the warm, (T_{ex} > 50 K), molecular gas immediately interior to these photodissociation regions, and not from the cold disk molecular cloud component as is commonly assumed. For the non-starburst galaxies in our sample, the line intensity ratio varies significantly from galaxy to galaxy but is always significantly less than the starburst value, in support of this model. The integrated line intensity ratios may thus be used as a sensitive probe of the physical conditions of the molecular gas in galaxies.

1. Introduction

Recent advances in far-infrared (FIR) technology have permitted FIR fine structure lines to be observed from several nearby galaxies (see Stacey et al. 1988a., and references therein). The $^2P_{3/2} \rightarrow {}^2P_{1/2}$ (157.7408 μm) transition of singly ionized carbon is observed to be among the brightest of these fine structure lines and is the primary coolant for much of the warm neutral interstellar medium. [CII] line emission has previously been reported from a sample of six nearby gas-rich infrared bright galaxies by Crawford et al. 1985, who found (1) the [CII] line radiation is bright, amounting to roughly .5% of the total FIR luminosity of the nuclear regions of these galaxies; (2) the [CII] line radiation arises in the warm dense photodissociated gas lying at the interface regions between giant molecular clouds

and fully ionized gas regions - it is not associated with atomic clouds or the diffuse interstellar medium; (3) the [CII] line intensity is sensitive to the local UV energy density, hence star formation activity; (4) the integrated [CII] to ^{12}CO (1 → 0) line intensity ratio is a constant for the observed galaxies and galactic star formation regions.

We have expanded the data set to include a much wider variety of galactic spectral types and luminosity classes ranging from the relatively low luminosity early RSab galaxy NGC 4736 through the mid luminosity late Scd galaxy NGC 6946 to the ultraluminous IRAS galaxies NGC 3690 and NGC 6240 (Table 1). The expanded data set confirm all of the conclusions of Crawford et al. but greatly extend their applicability to include the environs of both normal spiral galaxies (including those very similar to our own, e.g. NGC 891) and the ultraluminous galaxies. For this paper, we concentrate on comparisons between the observed ^{12}CO (1 → 0) and [CII] line emission. A more complete discussion may be found in Stacey et al. 1988a.

Table 1

Galaxy	R.A. (1950)	Dec. (1950)	Type	Distance (Mpc)	L(FIR) ($10^9 L_\odot$)	I([CII]) (10^{-5}erg s^{-1} cm^{-2} sr^{-1})	L([CII]) ($10^7 L_\odot$)	L([CII])/L(FIR)
NGC 660	$01^h40^m20.7^s$	13°23'32"	SB(s)a pec	12	22.	≤3.9 (3σ)	≤1.5	≤7 × 10^{-4}
NGC 891	$02^h19^m24.5^s$	42°07'13"	SA(s)b	9.6	9.	11.0 ± 1.1	2.8	3.1 × 10^{-3}
Maffei II	$02^h38^m10.1^s$	59°23'32"	SAB(rs)bc	5	4.2	19.0 ± 1.2	1.2	2.9 × 10^{-3}
NGC 2146	$06^h10^m40.1^s$	78°22'23"	SB(s)ab pec	14.4	49.	39.0 ± 0.8	22.3	4.6 × 10^{-3}
NGC 3079	$09^h58^m35.0^s$	55°55'17"	SB(s)c	16.	28.	11.3 ± 0.9	7.9	2.8 × 10^{-3}
NGC 3109	$10^h00^m49.0^s$	-25°55'00"	SB(s)m	1.7	0.02	≤3.4 (3σ)	≤0.03	≤1.6 × 10^{-2}
NGC 3628	$11^h17^m39.6^s$	13°51'48"	Sb/pec	9.6	7.2	7.9 ± 0.9	2.0	2.9 × 10^{-3}
NGC 3690 /IC 694	$11^h25^m44.2^s$	58°50'18"	IBm pec	44.	330.	9.4 ± 1.5	49.0	1.5 × 10^{-3}
NGC 4565	$12^h33^m52.2^s$	26°15'34"	SA(s)b	10.2	3.	3.0 ± 1.0	0.85	2.8 × 10^{-3}
NGC 4736	$12^h48^m32.0^s$	41°23'36"	RSA(r)ab	5.	1.8	7.3 ± 0.8	0.5	2.8 × 10^{-3}
NGC 5907	$15^h14^m36.8^s$	56°30'23"	SA(s)c	10.4	2.	6.0 ± 0.9	1.8	6.1 × 10^{-3}
NGC 6240	$16^h50^m28.0^s$	02°29'00"	IO pec	100.	620.	3.3 ± 0.66	90.0	1.5 × 10^{-3}
NGC 6946	$20^h33^m48.8^s$	59°58'50"	SAB(rs)cd	11.	8.9	7.6 ± 1.1	2.6	2.9 × 10^{-3}

2. Observations and Results

We made our observations during eleven separate flights on the Kuiper Airborne Observatory using three incarnations of the UC Berkeley Tandem Fabry-Perot spectrometer. The detective elements were stressed Ge:Ga photoconductors. The beam size at 158 μm was 55" (8.55×10^{-8}sr) and we typically chose a velocity resolution of ~ 100 km s^{-1}. We detected eleven of the thirteen new galaxies investigated, five of which we mapped with our new three element spatial array. Figure 1 shows representative spectra obtained on the starburst galaxy NGC 2146 and the normal spiral galaxy NGC 5907. The [CII] lines are bright in the nuclear regions of both galaxies totalling roughly 0.5% of the FIR luminosity. For comparision, we have superposed the ^{12}CO (1 → 0) spectra observed at the [CII] positions with similar sized beams. The spatial and spectral correlation between the two lines is very good indicating that they arise from in or about the same gas.

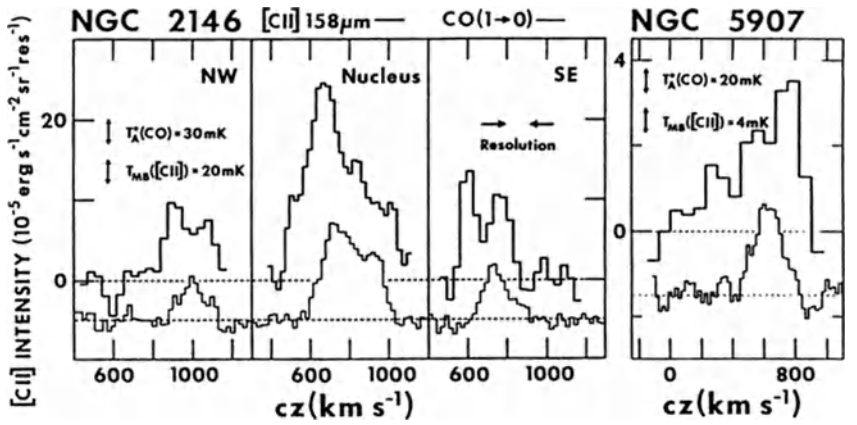

Figure 1. (left) Spatially multiplexed [CII] spectra (dark lines) of the starburst galaxy NGC 2146 obtained in 22 minutes of integration time. T_{MB}([CII]) is the main beam Raleigh Jeans brightness temperature scale for the (spectrally resolved) [CII] lines. The superposed ^{12}CO (1 → 0) spectrum (light lines) is from Young et al. 1988. (right) [CII] spectrum of the nuclear regions of the Sc galaxy, NGC 5907 obtained in 29 minutes of integration time. The superposed ^{12}CO spectrum is from Stacey et al. 1988a.

Figure 2 plots the integrated [CII] line intensities in the nuclear regions of the observed galaxies (★,●) against the integrated ^{12}CO line intensities observed in similar sized beams. For completeness, we also include the galaxies from Crawford et al., and selected galactic molecular clouds (○)and star formation regions (☆). There is a good general correlation between the line intensities for most of the observed objects. This correlation becomes much tighter when one restricts the objects to galactic star formation regions (☆), and external galaxies with dust temperatures (derived from FIR continuum measurements) in excess of 40 K (★). This latter restriction picks out those galaxies generally thought to be undergoing a starburst.

3. Discussion

The close association between [CII] and CO line emission is not too surprising. Both lines require similar gas densities ($\geq 10^3$ cm^{-3}) for excitation, and the [CII] line requires the presence of nearby ionization source (e.g. OB stars). Both requirements are well met by star forming giant molecular clouds. On galactic scales these clouds will presumably be well mixed with non-starforming clouds. What is surprising, however, is that the integrated line flux ratio is constant for the observed starburst galaxies, and this constant value is the same as that found for star formation regions in our own galaxy.

The CO (1 → 0) line emission in galaxies is presumed to be dominated by emission from the cold (T_{ex} ~ 10 K) molecular disk. This cold component should produce very little [CII] line radiation due to the lack of nearby ionizing radiation (c.f. Wolfire, Hollenbach, and Teilens 1988). The integrated [CII]/CO line intensity

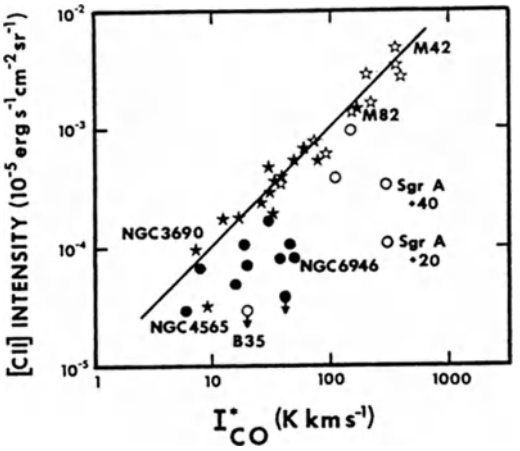

Figure 2. [CII] integrated line intensity vs ^{12}CO(1 → 0) line intensity for a variety of galactic and extragalactic regions. The solid line indicates a line intensity ratio $[CII]/I_{CO}$ = 6600.

ratio should therefore be substantially less in galaxies than in galactic star formation regions, and vary, depending on just how the UV energy density is distributed. This is exactly what we find (Figure 2) for the normal spiral galaxies and non-starforming clouds in the Galaxy. However, for the starburst galaxies the integrated line intensity ratio is the same as that for star formation regions in the Galaxy. This suggests that the CO line emission from these galaxies arises in the warm molecular gas associated with star formation regions and not from the cold disk component. This molecular gas is likely to have substantially elevated excitation temperatures ($T_{ex} \geq 50$ K) similar to those observed in galactic star formation regions (Harris et al. 1987, Jaffe et al. 1988, Stacey et al. 1988b). The ^{12}CO (1 → 0) integrated line intensity may thus be severely affected by gas excitation in these infrared bright galaxies and therefore not in of itself reliably trace molecular gas mass.

Acknowledgements We thank the staff of the KAO for their enthusiastic support. This research was supported by NASA grant NAG2-208.

References

Crawford, M.K., Genzel, R., Townes, C.H., and Watson, D.M. 1985, **Ap.J.**, 291, 755.

Harris, A.I., Stutzki, J., Genzel, R., Lugten, J.B., Stacey, G.J., and Jaffe, D.T. 1987, **Ap.J. (Letters)**, 322, L49.

Jaffe, D.T., Genzel, R., Harris, A.I., Lugten, J.B., Stacey, G.J., and Stutzki, J. 1988, submitted to **Ap.J.**.

Stacey, G.J., Genzel, R., Lugten, J.B., and Townes, C.H. 1988a in prep.

Stacey et al. 1988b in prep.

Young, J.S., Clausen, M.J., Kleinmann, S.G., Rubin, V.C., and Scoville, N.Z. 1988, **Ap.J. (Letters)**, 331, L81.

Wolfire, M.G., Hollenbach, D. and Tielens, A.G.G.M. submitted to **Ap.J.**.

A ^{12}CO SURVEY OF THE SMALL MAGELLANIC CLOUD

Monica Rubio and Guido Garay

Departamento de Astronomía, Universidad de Chile

In this contribution we summarize the results of a complete survey of the ^{12}CO emission, in the J=1 0 transition, from the Small Magellanic Cloud (SMC) made at an angular resolution of 8'8, corresponding to a linear resolution of 160 pc at 63 Kpc. The survey, made using the 1.2 m Columbia Millimeter-wave Telescope in Chile, covers the central 3°x2° region of the SMC with full resolution (angular spacing of 0º125). The spectral resolution was 1.3 km/s and the sensitivity in antenna temperature was 0.02 K.

We detected CO emission from two large complexes, located in the outermost southwest and northeast regions of the SMC bar. Table 1 gives the observed parameters of the ^{12}CO emission from these two complexes. There is good correspondance between the distribution of molecular emission and peaks in the 60 and 100μ IRAS infrared emission (Schwering 1988). Both CO complexes are projected toward regions of atomic gas having the largest column densities of HI (N(HI) $\sim 10^{22}$ cm^{-2}). In addition, the radial velocities of the CO and associated HI gas are similar. We suggest that molecular clouds in the SMC may be the dense cores of large regions of atomic gas. The theoretical critical HI column density required to shield the cloud interior from the external UV radiation field is $5x10^{20}$ $(Z/Z_\odot)$ cm^{-2}, where Z is the heavy element abundance (Franco and Cox 1986). For the SMC, $Z\sim 1/10\ Z_\odot$ and the critical column density is $5x10^{21} cm^{-2}$. The column densities of HI toward the CO complexes are $\sim 10^{22}$ cm^{-2} (Mc Gee and Newton 1981), which gives strong support to the contention that molecular clouds in the SMC are the UV shielded cores of large diffuse regions of atomic gas (Rubio and Garay 1988).

The antenna temperatures of the CO emission from the SMC are typically $\sim$ 0.03 K, about two orders of magnitude smaller than that of Galactic molecular couds. Possible explanations for the weakness of the CO emission are (Elmegreen, Elmegreen and Morris 1980; Israel et al. 1986): (i) optically thin ^{12}CO emission, (ii) low excitation temperatures; and (iii) small filling factors or beam dilution. We suggest that the extremely weak ^{12}CO antenna temperatures of the molecular clouds in

TABLE 1. Observed parameters of the ^{12}CO emission

Complex	T_A K	ΔV km s^{-1}	R pc	L_{CO} K km s^{-1} pc^2
SW	0.06	16.5	278	1.3×10^5
NE	0.03	20.4	254	1.1×10^5

the SMC are most likely due to small filling factors of the CO regions. Assuming that the ^{12}CO line emission is optically thick, we infer that the CO emission, within an antenna beam, should arise from clumps whose sizes are $\sim$10 times smaller than the typical size of the clumps making up giant molecular clouds in our Galaxy. Recently, Maloney and Black (1988) investigated the effects of changes in the metal abundance on the properties of molecular clouds and found that a decrease in the metallicity make the size of the CO region smaller relative to the size of the hydrogen molecular cloud. Thus, the small sizes of the CO clumps in the SMC are probably a consequence of the low dust content and low metallicity of the interstellar gas in this irregular galaxy.

To determine the molecular mass of the SMC we assume that, as in the Galaxy, the velocity integrated CO emission, W_{CO}, is a tracer of the molecular hydrogen column density, $N(H_2)$. However, for low metallicity systems, such as the SMC, the CO abundance in molecular clouds differs drastically from that in Galactic clouds, while their molecular hydrogen content is similar (Maloney and Black 1988). Thus, to apply the value of the $N(H_2)/W_{CO}$ ratio derived for Galactic clouds, X_G, to extragalactic clouds is probably not adequate. The conversion factor in the SMC can be derived by analysing the CO luminosity, L_{CO}, versus linewidth, Δv, relationship as we have already done for molecular clouds in the LMC (Cohen et al. 1988). Figure 1 shows this relation for molecular clouds in the SMC, LMC and a fit to the Galactic relationship. We note here that each molecular complex in the SMC has been dissected into two well defined clouds, whose observed parameters have been used in the correlation. The slope of the L_{CO} - Δv relations is similar, but for a given linewidth the clouds in the SMC appear $\sim$25 times fainter than Galactic clouds. We therefore adopt $X_{smc} = 25\ X_g$ or, with $X_g = 2.8 \times 10^{20}$ $cm^{-2}K^{-1}km^{-1}s$ (Bloemen et al. 1986), $X_{smc} = 7 \times 10^{21}$ $cm^{-2}K^{-1}km^{-1}s$. The cloud masses calculated using this conversion factor agrees with the virial masses to about a factor of two.

The total molecular mass of the SMC, determined with this calibration factor, is $3.5 \times 10^7 M_\odot$ and the ratio of molecular to atomic mass is 9%, about 10 times smaller than the ratio derived in our Galaxy.

This research has been supported by Universidad de Chile (DTI) grant E2604-8824 and FONDECYT grant 486/88.

References

Bloemen, J.B.G.M. et al., 1986. Astr. Ap., 154, 25.

Cohen, R.S., Dame, T.M., Garay, G., Montani, J., Rubio, M., and Thaddeus, P. 1988, Ap. J. (Letters), 311, L95.

Elmegreen, B.G., Elmegreen, D.M., and Morris, M. 1980, Ap. J., 240, 455.

Franco, J., and Cox, P.C. 1986, Pub. A.S.P., 98, 1076.

Israel, F.P., De Graauw, Th., Van de Stadt, H., and De Vries, C.P. 1986, Ap. J., 303, 186.

Maloney, P. and Black, J.H. 1988, Ap. J., 325, 389.

Mc Gee, R.X. and Newton, L.M., 1981, Proc. Astron., Soc., Australia, 4, 189.

Rubio, M., and Garay, G. 1988, Molecular Clouds in the Milky Way and External Galaxies, (Springer-Verlag), in press.

Schwering, P. 1988, Ph. D. thesis, Leiden University.

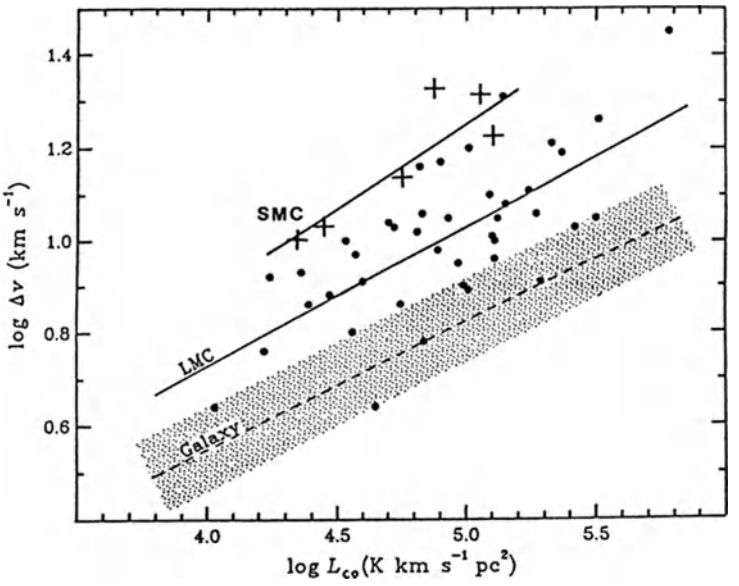

Figure 1. CO luminosity - linewidth relationship for the SMC, LMC, and bright Galactic molecular clouds.

MM OBSERVATIONS OF THE MAGELLANIC CLOUDS AND OF A FEW GALACTIC MOLECULAR CLOUDS

P. ANDREANI[1], G. DALL'OGLIO[1], L. MARTINIS[3]
L. PICCIRILLO[1,2], L. PIZZO[1], L. ROSSI[4], C. VENTURINO[1]

(1) – Dipartimento di Fisica, Università di Roma "La Sapienza", Roma
(2) – Istituto Superiore PP.TT., Roma
(3) – E.N.E.A. Tib. Frascati
(4) – Istituto Astrofisica Spaziale, Frascati

During a run of submillimetre observations from Antarctica, we detected the millimetric emission of the two Magellanic Clouds and a few galactic molecular clouds. The *mm* spectra does not match with the long wavelength tail of the thermal emission observed by IRAS and very likely represent a coexisting very cold dust component.

Millimetric and submillimetric observations from the ground are contaminated by the atmospheric emission and fluctuations, mainly due to the water vapour content. For this reason very cold and dry sites are preferred. During the 1987-88 expedition to the Italian Base at Terra Nova Bay (74° 41.61 S, 164° 06.89 E) in Antarctica, the good atmospheric conditions allowed an instrument, devoted to the search for the fluctuations on the CBR spectrum, to detect the millimetric emission of the Galaxy at about $8° \div 16°$ from the plane and the Magellanic Clouds, at a level well above the atmospheric noise.

The instrumental set-up, the observation procedure and the data analysis can be found in Andreani et al (1988a, 1988b)

A striking correlation between our measurements, at 1 and 2 millimetre wavelengths, and the IRAS $100\mu m$ emission in the same sky regions provides strong evidence for the detection of the IRAS clouds at $b \sim -8° \div 16°$ and $l \sim 290° \div 310°$ and the Magellanic Clouds.

As it is evident from the figures 1,2 and 3 at least two dust components are required in order to explain the IR/mm spectra of these sources.

REFERENCES

P. Andreani, G. Dall'Oglio, L. Martinis, L. Piccirillo, L. Pizzo, L. Rossi, C. Venturino, submitted to the Astroph. Journal (1988a)

P. Andreani, C. Ceccarelli, G. Dall'Oglio, L. Martinis, L. Piccirillo, L. Pizzo, L. Rossi, C. Venturino, submitted to the Astroph. Journal (1988b)

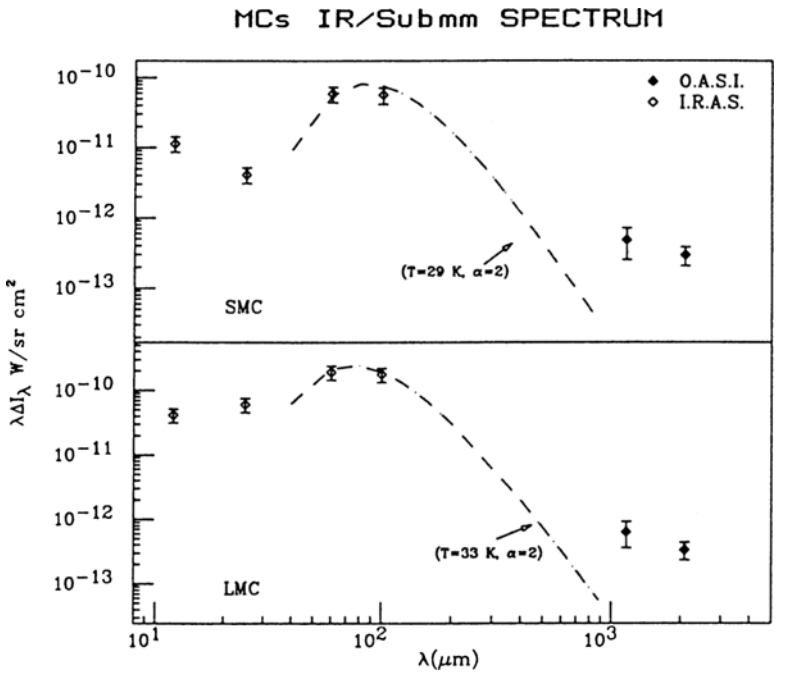

fig. 1 Far-infrared and submillimiter spectra of the Magellanic Clouds. The 12, 25, 60 and 100 μm intensities have been obtained by simulating the sky modulation on the IRAS high resolution maps.A grey body curve is reported for comparison (from Andreani et al 1988b).

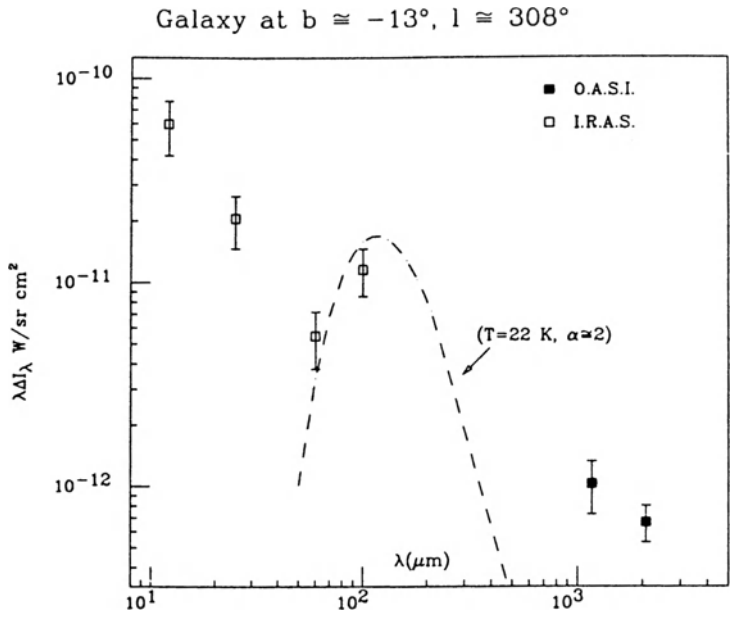

fig. 2 The far-infrared and submillimeter spectrum of the Chamaeleon Cloud. The 12, 25, 60 and 100 μm intensities have been obtained by simulating the sky modulation on the IRAS high resolution maps. A grey body curve is reported for comparison. (from Andreani et al 1988a)

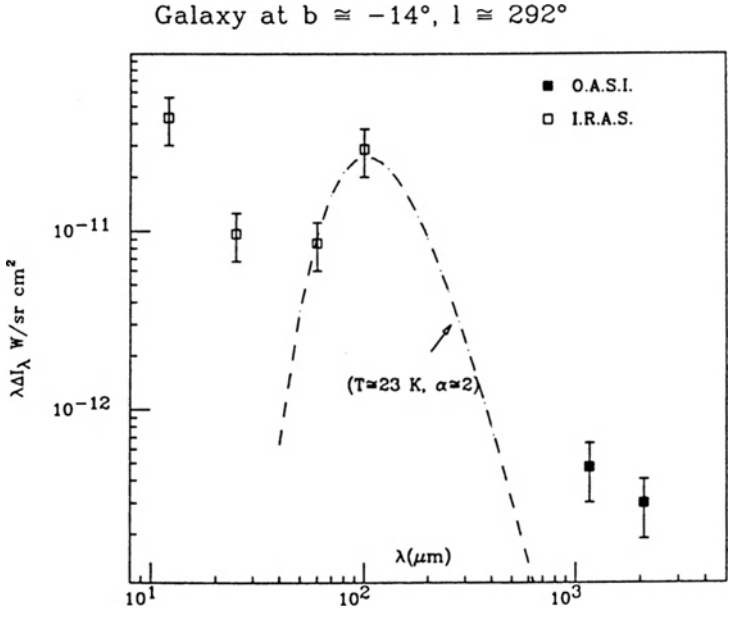

fig. 3 Far-infrared and submillimiter spectrum of a cluod in the Chamaeleon region. The 12, 25, 60 and 100 μm intensities have been obtained by simulating the sky modulation on the IRAS high resolution maps.A grey body curve is reported for comparison. (from Andreani et al 1988a)

GIANT MOLECULAR CLOUD COMPLEXES IN IRREGULAR GALAXIES

R. Becker[1)], C. Henkel[2)], P. Schilke[2)], T.L. Wilson[2)],
J.G.A. Wouterloot[2)], I. Appenzeller[1)]

1) Landessternwarte Heidelberg-Königstuhl, D-6900 Heidelberg
2) Max-Planck-Institut für Radioastronomie, Auf dem Hügel 69, D-5300 Bonn

1 Introduction

In the following we report CO observations of the two nearby irregulars IC 10 and NGC 3077. We have mapped giant molecular cloud complexes in both systems in the CO J=1-0 and J=2-1 transitions simultaneously, with the IRAM 30-m telescope, at angular resolutions of 21" and 13", respectively.

2 IC 10

IC 10 has been classified as a dwarf irregular galaxy of the Magellanic type with a barlike core (de Vaucouleurs and Freeman 1972). It has an optical diameter of 4 arcmin. Estimates of its distance range from 1 to 3 Mpc. We shall here assume a distance of 1 Mpc. The linear dimensions of IC 10 appear to be similar to those of the SMC, but otherwise this galaxy seems to be denser and brighter (more like NGC 4449; de Vaucouleurs and Ables 1965). Only its high surface brightness allows a detection of this galaxy, because it is close to the galactic plane (b^{II} = -3°.32). Huchtmeier (1979) found a huge HI shell around IC 10 extending to 80' in diameter at a surface density level of 3.8 10^{18} atoms cm^{-2}. This is 20 times the observed optical diameter. Interferometric measurements by Shostak and Skillman (1989) reveal that the HI distribution is characterized by a 7x10 arcmin disk of high surface brightness and the extended envelope of weaker emission, found in the single-dish study of Huchtmeier. According to Shostak and Skillman, the disk has several high surface density regions with peak column densities of 4.2 10^{21} atoms cm^{-2}, while the average column density there is about 1.5 10^{21} atoms cm^{-2}. IC 10 has two main centers of star-formation activity. One is located in the south-eastern part (IC 10/SE). Toward this region Henkel et al. (1986) detected CO emission and an unusually luminous interstellar H_2O maser. The first CO map was obtained in March 1987 with the Onsala 20-m telescope. In July 1988 simultaneous observations in the CO J=1-0 and J=2-1 transitions at 115.271 GHz and 230.538 GHz, respectively, were carried out with the IRAM 30-m telescope at Pico Veleta. In IC 10/SE we found a giant molecular cloud complex (GMC) that coincides with one of the peak positions of the HI distribution and with the position of the strongest radio continuum emission (Skillman 1988). The H_2O maser is located at the northern edge of this GMC, which has a deconvolved linear FWHP size of 130x120 pc^2. Line calibration was obtained by assuming T_A^*=100 K for both transitions toward Orion IRc2. For IC10/SE we measured peak line temperatures up to 1 K. A second very luminous H_2O maser was discovered in February 1987 towards the star-formation complex in the north west of IC10. This maser also coincides with a molecular cloud which appears to be compact ($\leq$ 40 pc) even when measured with a 13" beam. The detection of CO emission from additional positions in the HI disk, but outside the optical dimensions of IC 10, was first reported by Ohta et al. (1988). With the IRAM 30-m telescope we mapped a

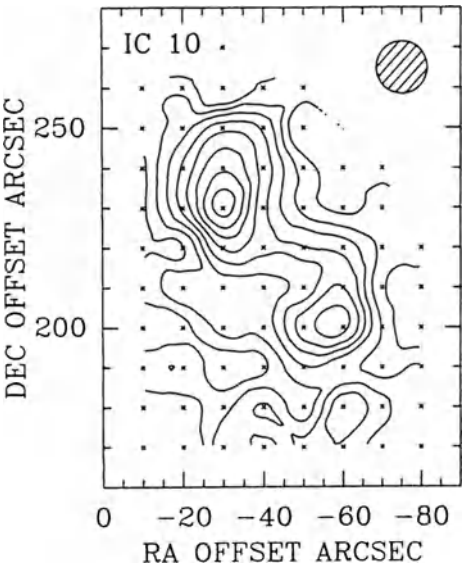

Figure 1: CO J=2-1 contour map of the molecular cloud complex in IC 10 located outside the optical radius. Contour levels are 0.5, 1, 1.5 ... 4 $Kkms^{-1}$ integrated over a velocity range of -345 to -320 kms^{-1}. The reference position is $\alpha_{50} = 00^h\,17^m\,44^s, \delta_{50} = 59^\circ\,00'\,48''$.

GMC outside the optical radius, which coincides with one of the dense HI peaks reported by Shostak and Skillman. In this CO complex we found two giant molecular clouds with deconvolved linear FWHP sizes of 90x160 pc^2 and 100x170 pc^2. As pointed out by Ohta et al. there are no counterparts in the optical, infrared or radio continuum. The peak line temperatures are $\approx$300 mK. Accounting for the different beam sizes, the $T_A^*(2\text{-}1)/T_A^*(1\text{-}0)$ line temperature ratio is 0.8 for all CO clouds. We determined the H_2 mass of the molecular clouds in IC 10 using the integrated J=1-0 line intensity, I_{co}, and a "galactic" conversion factor $N(H_2)/I_{CO}=4\ 10^{20}\ cm^{-2}\ (Kkms^{-1})^{-1}$ and compared these values to the virial H_2 masses that we derived. For IC10/SE we find that the virial mass is equal to the mass derived from I_{CO} and for the giant molecular clouds outside the optical disk the virial masses are larger only by a factor of two. This suggests that the conversion factor we used may be appropriate for IC 10. The $N(H_2)/I_{CO}$ conversion factor depends on the metallicity and the physical conditions within the molecular clouds (see e.g. Maloney and Black 1988). Therefore the use of a "galactic" value can significantly underestimate the H_2 mass of molecular clouds in low metallicity systems. The atomic hydrogen mass contained in the GMC's is about 20 % that of the molecular mass. CO has been observed also at another peak position in the HI disk of IC 10, where no optical counterpart is known, but this CO map is not yet completed. Molecular clouds can be formed from diffuse interstellar clouds only when the interior of the cloud is shielded from the external UV radiation field. Franco and Cox (1986) find that the required critical HI column density is $\approx 5\ 10^{20}\ (Z_\odot/Z)\ cm^{-2}$, where Z is the metallicity (see also Rubio and Garay 1987). Adopting the metallicity values given by Lequeux et al. (1979), the critical column density for IC 10 is $\approx 1.8\ 10^{21} cm^{-2}$. The peak HI column densities in IC 10 are well above this value (see Shostak and Skillman 1988). The metallicity is usually determined by the means of optical spectrophotometry of bright HII regions. These are found only in the innermost parts of IC 10. A lower metal abundance in the outer regions could be inferred by the fact that the virial H_2 masses are systematically larger than the H_2 masses derived via conventional $N(H_2)/I_{CO}$ conversion factors. More CO observations are needed for a more reliable conclusion.

3 NGC 3077

NGC 3077, an Irr II galaxy, is a member of the M81 group at a distance of 3.25 Mpc. It is embedded in a large dynamically complex cloud of neutral hydrogen (Appleton et al. 1981). The HI distribution near NGC 3077 shows two regions with enhanced emission: one at the nucleus with column densities up to 1.4 10^{21} cm^{-2} and the other approximately 4' SE of the nucleus with similarly high peak HI column densities (van der Hulst 1979). A prominent optical absorption region is located near the nucleus (Barbieri et al. 1974). Large quantities of dust are also suggested by the presence of an IRAS point source (L_{IR}=5 10^8 $L_\odot$). The metallicity of the gas near the center is approximately solar and at least a factor of two higher than what is expected for such a low mass galaxy (M_T=3.3 10^9 $M_\odot$; Heckman 1980). We discovered and mapped a giant molecular cloud complex (GMC) in NGC 3077. The position of the GMC coincides with the HI peak and the dust cloud near the center. Observed peak line temperatures are ≈200 mK. As for IC 10, the line temperature ratio T_A^*(2-1)/T_A^*(1-0) is 0.8, a value that is higher than in nearby galactic dark clouds, indicating that a substantial fraction of the gas may be heated to T_{kin} ≥10 K (see also Becker et al. 1989). The GMC has a deconvolved FWHP size of about 320 pc. Using the conversion factor $N(H_2)/I_{CO}$=4 10^{20} cm^{-2} $(Kkms^{-1})^{-1}$ (this may be appropriate for an interstellar medium with approximately solar metallicity; see e.g. Maloney and Black 1988) we obtain M_{H_2}=1.0 10^7 $M_\odot$. Adopting R=160 pc and ΔV=30 kms^{-1} the virial mass of the GMC is M_{vir}=3.0 10^7 $M_\odot$. The discrepancy between the virial mass and the mass derived from I_{CO} suggests that there may be a great deal of substructure not resolved with an angular resolution of 13" (=205 pc at 3.25 Mpc).

References

Appleton,P.N., Davies, R.D., Stephenson,R.J.: 1981, *Monthly Notices Roy. Astron. Soc.*, **195**,327

Barbieri,C., Bertola,F.,di Tullio,G.: 1974, *Astron. Astrophys*, **35**, 463

Becker,R., Schilke,P., Henkel,C.: 1989, *Astron. Astrophys.*, in press

de Vaucouleurs,G., Ables,H.: 1965, *Publ. Astron. Soc. Pacific*, **77**, 272

de Vaucouleurs,G., Freeman,K.C.: 1972, *Vistas in Astronomy* **14**,163

Franco,J., Cox,D.P.: 1986, *Publ. Astron. Soc. Pacific* **98**,1076

Heckman,T.M.: 1980, *Astron. Astrophys.* **87**, 142

Henkel,C., Wouterloot,J.G.A., Bally,J.: 1986, *Astron. Astrophys.*, **155**,193

Huchtmeier,W.K.: 1979, *Astron. Astrophys*, **75**,170

Lequeux,J., Peimbert,M., Rayo,J.F., Serrano,A., Torres-Peimbert,S.: 1979, *Astron. Astrophys.***80**,155

Maloney,P., Black,J.H.: 1988, *Astrophys. J.* **325**,389

Ohta,K., Sasaki,M.,Saito,M.: 1988, *Publ. Astron. Soc. Japan*, in press

Rubio,M., Garay.: 1987, *pre-publication, Departamento de Astronomia, Universidad de Chile*

Shostak,G.S., Skillman,E.D.: 1989, *Astron. Astrophys.*, submitted

Skillman,E.D.: 1988, in *The Interaction of Supernova Remnants with the Interstellar Medium*, IAU Coll. **101**,p465

van der Hulst,J.M.: 1979, *Astron. Astrophys*, **75**, 97

FINE STRUCTURE F.I.R. LINES: A TOOL TO INVESTIGATE THE CIRCUMSTELLAR ENVELOPE OF SOME YOUNG STARS.

C.Ceccarelli[1], G.Ingrosso[2], D.Lorenzetti[1], P.Saraceno[1], F.Strafella[1,2]

1. Istituto di Fisica dello Spazio Interplanetario C.N.R. - Frascati (Italy)
2. Dipartimento di Fisica Universita' di Lecce (Italy)

Ae/Be Herbig stars are known to be pre-main sequence stars. Some of these show evidence of mass ejection whose associated phenomenology comprises:

i) molecular outflows (CO mm lines)
ii) optical outflows (HH objects, jets)
iii) P Cyg profile (stellar winds)

These manifestations often coexist, suggesting the presence of correlated excitation mechanisms. Because the associated angular scales are very different (unresolved for stellar winds and several arcminutes for molecular outflows) it is worthwhile to identify suitable tools for investigating the possible continuity of the phenomenon at intermediate scales.

On the basis of their spectral types these stars are expected to produce a small HII region and a relatively extended region where photons with energies lower than the Lyman limit still ionize atoms as C,S,Fe,Si etc. and maintain the oxygen

mostly atomic preventing the formation of molecules. This region could be traced by means of the fine structure emission lines of [OI] 63μm , 145μm and [CII] 158μm. Among the more abundant ions in this region it is expected that only these lines could be collisionally excited. We have estimated the extent of the CII and OI regions surrounding a Herbig star considering the photoionization and photodissociation processes balanced by recombination and molecular formation respectively.

We assumed:

- spherical symmetry
- solar abundances
- far UV field as described by the Planck function at the stellar effective temperature.
- process rates given by Tielens and Hollenbach (1985).
- far UV photons absorbed according to the relation $A_V=5.9\ 10^{-22} N_{HI}$ mag (Savage and Mathis, 1979).

The extent of the CII and OI emitting regions is estimated according to the choice that the ratios CII/C and O/O_2 are 0.3. The aim is to compensate for the overestimation due to the neglecting of chemical processes depleting C and O.

The results are summarized in Table 1.

The flux densities requiring reasonable exposure times with the Long Wavelength Spectrometer (LWS) for the Infrared Space Observatory, are underlined. Taking into account the continuum IRAS observations of the Herbig stars, we obtain a line to continuum ratio in the limit of the read out accuracy of LWS.

MOD. N.	T_*(K) Sp	$n_H(R_*)$ (cm^{-3})	α	N_H (cm^{-2})	FLUX DENSITY IN LINE (W m^{-2}) [CII]158μm	[OI]63μm	[OI]145μm
1		$1\ 10^{10}$	0	1.0(22)	2.8(-24)	1.7(-21)	1.5(-22)
2	8100		1	5.0(22)	2.9(-22)	1.7(-16)	1.5(-17)
3	A5	$1\ 10^{11}$	0	1.0(22)	2.2(-25)	4.0(-23)	3.6(-24)
4			1	8.3(21)	2.4(-25)	1.6(-22)	1.4(-23)
5		$1\ 10^{10}$	0	1.3(22)	7.0(-24)	2.4(-21)	2.1(-22)
6	9700		1	6.8(22)	6.0(-22)	7.6(-17)	6.7(-18)
7	A0	$1\ 10^{11}$	0	1.2(22)	4.6(-25)	6.6(-23)	5.7(-24)
8			1	8.3(21)	5.3(-25)	1.7(-22)	1.5(-23)
9		$1\ 10^{10}$	0	3.2(22)	9.2(-23)	7.0(-21)	6.1(-22)
10	13800		1	2.2(23)	6.2(-20)	7.3(-16)	6.4(-17)
11	B5	$1\ 10^{11}$	0	3.2(22)	4.0(-24)	1.9(-22)	1.7(-23)
12			1	4.0(22)	7.0(-24)	7.0(-22)	6.2(-23)
13		$1\ 10^{10}$	0	5.0(23)	2.9(-20)	4.8(-19)	4.2(-20)
14	30900		1	5.3(24)	1.3(-14)	7.6(-15)	6.7(-16)
15	B0	$1\ 10^{11}$	0	1.0(24)	1.4(-21)	2.1(-20)	1.8(-21)
16			1	6.0(24)	1.1(-18)	2.1(-17)	1.8(-18)
$N_H(cm^{-2})/\Delta v_D$ (Km/s)					9.27(21)	2.62(20)	9.28(20)

Table 1

Column:

1) Model number
2) effective temperature according to the given spectral type.
3) density value at the stellar surface.
4) according to the density law:
   $n(r) = n_H(R_*)[(R_*/r)^{\alpha}]$ the α value is given
5) Hydrogen column density
6,7,8) Flux densities for the considered lines at a gas temperature of 1000 K and at a distance of 1000 pc.

At the bottom the values of the H column densities required to obtain the unit of optical depth in units of $N_H(cm^{-2})/\Delta v_D$(Km/s) where Δv_D is the line width.

REFERENCES

- ISO - Summary and Presentation Material compiled by M. Kessler. Revised March 1988 - ESA Space Sci. Dept.
- Savage,B.D., Mathis,J.S. 1979 Ann. Rev. Astron. Astrophys. 17,73.
- Tielens, A.G.G.M., Hollenbach, D., 1985 Ap.J. 291, 722.

Molecular Cloud Evolution and Star Formation

Joseph Silk
Department of Astronomy, University of California, Berkeley, CA 94720

Abstract

The origin and growth of molecular clouds is described and mechanisms for molecular cloud support are reviewed. Cloud disruption is discussed with emphasis on star formation efficiency. Issues pertaining to massive star enhanced star formation are summarized, and a mechanism for bimodal star formation is presented. Applications are made to the global star formation rate and to starburst galaxies.

1. INTRODUCTION

This conference has had as an important theme the role of small telescopes in millimetre–wave astronomy. I will in this review attempt to work with the theorist's analog of a small telescope, namely pen and paper, in order to give a broad review of molecular cloud evolution. Star formation issues are inseparable from molecular clouds, and some relevant aspects of star formation will also form a major part of this review. I will emphasize physical evolution of clouds, and describe cloud growth, support and disruption. Subsequently, I will examine the efficiency of star formation, discuss the initial mass function, and evaluate the star formation rate. A global model for star formation leads to consideration of starbursts in disk galaxies.

Molecular clouds with $A_v > 1$ can be divided into dark, and usually cold, clouds, and massive clouds or cloud complexes, which in spiral arms are warmer and associated with H II regions and massive star formation. The clouds are generally gravitationally bound, although subcondensations (cores or clumps) are not necessarily self–gravitating, and have supersonic line widths. I begin with a description of the origin, longevity and fate of these clouds.

2. Origin and Growth

A cloud becomes predominantly molecular when the total gas density exceeds $\sim 100\,\mathrm{cm}^{-3}$. The molecular gas is highly dissipative, and collisions between gas fragments lead to formation of small self–gravitating clouds. These clouds are likely to be below the critical mass $M_{crit} \sim \Phi G^{1/2}$, where Φ is the magnetic flux, required for magnetostatic support against gravitational collapse. Support of subcritical mass clouds can be maintained for a time of order the ambipolar diffusion time–scale, which is of order 30 cloud initial free-fall times (Nakano 1985) or $\sim 3 \times 10^7$ yr. If ensuing star formation involves low mass

stars, as argued below, cloud disruption is not likely to be catastrophic over a time–scale as long as a cloud–cloud collision time–scale, which for ~ 7.5 molecular clouds kpc^{-1} (averaging over the cloud mass spectrum) and velocity dispersion $6\,\mathrm{km\,s}^{-1}$ is $\sim 10^8\,\mathrm{yr}$. These clouds orbit the galaxy on ballistic trajectories, and grow as a consequence of cloud–cloud collisions and of orbit focussing by spiral density waves (Casoli and Combes 1982; Kwan and Valdes 1987). Cloud growth is favored as cloud collisions are likely to be highly dissipative, the collision rate being enhanced by cloud self–gravity and by large–scale density waves, whether in grand design or flocculent spirals. Numerical simulations show that giant molecular clouds or cloud complexes inevitably form along spiral arms in grand design spirals (Roberts and Stewart 1987). Typical masses are $10^5 - 10^6\,\mathrm{M}_\odot$, and densities are $100\text{–}300\,\mathrm{cm}^{-3}$, as observed in our galaxy. High resolution observations in ^{12}CO of the spiral galaxy M51 lend considerable support to such a model, revealing the non–circular motions acquired by gas clouds from the density wave, the formation of giant cloud complexes in the dust arms, and the delayed, downstream formation of OB stars that demarcate the grand design spiral arms (Vogel *et al.* 1988).

These massive clouds or cloud complexes certainly have mass $> \mathrm{M_{crit}}$, and the magnetic field can no longer regulate their collapse to form stars. However, we know observationally that these clouds, which contain the bulk of the molecular gas (Solomon and Rivolo 1987), are somehow supported against free–fall collapse in order to avoid an excessive rate of galactic star formation. Possible explanations are described in the following section, where I argue that energy input from forming stars provides the most plausible source of support, with ensuing disruption as massive stars form (*cf.* Oort 1954).

3. Support

For the cold dark clouds, with masses $10^3 - 10^4\,\mathrm{M}_\odot$, magnetic field support is indicated by the fact that measured field strengths are consistent with the cloud line widths being equal to the Alfvén velocity (Myers and Goodman 1988). The statistical correlations between line width, density and clump scale can then be explained with an approximately constant magnetic field, $\mathrm{B} \approx 30\,\mu\mathrm{G}$, if the clouds are assumed to be self–gravitating.

There is an additional contribution, however, to cloud support. Once stars begin to form, high velocity outflows from pre–main-sequence stars inject considerable momentum into the clouds. This is graphically illustrated in observations of the dark cloud L43, which is being disrupted by a high velocity bipolar flow (Mathieu *et al.* 1988). A study of NH_3 cores in cold clouds reveals that cores with embedded infrared objects tend to have broader lines on the average than the cores without such objects, these latter cores having near–thermal line widths (Myers 1983). Unfortunately, this does not constitute a good test of the role of outflows in cloud support, because the cold, dense ammonia cores rarely have very supersonic line widths and are also inferred to be in extremely early stages of low mass star formation. The ubiquity of optical jets, which are closely associated with high velocity molecular flows, suggests that with the presently available incomplete mapping of cold clouds, we may be missing many flows from low luminosity objects.

If outflows rather than magnetic fields are the primary agent of cold cloud support, then the original correlation between line width and core scale needs an explanation. Of course, even if magnetic support prevails, there is no fundamental reason why B should

be approximately constant over a wide range of scales. The observational dispersion in B is so large that one cannot directly test this hypothesis. Alternative explanations, which have similar degrees of plausibility, are that either the ambient pressure is approximately constant or that there is a column density through a molecular cloud, amounting to $A_v \approx 10$: these conditions actually are a consequence of the observed correlations if the clouds are in virial equilibrium. Models have been developed which require clouds to exist on the threshold of photodissociation, thereby limiting the column density to a narrow range (McKee 1988), or in a state of marginal stability to gravitational collapse, subject to a universal ambient pressure of $p/k = 10^4\,cm^{-3}\,K$ (Chieze 1987). Indeed, Elmegreen (1988) has combined the ambient pressure and internal magnetic support into a unified model of self–gravitating clouds, although attempts to apply this model to the LMC, where the scaling relations differ from those in galactic giant molecular clouds, have not had much success.

The situation with regard to the generally more massive warmer clouds, including the giant molecular clouds, is less well understood. Here the linewidths are larger (2–$5\,km\,s^{-1}$), the massive clouds are mostly very distant, and their structure is more complex. The role of energy input from the associated OB associations and embedded massive stars is extremely uncertain. If the masses of these cloud complexes considerably exceeds M_{crit}, as is suggested by the arguments of the previous section, then their linewidths cannot be attributed to internally generated Alfvén waves. If the giant clouds were magnetically coupled to the surrounding medium (Falgarone and Puget 1986), one could sustain greater Alfvén speeds, and perhaps explain the linewidths in this manner. Such a model might be appropriate if the clouds form by Parker instability, coagulating along field lines. However the correlation of the massive complexes with spiral structure argues against any dominant role for such magnetic coupling in cloud formation or structure.

What then supports the massive molecular clouds? One possibility is outflows from massive pre–main-sequence stars. Bally and Lada (1983) originally dismissed this possibility in their survey of high velocity outflows within 1 kpc of the sun. However recent observations provide a strong incentive to reconsider the earlier conclusion as unbiased surveys reveal more and more flows (Fukui *et al.* 1986; Margulis and Lada 1986). Higher resolution studies indicate the flows are more extended than previously realized (Moriarty-Schieven and Snell 1988). Mapping of the Orion molecular complex has revealed a remarkable patchwork of filaments, sheets and bubbles that is qualitatively suggestive of a cloud dynamically dominated by relic outflows (Bally, these proceedings). The only quantitative statement that can be made at present, however, comes from the results of the first unbiased (and fully sampled) studies of molecular clouds.

In the case of Mon OB1, Margulis *et al.* (1988) find between 5 and 9 flows with an aggregate momentum input of between 190 and $830\,M_\odot\,km\,s^{-1}$into this molecular cloud of mass $3 \times 10^4\,M_\odot$. The uncertainties enter because not all of the flows are unambiguous identifications of bipolar outflows and because of plausible corrections for inclination and flow lifetime that tend to increase the minimum estimates of momentum input. In order to assess the role of these flows in stirring up the Mon OB1 molecular cloud, one may simply compare the momentum injected over the momentum–dissipation time–scale t_{diss} with that required for cloud support. Since there can be several generations of flows over this time–scale, which is at least the free–fall time $\sim 5 \times 10^6$ yr, the relevant quantity to evaluate is the implied star formation efficiency of the molecular cloud. Let there

be at any given time N flows each of average momentum $\langle M_{flow} V_{flow} \rangle$ and of average duration $\langle t_{flow} \rangle$. Then if the cloud has mass M_{cloud} and linewidth ΔV, the cloud support hypothesis, assuming that momentum is conserved as the flows expand and dissipate, requires

$$N_{flow} \langle M_{flow} V_{flow} \rangle / t_{flow} = M_{cloud}\, \Delta V / t_{diss}.$$

The star formation efficiency, or the mass fraction of stars formed over the cloud lifetime t_{cloud}, is

$$SFE = \langle M_* \rangle \frac{N_{flow}\, t_{cloud}}{t_{flow}\, M_{cloud}},$$

where $\langle M_* \rangle$ is the average mass of the forming stars that drive the flows. One infers that

$$SFE = 0.03 \frac{(\langle M_* \rangle / 0.5\, M_\odot)(\Delta V / 1\, km\, s^{-1})}{(\langle M_{flow} V_{flow} \rangle / 50\, M_\odot\, km\, s^{-1})} \left(\frac{t_{cloud}/t_{diss}}{3} \right).$$

With a dissipation time–scale for the turbulence equal to the dynamical time, one obtains a cloud lifetime of $\sim 1.5 \times 10^7$ yr with star formation efficiency of 3 percent, which is consistent with observations of massive clouds, although a somewhat longer lifetime for the cloud may be preferable.

Alternatively, one can try to allow for undetected flows by utilizing the empirical correlation between flow and luminosity L of the embedded young stellar objects (YSO's) suspected of driving the flows. One may crudely fit the data on flows with $\dot{M}_{flow} V_{flow} \approx 100\, f\, L/c$, $f = O(1)$. Since $L \propto M_*^3$, this implies that the more luminous and massive YSO's play the most important role. One can integrate over the protostellar luminosity function to infer the net rate of momentum input and compare this with the cloud momentum observed, $M\Delta V$. If this integration yields a mean YSO luminosity–to–mass ratio $\langle L/M \rangle$, one obtains

$$SFE = \frac{c\, \Delta V}{100\, f\, \langle L/M \rangle\, t_{diss}} = \frac{0.002}{f} \left(\frac{100\, L_\odot/M_\odot}{\langle L/M \rangle} \right) \left(\frac{\Delta V}{1\, km\, s^{-1}} \right) \left(\frac{5 \times 10^6\, yr}{t_{diss}} \right).$$

This suggests that one could comfortably have 10 generations of flows with $\langle L/M \rangle = 10\, L_\odot/M_\odot$ (corresponding to $\langle M_* \rangle \approx 3\, M_\odot$) and support the cloud against collapse over its lifetime, ending up with a SFE of 2 percent.

There are additional complications that should be considered before any firm conclusion is reached. The flows may be deflected by inhomogeneities in the cloud or expand into lower density cavities, dumping their momentum into diffuse molecular gas and leaving the bulk of the dense molecular gas unaffected. Magnetic coupling should however play more of a role (although this is unlikely if $\dot{M}_{flow} V_{flow} \propto L$), and there may be more than one outflow episode during the lifetime of a pre–main-sequence star. However, the conclusion that massive cloud linewidths are largely due to outflows seems to be well within present uncertainties.

4. Disruption

If outflows are responsible for injecting momentum into massive clouds, one consequence is likely to be disruption. Theoretical arguments (§7) suggest that stirring by massive stars is likely to enhance rather than reduce the rate of massive star formation. Observationally, one finds that the number of H II regions increases proportionally with molecular cloud mass.

Other forms of energy input into molecular clouds by massive stars include main sequence winds, ionization fronts and supernova explosions. These probably arise too late to have had a large impact on observed clouds, which are younger than the adjacent OB associations whose nuclear turn–off ages are $\sim 3 \times 10^7$ yr. However these processes must play important roles in the late stages of cloud disruption. For example, a molecular cloud of mass M produces ~ 5 (SFE/0.01)(M/10^5 $M_\odot$) Type II supernovae, but only at a rate of 10^{-7} yr^{-1}. Disruption by ionization is probably the most important of these effects. It is most efficient via the "champagne" effect, with cavities being progressively excavated in the low density regions of the molecular clouds. Analytic estimates (Whitworth 1979 and Larson 1988) and simulations (Tenorio-Tagle *et al.* 1979) indicate that for a standard initial mass function, a SFE of about 5 percent is required for destruction of a molecular cloud. Allowance for clustering of the stars increases this by up to a factor of 2 (McKee 1982). This is rather high, and it may be either that predominantly massive stars are formed once OB star formation is initiated, a possibility discussed in the next section, or that pre–main-sequence outflows provide a more efficient destruction mechanism.

5. Efficiency

A critical role in the preceding discussion of cloud support and disruption is played by the SFE. It is helpful to define this in two ways. The *local* SFE refers to any individual molecular cloud, and is the mass in stars and long–lived dense stellar remnants at the end of the cloud's lifetime, relative to the initial gas mass of the cloud. In terms of the instantaneous star formation rate (SFR) in the cloud, which of course includes the short lived massive stars as well as the long lived low mass stars, we have

$$\mathrm{SFE} = (1 - \mathrm{R}) \frac{\mathrm{SFR}}{\mathrm{M_{cloud}}} \tau_{\mathrm{cloud}}$$

where τ_{cloud} denotes the cloud lifetime and $\mathrm{M_{cloud}}$ its mass. R is the mass fraction returned to the interstellar medium by massive stars and presumed to be retained in the cloud: for a solar neighborhood initial mass function, R = 0.4. To obtain the *global* SFE for the galactic disk, we replace τ_{cloud} by $\tau_{\mathrm{dynamical}}$, the time–scale appropriate for build–up of molecular clouds and also for triggering OB star formation; SFR now denotes the galactic star formation rate.

The observed efficiency in molecular clouds where OB stars have formed is between 1 and 3 percent. In cold cloud cores, it is higher, the most extreme nearby example being the ρ Oph core, where the SFE exceeds 20 percent (Lada and Wilking 1984). However, such SFE's are unrepresentative of larger–scale complexes: for example in Taurus–Auriga, the cold cores which have formed low mass stars with 5–10 percent efficiency only amount to a small fraction of the total gas mass. This indeed means that there must be several

generations of cold cores in a dark cloud complex of this size in order to end up with a low mass SFE of one percent. One consequence is that there should be a spread in the ages of low mass pre–main-sequence stars in associations, as a relic of such a history of early star formation. This age spread, which should amount to $\gtrsim 10^7$ yr, may manifest itself in the distribution of rotation velocities of T–Tauri stars (Hartmann *et al.* 1986), as well as in the occurrence of low mass stars above the main sequence in young star clusters (Stauffer *et al.* 1984; Stauffer and Hartmann 1987). The SFE is also inferred to be 20–40 percent in order to form a bound star cluster: again the presumption is that these are relatively rare, with most stars forming in expanding associations.

The global SFE for the galactic disk is, not surprisingly, similar to the local SFE. We estimate it by taking the galactic SFR to be $(3-5)\,M_\odot\,yr^{-1}$ and the mass of atomic and molecular gas to be $(4-6)\times 10^9\,M_\odot$. For a dynamical time appropriate to 4 kpc galactocentric distance, where the bulk of the molecular gas is located, namely 6×10^7 yr, the global SFE = 2 – 4 percent, suggesting that a mean cloud lifetime is $\sim 4\times 10^7$ yr, and hinting that the SFE may be marginally higher in the inner galaxy than in the solar neighborhood.

I shall subsequently adopt a mean galactic SFE of $3(\pm 1)$ percent. There is an immediate problem, recently quantified by Sandage (1986). The gas will be exhausted in τ_{dyn}/SFE or $\lesssim 3\times 10^9$ yr. In fact, this is the e–folding time for the gas mass to decrease in a closed system where the only gas sink is due to star formation with a standard IMF (R = 0.4). The gas amounts to at least 10 percent of the mass of the galactic disk, and so the age of the disk should be about 7.5×10^9 yr, an uncomfortably short age. The disk is generally believed to be between 10 and 12 billion years old, so that one might be able to have enough gas survive if the SFE is 1 or even 1.5 percent. While this low a global SFE can probably not be excluded, there is a further argument which suggests a serious deficiency in the assumptions of the model. We would have to be living at a very special epoch in the universe if our galaxy were just on the verge of being exponentially depleted of gas. It would then be difficult to understand why most luminous disk galaxies in the field are gas–rich. The implication is that one of the simple model assumptions is wrong: either the galaxy is not a closed system, so that gas infall replenishes the gas surplus, or else the IMF is biased towards massive stars, so that $R \approx 1$.

I will not consider possible gas infall here, because the evidence for infall in a sufficient amount to alleviate the gas exhaustion problem, $\sim 3\,M_\odot\,yr^{-1}$, is extremely uncertain. However the possibility that the mean galactic value of R is very different from the value observed locally merits being taken seriously, particularly in view of the implications for the rate of massive star formation.

6. Massive Star–Enhanced Star Formation

In the inner spiral arms of our galaxy, where the bulk of galactic star formation is occurring, we directly observe only massive star formation. If the IMF were deficient in low mass stars, we would not detect such a shortfall. To increase R significantly, to say 0.9, one has to truncate the IMF below $(2-4)\,M_\odot$. Most of our information about the IMF is based on measurements in the solar neighborhood, where we observe only the current rate of massive star formation as well as the time–integrated production of low mass stars. The massive SFR could have been much higher during the first several 10^9 yr of

the galactic disk. Even with regard to observations of nearby molecular clouds, we know that there are regions of exclusively low mass star formation, such as Taurus–Auriga, and regions where both massive and low mass stars are forming contemporaneously, as in Orion. Such questions as whether massive star formation is an inevitable consequence of low mass star formation in a given cloud, and whether massive stars can form without accompanying low mass star formation, have not yet been answered from studies of galactic molecular clouds and stellar associations.

It has been proposed that exclusively massive star formation is occurring in the inner spiral arms of our galaxy (Güsten and Mezger 1983). This result is motivated by the radial distribution of molecular gas and of massive star formation. However the inference that low mass star formation is suppressed in the spiral arms is indirect, and dependent on the slope and upper mass adopted for the IMF. Scalo (1987) argues that there is little necessity to invoke *spatially* bimodal star formation to account for the observations of galactic star formation, and the indirect consequences of a contemporaneous bimodal model, including radial abundance gradients and lowered gas consumption rate, are not unique to this model.

Larson (1986) argues that star formation is *temporally* as well as spatially bimodal, with the massive star forming mode dominating in the first 2 billion years or so of the galactic disk. This provides a solution to the G dwarf problem (the solar neighborhood naturally being deficient in metal–poor stars), and allows a high star formation rate in the inner galaxy while being consistent with the mass inferred from the galactic rotation curve. It is not unique, of course: for example, the star formation rate could be oscillatory, as in a bursting model. There are several potential problems with this model, including the possible overproduction of white dwarfs and of heavy elements. However, parameters can be adjusted (white dwarf cooling times, upper mass cut–off in the IMF at $\sim 20\,M_\odot$ instead of $100\,M_\odot$ in the massive star mode) to make the model acceptable. The bimodal model does account for the history of iron production in the disk, for the variation in mass–to–light ratio between spirals and luminous ellipticals, and for the large dispersion in radio galaxy colors at modest redshift (Wyse and Silk 1987), which otherwise suggests that intense star formation has occurred uncomfortably recently in many giant ellipticals if the IMF is unchanging in time and if the remote radio galaxies are the counterparts of the nearby ellipticals.

There is evidence in starburst galaxies that the IMF is truncated at low masses. A starburst may be defined as a greatly elevated ratio of star formation rate to gas mass in the star–forming region. One could achieve a starburst by enhancing the SFE by an order of magnitude or more above the galactic value of ~ 3 percent. It seems difficult to achieve a SFE of more than about 10 percent, however, when massive stars form, because of the disruption of molecular gas clouds by the ionizing photons from OB stars, as well as energy input from winds and supernova explosions. Formation of exclusively massive stars should not lower the global SFE very much, because there is now time for several generations of massive star formation over the local dynamical time–scale. The gas is still used up, in forming remnants of massive stars, over the duration of the burst. Nevertheless, the effect of a high returned fraction ($R = 0.9$, say) allows a substantially higher SFR (itself proportional to $(1 - R)^{-1}$.

Evidence for a truncated IMF has been found for the well–studied case of M82, where the inner 600 pc has been undergoing a starburst over the past 3×10^7 yr, and in a variety of other galaxies, including NGC 253, Mk 171, IC 2153, I Zw 36, ESO 338–IG04,

NGC 6240, and Arp 220, as reviewed by Scalo (1987). The SFE, defined in terms of the observed SFR, is, when corrected for the large returned fraction, not greatly different from the galactic value. The high SFR per unit gas mass means, however, that even with $R \approx 0.1$, the gas is exhausted within 10^9 yr or less, so that this high SFR cannot be sustained continuously. To enhance the SFR, in addition to increasing R, one also has to increase the amount and rate of supply of gas. A simple model for starbursts will be presented below: first, however, I address the issue of a physical mechanism for truncation of the IMF at the low mass end, thereby allowing bimodal star formation.

7. Mechanisms for Bimodal Star Formation

The relevant issue for bimodal star formation is how the minimum stellar mass in a star-forming region is determined. One approach has appealed to consideration of gravitational instability, utilizing an estimate of the Jeans mass. The opacity-limited Jeans mass reaches a minimum value of $\sim 0.01\,M_\odot$ in hierarchical fragmentation during quasi-spherically symmetric dynamical collapse, but the relevance of this to realistic fragmentation is unclear, numerical simulations lacking sufficient dynamical range to provide a satisfactory test. An alternative approach attempts to apply linearized gravitational instability calculations to molecular clouds in order to estimate clump masses. The most rapidly growing scale is again, to within numerical factors,the Jeans mass and is proportional to $T^2P^{-1/2}$, but now applies to a variety of geometries (sheets, filaments) and to non-thermal support (turbulence, magnetic fields), provided that T is suitably generalized (using ΔV or V_A) (Larson 1985). Non-linear collapse is initiated, subject to a given external pressure, at a similar scale. What is not clear, however, is the relation between the final stellar mass and molecular cloud parameters. Angular momentum is evidently a limiting factor, as is the coupling with the magnetic field which transfers angular momentum from the core to the cloud envelope. This certainly sets the scale of the dense clump from which a protostar forms, but the ultimate determinant of protostar mass is likely to involve the interaction of the protostellar wind with the accreting envelope. Indeed, the dense cores in which low mass stars form are directly observed in some cases to be dispersed by outflows (Mathieu *et al.* 1987; Myers *et al.* 1988).

An estimate of the typical stellar mass can be made from the following argument. A collapsing cloud tends to non-homologously develop a quasi-isothermal core. The accretion rate $\dot{M} \sim (\Delta V)^3/G$ in such a cloud core with velocity dispersion ΔV regulates the growth of the protostellar core and the protostellar luminosity (Shu 1977). Interpretation of the clustering of T-Tauri stars near a "birth-line" in the H-R diagram for a suitable choice of $\dot{M}$ lends support to a simple model according to which deuterium burning is identified with triggering the convective phase that heralds the optically visible emergence of protostars (Stahler 1988). To incorporate magnetic field-limited collapse, one can naively replace ΔV by the Alfvén velocity. Rotation is assumed to not be a limiting factor in modulating the accretion rate via disk formation: the empirical birth-line may justify this assumption. To determine the stellar mass, one has to specify a duration for the accretion phase. The mechanism for initiating a protostellar wind is poorly known: speculations span the range from initiation of convection at the onset of deuterium burning coupling with the excess angular momentum of the differentially rotating core to drive a dynamo which in turn powers a wind (Shu and Terebey 1984) to magnetically

(Uchido and Shibata 1984) or centrifugally (Pudritz and Norman 1986) driven outflows associated with disk formation. Common to all mechanisms, however, is the requirement for a central core to have formed.

The time–scale for core formation is the Kelvin–Helmholtz contraction time, and this must give a rough estimate of the time elapsed before the protostellar outflow phase gets underway. Thus I estimate a typical protostellar mass to be very approximately given by $M_* \approx \dot{M} t_{KH}$. To evaluate this expression, I take $t_{KH} = GM_*^2/R_*L$, with

$$L = \frac{64\pi}{3} \frac{M_*}{\kappa p_*} \sigma T_*^4 \frac{d \ln T_*}{d \ln p_*},$$

where κ is the Rosseland mean opacity, T_* is the core temperature at the onset of the outflow phase, which is plausibly identified with the D ignition temperature ($\sim 10^{6\circ}$ K) for $M_* \lesssim 2 M_\odot$, R_* is the effective radius, and p_* the interior pressure. For a polytropic model with index 3/2, appropriate to a convective protostar, one has $p = c_p GM^2/R^4$, $\rho = c_\rho M/R^3$, $T = c_T GMm/kR$, with $c_p = 0.77$, $c_\rho = 1.43$, $c_T = 0.54$ and mean molecular weight $m = 0.62\, m_H$. Taking $\kappa = \kappa_o \rho T^{-7/2}\, cm^2\, g^{-1}$ with $\kappa_o = 1.5 \times 10^{24}$, one obtains

$$M_* = 4.1(\Delta V/km\, s^{-1})^{3/5}(T_*/10^6\, K)^{1/10}\, M_\odot.$$

For cold cores in dark clouds, $\Delta V \approx 0.1\, km\, s^{-1}$ and $M_* \approx 1 M_\odot$, while in massive molecular clouds with $\Delta V \approx 3 - 5\, km\, s^{-1}$, $M_* \approx 8 - 10 M_\odot$. This critical mass motivates the rationale for bimodal star formation (*cf.* also Palla 1988). Dimensionally (if not conceptually) equivalent derivations of a critical protostar mass that distinguish massive cores dominated by gravitational free–fall from low mass cores undergoing quasi–hydrostatic contraction can be traced back to a pioneering paper by Gaustad (1963).

8. Global Star Formation and Starbursts

A simple model for the global star formation rate is given by

$$SFR = \frac{SFE}{1 - R} \frac{M_{gas}}{\tau_{dyn}}. \qquad (1)$$

The motivation for this comes from consideration of non–axisymmetric perturbations of a disk, necessary to drive angular momentum transfer involved in radial gas flows and responsible for spiral density wave propagation. A marginally unstable disk is heated by gravitational instabilities and cools by gas dissipation and star formation, maintaining $Q \equiv \kappa\sigma/\pi G\mu \approx 1$ where σ is the disk velocity dispersion and κ is the epicyclic frequency. The instability growth rate is $\kappa Q^{-1} \sim \tau_{dyn}^{-1}$. One can apply (1) to grand design spirals by replacing τ_{dyn}^{-1} by $\Omega(r) - \Omega_p$, where Ω_p is the pattern frequency, or to flocculent spirals by setting $\Omega_p = 0$. A similar formula, with $SFR \to \dot{\mu}_{H_2}$ and $M_{gas} \to \mu_{HI}$, describes the agglomeration of molecular cloud complexes, and successfully accounts for the radial H_2 distributions observed in nearby spiral galaxies (Wyse 1986). Global successes of the model for the SFR include production of metallicity gradients in disks, the increase of Ω ($\gtrsim r^{-1}$) in the inner regions enhancing star formation and metal production, and chemical evolution with disk age, the enhanced early rate of star formation being a simple consequence of the proportionality of SFR to gas surface density (Wyse and Silk

1987). Bimodal star formation with $R \approx 0.9$ during the first 2–3 billion years provides an explanation of the paucity of metal–poor dwarfs, and allows an ample gas supply to survive to the present epoch, especially if it prevails today in the inner spiral arms.

To obtain a starburst, inspection of equation (1) suggests that there are essentially three limiting factors. One can increase R to ≈ 0.9, or alternatively, increase the SFE by an order of magnitude. A massive star–dominated IMF must necessarily form stars at low SFE because of the energy feedback produced by the ionizing photons, winds and supernova explosions. In rare regions (cold clouds, formation of bound clusters) where incidentally $R \approx 0.4$, the SFE is known to exceed 20–40 percent, and this could be the situation in starbursts. The young globular clusters in the LMC may be examples of such activity. One additional uncertainty which would allow higher SFE in a bimodal model is that the IMF might also be truncated at the upper end: with considerable uncertainty this has been inferred for the starburst galaxies M82 and NGC 253 at $\sim 20\,M_\odot$ (Rieke 1988), and in the M83 spiral arms at $\sim 10 - 15\,M_\odot$ (Jensen *et al.* 1981). Interestingly, the bimodal hypothesis requires an upper mass cut–off in this range in order to avoid excessive metal production.

The remaining factors that limit the SFR are the gas surface density and the dynamical time–scale. In a gas–rich disk, $\mu_{\rm gas}$ can be increased by an order of magnitude relative to its value in our galaxy before it dominates the local gravity. In the inner regions of a disk, the dynamical time is an order of magnitude shorter at, say, 1 kpc galactocentric radius, and the surface density is enhanced by an additional order of magnitude. This suggests that one would expect to find a starburst occurring within the inner kpc, and to be triggered by a high gas surface density. The extreme starburst galaxy Arp 220 is a good example: the SFR is about $200\,M_\odot\,yr^{-1}$ for stars above $2\,M_\odot$ within the central kpc, where $\mu_{\rm gas} \sim 7000\,M_\odot\,pc^{-2}$ (Scoville 1988).

A more useful comparison involves the ratio L_{IR}/L_B, which measures the rate of current star formation to the past average SFR over $\sim 3 \times 10^9$ yr. This ratio is enhanced by a factor $\lesssim 3$ in starbursts associated with central bars, by 10–30 in tidally interacting systems, and by ~ 100 in systems that are undergoing mergers or contain AGN (Soifer *et al.* 1987). One understands this circumstantial evidence as follows: mergers and tidal interaction are driving radial gas flows, the mergers resupplying the gas, and swing amplification of non-axisymmetric gravitational instabilities (Toomre 1981) triggers the central starburst. Bars are presumed to represent the late phase of a merger, and the non–circular motions drive gas flows that help transfer angular momentum outward and drive gas into the central region (Combes 1988). One inference from numerical simulations is that once sufficient gas inflow occurs that gas self–gravity is important, the gas coagulation processes are greatly enhanced. Studies of molecular emission from M82 have shown that the pressure of the molecular gas is elevated by up to two orders–of–magnitude relative to that in galactic giant molecular clouds. Since for self–gravitating clouds, $p \sim G\mu^2$, this implies that $\mu_{\rm gas}$ is enhanced, thereby providing one of the necessary ingredients for the observed starburst. Of course, not all starbursts are nuclear, nor are all closely interacting galaxies undergoing starbursts. Nor is the role of the AGN clear: in extreme starbursts, as much as 50 percent of the infrared luminosity is attributed to the AGN. It is not known whether the AGN drives the starburst or whether the gas flow fuels both the starburst and the AGN.

9. Summary

Dynamical evolution of molecular clouds is governed by density–wave stimulated growth. Cloud support and disruption are plausibly governed by outflows. Magnetic support plays an important role for the less massive clouds, and a major contributor to giant cloud disruption is the ionizing photon output from massive stars. The star formation efficiency is about 3 percent, averaged either over the lifetime of a massive cloud or over a dynamical time–scale. Allowance for the gas fraction returned by massive stars means that even in extreme starbursts, the SFE need not greatly exceed the galactic value. In these galaxies, there are persuasive, if not conclusive, arguments that the IMF is truncated below several $M_\odot$, leading to a returned fraction as high as 90 percent. Bimodal star formation may have occurred in our own galaxy over the first 2–3 billion years, based on circumstantial arguments pertaining to chemical evolution. While the case for ongoing bimodal star formation in regions of vigorous star formation activity is weaker, one can still argue that predominantly low mass stars form in dark clouds while massive stars, possibly accompanied by low mass stars, form in massive molecular clouds. It would be of considerable interest to ascertain whether low mass star formation inevitably accompanies massive star formation to the extent inferred from the local IMF: the inference from starbursts is that it need not. Starbursts may be described by a simple model which allows either the SFE or the returned fraction, the gas surface density, and the rate of gas supply to increase. Plausible enhancements by an order of magnitude in each factor suggest that the most extreme starbursts undergone by a massive galactic disk should result in a SFR of order $10^3\,M_\odot\,yr^{-1}$. Such starbursts could be sustained for up to SFE^{-1} dynamical times, or 10^8 yr for a nuclear starburst, before the gas supply is depleted. This suffices to make a substantial fraction of a galactic mass.

Acknowledgements. I gratefully acknowledge many discussions on these topics with R.F.G. Wyse. Useful input was also provided by C. Lada. This research has been supported in part by grants from NASA and NSF.

References

Bally, J. and Lada, C.J. 1983, *Ap. J.*, **265**, 824.
Casoli, F. and Combes, F 1982, *Astr. Ap.*, **110**, 287.
Chieze, J.-P. 1987, *Astr. Ap.*, **171**, 225.
Combes, F. 1988. In *Galactic and Extragalactic Star Formation*, eds. R. Pudritz, M. Fich (Dordrecht: Kluwer), L75.
Elmegreen, B.G. 1988, preprint.
Falgarone, E. andPuget, J.-L. 1986, *Astr. Ap.*, **162**, 235.
Fukui, Y. *et al.* 1986, *Ap. J.*, **311**, 285.
Gaustad, J.E. 1963, *Ap. J.*, **138**, 1050.
Güsten, R. and Mezger, P.G. 1983, *Vistas in Astron.*, **26**, 159.
Hartmann, L. *et al.* 1986, *Ap. J.*, **304**, 275.
Jensen, E.B., Talbot, R.J. and Dufour, R.J. 1981, *Ap. J.*, **243**, 716.
Kwan, J. and Valdes, F. 1987, *Ap. J.*, **315**, 92.
Lada, C.J. and Wilking, B.A. 1984, *Ap. J.*, **287**, 610.
Larson, R. 1985, *M.N.R.A.S.*, **214**, 374.
Larson, R.B. 1986, *M.N.R.A.S.*, **218**, 409.
Larson, R. 1988. In *Galactic and Extragalactic Star Formation*, eds. R. Pudritz, M. Fich (Dordrecht: Kluwer), 459.
Margulis, M. and Lada, C.J. 1986, *Ap. J.*, **309**, L87.
Margulis, M., Lada, C.J., and Snell, R.L. 1988, *Ap. J.*, in press.

Mathieu, R.D. *et al.* 1988, *Ap. J.*, **330**, 385.
McKee C.F. 1988. Preprint.
Moriarty–Schieven, G.H. and Snell, R.L. 1988 *Ap. J.*, in press.
Myers, P.C. 1983, *Ap. J.*, **270**, 105.
Myers, P.C. and Goodman, A.A. 1988, *Ap. J.*, **326**, L27.
Oort, J.H. 1954. In *The Formation and Dynamics of Galaxies*, ed. J.R. Shakeshaft (Dordrecht: D. Reidel), 375.
Pudritz, R.E. and Norman, C.A. 1086, *Ap. J.*, **301**, 571.
Rieke, G. 1988. In *Galactic and Extragalactic Star Formation*, eds. R. Pudritz, M. Fich (Dordrecht: Kluwer), 561.
Roberts,W.W. and Stewart, G.R. 1987, *Ap. J.*, **314**, 10.
Sandage, A. 1986, *Astr. Ap.*, **161**, 89.
Scalo, J. 1987. In *Evolution of Galaxies*, ed. J. Palous (Prague: Astronomical Institute), 101.
Scoville, N. 1988. In *Galactic and Extragalactic Star Formation*, eds R. Pudritz, M..Fich (Dordrecht: Kluwer), 541.
Shu, F.H. 1977, *Ap. J.*, **214**, 488.
Shu, F.H. and Terebey, S. 1984. In *Cool Stars, Stellar Systems and the Sun*, eds. S. Baliunas, L. Hartmann (Berlin: Springer Verlag), 78.
Soifer, B.T. *et al.* 1987, *Ann. Rev. Astr. Ap.*, **25**, 187.
Solomon, P.M. and Rivolo, A.R. 1987. In *The Galaxy*, eds. G. Gilmore, B. Carswell (Dordrecht: D. Reidel), 105.
Stahler, S.W. 1983, *Ap. J.*, **274**, 822.
Stahler, S. 1988. Preprint.
Stauffer, J.R. *et al.* 1984, *Ap. J.*, **280**, 202.
Stauffer, J.R. and Hartmann, L.W. 1987, *Ap. J.*, **318**, 337.
Tenorio–Tagle, G. *et al.* 1988, *Ap. J.*, **330**, 385.
Toomre, A. 1981. In *Structure and Evolution of Normal Galaxies*, eds. S.M. Fall, D. Lynden–Bell (Cambridge: Cambridge University Press), 111.
Uchida, Y. and Shibata, K. 1984, *P.A.S.J.*, **36**, 105.
Vogel, S.N., Kulkarni, S.R. and Scoville, N.Z. 1988, *Nature*, **334**, 402.
Whitworth, A. 1979, *M.N.R.A.S.*, **186**, 59.
Wyse, R.F.G. 1986, *Ap. J.*, **311**, L41.
Wyse, R.F.G. and Silk, J. 1987, *Ap. J.*, **319**, L1.

MAGNETIC FIELDS IN MOLECULAR CLOUDS: REGULATORS OF STAR FORMATION

Telemachos Ch. Mouschovias
University of Illinois at Urbana-Champaign
Departments of Physics and Astronomy
Urbana, IL 61801, U. S. A.

ABSTRACT

Magnetic fields cause relatively violent behavior in diverse astrophysical systems. Yet they also mitigate would-be violent behavior. Although they destabilize the interstellar medium on scales ~ 1 kpc and lead to the formation of clouds, they also provide effective support against the self-gravity of interstellar clouds. On the one hand they allow gravitational contraction of clouds and star formation to take place by redistributing angular momentum (*magnetic braking*). Yet, on the other hand, they transform the would-be violent gravitational collapse of interstellar clouds to an almost quasistatic, but still rapid, contraction of their cores which often endures to densities > 10^8 cm^{-3}; this is achieved by a well controlled redistribution of mass in the central flux tubes of clouds (*ambipolar diffusion*). We show that *magnetic fields also unavoidably introduce a natural length scale in cloud interiors.* The *typical* mass inside this length scale is ~ 1 $M_\odot$ which, deprived of effective magnetic support due to ambipolar diffusion, contracts relatively rapidly, while the surrounding envelope is much better supported by magnetic forces. *Hence, magnetic fields may also play a crucial role in the determination of the initial (stellar) mass function* as they tend to inhibit accretion of the envelope onto a protostellar core. These quantitative results and the star formation scenario that they suggest are qualitatively different from current ideas concerning star formation in nonmagnetic clouds or in cores which have lost their magnetic support. The latter ideas *postulate* the *absence* of any characteristic length (or protostellar mass); we prove its existence and calculate its precise magnitude.

A new analytical determination of the ambipolar diffusion time scale, including the effect of thermal pressure, is given for both quasistatic and dynamical contraction of cloud cores, and the expected reduction of the flux-to-mass ratio is re-examined in light of these results.

I. INTRODUCTION

a) The Wide Front of Contact Between Theory and Observations

Observations of interstellar magnetic fields have been reviewed recently and have been compared with theoretical predictions (Heiles 1987; Mouschovias 1981, 1987a). Remarkable agreement is found between theory and observations concerning (1) the alignment of cloud complexes, OB associations, and giant H II regions like "beads on a string" separated by regular intervals ~ 1 kpc along spiral arms; (2) the enhancement of synchrotron radiation in spiral arms relative to the interarm region; (3) the relatively small variation of the intensity of synchrotron radiation along a spiral arm; (4) the relation between the magnetic field strength (B) and the gas density (ρ) in self-gravitating clouds; (5) the rate of rotation of H I and molecular clouds as well as that of their dense cores; (6) the support of extended cloud envelopes against self-gravity; (7) the retrograde rotation of some fragments in molecular clouds; (8) angular velocities of some dense fragments near or even above breakup; (9) the variation of the width of spectral lines with size of the observed object; (10) the narrowing and eventual thermalization of the

widths of molecular lines sampling regions of progressively larger density in one and the same cloud; (11) the existence of a single maximum in the period distribution of binary stars (as opposed to two peaks corresponding to short period spectroscopic binaries and wide visual pairs); (12) the rotational velocities of spectral type O5 - F5 main-sequence stars; and (13) the ease with which binary (and multiple) star systems can form, as opposed to single stars. The observational confirmation of so many theoretical predictions and the theoretical explanation of numerous previously unexplained observations coupled to the absence of a single contradiction between theory and observations leave little doubt that magnetic fields play a crucial role in star formation.

We summarize first in § II the key elements of the scenario for star formation in magnetic clouds presented recently (Mouschovias 1987a), which accounts for the results of the most recent calculations and observations and which thus represents a refinement of the original scenario proposed a decade ago (Mouschovias 1977, 1978). New quantitative results are presented which necessitate significant qualitative changes in current ideas concerning star formation in molecular clouds and, more specifically, in the notion that stellar masses are determined by the stars themselves *via* the onset of energetic stellar winds that reverse the infall of the envelopes. Then in § III we concentrate on the role of ambipolar diffusion in star formation. We obtain new expressions for the ambipolar diffusion time scale in cloud cores for both quasistatic and dynamical contraction and use them to study the reduction of the flux-to-mass ratio by ambipolar diffusion.

Since a new, potentially significant measurement of the magnetic field strength in the molecular cloud *Barnard 1* has been presented at this meeting (Goodman *et al.* 1988), we first compare this observation with theoretical predictions. Since, also, the role of magnetic fields in explaining quantitatively the supersonic widths of molecular lines has not been widely accepted yet, we summarize the theory and the observational evidence immediately below.

b) Theoretical Predictions and Recent Observations

The OH Zeeman observation presented by Goodman *et al.* has detected a magnetic field strength of 27 ± 4 μGauss in *Barnard 1*, where the number density is estimated to be $n \simeq 10^3$ cm^{-3}. In order to compare with theory, we use Mouschovias' (1976b) relation (which is a simple approximation but an approximation nevertheless to the exact result) between the field strength and the gas density in the cores of *self-gravitating* clouds with *frozen-in* fields, namely,

$$\frac{B_c}{B_0} = \left(\frac{\rho_c}{\rho_0}\right)^{\kappa}, \qquad \kappa = \frac{1}{2}, \tag{1a}$$

where the quantity ρ_0 is the gas density at which gravitational forces become comparable to magnetic forces and significant contraction perpendicular to field lines begins. Converted to a number density of *protons* (n_0), it is approximately given by

$$n_0 \simeq 137 \left(\frac{{B_0}^3}{M}\right)^{1/2}, \tag{1b}$$

where B_0, which is expected to be only slightly larger than its galactic value $\simeq 3$ μGauss, is measured in *microgauss* and the cloud's mass M in *solar masses* (see brief review by Mouschovias 1985). Equation (1b) yields a density range $n_0 \simeq 1$ - 320 cm^{-3} for $B_0 = 3$ μGauss and for M in the corresponding range 5×10^5 - 5 $M_\odot$. The slope κ is essentially zero below the density n_0 and becomes equal to 1/2 above n_0; the value $\kappa = 1/2$ corresponds to establishment of force balance *along* field lines, with gravitational contraction taking place only as rapidly as magnetic forces (perpendicular to the field lines) may allow. (For the spatial variation of κ within a cloud and its physical explanation, see Mouschovias 1978, § IIIa2.)

Using a mass of $\simeq 10^3$ $M_\odot$ for the (whole) cloud observed by Goodman *et al.*, equation (1b) yields $n_0 = 22.5$ cm^{-3}, and equation (1a) predicts a field strength $B_c = 28.3$ μGauss. This is in excellent agreement with the measured value of 27 ± 4 μGauss. This comparison, however, assumes that the full strength of the field is measured by the Zeeman observation. If, instead, there is a comparable component of the field perpendicular to the line of sight, then the excellent agreement between the predicted and measured field strength can be maintained only if either B_0 is somewhat larger than 3 μGauss or the mass of the whole cloud is larger than the estimated $M \simeq 10^3$ $M_\odot$, or both $B_0 > 3$ μGauss and $M > 10^3$ $M_\odot$.

In order to understand how the above theoretical result has unique implications on molecular line widths and their often observed virialization in magnetically supported clouds, we combine equations (1a) and (1b) and the definition of the Alfvén speed [$v_A \equiv B/(4\pi\rho)^{1/2}$] to find that

$$v_A \simeq 1.7 \left[\frac{B_0}{3\ \mu G}\ \frac{M}{10^4\ M_\odot}\right]^{1/4} \quad \text{km s}^{-1}, \tag{2a}$$

where, as above, B_0 is the field strength at the stage at which the gravitational energy of the cloud became comparable to its magnetic energy, and M is the total mass of the cloud. (Note that B_0 is not independent of M; the two quantities are related through equation [1b]. Note also that v_A is remarkably insensitive to the values of physical quantities characterizing a cloud up to the stage at which rapid ambipolar diffusion sets in; recall that equation [1a] is valid only under flux freezing or very slow ambipolar diffusion.) Since the field B_0 is certainly expected to be at least as large as the background field (i.e., $B_0 > 3$ μG) and since the *total* mass of a molecular cloud is seldom less than 10^3 $M_\odot$, it follows that the Alfvén speed is greater than or equal to the speeds implied by observed line widths after subtraction, wherever appropriate, of the contribution of systematic motions, such as rotation and outflow or inflow. It is always the case (for magnetically supported, self-gravitating clouds) that the value of v_A given by equation (2a) is consistent with

$$v_A \simeq \left[\frac{GM}{R}\right]^{1/2} \simeq (\pi G\sigma R)^{1/2} \simeq v_{ff}, \tag{2b}$$

where $\sigma = M/\pi R^2$ is the column (or, surface) density, and v_{ff} is the free-fall speed. It is clear from equation (2b) that virialized line widths are *naturally* expected in such clouds. *In other words, the motions responsible for the "unusually large" line widths are most likely long-wavelength hydromagnetic waves, which resemble large-scale oscillations (translational or rotational) within a cloud* (Mouschovias 1975b) *and which damp essentially on the ambipolar diffusion time scale.* The trapping and damping of these disturbances within fragments (or cores) and in the envelopes of molecular clouds have important observational consequences, aside from causing the observed spectral line widths, some of which were summarized in Mouschovias 1987a (§ 2.2.3) and 1987b.

The so-called "turbulence law" (Larson 1981; Myers 1985), namely, that the velocity dispersion Δv (as reflected by line widths) in a few tens of clouds varies as $\Delta v \propto R^{1/2}$, is thus seen from equation (2b) to have nothing to do with turbulence. It is a natural consequence of magnetic support of clouds having comparable surface densities σ. Also, the issue emphasized by Myers (1985, p.95) as an unexplained consequence of the so-called "condensation law" $\rho R \simeq const$ of Larson (1981), namely, that cloud surface densities seem to vary by less than a factor ~ 10, finds a natural explanation in this picture. Simply, self-gravitating clouds are expected to have surface densities comparable to σ_{crit}, given by equation (3b), which depends only on the mean field strength $\langle B \rangle$, which in turn is not expected to vary much from place to place in the interstellar medium under conditions suitable for the formation of self-gravitating clouds. It follows, therefore, that σ $(= 4\rho R/3) \simeq const$, but only to the extent that $\langle B \rangle \simeq const$ for different self-gravitating clouds.

II. SUMMARY OF THE SCENARIO FOR STAR FORMATION

The schematic diagram on the following page summarizes the key elements of the scenario for star formation recently described elsewhere in detail (see Mouschovias 1987a). A dashed line in the diagram signifies a possible but unlikely evolutionary path. *Collapse* means indefinite contraction, but not necessarily free fall.

Cloud Formation and Early Evolution. The most likely mechanism responsible for the formation of interstellar clouds and cloud complexes is the Parker (1966) instability triggered in the galactic disk by spiral density waves or by any other large-scale disturbance (Mouschovias 1974, 1975a; Mouschovias, Shu, and Woodward 1974; Shu 1974; Blitz and Shu 1980). The thermal instability (Field 1965) and the Jeans instability (Jeans 1928) cannot be responsible for the formation of typical clouds (see detailed discussion in the review by Mouschovias 1981, § 4). Regardless of the nature of this mechanism, its significance stems mainly from the fact that the mechanism determines the distribution of forces (such as gravitational, magnetic, thermal, and centrifugal) within a cloud. Soon after a cloud's formation, thermal-pressure and centrifugal forces lose memory of initial conditions. The temperature of an H I cloud is determined by the cloud's environment (heat input by ionizing cosmic rays and X-rays) and by its local density and composition (heat losses through collisional excitation of elements such as C II, and heat input through photoelectric emission from grains). Also, H I clouds are predicted to be in nearly synchronous galactocentric orbits ($\Omega \sim 10^{-15}$ rad s^{-1}) (see Mouschovias 1977). The differential mass-to-flux ratio $[dm(\Phi)/d\Phi)]$ determines the relative magnitude of gravitational and magnetic forces, and affects crucially the subsequent evolution of a cloud. One can obtain reasonable theoretical estimates for this function, but no observational determination exists as yet. Observations such as those by Bregman *et al.* (1983) and by Schwarz *et al.* (1986) should be pursued most vigorously if this important quantity is to cease to be treated as a free parameter by theoretical calculations.

For a cloud to collapse, its mass-to-flux ratio must exceed a critical value given by (see Mouschovias and Spitzer 1976)[1]

$$M_{\rm crit} = \frac{0.53}{3\pi}\left(\frac{5}{G}\right)^{1/2}\Phi_{\rm B} = \frac{0.126}{G^{1/2}}\Phi_{\rm B} \simeq \left(\frac{1}{63G}\right)^{1/2}\Phi_{\rm B}\,. \tag{3a}$$

This is also equivalently written in terms of a critical mean column density of matter, commonly referred to as *surface density*, as

$$\langle\sigma\rangle_{\rm crit} = \left(\frac{1}{63G}\right)^{1/2}\langle B\rangle = 2.4\times10^{-2}\,\frac{\langle B\rangle}{50\ \mu G}\quad {\rm g\ cm^{-2}}, \tag{3b}$$

where, with R being the cloud radius, $\sigma \equiv M/\pi R^2$. Other forms of this equation, for example, in terms of a critical visual extinction, are given in Mouschovias (1987a). *It follows from equation (3b) that clouds, as opposed to cores, with supercritical masses should be very rare.*

A cloud which has not contracted sufficiently to become self-gravitating could either disperse once the cause of its formation is removed or exist in pressure equilibrium with the intercloud medium. In the latter case, it will await an external disturbance (such as a supernova shock wave or an ionization front) to either disperse or implode it --or implode part of it and disperse the rest. Theoretical considerations, as seen above, and the observational fact that velocity fields characteristic of gravitational collapse are not observed suggest that very few, if

---

[1]In order for a cloud to collapse, the external pressure must also exceed a critical value given by $P_{\rm crit} = 1.89\ C^8G^{-3}M^{-2}\ [1 - (M_{\rm crit}/M)^2]^{-3}$, where $M \geq M_{\rm crit}$, $C \equiv (kT/\mu m_{\rm H})^{1/2}$ is the isothermal speed of sound in the gas, k the Boltzmann constant, and μ the mean mass per particle in units of the atomic hydrogen mass $m_{\rm H}$.

A SCENARIO FOR STAR FORMATION IN MAGNETIC CLOUDS

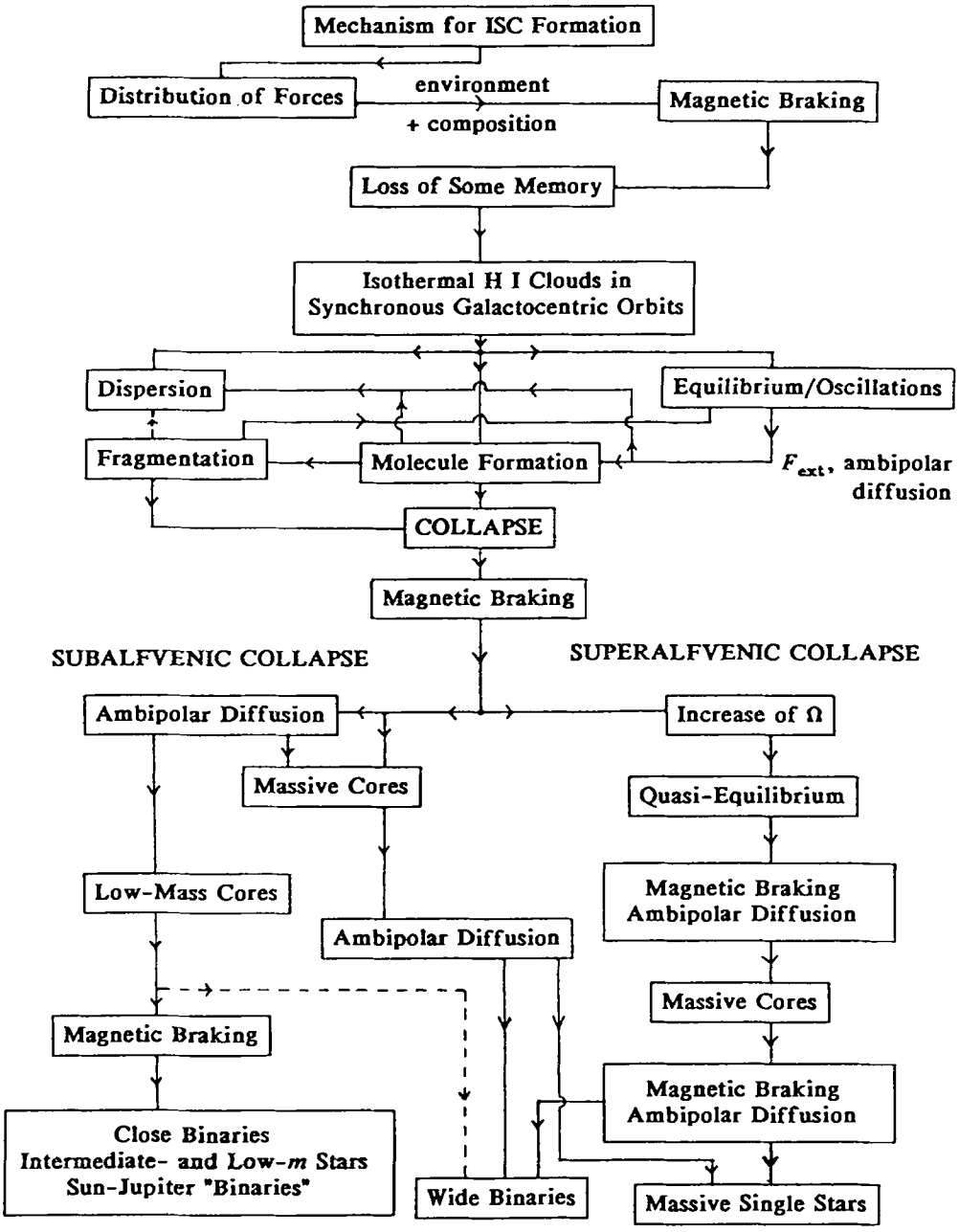

any, clouds acquire a supercritical mass-to-flux ratio from the outset and begin to collapse as a whole. Instead, *clouds reach first a relatively quiescent state* (near hydrostatic equilibrium with magnetic and thermal-pressure forces balancing gravity), with possible leftover stable oscillations about the equilibrium state. Centrifugal forces remain small at this stage due to magnetic braking, which operates over a time scale *strictly smaller* than (see review by Mouschovias 1987b)

$$\tau_{\parallel} = \frac{\rho_{cl}}{\rho_{ext}} \frac{Z}{v_{A,ext}} , \tag{4}$$

where ρ_{cl}, R, and Z, are the density, equatorial and polar radius, respectively, of a cloud (or fragment) rotating about its (z-) axis of symmetry which is aligned with the magnetic field. The matter density and Alfvén speed in the external medium (or envelope) are denoted by ρ_{ext} and $v_{A,ext}$, respectively. Since the magnetic braking time scale for a perpendicular rotator has been found to be $\tau_{\perp} << \tau_{\parallel}$ (see Mouschovias and Paleologou 1979; or summary in Mouschovias 1987b, § 2.3.2), most clouds and fragments tend to become aligned rotators in time.

Molecules form over time scales shorter than evolutionary time scales once the density becomes sufficiently large. Collapse may receive a boost or even be initiated by the decrease in sound speed due to the larger molecular weight and the possible decrease in temperature that may accompany the formation of molecules. The electrical conductivity is so large that the magnetic field remains frozen in the matter (Spitzer 1962) and lengthens the collapse time scale (even after the onset of ambipolar diffusion in the core; see below) by at least one order of magnitude compared to the characteristic free-fall time (Mouschovias 1983; Mouschovias, Paleologou, and Fiedler 1985).

Onset, Essence, and Consequences of Ambipolar Diffusion. Ambipolar diffusion is unavoidable in the core of a self-gravitating, magnetically supported cloud. The essence of ambipolar diffusion is to permit self-gravity to redistribute mass in the central flux tubes of a cloud and thereby induce fragmentation (Mouschovias 1977, 1978, 1979; see also discussion associated with eq. [6] below), recently being referred to as core formation (Paleologou and Mouschovias 1983; Shu 1983; Scott 1984; Mouschovias, Peleologou, and Fiedler 1985; Myers and Goodman 1988), followed eventually by gravitational collapse of dense cores that have exceeded the critical mass-to-flux ratio specified by equation (3) above. *If* ambipolar diffusion in cloud cores can prevent the magnetic field strength from increasing much above a few $\times$ 10^2 μGauss up to densities 10^{10-11} cm^{-3}, then the bulk of the (or even the entire) magnetic flux problem of star formation will be resolved. This is so because the ratio of the flux of a protostellar fragment and the flux of a magnetic star (of the same mass) is

$$\frac{\Phi_{fr}}{\Phi_*} = \frac{\pi B_{fr} R_{fr}^2}{\pi B_* R_*^2} = \frac{B_{fr}}{B_*} \left(\frac{\rho_*}{\rho_{fr}} \right)^{2/3} ; \tag{5a}$$

$$\lesssim \left(\frac{B_{fr}/(10^{-4}\ \mathrm{G})}{B_*/(10^4\ \mathrm{G})} \right) \left(\frac{10^{11}\ \mathrm{cm}^{-3}}{n_n} \right)^{2/3} , \tag{5b}$$

where we have taken $\rho_* \sim 1$ g cm^{-3} as a representative mean stellar density. *The distinction between the onset of rapid ambipolar diffusion and the actual resolution of the magnetic flux problem is of the essence.* Approximate analytical calculations (Mouschovias 1977, 1978, 1979) as well as one-dimensional collapse calculations (Paleologou and Mouschovias 1983; Mouschovias, Paleologou, and Fiedler 1985) have demonstrated that rapid ambipolar diffusion can indeed set in by the stage $n_n \sim 10^6$ cm^{-3} in cloud cores, and can have very important effects on the core's evolution. However, whether ambipolar diffusion can resolve the magnetic flux problem remains an open question due to lack of reliable multi-dimensional collapse calculations properly accounting for ambipolar diffusion (see, also, end of § IIIb below).

The Role of the Mass-to-Flux Ratio and of the External Pressure. The mass-to-flux ratio, the central-to-surface pressure ratio, and the chemical composition of a cloud determine the stages at which the angular momentum and magnetic flux problems will be resolved (see below), the stage at which fragmentation will take place and, consequently, the number and kinds of stars which will form; this includes the interaction between the forming protostars and the surrounding cloud material as well as the interaction among the protostars themselves. Once collapse begins, a cloud will usually evolve on its own time scale, affected only by objects to which it itself may give birth. It is therefore sensible to study physical processes in a single, but not necessarily isolated, collapsing cloud. However, the interaction among fragments (or cores) within one and the same cloud at least through torsional Alfvén waves cannot, in general, be ignored (see Mouschovias and Morton 1985a, b; review by Mouschovias 1987b).

Although collapse at subAlfvénic speeds in cloud cores should be the most common case (see Mouschovias 1978, Appendix B), Alfvénic or superAlfvénic collapse of a cloud or fragment (e.g., due to implosion, as discussed above) will lead to a very different sequence of events and, most likely, to a different IMF; i.e., more high-mass stars.

a) SubAlfvénic Collapse

Redistribution of Angular Momentum and Magnetic Flux, and Core-Envelope Separation. The tension of the field lines effectively supports the outlying portions of a cloud, thus forming an extended envelope, while allowing a dense central core to develop and a highly nonhomologous contraction to set in once gravitational forces become strong enough (see Mouschovias 1976b). During the initial stages of contraction, magnetic braking is so effective that the cloud contracts at nearly constant angular velocity, comparable to that of galactic rotation. (Thus the kinetic energy of rotation decreases as R^2.) Since magnetic braking becomes somewhat less efficient at densities $\sim 10^4$ cm^{-3} due to slow onset of ambipolar diffusion and the development of a larger density contrast between a core and the envelope (see Mouschovias 1978, § IId), two phenomena should reveal themselves at such densities. (i) A cloud core (or a molecular cloud with a dense envelope) should spin up noticeably above the rate of rotation that it would have if it remained in a synchronous galactocentric orbit at all stages of contraction --but still well below the rate of rotation implied by angular momentum conservation from an initial density of $n \sim 1$ cm^{-3} and angular velocity $\Omega \sim 10^{-15}$ rad s^{-1}. [Observed angular velocities are at least one (and usually two or more) order(s) of magnitude *smaller* than those implied by conservation of angular momentum (see Clark and Johnson 1978, 1981; Martin and Barrett 1978; Mattila, Winnberg, and Grasshof 1979; Young *et al.* 1981; Baudry *et al.* 1981; Schloerb and Snell 1984; Arquilla 1984; and Goldsmith and Sernyak 1984; see also review by Goldsmith and Arquilla 1985). There is little doubt that magnetic braking has been at work from scales larger than ~ 10 pc to scales smaller than $\sim 10^{-2}$ pc.] (ii) The central flux tubes of a cloud should keep increasing their mass-to-flux ratio due to ambipolar diffusion.

Fragmentation. Even with the magnetic field still frozen in the matter, fragments with $M_{fr} \sim 150\ M_\odot$ can separate out in a cloud of mass $M \sim 10^4\ M_\odot$ at a density $n\ (= n_p/2) \sim 10^4$ cm^{-3} -- recall that the critical mass for gravitational collapse (eq. [3a]) may also be written as

$$M_{crit} = 5.04 \times 10^5 \frac{(B/3\ \mu G)^3}{(n_p/1\ \mathrm{cm}^{-3})^2}\ M_\odot\ , \qquad (6)$$

(see Mouschovias and Spitzer 1976; Spitzer 1978; Mouschovias 1978). As ambipolar diffusion increases the mass-to-flux ratio in a fragment (or core) above the critical value for collapse, lower-mass fragments separate out gravitationally and begin to contract on their own. For example, even with a magnetic field as large as ~ 100 μGauss in a core in which ambipolar diffusion is in progress (and, consequently, with the magnetic field only partially coupled to the

neutrals), equation (6) implies that fragments with masses $M_{fr} \lesssim M_{crit} \simeq 3\ M_\odot$ can separate out at neutral densities $n_n \sim 4 \times 10^4\ cm^{-3}$. A plethora of low-mass, low-spin fragments (or cores) should therefore be forming preferentially in (and perhaps only in) the cores of self-gravitating clouds which (clouds) contract either subAlfvénically or not at all, while more massive fragments can form further out from a cloud's core (see also Mouschovias 1978 for the same, but somewhat less refined, prediction). This is consistent with observations of low-mass fragments in molecular clouds (see review by Myers 1985).

Disk Formation and Bipolar Outflows. That a contracting core should form a disk with its axis of symmetry aligned with the common direction of the magnetic field and the angular momentum vectors is an inevitable consequence of the inherent anistropy of magnetic and centrifugal forces. [Recall that magnetic braking is much more efficient in redistributing angular momentum in the case of a perpendicular rotator than in the case of an aligned rotator (see Mouschovias and Paleologou 1979, 1980), so that an initially oblique rotator will tend to become an aligned one relatively rapidly.] However, there is as yet no theory that can *predict*, as opposed to assume, what the distribution of mass in the disk should be and what fraction of that mass should eventually find its way into a protostar. Neither is there as yet a theory that can predict, or just explain, the commonly observed bipolar outflows in regions of low-mass star formation --although preliminary calculations and ideas, each with its own problems, abound (see review by Shu, Lizano, and Adams 1987; or Shu, Adams, and Lizano 1987).

Formation of Binary Stars and of Intermediate- and Low-Mass Stars in Cloud Cores. For these subAlfvénically contracting cores, it was demonstrated early on that magnetic braking followed by ambipolar diffusion can explain the entire range of periods of binary stars from 10 hr to 100 yr (Mouschovias 1977). Moreover, a single maximum in the distribution of the number of binaries as a function of (orbital) period was predicted, in disagreement with earlier but in agreement with more recent observations (see review by Abt 1983). It has also been shown very recently that, in subAlfvénically contracting cores, magnetic braking can be effective even while ambipolar diffusion is in progress, so that sufficient angular momentum is lost to the envelope for Sun-Jupiter "binaries" and single stars to form without interference from centrifugal forces (see Mouschovias and Paleologou 1986; or summary in Mouschovias 1987b, § 4). To the extent that microscopic physical processes in a cloud determine the degree of ionization (and the presence of small, charged grains), which in turn significantly affects the density at which ambipolar diffusion may reduce the effectiveness of magnetic braking (and, therefore, affect the leftover angular momentum in a protostellar fragment), *these microscopic processes may be nature's way of apportioning, with magnetic fields as its indispensable agent, collapsing interstellar mass between binary stars on the one hand and single stars on the other.*

In the case of magnetically connected fragments, the torsional Alfvén waves generated by the rotation of the fragments bounce back and forth among fragments and set each one of them in a series of (relatively) high-spin and low-spin states (see Mouschovias and Morton 1985a,b). Thus the angular momentum problem for each fragment may be resolved, recreated, and then resolved again, perhaps several times, before the torsional Alfvén waves reduce the angular momentum of the system of fragments sufficiently for star formation to take place.

Since low-mass fragments owe their existence to ambipolar diffusion, they reach the fully dynamical stage of contraction and protostar formation before the more massive, outlying fragments, which may have formed while the magnetic field is nearly frozen in the matter begin to evolve dynamically. However, once a massive star has formed, it evolves relatively rapidly and either the expansion of the resulting H II region or the eventual supernova explosion changes the evolution of other, especially massive, fragments substantially. In particular, a supernova may induce rapid collapse of nearby fragments with masses $\sim 10^1 - 10^3\ M_\odot$, while it may disperse the least massive ones, and may lead to more efficient star formation.

b) Alfvénic or SuperAlfvénic Collapse

Both theoretically and observationally such rapid collapse of a cloud as a whole should be a very rare phenomenon. It should happen, if at all, mostly in relatively massive fragments imploded by a sudden and large increase in the external pressure. [The sequence of events described here or in Mouschovias 1987a, § 3.6, differs qualitatively, quantitatively, and in specificity from ideas concerning "bimodal" star formation under the assumption that rapid collapse and the formation of massive stars are the result of $M > M_{\rm crit}$ (e.g., compare and contrast this discussion with that in Lizano and Shu 1987, § 3), in which case the magnetic tension force increases rapidly with contraction (see Mouschovias 1978).] During the rapid implosion of a clump with mass $M \simeq M_{\rm crit}$ in a cloud complex, magnetic tension cannot stop or significantly slow down the collapse and, in addition, the torsional Alfvén waves remain trapped within the clump. Contraction with angular momentum nearly conserved implies that centrifugal forces will become progressively more important. Depending, however, on the precise density at which rapid collapse begins, they may not increase sufficiently to prevent the formation of very wide binaries, including rapidly rotating, massive single stars as members. For example, if angular momentum begins to be conserved above a density $\simeq 10^4$ cm^{-3}, the angular momentum left over in a fragment (due to earlier efficient magnetic braking) is exactly what is required to form a relatively wide (visual) binary system, with a period $\tau_b \simeq 100$ yr. This argument does not depend on mass. In fact, a simple model shows that binaries forming according to this scenario will have periods scaling with the density $n_{\rm cr}$, above which angular momentum is nearly conserved, as

$$\left(\frac{\tau_b}{100\ \text{yr}}\right) \simeq \left[\frac{10^4\ \text{cm}^{-3}}{n_{\rm cr}}\right]^2 \tag{7}$$

(see Mouschovias 1977). Note that $n_{\rm cr}$ exceeds the density at which rapid ambipolar diffusion sets in (i.e., at a rate that significantly affects the evolution of a core) because magnetic braking continues to remove angular momentum, although at a reduced rate, even while ambipolar diffusion is in progress (see Mouschovias 1977; and Mouschovias and Paleologou 1986).

If Alfvénic or superAlfvénic contraction begins at $n < 10^3$ cm^{-3}, centrifugal forces will lead to a quasi-equilibrium configuration by balancing gravity perpendicular to the axis of rotation. Further contraction takes place only as rapidly as magnetic braking can remove angular momentum to the envelope. Since the fragment still has most of its magnetic flux trapped inside at this stage and since it was magnetically supported before implosion, magnetic forces will also contribute significantly to this quasi-equilibrium, and both magnetic braking and ambipolar diffusion are expected to occur simultaneously, probably over comparable time scales. Although this complex configuration has not been studied in any satisfactory fashion, it seems likely that stars which will form in such fragments will be characterized by both rapid rotation *and* strong magnetic fields. Since these are signatures of massive stars, it is tempting to suggest, at least tentatively, that this is how such stars form (see also § III below for a strengthening of this suggestion and for a scenario of high-mass star formation even in subAlfvénically contracting but very massive clouds).

Although calculations do exist, simplifying assumptions concerning the geometry do not presently allow definitive conclusions on the issue of whether a protostar (low-mass or massive) becomes opaque while possessing a relatively weak magnetic field which will be amplified by a dynamo process, or whether it does so while having too much magnetic flux which will be dissipated during this or subsequent stages of contraction. We believe, nevertheless, that it is during these relatively late stages of protostar formation that its magnetic field will detach from the background. This view is based on calculations (see Mouschovias 1976a, b; 1978) which show that conditions conducive to magnetic detachment do not arise during the earlier, relatively diffuse stages of fragment contraction and protostar formation. Once magnetic

detachment takes place, further loss of angular momentum becomes very inefficient (compared to earlier stages) and occurs through a magnetic wind.

c) Selection of ~ 1 $M_\odot$ as a Typical Stellar Mass

Detailed calculations have shown that there exists a characteristic length scale $\lambda_{A,cutoff}$ below which ambipolar diffusion is so effective that Alfvén waves in the neutrals cannot propagate at all [see summary in Mouschovias 1987a, § 2.2.6(b)]. In clouds with an Alfvén speed significantly larger than the sound speed (a common occurrence), this length scale is given by

$$\lambda_{A,cutoff} \simeq \pi v_A \tau_{ni} , \tag{8}$$

where v_A and τ_{ni} are the Alfvén speed and the neutral-ion collision time, which are given by equations (2a) and (12), respectively. The physical origin of $\lambda_{A,cutoff}$ lies in the fact that any disturbance in the magnetic field having wavelength $\lambda < \lambda_{A,cutoff}$ *diffuses* (or decays) before collisions between neutrals and ions have had time to transmit to the neutrals the magnetic force associated with the disturbance. For a core density of 10^4 cm^{-3} and $v_A \simeq 2$ km s^{-1} (see eq. [2a]), we find that $\lambda_{A,cutoff} \simeq 0.14$ pc and the mass in a core of this diameter is $\simeq 1$ $M_\odot$. Since v_A is relatively insensitive to (massive) cloud parameters (see eq. [2a]), *protostellar masses in the approximate range* 1 - 0.1 $M_\odot$ *are selected quite naturally in molecular cloud cores in the corresponding density range* 10^4 - 10^6 cm^{-3}.

The Jeans critical wavelength λ_J (in the presence of ambipolar diffusion) is comparable to $\lambda_{A,cutoff}$ and, as long as $v_A \simeq const$ (e.g., as a consequence of eq. [1a]), both $\lambda_{A,cutoff}$ and λ_J vary with density as $n_n^{-1/2}$. Both analytical calculations (Mouschovias, Morton, and Ciolek 1989) and numerical collapse calculations (Mouschovias and Morton 1989) show that ambipolar diffusion allows relatively rapid contraction of the mass inside this region to take place, while in the surrounding envelope at distances significantly larger than $\lambda_{A,cutoff}$ magnetic forces provide much more effective support against gravity. A natural core-envelope separation takes place. Although infall of some envelope material onto the rapidly formed high-density core still takes place, the preliminary results suggest that the amount of this material and perhaps even its accretion rate are limited by magnetic forces. Thus, although the onset of a stellar wind at a later stage may indeed reverse the infall, as suggested by Lada (1985, § 4.3.1) and by Shu, Lizano, and Adams (1987), it may be the effective magnetic support of the envelope, rather than the later onset of the wind, that determines the protostellar mass. Collapse calculations now under way with graduate students Robert Fiedler and Scott Morton should answer this central question of star formation.

The above considerations also hint on how massive stars may form even in subAlfvénically contracting clouds. Since the protostellar mass contained in a sphere of diameter $\lambda_{A,cutoff}$ goes as $M \propto v_A^3/n^{1/2}$, it appears that any mechanism which can increase the Alfvén speed at a given density is likely to lead to the formation of more massive stars. For example, since the Alfvén speed varies as $v_A \propto (B_0 M_{cl})^{1/4}$ (see eq. [2a]) in the cores of self-gravitating clouds, if such a cloud can form as (or by agglomeration become) a single entity, as opposed to a cloud complex, with mass $\simeq 10^5$ $M_\odot$ at an initial field strength $B_0 \simeq 6$ μGauss, then protostars with masses up to 10 $M_\odot$ can form in cores due to ambipolar diffusion. The formation of massive stars in this manner will be an inefficient process, just like the formation of low-mass stars in the cores of subAlfvénically contracting clouds discussed in § IIa above, and unlike the formation of massive stars by the spherical implosion of massive fragments. *We suggest that this kind of formation of massive stars (and consequent supernovae) in primordial proto-globular-cluster clouds is most likely responsible (since causes for implosion are not available) for metal contamination of the parent cloud and thus for explaining the observed presence of metals in globular cluster stars.* Since cluster masses are ~ 10^5 $M_\odot$, it follows that the protocluster clouds must have been at least as massive. Hence, assuming only that a magnetic field strength of a few microgauss was present in these clouds when they became self-gravitating, protostellar masses $\gtrsim 10$ $M_\odot$ would be selected naturally by the above mechanism --a necessary condition for metal contamination of the clouds by the resulting supernovae (see review by Wheeler *et al.* 1989).

III. AMBIPOLAR DIFFUSION TIME SCALES IN CLOUD CORES

We consider the contraction of a core having neutral and ion densities ρ_n and ρ_i, respectively, magnetic field strength B, and isothermal speed of sound C. Denoting the acceleration of gravity by g, the actual acceleration of neutrals by a, and the magnetic force per unit volume by F_m, we may employ cylindrical polar coordinates (r, ϕ, z) in an axisymmetric geometry and write the r-component of the equation of motion of the neutrals in the equatorial plane as

$$a_{n,r} = g_r + \frac{F_{m,r}}{\rho_n} - \frac{C^2}{\rho_n}\frac{\partial \rho_n}{\partial r}, \tag{9}$$

where $g_r < 0$ and $a_{n,r} \leq 0$. The magnetic force is, in general, given by

$$F_m = -\nabla_\perp\left(\frac{B^2}{8\pi}\right) + \hat{n}\frac{B^2}{4\pi R_c}, \tag{10}$$

where the subscript $\perp$ refers to a direction perpendicular to a field line, the unit vector $\hat{n}$ is normal to a field line and points toward the local center of curvature, and R_c is the local radius of curvature of the field line. In the equatorial plane, $\nabla_\perp = \hat{r}(\partial/\partial r)$, and $\hat{n} = \hat{r}$.

Due to the small ion inertia, the drift velocity between ions and neutrals in the equatorial plane is obtained by balancing the magnetic force and the collisional drag on the ions, i.e.,

$$v_D \equiv v_i - v_n = \rho_H^{-1}\tau_{ni}F_{m,r}, \tag{11}$$

where collisions of ions with He are neglected, the cosmic abundance of He is accounted for in ρ_n ($= 1.4\rho_H$), and the mean collision time of a neutral particle in a sea of ions is given by

$$\tau_{ni} = \frac{m_i + m_n}{m_i}\frac{1}{n_i\langle\sigma w\rangle_{in}}. \tag{12}$$

The quantity $\langle\sigma w\rangle_{in}$ is the average collisional rate between ions of mass m_i (and number density n_i) and neutrals of mass m_n; it is equal to 1.69×10^{-9} cm^3 s^{-1} for HCO^+-H_2 collisions (see McDaniel and Mason 1973) --note that $m_i/m_n = 14.4$ for this particle pair.

a) Cylindrical Collapse

In cylindrical geometry, we may write the force equation (9) near the axis of symmetry as

$$-\frac{1}{\tau_{dyn}^2} = -\frac{\pi}{2}\frac{1}{\tau_{ff}^2}\left(1 - \frac{2}{1.4\pi}\frac{\tau_{ff}^2}{\tau_{AD}\tau_{ni}} - \frac{2}{\pi}\frac{\tau_{ff}^2}{\tau_s^2}\right), \tag{13}$$

where the following definitions of the dynamical time scale τ_{dyn}, the ambipolar diffusion time scale τ_{AD}, and the sound crossing time τ_s have been used:

$$\tau_{dyn} = \left(\frac{r}{|a_{n,r}|}\right)^{1/2}, \qquad \tau_{AD} = \frac{r}{|v_{D,r}|}, \qquad \tau_s = \frac{r}{C}. \tag{14a, b, c}$$

The gravitational field near the axis is given by $g_r = -2\pi G\rho_{n,c} r$, where $\rho_{n,c}$ is the core (or, central) density, and the free-fall time near $r = 0$ in cylindrical geometry is

$$\tau_{ff} = (4G\rho_{n,c})^{-1/2} ; \tag{15}$$

it is 8% smaller than the free-fall time in a spherical geometry. The last term in the parentheses on the right-hand side of equation (13) may be rewritten, by using equations (14c) and (15), as

$$\frac{2}{\pi}\frac{\tau_{ff}^2}{\tau_s^2} = \frac{1}{4}\frac{m_{cr}}{m(r)} , \tag{16}$$

where $m(r)$ is the mass per unit length inside a radius r, and m_{cr} is the critical mass per unit length above which no thermal support against gravity is possible and is given by

$$m_{cr} = \frac{2C^2}{G} = 16.4\left(\frac{T}{10\ \mathrm{K}}\right) \quad M_\odot\ \mathrm{pc}^{-1} . \tag{17}$$

Quasistatic Contraction. It follows immediately from equation (13) and the definition (14b) that, for quasistatic contraction of the neutrals (i.e., $a_n \to 0$, hence $\tau_{dyn} \to \infty$), the ambipolar diffusion time scale is

$$\tau_{AD} = \frac{2}{1.4\pi}\frac{\tau_{ff}^2}{\tau_{ni}}\left(1 - \frac{2}{\pi}\frac{\tau_{ff}^2}{\tau_s^2}\right)^{-1} , \qquad \text{for} \quad \frac{2}{\pi}\frac{\tau_{ff}^2}{\tau_s^2} < 1. \tag{18}$$

If magnetic forces provide the main support against gravity, the second term in parentheses on the right-hand side of equation (18) is negligible; hence, $\tau_{AD} = (2/1.4\pi)(\tau_{ff}^2/\tau_{ni})$, which is the exact expression obtained by Mouschovias (1979) for a quasistatically contracting, cylindrically symmetric cloud (see also the review by Mouschovias 1987a, § 2.2.5). If thermal-pressure forces dominate the magnetic forces (a likely situation after ambipolar diffusion significantly reduces the flux-to-mass ratio in a core), then the difference of the two terms in parentheses becomes small, and consequently τ_{AD} becomes longer than its quasistatic contraction value. The physical meaning of this is that, when a cloud is mainly thermally supported against gravity, ambipolar diffusion is primarily due to ions moving outward with respect to the axis of symmetry (and relative to the nearly stationary neutrals). Such motion, however, is extremely slow because the magnetic force is weak by assumption and, consequently, v_D is very small (see eq. [11]).

It is clear from equation (13) that although the accelerations (at a given small distance r from the axis) due to gravity and thermal-pressure forces are proportional to τ_{ff}^{-2} and τ_s^{-2}, respectively, the magnetic acceleration on the neutrals is *not* proportional to τ_{AD}^{-2}; it varies instead as $(\tau_{AD}\tau_{ni})^{-1}$, where τ_{AD} is defined as in equation (14b) and is not, in general, equal to its quasistatic value given by equation (18).

Dynamical Contraction. If the acceleration of the neutrals cannot be neglected (i.e., if the left-hand side of equation (13) is a significant fraction of the first [gravitational] term on the right-hand side), the ambipolar diffusion time scale is given by

$$\tau_{AD} = \frac{2}{1.4\pi}\frac{\tau_{ff}^2}{\tau_{ni}}\left(1 - \frac{2}{\pi}\frac{\tau_{ff}^2}{\tau_{dyn}^2} - \frac{2}{\pi}\frac{\tau_{ff}^2}{\tau_s^2}\right)^{-1} . \tag{19}$$

If thermal-pressure forces are negligible and one takes $|a_{n,r}| \gtrsim (1/3)|g_r|$ as the condition at which quasistatic contraction breaks down, equation (19) would imply that when τ_{AD} exceeds its quasistatic value by about 50%, the dynamics of contraction cannot be ignored. Does it also become progressively more difficult for the collapsing core to lose magnetic flux beyond this stage? The answer depends on geometry.

In the case of one-dimensional rectilinear geometry (a slab-shaped cloud with the magnetic field parallel to the faces of the slab), the gravitational field at the comoving coordinate of a neutral fluid element is constant in time, while the magnetic acceleration (force per gram of *neutral* matter) increases upon compression (it would increase as z^{-2} if the field were frozen in the matter). Hence, even while ambipolar diffusion is in progress during contraction, it is not very difficult for the magnetic force to balance the gravitational force and thus ensure quasistatic contraction and, therefore, continued loss of flux at a significant rate, as found by Mouschovias, Paleologou, and Fiedler (1985). In the case of cylindrical symmetry, the gravitational acceleration at a shell of matter increases as r^{-1}, but the magnetic acceleration can still increase more rapidly (it would increase as r^{-3} under flux freezing). Thus, even in this geometry, in which the collapse is qualitatively different from the rectilinear case in that no thermally supported final equilibrium states can exist once the critical mass (per unit length along the axis of symmetry) m_{cr} is exceeded (see eq. [17]), the magnetic field may eventually enforce quasistatic contraction, despite the fact that dynamical evolution can precede that stage if $\tau_{ni} \sim \tau_{ff}$. The axisymmetric case, however, to which we now turn, is different from the above two cases in that magnetic forces cannot enforce quasistatic contraction of the core indefinitely because of the existence of a critical mass-to-flux ratio for gravitational collapse (see eq. [3a]).

b) Axisymmetric Collapse

Quasistatic Contraction. Up to the stage that ambipolar diffusion will increase the mass-to-flux ratio of the core above the critical value $(1/63G)^{1/2}$ (see eq. [3a]), the contraction will remain quasistatic and an expression for τ_{AD} similar to that given by equation (18) can be obtained:

$$\tau_{AD} = \frac{8}{1.4\pi^2}\frac{\tau_{ff}^2}{\tau_{ni}}\left[1 - \frac{8}{\pi^2}\frac{\tau_{ff}^2}{\tau_s^2}\right]^{-1}, \qquad \text{for} \quad \frac{8}{\pi^2}\frac{\tau_{ff}^2}{\tau_s^2} < 1, \tag{20}$$

where τ_{ff} is now the spherical free-fall time

$$\tau_{ff} = (3\pi/32G\rho)^{1/2}. \tag{21}$$

In deriving equation (20), no assumption was made as to the relative magnitude of the magnetic-pressure force and the magnetic tension. The gravitational field was taken as $g_r = -(4\pi/3)G\rho_{n,c}r$, corresponding to a spherical distribution of mass inside the core. A comparison of equations (20) and (18) reveals that the expression for the ambipolar diffusion time scale in the form $\tau_{AD} \sim \tau_{ff}^2/\tau_{ni}$, valid for quasistatic contraction, is indeed a property of the general equations governing ambipolar diffusion in magnetically supported clouds and does not depend on the dimensionality of a model (as shown earlier by Mouschovias 1987b from a more general point of view).

Dynamical Contraction. Equation (20) can easily be modified, by adding the term $-(8/\pi^2)(\tau_{ff}^2/\tau_{dyn}^2)$ in the parentheses on the right-hand side, to account for dynamical contraction. However, since τ_{dyn} would still need to be estimated from equation (9) and the corresponding expression for the z-direction, we revert to first principles. We consider, for simplicity, a spherical core which has just exceeded the critical mass-to-flux ratio due to earlier

quasistatic ambipolar diffusion, described by equation (20). Using the definition (14b) for τ_{AD} and the expression (11) for the drift velocity v_D, with the magnetic tension force taken as the dominant contribution in equation (10), we find that

$$\tau_{AD} = r \frac{\rho_H}{\tau_{ni}} \frac{4\pi r}{B^2}, \tag{22}$$

where we have taken $R_c \simeq r$, the radius of the core, as a reasonable estimate. We now multiply and divide the right-hand side of equation (22) by ρ_n and by the appropriate factors of π and r so as to introduce $M^2/\Phi_B{}^2$, and we use the definition (21) for τ_{ff} and equation (3a) for the critical flux at a given mass to write equation (22) as

$$\tau_{AD} = 0.27 \frac{\tau_{ff}^2}{\tau_{ni}} \left(\frac{\Phi_{B,crit}}{\Phi_B} \right)^2, \qquad \text{for} \quad \Phi_B \leq \Phi_{B,crit}; \tag{23a}$$

$$= 1.3 \times 10^3 \left(\frac{n_i/n_{H_2}}{10^{-10}} \right) \left(\frac{\Phi_{B,crit}}{\Phi_B} \right)^2 \quad \text{yr}, \tag{23b}$$

where Φ_B is the actual flux of the core at any stage past the onset of dynamical contraction, and $\Phi_{B,crit}$ is uniquely determined by the mass of the core from equation (3a) as $\Phi_{B,crit} = (63G)^{1/2}M$. The normalization of n_i/n_{H2} in equation (23b) refers to a neutral density $\sim 10^9$ cm^{-3}, above which n_i no longer increases with n_n (see Elmegreen 1979; Nakano 1979).

It should be emphasized that equation (23) refers to a core, not to the entire cloud. The cloud as a whole has $M \simeq M_{crit}$ because it is magnetically supported. However, a core of mass $\sim 1\ M_\odot$ has $M < M_{crit}$ or, equivalently, $\Phi_B > \Phi_{B,crit}$ for a relatively long time, i.e., until the quasistatic phase of ambipolar diffusion manages to reduce the flux of this (fixed) mass so as to make the mass-to-flux ratio equal to its critical value. *If* this marks the onset of accelerated contraction of the core (see § II, footnote 1 for the sufficient condition for such collapse), then equation (23) shows clearly that this will also mark the stage at which τ_{AD} begins to increase above its quasistatic contraction value by the factor $(\Phi_{B,crit}/\Phi_B)^2$. It therefore becomes more difficult to lose flux during this late phase of accelerated contraction. Although ambipolar diffusion may have reduced the flux of such a core by a few orders of magnitude prior to this stage, equation (3a) yields a critical flux for a $\sim 1\ M_\odot$ core which is larger than the observed fluxes of magnetic stars by a factor 10 - 50. Hence, unless one of the simplifying assumptions that we have made (such as ignoring flattening, which tends to enhance the magnetic force by reducing the radius of curvature of field lines) in order to obtain an analytical answer breaks down, it seems that ambipolar diffusion may not resolve the entire magnetic flux problem of star formation. To complete the task, then, one may need to appeal to another dissipative process (such as ohmic dissipation) that sets in at higher densities, at which the electron density becomes negligible and the negative charge is mainly carried by grains (Spitzer 1963). Ohmic dissipation at densities $\gtrsim 10^{12}$ cm^{-3} has recently been studied by Nakano and Umebayashi (1986), who conclude that it can reduce the protostellar flux to the desired level prior to flux re-freezing (originally studied by Pneuman and Mitchell 1965) due to thermal ionization. Detailed collapse calculations beyond the density $\sim 10^9$ cm^{-3}, accounting for the significant reduction in the electron density and the fact that collisions no longer permit the dominant charge carriers to remain attached to the magnetic field, are essential for understanding precisely how nature resolves the magnetic flux problem during star formation.

For the time being, equation (23) taken at face value implies that, if magnetic forces maintain quasistatic contraction up to a density $n_n \sim 10^9$ cm^{-3} (not an unreasonable proposition given the conclusions by Mouschovias [1976b, 1978] concerning the effective support against gravity by magnetic tension, confirmed also by Nakano's 1979 quasistatic calculation), it may be possible for ambipolar diffusion to reduce the core's flux by at least another order of magnitude prior to the stage $n_n \sim 10^{12}$ cm^{-3}. This is so because we now have that (i) $\tau_{AD}/\tau_{ff} \propto$

$\rho_n^{-1/2}\Phi_B^{-2}$ (since $n_i \simeq const$ above $n_n \simeq 10^9$ cm^{-3}), and (ii) the charged particles themselves are not well attached to the magnetic field. Hence, ambipolar diffusion may still have its day in resolving the magnetic flux problem...

IV. SUMMARY

Magnetic fields are instrumental in the formation of interstellar clouds, and they regulate a cloud's evolution up to densities ~ 10^{10} cm^{-3}. This regulatory action includes (1) the resolution of the angular momentum problem by effective magnetic braking even while ambipolar diffusion is in progress; (2) effective support against the self-gravity of molecular clouds; (3) core-envelope separation and self-initiated core collapse due to ambipolar diffusion; (4) introduction of a characteristic length scale and consequent selection of ~ 1 $M_\odot$ as a typical protostellar mass at a stage preceding stellar winds; (5) reduction of the flux-to-mass ratio of protostellar fragments by a few orders of magnitude; and (6) formation of close and wide binary stars as well as single low-mass and massive stars. Magnetic fields, by naturally selecting protostellar masses ≥ 10 $M_\odot$ in primordial clouds of mass $\geq 10^5$ $M_\odot$, may also be ultimately responsible for the observed metal contamination of globular clusters.

We have shown that ambipolar diffusion in quasistatically contracting cores progresses with a time scale $\tau_{AD} = 0.6\ \tau_{ff}^2/\tau_{ni}$, where τ_{ff} is the free fall time scale and τ_{ni} the mean collision time of a neutral particle in a sea of ions. When the critical mass-to-flux ratio $(M/\Phi_B)_{crit} = (63G)^{-1/2}$ is exceeded, dynamical contraction may ensue with ambipolar diffusion characterized by the time scale $\tau_{AD} = 0.3\ (\tau_{ff}^2/\tau_{ni})(\Phi_{B,crit}/\Phi_B)^2$, where $\Phi_{B,crit} = (63G)^{1/2}M$ is the critical flux below which a core of mass M may begin to contract dynamically. These results have been used to re-examine the resolution of the magnetic flux problem of star formation.

REFERENCES

Abt, H. A. 1983, *Ann. Rev. Astr. Ap.*, **21**, 343.

Arquilla, R. 1984, Ph. D. thesis, University of Massachusetts.

Baudry, A., Cernicharo, J., Perault, M., de la Noe, J., and Despois, D. 1981, *Astr. Ap.*, **194**, 101.

Blitz, L., and Shu, F. H. 1980, *Ap. J.*, **238**, 148.

Bregman, J. D., Troland, T. H., Forster, J. R., Schwarz, U. J., Goss, W. M., and Heiles, C. 1983, *Astr. Ap.*, **118**, 157.

Clark, F. O., and Johnson, D. R. 1978, *Ap. J.*, **220**, 550.

Elmegreen, B. G. 1979, *Ap. J.*, 232, 729.

Field, G. B. 1965, *Ap. J.*, **142**, 531.

Goldsmith, P. F., and Arquilla, R. 1985, in *Protostars & Planets II*, eds. D. C. Black, and M. S. Matthews (Tucson: Univ. of Arizona Press), p. 137.

Goldsmith, P. F., and Sernyak, M. I., Jr. 1984, *Ap. J.*, **283**, 140.

Goodman, A. A., Crutcher, R. M., Heiles, C., Myers, P. C., and Troland, T. H. 1988, *preprint* (also in this volume).

Heiles, C. 1987, in *Physical Processes in Interstellar Clouds*, eds. G. E. Morfill and M. Scholer (Dordrecht: Reidel), p. 429.

Jeans, J. H. 1928, *Astronomy and Cosmogony* (Cambridge: Cambridge Univ. Press).

Larson, R. B. 1981, *M. N. R. A. S.*, **194**, 809.

Lizano, S., and Shu, F. H. 1987, in *Physical Processes in Interstellar Clouds*, eds. G. E. Morfill and M. Scholer (Dordrecht: Reidel), p. 173.

Martin, R. N., and Barrett, A. H. 1978, *Ap. J. Suppl.*, **36**, 1.

Mattila, K., Winnberg, A., and Grasshof, M. 1979, *Astr. Ap.*, **78**, 275.

McDaniel, E. W., and Mason, E. A. 1973, in *The Mobility and Diffusion of Ions in Gases* (New York: Wiley).

Mestel, L., and Spitzer, L., Jr. 1956, *M. N. R. A. S.*, **116**, 503.

Mouschovias, T. Ch. 1974, *Ap. J.*, 192, 37.
____. 1975a, *Astr. Ap.*, **40**, 191.
____. 1975b, *Ph.D. Thesis*, Univ. of California at Berkeley.
____. 1976a, *Ap. J.*, **206**, 753.
____. 1976b, *Ap. J.*, **207**, 141.
____. 1977, *Ap. J.*, **211**, 147.
____. 1978, in *Protostars and Planets*, ed. T. Gehrels (Tucson: University of Arizona Press), p. 209.
____. 1979, *Ap. J.*, **228**, 475.
____. 1981, in *Fundamental Problems in the Theory of Stellar Evolution*, eds. D. Sugimoto, D. Q. Lamb, and D. N. Schramm (Dordrecht: Reidel), p. 27.
____. 1983, in *Solar and Stellar Magnetic Fields: Origins and Coronal Effects*, ed. J. O. Stenflo (Dordrecht: Reidel), p. 479.
____. 1985, *Astr. Ap.*, **142**, 41.
____. 1987a, in *Physical Processes in Interstellar Clouds*, eds. G. E. Morfill and M. Scholer (Dordrecht: Reidel), p. 453.
____. 1987b, in *Physical Processes in Interstellar Clouds*, eds. G. E. Morfill and M. Scholer (Dordrecht: Reidel), p. 491.
Mouschovias, T. Ch., and Morton, S. A. 1985a, *Ap. J.*, 298, 190.
____. 1985b, *Ap. J.*, **298**, 205.
____. 1989, *in preparation.*
Mouschovias, T. Ch., Morton, S. A., and Ciolek, G. 1989, *in preparation.*
Mouschovias, T. Ch., and Paleologou, E. V. 1979, *Ap. J.*, 230, 204.
____. 1980, *Ap. J.*, **237**, 877.
____. 1986, *Ap. J.*, **308**, 781.
Mouschovias, T. Ch., Paleologou, E. V., and Fiedler, R. A. 1985, *Ap. J.*, **291**, 772.
Mouschovias, T. Ch., and Spitzer, L., Jr. 1976, *Ap. J.*, 210, 326.
Mouschovias, T. Ch., Shu, F. H., and Woodward, P. R. 1974, *Astr. Ap.*, **33**, 73.
Myers, P. C. 1985, in *Protostars & Planets II*, eds. D. C. Black, and M. S. Matthews (Tucson: Univ. of Arizona Press), p. 81.
Myers, P. C., and Goodman, A. A. 1988, *Ap. J.*, **329**, 392.
Nakano, T. 1979, *Publ. Astr. Soc. Japan*, **31**, 697
Nakano, T., and Umebayashi, T. 1986, *M. N. R. A. S.*, **218**, 663.
Paleologou, E. V., and Mouschovias, T. Ch. 1983, *Ap. J.*, **275**, 838.
Parker, E. N. 1966, *Ap. J.*, **145**, 811.
Pneuman, G. W., and Mitchell, T. P. 1965, *Icarus*, **4**, 494.
Schloerb, F. P., and Snell, R. L. 1984, *Ap. J.*, 283, 129.
Schwarz, U. J., Troland, T. H., Albinson, J. S., Bregman, J. D., Goss, W. M., and Heiles, C. 1986, *Ap. J.*, **301**, 320.
Scott, E. H. 1984, *Ap. J.*, **278**, 396.
Shu, F. H. 1974, *Astr. Ap.*, **33**, 55.
____. 1983, *Ap. J.*, **273**, 202.
Shu, F. H., Adams, F. C., and Lizano, S. 1987, *Ann. Rev. Astr. Ap.*, **25**, 23.
Shu, F. H., Lizano, S., and Adams, F. C. 1987, in *Star Forming Regions*, eds. M. Peimbert and J. Jugaku (Dordrecht: Reidel), p. 417.
Spitzer, L., Jr. 1962, *Physics of Fully Ionized Gases*, 2nd ed. (New York: Interscience).
____. 1963, in *Origin of the Solar System*, eds. R. Jastrow and A. G. W. Cameron (New York: Academic Press), p. 39.
____. 1978, *Physical Processes in the Interstellar Medium* (New York: Wiley-Interscience).
Wheeler, J. C., Sneden, C., and Truran, J. W., Jr. 1989, *Ann. Rev. Astr. Ap., in press.*
Young, J. S., Langer, W. D., Goldsmith, P. F., and Wilson, R. W. 1981, *Ap. J. (Letters)*, **251**, 81.

On the Interaction between a Hypersonic Jet and the Interstellar Medium

Z. Y. Yue and B. Zhang
Department of Geophysics, Beijing University
and
G. Winnewisser
I. Physikalisches Institut der Universität zu Köln

Summary

We will give only a short outline of an analytical treatment for the "working surface" of the astrophysical jet associated with the early stage of star formation based on gas dynamics. Further details will be presented in a separate paper. For a general review of outflow and jet phenomena see [1]. For a detailed observational study of the typical "working surface" HH 34 see [2].

I. Analytical solutions for the case of non-radiating shocks

We first consider the following gas dynamical problem: a hypersonic jet forges its way through a uniform ambient medium which is assumed to be at rest before being disturbed by the jet. Because of the hypersonic speed and the finite lateral size of the jet, the boundary between the disturbed part and the undisturbed part of the medium must be a "bow shock." Since the bow shock is formed by the squeezing effect of the jet, it must move more slowly than the jet itself. The velocity behind the bow shock is even smaller than the speed of the bow shock, and the hypersonic jet has to pass through another shock, which is referred to as the rear shock hereafter, in order to reduce its velocity before getting close to the bow shock. Thus, in a reference frame comoving with the double shock structure, the flow pattern is as shown in Fig. 1. The two supersonic flows travel in opposite directions. After each crosses a shock, they meet in between and form a contact discontinuity.

The pressure balance at the stagnation point C and the strong shock approximations lead to the following relation between the shock velocity V_S and the central speed of the jet V_{J0}:

$$V_S = \frac{V_{J0}}{\left[1 + (\rho_\infty/\rho_J)^{1/2}\right]}, \tag{1}$$

where the ratio between the densities of the undisturbed medium ρ_∞ and the jet ρ_J is involved.

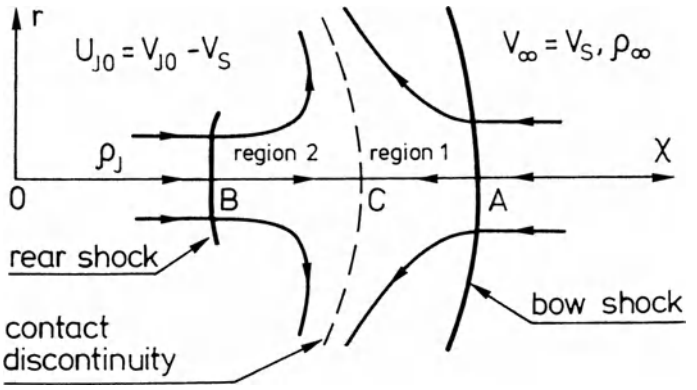

Fig. 1. A sketch of the flow pattern in the frame comoving with the double shock structure. The order of magnitude of the velocity of the hypersonic jet is $V_{J0} \sim 10^2\ \mathrm{km\,s^{-1}}$, whereas the bow shock velocity V_S is a density-dependent function of V_{J0} (Eq. 1).

We define a coordinate system in which R and θ are the spherical coordinates with the origin at the center of curvature of the contact discontinuity. For the neighborhood of the X axis, the constant-density approximation is valid for each side of the contact discontinuity [3]. Thus, we introduce the stream function $\psi(R, \theta)$, defined by $\psi(R, \theta) = (1/2\pi\rho)\dot{M}(R, \theta)$, where $\dot{M}(R, \theta)$ is the mass flux through the surface spanning the loop defined by a given (R, θ) pair. The stream functions ψ_1 and ψ_2, for region 1 and region 2 (Fig. 1) respectively, then satisfy

$$V_R = \frac{1}{R^2 \sin\theta}\frac{\partial\psi}{\partial\theta}, \qquad V_\theta = -\frac{1}{R\sin\theta}\frac{\partial\psi}{\partial R}, \tag{2}$$

By using an analysis similar to that for a hypersonic flow around a solid sphere [4] and that for the Hill vortex sphere [5], we obtain the equations governing the stream functions for both regions as follows:

$$\frac{\partial^2\psi_i}{\partial R^2} + \frac{\sin\theta}{R^2}\frac{\partial}{\partial\theta}\left(\frac{1}{\sin\theta}\frac{\partial\psi_i}{\partial\theta}\right) = A_i R^2 \sin^2\theta \qquad (i = 1, 2), \tag{3}$$

where $-A_i \equiv \Omega_i/r$, the ratio of the vorticity Ω_i in region i to the distance r from the X-axis. These equations allow solutions of the following form:

$$\psi_i = \left(\frac{B_i}{R} + C_i R^2 + \frac{A_i}{10}R^4\right)\sin^2\theta \qquad (i = 1, 2). \tag{4}$$

There are nine constants involved: A_1, B_1, C_1, A_2, B_2, and C_2, as well as R_C, R_S, and X_B, where R_C and R_S are respectively the radii of curvature of the contact discontinuity and the bow shock, which are assumed to share their center of curvature. X_B is the distance between the rear shock and this center of curvature. All these constants can be determined by the boundary conditions at the two shocks and the matching condition at the contact discontinuity. For $\gamma = c_P/c_V = 5/3$, which enters through the shock conditions, the final results are as follows:

$$\psi_1 = -0.1627\, V_S\, R_C^2\, \sin^2\theta \left[\left(\frac{R}{R_C} \right)^4 - \frac{R_C}{R} \right], \tag{5}$$

$$\psi_2 = 0.3677\, U_{J0}\, R_C^2\, \sin^2\theta \left[0.0702 \left(\frac{R_C}{R} \right) + 0.9298 \left(\frac{R}{R_C} \right)^2 - \left(\frac{R}{R_C} \right)^4 \right], \tag{6}$$

$$R_S/R_C = 1.176, \tag{7}$$

$$X_B/R_C = 0.8414, \tag{8}$$

$$R_C/H = 2.712, \tag{9}$$

where H is a scale factor for the half width of the jet and $U_{J0} = V_{J0} - V_S$ is the central speed of the jet observed in the comoving frame. The flow field and the temperature distribution based on the stream function are shown in Fig. 2. Since, strictly speaking, the approximations we used are valid only for the neighborhood of the X axis, we show the full side view of only the central high-temperature region in Fig. 3, which represents the basic features of the working surface to be compared with observed working surfaces such as HH 34.

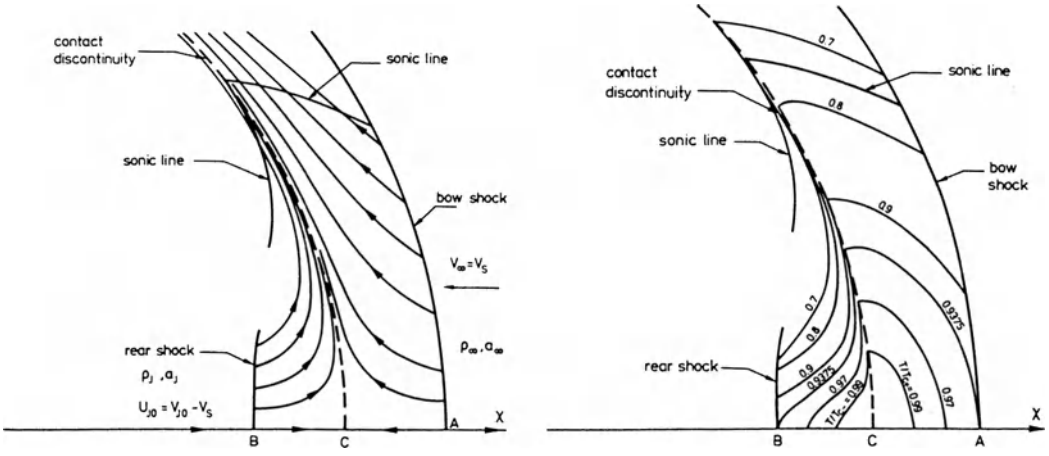

Fig. 2. a: The flow field between the two shocks. b: The temperature distribution. Contours are labelled in terms of $T_{C\pm}$, which are the temperatures immediately to the right (+) and left (−) of the stagnation point. The sonic line indicates where the flow between the shocks changes from subsonic to supersonic.

II. Analytical solutions for the case of radiating shocks

The effect of radiation cooling at the post shock regions is usually important for astrophysical jets. The mechanism of radiation cooling involves the processes of dissociation, ionization and excitation of various components of the gas. The detailed processes are so complicated that it is very difficult to give an analytical treatment of the flow field when radiation cooling is included. However, if the scale of radiation cooling is small compared to the size of the working surface, and if we are not concerned with the process of radiation cooling, but only with its influence on the flow field, we can approximate the

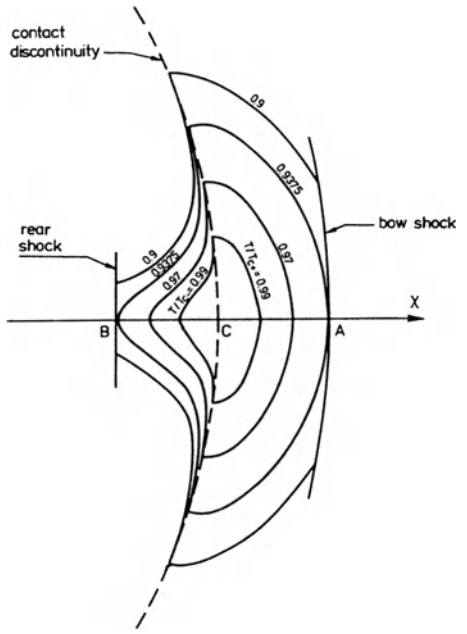

Fig. 3. The full side view of the central high-temperature region.

Table 1. The relation between the geometrical parameters and the radiation loss factor ζ

ζ	R_S/R_C	$(R_S - R_C)/H$	$(R_C - X_B)/H$	$(R_S - X_B)/H$	R_C/H
0	1.176	0.4773	0.4301	0.9074	2.712
0.1	1.147	0.4276	0.3922	0.8198	2.909
0.2	1.121	0.3802	0.3559	0.7361	3.142
0.3	1.099	0.3380	0.3214	0.6594	3.414
0.4	1.080	0.2996	0.2876	0.5872	3.746
0.5	1.063	0.2627	0.2548	0.5175	4.170
0.6	1.048	0.2269	0.2217	0.4486	4.726
0.7	1.034	0.1883	0.1867	0.3750	5.539
0.8	1.022	0.1513	0.1486	0.2999	6.878
0.9	1.010	0.0990	0.1020	0.2010	9.904
1	1.000	0	0	0	∞

radiation cooling region as a thin layer and combine it with the shock to form a radiating shock. We introduce a radiation loss factor ζ, defined by

$$\zeta = q \Big/ \left(\frac{u_-^2}{2} + \frac{a_-^2}{\gamma - 1} \right), \tag{10}$$

where q is the radiative energy loss from unit mass as the mass crosses the shock, and u_- and a_- are the propagating velocity of the shock and the sound speed immediately

before the shock, respectively. The denominator in Eq. (10) represents the upper limit of the energy loss q from the unit mass.

By following the same procedure as the last section, we can still obtain the analytical solutions of the flow field for given ζ. The relations between various geometrical parameters and the radiation loss factor ζ are listed in Table 1.

References

1. Lada, C.J.: 1985, Ann. Rev. Astron. Astrophys., 23, 267
2. Bührke, T., Mundt, R. and Ray, T.P.: 1988, Astron. Astrophys., 200, 99
3. Hayes, W.D. and Probstein, R.F.: 1966, Hypersonic Flow Theory, 2nd ed., Academic Press, New York and London
4. Lighthill, M.J.: 1957, J. Fluid Mech., 2, 1
5. Milne-Thomson, L.M.: 1955, Theoretical Hydrodynamics, 3rd ed., Macmillan, New York

A Non–local Model of Line Emission from Molecular Clouds

Alistair C.H. Glasse
Astrophysics Division, ESTEC, 2200AG Noordwijk, The Netherlands.

Abstract

A technique developed by Scharmer & Carlsson for finding accurate solutions to the multi-level line transfer problem in the presence of velocity fields has been adapted for modelling the submillimetre emission spectra of molecular clouds. Line profiles for transitions up to J=20–19 in CO and J=5–4 in HCO^+ can be modelled for slab or spherically symmetric atmospheres exhibiting spatial variations in temperature, density and bulk velocity. The technique is used here to reproduce the published observed profiles of HCO^+, CO and its isotopes, using a single physical model of the Bok globule B335.

Introduction

There are many radiation transport models available to the submillimetre astronomer who wishes to interpret spectral line observations of molecular clouds or circumstellar envelopes. Two of the more successful of these are the familiar LVG (for Large Velocity Gradient) or escape probability method (Goldreich & Kwan 1974, Scoville & Solomon 1974), and the ANR (for Approximate Newton–Raphson) technique, recently adapted for multi–level molecular emission line work by Schönberg and co–workers (Schönberg & Hempe 1986, Schönberg 1988). A common feature of these two techniques is the assumption that the emission is determined by local physical conditions, with no coupling between distant parts of the atmosphere through the line radiation field. This situation is realised when the atmosphere is optically thick, or when the change in the bulk velocity field across a region where the kinetic temperature and density are effectively constant is significantly greater than the intrinsic linewidth. In other physical situations, the emission process becomes non–local, and the interaction of all layers of the cloud must be taken into account.

In this paper we present the first results of a non–local model of molecular line emission which was originally developed to solve the line transfer problem in stellar atmospheres with velocity fields by G.B. Scharmer and M. Carlsson, (Scharmer & Carlsson 1985); we will only give a brief description of the technique here.

The model

The non–local effects of the radiation field are included using an approximate 'Λ' operator solution to the equation of radiative transfer in a perturbed grand rate equation which connects all energy levels and regions of the atmosphere. An accurate error vector is calculated which describes the departure of the perturbed rate equation from statistical equilibrium. Iterative solution of this rate equation for the population perturbations necessary to reduce the error vector then gives the accurate source function throughout the atmosphere.

Scharmer & Carlsson's original code has been modified to deal with the sub–millimetre spectra of molecular clouds by using rates for the rotational excitation of CO and HCO^+ by collisions with H_2. For CO at temperatures below 100K, the rates for para–H_2 (Flower & Launay 1985) were approximated by a linear interpolation formula, while at higher temperatures, rates were taken from Draine & Roberge (1984), with the authors factor 'α' set to zero in accordance with the recommendation of Viscuso & Chernoff (1988). Currently, transitions from levels up to J=20 can be modelled for CO. The rates for HCO^+ at $T_{kinetic} < 30K$ were taken from Monteiro (1985).

The original model's slab geometry was extended to treat spherically symmetric atmospheres by adopting a 'shell ray' approach (see for example Avrett & Loeser 1984); the details of this and other modifications will be described in a later paper.

Adapted for sub–millimetre line transfer problems, the technique allows atmospheres exhibiting wide variations with depth of bulk velocity, density, temperature and turbulent broadening to be modelled, producing accurate and physically realistic line profiles and intensities. It is particularly suited to solving problems where the more familiar LVG approximation is inappropriate, such as the envelopes of late-type stars, the early stages of cloud collapse and low–velocity shocks. Convergence problems have only been encountered so far in the presence of strong population inversions.

Modelling the Bok globule B335

The core of B335 has recently been the subject of an extensive millimetric survey by Frerking, Langer & Wilson (1987) (hereafter FLW), who model their data with LVG or microturbulent models, depending on the optical depth of the transition in question. Here, the power of Scharmer & Carlsson's technique is demonstrated by showing its ability to model FLW's data using a physically realistic model atmosphere which is common to all molecular species.

The radial variations of temperature and density that were used follow FLW's model of the region, with no radial velocity field. For the isotopic abundances, standard gas phase chemistry values were adopted for CO in the cloud core where $n(H_2) > 10^6 cm^{-3}$. In the envelope, either the values determined by FLW were used or, where these were unavailable, theoretical isotopic enhancement factors for regions of low A_V were taken from Glassgold, Huggins & Langer (1985). These physical parameters were defined at the surfaces of fourteen shells with varying thickness.

The predicted line profiles for the J=1–0 transition of the isotopes of CO in the core of B335 are plotted as the smooth curves in Figure 1, with the observed data reproduced for comparison; the observed broad line wings are due to an embedded outflow and so

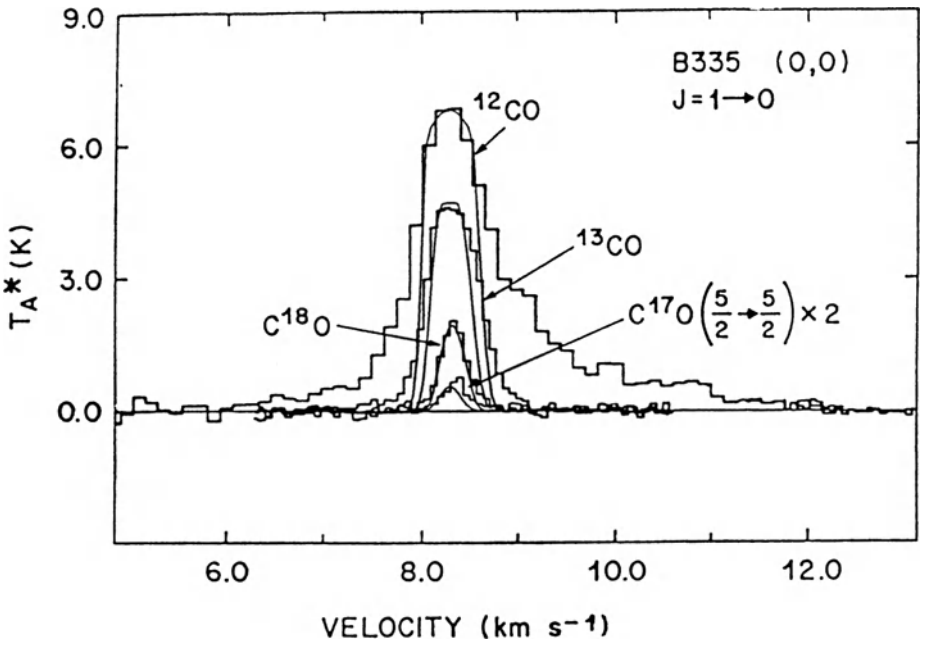

Fig. 1. Fitting the J=1–0 spectra of the isotopes of CO seen towards the core of B335; the observed spectra have been reproduced by permission of the authors

are not treated by our model. The ^{12}CO(1–0) line becomes very optically thick at line centre; the self-reversed profile that one might expect to see is 'filled-in' by external heating of the globule. This good agreement was also seen in the models fit to the observed self-reversed HCO^+(1–0) and ^{12}CO(2–1) profiles.

References

Avrett, E.H., Loeser, R., in 'Methods in Radiative Transfer', C.U.P., ed. Kalkoffen, 341.
Draine, B.T., Roberge, W.G. 1984, Ap.J., 282, 491.
Flower, D.R., Launay, J.M. 1985, M.N.R.A.S, 214, 271.
Frerking, M.A., Langer, W.D., Wilson, R.W. 1987, Ap.J., 313, 320.
Glassgold, A.E., Huggins, P.J., Langer, W.D. 1985, Ap.J., 290, 615.
Goldreich, P., Kwan, J., 1974, Ap. J., 189, 441.
Monteiro, T.S., 1985, M.N.R.A.S, 214, 419.
Scharmer, G.B., Carlsson, M. 1985, Journal of Comp. Phys., 59, 56.
Schönberg, K., 1988, Astron. Astrophys., 195, 198.
Schönberg, K., Hempe, K., 1986, Astron. Astrophys., 163, 151.
Scoville, N.Z., Solomon, P.M., Ap. J. Letters, 187, L67.
Viscuso, P.J., Chernoff, D.F., 1988, Ap. J., 327, 364.

Diffuse Reflected Light from High Latitude Dust Clouds

Ronald Stark
Sterrewacht, PO Box 9513, 2300 RA Leiden, The Netherlands

The transport of radiation in a spherical dust cloud has recently been revived in the context of the interpretation of the cirrus clouds observed by the IRAS satellite (de Vries 1986, van de Hulst 1987, Laureijs *et al.* 1987). Spherical models are also of obvious importance in the study of reflection nebulae because they supplement the more frequently discussed plane parallel models.

We used the exact results for spherical, homogeneous dust clouds (van de Hulst 1987) for isotropic scattering and uniform incident radiation and derived the Bond albedo, or cloud-albedo, as a function of the optical depth of the cloud and as function of the albedo, a, of the individual particles. This result gives us the possibility to derive the albedo, a, from the observations. There are two definitions possible for the cloud-albedo:

$$A = \frac{scattered\ light}{incident\ light}$$

$$A^* = \frac{scattered\ light}{(scattered + absorbed\ light)}$$

The second option excludes the zero-order (unscattered) light from the denominator.

In Figure 1 and 2 we plot both quantities A and A^* as functions of the optical depth, b, measured along the diameter of the cloud, and the albedo a. From Fig. 1 we see that for small optical depth, $b < 1$, the cloud-albedo A increases with b, most of the light is at most once scattered. At a certain optical depth multiple light scattering becomes important, and from there on the cloud-albedo decreases with increasing optical depth. Fig. 2 shows that the cloud-albedo A^* decreases continuously. For small optical depth the cloud-albedo approaches the albedo of a single particle. In Fig. 3 the cloud-albedo A^* is plotted for plane parallel layers (slabs).

High latitude dust clouds are good examples for modelling as above because they are isolated, optically thin and illuminated only by our Galaxy at a large distance ($\sim$ 100 pc). The option for the cloud-albedo without unscattered light describes this situation the best, since only scattered light is seen from our direction.

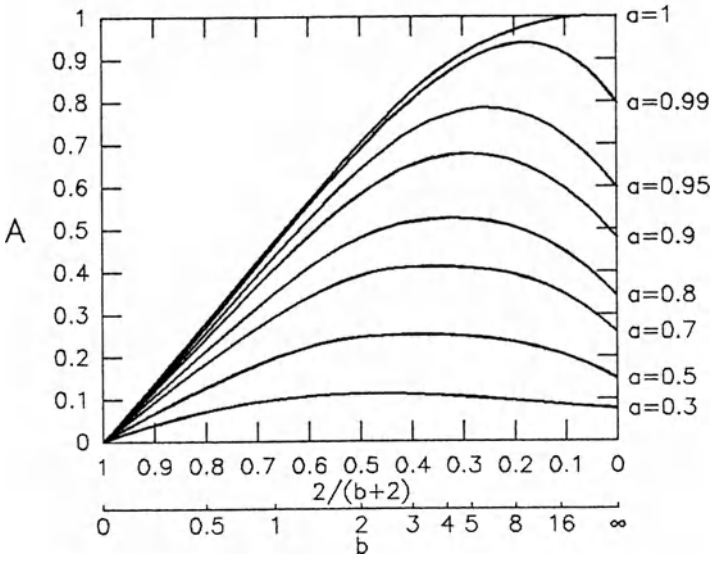

Fig. 1. The cloud-albedo A as function of the optical depth for spherical clouds

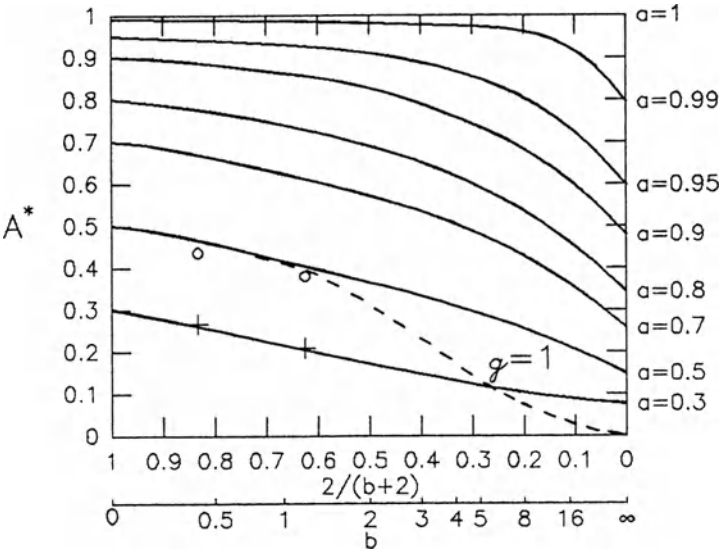

Fig. 2. The cloud-albedo A^* as function of the optical depth for spherical clouds, + indicating the data from de Vries (1986), o indicating the same data corrected for anisotropic scattering

De Vries (1986) studied two high latitude dust clouds (E025 and E487) and derived their optical depths and the total amount of scattered and absorbed light. His data are plotted in Fig. 2 and Fig.3 (as crosses). It is clearly seen that his results are consistent with **one** value for the albedo of the individual particles in both clouds. We find for a

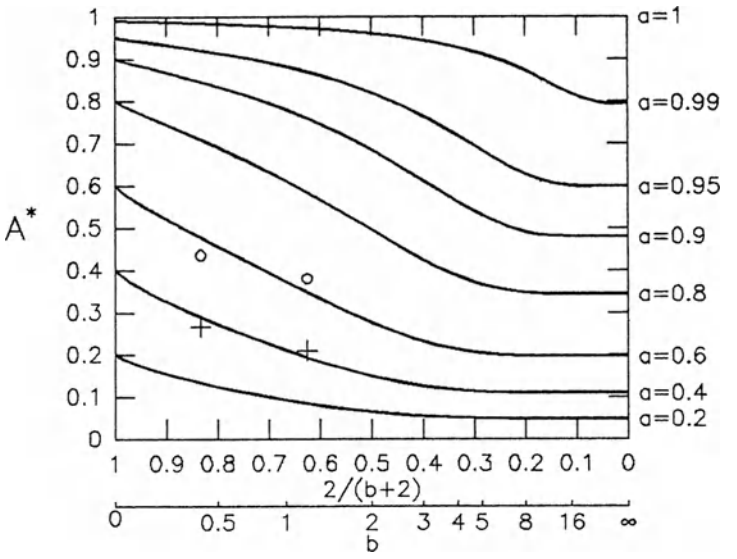

Fig. 3. The cloud-albedo A^* as function of the optical depth for slabs, + indicating the data from de Vries (1986), o indicating the same data corrected for anisotropic scattering

slab geometry a=0.40 ± 0.02 and for a spherical geometry a=0.30 ± 0.02. The spherical result is in agreement with Mattila's (1979) Monte Carlo modelling for L1780: a=0.30.

However interstellar dust particles have a non isotropic phase function. Assuming an anisotropy factor g (0.75) and a correction factor (Jura (1979): $A^* = A^*_{obs}[1-1.1g(sinb)^{\frac{1}{2}}]$ where b is the galactic latitude of the cloud) it then is possible to estimate the total amount of scattered light in other directions. In Fig. 2 and 3 the corrected data are plotted as open circles. In Fig. 2 the cloud albedo for $g = 1$, completely forward scattering, is also plotted for comparison. Since for small optical depth, b < 1, most of the light is singly scattered , the behaviour in that region is the same for any anisotropy factor. We find for a slab: a=0.60 ± 0.02 and for a sphere: a=0.48 ± 0.02. The latter value is in excellent agreement with the result of Laureijs *et al.* (1987) for L1642 : a=0.48 ± 0.03, but the coincidence is somewhat fortuitous.

A full calculation requires the use of an anisotropic model instead of a single correction factor. This will be developed soon.

References:

de Vries, C. P.: 1986 Thesis Leiden University
Jura, M.: 1979 Astrophys. J. **227**, 798
Laureijs, R. J., Mattila, K., Schnur, G.: 1987 Astron. Astrophys. **184**, 269
Mattila, K.: 1979 Astron. Astrophys. **78**, 253
van de Hulst, H. C.: 1987 Astron. Astrophys. **173**, 115

Laboratory Spectroscopy: The Rotation-Torsion Spectrum of Carbodiimide, HNCNH

Manfred Winnewisser

Physikalisch-Chemisches Institut, Justus-Liebig-Universität Giessen, Heinrich-Buff-Ring 58, D-6300 Giessen, Federal Republic of Germany

Abstract

The rotation-torsion spectrum of carbodiimide, HNCNH, a constituent of the vapour of the well-known interstellar molecule cyanamide, H_2NCN, was measured in the region from 20 GHz to 330 cm^{-1} using a high resolution Fourier transform spectrometer, a laser single sideband spectrometer, a millimeter wave and a submillimeter wave spectrometer. The spectral pattern of a perpendicular band system of an almost perfect accidental symmetric top, expected for skew-chain molecules, was observed. The principal axis b is parallel to the C_2 symmetry axis of HNCNH. The molecular constants obtained by fitting the positions of the torsional doublet centers with Watson's Hamiltonian in S-reduction are A = 379 244.493 (27) MHz, B = 10 366.9389 (18) MHz, and C = 10 366.0837 (25) MHz which yield $\kappa = -0.999\,995\,368\,(18)$. Small splittings of the observed rotational lines were found to be due to a torsional motion. Excerpts of the experimental data and the effective molecular constants of HNCNH relevant for radioastronomy are given.

Introduction

High resolution and high precision molecular spectroscopy in the terrestrial laboratory has been in the past and will be in the future an essential part of the information backbone of radioastronomy in its attempt to probe and understand the complex physics and chemistry of the interstellar medium. In my lecture at Zermatt I selected as a case study of current laboratory work the discovery and measurement of the high resolution spectrum of the molecule carbodiimide, HNCNH. In contrast to my lecture I shall not retrace in this paper all the steps of our work; I shall simply provide you with the hard data necessary for a radioastronomical search.

Carbodiimide, HNCNH, belongs to the group of isomers of the well-known interstellar molecule cyanamide, H_2NCN, which have been investigated in the Giessen laboratory

(*1-8*) by high resolution spectroscopic techniques in the vapour phase. Although carbodiimide was calculated to be the next most stable isomer after cyanamide (*9*), it has not been isolated chemically. We now know that this is due to the low tautomerisation barrier between carbodiimide and cyanamide: There is an equilibrium between the two molecules with the ratio of the molecular abundances determined by their difference in free energy. This difference is calculated *ab initio* to be 42 kJ/mol (*9*), which led in the past to the conclusion that the abundance of carbodiimide should be very low at room temperature in the terrestrial laboratory. As in the well-known case of the interstellar isomers HCN and HNC (*10*) an equilibrium between HNCNH and H_2NCN will certainly not exist in interstellar molecular clouds with their low particle densities and low kinetic temperatures. However, since cyanamide has been detected in the interstellar medium (*11,12*), and the ion-molecule reaction scheme predicts carbodiimide to be also a constituent of interstellar clouds, such an interstellar search is highly recommended, since accurate microwave, millimeter wave and sub-millimeter wave data are now available.

The first evidence for the existence of the free molecule carbodiimide in the gaseous phase was presented by King and Strope in 1971 (*13*). Four carbodiimide bands were identified in the IR matrix isolation spectrum of trapped cyanamide vapour. Confirmation that carbodiimide is present in the vapour phase in equilibrium with cyanamide was given in 1985 by Birk and Winnewisser (*14,15*) who detected three complex carbodiimide band systems corresponding to bands observed by King and Strope in the matrix spectrum. Two of these parallel bands were remeasured with Doppler-limited resolution (*16*). A complete analysis was impossible without prior knowledge of the spectroscopic constants for the ground vibrational state. In order to obtain this information, the observation and analysis of the rotational spectrum was mandatory.

The new Bruker IFS 120 HR Fourier transform spectrometer (FTS) in Giessen enabled us to measure the high resolution spectrum (0.0025 cm^{-1}) of cyanamide and carbodiimide in the far infrared region from 25 to 330 cm^{-1}. In addition, single sideband laser data in the far infrared, as well as submillimeter wave, millimeter wave and microwave data were obtained at the Jet Propulsion Laboratory in Pasadena. Further millimeter wave measurements were carried out in Giessen. The experimental details relevant in obtaining the spectra, the problems of finding the spectrum among the ubiquitous lines of cyanamide, as well as the theoretical analysis of our HNCNH data, in particular the torsional doubling, have already been published (*17,18,19*) elsewhere and are summarized by Birk (*16*).

Molecular Structure and Type of Spectrum

Carbodiimide belongs to the point group C_2. It is isoelectronic to the molecule allene, H_2CCCH_2, and therefore the dihedral angle Φ is nearly 90°. This gives rise to a very interesting situation as far as the inertial asymmetry of the molecule and its resulting spectrum are concerned. Carbodiimide is extremely close to an accidental symmetric top with its permanent electric dipole moment collinear with the C_2 axis, thus exhibiting as its rotational spectrum a perpendicular band system. A recent *ab initio* calculation (*18*) predicted the inertial asymmetry of the molecule to be so small that, within the estimated error, either the *b*- or the *c*-axis could be parallel to the C_2-axis. The analysis of our data

revealed without doubt that carbodiimide exhibits a *b*-type rotational spectrum with a small torsional splitting of the individual rotational lines. The permanent electric dipole moment was found to be 1.90 D. From this determination of the electric dipole moment and intensity measurements the abundance ratio of HNCNH to H_2NCN in the gas phase at 110°C was found to be 1 to 115(14). A detailed discussion of how we reached these conclusions can be found in Refs. (*17,18,19*).

Molecular Constants of HNCNH

Two different methods have been used in order to obtain effective molecular constants from the observed line positions of the rotation-torsion transitions and to predict the remaining part of the rotation-torsion spectrum. In the first method we considered the unperturbed rotational line positions only, i.e. the center positions of the torsional doublets. These were fitted using Watson's Hamilton operator in S-reduction (*20,21*). In this way 20 adjusted effective molecular constants were fitted to 335 center frequencies. From the rotational constants obtained via this procedure and listed in the abstract Wang's asymmetry parameter b_p and Ray's asymmetry parameter κ (*22*) were calculated:

$$b_p = \frac{\kappa + 1}{\kappa - 3} = -1.1580(45) \times 10^{-6}$$
$$\kappa = \frac{2B - A - C}{A - C} = -0.999\,995\,368(18).$$

Compared even to structurally related molecules carbodiimide is closest to an accidentally symmetric top molecule, since $\kappa(H_2O_2) = -0.991\,959\,22$ (*23*) and $\kappa(H_2S_2) = -0.999\,960\,8$ (*24*).

The fitting of molecular constants to the centers of the torsional doublets of the individual rotational lines has the disadvantage that the line positions themselves were not used or reproduced. It was initially essential, however, to determine the D_{JK} value in order to complete the assignment of the ${}^rQ_0$ rotational lines, as discussed in Ref. (*17*).

A more rigorous but still effective fitting procedure was also carried out, fitting the observed line positions directly though not accounting for the torsion explicitly in the energy operator. The selection rules for the rotation-torsion transitions and the group theoretical aspects were dicussed in great detail in Refs. (*16,17,19*). They allow transitions only to occur between the pairs of states denoted as A_{1s}, A_{1d} and A_{2s}, A_{2d}. Each pair of states was treated as an upper and lower vibrational (torsional) energy state,

$$\tilde{\nu}_1 = \frac{1}{hc}[E_{A_{1d}}(0,0) - E_{A_{1s}}(0,0)] + \frac{1}{hc}[E_{rot,A_{1d}}(J', K_a', K_c') - E_{rot,A_{1s}}(J'', K_a'', K_c'')]$$
$$\tilde{\nu}_2 = \frac{1}{hc}[E_{A_{2s}}(0,0) - E_{A_{2d}}(0,0)] + \frac{1}{hc}[E_{rot,A_{2s}}(J', K_a', K_c') - E_{rot,A_{2d}}(J'', K_a'', K_c'')],$$

with

Table 1. Observed and Calculated Rotation–Torsion Transitions of HNCNH

Γ'_{tors} $J'(K'_a, K'_c)$ - Γ''_{tors} $J''(K''_a, K''_c)$	ν_{obs}/MHz	$(\nu_{obs} - \nu_{calc})$/MHz
	$^rQ_0$-branch	
A_{1d} 3(1, 2) - A_{1s} 3(0, 3)	368 940.294	0.089
A_{1d} 4(1, 3) - A_{1s} 4(0, 4)	368 939.296	-0.022
A_{1d} 5(1, 4) - A_{1s} 5(0, 5)	368 938.190	-0.019
A_{1d} 6(1, 5) - A_{1s} 6(0, 6)	368 936.866	-0.010
A_{1d} 7(1, 6) - A_{1s} 7(0, 7)	368 935.310	-0.010
A_{1d} 8(1, 7) - A_{1s} 8(0, 8)	368 933.533	-0.005
A_{1d} 9(1, 8) - A_{1s} 9(0, 9)	368 931.530	0.000
A_{1d} 10(1, 9) - A_{1s} 10(0, 10)	368 929.298	0.003
A_{1d} 11(1, 10) - A_{1s} 11(0, 11)	368 926.845	0.014
A_{1d} 12(1, 11) - A_{1s} 12(0, 12)	368 924.152	0.015
A_{1d} 13(1, 12) - A_{1s} 13(0, 13)	368 921.234	0.023
A_{1d} 14(1, 13) - A_{1s} 14(0, 14)	368 918.101	0.050
A_{1d} 15(1, 14) - A_{1s} 15(0, 15)	368 914.700	0.044
A_{1d} 16(1, 15) - A_{1s} 16(0, 16)	368 911.085	0.061
A_{1d} 17(1, 16) - A_{1s} 17(0, 17)	368 907.210	0.058
A_{1d} 18(1, 17) - A_{1s} 18(0, 18)	368 903.074	0.035
A_{1d} 19(1, 18) - A_{1s} 19(0, 19)	368 898.743	0.062
A_{1d} 20(1, 19) - A_{1s} 20(0, 20)	368 894.120	0.044
A_{1d} 21(1, 20) - A_{1s} 21(0, 21)	368 889.172	-0.050
A_{1d} 22(1, 21) - A_{1s} 22(0, 22)	368 884.127	0.011
A_{1d} 23(1, 22) - A_{1s} 23(0, 23)	368 878.764	0.009
A_{1d} 24(1, 23) - A_{1s} 24(0, 24)	368 873.143	0.008
A_{1d} 25(1, 24) - A_{1s} 25(0, 25)	368 867.237	-0.016
A_{1d} 26(1, 25) - A_{1s} 26(0, 26)	368 861.061	-0.046
A_{1d} 27(1, 26) - A_{1s} 27(0, 27)	368 854.585	-0.107
A_{1d} 28(1, 27) - A_{1s} 28(0, 28)	368 847.874	-0.132
A_{1d} 29(1, 28) - A_{1s} 29(0, 29)	368 840.905	-0.138
A_{1d} 30(1, 29) - A_{1s} 30(0, 30)	368 833.732	-0.069
A_{1d} 31(1, 30) - A_{1s} 31(0, 31)	368 826.149	-0.127
A_{1d} 32(1, 31) - A_{1s} 32(0, 32)	368 818.505	0.043
A_{1d} 33(1, 32) - A_{1s} 33(0, 33)	368 810.450	0.093
A_{1d} 34(1, 33) - A_{1s} 34(0, 34)	368 802.046	0.091
A_{1d} 35(1, 34) - A_{1s} 35(0, 35)	368 793.293	0.042
A_{1d} 36(1, 35) - A_{1s} 36(0, 36)	368 784.270	0.028
A_{1d} 37(1, 36) - A_{1s} 37(0, 37)	368 774.969	0.047
A_{1d} 38(1, 37) - A_{1s} 38(0, 38)	368 765.314	0.027
A_{1d} 39(1, 38) - A_{1s} 39(0, 39)	368 755.430	0.099
A_{1d} 40(1, 39) - A_{1s} 40(0, 40)	368 745.123	0.074
A_{1d} 41(1, 40) - A_{1s} 41(0, 41)	368 734.488	0.053
A_{1d} 42(1, 41) - A_{1s} 42(0, 42)	368 723.407	-0.078
A_{1d} 43(1, 42) - A_{1s} 43(0, 43)	368 712.207	0.015
A_{1d} 45(1, 44) - A_{1s} 45(0, 45)	368 688.572	0.016
A_{1d} 46(1, 45) - A_{1s} 46(0, 46)	368 676.176	-0.024
A_{1d} 47(1, 46) - A_{1s} 47(0, 47)	368 663.518	0.040
A_{1d} 48(1, 47) - A_{1s} 48(0, 48)	368 650.392	0.009

Table 1. continued (a)

Γ'_{tors} $J'(K'_a, K'_c)$ - Γ''_{tors} $J''(K''_a, K''_c)$	ν_{obs}/MHz	$(\nu_{obs} - \nu_{calc})$/MHz
$^rQ_0$-branch		
A_{1d} 49(1, 48) - A_{1s} 49(0, 49)	368 636.921	0.012
A_{1d} 50(1, 49) - A_{1s} 50(0, 50)	368 622.971	-0.078
A_{1d} 51(1, 50) - A_{1s} 51(0, 51)	368 608.952	0.155
A_{1d} 52(1, 51) - A_{1s} 52(0, 52)	368 593.969	-0.176
A_{1d} 53(1, 52) - A_{1s} 53(0, 53)	368 579.072	-0.014
A_{1d} 54(1, 53) - A_{1s} 54(0, 54)	368 563.553	-0.062
A_{1d} 55(1, 54) - A_{1s} 55(0, 55)	368 547.845	0.123
$^rP_0/^pR_1$-branch		
A_{1d} 5(1, 5) - A_{1s} 6(0, 6)	244 529.640	-0.067
A_{1d} 7(1, 7) - A_{1s} 8(0, 8)	203 053.264	-0.018
A_{1d} 8(1, 8) - A_{1s} 9(0, 9)	182 314.382	0.049
A_{1d} 9(1, 9) - A_{1s} 10(0, 10)	161 575.008	0.008
A_{1d} 10(1, 10) - A_{1s} 11(0, 11)	140 835.282	-0.077
A_{1d} 11(1, 11) - A_{1s} 12(0, 12)	120 095.458	-0.035
A_{1d} 11(1, 11) - A_{1s} 12(0, 12)	120 095.498	0.006
A_{1d} 12(1, 12) - A_{1s} 13(0, 13)	99 355.449	-0.029
A_{1d} 15(1, 15) - A_{1s} 16(0, 16)	37 135.395	0.048
A_{1d} 16(1, 16) - A_{1s} 17(0, 17)	16 395.527	-0.014
A_{1s} 19(0, 19) - A_{1d} 18(1, 18)	25 083.265	0.028
A_{1s} 20(0, 20) - A_{1d} 19(1, 19)	45 822.046	-0.002
A_{1s} 23(0, 23) - A_{1d} 22(1, 22)	108 035.184	-0.020
A_{1s} 25(0, 25) - A_{1d} 24(1, 24)	149 507.092	-0.015
A_{1s} 27(0, 27) - A_{1d} 26(1, 26)	190 975.466	0.039
A_{1s} 29(0, 29) - A_{1d} 28(1, 28)	232 439.504	-0.016
$^rR_0$-branch		
A_{1d} 5(1, 5) - A_{1s} 4(0, 4)	472 588.762	0.016
$^rQ_3$-branch		
A_{1s} 10(4, 7;6) - A_{1d} 10(3, 8;7)	2 553 650.970	0.212
A_{1s} 11(4, 8;7) - A_{1d} 11(3, 9;8)	2 553 599.170	0.083
A_{1s} 12(4, 9;8) - A_{1d} 12(3, 10;9)	2 553 542.850	0.130
A_{1s} 13(4, 10;9) - A_{1d} 13(3, 11;10)	2 553 482.280	0.621
A_{1s} 14(4, 11;10) - A_{1d} 14(3, 12;11)	2 553 415.940	0.035
A_{1s} 15(4, 12;11) - A_{1d} 15(3, 13;12)	2 553 345.600	0.144
A_{1s} 16(4, 13;12) - A_{1d} 16(3, 14;13)	2 553 270.450	0.135
A_{1s} 17(4, 14;13) - A_{1d} 17(3, 15;14)	2 553 191.170	0.687
A_{1s} 18(4, 15;14) - A_{1d} 18(3, 16;15)	2 553 106.040	0.081

Table 1. continued (b)

Γ'_{tors} $J'(K'_a, K'_c)$ - Γ''_{tors} $J''(K''_a, K''_c)$	ν_{obs}/MHz	$(\nu_{obs} - \nu_{calc})$/MHz
$^rQ_0$-branch		
A_{2d} 3(1,2) - A_{2s} 3(0,3)	368 476.604	0.106
A_{2d} 4(1,3) - A_{2s} 4(0,4)	368 475.504	-0.065
A_{2d} 5(1,4) - A_{2s} 5(0,5)	368 474.452	0.045
A_{2d} 6(1,5) - A_{2s} 6(0,6)	368 472.998	-0.013
A_{2d} 7(1,6) - A_{2s} 7(0,7)	368 471.358	-0.023
A_{2d} 8(1,7) - A_{2s} 8(0,8)	368 469.498	-0.016
A_{2d} 9(1,8) - A_{2s} 9(0,9)	368 467.384	-0.028
A_{2d} 10(1,9) - A_{2s} 10(0,10)	368 465.065	-0.006
A_{2d} 11(1,10) - A_{2s} 11(0,11)	368 462.454	-0.037
A_{2d} 12(1,11) - A_{2s} 12(0,12)	368 459.648	-0.023
A_{2d} 13(1,12) - A_{2s} 13(0,13)	368 456.684	0.076
A_{2d} 14(1,13) - A_{2s} 14(0,14)	368 453.285	-0.016
A_{2d} 15(1,14) - A_{2s} 15(0,15)	368 449.750	0.002
A_{2d} 16(1,15) - A_{2s} 16(0,16)	368 445.962	0.014
A_{2d} 17(1,16) - A_{2s} 17(0,17)	368 441.936	0.039
A_{2d} 19(1,18) - A_{2s} 19(0,19)	368 433.059	0.023
A_{2d} 20(1,19) - A_{2s} 20(0,20)	368 428.266	0.045
A_{2d} 21(1,20) - A_{2s} 21(0,21)	368 423.188	0.042
A_{2d} 22(1,21) - A_{2s} 22(0,22)	368 417.820	0.011
A_{2d} 23(1,22) - A_{2s} 23(0,23)	368 412.174	-0.031
A_{2d} 24(1,23) - A_{2s} 24(0,24)	368 406.287	-0.046
A_{2d} 25(1,24) - A_{2s} 25(0,25)	368 400.171	-0.018
A_{2d} 26(1,25) - A_{2s} 26(0,26)	368 393.741	-0.029
A_{2d} 27(1,26) - A_{2s} 27(0,27)	368 387.086	0.014
A_{2d} 28(1,27) - A_{2s} 28(0,28)	368 380.127	0.036
A_{2d} 29(1,28) - A_{2s} 29(0,29)	368 372.868	0.044
A_{2d} 30(1,29) - A_{2s} 30(0,30)	368 365.279	0.012
A_{2d} 31(1,30) - A_{2s} 31(0,31)	368 357.455	0.038
A_{2d} 32(1,31) - A_{2s} 32(0,32)	368 349.316	0.048
A_{2d} 33(1,32) - A_{2s} 33(0,33)	368 340.772	-0.044
A_{2d} 34(1,33) - A_{2s} 34(0,34)	368 332.039	-0.019
A_{2d} 35(1,34) - A_{2s} 35(0,35)	368 322.788	-0.200
A_{2d} 36(1,35) - A_{2s} 36(0,36)	368 313.629	0.027
A_{2d} 39(1,38) - A_{2s} 39(0,39)	368 283.539	0.041
A_{2d} 40(1,39) - A_{2s} 40(0,40)	368 272.793	-0.004
A_{2d} 41(1,40) - A_{2s} 41(0,41)	368 261.818	0.062
A_{2d} 42(1,41) - A_{2s} 42(0,42)	368 250.385	0.018
A_{2d} 43(1,42) - A_{2s} 43(0,43)	368 238.642	0.017
A_{2d} 44(1,43) - A_{2s} 44(0,44)	368 226.615	0.090
A_{2d} 45(1,44) - A_{2s} 45(0,45)	368 214.042	-0.018

Table 1. continued (c)

Γ'_{tors} $J'(K'_a, K'_c)$ - Γ''_{tors} $J''(K''_a, K''_c)$	ν_{obs}/MHz	$(\nu_{obs} - \nu_{calc})$/MHz
$^rP_0/^pR_1$-branch		
A_{2d} 5(1, 5) - A_{2s} 6(0, 6)	244 066.575	-0.048
A_{2d} 7(1, 7) - A_{2s} 8(0, 8)	202 590.600	-0.006
A_{2d} 8(1, 8) - A_{2s} 9(0, 9)	181 851.900	-0.004
A_{2d} 9(1, 9) - A_{2s} 10(0, 10)	161 112.838	-0.008
A_{2d} 10(1, 10) - A_{2s} 11(0, 11)	140 373.511	0.002
A_{2d} 11(1, 11) - A_{2s} 12(0, 12)	119 633.950	-0.024
A_{2d} 11(1, 11) - A_{2s} 12(0, 12)	119 634.030	0.056
A_{2d} 12(1, 12) - A_{2s} 13(0, 13)	98 894.322	0.001
A_{2d} 15(1, 15) - A_{2s} 16(0, 16)	36 675.469	0.025
A_{2d} 16(1, 16) - A_{2s} 17(0, 17)	15 936.094	-0.019
A_{2s} 19(0, 19) - A_{2d} 18(1, 18)	25 541.620	-0.010
A_{2s} 20(0, 20) - A_{2d} 19(1, 19)	46 279.903	0.022
A_{2s} 23(0, 23) - A_{2d} 22(1, 22)	108 491.198	0.006
A_{2s} 25(0, 25) - A_{2d} 24(1, 24)	149 961.723	-0.006
A_{2s} 27(0, 27) - A_{2d} 26(1, 26)	191 428.580	0.000
A_{2s} 29(0, 29) - A_{2d} 28(1, 28)	232 891.096	-0.006
$^rR_0$-branch		
A_{2d} 5(1, 5) - A_{2s} 4(0, 4)	472 125.506	0.143
$^rQ_3$-branch		
A_{2s} 13(4, 10;9) - A_{2d} 13(3, 11;10)	2 553 642.190	0.003
A_{2s} 14(4, 11;10) - A_{2d} 14(3, 12;11)	2 553 576.950	0.336
A_{2s} 15(4, 12;11) - A_{2d} 15(3, 13;12)	2 553 506.000	-0.355
A_{2s} 16(4, 13;12) - A_{2d} 16(3, 14;13)	2 553 431.200	-0.211
A_{2s} 17(4, 14;13) - A_{2d} 17(3, 15;14)	2 553 352.160	0.379
A_{2s} 18(4, 15;14) - A_{2d} 18(3, 16;15)	2 553 267.560	0.095
A_{2s} 19(4, 16;15) - A_{2d} 19(3, 17;16)	2 553 179.390	0.928
A_{2s} 21(4, 18;17) - A_{2d} 21(3, 19;18)	2 552 986.310	-0.085

Table 2. Effective Molecular Constants in MHz for the Torsional Levels of HNCNH in the Vibrational Ground State

Constants	Irreducible representations of the torsional levels			
	A_{1s}	A_{1d}	A_{2s}	A_{2d}
A	379 267.27(59)	379 246.72(54)	379 220.61(53)	379 237.95(48)
B	10 366.956 7(19)	10 366.956 7(26)	10 366.925 4(22)	10 366.925 4(17)
C	10 366.085 8(31)	10 366.085 8(26)	10 366.091 5(22)	10 366.091 5(26)
$D_J \times 10^2$	0.324 66(64)		0.326 03(56)	
D_{JK}	0.328 22(35)		0.324 06(30)	
D_K	169.856(53)	168.850(40)	167.309(48)	168.003(36)
$d_1 \times 10^5$	-0.622(24)		-0.573(19)	
$H_J \times 10^8$	0.53(33)		0.61(27)	
$H_{JK} \times 10^6$	0.61(24)		0.14(19)	
$H_{KJ} \times 10^3$	-0.144(24)		-0.336(22)	
H_K	0.459 9(18)	0.438 6(13)	0.389 7(16)	0.402 1(12)
$L_{JK} \times 10^7$	0.179(92)		0.162(79)	
$L_{KJ} \times 10^5$	0.875(71)		0.445(66)	
$L_K \times 10^2$	0.192 6(24)	0.177 8(20)	0.105 8(22)	0.113 4(19)
$S_{JK} \times 10^9$	0.261(80)		0.300(72)	
$S_{KJ} \times 10^7$	0.620(92)		0.174(85)	
$S_K \times 10^5$	0.552(11)		0.173(10)	
$T_{KJ} \times 10^9$	0.578(40)		0.412(38)	
$(1/h)\Delta E_{trans}(0,0)$	229.75(50)		225.96(45)	
σ	0.107		0.098	

$$E_{A_{1d}}(0,0) - E_{A_{1s}}(0,0) = \Delta E_{trans}(K_a = 0, J = 0)$$
$$E_{A_{2s}}(0,0) - E_{A_{2d}}(0,0) = \Delta E_{trans}(K_a = 0, J = 0)$$

and $E_{rot,A_{1s}}(J'', K_a'', K_c'')$, $E_{rot,A_{1d}}(J', K_a', K_c')$, etc. being the rotational energies in the different torsional states, calculated again using Watson's S-reduced Hamiltonian. For the torsional transitions $E_{A_{1d}} \leftrightarrow E_{A_{1s}}$ 351 individual rotational lines were analysed while for the torsional transitions $E_{A_{2s}} \leftrightarrow E_{A_{2d}}$ 345 lines could be included in the fit. This analysis yielded 23 effective spectroscopic constants for the set of four torsional states. The observed line positions ν_{obs} and $\tilde{\nu}_{obs}$ and the differences in observed minus calculated line positions of the combined microwave, MMW, SubMMW and FIR laser data are given in Table 1. The Fourier transform data were included in the global fit but they are not entered in Table 1 since they are not yet of direct interest to radioastronmy. The unabriged list of assigned HNCNH line positions can be found in Refs. (*16,19*). The resulting molecular constants are given in Table 2. The J and K_a dependence of the observed doublet splitting is incorporated into the slightly different set of constants obtained for each torsional state without being related to the torsional potential function or the rotation-torsion interaction. However, the adjusted spectroscopic constants given in Table 2 enable us to provide accurate predictions of the HNCNH ground state rotation-torsion transitions throughout the entire MW, MMW, SubMMW and FIR regions, thus providing the basis for a radioastronomical search for this important isomer of cyanamide. They will also be essential in the analysis of vibration-rotation bands of the molecule.

Acknowledgements. The author expresses his sincere thanks to Dr. Brenda P. Winnewisser for valuable comments, and Dr. Frank Holland for his help in TeXing the manuscript. The laboratory and computational work was supported in Giessen in part by the Deutsche Forschungsgemeinschaft and the Fonds der Chemischen Industrie.

References

1. M. Winnewisser, K. Möller and A. Gambi, The Microwave, Infrared and Ultraviolet Spectra of Diazirines: Interpretation and Physical Aspects in "The Chemistry of Diazirines" (M. T. H. Liu, Ed.), CRC Press, Boca Raton, 1987.
2. M. Bogey, M. Winnewisser and J. J. Christiansen, Can. J. Phys. 62, 1198-1216 (1984).
3. U. P. Verma, K. Möller, J. Vogt, M. Winnewisser and J. J. Christiansen, Can. J. Phys. 63, 1173-1183 (1985).
4. E. Schäfer and M. Winnewisser, J. Mol. Spectrosc. 97,154-164 (1983).
5. J. Vogt, M. Winnewisser, K. Yamada and G. Winnewisser, Chem. Phys., 83, 309-318 (1984).
6. E. Schäfer and M. Winnewisser, Ber. Bunsenges. Phys. Chem. 86, 780-790 (1982).
7. P. Jensen and M. Winnewisser, Collect. Czech. Chem. Commun. 51, 1373-1381 (1986).
8. M. Winnewisser and J. Reinstaedtler, J. Mol. Spectrosc. 120, 28-48 (1986).
9. C. Thomson and C. Glidewell, J. Comput. Chem. 4, 1-8 (1983).
10. T. L. Allen, J. D. Goddard and H. F. Schaefer III, J. Chem. Phys. 73, 3255-3263 (1980).
11. B. E. Turner, A. G. Kislyakow, H. S. Liszt, and N. Kaifu, Astrophys. J. 201, L149-L152 (1975).
12. H. E. Matthews and T. J. Sears, Astrophys. J. 300, 766-772 (1986).
13. S.T. King and J.H. Strope, J. Chem. Phys. 54, 1289-1295 (1971).
14. M. Birk and M. Winnewisser, Chem. Phys. Lett. 123, 382-385 (1986).
15. M. Birk and M. Winnewisser, Chem. Phys. Lett. 123, 386-389 (1986).
16. M. Birk, Dissertation Justus-Liebig-Universität Giessen (D26), D-6300 Giessen, Federal Republic of Germany.
17. M. Winnewisser and M. Birk, J. Chem. Soc., Faraday Trans. 2, 84, 1341-1363 (1988).
18. M. T. Nguyen, N. V. Riggs, L. Radom, M. Winnewisser, B. P. Winnewisser and M. Birk, Chem. Phys. 122, 305-315 (1988).

19. M. Birk, M. Winnewisser and E. A. Cohen, J. Mol. Spectrosc., in press (1989).
20. J. K. G. Watson, J. Chem. Phys. 46, 1935-1949 (1967).
21. J. K. G. Watson, J. Chem. Phys. 48, 4517-4524 (1968).
22. W. Gordy and R. L. Cook, Microwave Molecular Spectra in "Techniques of Chemistry" (A. Weissberger, Ed.), John Wiley & Sons, New York, Vol. XVIII, 1984.
23. P. Helminger, W. C. Bowman and F. C. DeLucia, J. Mol. Spectrosc. 85, 120-130 (1981).
24. G. M. Plummer, G. Winnewisser, M. Winnewisser J. Hahn and K. Reinartz, J. Mol. Spectrosc. 122, 255-269 (1987).

MOLECULAR ABUNDANCES IN THE DENSE INTERSTELLAR AND CIRCUMSTELLAR CLOUDS

M. Guélin[†] and J. Cernicharo[†,‡]
[†]IRAM, Domaine Universitaire, F-38406 St-Martin-d'Hères, France
and IRAM, Divina Pastora 7, 18012 Granada, Spain
[‡]Centro Astronomico de Yebes, OAN, Ap. 148, 19080, Spain

ABSTRACT

The abundances of a variety of astrophysical molecules, ranging from H_2 and CO to urea and glycine, are reconsidered in the light of new astronomical and laboratory data. Emphasis is given on the sources HCL2(TMC1) and IRC+10216.

1 Introduction

The determination of molecular abundances in the dense interstellar clouds is a difficult task. H_2 cannot be observed, except on the line of sight to a few bright infrared sources. CO, the next most abundant molecule, is easily observable through its millimetre lines, but these are so optically thick that they seldom probe deeper than the outermost layers. The polar species CS, HCN, HCO^+, H_2CO, NH_3 have also optically very thick lines, while N_2, C_2, CO_2,C_2H_2 and CH_4 have no detectable radio transition. Finally, O_2 cannot be observed from the ground or from airplane, due to atmospheric absorption. The abundances of these important species have to be derived indirectly from the dust column density, assuming a constant dust-to-H_2 or CO ratio, from rare isotopic species, neglecting isotopic fractionation, from delicate radiative transfer calculations, or from chemistry models. Progress has thus been slow in the recent years; it has come mainly from the access to the far-infrared dust radiation, using IRAS and airborne telescopes, from higher resolution millimetre wave observations, and from a better understanding of isotope-selective photodissociation of CO at the edges of the clouds.

Paradoxically, abundance determinations are somewhat easier for the heavier and less abundant species, which have a rich spectrum of optically thin microwave lines. These species' rotational level populations can be properly sampled and their abundances derived without detailed knowledge of the excitation conditions. This latter point is particularly valuable, since the gas density and temperature vary along the line of sight and across the antenna beam, and since, except for CO, OH, H_2CO and NH_3^1, the excitation rates for collisions with H_2 are not well known (most excitation rates reported in the literature are very uncertain at low temperatures, even in the case of collisions with He, as attested by the recent redeterminations of H_2O–He [2]). It is for

this type of molecules, in particular for the acetylenic chains, that our knowledge of the abundances has progressed the most.

In this article, we will focus on a few recent advances, referring the reader to other reviews[3,4] for a general survey of the subject.

The H_2, CO and dust abundances

Because H_2 is difficult to observe, dust and CO are used as the main gas tracers in dense molecular clouds. The far-IR and sub-mm continuum radiation emitted by dust grains is mostly optically thin, and can be observed throughout the densest clouds. Its intensity depends on the grain composition, size and temperature and is not easy to relate to the dust column density. The emission of dusty clouds embedded in the "standard" interstellar radiation field (ISRF) have nevertheless been modeled [5,6]. Of special interest is the model by Boulanger and Perault[6] of HCL2, a dark cloud in Taurus which contains TMC1, one of the richest interstellar molecular sources. HCL2 is a nearby "translucent" cloud (average A_v=3.5 mag), for which data are available on star counts, FIR radiation, and molecular line emission, allowing a detailed comparison between dust visual extinction, dust FIR emission, and CO (1-0) line emission[7]. There is a good proportionality relation between the 100μm flux and A_v, up to $A_v \simeq 4$ mag, with a slope $F(100\mu)/A_v = 5$ MJy sr^{-1} per mag of extinction (see Cernicharo and Guélin[7]; the same relation is also derived by Langer et al.[8] in the dark cloud B5). This behaviour is consistent with predictions[6] in the case of a cloud containing a mixture of silicate and graphite grains[5], when the ISRF of Mathis et al.[5] is attenuated by a 0.5 mag. dusty halo (the existence of such a halo is in fact suggested by the stellar reddening data[7]). Assuming the standard diffuse cloud $A_v/N(H+H_2)$ relation still holds up to A_v=4 (see ref. [7]), Boulanger and Perault[6] derive an infrared luminosity to molecular hydrogen mass ratio r=0.6 $L_\odot/M_\odot$. Obviously, this ratio is not constant from cloud to cloud, or even within one cloud (it is three times higher in the Galactic cirrus clouds[6]). The scatter is however not that large (e.g. same values for B5[8] and HCL2), so an "average" value of r=1 $L_\odot/M_\odot$ may provide an interesting way to estimate the H_2 mass of dense clouds devoid of internal sources.

The empirical ^{12}CO(1-0) integrated line intensity–H_2 column density relation, $W(^{12}CO)/N(H_2) = C^st$, offers another way to estimate the molecular hydrogen mass. This rough proportionality law as been "calibrated" using the virial theorem[9], the gamma-rays flux[10] and star counts[11], yielding for local cloud complexes $W(^{12}CO)/N(H_2) = 1 - 3 \cdot 10^{20}$ K kms^{-1}cm^2. That the CO abundance follow that of H_2 is not surprising, since CO is one of the most easily formed molecule and one of the most difficult to destroy or condense; but that the CO (1-0) line may trace the H_2 column density is puzzling, since this line is optically thick in dense clouds. This has been tentatively explained by assuming that the clouds have roughly the same temperature (which is obviously wrong) and are virialized[12] or, alternately, by assuming that the bulk of the molecular mass in cloud complexes is in a low density halo, rather than in the dense clumps[11]. The latter view is probably correct for the Taurus cloud complex, which surrounds HCL2. The halo component, which is barely detectable in ^{13}CO and not at all in C^{18}O, dominates completely the ^{12}CO(1-0) emission and contains, according to star counts, more than 50% of the mass of the complex; its temperature is set by the ambient

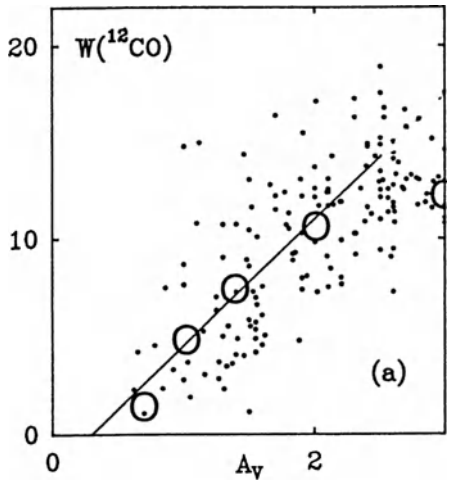

Fig. 1 The ^{12}CO velocity-integrated brightness temperature (in K·kms^{-1}) observed in HCL2 in directions of small visual extinction (A_v in mag.–from Guélin and Cernicharo[11]). The straight line corresponds to W(^{12}CO = 6.5·(A_v-0.3). Open dots are the results of radiative transfer calculations (see text).

radiation field. In the halo surrounding HCL2, where the CO–A_v correlation has been studied the most in detail[11], W(^{12}CO) (in K·kms^{-1}) is indeed found to increase roughly as 6.5 A_v (mag.), i.e. as $1.5 \cdot 10^{20}$ N(H_2) (cm^{-2}) (see Fig 1).

The slope of the W(^{12}CO)/N(H_2) relation and the weakness of W($C^{18}O$) in the halo can be accounted for in the light of the new laboratory data on CO photodissociation[13,14]. CO photodissociation is known now to occur essentially in the lines, so that self-shielding is very efficient. The new data yield a global photodissociation rate 10 times higher than previously thought; self-shielding, on the other hand, drastically reduces this rate for A_v >1 mag, and the CO fractional abundance increases very fast between A_v=0.5 and 2 mag[14,15]. The abundance increase is partly compensated by an increase of the opacity of the (1-0) CO line, so that W(^{12}CO) scales very roughly as N(H_2), for A_v between 0.7 and 2 mag. This behaviour is illustrated in Fig. 1, where the integrated intensities W(^{12}CO), observed in the halo of HCL2, are reproduced by radiative transfer calculations in a cloud with n_{H_2}= 150 cm^{-3} and T_K=10 K, using the CO abundances derived by van Dishoeck and Black[14] in the case of an attenuated IS radiation field (I_{UV}=0.5).

Another interesting result of the laboratory photodissociation measurements is that CO seems mostly dissociated in lines with non-zero vibrational quantum numbers, thus presenting large isotope shifts. Shielding of ^{13}CO and $C^{18}O$ by ^{12}CO should not be efficient, so that ^{13}CO and, mostly, $C^{18}O$ could be largely dissociated in the halo. Observations show indeed little or no ^{13}CO and $C^{18}O$ emission in the halo, in qualitative agreement with the above. These species, however, start to be detected at 0.7 and 1.5 mag of extinction respectively[7], i.e. earlier than the new ^{12}CO photodissociation rates would tend to suggest (1.2 and 4 mag, respectively, according to van Dishoeck and Black[14]. The $C^{18}O$ data in Taurus could be matched for a cloud with little carbon depletion in an attenuated UV flux. The ^{13}CO data, on the other hand suggest a normal cloud and a high carbon depletion[14]. Measurements of the photodissociation rates of ^{13}CO and $C^{18}O$ and more astronomical data would be needed before meaningful constraints on the ISRF and the gas depletion can be set by this method.

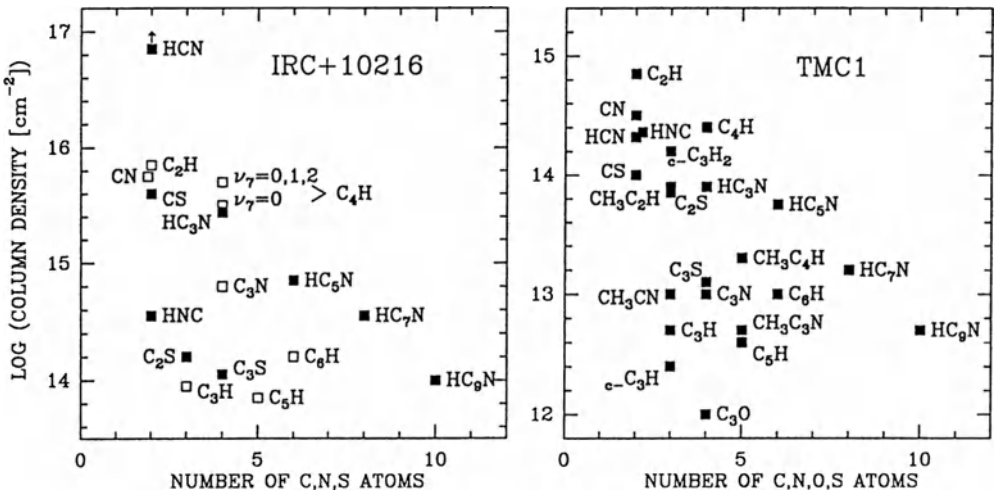

Fig. 2 Column densities of carbon chains and related molecules in IRC+10216 (from refs. [16,17] and from unpublished data) and TMC1 (from ref. [16] and a compilation of recent literature). Two diameters were assumed for the molecular sources in IRC+10216: 25"(white squares) and 50"(black squares). The H_2 column density in TMC1 is about 10^{22} cm^{-2}

Abundance of carbon chain molecules

Several families of polar carbon chain molecules are known to be abundant in dark clouds (mostly TMC1) and in the carbon star envelope IRC+10216. These are the cyanopolyynes, $HC_{2n+1}N$ (n=0–5), and their fragments $C_{2n+1}N$ (n=0–1), the polyacetylenic radicals HC_n (n=1–6), and the sulfur-bearing carbon chains C_nS (n=1–3), to which we may add cyclic C_3H_2 and C_3H and, in TMC1, H_2CCN and C_2O. Fig. 2 gives the relative abundances of these species in function of the length of their carbon chain. Except for the lightest and the heaviest species, these abundances are relatively accurate, at least in IRC+10216, because many optically thin lines, sampling a fair fraction of the populated rotational levels, were observed (including, in the case of IRC+10216, upper fine structure levels for the radicals C_3H, C_5H and C_6H, and excited bending states for HC_3N and C_4H).

Whereas all linear chains with an odd number of carbon atoms and terminated by a nitrogen atom are abundant, none with an even number of C atoms is detected (including HCCN and CCN, whose rotational frequencies are known). The bond structure of the "odd" species can be described by an alternation of single and triple covalent bonds, which probably leads to more stable compounds. Even and odd polyacetylenic radicals are detected, although with higher and lower abundances respectively. The high abundances of C_2S and C_3S in TMC1 are quite surprising, compared to that of C_3O. The general abundance decrement with lengthening of the carbon chain is similar for the closed-shell cyanopolyynes and the C_nH radicals, and is roughly the same in TMC1 and

IRC+10216. A larger decrement is observed in SgrB2 and, mostly Orion(KL), where HC_5N is the heaviest species detected.

C_4H in its lowest excited bending mode, ν_7, has been detected in the envelope IRC+10216[18,19]. Unexpectedly, the ν_7 and $2\nu_7$ rotational lines are observed to be not much weaker than the ground level lines and are seen to extend far over the outer envelope. This is especially surprising, because the energies of the ν_7 and $2\nu_7$ levels are probably $\geq$150 K and 300 K, whereas the dust temperature in the outer envelope was previously thought to be <100 K. The abundance of C_4H calculated from the ground level line intensities should be increased by at least 50%, to take into account the molecules in excited bending levels (se Fig. 2). Other cases where the population of the excited bending modes is probably a large fraction of that of ground level are those of the heavy cyanopolyynes in IRC+10216 and HC_3N in the planetary nebula CRL 618[20]

Metal-bearing molecules

A remarkable result of the last few years has been the first detection of rotational lines from inter- and circumstellar molecules containing heavy elements. Besides PN[21,22] and, perhaps, HCl[23], which are observed in interstellar clouds, there are also highly refractive species, detected in the circumstellar shell IRC+10216: NaCl, AlCl, KCl and AlF[24] (we do not consider here molecules present only in stellar atmospheres). The AlF and AlCl sources are clearly resolved with the 12"beam of the IRAM 30m telescope and are seen to extend into the outer envelope, i.e. in a region where the gas temperature is much lower than their temperature of condensation. Probably, these molecules are formed at thermodynamic equilibrium in the atmosphere of the inner star and expelled into the envelope. Their relative abundance with respect to those of SiS, SiC_2 and CS, as well as with respect to each other, is consistent with Tsuji's equilibrium calculations[25] in a carbon-rich atmosphere at 1200-1500 K.

Several other metal-bearing molecules have been sought for with the 30-m telescope in IRC+10216 and in the envelopes of other carbon-rich or oxygen rich red giants, without success. These include CCl, SiCl, SiN, ClCN, CaCl, NaF, KF, MgCl, FeO, MgO and TiO. The limits on CaCl, NaF and KF, which have very large dipole moments are particularly low ($\leq few \times 10^{12}$ cm^{-2}). AlF, AlCl, NaCl and KCl, have also been sought without success in stellar envelopes other than IRC+10216. AlF, on the other hand, is tentatively detected with the 30-m telescope (on the basis of a single line) toward Orion IRC2.

Table 1: Abundances of "Metal"-bearing Molecules in IRC+10216
(column densities in cm^{-2} for a 15" diameter source)

Sulfur compounds		Silicon compounds		Metal halides	
SiS	$7\ 10^{15}$	SiS	$7\ 10^{15}$	AlCl	$2\ 10^{14}$
CS	$4\ 10^{15}$	SiO	$2\ 10^{15}$	AlF	$4\ 10^{13}$
C_2S	$1.5\ 10^{14}$	SiC_2	$2\ 10^{15}$	NaCl	$5\ 10^{12}$
C_3S	$1.1\ 10^{14}$	SiC	$6\ 10^{13}$	KCl	$2\ 10^{12}$
H_2S	$1\ 10^{13}$				

Table 1 summarizes the abundances (and limits to the abundances) of sulfur, silicon and "metal" compounds in IRC+10216, derived from the IRAM 30 m telescope spectral survey[17,23,26].

Glycine and Urea

Urea, $(NH_2)_2CO$, and glycine, NH_2CH_2COOH, are the two simplest molecules of biological significance and, to date, the only such molecules which we can reasonably hope to identify in interstellar space. Their microwave spectrum is fairly well known and they have been sought for several times. The latest and most sensitive search was made two years ago with the IRAM 30 m telescope (Guélin and Cernicharo, unpublished). A dozen of millimetre lines of each species have been surveyed in Orion A (at the peak of $HCOOCH_3$ emission), Sgr B2 (M and N–OH maser positions) and W3(OH). Several strong transitions of urea coincide with unidentified lines of $\simeq$ 0.05–0.1 K in Sgr B2, but others seem to have no counterpart down to 0.03 K. A similar situation exists for glycine. The Orion data is particularly difficult to interpret, due to a forest of unidentified lines at the level 0.05–0.1 K (e.g. Fig 3). The limits to the column densities of urea and glycine (or of any heavy molecule) in these sources are consequently not that low (few$\times 10^{12} - 10^{13}$ cm^{-2}, or 10^{-10}–10^{-11} of $N(H_2)$).

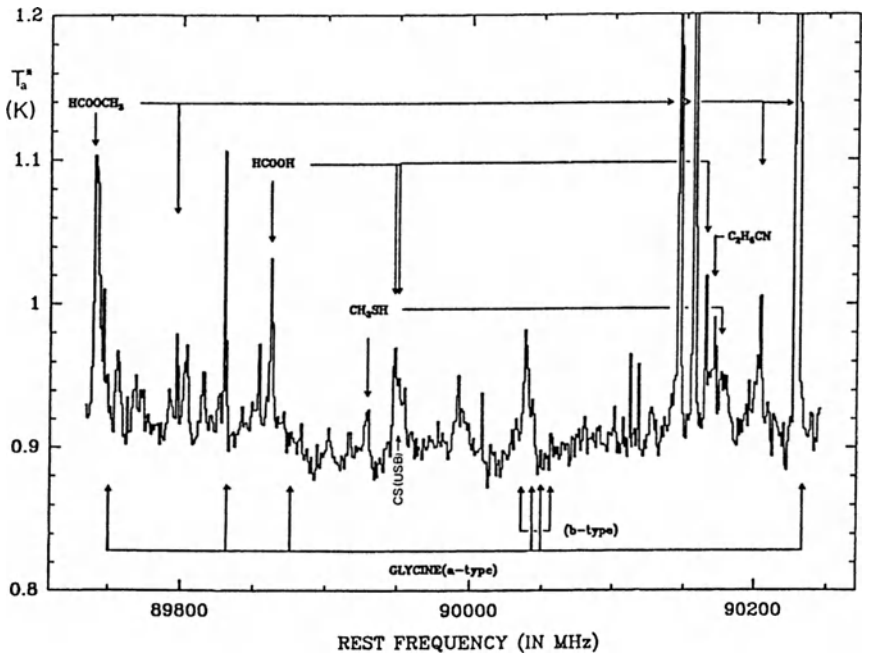

Fig. 3 A portion of the 3-mm spectrum observed in the direction of Orion IRC2 with the IRAM 30-m telescope during the search for the lowest energy conformer of glycine. The r.m.s. fluctuation in one 1 MHz channel is 9 mK: all the weak (50–200 mK) unidentified features are real. The position of the strongest glycine transitions are indicated by upward arrows. The broad feature denoted "CS" is the 2–1 line of CS, observed in the receiver image sideband with a rejection 30 dB.

The spectrum of Fig 3 (which is atypical because it is devoid of strong lines) is remarkable in that it probably does not reach the continuum level. Most of its lines are unidentified, and many probably come from excited bending states of heavy molecules. A large fraction of the identified lines arise from levels with energies higher than 150 K, showing that the Orion molecular core is indeed quite hot.

We thank D. Downes for comments on the manuscript.

References

[1] Danby, G., Flower, D.R., Valiron, P., Schilke, P. and Walmsley, C.M. 1988, *Mon. Not. Royal Astron. Soc.* **235**, 229.

[2] Palma, A., Green, S., DeFrees, D.J. and McLean, A.D. 1988, *Astrophys. J. (Supplements)* **68**, 287

[3] Guélin M. 1985, in: Molecular Astrophysics, p. 23, ed. Diercksen et al., *NATO ASI Series C*, **Vol 157**, (Dordrecht: Reidel)

[4] Winnewisser, G. and Herbst, E. 1987, in *Topics in Current Chemistry*, Vol **139**, (Berlin: Springer)

[5] Mathis, J.S., Mezger, P.G. and Panagia, N. 1983, *Astron. Astrophys.*, **128**, 212.

[6] Boulanger, F. and Pérault, M. 1988, *Astrophys. J.*, **330**, 964.

[7] Cernicharo, J. and Guélin, M. 1987, *Astron. Astrophys.*, **176**, 299.

[8] Langer, W.D., Wilson, R.W., Goldsmith, P.F. and Beichman, C.A. 1989, *Astrophys. J.*, **337**, 355.

[9] Solomon, P.M., Rivolo, A.R., Barrett, J. and Yahil, A. 1987, *Astrophys. J.*, **319**, 730.

[10] Strong, A.W., Bloemen, J.G., Dame, T. M., Grenier, I.A., Hermsen, W., Lebrun, F., Nyman, L. A., Pollock, A.M., Thaddeus, P. 1988, *Astron. Astrophys.*, **207**, 1.

[11] Guélin, M. and Cernicharo, J. 1988, in *Proc. Conf. Molecular Clouds in the Milky Way and External Galaxies*, ed Dickman et al. (Dordrecht: Reidel)

[12] Dickman, R.L., Snell, R.L. and Schloerb, F.P. 1986, *Astrophys. J.*, **309**, 326.

[13] Letzelter, C., Eidelsberg, M., Rostas, F., Breton, J., and Thieblemont, B., 1987, *Chem. Phys.*, **114**, 273.

[14] van Dishoeck, E.F. and Black, J.H. 1989, *Astrophys. J.*, in press.

[15] Viala, Y.P., Letzelter, C., Eidelsberg, M. and Rostas, F. 1988, *Astron. Astrophys.*, **193**, 265.

[16] Cernicharo. J., Guélin, M., Menten, K. and Walmsley, C.M. 1987a, *Astron. Astrophys.*, **181**, L1.

[17] Cernicharo. J., Guélin, M., Hein, H., and Kahane, C. 1987b, *Astron. Astrophys.*, **181**, L9.

[18] Guélin, M., Cernicharo, J., Navarro, S., Woodward, D.R., Gottlieb, C.A., and Thaddeus, P. 1987, *Astron. Astrophys.*, **182**, L37. *Astron. Astrophys.*, **189**, L3.

[19] Yamamoto, S., Saito, S., Guélin, M., Cernicharo, J., Suzuki H. and Ohishi, M. 1987, *Astrophys. J.*, **323**, L149.

[20] Bujarrabal, V., Gomez-Gonzales, J., Bachiller, R. and Martin-Pintado, J. 1988, *Astron. Astrophys.*

[21] Turner, B.E., Bally, J. 1987, *Astrophys. J.*, **321**, L75.

[22] Ziurys, L.M. 1987, *Astrophys. J.*, **321**, L81.

[23] Blake, G.A., Keene, J. and Phillips, T.G. 1985, *Astrophys. J.*, **295**, 501.

[24] Cernicharo, J. and Guélin, M. 1987, *Astron. Astrophys.*, **183**, L10.

[25] Tsuji, T. 1973, *Astron. Astrophys.*, **23**, 411.

[26] Cernicharo, J., Gottlieb, C.A., Guélin, M., Thaddeus, P. and Vrtilek, J.M. 1989, submitted for publication to the Astrophys. J.

FORMATION OF MOLECULES IN THE GAS PHASE

Eric Herbst
Department of Physics, Duke University
and
I. Physikalisches Institut, Universität zu Köln

SUMMARY

The gas phase reactions that produce polyatomic molecules in dense interstellar clouds are reviewed. The production of complex molecules and the extent of deuterium fractionation in dense clouds are discussed in the context of detailed models.

I. ION-MOLECULE REACTIONS

This review is concerned with the chemistry occurring in portions of dense interstellar clouds distant from star forming activity. In such regions, the gas phase chemistry is dominated by exothermic ion-molecule reactions that can produce a wide assortment of polyatomic molecules (Winnewisser and Herbst 1987) once a sufficient amount of gaseous H_2 has been produced via reactions on grain surfaces. Reactions between neutral gas phase species, even if exothermic, are normally unmeasurably slow at the low temperatures of dense clouds because they possess activation energy barriers (Herbst 1987a). Exceptions to this rule exist; atoms and especially reactive species labelled "radicals," in non-singlet electronic ground states, often react without activation energy. However, if the gas phase chemistry of dense interstellar clouds were confined to reactions involving atoms and/or neutral radicals, it would not be of much significance.

Reactions between ions and molecules, if exothermic, occur typically without activation energy due, in part, to strong long range forces (Herbst 1987a). There are exceptions to this rule as well so that there is no substitute for laboratory measurements to confirm the rapidity of a particular reaction and to determine the specific products. Thousands of ion-molecule reactions have been studied in the laboratory by groups headed by Smith and Adams, Bohme, Huntress, McEwan and others. The rate coefficients k of rapid ion-molecule reactions are quite large; at room temperature k is in the range 10^{-8} - 10^{-9} cm^3 s^{-1} (Anicich and Huntress 1986), which is one to two orders of magnitude larger than the rate coefficients of the fastest neutral-neutral reactions. These measured ion-molecule rate coefficients are in agreement with the results

of simple long-range theories (Clary 1988; Herbst 1987a). At lower temperatures, the rate of an ion-molecule reaction depends strongly on the dipole moment of the neutral species. For non-polar reactants, there is little temperature dependence, as has been demonstrated by experiments down to 8 K (Rowe 1988). For polar reactants, the rate coefficient often increases with decreasing temperature according to both theory (Clary 1988) and experiment (Clary, Smith, and Adams 1985; Rowe 1988).

The primary ionization step in the ion-molecule chemistry of dense interstellar clouds is caused by the collisions of cosmic rays with molecular hydrogen to produce H_2^+; another important ionization is caused by collisions of cosmic rays with atomic helium to produce He^+. The H_2^+ ion "immediately" reacts with ubiquitous H_2 to form the simplest polyatomic species H_3^+:

$$H_2^+ + H_2 \rightarrow H_3^+ + H, \tag{1}$$

which can then react with a variety of atoms present in the primeval gas. The reaction with atomic oxygen leads to the formation of the protonated water ion H_3O^+ via the well-studied reactions

$$H_3^+ + O \rightarrow OH^+ + H_2 \tag{2}$$

$$OH^+ + H_2 \rightarrow OH_2^+ + H \tag{3}$$

$$OH_2^+ + H_2 \rightarrow H_3O^+ + H. \tag{3}$$

Since it is chemically saturated, the H_3O^+ ion does not react with H_2. It does recombine dissociatively with electrons to form neutral fragments. The rates of dissociative recombination reactions have been well studied in the laboratory (Adams and Smith 1988), although there is little experimental evidence available concerning what the neutral products are. With few exceptions, these reactions are very rapid at room temperature with rate coefficients k in excess of 10^{-7} cm^3 s^{-1}. In addition, they increase in rate with decreasing temperature, typically as $T^{-0.3} - T^{-0.5}$. In the particular case of $H_3O^+ - e$, there is some recent experimental evidence concerning the relative abundances (branching ratio) of neutral products which demonstrates directly that OH (+ H_2 or 2H) is formed 80 percent of the time and indirectly that H_2O (+ H) is formed 20 percent of the time (Smith 1988). Once produced, H_2O can be destroyed only by ion-molecule reactions since it is a stable neutral species, whereas OH, a reactive radical, can also be depleted by neutral-neutral reactions such as

$$OH + O \rightarrow O_2 + H, \tag{5}$$

although it must be conceded that neutral-neutral reactions have not been studied at low interstellar temperatures and the possibility of small activation energy barriers cannot be ruled out.

If neutral atomic carbon is present in the gas, it can react with H_3^+ to initiate a chain of reactions leading to hydrocarbons:

$$H_3^+ + C \rightarrow CH^+ + H_2. \tag{6}$$

Reaction (6) has not been studied in the laboratory due to the difficulty of producing atomic carbon, but should proceed as shown. For carbon present in its singly ionized

form, the initial reaction in hydrocarbon production is thought to be the radiative association (Black and Dalgarno 1973)

$$C^+ + H_2 \rightarrow CH_2^+ + h\nu \qquad (7)$$

because the regular ion-molecule reaction leading to $CH^+ + H$ is endothermic by 0.39 eV and cannot occur in cold regions. (It is most important in shock chemistry however – for a recent review see Flower *et al.* 1988). Although this radiative association is too slow to be measured directly in the laboratory (Luine and Dunn 1985) and is calculated to occur on only one of every 10^6 collisions at 10 K (Herbst 1982a), the large amount of H_2 in dense clouds renders it important. Once produced, CH^+ and CH_2^+ react to form CH_3^+ via rapid hydrogenation reactions analogous to (3) and (4). The CH_3^+ ion, however, does not react rapidly with H_2. It undergoes a slow but important radiative association reaction with H_2 that has been studied in the laboratory by two different groups (Barlow *et al.* 1984 a,b; Gerlich and Kaefer 1988). The resultant CH_5^+ ion is a precursor of methane (CH_4), which is formed either via dissociative recombination or via an exothermic reaction with CO, itself an abundant interstellar molecule:

$$CH_5^+ + CO \rightarrow CH_4 + HCO^+. \qquad (8)$$

(Reaction (8) is unusual in the sense that protonation reactions involving HCO^+ – here the endothermic right-to-left reaction – are normally exothermic.) Dissociative recombination of CH_5^+ produces other one-carbon species such as CH_3 and CH_2, although branching ratios have not yet been measured. Once one-carbon hydrocarbons are produced, more complex species can be synthesized. The reactions that produce selected types of complex molecules are discussed in the next section.

II. SYNTHESIS OF COMPLEX MOLECULES

Ion-molecule pathways leading to most of the complex molecules detected unambiguously in dense interstellar clouds have by now been suggested. Here we consider only the syntheses of hydrocarbons and cyanopolyynes. For other species, the reader is advised to consult Herbst and Leung (1988), Smith *et al.* 1988, Herbst (1987b), and Bohme *et al.* (1988). A more thorough treatment than presented here has been undertaken by Bohme (1988).

Hydrocarbon synthesis commences with the reactions discussed in Section I leading to CH_n species. Once these are produced, three types of reactions lead to more complex molecules. These are carbon insertion reactions, condensation reactions, and radiative association reactions. In carbon insertion reactions, either C^+ or C inserts itself into a hydrocarbon neutral or ion to produce a larger carbon skeleton with the concomitant removal of one or more hydrogen atoms. In general terms, these reactions can be written as:

$$C^+ + C_nH_m \rightarrow C_{n+1}H_{m-1}^+ + H \qquad (9)$$

$$C + C_nH_m^+ \rightarrow C_{n+1}H_{m-1}^+ + H \qquad (10)$$

where it has been assumed that only one hydrogen atom is removed. Many reactions of type (9) have been studied in the laboratory (Anicich and Huntress 1986); one example is

$$C^+ + CH_4 \rightarrow C_2H_3^+ + H; \quad C_2H_2^+ + H_2. \tag{11}$$

Because of the difficulty of generating neutral C, reactions of type (10) have yet to be studied. Once synthesized, more complex hydrocarbons ions such as the acetylenic species $C_2H_2^+$ and $C_2H_3^+$ will react predominantly with molecular hydrogen if the reactions occur with rate coefficients larger than $\approx 10^{-13}$ cm^3 s^{-1} (Herbst, DeFrees *et al.* 1987). However, it is most often the case that hydrogenation reactions are endothermic or, even if exothermic, show sufficient activation energy that k is much less than this value. Even association reactions most often fail to occur. The interesting result is that carbon insertion ion-molecule reactions do not lead to relatively saturated (hydrogen-rich) hydrocarbon neutrals and ions for species with more than one carbon atom. For the case of the acetylenic ions, $C_2H_2^+$ undergoes only an association reaction with H_2 to form $C_2H_4^+$ whereas $C_2H_3^+$ and $C_2H_4^+$ undergo no reaction at all with H_2. Therefore the dissociative recombination reaction

$$C_2H_3^+ + e \rightarrow C_2H_2 + H; \quad C_2H + 2H \tag{12}$$

and the corresponding reaction involving $C_2H_4^+$ are of some importance. The radiative association reaction involving $C_2H_2^+$ and H_2 has not been studied in the laboratory. Rather, as is most frequently the case, the system has been studied under high pressure when three-body association dominates. Theory must then be utilized (Bates and Herbst 1988) to determine the corresponding radiative association rate.

Carbon insertion reactions between neutrals such as C_2H_2 or C_2H and C^+ or between ions such as $C_2H_3^+$ and $C_2H_4^+$ and C subsequently lead to three-carbon hydrocarbons. For example, the reaction

$$C^+ + C_2H_2 \rightarrow C_3H^+ + H \tag{13}$$

has been well studied (Anicich and Huntress 1986). The product ion is known to undergo a three-body association to produce the ion $C_3H_3^+$ (Adams and Smith 1987), which does not undergo subsequent reaction with hydrogen. Presumably the corresponding radiative association reaction occurs in dense interstellar clouds. The laboratory association reaction has been shown to produce a mixture of the normal and cyclic (c-) forms of the $C_3H_3^+$ ion. The cyclic ion is the precursor of the widespread species C_3H_2, which is produced via dissociative recombination of c-$C_3H_3^+$ if the skeletal structure of the ionic species is preserved in the neutral fragment.

Carbon insertion reactions leading to species as complex as C_9 have now been proposed (Herbst and Leung 1988). In general, for $n \geq 4$, hydrogenation reactions involving the ions C_n^+ and occasionally C_nH^+ occur, whereas ions with two or more hydrogen atoms do not react with H_2. Since only ions as saturated as $C_nH_2^+$ are formed, the carbon insertion mode of synthesis cannot produce neutral hydrocarbons via dissociative recombination with more than one hydrogen atom.

A second mode of complex hydrocarbon production can lead to more saturated hydrocarbons. This mode consists of condensation reactions, in which a hydrocarbon

neutral and ion react to form a more complex ion with either one or two hydrogen atoms being ejected; *i.e.*,

$$C_nH_m^+ + C_iH_j \rightarrow C_{n+i}H_{m+j-1}^+ + H \quad (14a)$$

$$C_nH_m^+ + C_iH_j \rightarrow C_{n+i}H_{m+j-2}^+ + H_2. \quad (14b)$$

A well-studied example (Anicich and Huntress 1986) is the reaction

$$C_2H_2^+ + C_2H_2 \rightarrow C_4H_3^+ + H; \quad C_4H_2^+ + H_2. \quad (15)$$

Condensation reactions are not as important as carbon insertion reactions for those species which can be produced via both pathways, since in general there are lower concentrations of more complex species than of simple ones such as C and C^+. However, the production of a relatively saturated ion such as $C_4H_5^+$ via the condensation reaction (Anicich and Huntress 1986)

$$C_2H_4^+ + C_2H_2 \rightarrow C_4H_5^+ + H \quad (16)$$

can clearly not occur via the insertion method.

A final mode for the production of complex hydrocarbon molecules is radiative association between small hydrocarbon ions and neutrals. For these reactions to compete with condensation processes such as (16), the rate coefficents must be very large. There is some evidence from low pressure studies (Anicich and Huntress 1986) that such can be the case. A particularly interesting reaction is

$$C_4H_3^+ + C_2H_2 \rightarrow C_6H_5^+ + h\nu, \quad (17)$$

in which the product is at least partially cyclic (Anicich *et al.* 1986).

The production of cyanopolyynes ($HC_{2n+1}N$) occurs by several routes (Bohme 1988) but, in analogy with the synthesis of hydrocarbons, the dominant process appears to be insertion reactions involving neutral atomic nitrogen and hydrocarbon ions (Herbst and Leung 1988). A variety of such reactions has been studied by the Innsbruck group (Federer *et al.* 1986). An example is

$$N + C_3H_3^+ \rightarrow H_2C_3N^+ + H, \quad (18)$$

which presumably leads to HC_3N via dissociative recombination of the product ion.

Herbst and Leung (1988) have utilized reactions such as those discussed here in a large chemical model of dense interstellar clouds that contains hydrocarbons through nine carbon atoms in complexity and cyanopolyynes as complex as HC_9N. The products and rates of many reactions in their model had to be estimated based on analogous reactions involving smaller species due to a paucity of experimental studies. The model is of the pseudo-time-dependent type, in which chemical abundances evolve under constant physical conditions. The results are in accord with previous pseudo-time-dependent models which show that large abundances of most carbon-containing molecules occur only at so-called early times well before steady-state conditions are achieved and the available carbon has mainly gone into the chemically inert carbon monoxide. At

these early times, the results of Herbst and Leung (1988) show that gas phase reactions starting from C and C^+ can produce copious amounts of complex hydrocarbon molecules although there appears to be a slight underproduction of the more complex cyanopolyynes compared with observed abundances in TMC-1. Other mechanisms for producing complex cyanopolyynes should be investigated.

III. DEUTERIUM FRACTIONATION

Deuterium fractionation of gas phase molecules in dense interstellar clouds is a dramatic effect which can be explained in terms of ion-molecule reactions. A primer has been given by Watson (1976) and a more recent discussion by Wootten (1987). Fractionation effects in trace species arise from three main systems of reactions:

$$H_3^+ + HD \rightleftharpoons H_2D^+ + H_2 \quad (19)$$

$$CH_3^+ + HD \rightleftharpoons CH_2D^+ + H_2 \quad (20)$$

$$C_2H_2^+ + HD \rightleftharpoons C_2HD^+ + H_2, \quad (21)$$

in which the right-to-left reactions are endothermic by amounts ranging from 230 K (reaction 19) to 550 K (reaction 21) and therefore occur slowly at low interstellar temperatures (Herbst 1982b; Herbst, Adams *et al.* 1987). The result is that the relative abundances of the deuterated ions are enhanced vis-a-vis the HD/H_2 abundance ratio. The deuterated ions produced in reactions (19) – (21) then react with other neutral species to propagate deuterium fractionation effects. For example, H_2D^+ reacts with CO to form DCO^+; DCO^+ recombines with electrons to form atomic D; atomic D reacts with many species to enhance deuteration, *etc.* Although relative abundances of deuterated to normal species have often been estimated in the literature by the use of small numbers of reactions directly relevant to the molecules being considered, it is more accurate to utilize comprehensive model calculations. Such calculations are especially useful in determining the time and temperature dependence of deuterium fractionation. This latter dependence was once thought to be simple; the higher the temperature, the more rapid the endothermic reactions in (19) – (21), the less the fractionation. Since the right-to-left reactions in (20) and (21) are much more endothermic than in (19), hydrocarbon fractionation was thought to be significant up to higher temperatures than fractionation based on H_2D^+. It is now known that the first of these viewpoints has to be heavily qualified and the second, although true, can be misleading since one must make sure that the fractionation of a particular species does indeed derive from H_2D^+. The temperature dependence of the abundance ratio of deuterated hydrocarbon species to their normal counterparts is not simple; both CH_2D^+ and C_2HD^+ react with H_2 at low temperatures, not by the endothermic processes shown in (20) and (21) but by radiative association processes, the three body analogs of which have been studied in the laboratory (Herbst, Adams *et al.* 1987). Radiative association reactions occur more rapidly at lower temperatures, introducing a complexity into the simple temperature dependence previously thought to pertain to deuterium fractionation. Recent calculations (Millar *et al.* 1989) show that in the 10 K – 70 K range, deuterium fractionation can increase with increasing temperature for selected species,

in accord with the large CCD/CCH abundance ratio observed by two groups in the extended Orion source (Vrtilek *et al.* 1985; Combes *et al.* 1985).

Following a previous model of deuterium fractionation by Brown and Rice (1986), Millar *et al.* (1989) have produced a detailed pseudo-time-dependent model of dense interstellar clouds that includes all of the currently known deuterium fractionation reactions and the important radiative association reactions discussed above. Their results can be compared with observations in cold dark clouds and in extended portions of giant molecular clouds distant from star forming activity. One of their more interesting findings is that at high temperatures ($\approx$ 50 K – 70 K) there is a strong time dependence to the DCO^+/HCO^+ abundance ratio. At times well before steady state is achieved ("early time"), this ratio is much larger than at steady state. The reason is that at steady state the dominant precursor of DCO^+ is H_2D^+ which is not abundant at high temperatures, whereas at earlier times the high hydrocarbon abundance and relatively large hydrocarbon fractionation lead to large amounts of DCO^+ being produced from precursors such as CH_4D^+. Another interesting finding is that the temperature dependence of the abundance ratio DCN/HCN (at early time) is such that it first decreases dramatically as the temperature is raised from 10 K to 30 K and then increases slightly as the temperature is further increased to 70 K. Preliminary observations for DCN/HCN seem to show this effect (Wootten 1987), but more detailed observations would be useful. The effect is obtained theoretically only if the branching ratios for dissociative recombination reactions are estimated using the ideas of Green and Herbst (1979) rather than those of Bates (1987). The two sets of branching ratios and the theories from which they come have been contrasted by Millar *et al.* (1988). Superimposed on these two theories in the model of Millar *et al.* (1989) is the additional assumption that there is no product selectivity based on isotope effects. On the other hand, Bell *et al.* (1988), in order to explain the very large value observed for the abundance ratio C_3HD/C_3H_2, have assumed that deuterated molecules are strongly favored over their normal counterparts as products in dissociative recombination reactions. For example, in the dissociative recombination of C_2HD^+, such selectivity would favor CCD + H over CCH + D. There is some evidence for this selectivity in dissociative charge transfer reactions (Gellene and Porter 1983), although these systems have less energy than is available in dissociative recombination reactions. Calculations on this point are planned using the phase space treatment (Herbst 1978) which does predict correctly the neutral product branching ratio obtained in the experimental measurement of $H_3O^+ + e$.

IV. CONCLUSIONS

Gas phase reactions can produce large amounts of complex molecules under the physical conditions extant in dense interstellar clouds if a significant portion of the carbon abundance does not exist in the form of carbon monoxide. In the simple pseudo-time dependent approach which considers clouds to be homogeneous entities that exclude UV radiation, this condition occurs only at times significantly earlier than steady state when there is a large abundance of neutral atomic carbon, a precursor of complex molecules. Of course, large abundances of neutral atomic carbon can arise by a num-

ber of other mechanisms, including penetrating UV radiation or a surplus of elemental carbon compared with oxygen in the gas phase. The dramatic enhancements in the ratios of the abundances of deuterated to normal species over the HD/H_2 ratio seen for many molecules in dense clouds are understandable in terms of gas phase chemistry. However, the temperature dependence of the fractionation is not as simple as previously thought and the time dependence can be large, especially at the higher temperatures of extended giant molecular clouds. More observational data on the temperature dependence of deuterium fractionation would be most helpful.

Acknowledgements. The author wishes to acknowledge the support of his theoretical program by the National Science Foundation (U.S.) through grant AST-8715446. The award of a fellowship by the Alexander von Humboldt Stiftung is gratefully acknowledged.

REFERENCES

Adams, N. G. and Smith, D. 1987, *Astrophys. J. Letters*, **317**, L25.

Adams, N. G. and Smith, D. 1988, in *Rate Coefficients in Astrochemistry*, eds. T. J. Millar and D. A. Williams (Kluwer: Dordrecht), p. 173.

Anicich, V. G. and Huntress, Jr., W. T. 1986, *Astrophys. J. Suppl.*, **62**, 553.

Anicich, V. G., Huntress, Jr., W. T., and McEwan, M. J. 1986, *J. Phys. Chem.*, **90**, 2446.

Barlow, S. E., Dunn, G. H., and Schauer, K. 1984a, *Phys. Rev. Letters*, **52**, 902.

Barlow, S. E., Dunn, G. H., and Schauer, K. 1984b, *Phys. Rev. Letters*, **53**, 1610.

Bates, D. R. 1987, in *Modern Applications of Atomic and Molecular Processes*, ed. A. E. Kingston (Plenum: London), p. 1.

Bates, D. R. and Herbst, E. 1988, in *Rate Coefficients in Astrochemistry*, eds. T. J. Millar and D. A. Williams (Kluwer: Dordrecht), p. 17.

Bell, M. B., Avery, L. W., Matthews, H. E., Feldman, P. A., Watson, J. K. G., Madden, S. C., and Irvine, W. M. 1988, *Astrophys. J.*, **326**, 924.

Black, J. H. and Dalgarno, A. 1973, *Astrophys. Letters*, **15**, 79.

Bohme, D. K. 1988, in *Rate Coefficients in Astrochemistry*, eds. T. J. Millar and D. A. Williams (Kluwer: Dordrecht), p. 117.

Bohme, D. K., Wlodek, S., and Fox, A. 1988, in *Rate Coefficients in Astrochemistry*, eds. T. J. Millar and D. A. Williams (Kluwer: Dordrecht), p. 193.

Brown, R. D. and Rice, E. H. N. 1986, *Mon. Not. Roy. Astron. Soc.*, **223**, 429.

Clary, D. C. 1988, in *Rate Coefficients in Astrochemistry*, eds. T. J. Millar and D. A. Williams (Kluwer: Dordrecht), p. 1.

Clary, D. C., Smith, D., and Adams, N. G. 1985, *Chem. Phys. Lett.*, **119**, 320.

Combes, F., Boulanger, F., Encrenaz, P. J., Gerin, M., Bogey, M., Demuynck, C., and Destombes, J. L. 1985, *Astron. Astrophys.*, **147**, L25.

Federer, W., Villinger, H., Lindinger, W., and Ferguson, E. E. 1986, *Chem. Phys. Lett.*, **123**, 12.

Flower, D. R., Monteiro, T. S., Pineau des Forets, G., and Roueff, E. 1988, in *Rate*

Coefficients in Astrochemistry, eds. T. J. Millar and D. A. Williams (Kluwer: Dordrecht), p. 271.
Gellene, G. I. and Porter, R. F. 1983, *Accounts of Chemical Research*, **16**, 200.
Gerlich, D. and Kaefer, G. 1988, at a talk given at the Symposium on Atomic and Surface Physics, La Plagne, France.
Green, S. and Herbst, E. 1979, *Astrophys. J.*, **229**, 121.
Herbst, E. 1978, *Astrophys. J.*, **222**, 508.
Herbst, E. 1982a, *Astrophys. J.*, **252**, 810.
Herbst, E. 1982b, *Astron. Astrophys.*, **111**, 76.
Herbst, E. 1987a, in *Interstellar Processes*, eds. D. J. Hollenbach and H. A. Thronson, Jr. (Reidel: Dordrecht), p. 611.
Herbst, E. 1987b, *Astrophys. J.*, **313**, 667.
Herbst, E., Adams, N. G., Smith, D., and DeFrees, D. J. 1987, *Astrophys. J.*, **312**, 351.
Herbst, E., DeFrees, D. J., and McLean, A. D. 1987, *Astrophys. J.*, **321**, 898.
Herbst, E. and Leung, C. M. 1988, *Astrophys. J. Suppl.*, in press.
Luine, J. A. and Dunn, G. H. 1985, *Astrophys. J. Letters*, **299**, L67.
Millar, T. J., Bennett, A., and Herbst, E. 1989, submitted for publication.
Millar, T. J., DeFrees, D. J., McLean, A. D., and Herbst, E. 1988, *Astron. Astrophys.*, **194**, 250.
Rowe, B. R. 1988, in *Rate Coefficients in Astrochemistry*, eds. T. J. Millar and D. A. Williams (Kluwer: Dordrecht), p. 135.
Smith, D. 1988, in a talk presented at the International Conference on Molecular Astrophysics held in Brioni, Yugoslavia, 5-9 September.
Smith, D., Adams, N. G., Giles, K., and Herbst, E. 1988, *Astron. Astrophys.*, **200**, 191.
Vrtilek, J. M., Gottlieb, C. A., Langer, W. D., Thaddeus, P., and Wilson, R. W. 1985, *Astrophys. J. Letters*, **296**, L35.
Watson, W. D. 1976, *Rev. Mod. Phys.*, **48**, 513.
Wootten, A. 1987, in *Astrochemistry*, eds. M. S. Vardya and S. P. Tarafdar (Reidel: Dordrecht), p. 311.
Winnewisser, G. and Herbst, E. 1987, *Topics in Current Chemistry*, **139**, 119.

FORMATION OF MOLECULES ON GRAIN SURFACES

W.W. Duley
Physics Department
York University
4700 Keele St.
North York
Ontario, Canada M3J 1P3

Summary

After a review of the role of grain reactions in forming molecules such as CO, H_2O, CH_4 and NH_3, the contribution of grain erosion to PAH formation is discussed.

The role of grain reactions in forming interstellar molecules is a poorly understood and controversial matter at the present time. The only gaseous interstellar molecule unambiguously known to derive from grain reactions is H_2. The possibility that more complex molecular species could be formed on dust has been often discussed (cf. Watson and Salpeter [1-2]. Recent reviews have been published by Williams [3] and by Winnewisser and Herbst [4].

The relation between molecule formation on grains and the composition of the molecular mantles that are seen in denser interstellar clouds [5,6] is a subject of special interest, particularly since Jones and Williams [7] have shown that such molecules may be retained on the surface of dust when formed. If reactions on grain surfaces lead directly to the growth of grain mantles then there may be little direct contribution of grain reactions to gas phase chemistry unless some mechanism exists for returning these molecules to the gas phase on a regular basis.

To explore this possibility we should first examine the likely reaction routes for 'heavy' atoms such as C, N and O on dust. Table 1 summarizes these reaction routes

Table 1. Reaction routes: C,N, O on dust

Reaction	Product
C + grain	CH_4
	CO, CN, ...
	aC/HAC
O + grain	H_2O
	O_2, CO, NO ...
	"silicates"
N + grain	NH_3
	N_2, CN, ...

In this table the 'traditional' products of grain reaction are listed in the first two rows for each channel. These products tend to be volatile and might return immediately to the gas phase. However, other products such as amorphous carbon (aC) or hydrogenated amorphous carbon (HAC) and silicates are also possible reaction products and are refractory, locking these elements up in dust. Laboratory data (cf. Robertson and O'Reilly (8)) show unequivocally that the reaction

$$C + \text{grain} \xrightarrow{H} \text{aC/HAC}$$

is the dominant channel for C atom reactions on a substrate under plasma conditions and that CH_4 is therefore unlikely to form as traditionally assumed when C atoms encounter dust grains under interstellar conditions. Ogmen and Duley (9) have recently shown that HAC condensates form readily under simulated interstellar conditions and that these materials have IR spectra that are quite similar to those seen in galactic sources.

As discussed by Jones and Williams (7) is also apparent that H_2O molecules formed in the reaction

$$O + \text{grain} \xrightarrow{H} H_2O$$

are also retained by dust at least in the Taurus cloud.

Since there is little spectroscopic evidence for the existence of NH_3 on dust (10) it is likely that the reaction

$$N + \text{grain} \xrightarrow{H} NH_3$$

results in the direct evolution of NH_3.

A decision as to whether or not a particular molecule is retained on dust or returned to the gas can be obtained by looking at the heat of vaporization ΔH_v as summarized in table 2. Since H_2O is found to be retained on dust when formed via grain reaction between O and H, while there is little evidence that this occurs for the reaction C + O + grain -> CO, the critical range for H_v would appear to be $0.06 < \Delta H_v \lesssim 0.42$ eV. In fact, if the critical value for ΔH_v is close to that for H_2O, then

Table 2. ΔH_v (eV/molecules) for various molecules

Molecule	Boiling Temperature	ΔH_v
graphite	4200°K	7.4eV
tetracene	710	1.3
perylene	680	1.3
napthalene	490	0.77
H_2O	373	0.42
C_6H_6	353	0.35
NH_3	240	0.24
CO_2	195	0.26
CH_4	110	0.085
CO	82	0.063
H_2	20	0.0094

$\Delta H_v(NH_3)$ may be too small to permit the retention of ammonia on dust during grain catalyzed reactions.

The data in table 2 can also be used to estimate the probability that mantles form through condensation of gaseous molecules on grain surfaces. The rate of accretion of a molecule present at gas phase density n_x on a grain of radius, a is $vn_x\pi a^2$ where v is the speed of the molecule. The desorption rate depends on grain temperature T_g and a vibrational frequency ν. This rate is $\nu \exp[-\Delta H_v/kT_g]$. The critical gas phase density for condensation of a mantle is then

$$n_x = \frac{\nu}{v\pi a^2} \exp[-\Delta H_v/kT_g]$$

with $\nu \sim 10^{12}\text{sec}^{-1}$, $v = 10^{4}\text{cm sec}^{-1}$ and $\pi a^2 \sim 10^{-10}\text{cm}^2$ this becomes

$$n_x = 10^{18} \exp[-\Delta H_v/kTg].$$

The sensitivity of this solution to grain temperature can be seen in the data of table 3. It is apparent from these data, that if T_g is low enough to permit CO to condense, then H_2O and NH_3 should also be observed on dust. On the other hand, if only an H_2O ice band is observed then neither CO nor NH_3 need be present.

Table 3. Conditions for mantle formation by accretion of CO, NH_3 and H_2O

Molecule	$n_H(cm^{-2})$	$n_x(cm^{-3})$	$T_g(°K)$	Mantle
CO	10^3	10^{-2}	15	Yes
			18	No
	10	10^{-4}	15	No
NH_3	10^3	10^{-5}	50	Yes
			60	No
H_2O	10^3	10^{-5}	90	Yes
		10^{-3}	100	No

The use of an equilibrium grain temperature in the above analysis may, however, be misleading. Many grain materials will be amorphous and these materials respond differently when absorbing photons. It has been shown [11-13] that in such materials the absorption energy is localized within a volume $10^{-21} - 10^{-22}$ cm^3 around the primary site. Such localization can lead to temperature excursions $\Delta T = h\nu/k(3N-6)$ where $h\nu$ is the original photon energy, N is the number of atoms in the localized volume and k is Boltzmann's constant. The contribution of such fluctuations to desorption of CO and H_2O from grains is discussed elsewhere [14]. Since $\Delta H_v \sim 0.06$ eV for CO even IR photons can lead to thermal desorption of this molecule through temperature spiking. It should be noted that this mechanism does not require small grains to be present [13].

Under more energetic conditions, for example adjacent to HII regions, temperature spiking can be sufficiently large that fragments

of grains can be desorbed. This is particularly likely when HAC dust is exposed to VUV photons. The structure of HAC and aC has been discussed by Robertson and O'Reilly [8]. These materials behave as if they consist of cluster of PAH rings with the cluster size being 1-8 rings in HAC and $\sim$ 20-40 rings in aC. It is these clusters that exhibit temperature spiking [15]. The amplitude of these spikes is such that smaller clusters will be removed from HAC dust under interstellar conditions.

The desorption rate p for a PAH cluster bonded with energy Δ to HAC will be

$$p = \nu_s \exp[-\Delta/kT^*]$$

where ν_s is a vibrational frequency ($\sim 10^{11}$ Hz) and T^* is the temperature achieved in a photon-induced spike. The value of Δ can be approximated from

$$\Delta \sim 0.3R \text{ eV}$$

where R is the number of rings in the cluster. Data on Δ and T^* for various PAH molecules are summarized in table 4.

Table 4. Bond energy on HAC for PAH molecules of various size. T^* is calculated using $h\nu$=8eV

R	Molecule	Δ(eV)	N	T^*(°K)
8	Benzocoronene	2.4	39	835
7	Coronene	2.1	36	900
6	Benzoperylene	1.8	34	960
5	Perylene	1.5	32	1032
4	Pyrene	1.2	26	1276
3	Anthracene	0.9	24	1390
2	Napthalene	0.6	18	1930

The desorption rate p (sec^{-1}) is a strong function of cluster size through Δ and T^*. With $h\nu$ = 8eV as typical of diffuse cloud conditions p varies from $\sim 3 \times 10^9$ sec^{-1} for a two ring cluster (eg napthalene) to $\sim 1.3 \times 10^1$ sec^{-1} for a six ring cluster, p $\sim 5 \times 10^3$ sec^{-1}.

Efficient desorption of a cluster requires that
to be found in abundance only in regions of grain disruption.

$$p\,\tau_{relax} \gtrsim 1$$

where τ_{relax} is the localization time for the temperature spike. Phillips [11] has shown that τ_{relax} may be $10^{-2} - 10^{-3}$ sec in amorphous solids. If this were also true for interstellar carbons then the above condition would imply that only clusters with greater than 5 rings would be retained on HAC dust in diffuse clouds. A similar result has also been obtained using an analysis of growth rates of HAC dust in diffuse clouds [15].

Clusters that remain on HAC (and in aC) after photoprocessing in this way will still be subject to temperature spiking. A variety of non-equilibrium emission excesses are expected from this material extending from the IR (UIR and cirrus emissions) to NIR and ERE emissions [13,15].

Clusters liberated from HAC return to the gas phase and represent a possible source of gaseous PAH molecules or molecular fragments. The reaction scheme for forming gaseous PAH in this way is

$$C + \text{grain} \xrightarrow{H} HAC$$

$$HAC + UV \rightarrow PAH\ (gas)$$

The accretion rate of C on dust is

$$R_C = n_C \pi a^2 v_C$$
$$\sim 3 \times 10^{-10} n \text{ sec}^{-1}$$

under diffuse cloud conditions. When $p\tau \gtrsim 1$ all clusters less than a threshold size will be returned to the gas. The formation rate of gaseous PAH is then

$$R_{PAH} = \frac{R_C}{N} n_g$$

where N is the average number of carbon atoms in the cluster released. With $n_g \sim 10^{-12} n$

$$R_{PAH} \sim 2 \times 10^{-23} n^2 \text{ cm}^{-3} \text{sec}^{-1}$$

If β is the destruction rate for <u>gaseous</u> PAH then

$$\frac{n_{PAH}}{n} \sim \frac{2 \times 10^{-23} n}{\beta}$$

This result shows that when $n = 10^2 \text{cm}^{-3}$ as appropriate for diffuse cloud conditions, $n_{PAH}/n = 10^{-6}$ would imply $\beta \lesssim 2 \times 10^{-15}$ sec^{-1}. A value of β this small would seem to be unlikely even for PAH under diffuse cloud conditions. This suggests that gaseous PAH are likely

A more widespread product of these photoreactions on dust may be the simple ring molecule C_3H_2. The formation rate for this molecule

$$R_{C_3H_2} \sim 10^{-22}\ cm^{-3}sec^{-1}$$

Then as before

$$\frac{n_{C_3H_2}}{n} \sim \frac{10^{-22}n}{\beta}$$

with $n = 10^2\text{-}10^3 cm^{-3}$ and $\beta = 10^{-11} sec^{-1}$, $n_{C_3H_2}/n = 10^{-8}\text{-}10^{-9}$. This is compatible with the abundances observed by Cox et al [16] suggesting that C_3H_2 may be a tracer for UV photodegradation of HAC dust in the ISM.

In conclusion, I have shown that temperature fluctuations in amorphous grain materials may be significant with respect to the desorption of molecules from grain surfaces. For volatile molecules such as CO and H_2O even modest photon energies can be important in desorption. However, in amorphous carbonaceous materials such as HAC temperature spikes can be in excess of 1000°K leading to the evolution of PAH molecules or their fragments from dust. Since these ring molecules form naturally when carbon condenses on dust under low temperature conditions, a balance exists between the formation of these molecules on dust and their return to the gas phase. This balance may lead to an appreciable gaseous PAH abuncance in regions of grain disruption. A more general indicator of these temperature spike driven desorption processes may be the observation of the simplest ring molecule, C_3H_2. This molecule would appear as the degradation product of PAH liberated from HAC.

Acknowledgement

This research was supported by a grant from the NSERCC.

References

1. W.D. Watson and E.E. Salpeter. Ap.J. 174, 321 (1972).
2. W.D. Watson and E.E. Salpeter. Ap.J. 175, 659 (1972).
3. D.A. Williams. Proc. NATO ASI "Physical Processes in Interstellar Clouds" 1986.
4. G. Winnewisser and E. Herbst. Topics in Current Chemistry 139 119 (1987).
5. D.C.B. Whittet, M.F. Bode, A.J. Longmore, D.W.T. Baines and A. Evans. Nature 303, 218 (1983).

6. D.C.B. Whittet, A.J. Longmore and A.D. McFadzean. M.N.R.A.S. 216, 45P (1985).
7. A.P. Jones and D.A. Williams. M.N.R.A.S. 209, 955 (1984).
8. J. Robertson and E.P. O'Reilly. Phys. Rev. B35, 2946 (1987).
9. M. Ogmen and W.W. Duley, Ap.J. (Letters) (1988).
10. R.G. Smith, K. Sellgren and A.T. Tokunaga. Ap.J. 334, 209 (1988).
11. J.C. Phillips. Phys. Rev. B25, 1397 (1986).
12. V.K. Malinovsky J. Non-Crystalline Solids 90, 37 (1987).
13. W.W. Duley and D.A. Williams M.N.R.A.S. 231, 969 (1988).
14. W.W. Duley, A.P. Jones, D.C.B. Whittet and D.A. Williams M.N.R.A.S. (submitted)
15. W.W. Duley M.N.R.A.S. 234,61P (1988).
16. P. Cox, M. Walmsley and R. Güesten, Astron. Astrophys. (in press) 1988.

CIRCUMSTELLAR CHEMISTRY

Alain OMONT
Observatoire de Grenoble.
Université Joseph Fourier.
BP 53X, F-38041 Grenoble-Cedex.

ABSTRACT. The chemistry of circumstellar envelopes around evolved stars is extremely rich, especially for C-rich ones. The discussion of the chemistry of inner layers is very difficult because of their complexity. Modelling of radical and ion photochemistry in the outer shells is now successful in accounting for the species, often complex, there observed by radioastronomy. The chemistry of sulfur and carbon bearing molecules in O-rich envelopes, and that of molecular ions in C-rich ones, are especially discussed.

I. INTRODUCTION

Circumstellar envelopes (CSEs) occupy a prominent position in cosmochemistry: they display a broad variety of element abundances that reflects nucleosynthesis and dredge-up in red giants and the complexity of grain formation. In particular, C-rich CSEs harbor a wealth of exotic complex molecules, a large proportion of which were observed there even before laboratory detection (see Guelin's contribution in these proceedings). CSEs span a broad range of physical conditions, from their photosphere to the dissolution of their outer layers in the interstellar medium, with extremely short characteristic times of evolution. Despite the variety of chemical processes and the complexity of some of them, such as grain formation, the modelling of circumstellar chemistry is favored by the relatively well defined physical conditions, the simple geometry, and the rapid evolution.

There exist several recent reviews of circumstellar chemistry (1-6) and of the general properties, physical conditions, and molecular observations relevant for modelling CSEs (see e.g. 7-13). In particular, I will not reproduce here most of the recent discussions I wrote on these topics and on the general features of circumstellar chemistry (5,6,11) but will only stress the relevance of some recent observational results. These have been made possible by the gains in sensitivity and in angular resolution of millimeter wave facilities, particularily important for these relatively compact objects. Together with some information on the complex chemistry of CSEs' inner layers, where most of the simple stable molecules are generated, these new results prove the importance of photochemistry in exotic species formation in the outer layers, and the success of recent models.

Without returning to the importance of the new detections of radical carbon chains and of metal molecules (13), I will discuss in turn : i) Observations of sulfur- and carbon-bearing molecules in O-rich CSEs (Sections II and III) and related radical reactions; ii) The first detections of molecular ions in CSEs (Section IV), and their dominant role in circumstellar chemistry as shown by the recent demonstration that species such as HNC and HC_3N are mostly synthesized in the outer shells.

II. SULFUR-BEARING MOLECULES IN O-RICH CSEs.

Because most of their carbon is locked in CO, the chemistry of O-rich CSEs is obviously much less rich than that of C-rich CSEs. For a long time, only OH, H_2O and SiO masers, and thermal CO and SiO were detected in O-rich CSEs. Sulfur oxides and H_2S were the next obvious candidates, but despite active searches (14,15), only H_2S was detected in a unique envelope, OH 231.8+4.2, known as exceptional (15). Indeed, it is now realised that SO_2, and to a smaller degree SO, are also exceptionally strong in this object, where OCS is also detected (16). Interferometric observations of SO_2 have lead Jackson and Nguyen-Q-Rieu (17) to propose that it originates from sulfur desorption from grains in shocks.

Indeed, the detection of SO_2 and SO, and the detection of H_2S in other stars had to wait for the first observations with the IRAM 30m telescope (18,19, see also 20). We have recently made a systematic study of these three molecules in O-rich CSEs (21). Our sample was 15 prominent massive CSEs: IRC-OH stars (such as IRC+10011), OH-IR stars (such as OH 26.5+0.6), and OH supergiants (VY CMa, NML Cyg and IRC+10420). In almost all of them two lines of H_2S (1_{10}-1_{01} of ortho-H_2S at 169 GHz, and 2_{20}-2_{11} of para-H_2S at 217 GHz) and at least two lines of SO_2 (among 3_{13}-2_{02} at 104.0 GHz, $10_{0,10}$-$9_{1,9}$ at 160.8 GHz and $10_{1,9}$-$10_{0,10}$ at 104.2 GHz) were detected, as well as the 2_2-1_1 line of SO at 86 GHz in about half of them. SO_2 was also marginally detected in a couple of semi-regular variables, and H_2S in IRC+10216 and AFGL 2343.

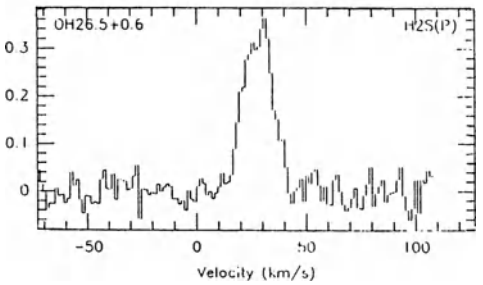

Figure 1. Spectra of OH 26.5+0.6
Lines :
1_{10}-1_{01} of ortho-H_2S at 169 Ghz
2_{20}-2_{11} of para-H_2S at 217 GHZ
$10_{0,10}$-$9_{1,9}$ of SO_2 at 161 GHZ

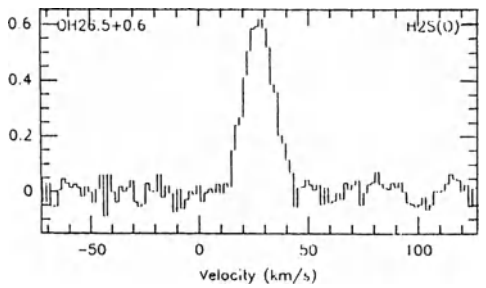

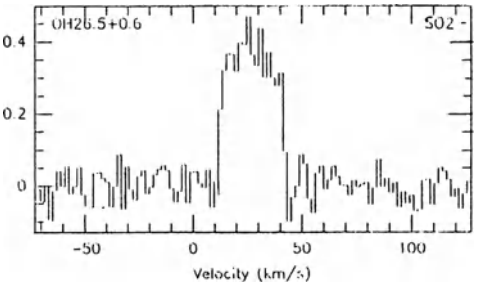

When the signal-to-noise ratio is good enough the SO_2 profile generally appears squared, characteristic of unresolved optically thin lines (Figure 1). The SO_2 excitation temperature lies in the range 20-40 K, increasing with the near infrared luminosity of the star. These characteristics appear in good agreement with chemical modelling that predicts SO_2 is formed in reactions with photoproduced OH in the outer shells (22,23,24) :

$$\begin{aligned} S + OH &\rightarrow SO + H \\ SO + OH &\rightarrow SO_2 + H \end{aligned} \qquad (1)$$

Assuming SO_2 is coextensive with OH yields an abundance $\approx 10^{-6}$ within a factor 3, a good order of magnitude smaller than the solar abundance. As the chemical models predict a substantial fraction of the sulfur is in SO_2 in these outer layers, it seems one can conclude sulfur is depleted in O-rich CSEs, although more work on sulfur photochemistry is probably needed.

The data concerning SO are less complete and conclusive. However, they give smaller abundances than for SO_2, in line with chemical models.

The line profiles of H_2S generally appear quite different from those of SO_2. This is particularily striking in the case of OH 26.5+0.6 (Figure 1). The central part is clearly enhanced, suggesting the possibility that the emission comes partly from the warm internal dust formation layers that are not yet fully accelerated. However, the profiles are probably not incompatible with the usual parabolic profiles of optically thick lines. Despite the difficulty introduced by the existence of the ortho and para varieties, the excitation temperature of H_2S appears much larger than that of SO_2 for the most massive CSEs (in the range 50-100K), but comparable for the OH-IRC sources. Such a high excitation temperature also indicates internal emission, although a clear view of its distribution is not presently possible. It is thus neither possible to identify i) the respective contributions of the different destruction processes of H_2S: accretion onto grains, reaction with atomic H, or photodissociation; nor ii) the precise origin of atomic sulfur used in reactions (1) to form SO_2 in the outer shells.

III. CARBON-BEARING MOLECULES IN OXYGEN-RICH ENVELOPES.

Thermodynamical chemical equilibrium in the cool photosheres of O-rich CSEs implies a negligible amount of C-bearing molecules other than CO. The CO molecule is so stable it will not release carbon to form other molecules without energetic processes such as shocks or UV photodissociation. HCN is however currently observed in O-rich CSEs with appreciable abundance $\approx 2\ 10^{-7}$ (with respect to the H nuclei) within a factor 3, as well as in OH 231.8+4.2, in OH supergiants, in prominent IRC objects, and in related stars (NML Tau, TX Cam, etc) (25,26,27,16,28,29).

Other C-bearing molecules (CS, HNC, HCO^+) have also been detected, first in OH 231.8+4.2 (16), and then in TX Cam and NML Tau (29) (as well as SiS in TX Cam).

The origin of these C-bearing molecules is not yet clear. Their photochemical formation in the outer layers has been investigated in detail (24,28). If one assumes the internal layers are in

thermodynamical equilibrium, photodissociation of CO fails by several orders of magnitude to provide enough C for the observed abundance of HCN. Nejad and Millar (24, see also 28) have proposed that carbon is released by photodissociation of CH_4 coming from the inner layers, through the reactions

$$\begin{aligned} CH_4 + h\nu &\longrightarrow CH_n \\ N_2 + h\nu &\longrightarrow N \\ N + CH_n &\longrightarrow HCN \end{aligned} \qquad (2)$$

One has to justify however the formation of CH_4 in the inner layers; and anyway one needs extremely large CH_4 abundances ($\approx 10^{-5}$), relatively implausible, to explain the large observed HCN abundances (28). Other explored processes, such as the ionic reaction $C^+ + NH_3$, are still less efficient. Accordingly, it is quite possible that HCN (and CS) are directly formed in the inner layers, by a process still unknown.

IV. OBSERVATIONS OF HCO^+.

The identifiation of HCO^+ is known as the cornerstone of the understanding of the role of ionic reactions in interstellar chemistry. However, HCO^+ was long sought without success in CSEs. Theoretical models (30,31,32) have shown there is no fundamental difference between the interstellar and circumstellar chemistry and abundance of HCO^+. In C-rich CSEs, HCO^+ is believed to be formed by cosmic ray ionization through

$$C\,R + H_2 \longrightarrow H_2^+ \xrightarrow{H_2} H_3^+ \xrightarrow{CO} HCO^+, \qquad (3)$$

and to be destroyed by dissociative recombination, exactly as in the interstellar medium. The difficulty of its detection is due to a slightly lower abundance and to the smaller masses of CSEs compared to interstellar clouds. However, these models predicted the expected line intensity in IRC+10216 should be just comparable to the sensitivity of the new large millimeter wave telescopes (30,31).

The maximum expected intensities in regular O-rich CSE are comparable (32), although the dominant processes are believed to be different. The formation of HCO^+ should mostly occur through

$$CO + h\nu \longrightarrow C \xrightarrow{h\nu} C^+ \xrightarrow{H_2O,OH} HCO^+, \qquad (4)$$

and the main destruction process is

$$HCO^+ + H_2O \longrightarrow H_3O^+ + CO. \qquad (5)$$

Indeed, HCO^+ is only marginally detected in IRC+10216, and not detected in any normal O-rich CSE. In IRC+10216, furthermore it is not impossible that the weak line detected at the HCO^+ J=1-0 frequency (33) with an intensity comparable to the theoretical expectations, could be due to some other unidentified species.

Much stronger HCO^+ lines have been detected in other peculiar CSE. The first detection was made in OH231.8+4.2 (16), known for the presence of very strong shocks, and there is some indication that the line profile displays the large velocities associated with these shocks.

Strong lines (0.5-1 K) were also detected in the very young planetary nebulae CRL 618 (33,34) and NGC 7027 (33). In the latter, the J=3=2 line is also detected and there is some evidence that the HCO^+ emission is associated with a bipolar outflow at relatively high velocity. HCO^+ is also detected at a lower level in another young PN, IRAS 21282+5050 (35) and in CIT 6 and VY CMa (33).

The processes described above are probably unable to explain the relatively strong emission in all these peculiar CSEs. It is likely that other processes are present in the inner layers, associated with shocks or photoionization by internal UV radiation from the PN or the chromosphere.

V. IONIC PHOTOCHEMISTRY.

As already mentioned, photoionization by galactic UV is a major source of ions in the outer layers of CSEs. The main primary ions are $C_2H_2^+$ in C-rich CSEs, H_2O^+ (immediately transformed into H_3O^+) in O-rich CSEs, and C^+ in all of them. Such ions quickly react with such abundant molecules as C_2H_2, HCN, H_2O, etc. In particular, they can enter condensation reactions and start the synthesis of complex species (30). The most important paths seem the following :

$$C^+ + C_2H_2 \longrightarrow C_3H_2^+ \longrightarrow C_3H,\ C_3H_2,\ C_3, \quad (6)$$

as proposed by Nejad and Millar (36). It seems that one can explain in this way the observed abundance of C_3H in IRC+10216, and possibly those of C_3H_2 and C_3.

Again in IRC+10216, the ion $C_2H_2^+$ can initiate the formation of the long carbon chains by joining two carbon atoms (30,31):

$$C_2H_2^+ + C_2H_2 \longrightarrow C_4H_3^+,\ C_4H_2^+ \longrightarrow C_4H_2,\ C_4H \quad (7)$$

The abundance of C_4H formed in this way agrees in order of magnitude with observations of IRC+10216. A similar reaction with HCN can give:

$$C_2H_2^+ + HCN \longrightarrow H_2CN^+ \longrightarrow HCN,\ HNC \quad (8)$$

$$\longrightarrow H_2C_3N^+ \longrightarrow HC_3N \quad (9)$$

The amount of HNC formed in this way in IRC+10216 (31) is in excellent agreement with the observations. As concerns HC_3N, Glassgold and Mamon (37) have shown that this process should be a more efficient synthesis than others proposed by Millar (4).

The theoretical expectation for the amount of HC_3N in the inner layers is not yet clear (see 38 and 39 for contradictory points of view), but recent interferometric observations by Bieging and Rieu (40) strongly support the idea that most of the exotic species are generated in the outer layers, probably by ionic photochemistry. Not only does the radical C_2H, a photodissociation product of C_2H_2, appear distributed in

a hollow shell as expected, but HNC and HC_3N also have similar distributions as expected if they are formed through reactions (8 and 9) (for HC_3N, Likkel et al. (41) reached also the same conclusion). There is also good evidence, although with less angular resolution, that other molecules, such as CN, C_4H, etc, have a similar distribution.
Accordingly, there is a good chance that photochemistry can account for all the complex and exotic species observed in IRC+10216 and other C-rich CSEs. Modelling of this part of circumstellar chemistry appears now in very good shape, and one can still expect rapid progress with the development of observations and millimeter facilities, and possibly with improvements to the values of the various implied reaction rates.

REFERENCES

1. A.E. Glassgold and P.J. Huggins: In M, S and C Stars, ed. by H.R. Johnson and F. Querci (NSF-CNRS 1988)
2. A. Omont: In Mass Loss in Red Giants, ed. by M. Morris and B. Zuckerman (Reidel, Dordrecht 1985) p.269
3. A. Omont: In Astrochemistry, ed. by M.S. Vardya and S.P. Tarafdar (Reidel, Dordrecht 1987) p.357
4. T.J. Millar: In Rate Coefficients in Astrochemistry, ed. by T.J. Millar and D.A. Williams (Kluwer Academic Pub. 1988) p.287
5. A. Omont: In Cosmic Chemistry, AG Meeting Koln, ed. by G. Klare. Lecture Notes In Physics (Springer-Verlag, Heidelberg 1988)
6. A. Omont: In Atomic and Molecular Data for Astrochemistry. IAU Highligths in Astronomy (Reidel, Dordrecht 1988)
7. B. Zuckerman: Ann. Rev. Astron. Astrophys. 18, 263 (1980)
8. H. Olofsson: In (Sub)millimeter Astronomy, ed. by P.A. Schaver and K. Kjar (ESO Publications, Garching 1985)
9. H. Olofsson: Space Sci. Rev., in press (1988)
10. H. Olofsson: In Evolution of Peculiar Red Giants, IAU Coll. N. 106, eds H.R.Johnson and B. Zuckerman. Cambridge University Press (1988).
11. A. Omont: In "Modelling the Stellar Environment: How and Why?", ed. P. Delache, S. Laloe, C. Magnan (Ed. Frontieres, Gif-sur-Yvette 1989)
12. H. Habing: In these proceedings
13. M. Guelin: In these proceedings
14. B. Zuckerman: Astron. J. 86, 1 (1980)
15. N. Ukita, M. Morris: Astron. Astrophys. 121, 15 (1983)
16. M. Morris, S. Guilloteau, R. Lucas, A. Omont: Astrophys. J. 321, 888 (1987)
17. J.M. Jackson, Nguyen-Q-Rieu: Astrophys. J. Lett. in press (1988)
18. R. Lucas, A. Omont, S. Guilloteau, Nguyen-Q-Rieu: Astron. Astrophys. 154, L12 (1986)
19. S. Guilloteau, R. Lucas, Nguyen-Q-Rieu, A. Omont: Astron. Astrophys. 165, L1 (1986)
20. R. Sahai, J. Howe: In "Late Stages of Stellar Evolution", eds S. Kwok and S.R. Pottasch, Reidel (1987), p 167
21. A. Omont, R. Lucas, S. Guilloteau, M. Morris: in preparation (1989)
22. J.M. Scalo, D.B. Slavsky: Astrophys. J. Lett. 239, L73 (1980)
23. D.B. Slavsky, J.M. Scalo: Preprint (1986)
24. L.A.M. Nejad, T.J. Millar: Mon. Not. Roy. Astr. Soc. 230, 79 (1988)
25. S. Deguchi, P.F. Goldsmith: Nature, 317, 336 (1985)
26. S. Deguchi, M.J. Claussen, P.F. Goldsmith: Astrophys. J. 303, 810 (1986)
27. P.R. Jewell, L.E. Snyder, M.S. Schenewerk: Nature 323, 322 (1986)
28. E. Nercessian, S. Guilloteau, A. Omont, J.J. Benayoun: Astron. Astrophys. in press (1988)
29. M. Lindqvist, L.-A. Nyman, H. Olofsson, A. Winnberg: Astron. Astrophys. 205, L15 (1988)

30. A.E. Glassgold, R. Lucas, A. Omont: Astron. Astrophys. 157, 35 (1986)
31. A.E. Glassgold, G.A Mamon, A. Omont, R. Lucas: Astron. Astrophys. 180, 183 (1987)
32. G.A. Mamon, A.E. Glassgold, A. Omont: Astrophys. J. 323, 306 (1987)
33. S. Guilloteau, A. Omont, R. Lucas, J. Cernicharo, M. Guelin: in preparation (1989)
34. R. Bachiller, J. Gomez-Gonzalez, V. Bujarrabal, J. Martin-Pintado, Astron. Astrophys. 196, L5 (1988)
35. L. Likkel, T. Forveille, A. Omont, M. Morris: Astron. Astrophys. 198, L1 (1988)
36. L.A.M. Nejad, T.J. Millar: Astron. Astrophys. 183, 279 (1987)
37. A.E. Glassgold, G.A. Mamon: In "Second Haystack Conference on Interstellar Matter", ed. J.M. Moran (1987)
38. S. Lafont, R. Lucas, A. Omont: Astron. Astrophys. 106, 201 (1982)
39. I.K. Shmeld, V.S. Strellnitskii, L.V. Gurvich: Sov. Astron. Lett. 11, 254, (1985)
40. J.H. Bieging, Nguyen-Q-Rieu: Astrophys. J. Lett. 329, L107 (1988)
41. L. Likkel, M. Morris, C. Masson, A. Wootten: Bull. Am. Astron. Soc. 19, 755, (1987)

CHEMICAL MODELS OF HOT MOLECULAR CORES

T. J. Millar[1] and P. D. Brown[1,2]

[1]Mathematics Department, UMIST, PO Box 88, Manchester M60 1QD
[2]CITA, University of Toronto, 60 St. George Street, Toronto

SUMMARY. We argue that the observation of molecules such as NH_3, CH_3OH, HDO and NH_2D in hot molecular cores indicates that surface reactions on interstellar grains must play an important role in determining the gas phase abundances in such regions. The detection of large saturated molecules in hot cores suggests that the surface chemistry might be extremely complex.

1. INTRODUCTION

Hot molecular cores are observed as small (size < 1 pc), dense ($n(H_2) \sim 10^7$ cm^{-3}), hot (T ~ 100-200 K) clumps within giant molecular clouds and appear to be associated with regions of active star formation. Although various mechanisms may be responsible for their formation we shall consider, for the purposes of the calculations described herein, a zero-order model in which the cores are considered to be remnants of a cloud which has collapsed to form a star (or stars). The cores themselves are assumed to be "failed stars" and are hot because of heating, probably via infrared radiation, from a nearby star. Such a scenario appears reasonable for the most well studied hot core, the so-called Orion Hot Core, situated near IRc2. Unlike cold interstellar clouds such as TMC-1, in which highly unsaturated molecules are observed - a statement true also for the envelope of the carbon-rich star IRC+10216 - hot cores are dominated by the presence of saturated molecules including NH_3, H_2O, CH_3OH and CH_3OCH_3 which have abundances much larger than those observed in cold clouds. A study of NH_3 in Orion led Sweitzer (1978) to propose that the large fractional abundance observed, ~ 10^{-5} - 10^{-6}, was due to the evaporation of NH_3 ice from the surface of dust grains. Likewise, the large abundaces of CH_3OH and H_2O, the latter inferred from observations of HDO and $H_2{}^{18}O$, have also been taken to be indicative of surface processes. Even if surface processes are not involved, there is overwhelming evidence that abundances in the Orion Hot Core reflect a previous cold phase. This includes the degree of fractionation observed in NH_2D/NH_3, HDO/H_2O, CH_3OD/CH_3OH and the A- to E-torsional state abundance ratio in CH_3OH (see Walmsley 1989 for a review). In this article we shall summarise detailed modelling of the chemistry of the Orion Hot Core in terms of cold gas phase and surface processes (Brown, Charnley and Millar 1988, Brown and Millar 1989).

2. THE CHEMICAL MODEL

We have followed the gas phase chemistry in a cold (T = 10 K) cloud undergoing a free-fall collapse from an initial density, $n_i(H_2)$ = 1500 cm^{-3}, to a final density, $n_f(H_2)$ = 10^7 cm^{-3}, which occurs in a time-scale, t_{ff} ~ 8 10^5 yr. Since the grain chemistry is thought to influence hot core abundances, we have incorporated accretion of the gas on to the dust grains and investigated the effects of a simple surface chemistry, namely hydrogenation and deuteration, in an explicit fashion. Since, for a normal gas-to-dust ratio, the accretion time-scale, t_{acc}, is ~ 3 $10^7/n$ yr, all of the gas, with the exception of H_2, HD, H, D, He and their associated ions, freezes on to the grains before the end of the collapse phase. At this stage the H_2D^+/H_3^+ abundance ratio is greater than 1 since, at 10 K, HD destroys H_3^+ (to form H_2D^+) whereas neither HD nor H_2 destroy H_2D^+. Because of the absence of more complex molecules, the fractional abundance of H_2D^+ can be large (~ 10^{-6}) and should be detectable in regions in which accretion dominates. This result assumes that H_2D^+ and H_3^+ do not recombine with electrons (Smith and Adams 1984); if they do so (Amano 1988), their abundances will be reduced. At this stage in the calculation, it is assumed that a heating event liberates the molecular mantles, which have accumulated on the grains during the cold phase. The resulting hot gas - observationally a hot molecular core - contains large abundances of simple hydrides such as H_2O, NH_3 and CH_4 initially. We have also followed the chemical evolution of this gas but find it to be chemically inert for a period of at least 10^4 yr, due to (i) the lack of atoms and radicals in the hot gas, all having been converted to saturated molecules on the grain surface, and (ii) the lack of ionising radiation deep in the hot core which keeps the ionisation fraction small. The high visual extinction, > 300 mag., at the centre of the Orion Hot Core ensures that ultraviolet and X-ray radiation cannot penetrate, although a "skin depth" around a hot core would show a larger fractional ionisation than that which we calculate at the centre (~ 10^{-13}).

3. RESULTS AND DISCUSSION

In addition to t_{ff} and t_{acc}, a third time-scale, the chemical time-scale, t_{ch}, is important in determining the final abundances in the hot core. This time-scale is that for processing atoms into molecules and is typically ~ 10^6 yr in a dense cloud (Leung, Herbst and Huebner 1984, Millar and Nejad 1985, Millar, Leung and Herbst 1987). A comparison of these three time-scales shows that before t_{ff} is reached, accretion is complete and that, since $t_{acc} < t_{ch}$, the accreted species are mainly atoms with traces of molecules such as CO, HCN, CH_3OH, etc. Hydrogenation of atoms on the grain surface leads to the major mantle species being (with percentage by

number density give in parentheses): H_2O (62%), NH_3 (14%), CH_4 (15%), CO (9%). Other molecules frozen onto grains can do so with fractional abundances much larger than those given by steady state calculations. That is, at early times, the large CI gas phase abundance ensures effective formation of molecules such as CH_3OH, CH_3CN, H_2CO and HC_3N which are frozen with fractional abundances ~ 10^{-6} - 10^{-7}.

The gas phase deuterium chemistry in the collapsing and accreting gas has some important differences from that occuring in a static cloud. Although the basic fractionation processes are similar, the degree of deuterium enhancement, particularly in radicals, can be much larger. Consider, for example, OD which in a static cloud at 10 K has an abundance ratio [OD]/[OH] ~ 0.5 (Millar, Bennett and Herbst 1989). In common with most radicals, OD is destroyed predominatly by neutral-neutral reactions involving atoms. As accretion takes place, however, the abundance of reactive atoms, such as O, C and N, decreases and destruction by D atoms, which are not removed from the gas upon collisions with grains, occurs. These D atoms destroy OH to form OD (Croswell and Dalgarno 1985) but do not destroy OD. Since the destruction of OH and OD by H atoms is negligible at 10 K, the overall effect is to give [OD]/[OH] > 1 in the gas phase. Eventually, of course, the large abundance of OD accretes on to the dust on which it is hydrogenated to from HDO. The accretion of O and OH leads to the formation of H_2O and HDO through surface reaction with H and D atoms. Our detailed numerical calculation (Brown and Millar 1989) shows that some deuteration must take place on the grain surface but that the accretion and subsequent hydrogenation of deuterated radicals is the major influence in determining the HDO and NH_2D abundances observed in hot cores.

Upon heating, to 200 K, the grain mantle evaporates rapidly and loads the hot core with processed material. Since we find the hot core gas to be chemically inert for a least 10^4 yr it appears that observations of the gas in hot cores gives information on the grain mantle composition of cold clouds.

Although our model has a relatively simple surface chemistry, there is evidence that it may be more complex. Firstly, despite sensitive searches, there is no evidence from infrared spectroscopy for CH_4 in grain mantles. Rather it appears that after H_2O, methanol is the most abundant mantle constituent (Tielens and Allamandola 1987). Secondly, the detailed calculations predict too much H_2O and NH_3, typically by an order of magnitude compared to hot core observations, implying reactions other than hydrogenation may take place on the grains. Thirdly, a number of complex molecules appear in hot cores with abundances larger that those which can be formed in cold gas phase chemistry. For example, Millar et al. (1988) have detected ethanol, CH_3CH_2OH, in the W51M hot core and estimated the fractional

abundances of CH_3OH, CH_3OCH_3 and CH_3CH_2OH to be 10^{-7}, 10^{-8} and 10^{-8}, respectively, assuming a source size of 10" as derived from CH_3OH observations (Menten et al. 1986). The abundances of the latter two species are more than three orders of magnitude greater than the best estimates using gas phase chemistry (Herbst 1987). Since O atom reactions have been poorly studied in the laboratory it is possible that the correct gas phase chemistry has yet to be identified. Alternatively, the presence of large saturated molecules with unexpectedly large abundances, together with the presence of small saturated molecules with large abundances argues for surface formation of these species and their subsequent release into the hot core gas. Millar et al. (1988) have outlined a possible mechanism for the formation of these complex species on grains but quantitative, rather than qualitative, results will be difficult to obtain due to the many problems associated with specifying the details of the surface chemistry.

REFERENCES

Amano, T. 1988, Astrophys. J., 329, L121.

Brown, P.D., Charnley, S.B. & Millar, T.J. 1988, MNRAS, 231, 409.

Brown, P.D. & Millar, T.J. 1989, MNRAS, in press.

Croswell, K. & Dalgarno, A. 1985, Astrophys. J. 289, 618.

Herbst, E. 1987, Astrophys. J., 313, 867.

Jacq, T., Jewell, P.R., Henkel, C., Walmsley, C.M. & Baudry, A. 1988, Astron. Astrophys., 199, L5.

Leung, C., Herbst, E. & Huebner, W.F. 1984, Astrophys. J. Suppl., 56, 231.

Menten, K.M., Walmsley, C.M., Henkel, C. & Wilson, T.L. 1986, Astron. Astrophys., 157, 318.

Millar, T.J., Bennett, A. & Herbst, E. 1989, Astrophys. J., in press.

Millar, T.J., Leung, C.M., & Herbst, E. 1987, Astron. Astrophys., 183, 109.

Millar, T.J. & Nejad, L.A.M. 1985, MNRAS, 217, 507.

Millar, T.J., Olofsson, H., Hjalmarson, A. & Brown, P.D. 1988, Astron. Astrophys., in press.

Smith, D. & Adams, N.G. 1984, Astrophys. J., 284, L13.

Sweitzer, J.S. 1978, Astrophys. J., 225, 116.

Tielens, A.G.G.M. & Allamandola, L.J. 1987, In "Physical Processes in Interstellar Clouds" eds G.Morfill & M.Scholer (D.Reidel, Dordrecht), p.333.

Walmsley, C.M. 1989, In "Interstellar Dust" eds. L.J. Allamandola & A.G.G.M. Tielens (Kluwer Academic Press, Dordrecht), in press.

COSMIC RAY INDUCED PHOTODESTRUCTION OF INTERSTELLAR MOLECULES

R. Gredel[1,2], S. Lepp[1], A. Dalgarno[1] and E. Herbst[3,4]
[1]Harvard-Smithsonian Center for Astrophysics
[2] European Southern Observatory
[3]Department of Physics, Duke University
[4]I. Physikalisches Institut, Universität zu Köln

ABSTRACT

Ultraviolet photons are created in the interior of dense interstellar clouds by the impact excitation of molecular hydrogen by secondary electrons generated by cosmic ray ionization. The resulting photodissociation and photoionization rates of a wide range of interstellar molecules are calculated. The effects on the equilibrium chemical composition of dense clouds are briefly discussed.

1. Introduction

In dense molecular clouds, cosmic rays with energies between 10 and 100 MeV ionize H_2 and generate secondary electrons with a mean energy around 30 eV (Cravens and Dalgarno 1978). Because the fractional ionization is generally low, the electrons lose their energy mainly by exciting, dissociating and ionizing H_2. The subsequent decay of the electronically excited states of H_2 produces UV photons within the clouds.

The idea of molecular hydrogen emission was invoked by Prasad and Tarafdar (1983) to explain the large abundance of atomic carbon which exists in several molecular clouds. In their mechanism, CO is photodissociated by the internal photons.

A detailed calculation of the cosmic ray induced ultraviolet spectrum of H_2 has been given by by Gredel, Dalgarno and Lepp (1987), who employed it in a calculation of the photodissociation rate of CO. We use their spectrum to derive the internal photodissociation rates of a wide range of interstellar molecules for which photodissociation cross sections are available. We briefly discuss the effects on the equilibrium chemical composition of dense clouds, extending the models of Sternberg, Dalgarno and Lepp (1987).

2. Photodestruction of Interstellar Molecules

The photodissociation and photoionization rate $R_{\rm M}$ of a molecular species M with density $n({\rm M})$ corresponding to a total cosmic ray ionization rate of ζ s^{-1} is given by

$$R_{\rm M} = \zeta n({\rm M}) \int \frac{\sigma_{\rm M}(\nu) P(\nu)}{\sigma_{\rm tot}(\nu)} d\nu. \tag{1}$$

$P(\nu)$ is the probability for the emission of a photon at frequency ν as given by Gredel *et al.* (1987). $\sigma_{\rm M}(\nu)$ is the photodissociation or photoionization cross section and $\sigma_{\rm tot}(\nu)$ is the total absorption cross section. It may be written in the form

$$\sigma_{\rm tot}(\nu) = \sigma_{\rm g}(1-\omega) + \sum_{\rm M'} \kappa_{\rm M'} \sigma_{\rm M'}(\nu) \tag{2}$$

where $\sigma_{\rm g} = 2 \times 10^{-21}$ cm^{-2} is the grain extinction cross section per hydrogen nucleus, ω is the grain albedo, and $\kappa_{\rm M} = n({\rm M})/n_{\rm H}$. In practice, for molecules in interstellar clouds, with the exception of CO (Gredel *et al.* 1987), $\sigma_{\rm tot}$ is dominated by $\sigma_{\rm g}(1-\omega)$ and for them we may write

$$R_{\rm M} = \frac{\zeta n({\rm M})}{(1-\omega)}\, p \text{ cm}^{-3} \text{ s}^{-1} \tag{3}$$

where the efficiency p is given by

$$p = \int \frac{\sigma_{\rm M}(\nu) P(\nu)}{\sigma_{\rm g}} d\nu. \tag{4}$$

3. The Steady State Abundances of Interstellar Molecules

We briefly explore the effects of the cosmic ray induced photons on the abundances of interstellar molecules, using a version of the chemistry of Sternberg *et al.* (1987), modified by the incorporation of the rate coefficients of dissociative recombination recommended by Bates (1986, 1987) and Millar, DeFrees, McLean and Herbst (1988). We present results for a uniform cloud of total hydrogen density $n_{\rm H} = 10^4$ cm^{-3}, a temperature of 50 K, abundances relative to H_2 for carbon of 1.46×10^{-4}, for oxygen of 3.52×10^{-4} and for nitrogen of 4.5×10^{-5}, a cosmic ray ionization rate of $\zeta = 10^{-17}$ s^{-1}, a total metal abundance ratio relative to hydrogen of 1.5×10^{-8} and an albedo ω of 0.5.

In the first two columns of Table 1, we show the effects on the steady-state abundances including cosmic ray induced photodissociation and photoionization, but ignoring the photodissociation of CO. The inclusion of the photon field severely diminishes the steady-state abundances of the more complex species because photodissociation is an effective destruction process at many points in the formation sequence (Sternberg *et al.* 1987). The destructive effects are mitigated when the photodissociation of CO is included, as the third column of Table 1 demonstrates. The additional source of neutral carbon enhances the supply of complex hydrocarbons. Large molecules, if they exist in significant amounts in dense interstellar clouds, also enhance the abundances of the

complex hydrocarbons (Lepp and Dalgarno 1988). The addition of a large molecule component with an abundance relative to hydrogen of 10^{-7} yields in our model chemistry the steady state concentrations given in column 4 of Table 1. With the inclusion of the photodissociation of CO as a source of neutral carbon, the additional source from charge transfer to large molecules and mutual neutralization to large molecular negative ions (Lepp and Dalgarno 1988) has but small consequences.

Because the time scales of the internal photodestruction processes are longer than the time scales to form molecules, the maximum abundances are not significantly affected by the presence of the internally generated photons.

References

Bates, D.R. 1986, *Ap. J. (Letters),* **306**, L45.
Bates, D.R., 1987, *Recent Studies in Atomic and Molecular Processes,* ed. A.E. Kingston (Plenum Press).
Cravens, T., and Dalgarno, A. 1978, *Ap. J.,* **219**, 750.
Gredel, R., Dalgarno, A., and Lepp, S. 1987, *Ap. J. (Letters),* **323**, L137.
Lepp, S., and Dalgarno, A. 1988, *Ap. J.,* **324**, 553.
Prasad, S.S., and Tarafdar, S.P. 1983, *Ap. J.,* **267**, 603.
Millar, T.J., DeFrees, D.J., McLean, A.D., and Herbst, E. 1988, *Astr. Ap.,* **194**, 250.
Sternberg, A., Dalgarno, A., and Lepp, S. 1987, *Ap. J.,* **320**, 676.

Table 1: Fractional Abundances $n(M)/n_H$ at Steady State

	(a)	(b)	(c)	(d)
O	7.9(-5)	1.2(-4)	1.2(-4)	1.1(-4)
OH	3.3(-9)	1.4(-8)	1.3(-8)	1.4(-8)
H_2O	5.4(-5)	2.5(-5)	2.5(-5)	2.5(-5)
O_2	3.7(-5)	3.1(-5)	3.0(-5)	3.3(-5)
C^+	1.8(-10)	4.3(-10)	4.4(-10)	4.2(-10)
C	4.5(-9)	6.5(-9)	6.1(-7)	7.9(-7)
C_2H_2	4.2(-9)	7.2(-11)	7.5(-10)	1.9(-9)
CH_4	6.6(-8)	9.6 (-9)	9.5(-8)	1.7(-7)
C_2H	1.5(-10)	4.2(-11)	4.2(-10)	8.3(-10)
C_3H_2	2.1(-11)	8.8(-13)	9.4(-12)	1.2(-12)
NH_3	4.7(-8)	4.4(-8)	4.1(-8)	3.3(-8)
HCN	1.9(-10)	2.7(-10)	1.2(-9)	6.0(-10)

(a) no photons, no large molecules
(b) photons but no photodissociation of CO, no large molecules
(c) photons, no large molecules
(d) photons, large molecules at $n(\mathrm{LM})/n(\mathrm{H}) = 10^{-7}$

AB INITIO CALCULATIONS ON MOLECULES OF ASTROCHEMICAL INTEREST

Peter Botschwina and Peter Sebald
Fachbereich Chemie, Universität Kaiserslautern
D–6750 Kaiserslautern

Among the about 80 molecules which have so far been detected in interstellar clouds there are many reactive neutral and charged species which are difficult to investigate in the laboratory. In fact, some ions such as HCO^+, HN_2^+, or HCS^+ were first observed by radioastronomy. Ab initio calculations may be of substantial help in making predictions for spectroscopic properties of such unstable species. In this contribution we will report on the results of large–scale ab initio calculations for a number of reactive molecules which are of interest to interstellar chemistry. For the electronic structure calculations, the coupled electron pair approximation (CEPA) of Meyer [1] was employed which has proven to yield quite accurate results for a variety of spectroscopic properties (see, e.g., [2–4] for reviews).

Results for two neutral species and three cations, all with linear equilibrium geometry, are given in table 1. Cyanoacetylene, which is well–known from laboratory studies and which is a constituent of many interstellar clouds, may serve as a benchmark case. In the calculations on the other four molecules basis sets of comparable size have been employed and the results should be of similar accuracy.

The calculated equilibrium rotational constant B_e for HC_3N is smaller than the experimental value of Mallinson and DeZafra [5] by 25 MHz; due to neglect of Fermi resonance between ν_4 and $4\nu_7^0$ the experimental value is probably too small by 2–3 MHz. The calculated equilibrium centrifugal distortion constant is smaller than the experimental ground–state value [5] by 6%. The calculated stretching vibrational frequencies, obtained variationally from an approximative vibrational Hamiltonian which neglects the anharmonic coupling between stretching and bending motions [6], have deviations of 0–34 cm^{-1} from experiment [7]. Good agreement with experiment (3–6% differences) is also obtained for the vibration–rotation coupling constants α_1, α_2, and α_3. The present α_4 value is larger than the valne reported by Mallinson and DeZafra [5] by 76%. This large difference is a clear indication for anharmonic interaction between ν_4 and $4\nu_7^0$ which was not taken into account by Mallinson and DeZafra.

Our ab initio results for protonated cyanoacetylene, the anticipated astrochemical precursor of cyanoacetylene, were partly published previously [8]. Recently, Lee and Amano [9] observed the ν_1 band of HC_3NH^+ with a difference frequency laser system and Kawaguchi, Kajita, Tanaka, and Hirota [10] detected the ν_3 band by means of IR diode laser spectroscopy. These were predicted to be the two strongest stretching vibrational bands. The uncorrected ab initio band origins turned out to be too high by 22 and 28 cm^{-1}, respectively. Corrected values, which made use of three experimental data for $HCNH^+$, were also given in our previous paper [8] and these predictions turned out to be too small by 1 cm^{-1} (ν_1) and 5 cm^{-1} (ν_3). The calculated vibration–rotation

coupling constants α_1 and α_3 of 7.19 and 18.73 MHz are also in excellent agreement with the corresponding experimental values of 7.10 MHz [9] and 18.41 MHz [10].

Using a smaller basis set of 96 contracted Gaussian type orbitals, the bending vibrational frequencies of HC_3NH^+ were calculated within the harmonic approximation. The results are (in cm^{-1}): $\omega_6 = 772$, $\omega_7 = 544$, $\omega_8 = 476$, and $\omega_9 = 190$. Analogous calculations for cyanoacetylene yielded harmonic bending vibrational frequencies of 686 (663), 502 (499), and 223 (222) cm^{-1}, where the experimental anharmonic values [7] are given in parentheses. We expect that the present values for ω_7, ω_8, and ω_9 of protonated cyanoacetylene will differ from the so-far unknown experimental anharmonic values by about 10 cm^{-1}. Assuming the same ratio between calculated harmonic and experimental anharmonic value as for cyanoacetylene we arrive at ν_6 (HC_3NH^+) = 747 cm^{-1}, which should be accurate to about 5 cm^{-1}.

Table 1: Calculated spectroscopic properties for some linear neutral molecules and cations of astrochemical interest[a]

	$H^{12}C_3{}^{14}N$[b]	$H^{12}C_3{}^{14}NH^+$	$^{12}C_3{}^{16}O$	$H^{12}C_3{}^{16}O^+$	$H^{12}C_3{}^+$
B_e (MHz)	4523 (4548)[b]	4305[f]	4781[h]	4434	11149
D_e (kHz)	0.513[c]	0.406[f]	0.529[h]	0.445	4.192
ν_1 (cm^{-1})	3340 (3327)[d]	3536 (3514)[f]	2229[i]	3253	3192
ν_2 (cm^{-1})	2305 (2274)[d]	3285	1919[i]	2318	2112
ν_3 (cm^{-1})	2113 (2079)[d]	2343 (2315)[g]	943	2099	1175
ν_4 (cm^{-1})	864 (864)[d]	2109		905	
ν_5 (cm^{-1})		901			
α_1 (MHz)	6.89 (7.33)[b]	7.19 (7.10)[f]	29.35	7.05	32.28
α_2 (MHz)	20.97 (21.53)[b]	6.76	19.12	22.38	-84.96
α_3 (MHz)	13.25 (14.31)[b]	18.73 (18.41)[g]	8.69	14.44	38.04
α_4 (MHz)	11.04 (6.26)[b]	13.24		9.28	
α_5 (MHz)		9.51			
μ_e (D)	-3.751[e]	1.750	2.535[j]	-3.103	-2.761
$\lvert\mu_1\rvert$ (D)	0.087	0.328	0.539	0.095	0.122
$\lvert\mu_2\rvert$ (D)	0.051	0.100	0.110	0.372	0.395
$\lvert\mu_3\rvert$ (D)	0.023	0.253	0.004	0.155	0.175
$\lvert\mu_4\rvert$ (D)	0.015	0.162		0.079	
$\lvert\mu_5\rvert$ (D)		0.107			

[a] Experimental values are given in parentheses. [b] Ref. [5] [c] Ground-state value [5]: 0.5444(15) kHz. [d] Ref. [7] [e] Ground-state value [11]: -3.724(30) D. [f] Ref. [9] Ground-state values are B_0 = 4328.892(71) MHz and D_0 = 0.445(23) kHz. [g] Ref. [10] [h] Ground-state values [12]: B_0 = 4810.88624(65) MHz and D_0 = 0.77707(130) kHz. [i] Argon matrix values [13]: ν_1 = 2242.6 cm^{-1} and ν_2 = 1907.2 cm^{-1}. [j] Ground-state value [14]: 2.391(5) D.

Upon protonation of cyanoacetylene, the electric dipole moment experiences a large change of 5.501 D and a change of sign occurs. The calculated equilibrium dipole moment for HC_3N differs from the experimental ground-state value [11] by 0.027 D.

Tricarbon monoxide, C_3O, has a rather shallow potential for CCC bending which manifests itself in significant differences between the calculated equilibrium and experimental ground-state values for the centrifugal distortion constant and the electric dipole moment. The calculated stretching vibrational frequencies ν_1 and ν_2 are in good agreement with matrix values [13]; due to its very low intensity ν_3 could not yet be observed. The calculated harmonic bending vibrational frequencies [15], obtained with a large basis set of 132 contracted GTOs, are $\omega_4 = 596$ and $\omega_5 = 124$ cm^{-1}. The former compares well with the anharmonic matrix value of 579.6 cm^{-1} [13].

The most stable form of protonated tricarbon monoxide is linear HC_3O^+; the corresponding proton affinity at 298 K was calculated to be 885 $kJ \cdot mol^{-1}$ [15]. Results referring to the stretching vibrations are given in Table 1; the bending vibrational frequencies are predicted as $\nu_5 = 765$, $\nu_6 = 551$, and $\nu_7 = 179$ cm^{-1}.

HC_3^+ has a linear equilibrium geometry, but a very shallow CCC bending potential. The calculated harmonic bending vibrational frequencies are $\omega_4 = 576$ and $\omega_5 = 105$ cm^{-1}. Similar to C_3 [16], its vibration-rotation coupling constant α_2 has a negative value. Its equilibrium dipole moment is rather large which should facilitate the radioastronomical detection.

Acknowledgement: Thanks are due to the Regionales Hochschulrechenzentrum Kaiserslautern for providing computation time and to the Fonds der chemischen Industrie for financial support.

[1] W. Meyer, J. Chem. Phys. 58, 1017 (1973).
[2] W. Meyer, in: Modern Theoretical Chemistry, Vol. 3, ed. H. F. Schaefer III (Plenum, New York, 1977).
[3] W. Meyer, P. Botschwina, P. Rosmus, and H.-J. Werner, in: Computational Methods in Chemistry, ed. J. Bargon (Plenum, New York, 1980).
[4] P. Botschwina, in: Ion and Cluster-ion Spectroscopy and Structure, ed. J. P. Maier (Elsevier, Amsterdam, 1989).
[5] P. D. Mallinson and R. L. De Zafra, Mol. Phys. 36, 827 (1978).
[6] P. Botschwina, Chem. Phys. 68, 41 (1982).
[7] P. D. Mallinson and A. Fayt, Mol. Phys. 32, 473 (1976).
[8] P. Botschwina, Chem. Phys. Lett. 139, 255 (1987).
[9] S. K. Lee and T. Amano, Ap. J. 323, L145 (1987).
[10] K. Kawaguchi, M. Kajita, K. Tanaka, and E. Hirota, to be published.
[11] W. F. Lafferty and F. J. Lovas, J. Phys. Chem. Ref. Data, 7, 441 (1978).
[12] T. B. Tang, H. Inokuchi, S. Saito, C. Yamada, and E. Hirota, Chem. Phys. Lett. 116, 83 (1985).
[13] R. D. Brown, D. E. Pullin, E. H. N. Rice, and M. Rodler, J. Am. Chem. Soc. 107, 7877 (1985).
[14] R. D. Brown, F. W. Eastwood, P. S. Elmes, and P. D. Godfrey, J. Am. Chem. Soc. 105, 6496 (1983).
[15] P. Botschwina, J. Chem. Phys, in press.
[16] K. Matsumura, A. Kanamori, K. Kawaguchi, and E. Hirota, J. Chem. Phys. 89, 3491 (1988).

MICRODYNAMICS OF ADSORBED POLYAROMATIC HYDROCARBONS ON SMALL GRAPHITE PARTICLES

G.Neue
Lehrstuhl für Phys.Chem.II, Universität Dortmund
Postfach 500500, D-4600 Dortmund 50, F.R.G.

SUMMARY

A laboratory NMR study of the dynamics of polycyclic aromatic hydrocarbons (PAH) adsorbed on small graphitic grains is presented. High surface mobilities were found and expressions for the temperature dependence for several types of motion are given.

EXPERIMENTAL AND DISCUSSION

In recent years large efforts have been made to elucidate the role of grain surfaces in the synthesis of interstellar molecules [1,2,3,4,5] . Up to now polycyclic aromatic hydrocarbons (PAH) have not been detected unambiguously in space though several investigators suggested them to explain some observations [6,7]. Their ease of formation from carbon radicals [8] and their interaction with charged particles [9] makes them an attractive class of interstellar molecules. A key property for chemical reactions on surfaces is mobility of the adsorbed species as it determines collision rates. The present work used nuclear magnetic resonance (NMR) to study the dynamics of adsorbed naphthalene, anthracene, fluoranthene, and pyrene on small graphite particles (diameter 40 nm). In each case samples containing 80% of a monolayer PAH were prepared by mixing the required amounts of graphite (0.5 g) and the respective PAH in a pyrex tube which was sealed under UHV conditions. To accelerate equilibration the sample was heated to about 200°C. To achieve good sensitivity for rotational motions fully deuterated PAHs were used and the D-resonance was observed at 52.72 MHz. A temperature range of 70 K to 300 K was investigated which is close to conditions in circumstellar en-

velopes and at the lower end close to the densest cores of giant molecular clouds. Due to the high surface area of the samples (40 m^2) contaminations by remaining gases can be regarded as insignificant. All PAHs were found to form thermodynamically stable surface phases implying adsorption enthalpies exceeding the heats of vaporization [10], i.e. 70-100 kJ/mol (8000-12000 K).

NMR lineshapes as well as longitudinal relaxation were observed covering a range of frequencies of (hindered) molecular reorientations of 1 kHz to 1 GHz. As an representative example observed lineshapes of adsorbed naphthalene are shown in Figure 1.

Figure 1:

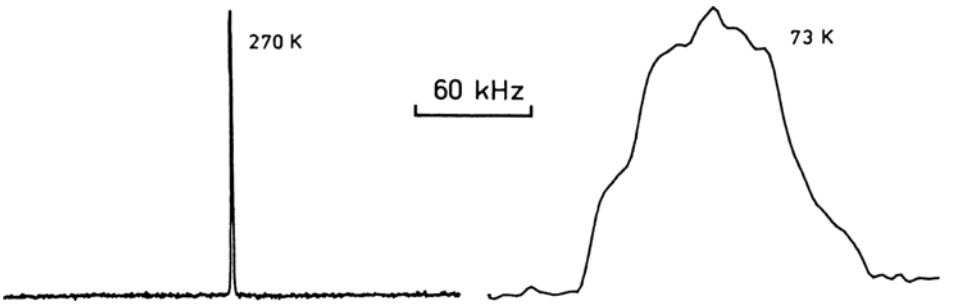

At high temperature the signal is averaged to a narrow line by fast isotropic rotations which can be identified with fast two-dimensional traslation around the almost spherical grains [11]. If this translational motion is sufficiently slowed down (73 K) the signal is much broader and, in addition, asymmetries caused by the strong anisotropic diamagnetic susceptibility of graphite show up which can be used to deduce that the molecules lie flat on the surface while rotating fast around an axis perpendicular to the surface [12]. A detailed quantitative discussion [13] yields expressions for the temperature dependence of the dynamical parameters.

Translational surface diffusion coefficients:

naphthalene	$6.4 \cdot 10^{-7}$ m^2/s exp(-6.6 kJ/mol /RT)	300 K - 100 K
anthracene	$4.3 \cdot 10^{-7}$ m^2/s exp(-6.6 kJ/mol /RT)	300 K - 75 K
fluoranthene	$1.8 \cdot 10^{-7}$ m^2/s exp(-6.6 kJ/mol /RT)	300 K - 90 K
pyrene	$1.5 \cdot 10^{-7}$ m^2/s exp(-6.6 kJ/mol /RT)	300 K - 100 K

Rotational correlation times (axis perpendicular to the surface):

naphthalene	$2.0 \cdot 10^{-12}$ s exp(4.7 kJ/mol /RT)	125 K - 75 K
fluoranthene	$3.7 \cdot 10^{-12}$ s exp(5.7 kJ/mol /RT)	200 K - 70 K

Anthracene does not show a rotation but instead a libration with respect to the surface with a correlation time given below

anthracene	$1.0 \cdot 10^{-11}$ s exp(4.3 kJ/mol /RT)	150 K - 70 K.

It should be remarked that the temperature ranges given are those where the respective motions show up in the data. Their existence may well extend beyond the stated limits.

It can be concluded that despite of their strong adsorption big molecules nevertheless can be remarkably mobile on surfaces even at low temperatures and rather high coverages.If the molecules are more diluted an even higher mobility has to be expected. Due to a wealth of reaction mechanisms PAHs are then perhaps able to influence the chemistry of small molecules on the surfaces of interstellar grains.

REFERENCES

1. Tielens, A.G.G.M., Hagen, W. : Astron. Astrophys. ***114***, 245 (1982)
2. d'Hendecourt, L.B., Allamandola, L.J., Baas, F., Greenberg, J.M. : Astron. Astrophys. ***109***, L12 (1982)
3. Greenberg, J.M. : Scientific American ***250*** , 124 (1984)
4. Duley, W.W., Williams, D.A. : Interstellar Chemistry, Academic Press, London (1984)
5. Winnewisser, G., Herbst, E. : Topics in Current Chemistry ***139***, 119 (1987)
6. Duley, W.W., Williams, D.A. : M.N.R.A.S. ***196*** , 269 (1981)
7. Allamandola, L.J., Tielens, A.G.G.M., Barker, J.R. : Astrophys. J. (Letters) ***290*** , L25 (1985)
8. Zander, M. : Intern. J. Environ. Anal. Chem. ***4***, 109 (1975)
9. Lepp, S., Dalgarno, A., Van Dishoeck, E.F., Black, J.H. : Astrophys. J. ***329*** ,418 (1988)
10. Sonnefeld, W.J., Zoller, W.H., May, W.E. : Anal. Chem. ***55*** , 275 (1983)
11. Neue, G. : Z. Naturforsch. ***43a*** , 30 (1988)
12. Boddenberg, B., Neue, G. : Z. Naturforsch. ***42a*** , 948 (1987)
13. Neue, G. : in preparation

A NON-CIRCUMSTELLAR ORIGIN OF THE HUMP

P.M.M. Jenniskens, M.S. De Groot
Laboratory for Astrophysics, P.O. 9504, 2300 RA Leiden, The Netherlands

SUMMARY

The particles responsible for the 217.5 nm interstellar extinction feature may originate from photoprocessed organic material on dust grains.

INTRODUCTION

The interstellar extinction curve has a broad and strong absorption at 217.5 nm called the "hump". Proposed candidates for its origin are graphite (Hoyle and Wickramasinghe, 1962; Stecher and Donn, 1965), amorphous carbon (Borghesi et al., 1985), quenched carbonaceous composite (Sakata et al., 1983) and polycyclic hydrocarbons (Donn, 1968; Leger, 1984), all assumed to have a circumstellar origin, and unsaturated linear carbon chain molecules (Hoyle and Wickramasinghe, 1977) and O^{2-} ions in oxide grains (Duley et al., 1979).

The hump is nearly constant in position and shape for different lines of sight and therefore for different environmental conditions. Any origin that is stronly particle size dependent is unlikely. To have an efficient absorption at 217.5nm, the hump particles must be at least an order of magnitude smaller on average than the particles responsible for the visual extinction. The strength of the hump correlates with visual extinction but not with the far UV part of the extinction curve (Greenberg and Chlewicki, 1983). This suggests a generic link between the hump particles and the dust responsible for the visual extinction.

We investigate the possibility that the hump is caused by organic matter originating from the mantles of the large visual particles. A more extended report is given by De Groot et al. (1988). The organic matter (organic refractory) is formed by photoprocessing of small molecules frozen on the surface of these large grains in dense clouds and subsequent photolysis and heating when the grains enter the diffuse medium (Hagen et al., 1979). Grain-grain collisions may scatter the mantles into small pieces which are further photoprocessed. This mechanism forms hump particles in situ, in the interstellar medium, contrary to models in which the particles are formed in circumstellar shells.

EXPERIMENTAL RESULTS AND DISCUSSION

Small molecules like ortho-xylene ($C_6H_6(CH_3)_2$), isolated in an argon matrix at 12 K and $3x10^{-8}$ mbar pressure, form a number of reactive intermediates upon irradiation by UV photons ($\lambda > 150$ nm). The intermediates have many narrow absorptions in the measured wavelength range of 500 to 200 nm as shown in figure 1 (left). The matrix is heated to the point where the argon evaporates (28K). The intermediates react to some polymeric substance that has a single broad absorption with a peak at 222 ± 8 nm as shown in figure 1 (right). This absorption feature resembles the hump that is seen

in the average diffuse interstellar extinction curve as published by (Chlewicki, 1985) and reproduced as a reference in both parts of figure 1. Less than 24% of the available carbon in space is needed to account for the interstellar hump with a similar polymeric substance as made in our experiment from ortho–xylene.

REFERENCES

Borghesi A., Bussoletti E., Colangeli L.; 1985. Astron. Astrophys. **142**, 225

Chlewicki G.; 1985. *Observational Constraints on Multimodal Interstellar Grain Populations*; thesis, Leiden University, p. 72

De Groot M.S., Van der Zwet G.P., Jenniskens P.M.M., Bauer R., Baas F., Greenberg J.M.; 1988. Submitted to the proceedings of the meeting *Dust in the Universe*; Bailey M.E., Williams D.A. (eds.), Manchester 1987 December 14–18.

Donn B.; 1968. Astrophys. J. **152**, L129

Duley W.W., Millar T.J., Williams D.A.; 1979. Astrophys. Space Science bf 65, 69

Greenberg J.M., Chlewicki G.; 1983. Astrophys. J. **272**, 563

Hagen W., Allamandola L.J., Greenberg J.M.; 1979. Astrophys. Space Science **65**, 215

Hoyle F., Wickramasinghe N.C.; 1962. M.N.R.A.S. bf 124, 417

Hoyle F., Wickramasinghe N.C.; 1977. Nature **266**, 241

Leger A., Puget J.L.; 1984. Astron. Astrophys. **137**, L5

Sakata A., Wada S., Okutsu Y., Shintani H., Nakada Y.; 1983. Nature **301**, 493

Stecher T.P., Donn B.; 1965. Astrophys. J. **142**, 1681

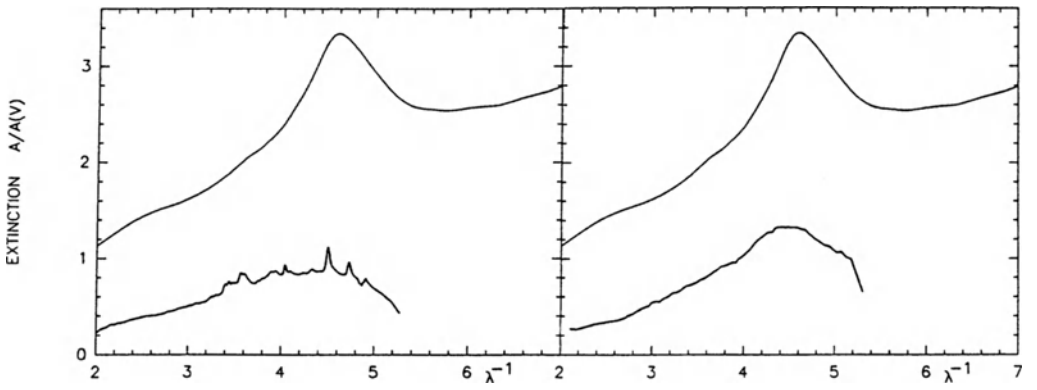

Figure 1: *Left: UV spectrum of reactive intermediates produced by photoprocessing of in argon isolated ortho–xylene molecules.*

Right: UV spectrum of the thin layer of polymeric product that forms when the matrix is heated to the point where the argon evaporates (28K).

In both figures the average extinction curve for the diffuse medium is given as published by Chlewicki (1985). The hump is the feature near $4.6\mu m^{-1}$.

CHEMICAL PATHWAYS FROM ATOMIC SILICON IONS TO COMPOUNDS OF SILICON

Diethard K. Bohme, Stanislaw Wlodek, and Arnold Fox
Dept. of Chemistry/Centre for Research in Experimental Space Science
York University, North York, Ontario, Canada M3J 1P3

SUMMARY

Ions and their reactions are an integral part of the composition and chemistry of interstellar and circumstellar molecular regions. Here we report results of laboratory studies of ion chemistry which is initiated by ground-state atomic silicon ions. The results improve our understanding of interstellar molecular clouds and the molecular outflows of stars by showing how known silicon-bearing molecules may be formed, how other silicon-bearing molecules may evolve, and how gas-phase ion chemistry can ultimately lead to the formation of silicon-bearing molecular aggregates such as silicon-carbide and silicate "grains".

Formation and growth of silicon-bearing molecules and particles from atomic silicon may occur either directly through neutral chemistry triggered by reactions of silicon atmos or indirectly through ion chemistry triggered by reactions of atomic silicon ions as illustrated below.

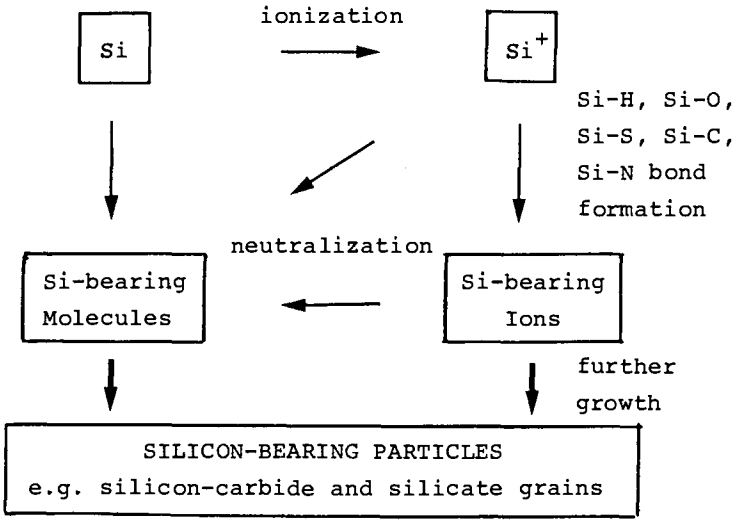

Here we report results of ongoing laboratory studies designed to track the chemistry initiated by ground-state atomic silicon ions. We are particularly interested in the identification and characterization of chemical reactions of $Si^+(^2P)$ which trigger the formation of Si-H, Si-O, Si-S, Si-C and Si-N bonds and chemical pathways which lead to further growth of ions and molecules containing these bonds. A variety of interstellar and related molecules were chosen as neutral reactants in the studies completed so far including H_2, O_2, CO, NO, NO_2, N_2O, CO_2, SO_2, COS, CS_2, H_2O, H_2S, NH_3, CH_4, acetylenes, alcohols, acetone, carboxylic acids, amines and cyanides. The laboratory technique which is being employed in these studies is the Selected-Ion Flow Tube or SIFT technique available in the Ion Chemistry Laboratory at York University. The SIFT technique allows the determination of rate constants, products and product distributions for selected-ion/selected-molecule reactions proceeding in a helium carrier gas at 0.35 Torr and 296 K.[1] Atomic silicon ions are generated by electron impact on tetrachloro- or tetramethylsilane.[1,2]

We have found that ground-state atomic silicon ions are generally quite reactive and can initiate a rich primary and higher-order chemistry which establishes chemical bonds between silicon and a variety of heteroatoms:

Silicon/Hydrogen Bonds: $Si^+(^2P)$ does not react rapidly with H_2 in a bimolecular fashion but may react with other hydrogen-bearing molecules by hydride transfer to form directly the neutral molecule SiH.[1,2] We have shown that methylamines transfer a hydride ion to Si^+ to form SiH in reactions driven by the stability of the resulting immonium ion.[2] Also we have seen that diacetylene reacts exclusively by hydride transfer to yield SiH.[3]

Silicon/Oxygen Bonds: We have found that the bimolecular oxidation of $Si^+(^2P)$ to form SiO^+ or SiO is thermodynamically controlled. It does not occur with molecules having a more tightly bound O atom or O^- anion such as O_2, CO, NO, CO_2 and OCS but has been observed to occur with NO_2 and N_2O which have less tightly bound O atoms and with NO_2 and SO_2 which have less tightly bound O^- anions.[4] Sequential O atom transfer reactions in N_2O appear to establish SiO_2^+, SiO_3^+ and SiO_4^+.[4]

Ground-state silicon ions react with hydroxyl-containing molecules and acetone to produce the silene cation $SiOH^+$ which may neutralize by proton transfer or recombination with electrons to form silicon monoxide.[1] $SiH_3O_2^+$, which may neutralize to produce silanoic acid, is the predominant product in reactions of $SiOH^+$ with water, ethanol and formic acid molecules, while direct formation of silanoic acid is likely in the reaction with acetic acid. The $SiH_3O_2^+$ ion is solvated in reactions

with water and ethanol, while $SiCH_3O_3^+$ and $SiH_5O_3^+$ are the predominant products in the reaction with formic acid. Several reaction sequences occur in methanol, ethanol and formic acid which can lead to the complete saturation of Si^+ forming ions of the type $HSi(OCH_3)_3H^+$, $HSi(OC_2H_5)_3H^+$ which may neutralize to generate trimethoxysilane, triethoxysilane and trihydroxysilane, respectively.[1]

Silicon/Sulfur Bonds: The ion $SiSH^+$ which may neutralize to form SiS has been observed as the product of the reaction of $Si^+(^2P)$ with H_2S.[5] Also, ground-state silicon ions will abstract an S atom from OCS to form SiS^+ while sequential S-atom transfer reactions with the same molecule can lead to polysulphide ions of the type SiS_n^+.[4,5] Charge transfer reactions of these ions will establish neutral polysulfide molecules of the type SiS_n.

Silicon/Nitrogen Bonds: We have reported previously that the reaction of Si^+ with ammonia produces $SiNH_2^+$ which may neutralize to form hydrogen silaisocyanide, SiNH.[6] A similar reaction with methylamine produces $SiNH_2^+$.[2] Related reactions were observed to occur with mono- and dimethylamine which yield the ion $SiNHCH_3^+$.[2] This latter ion may lose a proton to produce $SiNCH_3$. Other syntheses are indicated by the observed secondary products. With methylamine $SiNH_2^+$ appears to produce $H_2SiNH_2^+$ which may deprotonate to form the simplest silanimine, $H_2Si{=}NH$, or aminosilylene, $HSiNH_2$.[2] Si-N bond formation also seems to prevail in the reactions of Si^+ with HCN and C_2N_2 which are possible sources for the CNSi molecule.[7]

Silicon/Carbon Bonds: Reactions of Si^+ with the unsaturated hydrocarbon molecules acetylene, ethylene and methylacetylene have been observed to lead to Si-C bond formation by C-H bond insertion with H-atom elimination.[3] Neutralization of the resulting ions SiC_2H^+, $SiC_2H_3^+$ and $SiC_3H_3^+$ can lead to the silicon-carbide molecules SiC_2, SiC_2H_3 and SiC_3H_2. Methylamines and acetone can lead directly to the neutral silicon-carbide molecules SiCH (HSiC) and $SiCH_3$ ($HSiCH_2$). A secondary reaction of SiC_2H^+ with acetylene acts to enhance the carbon content as it produces SiC_4H^+ which may neutralize to SiC_4.[3]

Our laboratory studies so far clearly indicate that when followed by neutralization, or sometimes without neutralization, many of the primary and higher-order reactions which were observed and characterized provide ion/molecule pathways towards the formation of the known interstellar silicon-bearing molecules SiO and SiS and a variety of new silicon-bearing molecules including SiH, SiCH, $SiCH_3$, SiC_2, SiC_4, SiC_2H_3, SiC_3H_2, SiO_2, SiS_2, HSiOOH, $HSi(OH)_3$, $HSi(OCH_3)_3$, $HSi(OC_2H_5)_3$, SiNH, $SiNH_3$, and CNSi. The observed ion chemistry also has implications for still further molecular growth. Many of the larger ions and

molecules are likely precursors important in the formation of silicon carbide and silicate particles or grains. For example, we have speculated elsewhere that trihydroxysilane may spawn tetrahydroxysilane which is a known building block for the condensational synthesis of hydrated silicate networks.[3] Also, association reactions were observed which lead to the sequential addition of molecules to ions. In the helium buffer gas of our experiments these adduct ions are likely to be stabilized by collisions with helium atoms. In the much less dense interstellar environment stabilization must occur by radiative association. Little is known about the efficiency of these latter reactions so that it is difficult to assess the importance of such processes in interstellar molecular growth.

Acknowledgment: We thank the Natural Sciences and Engineering Research Council of Canada for the financial support of this research.

References:

1. W/odek, S., Fox, A., Bohme, D.K.: J. Am. Chem. Soc. 109, 6663 (1987).
2. W/odek, S., Bohme, D.K.: J. Am. Chem. Soc. 110, 2396 (1988).
3. Bohme, D.K., W/odek, S., Fox, A.: "Rate Coefficients in Astrochemistry", T.J. Millar and D.A. Williams (Eds.), Kluwer Academic Press, 193 (1988).
4. W/odek, S., Bohme, D.K.: Proceedings of the 11th International Mass Spectrometry Conference, 28 August - 2 September, 1988, Bordeaux, France.
5. Bohme, D.K., W/odek, S., Fox, A.: Proceedings of the IAU Symposium 135, July 26 - 30, 1988, Santa Clara, California.
6. W/odek, S., Rodriquez, C.F., Lien, M.H., Hopkinson, A.C., Bohme, D.K.: Chem. Phys. Lett. 143, 385 (1988).
7. W/odek, S., Bohme, D.K.: J. Am. Chem. Soc.: in press (1989).

FOCAL PLANE IMAGING ARRAY FOR ASTRONOMICAL SPECTROSCOPY AT 3MM WAVELENGTH

P.F. Goldsmith, N.R. Erickson, C.R. Predmore, P. J. Viscuso and G. Novak
Five College Radio Astronomy Observatory
Department of Physics and Astronomy
University of Massachusetts, Amherst MA 01003

INTRODUCTION

Millimeter wavelength astronomy technology has matured to the point that individual receivers are approaching the sensitivity limit set by the atmosphere. Consequently, the only way to achieve a major increase in the rate of data collection for the study of extended sources is by using multiple detectors. While not the only possible approach, a detector array in the telescope focal plane is by far the most straightforward means of increasing the rate at which information is gathered. For the molecular line observations which dominate millimeter wavelength astronomy, the requirement that spectral analysis be carried out for each pixel of the array is a major deterrent in terms of both system complexity and cost. This is one important reason that most focal plane array systems envisioned or built for millimeter wavelength spectroscopy have been instruments with essentially a single frequency channel [1],[2]. While this eases the "backend" problem, a major penalty is paid in overall sensitivity, since simultaneous analysis of multiple frequency channels is as valuable as simultaneous analysis of pixels corresponding to different directions on the sky. Various technologies have been developed for imaging arrays; the general subject is reviewed in [3] and [4], and recent developments summarized in [5].

The Five College Radio Astronomy Observatory at the University of Massachusetts has undertaken a major instrumentation project to develop a focal plane array for use on the 14 m radome enclosed telescope located in the Quabbin watershed; hence the acronym QUARRY. In this effort we have sought to increase the effective speed of the facility by at least an order of magnitude, while retaining good frequency agility and coverage throughout the 3mm wavelength range, 85-115 GHz, in which the antenna is highly efficient and in which observations can be carried out for a large portion of the year. The QUARRY system has been described in some detail previously [6], and the purpose of the present communication is to summarize the project and indicate its present status.

FRONTEND COMPONENTS AND OPTICS

The requirement of currently available technology of proven reliability indicated the use of cooled Schottky mixers. Previous efforts at FCRAO have resulted in good performance [7], and the necessity of cooling only to 15 K greatly facilitates system design and maintenance. A great advantage of Schottky diode mixers compared to alternative nonlinear devices is that they offer good performance over a large frequency range without the need of mechanical adjustment. We have determined that a fixed-tuned mixer varies in noise temperature by less than 25% over the 80 to 115 GHz range. For a focal plane array, this drastically simplifies both the thermal and mechanical design. Tests of a prototype mixer have yielded DSB receiver temperatures between 80 and 120 K with an IF noise temperature of 15 K. The 6 dB conversion loss implies that a receiver noise temperature well under 100 K should be achieved in the array with lower-noise IF amplifiers and reduced input loss.

Currently available low capacitance Schottky diodes also require sufficiently low local oscillator power, on the order of 30 microwatts, that providing the local oscillator for a focal plane array of moderate size is not a major problem. In the QUARRY system the local oscillator will be injected with a multiple crossguide directional coupler, with a coupling of approximately -18 dB for each mixer. This approach, which is quite inefficient for a single mixer, ends up being reasonably efficient for an array with more than ten elements.

To achieve minimum receiver noise temperature as well as facilitate the packing of the mixers, the first IF amplifier is integrated with the mixer and DC bias circuit. The IF covers the 1.25-1.65 GHz range, and the first stage of the amplifier is a HEMT transistor while the following two stages are FETs. A second amplifier for each array element is also included in the dewar, but is physically separated from the mixer/first IF amplifier assembly and is at room temperature.

The QUARRY system includes fifteen elements, each being fed by a corrugated feedhorn in order to obtain high illumination efficiency of the antenna. To obtain the lowest possible single sideband system temperature and good calibration accuracy, a single sideband filter [8] cooled to 15 K is included, which is common to all array elements. The feedhorns, shown in Figure 1, are circumscribed by four planes, resulting in a square envelope with rounded corners. The truncation reduces the horn center to center distance for square packing by 20 % compared to horns with full walls and corrugations. The improvement in the packing efficiency is obtained without significantly affecting the radiation patterns. The feedhorns are arranged in a 5x3 array with equal spacing in the two principal planes.

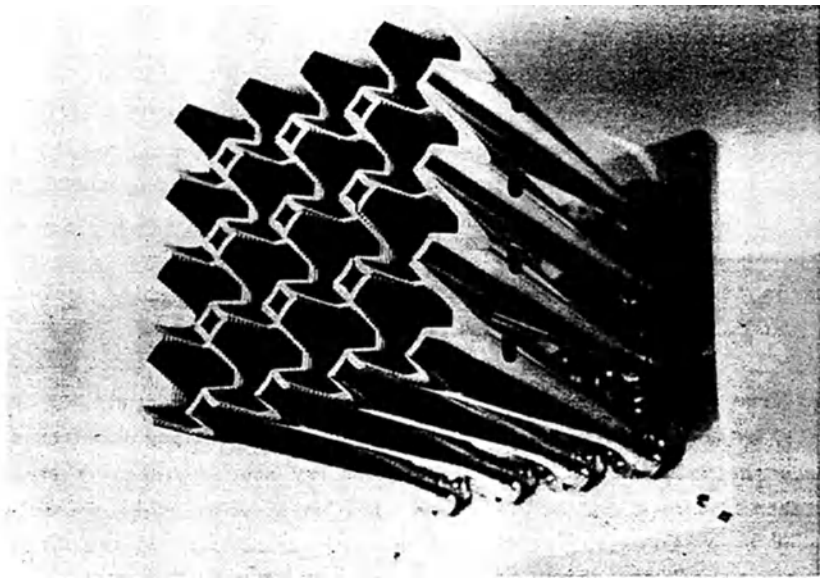

Figure 1 QUARRY Cutoff Corrugated Feedhorns

The optics in the QUARRY system are shown in Figure 2. Their first function is to guide the beams from the individual feedhorns to the single sideband filter. This is carried out by a field lens located just in front of the feedhorns. This lens is made from boron nitride (BN), which we have found to have very low absorption,

Figure 2 QUARRY Optics

and which is readily machinable. The index of refraction of BN is close to 2, so that it is efficiently anti-reflection coated by materials such as polyethylene and teflon. We have used teflon fabric laminated with epoxy for antireflection coating cooled lenses. The single sideband filter is preceded by a wire grid, and by a second lens, which collimates the beam propagating in the filter, in order to reduce diffraction loss. The polarization-rotating properties of the filter result in energy at the signal frequency passing through the grid and being coupled from the feedhorns to the antenna, while energy at the image frequency is not rotated and thus is reflected from the grid and then to a termination cooled to 15 K located just below the field lens and feedhorn array.

The beams from all 15 feedhorns have the same linear polarization, and are treated identically by the single sideband filter. Just before exiting from the dewar, the beams from the 3x3 subarray and the 2x3 subarray are separated (there is a gap between the subarrays in the feedhorn array which makes this possible without significant beam truncation). The 2x3 subarray beams are rotated 90 degrees in polarization by a reflective half wave plate. The beams from the two subarrays, now having orthogonal polarizations, can be combined by a wire grid polarizer in a manner such that the beams from the small subarray are interleaved with those from the large subarray. These elements are shown in the left hand side of Figure 2. The resultant footprint of the array in the antenna focal plane is again 5x3 elements, but with the beams in rows of 5 having alternating polarizations, and just over one FWHM beamwidth spacing, while the 3 rows of beams have just over two FWHM beamwidth spacing.

FRONTEND SYSTEM

The front end of the QUARRY system has to perform a number of functions in addition to collecting energy from the pixels of the array and down-converting and amplifying the signals. These are shown schematically in the system diagram given in Figure 3. The first task is maintaining a constant position angle for the pixels of the array during long integrations; this ability also facilitates mosaicing to create large maps. This function is carried out by rotation of the entire dewar, which is accomplished by a servo system employing two opposing DC motors. The mixer bias supplies and local oscillator system rotate with the dewar, and a cable wrap is used to bring the IF cables and refrigerator hoses from the dewar to the non-rotating portion of the receiver.

QUARRY

FOCAL PLANE IMAGING SYSTEM FOR SPECTRAL LINE ASTRONOMY

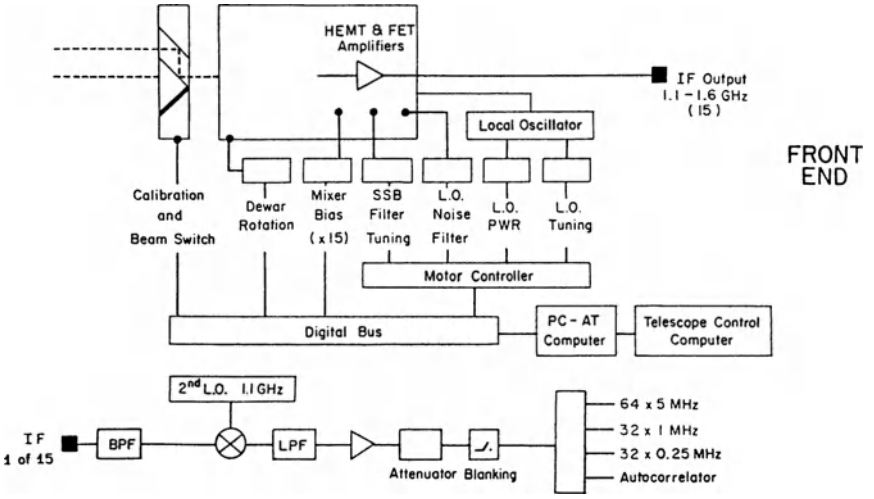

Figure 3 QUARRY System Diagram

Calibration of the QUARRY elements is obtained by means of an ambient temperature load which can be moved in front of the dewar signal input window by a linear stepper motor. This system can also move a 45 degree mirror into the beam, which results in a set of reference beams displaced by 6 inches in the focal plane (corresponding to an angular shift of 10′ on the sky). The receiver can switch between main and reference beams at a 1 Hz rate, making this system useful for pointing measurements, albeit less than ideal for continuum observations.

The receiver functions are controlled by an instrument computer, which is an IBM PC AT-compatible unit. Commands for receiver tuning and observing mode are received from the MODCOMP telescope control computer, and operating parameters including dewar rotation angle, position of the calibration system, local oscillator frequency and power, single sideband filter tuning, and mixer bias levels are set by the instrument computer via a digital bus.

SPECTROMETERS

The range of astronomical projects for which QUARRY will be a powerful tool is very wide, since most objects at millimeter wavelengths are extended on the scale of the

3 arcminute x 3 arcminute footprint of the array beams on the celestial sphere. Several hundred nearby galaxies are prime candidates for study in an extension of the FCRAO external galaxy survey. Thus, a velocity coverage of 500 km/s is the minimum that is acceptable. Nearby dark clouds have extremely large angular extents, and require a velocity resolution of less than 0.1 km/s for detailed analysis of their kinematic structure. The demands on the spectral analysis system are thus considerable and a two part program has been adopted to reduce cost and manpower impact while the frontend is being constructed, while allowing some significant astronomical utilization of QUARRY in the immediate future.

In the first phase, we have modified our existing 512 channel x 250 kHz resolution filter spectrometer to have 32 channels for each pixel of QUARRY. The velocity resolution of 0.65 km/s and coverage of 21 km/s at CO J-1-0 are adequate for observations of nearby cloud complexes, but not for detailed study of dark clouds. For observations of galaxies, we have developed a low-cost spectrometer with 64-5 MHz filters for each pixel [6]. The total velocity coverage is 830 km/s, which should make this efficient system well-suited for almost all extragalactic observations.

The galactic observations will, however, be severely limited by the initial spectrometer system, and any multi-line observations will be essentially precluded as a result of the limited bandwidth analyzed. To provide a backend system that can really take advantages of the full capability of the QUARRY system, we intend to construct an autocorrelation spectrometer for each pixel, based on the design of A. Bos [9]. There will be 1024 channels for each element of the array, covering 4 bands each up to 25 MHz wide. With this system, we will be able to carry out projects such as detailed mapping of dark clouds, sensitive searches for outflow sources, and mapping of the emission throughout the galaxy with high efficiency and the appropriate velocity resolution and coverage.

PRESENT STATUS

The basic design work for the QUARRY system is complete, and the optical system including the single sideband filter and feedhorn array has been constructed and tested at room temperature. The performance agrees with expectations in all regards, except that no loss measurements have been made. Previous experiments indicated that the loss of boron nitride is appreciably lower at liquid nitrogen temperature than at ambient temperature, so that representative measurements will have to await cooling of the complete system, which should be carried out before

the end of 1988. The local oscillator injection coupler, calibration system, and dewar rotation system have also been built and shown to operate properly.

As indicated above, a prototype mixer has been constructed and tested. At the present time, the 15 array mixers are being built, and the HEMT IF amplifiers are being finalized and integrated with the mixers. The conversion of the 250 kHz filter spectrometer is complete, and the 5 MHz resolution filterbanks are in production, with all of the filter units already finished. QUARRY is expected to be operational by mid-1989.

This project has been critically dependent on the efforts of many of the F.C.R.A.O. technical staff. We would in particular like to acknowledge the important contributions of D. McGonagle and R. Grosslein, in the areas of mixer testing and optics fabrication and testing. S. Han, A. Hartai, J. Karakala, T.-C. Li, and P. Luippold have made significant contributions of time and ideas to QUARRY.
This work was supported by the National Science Foundation (grant AST 85-12903), and is contribution 671 of the Five College Astronomy Department.

REFERENCES

[1] A.R. Gillespie and T.G. Phillips, "Array Detectors for Millimetre Line Astronomy", *Astron. Astrophys.*, **73**, 14-18, 1978.

[2] J.A. Murphy, R. Padman, and R.E. Hills, "An Experimental submillimeter Heterodyne Array Receiver", *Int. J. Infrared and Millimeter Waves*, **9**, 325-350, 1988.

[3] K.S. Yngvesson, *Near-Millimeter Wave Imaging with Integrated Planar Receptors*, Chapter 1 of Infrared and Millimeter Waves, vol. 10, K.J. Button, ed. New York: Academic, 1983.

[4] J.A. Murphy and R. Padman, "Focal Plane and Aperture Plane Array Receivers for Millimeter Wave Radio Astronomy",*Int. J. Infrared and Millimeter Waves*, **9**, 667-704, 1988.

[5] K.S. Yngvesson, "MMW Radio Astronomical Imaging Instrumentation", *Microwave Systems News*, December 1988, in press.

[6] N.R. Erickson, P.F. Goldsmith, C.R. Predmore, and P.J. Viscuso, "A 3mm Wavelength Imaging Array for Astronomical Spectroscopy", Proc. UMass Conf. Molecular Clouds in the Milky Way and Other Galaxies, J. Young, R. Dickman, and R. Snell, eds. Dordrecht: Reidel, 1989.

[7] C.R. Predmore, A.V. Raisanen, N.R. Erickson, P.F. Goldsmith, and J.L.R. Marrero, "A Broad-Band Ultra-Low-Noise Schottky Diode Receiver from 80 to 115 GHz," *IEEE Trans. Microwave Theory Tech.*, **MTT-32**, 498-507, 1984.

[8] N.R. Erickson, "A New Quasi-Optical Filter, the Reflective Polarizing Interferometer," *Int. J. Infrared and Millimeter Waves*, **8**, 1015-1025, 1987.

[9] A. Bos,"The N.F.R.A. Correlator Chip", Netherlands Foundation for Radio Astronomy Internal Technical Report nr. 176, 1986.

THE U.C. BERKELEY INFRARED SPATIAL INTERFEROMETER: INSTRUMENTATION AND FIRST RESULTS

M. Bester [1, 2], W.C. Danchi [1], P.R. McCullough [1], C.H. Townes [1]

[1] Space Sciences Laboratory and Physics Department
University of California at Berkeley, Berkeley, CA 94720, USA

[2] I. Physikalisches Institut der Universität zu Köln
Zülpicher Str. 77, D-5000 Köln 41, West Germany

INTRODUCTION

In the mid-infrared region, at a wavelength of 10 μm, the diffraction limited beamwidth of a single telescope with a typical aperture of 3 m diameter is approximately 0.8 arc sec. For substantially higher angular resolution multiple apertures are required. In the early 1970's a prototype interferometer for the 9-12 μm atmospheric window was developed by our group and was successfully operated [1],[2]. Based on this experience a new Infrared Spatial Interferometer (ISI) has been designed for high-resolution imaging [3], using Earth rotation aperture synthesis techniques that are well known from radio interferometry. Optimized for high mechanical stability and high precision performance the new long-baseline interferometer has been constructed and assembled at Berkeley during the past 5 years and was moved to Mt. Wilson (1742 m), California, in January 1988.

ISI - THE NEW SPATIAL INTERFEROMETER

Each of the two novel-design Pfund-type telescopes (figure 1) consists of a fixed f/3.14 parabolic mirror with 1.65 m diameter and a 2 m diameter flat mirror in an alt-az fork mount [4]. The flat mirror reflects the signal from the sky onto the parabola which in turn focuses it onto an optics table behind the flat mirror. An advantage of this particular geometry besides compactness is that it has no support struts for a secondary mirror which usually give rise to diffraction effects and partly block the aperture. The diffraction limited aperture of 1.65 m corresponds to a half-power beamwidth of about 1.4 arc sec at a wavelength of 11 μm. Another advantage of the Pfund geometry is the absence of the singularity in the zenith that is common for conventional alt-az mounts. A disadvantage is limited sky coverage, but this can be eliminated by rotating the trailers by 180°. This compact telescope design allows all optics and electronics to be contained in one standard-size semi-trailer per telescope. The trailers weigh less than 20 tons each.

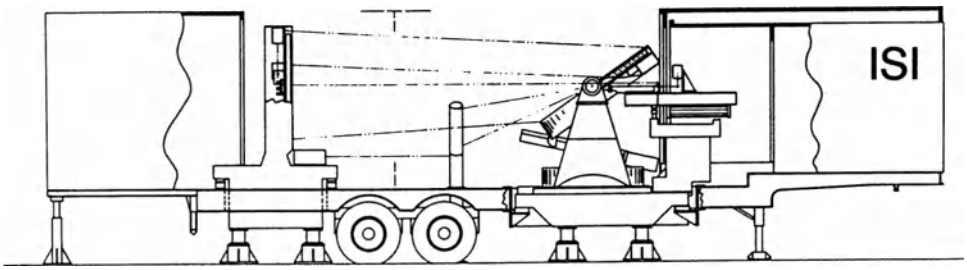

Figure 1: Schematic outline of one ISI semi-trailer.

At present there are seven stations where the telescopes can be positioned; the non-redundant baselines range in length from 4 m to 34 m, yielding angular resolutions as fine as 0.03 arc sec (fringe separation of 0.06 arc sec). However, the interferometer is designed for a maximum baseline of 1000 m which would give an angular resolution of nearly 0.001 arc sec. Each station consists of a pair of concrete pads, one for each mirror mount. When positioned on the concrete pads all mirror mounts are resting on three kinematic supports in order to allow for stress-free expansion or contraction with temperature changes. The mirror mounts are also mechanically decoupled from the trailers. They can be lifted by the trailers for moving from one station to another one.

We employ HeNe laser metrology systems that consist of 7 laser distance interferometers (LDI) per telescope (see dotted lines in figure 1): 2 LDI's for measuring the relative angles between the flat mirror and the parabolic mirror while tracking a source across the sky; 2 for monitoring the critical distances from the parabolic mirror to the flat mirror and to the optics table, and 3 others for measuring the position of the center of the flat mirror in space by triangulation [5]. The advantage of the LDI tracking system over a conventional encoder system is that the relative angles between the flat mirror and the parabolic mirror are measured directly. No backlash or other mechanical inaccuracies exist that otherwise would degrade the pointing. Theoretically the pointing precision attainable with this laser metrology system is 0.004 arc sec in the rotation angle of the flat mirror or 0.008 arc sec on the sky. However, atmospheric effects on optical pathlengths in the telescope structure can affect the precision of the measurements. Under good seeing conditions, this system allows a telescope to be pointed to a precision of about 0.1 arc sec on the sky. The telescopes are equipped with a fully redundant back-up system consisting of conventional incremental optical encoders with a resolution of 0.24 arc sec in azimuth and 0.07 arc sec in altitude on the sky.

After the initial positioning of the trailers, we observed a set of more than 100 FK5 stars all over the visible sky, using the conventional encoder system. Fitting an 11-parameter pointing model for either telescope to these observations yields a blind pointing accuracy for each telescope of less than 10 arc sec (rms) in azimuth and less than 3 arc sec (rms) in altitude on the sky. The laser metrology system has not yet been implemented for tracking control.

The main computer is a SUN Microsystems Workstation which serves as the user interface and runs the operating system UNIX (Berkeley UNIX 4.2BSD). The real-time interface between the workstation and the telescope hardware consists of three 68020-based single-board microcomputers. A digital servo system controls the tracking of the flat mirrors. Algorithms for telescope control, tracking, and data acquisition have been written in "C" code. The astronomical coordinate transformations, referred to the epoch J2000.0, employ the vector/matrix method (*The Astronomical Almanac*, 1988), yielding an overall precision of 0.01 arc sec for the apparent place of a star outside the Earth's atmosphere.

INFRARED DETECTION SYSTEM

As in many radio interferometers, ISI employs heterodyne detection and IF signal processing and correlation [6]. A schematic diagram of the infrared optics and the detection system is shown in figure 2. It is comprised of four functional blocks: the two detection systems, one per telescope; the laser phaselock system; and the pathlength control system. Heterodyne detection is achieved using LN_2 cooled HgCdTe photodiodes [7] and CO_2 laser local oscillators (LO). We use a laser line of $^{13}CO_2$ at 11.149 μm to avoid attenuation in the atmosphere due to $^{12}CO_2$ absorption lines. The Gaussian beam shape of the laser local oscillator is modified to match the profile of the sky signal, in order to get optimum heterodyne mixing efficiency. This is accomplished with a set of mirrors, lenses and aperture stops. The quantum efficiency of the detectors including telescope transmission losses is about 25% at 11 μm ($T_{sys}^{SSB} \approx 5200$ K). The IF passband is 200-2000 MHz. The first cooled FET IF amplifiers have noise temperatures of about 80 K and a gain of 25 dB.

The LO signal from one telescope is transferred by a parallel beam to the other telescope in order to phaselock the two LO's. Phase fluctuations due to the atmosphere or other causes on the transferred LO signal are compensated with the pathlength control system. It measures the round-trip phase of the LO signal on the path through the open air and corrects it with a servo loop.

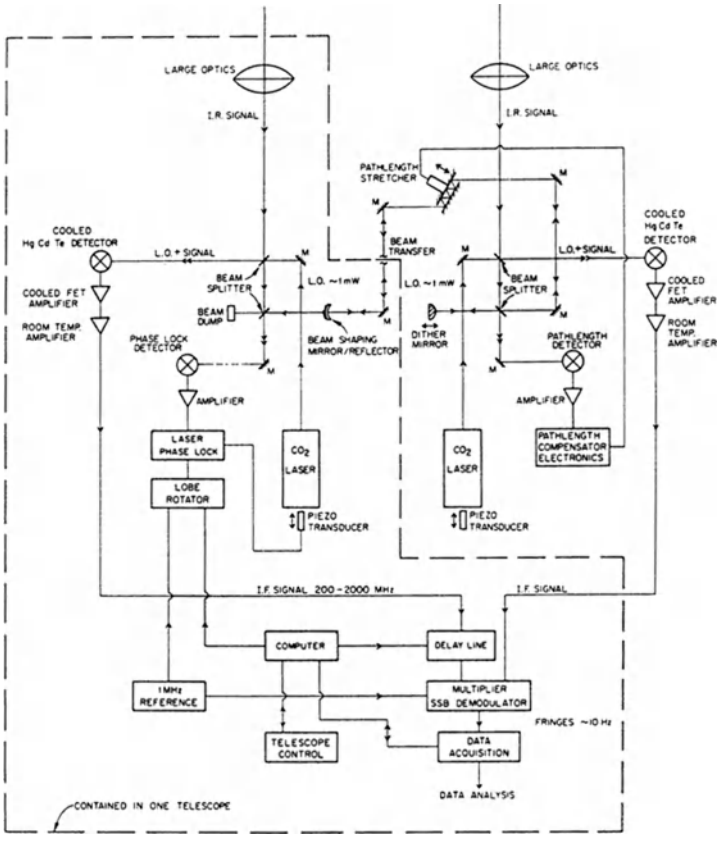

Figure 2: Schematic diagram of the heterodyne detection system.

While a source is tracked across the sky, the correlation of the received signals is maintained with the computer-controlled delay line in the IF chain. This is accomplished by switching binary multiples of 1-cm pieces of cable into the IF branch of one of the telescopes. Due to the rotation of the Earth, the signals received by the two telescopes beat together at a frequency dependent on the baseline. This beat frequency ranges from 0 Hz up to about 6.6 kHz for a 1000 m baseline. Therefore, as in many radio interferometers, the fringes are stopped with a lobe rotator acting on the laser phaselock system. The lobe rotator basically is a frequency synthesizer that tracks the differential Doppler shift and the corresponding change in phase with an accuracy of about 5°. The LO system and the correlator are set up in a way to always provide a fringe signal at 10 Hz (cf. figures 3 and 4) which in turn is digitally sampled a rate of 100 Hz. Controlling both the delay line and the lobe rotator makes the interferometer track a white-light fringe.

FIRST INTERFEROMETRY RESULTS

To perform an overall system test, we generated an artificial fringe signal on the ground. This allowed us to optimize the detection system, the delay line, and the correlator. The first fringes on a celestial source were obtained on June 29, 1988 on IRC +10216 with the initial 4-m east-west baseline. A more recent fringe spectrum obtained on this source is shown in figure 3. The width of the central peak is about 50 mHz, which indicates that the coherence time was at least 10 sec during this observation. Figure 4 shows a fringe spectrum of α Ori, taken in only 10.24 sec integration time on September 13, 1988. The width of the central spike here corresponds to the resolution of the Fourier

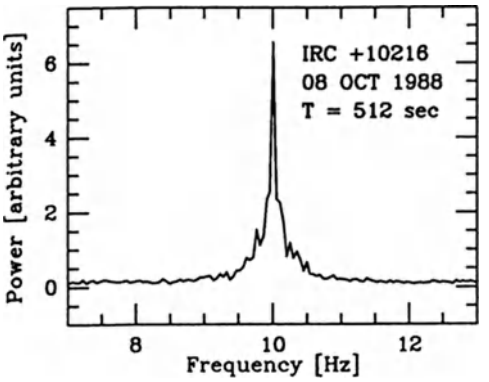

Figure 3: Fringe spectrum of IRC +10216.

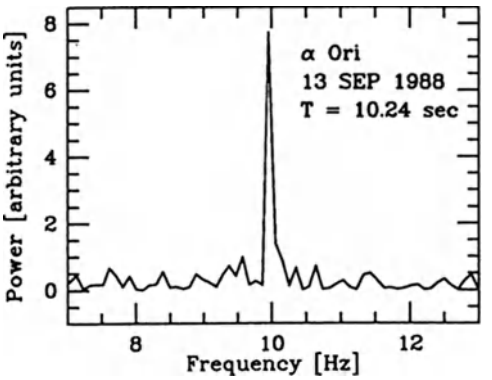

Figure 4: Fringe spectrum of α Ori.

transform, or 1/10.24 Hz, again indicating a rather long coherence time. Fringes have so far been detected on 10 other sources: VY CMa, α Sco, o Cet, R Leo, VX Sgr, α Her, χ Cyg, R Aqr, α Tau, and U Ori. Detailed results will be communicated elsewhere.

ASTROPHYSICS AND FUTURE PLANS

The sensitivity of the present detection system is such that a one hour integration time should be adequate to detect fringes on sources 6 mag fainter than the brightest IR sources. Consequently, there are several thousand infrared sources available for study at high angular resolution with the instrument described. Among those are protostellar objects imbedded in dark clouds, evolved stars, and the Galactic center. Other goals include astrometric work, characterizing atmospheric seeing at 10 μm, and observations with high angular resolution on spectral lines. The heterodyne interferometer described is well suited to expansion to more than 2 elements; with n telescopes there are n(n-1)/2 baselines which can provide data simultaneously. In addition, with 3 or more telescopes, phase closure techniques may be applied on the brighter sources, thus allowing one to correct the deleterious effects of the atmosphere on the images synthesized with such an array.

ACKNOWLEDGMENTS

This work was supported in part by the United States Office of Naval Research Contract N00014-82-C-0700 and grants from the California Space Institute and the Perkin Fund. One of the authors (WCD) has been supported in part by the L.W. Frohlich Research Fellowship of the New York Academy of Sciences. Another author (PRM) acknowledges support by the NASA GSRP grant.

REFERENCES

[1] Johnson, M.A., Betz, A.L., Townes, C.H., *Phys. Rev. Lett.*, **33**, 1617 (1974)

[2] Sutton, E.C., Storey, J.W.V., Betz, A.L., Townes, C.H., and Spears, D.L., *Ap. J. (Letters)*, **217**, L97 (1977)

[3] Townes, C.H., *J. Astrophys. and Astron.*, **5**, 111 (1984)

[4] Townes, C.H., Danchi, W.C., Sadoulet, B., and Sutton, E.C., *Proc. of a SPIE Conference on Advanced Technology Optical Telescopes III*, **628**, 281 (1986)

[5] Danchi, W.C., Arthur, A., Fulton, R., Peck, M., Sutton, E.C., Townes, C.H., and Weitzmann, R.H., *Proc. of a SPIE Conference on Advanced Technology Optical Telescopes III*, **628**, 422 (1986)

[6] Danchi, W.C., Bester, M., and Townes, C.H., *Proc. of a NOAO-ESO Conference on High-Resolution Imaging by Interferometry*, Garching, West Germany (March 14-18, 1988)

[7] Spears, D.L., *Infrared Phys.*, **17**, 5 (1977)

THE SWEDISH-ESO SUBMILLIMETRE TELESCOPE

R.S. Booth and L.E.B. Johansson
Onsala Space Observatory, Chalmers University of Technology,
S-43900 Onsala, Sweden.

Introduction.

The Swedish-ESO Submillimetre Telescope, acronym SEST, was opened for scheduled observing on April 1st, 1988, and has just completed six months of successful exploration of the southern sky. The SEST project (Booth et al.,1987) is a collaboration between the Swedish Research Council (NFR) and the European Southern Observatory (ESO). It is the only large submillimetre telescope in the Southern Hemisphere.

The Telescope

SEST is a 15m antenna, for use at wavelengths as short as 0.8mm, built on the ESO site of La Silla at a height of 2300m in the Chilean Andes. It is an IRAM design antenna with a similar specification to the interferometer antennae under construction on Plateau de Bure (Dellanoy, 1985), but on a fixed base. Like those telescopes, it is designed and constructed to operate in the open, wihout a protective astrodome, and achieves its specification by careful design and the use of carbon fibre technology in its backing structure and surface panels. It can operate in winds up to 14m/s.

A full description of SEST and the results of its commissioning tests have been given by Booth et al., (1988) and so only a brief account will be given here. SEST is a Cassegrain antenna with an alt-az mount. The main reflector consists of 176 panels, each formed from aluminium honeycomb material sandwiched between carbon fibre reinforced plastic skins and finished with a layer of aluminium, protected by a thin transparent teflon sheet bonded to the outer surface. The panel accuracy is typically 15 microns, rms.

Each panel is attached to the backing structure at five points. The height of each support point may be adjusted using remotely controlled motors, thus

allowing a rapid adjustment of the reflector. The reflector surface has been adjusted in this way and measured, while pointing at the zenith, using the theodolite-tape technique (Greve, 1986), resulting in a surface accuracy of 65 microns, rms. This level of accuracy probably represents the limit of this measuring technique and "holographic" measurements are planned to allow final adjustment of the reflector to its specified accuracy of 50 microns, rms. The measured performance of SEST is shown below in Table 1.

The homology principle has been used in the design; the subreflector vertical tilt and position are remotely controlled and pre-programmed to compensate for gravity deformation of the main reflector.

The telescope pointing parameters have been determined through observations of 86 GHz SiO masers, some of which are newly detected using SEST at the positions of southern Mira variables. In these cases it is assumed that the stellar positions from the SAO catalogue are correct. The rms residuals from the pointing model, essentially that described by Ulich (1981), are 3 arc seconds in both azimuth and elevation.

Table 1: Measured antenna parameters (October 1988)

	86 GHz	230 GHz
Main beam efficiency	0.76	0.51
Aperture efficiency	0.60	0.3 (approx.)
Half power beam width(arcsec)	57	25

Receivers.

SEST is furnished with dual polarization Schottky diode mixer receivers, built at Onsala Space Observatory (Chalmers University of Technology), for frequencies in the range 80-117 GHz and 220-270 GHz. The spectral line back-end consists of two acousto-optic spectrometers (AOS): one a high resolution AOS with a bandwidth of 100 MHz and resolution of 50 kHz and the other a wide band AOS with a total bandwidth of 1 GHz (2 x 500 MHz) and resolution 0.6 MHz. These spectrometers were built by Guisbert Winnewisser's group at the University of Cologne. Continuum observations are also supported.

Some astronomical results.

Many interesting and significant observing programmes have already been carried out with SEST in all the established areas of millimetre astronomy.

In the field of evolved stars, new results include the detection of several new SiO masers (in connection with pointing observations) and the confirmation of the suggestion by Meadows et al. (1987) that IRAS 15194-5115 is similar to IRC+10216 through the detection of some eight molecules which are seen in 10216 (Booth et al., 1988).

The southern sky is rich in optical signposts of protostellar evolution and bipolar flows. Studies of such regions in the lines of carbon monoxide are confirming the optical measurements and giving new spatial and dynamical details of the flows. An example of this work may be found in the paper by Olberg et al.,1988, published in these proceedings.

In some nearby galaxies we also have interesting results, including the detection of CO in absorption in the centre of Centaurus A by Eckart et al.(1988). Mirabel et al.,(1988) have detected CO in several luminous far infrared galaxies, including IRAS 0602-63 at a redshift, z=0.091.

Finally, we turn to observations of the Large Magellanic Cloud (LMC). Chini et al. (1988) recently made some test continuum observations at 1 mm wavelength, using the MPI bolometer built by E. Kreysa. Among other things, they detected the supernova 1987A in the LMC and report a flux density of 29 mJy. This probably represents emission from heated dust surrounding the SNR.

Following the Columbia survey of the LMC, reported in the interesting paper by Dame et al. (1988) (these proceedings), we report some high spatial resolution measurements in the ^{12}CO (1-0) line with SEST in two small areas: one area measuring 14' x 11' and centred on 30 Dor, and a second (11' x 27'), including the HII regions N159, N160 and N158 (Johansson et al. 1988). The grid spacing used was 1 arc min. In these areas we found 20 well defined molecular clouds. The SEST beam is 45" at 115 GHz, and corresponds to 11 parsecs in the LMC.

For this sample we have calculated CO luminosities, sizes, velocity dispersions, and virial masses, assuming the clouds to be spherical. A statistical comparison of the virial mass with a cloud mass determined from the CO luminosity, implies that the CO to molecular hydrogen conversion factor is about 5 times higher in the LMC than in the Galaxy. This result, based on

smaller size molecular clouds, is consistent with the "broad brush" result of the Columbia survey.

References

Booth, R.S. de Jonge, M.J., and Shaver, P.A., 1987, *ESO Messenger*, 41, 2

Booth, R.S., Delgado, G., Hagström, M., Johansson, L.E.B., Murphy, D., Olberg, M., Whyborn, N.D., Greve, A., Hansson, B., Lindström, C.O. and Rydberg, A., 1988, *Astron. Astrophys.*, (in press).

Chini, R., 1988, (private communication).

Dame, T.M., Cohen, R.S., Garay, G., Montani, J., Rubio, M., and Thaddeus, P., 1988, (these proceedings).

Dellannoy, J., 1985, Proc. ESO-IRAM-Onsala Workshop on (Sub)millimeter Astronomy, ESO Conference and Workshop Proceedings No. 22, eds., P.A. Shaver and K. Kjär, p 25.

Eckhart, A., 1988, (private communication).

Greve, A., 1986, *Int. J. Infrared and Millimetre Waves*, **7**, 121.

Johansson, L.E.B., Booth, R.S., Murphy, D., and Olberg, M., 1988, Proc. Hawaii Conference on Millimetre Astronomy.

Meadows, P.J., Good, A.R., Woolstencroft, R.D., 1987, *Mon. Not. Roy. Astron. Soc.*, **225**, 43.

Mirabel, I.F., Booth, R.S., Garay, G., Johansson, L.E.B., and Sanders, D.B., 1988, *Astron. Astrophys.*, **206**, L20.

Olberg, M., Reipurth, B., and Booth, R.S., 1988, (these proceedings).

Ulich,B.L., 1981, *Int. J. Infrared and MillimetreWaves*, **2**, 293.

THE 10 m SUBMILLIMETER TELESCOPE (SMT)

Jacob W.M. Baars
Max-Planck-Institut für Radioastronomie, Auf dem Hügel 69, 5300 Bonn, FRG
Robert N. Martin
Steward Observatory, University of Arizona, Tucson, Arizona 85721, USA

ABSTRACT. The SMT is a highly accurate telescope of 10 m diameter with a reflector quality of 15 μm rms and a pointing/tracking accuracy of 1 arcsec. It provides excellent performance at 350 μm, the shortest wavelength submillimeter atmospheric window. The SMT will be located on Mt. Graham, Arizona at an altitude of 3200 m. The performance of the SMT is attained through extensive use of carbon fiber reinforced plastic in the structure, allowing unimpaired use of the instrument under various environmental conditions. Both the site and the telescope design allow submillimeter observations during the day as well as the night. We summarize here the technical features of the telescope. The project organisation and the site characteristics have been described in the proceedings of the Kona Symposium (Baars, Krügel and Martin, 1989).

1. INTRODUCTION

Under favourable weather conditions at a high site, it is possible to make observations through the submillimeter wavelength atmospheric windows down to 330 μm. Since at best a 50 % transmission through the atmosphere is expected at the shortest wavelength, it is important that the telescope have full efficiency over the entire submillimeter wavelength range. This requires a reflector accuracy of 15 μm rms under all operational conditions and a pointing accuracy of 1 arcsec for a reflector diameter of 10 m (beamwidths are 8-25"). In a collaboration between the Max-Planck-Institut für Radioastronomie (MPIfR) and the Steward Observatory (SO), a 10 m Submillimeter Telescope (SMT) has been designed and is under construction at the firms Krupp Industrietechnik and M.A.N. Technologie, both of Germany. The SMT will be operated jointly by the MPIfR and SO (cf. Baars et al., 1989) and both institutes are developing receiver instrumentation for the telescope. The fabrication of the SMT mount and reflector will be finished in early 1989. Erection of the enclosure and telescope structure on site will begin in the spring of 1989.

With present day structural design techniques, operating on the principle of homology, residual gravitational deformations can be limited to such small values, that other influences become dominant. The most severe limitation is temperature gradients through the structure (Baars, 1983). By using carbon fiber reinforced plastic (CFRP) for the members of the reflector support structure, as well as for the reflector panels, thermal deformations are reduced by about an order of magnitude, compared to standard materials like steel or aluminium. The coefficient of thermal expansion for CFRP is about $10^{-6}\,K^{-1}$ and can be customized to a specific value during the manufacturing process. In addition, the specific stiffness (strength to density ratio) is three times greater than that of steel. This results in a lighter weight structure which is more responsive to the servo drive system. The final result is a telescope which will be operational in a variety of thermal loading conditions, both day and night. This is particularly important since our site, Mt. Graham, does not appear to exhibit diurnal variations in the atmospheric conditions at submillimeter wavelengths.

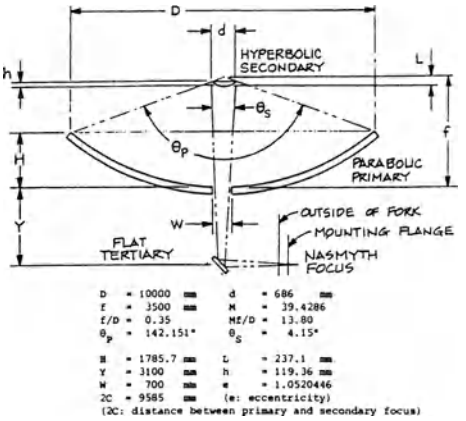

Fig. 1. The optical layout of the SMT

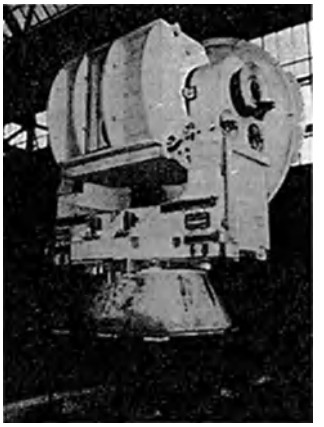

Fig. 2. The SMT mount in the workshop

2. TELESCOPE GEOMETRY AND LAYOUT

The geometry and the basic design of the SMT are summarized in Tab. 1, while the optical layout is illustrated in Fig. 1. A tertiary mirror brings the focus to the outboard side of the mount through either hollow elevation bearing. On the right side, either a bent Cassegrain or Nasmyth mounting can be used for the receiver (i.e. the equipment is fastened to either the inside or outside of the elevation bearing). On the left side, the elevation encoder restricts the field of view and allows only a Nasmyth mounting position. The preassembled mount is shown in Fig. 2 during tests of the servo drive system. The azimuth bearing on top of a support ring carries the elevation fork. The moveable elevation section is driven at both sides. Its 4.5 m diameter upper disc supports the spaceframe reflector structure through a special connection, which absorbs differences in thermal expansion between the CFRP space frame and the steel mount without introducing tensions in the former. A CAD drawing is shown in Fig. 3, while Fig. 4 shows a part of the preassembled space frame.

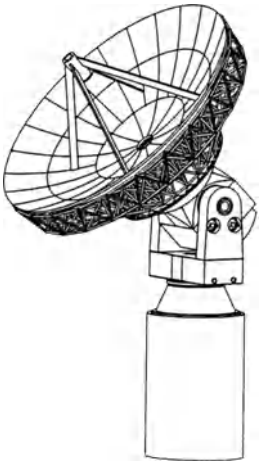

Fig. 3. CAD drawing of reflector structure

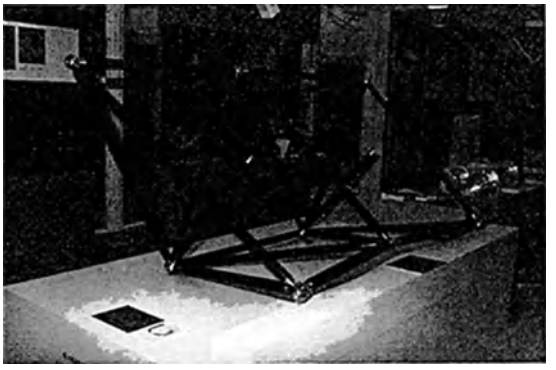

Fig. 4. A section of the CFRP space frame

Table 1: SMT geometry and basic desing

Geometry:	main reflector - paraboloid D = 10 m, F/D = 0.35	
	subreflector - hyperboloid d = 0.69 m, F_2/D = 13.8	
	Nasmyth and bent Cassegrain foci - outside elevation bearings	
Mounting:	azimuth/elevation type, steel, thermally insulated on outside,	weight 41500 kg
	angular range: azimuth 540°, elevation -3° to 90°, placed on cylindrical, concrete pier	
Reflector:	spaceframe support - CFRP tubular members with invar steel joints	weight 3040 kg
	panels and subreflector - composite of CFRP skins and aluminium honeycomb,	weight 1150 kg
	subreflector support (quadrupod) - rectangular CFRP tubes,	weight 110 kg

The reflector consist of three concentric rings of pyramidal panels - 12, 24 and 24 per ring, respectively. The panels are a composite structure with a 90 mm thick honeycomb aluminium core to which top and bottom skins of 1.2 mm thick CFRP are bonded. Aluminium foil of 40 μm thickness is bonded to the CFRP skin to provide a reflective surface. Each panel has an area of 1.0 - 1.7 m^2 and a maximum diagonal dimension of less than 2 m. The panel mass per unit area is about 10 kg/m^2. The accurate surface contour is achieved by replication from a mold of pyrex glass. These molds were ground to a 3 μm rms precision at the Optical Sciences Center of the University of Arizona. The panels are supported by the space frame through five or six adjustable scews (depending on the ring). A photo of a panel is shown in Figure 5. The fabrication of the panels will be completed by February 1989.

Considerable effort has been expended on the structural optimisation of the telescope design. The effects of gravity, wind and thermal variations have all been considered. The final design results, most of which surpass the original specification, are assembled in Table 2. Our goal of a 15 μm reflector accuracy will be reached, provided we can measure and set the surface with 10 μm accuracy. This we plan to achieve by the method of amplitude interferometry, as described by Ulich et al. (1985). It should be noted that the specified temperature gradients in Table 2 are larger than are expected in reality. The quoted performance will be reached under all operational conditions both day and night.

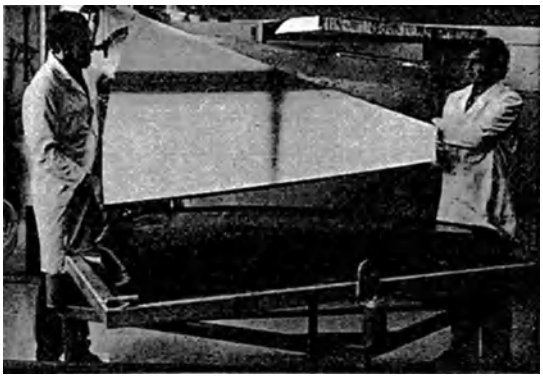

Fig. 5. Testpanel (just) removed from pyrex mold

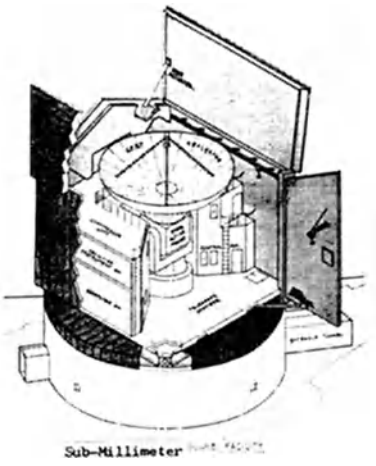

Fig. 6. The SMT in its rotating enclosure

Table 2. Performance: computed deformations and pointing error

Load condition		rms profile deformation (μm) spaceframe	panel	Pointing error (arcsec)
Gravity	- horizon	7.0(4.2)*	-	12.8**
	- zenith	6.8(4.2)*	2.0	0
Wind 12 m/s	- elevation 0°	2.0	2.0	0
	- elevation 50°	2.3	-	-0.3
	- elevation 90°	3.7	-	-0.6
Temperature	- ambient change 20°C	5.1	2.0	0
	- grad across 6°C	0.8	-	2.7
	- grad through 4°C	2.2	4.5	-
	- time grad 5°C/h	3.0	0	0
Total (root sum squared)		8 μm	5.5 μm	

* effective values after optimal panel setting at 45° elevation

** systematic elevation dependent effect, to be calibrated to 1 arcsec.

The telescope structure is surrounded by a co-rotating enclosure, designed at Steward Observatory. A "cut away" view of the installation is shown in Figure 6. The space around the telescope mount is utilized by the co-rotating enclosure. Receiver rooms are located at the foci near the mounting plates on the elevation bearings, which protrude into the rooms. This allows the receivers to be easily accessed in a controlled environment. Immediately below the receiver rooms are the control room and computer equipment rooms. The two lower, stationary levels of the enclosure provide office space, living quarters, workshop and laboratory space.

3. CONCLUSION

A set of initial "facility" receivers is under construction at MPIfR. These will be cooled Schottky-diode mixers for the windows at 340, 460, 700 and 800 GHz. Several AOS are being constructed for backends. Cooled He bolometers with filters optimized for the submm windows will be used for continuum measurements. Development of further, advanced receivers is being carried out at both institutes. A focus translation and subreflector chopping mechanism has been designed and built at SO. It provides 4' beamchop at 10 Hz and 25" beamchop at 30 Hz with an 80 % duty cycle. Our schedule forsees the erection of the enclosure during 1989 and 1990 followed by the installation of the telescope and the associated equipment in 1990. We hope to begin astronomical commissioning in the winter 1990/91.

REFERENCES

Baars, J.W.M., 1983, in Infrared and Millimeter Waves, Vol. 9, 241; E. Button (Ed.), Academic Press

Baars, J.W.M., Krügel, E., Martin, R.N., 1989, in Proccedings Kona Symposium; A. Webster (Ed.), Kluwer Press

Ulich, B.L., et al. 1986, Proceedings SPIE: Optical Alignment, Vol. 608, 55

The KOSMA Observatory

R. Schieder
I. Physikalisches Institut, Universität zu Köln, FRG

Summary

The present situation of the frontends and backends of the 3 m KOSMA radio telescope on Gornergrat near Zermatt, Switzerland, is discussed. Three receivers are available, two Schottkys (78 – 116 GHz and 345 GHz) and one SIS (125 – 170 GHz). The backends are a continuum backend, one filterbank (256 channels, 256 MHz total bandwidth) and two AOSs (HRS: 64 MHz, 2048 channels, MRS: 287 MHz, 1700 channels). A 1 GHz AOS (LRS: 1400 channels) is used in for testing receivers in Cologne. Future developments in SIS array receivers, array AOSs and variable resolution AOSs are briefly discussed.

1. The Location at Gornergrat

Since early 1986, the Observatory at Gornergrat has been in successful operation. The weather conditions have been found to be very good by European standards. On the average, we have had about 70% usable observing time. The atmospheric opacity is found to be extraordinarily good. This is partly due to the fact that the site is surrounded by very high mountains and lower-lying glaciers. They keep the air cold and reduce the water content even in summer. During winter 1988/89, the water content was below 1 mm precipitable water vapor most of the time. The observatory is easily supported because of the excellent infrastructure available on the mountain and the reliable access by train.

2. The Telescope

The telescope is a 3 m Cassegrain system with a surface accuracy of 30 μm rms [1]. The pointing accuracy has been recently improved by means of an optical telescope together with a CCD camera. From these optical measurements, pointing constants have been derived that give an overall pointing accuracy of 12 arcsec rms. The small scale accuracy can be made much better by measuring the actual pointing on nearby stars. The beam profile of the 3 mm receiver was measured with a transmitter set on the Klein Matterhorn at a distance of about 6 km at 3900 m altitude. During these measurements the subreflector was carefully adjusted for best focusing and symmetrical beam profile. This procedure worked very well, and we plan to repeat this procedure with all other receivers.

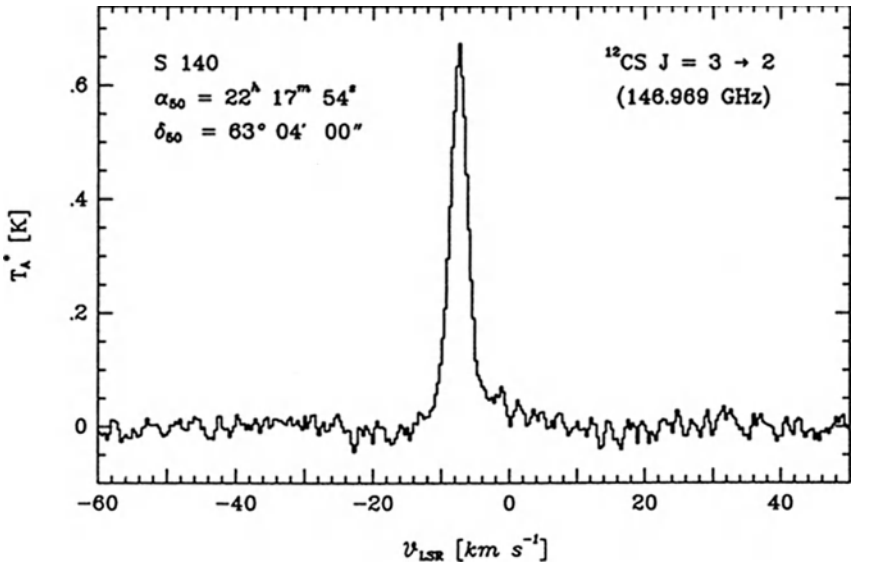

Fig. 1. Spectrum of CS $J = 3 - 2$ in S140, recorded with the 145 GHz receiver and the KOSMA MRS. The spectrum was measured in the position switching mode with 50 s integration time per position and 6000 s total integration time. The receiver was built and installed by Dr. B. Vowinkel, K. Eigler, W. Hilberath and Ph. Müller.

3. The Frontends

The frontends used on Gornergrat were all built at Cologne University. Our first receiver has been in operation since 1985 [2]. It has a Schottky barrier mixer and two tunable Gunn oscillators, one for the frequency range 78 to 100 GHz (GaAs) and the other for 100 to 116 GHz (InPh). The other data are as follows:

Frequency range	78–116 GHz
IF bandwidth	600 MHz
IF center frequency	1400 MHz
Receiver temperature (DSB)	200–300 K
Observing modes	Frequency switch, Beam switch, Total power

The second frontend is a $\lambda 2$ mm SIS receiver, in operation since summer 1988 [2,3]. The SIS junction was manufactured by IRAM. The receiver has a closed cycle cooling system operating at 2.8 K. One of the first spectra obtained with this receiver is shown in Fig. 1. The other data for this receiver are as follows:

Frequency range	125–170 GHz
IF bandwidth	600 MHz
IF center frequency	1400 MHz
Receiver temperature (DSB)	50–200 K
Observing mode	Total power

The most recently developed frontend is a 345 GHz Schottky receiver [2]. It has been in operation since December 1988. With this first sub-mm receiver we have been able to demonstrate the good quality of the atmosphere on Gornergrat at least during winter. One of the first spectra measured is shown in Fig. 2. The other data for this receiver are as follows:

Frequency range	345 GHz (CO 3 – 2)
IF bandwidth	500 MHz
IF center frequency	1400 MHz
Receiver temperature (DSB)	600 K
Observing mode	Total power

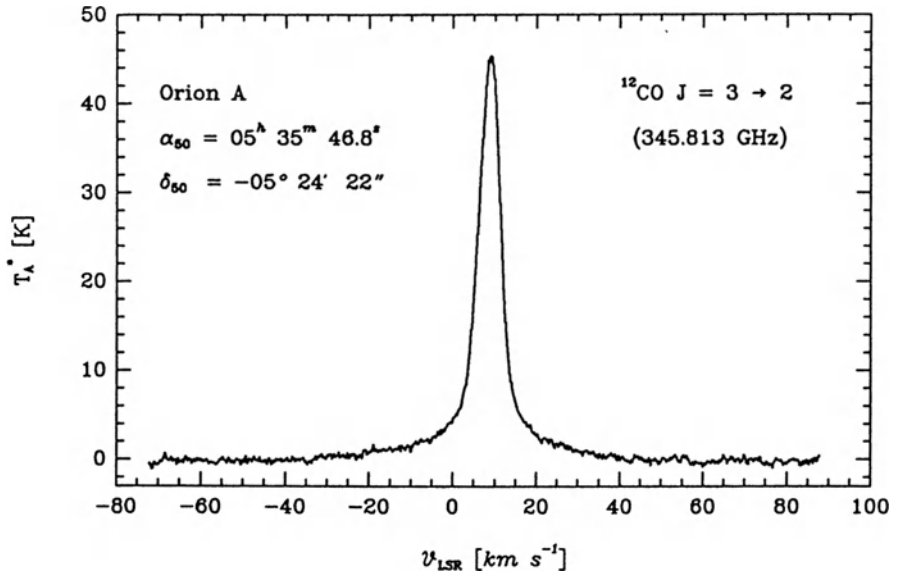

Fig. 2. First sub-mm observation from Gornergrat. The spectrum shows the ^{12}CO $J = 3 - 2$ emission from Orion at 345.796 GHz obtained with the KOSMA MRS in the position switching mode. The integration time was 50 s per position and 750 s in total. The receiver was built and installed by Dr. P. Zimmermann and J. Hernichel of our group.

All receivers and spectrometers are tested in Cologne very carefully before they are shipped to the site. We apply several different test procedures. In order to determine the best possible measuring mode for observations, the stability is precisely analyzed by means of the Allan variance method [4]. For this we use a 1 GHz bandwidth AOS, also developed in Cologne, which has proven to be extremely stable (see below). The results of the Allan plot are used to determine the best possible integration time for the receiver in the total power mode [5].

The problems of baseline ripple are also analyzed in detail in the laboratory by measuring simulated spectra with the AOS. As it turns out, one of the most important requirements is to remove standing waves occurring on the loads and in the quasioptics

of the telescope. Usually they are not stable in time and cause severe problems when observing. Another procedure applied regularly is to observe absorption spectra of gases like CO in the laboratory. For this, a white noise source is placed in front of an absorption cell (about 3 m long) and the spectrum is measured the same way as at the telescope.

4. The Spectrometers

At Gornergrat four different backends are available. The first is a continuum backend designed for chopping frequencies up to five cycles per second. The pointing of the telescope is regularly checked on the planets using this backend.

The second is a 256×1 MHz filterbank, one of the first spectrometers built in Cologne. Two additional AOSs are also available; one is a high resolution (HRS) and the other a medium resolution AOS (MRS) [6,7,8]. The data of these spectrometers are as follows:

HRS	
Total bandwidth	64.7 MHz
Channel spacing	31.6 kHz
Number of channels	2048
Resolution bandwidth	46 kHz
Reception bandwidth	66 kHz
Laser source	HeNe (633 nm)
Allan variance minimum time	500 s
MRS	
Total bandwidth	287 MHz
Channel spacing	166.6 kHz
Number of channels	1700
Resolution bandwidth	287 kHz
Reception bandwidth	406 kHz
Laser source	Laser diode (790 nm)
Allan variance minimum time	120 s

A third AOS with 1 GHz bandwidth and 1400 channels (LRS) is in operation in Cologne. It is a similar design to the LRS built by us for the ESO SEST telescope in Chile [6,8]. The Allan variance minimum time is 100 s. This AOS is used at present for testing the frontends in Cologne. A copy of this AOS will be also stationed on Gornergrat when further sub-mm receivers with 1 GHz IF bandwidth are available at the KOSMA telescope.

5. Future Developments

Three other receivers are at present under development in Cologne. The first is a Schottky 230 GHz receiver, which should be operational in the course of 1989. A second is a

TIRGO on Gornergrat-Nord very soon. A third is a 600 GHz Schottky receiver. With these developments we will try to explore the whole frequency range accessible with the KOSMA telescope as fast as possible.

One of the major new projects starting now at Cologne University is the installation of our own SIS laboratory. It is meant to fabricate dedicated designs of SIS structures together with planar antennas, etc. The main goal is to open up the sub-mm range as a regular application of SIS mixers in our laboratory. In future we hope to be able to build array receivers based on this technique.

Further activities are planned for novel developments of acousto-optical spectrometers. At present we have started to design a variable resolution AOS (VRS). The idea is to have spectrometers available which allow matching the resolution of the spectrometer to the linewidth of the astronomical molecular line signal. This could be extremely useful when measuring at different frequencies and comparing the line features with each other. Adding the contents of adjacent channels of a fixed resolution AOS would not be suitable, because in most cases only fractions of neighbouring channels would have to be added. Another important development for the future is to construct array spectrometers with several different IF inputs to meet the requirements of future array receivers. The present situation is that there are no such spectrometers available. We believe that this is the most important task for spectrometer developments in near future.

Acknowledgements. The KOSMA 3 m radio telescope at Gornergrat-Süd Observatory is operated by the University of Cologne and supported by the Deutsche Forschungsgemeinschaft – DFG – through grant SFB-301, as well as special funding from the Land NRW. The Observatory is administered by the Hochalpine Forschungsstationen Jungfraujoch and Gornergrat, Bern. The details presented in this paper are the result of the work of all members of the KOSMA group. The author is giving only a report about the results achieved so far.

References

[1] G. Winnewisser et al., *Astron. Astrophys.* **167**, 207 (1986)
[2] K. Eigler et al., this volume.
[3] B. Vowinkel, K. Eigler, W. Hilberath, K. Jacobs, Ph. Müller, *Int. J. IR and MM Waves*, accepted for publication (1989)
[4] R. Schieder, B. Vowinkel, G. Rau, Proc. SPIE Conf. on Submillimeter Spectroscopy, Cannes, France, p. 598 (1985)
[5] R. Schieder, J. T. Armstrong, A. Piciorgros, and L. Haikala, this volume.
[6] V. Tolls, R. Schieder, and G. Winnewisser, this volume.
[7] W. Zensen, A. Piciorgros, R. Schieder, G. Winnewisser, Proc. SPIE Conf. on Submillimeter Spectroscopy, Cannes, France, p. 598 (1985)
[8] R. Schieder, V. Tolls, G. Winnewisser, Experimental Astronomy, **1**, accepted for publication (1989)

Optimizing the Use of Telescope Time

R. Schieder, J.T. Armstrong, A. Piciorgros, L. Haikala
I. Physikalisches Institut, Universität zu Köln, FRG

SUMMARY

We show how to determine the most efficient switching rate for observations with "dead" time between switching cycles and in the presence of a combination of white and non-white noise. The most efficient switching rate depends strongly on the dead time, but only weakly on the exact character of the noise. We present recommendations for optimal strategies for either one or many ON-position observations per OFF-position observation.

I. Introduction and Mathematical Approach

As is well known, the noise in a system dominated by white noise declines as the square root of the integration time. However, the total amount of time needed to attain a given rms noise level is also affected by non-white noise contributions such as instrumental drifts and by the proportion of unused "dead" time. These noise contributions are commonly represented as proportional to $f^{-\alpha}$, where f is the sampling frequency. White noise corresponds to $\alpha = 0$.

The tradeoff between system instability and excessive dead time is shown in Fig. 1. The spectrum taken with one ON-OFF pair has baseline features due to slow drifts in the receiver-spectrometer system, while the spectrum taken with seven ON-OFF pairs has a higher-than-optimal rms because of lost time. The optimal t_{int} of 30 to 40 s is a measure of the stability of the receiver-spectrometer system.

We discuss here a simple example of alternate OFF- and ON-source measurements with both white noise and f^{-3} noise. The total number K of ON-OFF cycles is determined by t_R and t_S, the integration times OFF- and ON-source; by t_D, the dead time between consecutive scans; and by t_B, the total time available. We express these times in terms of the Allan variance minimum time t_A, (see below): $r \equiv t_R/t_A$, $s \equiv t_S/t_A$, $d \equiv t_D/t_A$, and $b \equiv t_B/t_A$. The OFF- and ON-source measurements are given by

$$R(t) = \frac{1}{t_R}\int_t^{t+t_R} p(t')dt' \qquad S(t) = \frac{1}{t_R}\int_{t+t_R+t_D}^{t+t_R+t_D+t_S} p(t'')dt''. \qquad (1)$$

$R(t)$ and $S(t)$ represent the OFF- and ON-source data; $p(t)$ is the signal strength. The desired spectrum is $R - S$; its variance $\sigma^2(r,s,d) = \langle (R-S)^2 \rangle$. We will show elsewhere that $\sigma^2(r,s,d)$ is related to the Allan variance (Allan 1966), $\sigma_A^2(t)$, by $\sigma^2(r=s, d=0) = 2\sigma_A^2(t_S)$. The Allan variance shows a minimum at a time t_A; for shorter times, white noise is dominant, but for longer times, $f^{-\alpha}$ noise dominates, and σ_A^2 rises.

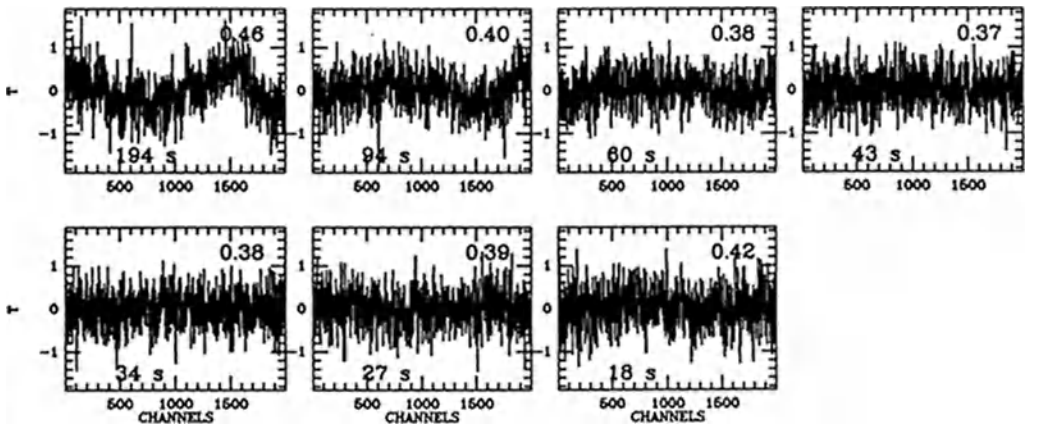

Fig. 1. *a)* Results of 400 s total observation time (ON- + OFF- + dead time) on the inside of the dome with the 3 mm receiver and the high-resolution spectrometer on the KOSMA 3 m telescope. For each spectrum, the ON time per *ON-OFF pair* and the final rms are shown. The number of ON-OFF pairs ranges from one to seven.

For the present example, we use $g(t'' - t') = A\delta(t'' - t') + B_1 - B_2|t'' - t'|^2$ as the correlation function $\langle p(t')p(t'')\rangle$. The total observation time t_B in terms of t_A for K cycles is $b = K(r + s + 2d)$. If we assume a lower cutoff frequency for the noise power spectrum, the variance of a series of K cycles becomes

$$\sigma_K^2 = \frac{1}{K}\sigma^2(r,s,d) = \frac{2}{3}\frac{\sigma_A^2(t_A)}{b}\left[\frac{1}{r} + \frac{1}{s} + \left(\frac{r+s}{2} + d\right)^2\right](r + s + 2d). \qquad (2)$$

II. Recommendations for Observing Strategy

For one ON per OFF, the integration times shown in Fig. 2, with $r = s$, are optimal. For small t_D, the best t_S is short in order to reduce the drift contribution. If t_D is a significant fraction of For small t_D, the best t_S is short in order to reduce the drift contribution. If t_D is a significant fraction of t_A, however, the optimal t_S is longer in order to avoid losing too much to dead time. Dead time is more harmful than one might expect: for $t_D = 0.1\,t_A$ and $\alpha = 3$, one needs 30% more time to attain the rms attainable if $t_D = 0$. The results of the same analysis for multiple ONs per OFF are summarized in Fig. 3.

We recommend the following for choosing the optimum observing strategy. The Allan variance minimum time t_A of the system under the current observing conditions should be measured or estimated. For techniques of measuring the Allan variance, see Tolls *et al.* (1988) or Winnewisser *et al.* (1986).

1. One ON per OFF: Choose the optimum t_S $(= t_R)$ from Fig. 2.
2. Many ONs per OFF:
   a) If you are free to choose N, do so from Fig. 3*a*; then choose t_R and t_S from Fig. 3*b*. A good rule of thumb is $t_R = \sqrt{N}\,t_S$.
   b) If you are not free to choose N, then choose the optimal t_R from Fig. 3*b* and calculate t_S from $t_S = \sqrt{1/N}\,t_R$.

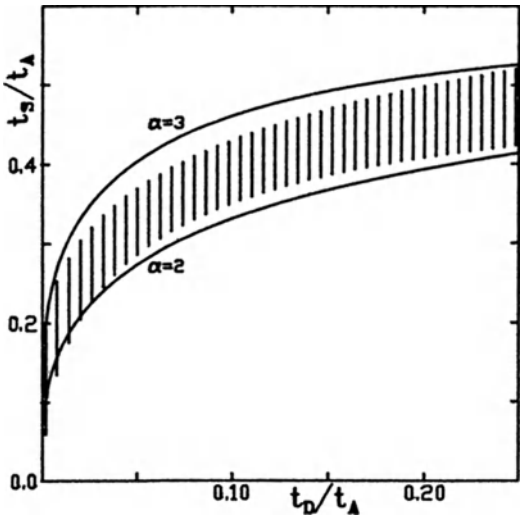

Fig. 2. The optimal ON-source observation time t_S $(= t_R)$ as a function of dead time t_D for one ON per OFF, for drift-noise contributions proportional to $f^{-\alpha}$ with $\alpha = 2$ and $\alpha = 3$. Both t_S and t_D are normalized to the Allan variance minimum time t_A. The shaded region shows the region within which the rms is within 1% of the optimal rms for *both* $\alpha = 2$ and $\alpha = 3$.

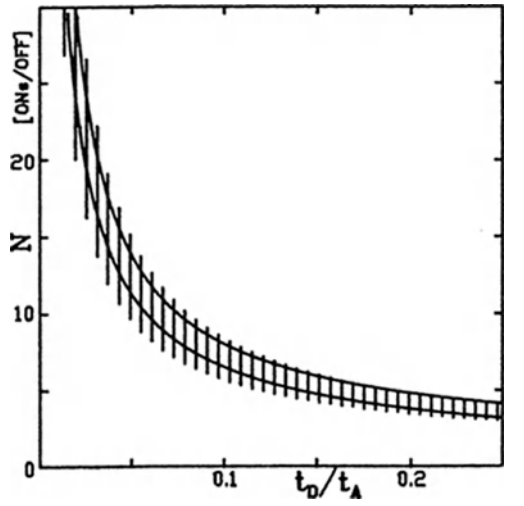

Fig. 3. *a)* The optimal number N of ONs per OFF as a function of the normalized dead time t_D. *b)* The optimal ON- and OFF-source integration times as functions of the normalized dead time t_D. The cases $\alpha = 2$ and $\alpha = 3$ are shown, as well as the overlap of the 1% tolerance regions as in Fig. 2.

References

Allan, D. W.: 1966, *Proc. IEEE* **54**, 221

Rau, G., Schieder, R., and Vowinkel, B. 1984, Proc. 14th European Microwave Conf., Liège, p. 248

Schieder, R., Rau, G., and Vowinkel, B. 1985, Proc. SPIE **598**, Instrumentation for Submillimeter Spectroscopy, Cannes, p. 189

Winnewisser, G., Bester, M., Ewald, R., Hilberath, W., Jacobs, K., Krotz-Vogel, W., Miller, M., Olberg, M., Pauls, T., Pofahl, E., Rau, G., Schieder, R., Stubbusch, H., Vowinkel, B., Wieners, C., Zensen, W.: 1986, *Astron. Astrophys.* **167**, 207

THE COLOGNE 3 m RADIO TELESCOPE: ITS ASSOCIATED ELECTRONICS AND OPERATION

A. Piciorgros[1)] and R. Ewald[1,2)]
1) I. Physikalisches Institut, Univ. of Cologne, D-5000 Köln 41
2) German Aerospace Research Establishment DFVLR, D-5000 Köln 90

Introduction

Since the end of 1986, the Cologne 3 m radio telescope on the Gornergrat has been in continuous operation for mm-wavelength astronomical observations, following an initial two-year test period on the roof of the Ist Physikalisches Institut in Cologne. Most of the system electronics were developed and constructed at the Institut during this period. Initial test measurements and subsequent astronomical observations have demonstrated the equipment's usefulness for long-term integrations with high spectral resolution. A short description of the overall system and operation concept is given here; examples of recent astronomical results are to be found throughout this volume.

The telescope and the observatory

The telescope was designed in two parts to facilitate its transport from Cologne to the Gornergrat. One part consists of the four-panel main reflector and feed support legs; the other is the telescope pedestal. The four fibreglass-reinforced epoxy panels have an overall rms accuracy of about 30 μm deviation from the best fit parabola (Fig. 1), suitable for observations at wavelengths down to ~0.5 mm. Further telescope parameters are given in Tables 1 and 2.

In 1985, the telescope and pedestal were transported by train and helicopter from Cologne to the new site on the south tower of the Kulmhotel Gornergrat, Switzerland, near Zermatt in canton Wallis. The site, at 3130 m altitude, administered by the Stiftung Hochalpine Forschungsstationen at Bern, has low precipitable atmospheric water vapor conditions, and should be well suited for submillimeter observations. The observatory was formerly used by the University of Geneva for optical observations; a new dome was needed to house the larger radio telescope.

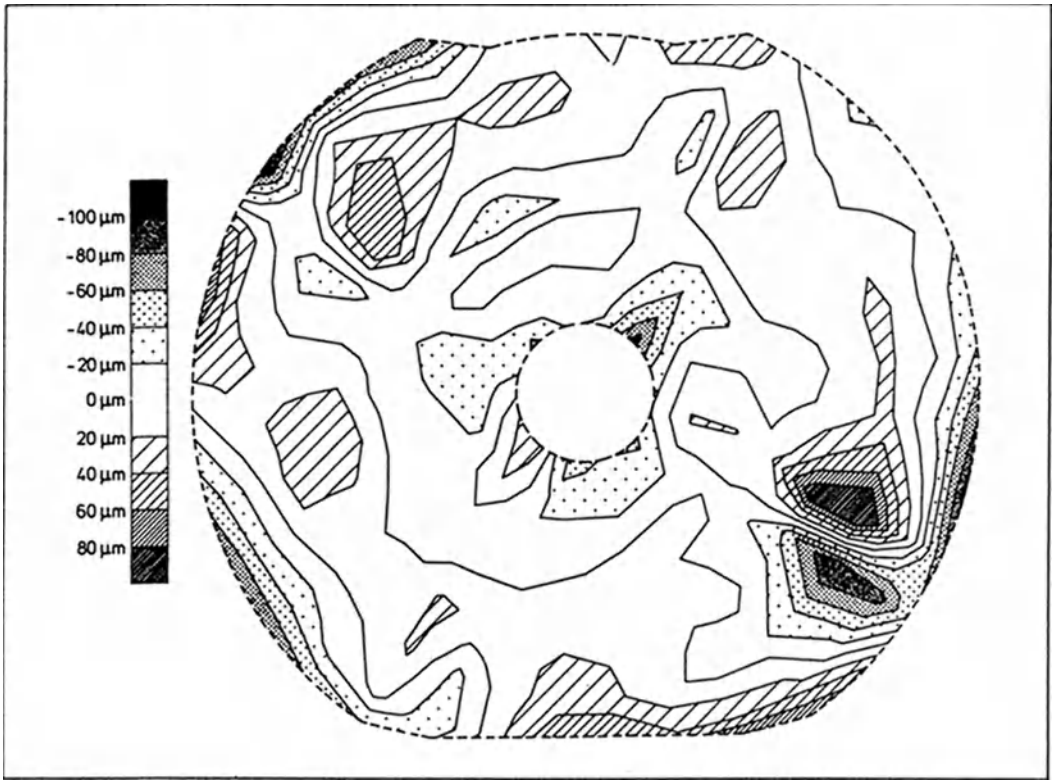

Fig. 1. The telescope surface accuracy

The system concept and the electronic equipment

As with the telescope itself, the system control and data-taking electronics have a modular design, which enables testing of individual components independent of the rest of the system. The various components of the telescope system, including the telescope drive, receivers, spectrometers and data-handling hardware are controlled by dedicated microprocessors, developed in the Institut in Cologne, based on 8085 and 6809 CPU's.

The overall concept is shown in Fig. 2. The control and data acquisition modules are connected via asynchronous 9.6 kBaud or 16 bit parallel lines to the central real-time processing unit of DEC PDP type running under the RSX operating system. The original PDP 11/34a has now been replaced by a more efficient successor, an 11/53.

The mm and submm front ends are described by B. Vowinkel in this volume.

the telescope	
primary reflector	
shape	parabolic
diameter	3 m
f/D	0.4
surface accuray	$\leq 30\,\mu$m rms
secondary reflector	
shape	hyperbolic
diameter	38 cm
pedestal	
mount	elevation-azimuth
rotation range azimuth	$\pm$ 200°
rotation range elevation	0° – 92°
max. slew rate	$1°s^{-1}$
max. tracking rate	$0.2°s^{-1}$
acceleration	$0.^{\circ}3\,s^{-2}$
pointing and tracking accuracy	$\leq 0.001°$
position accuracy	ca. 10″
max. wind speed	$21\,m\,s^{-1}$
max. wind speed allowed during measurements	$15\,m\,s^{-1}$
temperature range	−20°C to +30°C
total weight	2.7 t
the dome	
diameter	7.5 m
max. slew rate	$1°s^{-1}$
angle accuracy	$0.^{\circ}1$
weight	18 t

Table 1. The Telescope and the dome

The backends comprise two acousto-optical spectrometers, a filterbank and a digital continuum backend (Table 2). A third low resolution AOS will have a bandwidth of 1 GHz and a channel spacing of 0.6 MHz. Test procedures for the backends follow an extension of a statistical approach to the problem by Allen (see R. Schieder et al., this volume) and are directly incorporated into the controlling microprocessors.

The rapid evolution of powerful minicomputers has let to a large enhancement of data handling and reduction abilities at Gornergrat. The current VAX 11/730 for data analysis with an Ethernet connection to the PDP will soon be replaced by a MicroVAX II, leading possibly to a cluster and, later on, the possibility of remote operation.

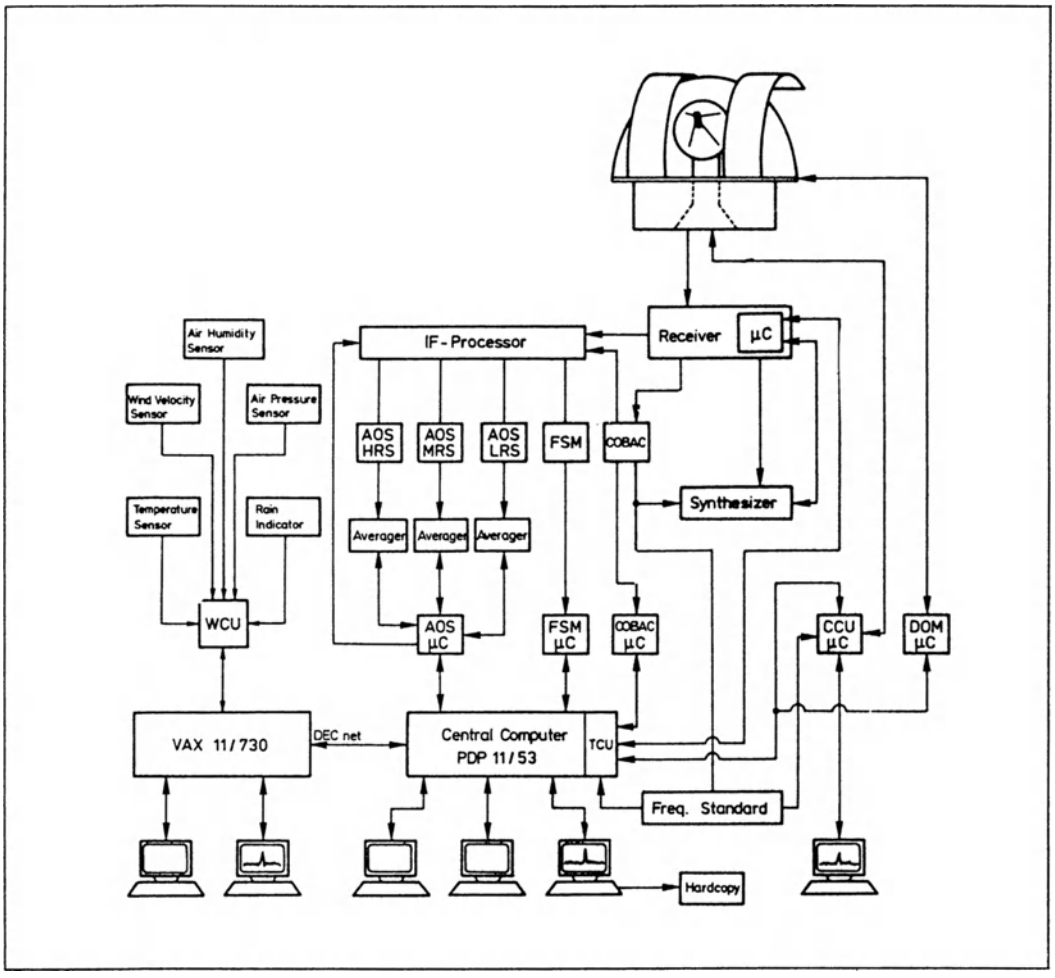

Fig. 2. The telescope concept

Observatory operation and funding

At present, the observatory is operated year around by research staff of the Cologne institute with an increasing amount of observing time given to outside observers (20% in 1987). Observation proposals are welcome. Financial support for the observatory is granted by the Deutsche Forschungsgemeinschaft SFB 301, the Land Nordrhein-Westfalen, the Minister of Research and Technology and federal funds for university promotion (HBFG). A donation from the Krupp Foundation enabled the construction of the new dome.

the backends	
channel spacing	30 kHz, 166 kHz, 1 MHz
bandwidth	64 MHz, 190 MHz, 256 MHz
the receivers	
cooled Schottky diode mixer	70 – 116 GHz
SIS	130 – 170 GHz
end of 1988 (submillimeter)	345 GHz
1989	230 GHz
in planning	460 GHz
the computers	
control unit	PDP 11/53
data reduction at Gornergrat	VAX 11/730
data reduction at Cologne	μVAX II, III cluster
μcomputers	8085 and 6809 systems

Table 2. The backends, frontends and computer

References

Winnewisser,G., Bester,M., Ewald,R., Hilberath,W., Jacobs,K., Krotz-Vogel,W., Olberg,M., Pauls,T.A., Pofahl,E., Rau,G., Schieder,R., Stubbusch,H., Vowinkel,B., Wieners,C., Zensen,W.,: 1986,"The University of Cologne 3 m Radio Telescope", Astron.Astrophys. **167**, 207

THE STRATOSPHERIC OBSERVATORY FOR INFRARED ASTRONOMY - A 3m CLASS AIRBORNE TELESCOPE

R. Ewald, A. Himmes, A.F. Dahl
German Aerospace Research Establishment (DFVLR)
Linder Höhe, 5000 Koeln 90, FRG

Summary

In cooperation with NASA, the German Minister for Research and Technology, BMFT, conducts studies to provide a 3m class airborne telescope for SOFIA, a successor to the extremely successful Gerard Kuiper Airborne Observatory, KAO. In the next decades, SOFIA could provide a continuing and readily deployable observation possibility at heigths above 12.5 km for sophisticated instrumentation from the submm well into the optical spectral range.
After studying feasible telescope concepts BMFT has now proceeded into the definition phase. Required characteristics and anticipated performance of the planned telescope are given together with the current time schedule.

Airborne Astronomy

Starting with an CV-990 aircraft in the 1960's, NASA now has the experience of almost a quarter of century in airborne astronomy. A 30cm open-port telescope in a Lear Jet paved the way for the Gerard Kuiper Airborne Observatory, KAO, with its 91cm diameter telescope, that provides up to now the only permanent observation facility for infrared astronomy above the water vapor layer of Earth's atmosphere. Plans for a "Large Airborne Telescope" finally led to the initiation of studies for a 3m class open-port telescope in a Boeing 747 aircraft, which will be named SOFIA. In 1986 NASA invited the German Minister for Research and Technology, BMFT, to contribute the telescope system to this observatory, acknowledging the high standard of astronomy and telescope tecnology in the FRG and the great interest shown in the participation in the KAO program. After the feasibility of a 3m primary dish in a 747 has been proven in a phase A study, NASA and BMFT are now conducting definition

studies for the aircraft modifications and the telescope system in parallel. If funds are provided, SOFIA's development can have a new start in 1991 with the goal of beginning astronomy operations in 1994. Thus the successful, but aging KAO will have a much more powerful successor to match the ever growing interest in the field of submm & infrared astronomy as well as to provide a larger number of science flights to the now numerous groups with sophisticated instrumentation.

The Observatory

The definition study concepts foresees a very thin Zerodur meniscus parabolic mirror of around 3m diameter and 50 mm thickness as primary mirror. The mirror has to be very fast with a ratio of f/1 in order to have no parts of the telescope exposed to the air flow outside the cavity. The optical configuration will be of Nasmyth type with a chopping lightweight secondary and dichroic tertiary to allow focal plane tracking simultaneously with the observations. The telescope will be balanced with a spherical bearing supported by the bulkhead that separates the pressurized cabin from the open cavity thus taking over the well-proven KAO design, which allows in-flight access to the science instruments.

The new technology for the fast thin mirror and the bearing concept are primary concerns for the study conducted in Germany while the US side will define the necessary modifications to the aircraft of choice, a 747-SP and other critical mission aspects as f.e. the control of the shear layer streaming over the cavity causing seeing degradations.

For a total payload weight of around 32 tons (70000 lb) the 747-SP provides the longest flight time at and above 41000 feet due to its steep ascent and long range capabilities. As additional weight will have to be balanced by ballast in the aft section of the plane, the telesope system shall not contribute more than 13.5 tons (30000 lb) to the budget.

Science Requirements

The current definition esp. of the telescope system has the aim of maximizing telescope performance in order to meet the science requirements, set up by an international Science Working Group. With a 3m diameter telescope SOFIA will have 10 times the sensitivity of the KAO for detecting compact sources. All the IRAS 60 and 100 μm

sources will then become observable. With its factor of three in spatial resolution improvement over KAO, SOFIA can probe the connection of bipolar outflows and disk formation to the process of starbirth. Meeting the pointing and tracking stability requirements means high resolution infrared spectroscopy and photometric occultation observations of the giant planets will become possible throughout a spectral range of 0.3-350 μm, revealing new findings on the structure, composition and chemistry of planetary atmospheres.

SOFIA COMPARISON WITH KAO

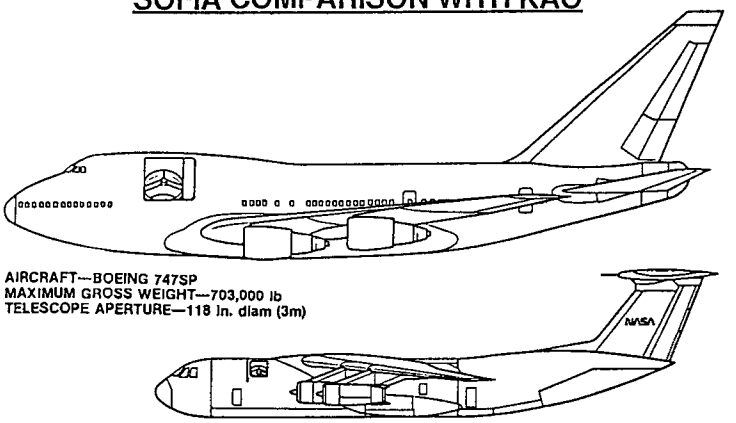

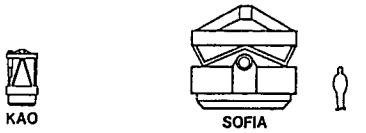

OBSERVATORY PLATFORM		
• Aircraft	Lockheed C-141	Boeing 747SP
• Operating Altitude	41-45,000 feet	41-46,000 feet
• Endurance for research (≥41,000 ft.)	5 hours	> 7 hours
• Range	3,300 n. miles	> 3,500 n. miles
• Payload (typical)	60,000 lb	80,000 lb
• Investigator team accommodation	≤ 10 people	≥ 10 people
OBSERVATORY TELESCOPE		
• Aperture	36 inch (91cm)	~118 inch (3m)
• Spectral range	0.3 - 1600 μm	same
• Diffraction limited wavelength	λ< 10 μm	λ< 30 μm
• Pointing stability	0.3 arcsecond	0.2 arcsecond
• Elevation range	35 -75 degrees	20 - 60 degrees

(courtesy of Ames Research Center)

Acknowledgements

Responsibility of the study activities for SOFIA in the US lies with NASA / Ames Research Center; studies in Germany are funded by BMFT and supervised by DFVLR-PT WRF/WRT. Thanks to E. Erickson and G. Thorley (ARC) for their contributions.

The Receivers of the University of Cologne 3 m Radio Telescope

K. Eigler, J. Hernichel, K. Jacobs, F. Leven, Ph. Müller, Th. Rose, B. Vowinkel, P. Zimmermann

I. Physikalisches Institut, Universität zu Köln,
Zülpicher Str. 77, D-5000 Köln 41, FRG

Abstract

The University of Cologne 3 m radio telescope at the Gornergrat Observatory has a surface accuracy of 30 μm (rms). It is therefore useful for frequencies up to about 600 GHz. At present three receivers are available: (1) a cryogenic Schottky-mixer receiver that covers a frequency range of 80 - 115 GHz, (2) a receiver for the frequency range 125 - 170 GHz using an SIS mixer, and (3) a cryogenic Schottky-mixer receiver for frequencies around 345 GHz. Receivers for the frequency regions around 230 GHz and 460 GHz are under development.

80 – 115 GHz Schottky receiver

The 80 – 115 GHz receiver uses a cooled Schottky diode (University of Virginia) as the mixing element. The local oscillator system consists of a tunable cross-guide harmonic GaAs Gunn oscillator operating between 80 and 100 GHz and an InP Gunn oscillator for the 105 to 115 GHz range [1]. Tuning of the receiver and selection of the oscillator system are remotely controlled from a terminal. The first IF amplifier is a two-stage FET amplifier with a center frequency of 1.4 GHz and a bandwidth of 500 MHz. The double-sideband receiver noise temperature is between 200 K and 300 K over the tuning range. Beamswitching is accomplished with a commercially available loudspeaker system which incorporates a flat aluminium membrane stiffened by a honeycomb backstructure (see Fig. 1). An ambient hot load and a cold absorber connected to the CTI 20 refrigerator are used for receiver calibration.

125 – 170 GHz SIS receiver

This receiver is mechanically tunable over the frequency range from 125 to 170 GHz and is remotely controlled from a terminal. The local oscillator power from the GaAs Gunn oscillator with doubler is directly injected in the mixer using a 20 dB directional coupler (see Fig. 2). To ensure impedance matching, a linear tapered standard waveguide in the 110 – 170 GHz frequency range shorted with a movable non-contacting backshort is used as the signal waveguide.

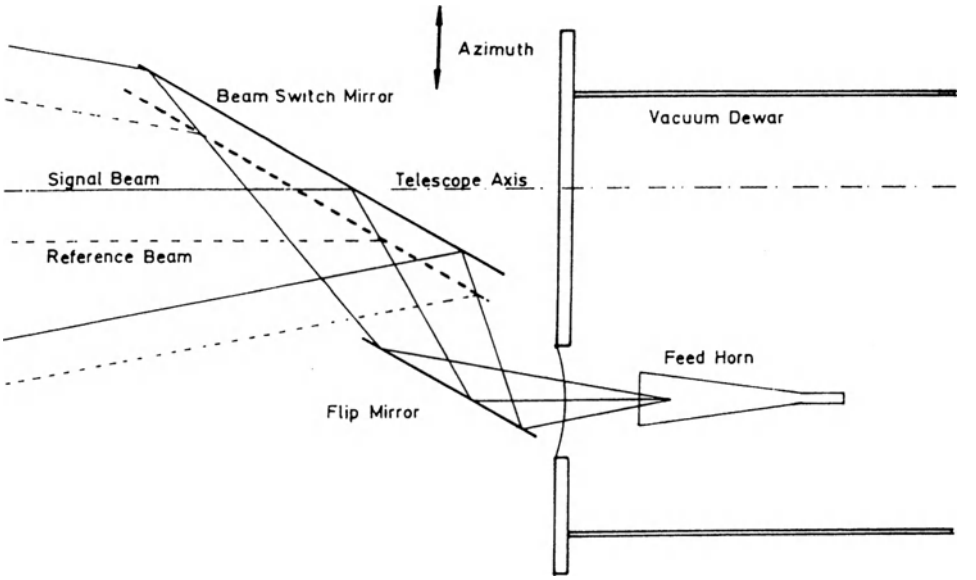

Fig. 1. Optics of the 80 – 115 GHz and 125 – 175 GHz receivers

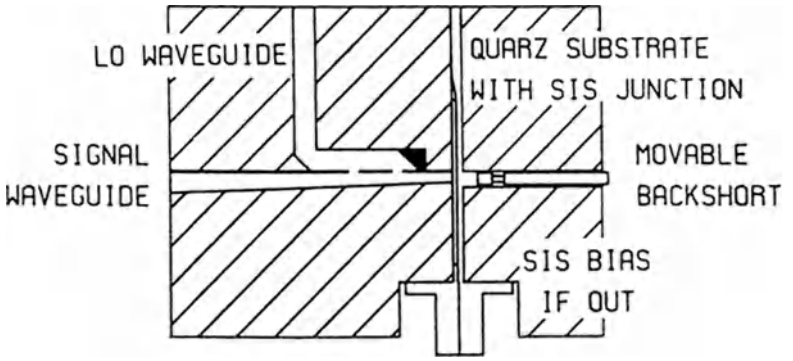

Fig. 2. Cross-sectional view of the SIS mixer

The mixer must be cooled to 2.8 K in order to get useful results. For this pupose a closed cycle refrigeration system has been developed [2][3] that has a cooling power of 350 mW at 2.8 K. The IF is centered at 1.4 GHz with a bandwidth of 600 MHz. For preamplification, a cryogenic two-stage HEMT amplifier has been developed that has a noise temperature of about 7 K. The best narrow-band (50 MHz) spot noise temperature of the receiver is 28 K (DSB) at 133 GHz. Typical broadband (600 MHz) values are between 55 and 200 K depending on the frequency.

345 GHz Receiver

The sensitive input element of the 345 GHz receiver is a cooled Schottky-diode mixer followed by a 1.4 GHz ± 300 MHz HEMT amplifier, both at the 20 K stage of a CTI refrigerator. Local oscillator power is provided by a 115 GHz Gunn oscillator (PLL

stabilized) followed by a varactor tripler. Mixer and multiplier use University of Virginia Schottky diodes of type 2I1-150 and 6P4 respectively. Signal power and local oscillator power are combined through a polarization-rotating Martin-Puplett interferometer (see Fig. 3).

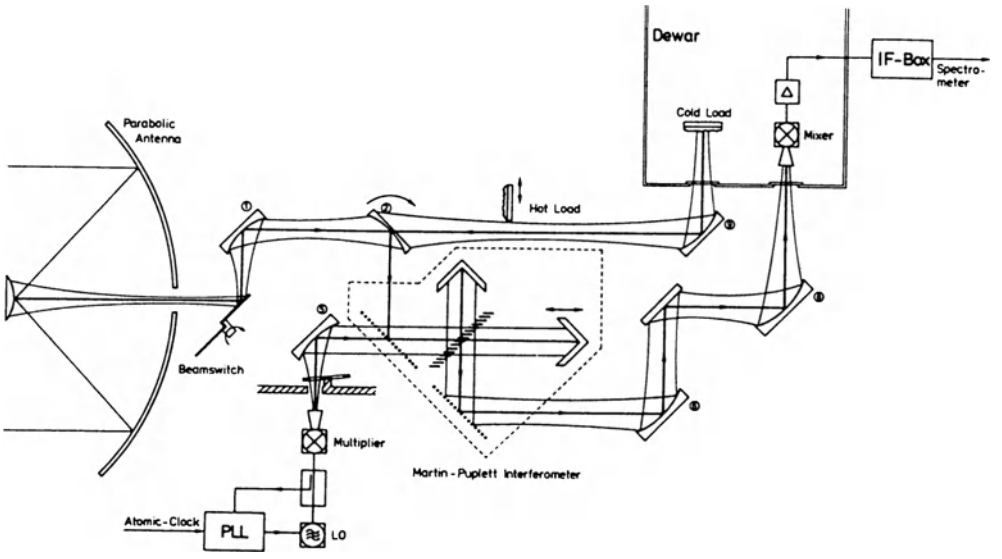

Fig. 3. 345 GHz receiver

For calibration the system can be switched by mirror 2 to hot and cold absorbers at 295 K and 50 K respectively. A rotating mirror at the input allows beam switching. Another device, a phase-wobbling dielectric sheet (not shown), may be used to reduce baseline ripple. The receiver temperature measured in the laboratory was in the range 650 $\pm$ 30 K when the mixer diode was pumped between 0.2 mA and 0.8 mA.

References

1. K. Jacobs, B.Vowinkel: "Solid state mm-wave oscillators with large tuning range," IEEE International Microwave Symposium Digest, MTT-S, 863-866 (1987)
2. W. Hilberath, B.Vowinkel: "An automatic low temperature heat switch," Cryogenics 23, 467-468 (1983)
3. W. Hilberath, B. Vowinkel: "Closed cycle refrigerator for superconducting mm-wave mixers," Cryogenics 25, 573-577 (1985)

HIGHLY PRECISE REFLECTORS AND MIRROR IN FIBRE-COMPOSITE TECHNOLOGY

Bernd Abt, Gunter Helwig, Dietmar Scheulen
Dornier-System GmbH, D 7990 Friedrichshafen

Reflectors for antennas using fibre-composite technology today represent the state of the art, and mirrors for radio telescopes occasionally are already made using this technology. For even shorter wavelengths, including the visible light, glass mirrors have been used almost exclusively and, rarely, metal mirrors (for example made of beryllium). In general a surface contour accuracy of about one twentieth of the wavelength is required. After years of development work based on experience gained in aircraft construction and space technology, Dornier succeeded in improving fibre-composite technology to such an extent that a substitute for heavy glass has become feasible, opening up new applications for lighter and/or larger mirrors.

Ultraprecise reflectors and mirrors using fibre-composite technology are produced by the replica process. To do this, a female mould is needed whose contour accuracy essentially determines the attainable precision of the componenet formed with this mould. This process has the big advantage that the precision has to be achieved only once, and then any given number of the same quality can be produced.

Fibre-composite technology for reflectors and mirrors offer the following advantages:

- high mechanical strength and stiffness
- low weight
- thermal stability
- long service life
- simpler and faster production.

More than ten years ago, Dornier developed the first carbon-fibre reinforced plastic (CFRP) sandwich reflector for a 2-metre offset satellite antenna. As CFRP is electrically conductive, no coating is necessary for wavelengths above 15 mm (below 20 GHz). For shorter wavelengths resp. higher frequencies, all fibre-composite mirrors must have a metallic coating. When developing the antennas for Kopernikus, the German communications satellite (DFS), Dornier qualified the vacuum depositing of aluminium on CFRP for space applications. Highly mobile ground stations with segmented reflectors 3.3 to 4.5 metres in diameter were also developed by Dornier for satellite communications.

By a combination and improvement of these very different developments, increasingly ambitious projects can be performed. For the 30-metre radio telescope on Pico Veleta in Spain, for

example, 420 aluminium sandwich panels were developed and delivered as well as the 2-metre metal-coated CFRP sandwich subreflector with a manufacturing accuracy of 15 micron rms.

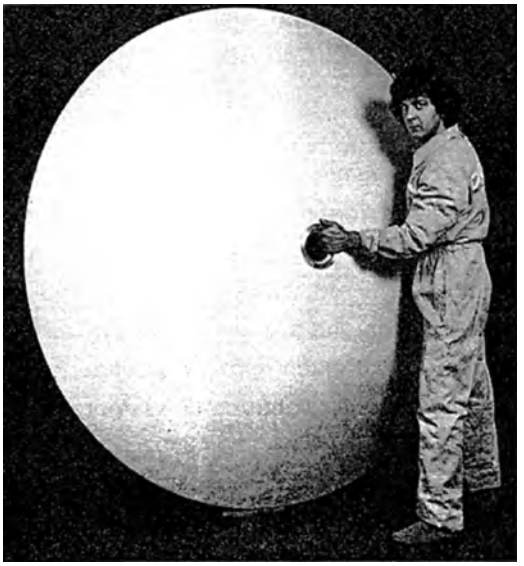

2 m Sandwich Subreflector

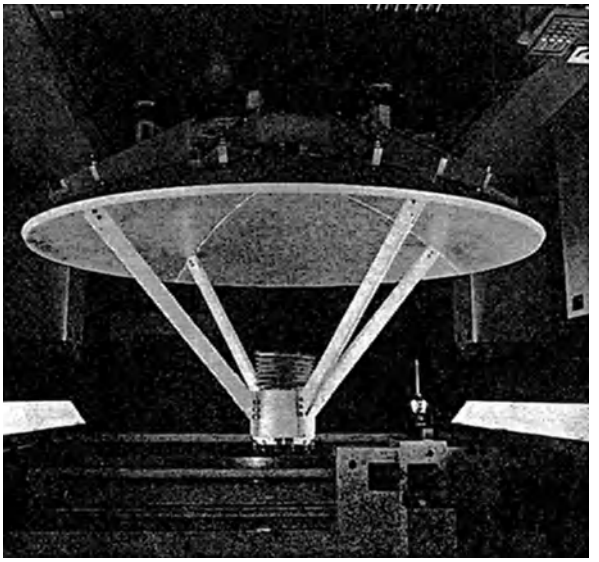

3 m Reflector for mm-Radiotelescope

The design of the mirror for the 3-metre telescope of Cologne University is similar to that of the mobile 3.3-metre ground antennas. But the four segments have been produced on preciser moulds and in addition they can be adjusted within certain limits leading to a contour accuracy of 25 micron rms.

For the sub-millimeter and far infrared wavelength ranges, the accuracy must be better by a factor of 10. In several feasibility studies for different projects, it was proven that fibre-composite technology could be an attractive alternative for these wavelengths as well.
For two corresponding projects, the "3-metre Far-Infrared and Submm Balloon Telescope" for the University of Arizona in the United States and the "Large Deployable Reflector" (about 20 metres in diameter) for NASA's Jet Propulsion Laboratory, Dornier built several panels of identical geometry with nearly identical requirements as to manufacturing accuracy (better than 2 micron, mass below 10 kp/m^2) and operating temperature range. They were all tested at the Steward Observatory of the University of Arizona, especially with regard to their temperatur behaviour down to about -60°C.
Within this development series, analytical methods were significantly improved, enabling a precise prediction of the panel behavior under such loads as

- manufacture
- temperature changes
- humidity
- gravity

Thus it was possible to optimally balance the design parameters, fibre material and orientation of the fibre layers, as well as type, material and orientation of the core structure.A ground glass mould (contour accuracy 1.5 micron rms) was used to produce panels, the manufacturing accuracy of which was improved in steps up to 1.8 micron rms and the thermostability for a temperature difference of $\Delta T \approx -80°C$ to a deformation of only 0.6 micron rms. The mass of the panels was only 6 kp/m^2. Thus it could be demonstrated that fibre-composite technology can be used for the submillimeter and the far-infrared ranges.

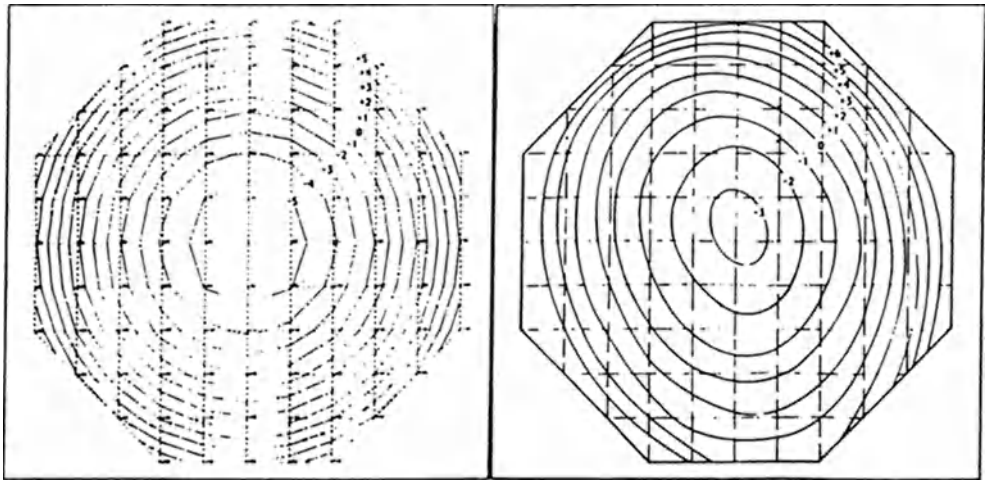

Thermal distortions as predicted (left) and as measured, iso-contour lines in micron

A feasibility study undertaken for ESA investigated wether this technology can be transferred to ESA's ambitious FIRST (Far Infrared and Submm Space Telescope) project. For a diameter of 8 metres, a contour accuracy including all errors of less than 10 micron rms is to be reached. A test panel of nearly the original size has been built and tested.

For the SOFIA (Stratospheric Observatory for Infrared Astronomy) project planned together by BMFT and NASA, a lightweight mirror about 3 metres in diameter is required for installation in a Boeing 747. Due to the even higher precision requirements (infrared to visible light), the replica process employed until now is no longer sufficient. First trials in cooperation with the University of Arizona have shown that it is possible to apply coatings on CFRP which can be ground and polished with less polishing pressure and faster than glass to obtain the required precision.

A novel support system linked with the design for homologous deformation, that is, the deformation generated under load forms a new paraboloid and thus only an uncritical focal length change, entails weight advantages if compared to a lightweight glass mirror with an 80% cent weight reduction (as compared to a solid glass mirror).

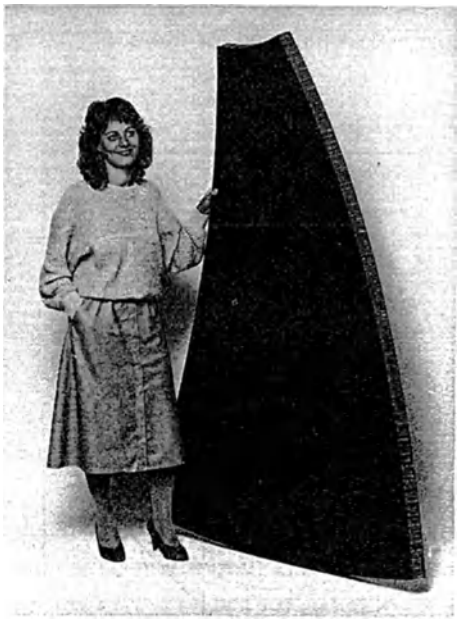

Test Panel for FIRST

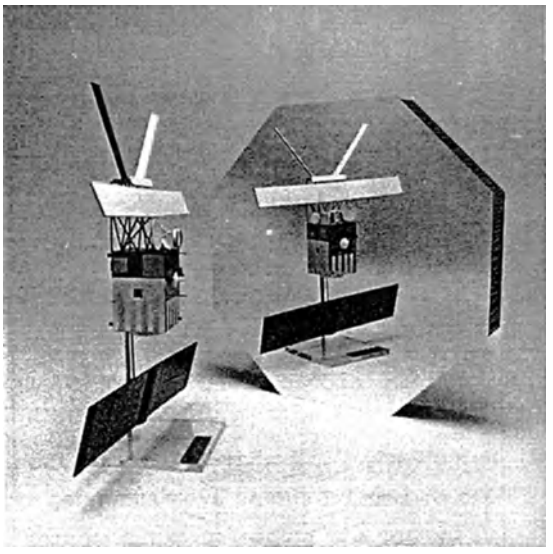

Sandwich Mirror

The Wolter-I telescope for the ESA XMM (X-Ray Multi-Mirror Satellite) is to reflect even shorter wavelengths. Each of the three mirror modules consists of 58 nested doublecone cylindrical mirrors 600 mm long and up to 700 mm in diameter. The global deviations from the ideal contour must not exeed 5 micron, and the surface quality must be better than 10 Å (= 0.001 micron). These a.m. requirements cannot be fulfilled for a planned wall thickness of only about one millimeter with a glass mirror, but it can be achieved using CFRP material.
In order to meet the extreme requirements for surface quality, the already very smooth CFRP surface must be coated with different materials in a second replica process on a superpolished form. The optimum coating sequence was calculated by Dornier by a micromechanical model. On samples produced in cooperation with Zeiss using this process, surface qualities better than 5 Å could be reached.

These last few examples impressively demonstrate the possibilities of fibre-composite technology in the optical field, and a considerable application potential still remains uncovered.

THE STATUS OF THE IRAM TELESCOPES

Robert LUCAS
IRAM, Domaine Universitaire
38406 Saint-Martin-d'Hères
FRANCE

Abstract

We give here a brief report on the status of the IRAM telescopes.

1 Introduction

IRAM (Institute for Radio Astronomy in the Millimeter Range) is a French-German institute, founded in 1979 by the Centre National de la Recherche Scientifique (CNRS) and the Max Planck Gesellschaft (MPG), with the contribution of the Instituto Geografico Nacional (IGN, Spain), to provide astronomers from these countries with first class facilities for millimeter wavelength astronomy. The 30-meter telescope on Pico Veleta in the Sierra Nevada has been in operation since 1985. A four element interferometer is being built on the Plateau de Bure, 90 km south of Grenoble (France).

2 The 30-m telescope

The 30-m telescope is built on the North slopes of Pico Veleta, at an altitude of 2870 m, and at a distance of 45 km from Granada. The site was chosen for its low latitude (37 degrees), the low water vapor content (on average 2mm in winter, to 4mm in summer), and the number of clear days (200 per year). The telescope itself was described by Baars *et al.* (1887). It is a paraboloid of 30m diameter, with a focal ratio of 0.35. The hyperbolic subreflector has a diameter of 2m, and flat third and fourth mirrors, at 45 degrees on the elevation axis, send the beam horizontally to a Nasmyth focus, situated in the receiver room, between the elevation bearings in the azimuth section. The reflector structure is of homologous design, thermally insulated, with an active system of temperature control, designed to achieve a temperature uniformity within one degree, between the structure itself, the yoke, and the quadrupod. This performance is actually reached (Baars *et al.* 1988). The telescope surface is a mosaic of 420 panels, roughly 1m × 2m in size, made of stretched aluminium skins bonded to aluminium honeycomb. The panels are mounted by pairs on steel subframes. The panel accuracy is 26 μm rms. The panels were adjusted on the structure to approach a parabolic shape by means of radio holography (Morris *et al.*

1988). The water-vapor maser source in Orion was first used, with a reference antenna built in the prime focus cabin, then phase retrieval holography was made using a remote transmitter on Pico Veleta. The final surface accuracy is about 65 μm rms. The tracking accuracy is about 1" rms for wind velocities up to 12 m/s. The absolute pointing accuracy is 3" rms; this is obtained by updating the pointing model every week to compensate for long-term drifts.

The telescope performance is summed up in the following table:

Frequency (GHz)	Aperture Efficiency	Main-beam Efficiency	Forward Efficiency	Beamwidth (")
90	0.50	0.60	0.90	26
110	0.50	0.60	0.90	21
140	0.50	0.60	0.90	17
230	0.27	0.45	0.95	12.5
345	0.10	$\simeq$0.20	0.84	8.4

Three SIS receivers, built at IRAM, are available in the 3mm, 2mm and 1mm ranges, with typical double side-band noise temperatures of 140 to 240 K (3mm and 2mm receivers) and 100 to 250 K (1mm receiver) (Blundell *et al.* 1983, 1984, 1988). A 345 GHz Shottky receiver with 900 K double side-band temperature, built by the MPIfR, is under test at the telescope.

Backends include two filter banks (512 $\times$1 MHz and 256 $\times$ 100kHz), a spectrum expander (128 channels), and a 1024-channel autocorrelator.

The system is now controlled by two micro-VAX computers, one for telescope control and data acquisition, the second for data analysis and backup.

3 The Interferometer

The interferometer is being built on Plateau de Bure, at 2553 m of altitude, in the southern French Alps. The site latitude is 44.5 degrees. Access is via a cable car operated by IRAM.

The antennas are 15 meters in diameter, with a focal ratio of 0.325 . The subreflector has a diameter of 1.5 m. The receivers are in a cabin at the Cassegrain focus. The backup structure is made of carbon fiber tubes, and the reflecting surface consists of 176 panels (carbon fiber plates on aluminium honeycomb). The current measured accuracy of the surface is typically 70 μm rms. Holographic measurements are planned in the future to improve this figure to reach the design goal of 50 μm. Two of the four antennas have being built and tested, the third one has been assembled and will be tested next winter. Tracking is good for winds speeds up to 10 m/s. The pointing accuracy is 3" rms over the full sky. The fourth antenna will be available in 1992.

The antennas may be placed on 26 stations on a T-shaped track, with arms in the North-South and East-West directions, of lengths 160m and 288m respectively. The tracks might later be extended to reach 1 km EW baselines. The local oscillator reference and intermediate frequencies are transported through high-Q coaxial cables. The electrical lengths of the cables are monitored in real time by a round-trip phase measurement at 1.8 GHz. Phase rotators on the first and third local oscillators are used to stop the fringes;

delays are digital and applied on the third local oscillators. The phase of the first local oscillator is switched by Walsh waveforms of π and $\pi/2$ amplitude to eliminate offsets and enable separating the upper and lower sidebands. Two digital correlators are available: a continuum correlator, of total bandwith 500 MHz (divided into ten 50 MHz sub-bands), with 4-bit multipliers, computing both the cosine and sine components of the visibilities; a spectral correlator with currently 128 channels per baseline (bandwidth up to 2×80 MHz).

The receivers are now two SIS receivers (with double-sideband temperatures 80 and 110 K) and one Shottky receiver (120 K). The whole system is controlled by a PDP 11/44 computer.

First fringes were obtained on 3C273 and the Orion SiO maser in December 1988, at 86 GHz with two antennas on a 48 m baseline. Regular operation with three antennas is planned for the fall of 1989.

References

Baars, J.W.M., Hooghoudt, B.G., Mezger, P.G., and de Jonge, M.J. 1987, *Astron. Astrophys.* **175**, 319

Baars, J.W.M., Greve, A., Hooghoudt, B.G., and Penalver, J. 1988, *Astron. Astrophys.* **195**, 371

Blundell, R., Gundlach, K.H., and Blum, E.J., 1983, *Electronics Letters*, **19**, 198

Blundell, R., Ibrügger, J., Gundlach, K.H., and Blum, E.J., 1984, *Electronics Letters*, **20**, 476

Blundell, R., Carter, M., and Gundlach, K.H., 1988, *Int. Journ. Infrared and Millimeter Waves*, **9**, 361

Morris, D., Baars, J.W.M., Hein, H., Steppe, H., and Wohlleben, R. 1988, *Astron. Astrophys.* **203**, 399

The Cologne Acousto-Optical Spectrometers

V. Tolls, R. Schieder, and G. Winnewisser
I. Physikalisches Institut, Universität zu Köln, FRG

I. Introduction

The general acceptance of acousto-optical spectrometers (AOS) as reliable spectroscopic tools for astronomical line observations was dependent on their integration capabilities, which posed problems in the past. The major problems arise from laser "speckles", which produce severe baseline variations and thus limit the ultimate performance. All optical surfaces and scattering centers within the optical path produce scattered light. Part of the AOS development at Cologne University was to find suitable techniques for removal of scattered background laser light [1].

For the design of a stable AOS, two basic principles must be considered:

1. Bragg cells that switch the polarization must be used, and
2. the optics must be suitable to the deflector used.

Design Characteristics

Two examples of Cologne-built AOSs are shown in Figure 1, which shows the medium resolution spectrometer (MRS) of the KOSMA Observatory on the Gornergrat near Zermatt (bandwidth 287 MHz, 1700 channels) and the low resolution spectrometer (LRS) which is now in operation at the ESO-SEST telescope in Chile (bandwidth 1.1 GHz, 1600 channels). The performance characteristics of all Cologne-built AOSs are summarized in Table 1 [2].

The AOSs are extremly stable and can be used for more than 100 s integration time for a single scan per position in position-switching mode. The spectroscopic Allan variance has been developed in our laboratory as a critical performance test and is used as a criterion for the AOSs and for the whole system ([3],[4]).

The main difference between the AOSs is the illumination of the Bragg cell. The laser diodes (Hitachi HL 7802 E) are oriented so that the long axis of the elliptical beam is horizontal and the polarisation vertical. Special collimation optics are used to produce a well-defined parallel laser beam. For the LRS, no further expansion of the beam is needed because of the small 3.5 mm length of the active zone of the Bragg cell (Marconi Y-35-2761). The beam is collimated horizontally by means of a cylindrical lens ($f = 60$ mm) to properly illuminate the small height of the acoustic wave in the deflector (50 μm). Although the divergence in the vertical direction is rather large, no additional

collimation with another cylindrical lens is necessary because of the small focal length of the imaging optics ($f = 80\,\mathrm{mm}$).

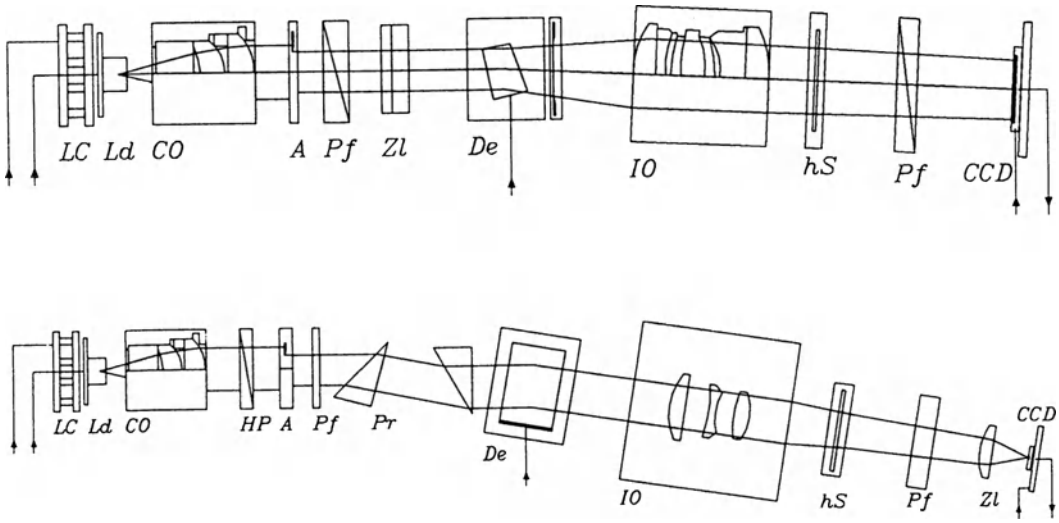

Fig. 1. Optical layout of the SEST LRS (above) and the KOSMA MRS (below). The components are: LC = Laser Cooling, Ld = Laser Diode, CO = Collimation Optics, A = Aperture, Pf = Polarizer, Zl = Cylindrical lens, De = Deflector, IO = Imaging Optics, hS = Slit Aperture, HP = Halfwave Retarder, $Pr = 30°$ Prism.

Table 1. Cologne AOS characteristics

	KOSMA HRS	KOSMA MRS	SEST LRS
bandwidth	64.7 MHz	287 Mhz	1100 MHz
center frequency	87.4 MHz	324.6 MHz	2072 MHz
number of channels	2048	1700	1600
channel spacing	31.6 kHz	166.6 kHz	689 kHz
resolution bandwidth	46 kHz	287 kHz	1070 kHz
reception bandwidth	66 kHz	407 kHz	1530 kHz
max. integration time	500 s	120 s	100 s
deflector	Matsushita EFL-D-2000S1	Crystal Tech. 4400S-GaP	Marconi Y-35-2761
laser	5 mW HeNe	laser diode: Hitachi HL 7802 E	laser diode: Hitachi HL 7802 E
detector	Fairchild CCD 142 CD	Fairchild CCD 122 CD	Fairchild CCD 122 CD

The optics of the MRS look quite different. A low loss beam expander (3-fold

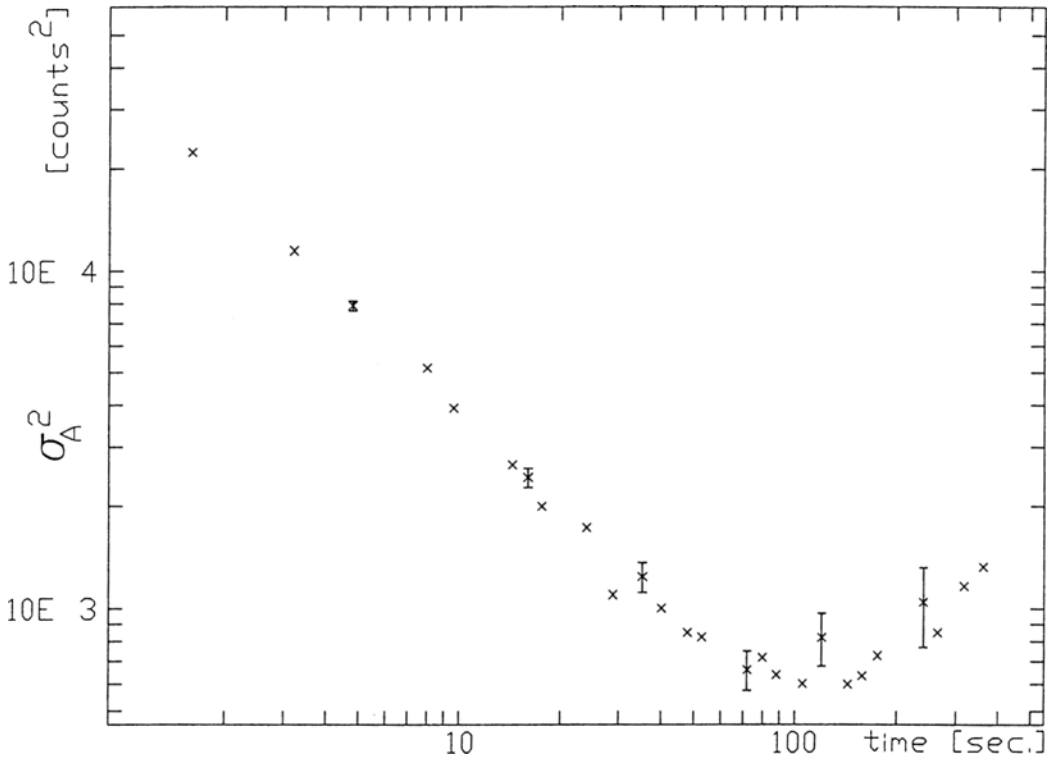

Fig. 2. Allan plot of the SEST LRS. The integration time at minimum variance is above 100 s. Below this time the variance behaves as expected from the radiometer formula (white noise; slope -1), while above this time it is dominated by drifts (slope > -1).

expansion) in the horizontal plane made of two 30° prisms (material SF10)[5] is needed to illuminate the deflector (Crystal Technology 4400S-GaP, active area $0.05 \times 17\,\mathrm{mm}^2$). Both the beam expander and the deflector require horizontal polarization, so a half-wave retarder rotates the polarization of the laser beam. No further vertical collimation by means of a cylindrical lens is applied, but a cylindrical lens is used for additional focusing in the vertical direction in front of the CCD (Fairchild CCD 122/142) because of the much longer focal length of the imaging optics ($f = 400\,\mathrm{mm}$). In both AOSs, a slit aperture made of razor blades directly behind the imaging optics is inserted to reduce the laser scatter.

In our experience, the laser scatter is the most important single factor limiting the stability of an AOS [6,4]. Integration times for good and stable AOSs as derived from the minimum of the spectroscopic Allan variance are of the order of minutes. A long integration time is a severe requirement for a broadband AOS but easy to achieve for high resolution AOS (see Table 1).

For the SEST LRS we obtained a maximum integration time of the spectrometer of about 100 s (see Fig. 2) and for the MRS at Gornergrat of about 120 s. These numbers refer to pure spectrometer performance. If there are other instabilities in the frontend system or elsewhere, e.g. the atmosphere, these times will be reduced significantly.

A transportable low resolution spectrometer for observations at other telescopes or for airborne observations is under construction. The optics of this AOS are similar to the optics of the LRS, but its mechanical stability is considerably improved to reach the same performance limits as a stationary AOS.

Acknowledgements. This work was supported by the Deutsche Forschungsgemeinschaft through grant Wi-391/2-1 and grant SFB 301. We also want to thank ESO and the SEST group in Chile for their help during the installation of the AOS at the La Silla site.

References

[1] R. Schieder, V. Tolls, G. Winnewisser, *Experimental Astronomy*, **1** (1989), in press
[2] W. Zensen, A. Piciorgros, R. Schieder, G. Winnewisser, Proc. SPIE Conf. on Submillimeter Spectroscopy, Cannes, p. 598 (1985)
[3] G. Rau, R. Schieder, B. Vowinkel, Proc. 14th European Microwave Conf., Liege (1984)
[4] R. Schieder, B. Vowinkel, G. Rau, Proc. SPIE Conf. on Submillimeter Spectroscopy, Cannes, p. 598 (1985)
[5] E. Hecht, *Optics*, Addison-Wesley Publishing Company, 2nd edition (1987)
[6] A. Piciorgros, Ph. D. Thesis, University of Cologne (1988)

Measurements of CO in the Terrestrial Mesosphere

R. M. Bevilacqua, T. Pauls, and P. R. Schwartz
E. O. Hurlburt Center for Space Research,
Naval Research Laboratory, Washington, D. C. 20375
and
J. T. Armstrong and H. Ungerechts
I. Physikalisches Institut, Universität zu Köln

Introduction

Because the photochemical lifetime of CO in the mesosphere (50–85 km) is comparable to atmospheric transport timescales, it is an excellent tracer of poorly understood dynamical activity and transport mechanisms in this altitude region. Ground-based mm-wave techniques are nearly ideally suited to measuring the CO abundance as a function of altitude in the mesosphere, and several observations have been reported using standard radio astronomy instrumentation and techniques. The technique invoves making high spectral resolution measurements of pure rotational lines. Because these lines are pressure broadened in the middle atmosphere, the measured shape of the line can be deconvolved to provide information concerning the constituent abundance as a function of pressure or, equivalently, altitude.

We have begun an experiment in which we plan to make periodic measurements of CO in the mesosphere using spectral observations of the terrestrial $J = 1 \rightarrow 0$ CO line at 115.2 GHz, obtained using the University of Cologne mm-wave telescope at the Gornergrat Observatory. The primary goal of the experiment is to resolve the details of the seasonal variation of mesospheric CO densities. The magnitude and phase of this variation contains important information concerning the interaction of dynamical transport and photochemistry in establishing the distribution of trace constituents in the middle atmosphere.

In this paper we report the first two observations we have made as part of this study. These observations, which were obtained in May 1987 and January 1988, are noteworthy because they suggest a large seasonal variation in CO abundances which is generally consistent with photochemical model calculations.

Results

In Figure 1 we plot the folded spectra obtained in May 1987 and January 1988. The integration time of the May observation is roughly five hours and the elevation angle is 20°; the integration time of the January spectrum is about 20 hours at an elevation angle 12?5. In both cases the smooth curve is a cubic spline fit to the spectra which was used in the spectral retrieval process. The total amplitude of the spectral line is a measure of the CO column density, and the shape of the line is dependent on the vertical distribution. The amplitude of the spectrum obtained in the January measurement is more than a factor of 3 larger than the May result. In addition, it is considerably broader. The total width of the May spectrum is about equal to the Doppler line width, which indicates that most of the CO was located at altitudes at which Doppler broadening is the predominant line broadening mechanism. For the $J = 1 \rightarrow 0$ CO line, this implies altitudes above about 75 km. However, the January spectrum contains significant pressure-broadened shoulders, which indicates the presence of significant CO abundances below 75 km.

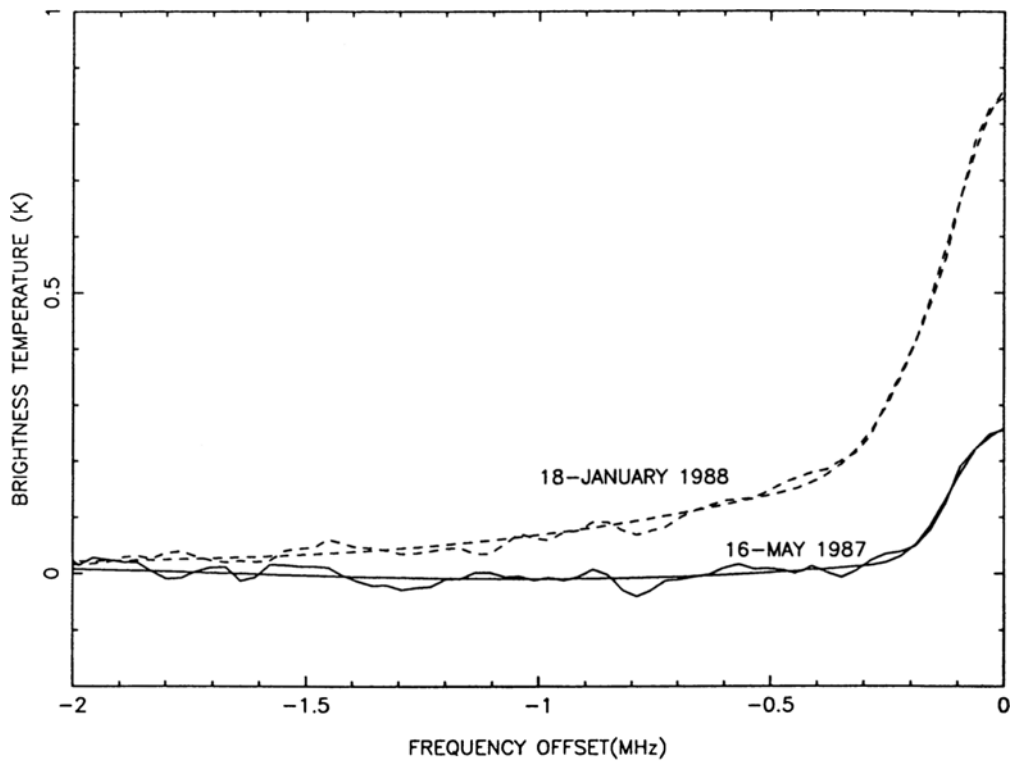

Fig. 1. Measured terrestrial $J = 1 \rightarrow 0$ CO spectra (folded about the line central frequency) obtained on the indicated dates. In both cases the smooth curve is a cubic spline fit to the measured spectrum.

In order to retrieve the vertical distribution of CO from the measured spectra, we use the Twomey modified Chahine inversion technique (Twomey *et al.*, 1977). This numerical retrieval algorithm is a simple iterative technique in which we start with an

initial CO profile and calculate a synthetic spectrum using a radiative transfer model. The CO profile is then varied based on the difference between the simulated and actual spectra. The solution is assumed to have converged when this difference is just equal to the noise level of the measurement. The altitude range of the measurements is 60 to 80 km, and the vertical resolution varies between 6 and 8 km.

In Figure 2, we show the spectral retrieval results in the form of CO abundance mixing ratios in parts per million by volume (ppmv), plotted as a function of altitude. The absolute error level of the retrieved profiles is about 20–30%. These results verify the points made above from examination of the spectra. At 60 and 65 km the January mixing ratios are more than a factor of 50 larger than the May results. However, the difference between the two profiles is a decreasing function of altitude. At 80 km, the discrepancy is reduced to less than a factor of 2.

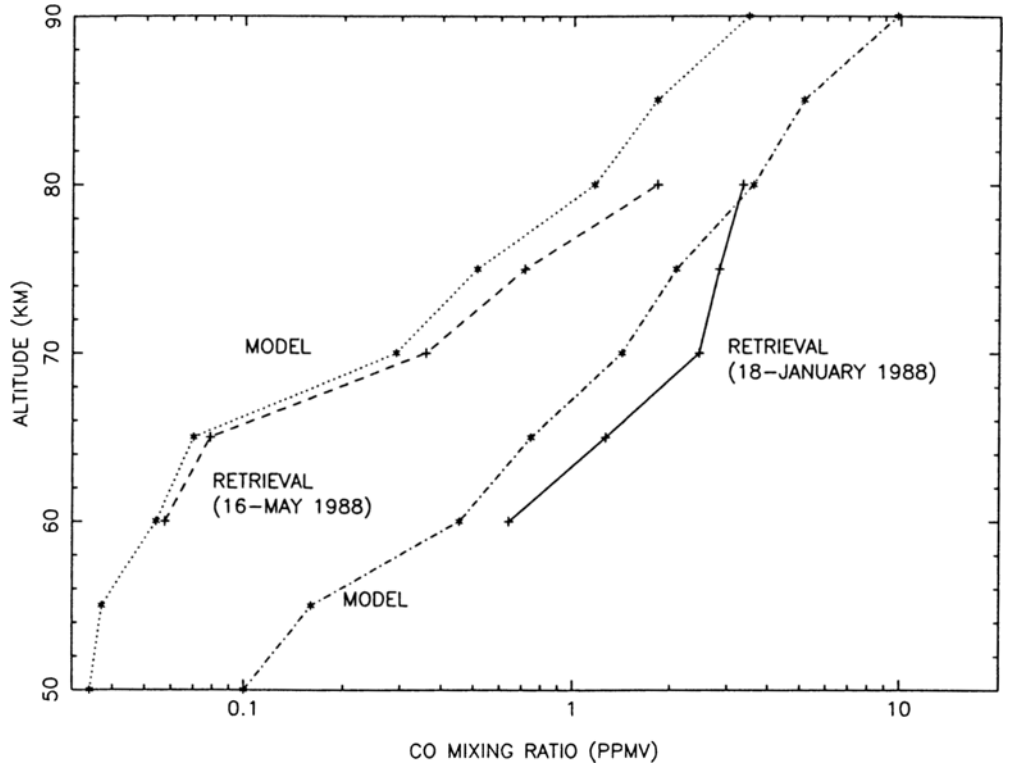

Fig. 2. CO mixing ratio retrievals, in parts per million by volume (ppmv), for the spectra shown in Figure 1, compared to winter and summer theoretical profiles for 45°N obtained from Solomon *et al.* (1985).

Also shown in Figure 2 are theoretical profiles taken from the two-dimensional photochemical/dynamical calculations of Solomon *et al.* (1985) for 45°N latitude summer and winter. The large seasonal variation indicated in the calculations is caused by a coincident variation in transport timescales. Carbon monoxide in the middle atmosphere is produced by the photodissociation of CO_2, which occurs predominantly above 85 km.

It is then transported down to lower altitudes where it is eventually converted back to CO_2 via reaction with OH. The vertical velocity in the middle atmosphere undergoes an annual variation at mid latitudes, with upward motion in summer and downward motion in winter. Thus CO is transported into the lower mesosphere from its thermospheric source region much more rapidly in winter than in summer. This results in much larger CO densities in the 60 to 70 km region during winter. Our measurements are in good general agreement with the model calculations, thus qualitatively corroborating this large seasonal variation.

References

Solomon, S., Garcia, R. R., Olivero, J. J., Bevilacqua, R. M., Schwartz, P. R., Clancy, R. T., and Muhleman, D. O. 1985, "Photochemistry and transport of carbon monoxide in the middle atmosphere," *J. Atmos. Sciences*, **42**, 1072-1083.

Twomey, S., Herman, B., and Rabinoff, R. 1977, "An extension to the Chahine method of inverting the radiative transfer equation," *J. Atmos. Sciences*, **34**, 1085-1090.

INDEXES

(Note: Paper of P. Thaddeus not indexed due to late arrival.)

Index of Authors

Index of Atoms, Ions and Molecules

Object Index

Subject Index

Zermatt Symposium Participants

Aalto, S. (Onsala Space Observatory)
Abt, B. (Dornier-System)
Achenbach, S. (Universität zu Köln)
Aiello, s. (University of Florence)
Andreani, P. (University of Rome)
Armstrong, Dr. J. T. (Universität zu Köln)
Assendorp, R. (Laboratory for Space Research, Groningen)
Baars, Dr. J. (MPI für Radioastronomie, Bonn)
Bally, Dr. J. (AT&T Bell Laboratories)
Becker, R. (Landessternwarte Heidelberg)
Bergmann, P. (Onsala Space Observatory)
Bester, Dr. M. (University of California, Berkeley)
Bloemen, Dr. J. B. G. M. (Sterrewacht Leiden)
Bloemhof, Dr. E. (Harvard-Smithsonian Center for Astrophysics)
Booth, Dr. R. (Onsala Space Observatory)
Botschwina, Prof. Dr. P. (Universität Kaiserslautern)
Boulanger, F. (Caltech, Pasadena)
Braine, J. (C. N. R. S., Paris)
Brand, J. (MPI für Radioastronomie, Bonn)
Bronfman, L. (University of Chile)
Büttgenbach, T. (Caltech, Pasadena)
Calamai, G. (TIRGO, Arcetri)
Castets, A. (Observatory of Grenoble)
Ceccarelli, C. (IFSI-CNR, Rome)
Cecchi-Pestellini, C. (University of Florence)
Churchwell, Dr. E. (MPI für Radioastronomie, Bonn)
Cox, P. (MPI für Radioastronomie, Bonn)
Dame, Dr. T. (Harvard-Smithsonian Center for Astrophysics)
Debrunner, Prof. Dr. H. (Int. Stiftung Hochalpine Forschungsstationen)
Dreizler, Prof. Dr. H. (Universität Kiel)
Dreizler, S. (Universität Kiel)
Duley, Dr. W. W. (York University, Ontario)
Duvert, G. (Observatory of Grenoble)
Ehrlichmann, H. (Universität Kiel)
Ewald, Dr. R. (DFVLR, Köln)
Feldman, P. (NRC of Canada)
Fiebig, D. (MPI für Radioastronomie, Bonn)
Fridlund, M. (ESTEC, Noordwijk)
Genzel, Prof. Dr. R. (MPI für Extraterrestrische Physik, Garching)
Gerharz, Dr. R. (U. S. Dept. of Commerce)
Glasse, A. C. H. (ESA/ESTEC, Noordwijk)
Goldsmith, Dr. P. (Five College Radio Astronomy Observatory)
Goodman, A. A. (Harvard-Smithsonian Center for Astrophysics)
Graf, U. (MPI für Extraterrestrische Physik, Garching)

Gredel, Dr. R. (ESO Chile)
Grenier, I. (CEN Saclay, Gif)
Gripp, J. (Universität Kiel)
Guarnieri, A. (Universität Kiel)
Guélin, Dr. M. (IRAM)
Güsten, Dr. R. (MPI für Radioastronomie, Bonn)
Habing, Prof. Dr. H. (Sterrewacht Leiden)
Haikala, Dr. L. (Universität zu Köln)
Hanau, Prof. Dr. P. (Universität zu Köln)
Harjunpää, P. (University of Helsinki)
Heineking, N. (Universität Kiel)
Heithausen, A. (Universität Bonn)
Helou, G. (Caltech, Pasadena)
Herbst, Dr. E. (Universität zu Köln)
Herbstmeier, U. (Universität Bonn)
Herzberg, Prof. Dr. G. (NRC Canada)
Hills, Dr. R. (Cambridge University)
Hjalmarson, Dr. A. (Onsala Space Observatory)
Jacobs, Dr. K. (Universität zu Köln)
Jenniskens, P. M. M. (Sterrewacht Leiden)
Junkes, N. (MPI für Radioastronomie, Bonn)
Kirste, Dr. E. (Deutsche Forschungsgemeinschaft)
Knee, L. B. G. (Onsala Space Observatory)
Kranski, B. (Universität zu Köln)
Lane, A. P. (Boston University)
Liljeström, T. (University of Helsinki)
Lorenzetti, D. (IFSI-CNR, Rome)
Lucas, R. (IRAM)
Mattila, Prof. Dr. K. (University of Helsinki)
Mebold, Prof. Dr. U. (Universität Bonn)
Melen, F. (Inst. d'Astrophys. de Liège)
Meyer, M. (Universität Kiel)
Millar, T. (UMIST)
Miller, Dr. M. (Universität zu Köln)
Mouschovias, Dr. T. (University of Illinois, Urbana)
Mundt, Dr. R. (MPI für Radioastronomie, Bonn)
Myers, Dr. P. (Harvard-Smithsonian Center for Astrophysics)
Müller, P. (Universität zu Köln)
Neue, Dr. G. (Universität Dortmund)
Olberg, M. (ESO Garching)
Omont, Dr. A. (University of Grenoble)
Pagani, L. (Observatoire de Meudon)
Palumbo, G. G. C. (University of Bologna)
Pauls, Dr. T. (Naval Research Laboratory, Washington)
Penselin, Dr. S. (Universität Bonn)
Phillips, Dr. J. P. (Queen Mary College, London)
Poglitsch, A. (MPI für Extraterrestrische Physik, Garching)

Prusti, T. (Laboratory for Space Research, Groningen)
Robberto, M. (Observatory of Turin)
Rubio, M. (University of Chile)
Ruggero, S. (University of Florence)
Saraceno, P. (IFSI-CNR, Rome)
Schieder, Prof. Dr. R. (Universität zu Köln)
Schmidt-Kaler, Dr. T. (Ruhr-Universität Bochum)
Schwartz, Dr. P. R. (Naval Research Laboratory, Washington)
Silk, Dr. J. (University of California, Berkeley)
Stacey, G. J. (University of California, Berkeley)
Stark, A. A. (AT&T Bell Laboratories)
Strafella, F. (IFSI-CNR, Rome)
Stutzki, Dr. J. (MPI für Extraterrestrische Physik, Garching)
Sugitani, K. (Nagoya City University)
Thaddeus, Prof. Dr. P. (Harvard-Smithsonian Center for Astrophysics)
Tofani, G. (Observatory of Florence)
Townes, Prof. Dr. C. H. (University of California, Berkeley)
Ungerechts, Dr. H. (Universität zu Köln)
Vidal, Dr. (MPI für Extraterrestrische Physik, Garching)
Vormann, K. (Universität Kiel)
Vowinkel, Dr. B. (Universität zu Köln)
Walmsley, C. M. (MPI für Radioastronomie, Bonn)
Walter, Y. (Universität Frankfurt am Main)
Weikard, H. (University of Grenoble)
Weiland, H. (Universität Bonn)
Welch, Prof. Dr. W. J. (University of California, Berkeley)
Wendker, Prof. Dr. H. J. (Hamburger Sternwarte)
White, Dr. G. (Queen Mary College, London)
Winnewisser, Dr. B. (Justus-Liebig-Universität Giessen)
Winnewisser, Prof. Dr. G. (Universität zu Köln)
Winnewisser, Prof. Dr. M. (Justus-Liebig-Universität Giessen)
Wootten, Dr. H. A. (NRAO)
Wouterloot, J. (MPI für Radioastronomie, Bonn)
Yamada, Dr. K. (Universität zu Köln)
Young, J. S. (Five College Radio Astronomy Observatory)
Yue, Z.-Y. (Beijing University)
Zimmermann, Dr. P. (Universität zu Köln)
Zinnecker, H. (MPI für Extraterrestrische Physik, Garching)

Lecture Notes in Mathematics

Vol. 1236: Stochastic Partial Differential Equations and Applications. Proceedings, 1985. Edited by G. Da Prato and L. Tubaro. V, 257 pages. 1987.

Vol. 1237: Rational Approximation and its Applications in Mathematics and Physics. Proceedings, 1985. Edited by J. Gilewicz, M. Pindor and W. Siemaszko. XII, 350 pages. 1987.

Vol. 1250: Stochastic Processes – Mathematics and Physics II. Proceedings 1985. Edited by S. Albeverio, Ph. Blanchard and L. Streit. VI, 359 pages. 1987.

Vol. 1251: Differential Geometric Methods in Mathematical Physics. Proceedings, 1985. Edited by P.L. García and A. Pérez-Rendón. VII, 300 pages. 1987.

Vol. 1255: Differential Geometry and Differential Equations. Proceedings, 1985. Edited by C. Gu, M. Berger and R.L. Bryant. XII, 243 pages. 1987.

Vol. 1256: Pseudo-Differential Operators. Proceedings, 1986. Edited by H.O. Cordes, B. Gramsch and H. Widom. X, 479 pages. 1987.

Vol. 1258: J. Weidmann, Spectral Theory of Ordinary Differential Operators. VI, 303 pages. 1987.

Vol. 1260: N.H. Pavel, Nonlinear Evolution Operators and Semigroups. VI, 285 pages. 1987.

Vol. 1263: V.L. Hansen (Ed.), Differential Geometry. Proceedings, 1985. XI, 288 pages. 1987.

Vol. 1265: W. Van Assche, Asymptotics for Orthogonal Polynomials. VI, 201 pages. 1987.

Vol. 1267: J. Lindenstrauss, V.D. Milman (Eds.), Geometrical Aspects of Functional Analysis. Seminar. VII, 212 pages. 1987.

Vol. 1269: M. Shiota, Nash Manifolds. VI, 223 pages. 1987.

Vol. 1270: C. Carasso, P.-A. Raviart, D. Serre (Eds.), Nonlinear Hyperbolic Problems. Proceedings, 1986. XV, 341 pages. 1987.

Vol. 1272: M.S. Livšic, L.L. Waksman, Commuting Nonselfadjoint Operators in Hilbert Space. III, 115 pages. 1987.

Vol. 1273: G.-M. Greuel, G. Trautmann (Eds.), Singularities, Representation of Algebras, and Vector Bundles. Proceedings, 1985. XIV, 383 pages. 1987.

Vol. 1275: C.A. Berenstein (Ed.), Complex Analysis I. Proceedings, 1985–86. XV, 331 pages. 1987.

Vol. 1276: C.A. Berenstein (Ed.), Complex Analysis II. Proceedings, 1985–86. IX, 320 pages. 1987.

Vol. 1277: C.A. Berenstein (Ed.), Complex Analysis III. Proceedings, 1985–86. X, 350 pages. 1987.

Vol. 1283: S. Mardešić, J. Segal (Eds.), Geometric Topology and Shape Theory. Proceedings, 1986. V, 261 pages. 1987.

Vol. 1285: I.W. Knowles, Y. Saitō (Eds.), Differential Equations and Mathematical Physics. Proceedings, 1986. XVI, 499 pages. 1987.

Vol. 1287: E.B. Saff (Ed.), Approximation Theory, Tampa. Proceedings, 1985–1986. V, 228 pages. 1987.

Vol. 1288: Yu. L. Rodin, Generalized Analytic Functions on Riemann Surfaces. V, 128 pages, 1987.

Vol. 1294: M. Queffélec, Substitution Dynamical Systems – Spectral Analysis. XIII, 240 pages. 1987.

Vol. 1299: S. Watanabe, Yu.V. Prokhorov (Eds.), Probability Theory and Mathematical Statistics. Proceedings, 1986. VIII, 589 pages. 1988.

Vol. 1300: G.B. Seligman, Constructions of Lie Algebras and their Modules. VI, 190 pages. 1988.

Vol. 1302: M. Cwikel, J. Peetre, Y. Sagher, H. Wallin (Eds.), Function Spaces and Applications. Proceedings, 1986. VI, 445 pages. 1988.

Vol. 1303: L. Accardi, W. von Waldenfels (Eds.), Quantum Probability and Applications III. Proceedings, 1987. VI, 373 pages. 1988.

Lecture Notes in Physics

Vol. 308: H. Bacry, Localizability and Space in Quantum Physics. VII, 81 pages. 1988.

Vol. 309: P.E. Wagner, G. Vali (Eds.), Atmospheric Aerosols and Nucleation. Proceedings, 1988. XVIII, 729 pages. 1988.

Vol. 310: W.C. Seitter, H.W. Duerbeck, M. Tacke (Eds.), Large-Scale Structures in the Universe – Observational and Analytical Methods. Proceedings, 1987. II, 335 pages. 1988.

Vol. 311: P.J.M. Bongaarts, R. Martini (Eds.), Complex Differential Geometry and Supermanifolds in Strings and Fields. Proceedings, 1987. V, 252 pages. 1988.

Vol. 312: J.S. Feldman, Th.R. Hurd, L. Rosen, "QED: A Proof of Renormalizability." VII, 176 pages. 1988.

Vol. 313: H.-D. Doebner, T.D. Palev, J.D. Hennig (Eds.), Group Theoretical Methods in Physics. Proceedings, 1987. XI, 599 pages. 1988.

Vol. 314: L. Peliti, A. Vulpiani (Eds.), Measures of Complexity. Proceedings, 1987. VII, 150 pages. 1988.

Vol. 315: R.L. Dickman, R.L. Snell, J.S. Young (Eds.), Molecular Clouds in the Milky Way and External Galaxies. Proceedings, 1987. XVI, 475 pages. 1988.

Vol. 316: W. Kundt (Ed.), Supernova Shells and Their Birth Events. Proceedings, 1988. VIII, 253 pages. 1988.

Vol. 317: C. Signorini, S. Skorka, P. Spolaore, A. Vitturi (Eds.), Heavy Ion Interactions Around the Coulomb Barrier. Proceedings, 1988. X, 329 pages. 1988.

Vol. 318: B. Mercier, An Introduction to the Numerical Analysis of Spectral Methods. V, 154 pages. 1989.

Vol. 319: L. Garrido (Ed.), Far from Equilibrium Phase Transitions. Proceedings, 1988. VIII, 340 pages. 1988.

Vol. 320: D. Coles (Ed.), Perspectives in Fluid Mechanics. Proceedings, 1985. VII, 207 pages. 1988.

Vol. 321: J. Pitowsky, Quantum Probability – Quantum Logic. IX, 209 pages. 1989.

Vol. 322: M. Schlichenmaier, An Introduction to Riemann Surfaces, Algebraic Curves and Moduli Spaces. XIII, 148 pages. 1989.

Vol. 323: D.L. Dwoyer, M.Y. Hussaini, R.G. Voigt (Eds.), 11th International Conference on Numerical Methods in Fluid Dynamics. XIII, 622 pages. 1989.

Vol. 324: P. Exner, P. Šeba (Eds.), Applications of Self-Adjoint Extensions in Quantum Physics. Proceedings, 1987. VIII, 273 pages. 1989.

Vol. 327: K. Meisenheimer, H.-J. Röser (Eds.), Hot Spots in Extragalactic Radio Source. Proceedings, 1988. XII, 301 pages. 1989.

Vol. 328: G. Wegner (Ed.), White Dwarfs. Proceedings, 1988. XIV, 524 pages. 1989.

Vol. 329: A. Heck, F. Murtagh (Eds.), Knowledge Based Systems in Astronomy. IV, 280 pages. 1989.

Vol. 330: J.M. Moran, J.N. Hewitt, K.Y. Lo (Eds.), Gravitational Lenses. Proceedings, 1988. XIV, 238 pages. 1989.

Vol. 331: G. Winnewisser, J.T. Armstrong (Eds.), The Physics and Chemistry of Interstellar Molecular Clouds mm and Sub-mm Observations in Astrophysics. Proceedings, 1988. XVIII, 463 pages. 1989.

M. Stix, Kiepenheuer Institut
für Sonnenphysik,
Freiburg, FRG

The Sun

An Introduction

1989. XIII, 390 pp. 192 figs. (Astronomy and Astrophysics Library). ISBN 3-540-50081-2

Contents: Introduction: The Sun's Distance, Mass, Radius, Luminosity. - Internal Structure. - Tools for Solar Observation. - The Atmosphere. - Oscillations. - Convection. - Rotation. - Magnetism. - Chromosphere, Corona, and Solar Wind. - List of Symbols. - References. - Subject Index.

H. Scheffler, Landessternwarte;
H. Elsässer, Max-Planck-Institut
für Astronomie,
Heidelberg, FRG

Physics of the Galaxy and Interstellar Matter

Translated from the German by A. H. Armstrong

1988. XI, 492 pp. 207 figs. (Astronomy and Astrophysics Library). ISBN 3-540-17315-3

Contents: Introductory Survey. - Positions, Motions and Distances of the Stars - Concepts and Methods. - Structure and Kinematics of the Stellar System. - Interstellar Phenomena. - Physics of the Interstellar Matter. - Dynamics of the Galaxy. - Appendix. - Astronomical and Physical Constants. - Latin Names of Constellations. - References. - Supplementary and Advanced Literature. - Sources of Tables. - Sources of Figures. - Subject Index.

K. Rohlfs, Ruhr-University
of Bochum, FRG

Tools of Radio Astronomy

1986. XII, 319 pp. 127 figs. (Astronomy and Astrophysics Library). ISBN 3-540-16188-0

Contents: Radio Astronomical Fundamentals. - Electromagnetic Wave Propagation Fundamentals. - Wave Polarization. - Fundamentals of Antenna Theory. - Filled Aperture Antennas. - Interferometers and Aperture Synthesis. - Receivers. - Emission Mechanisms of Continuous Radiation. - Some Examples of Thermal and Nonthermal Radio Sources. - Line Radiation Fundamentals. - Line Radiation of Neutral Hydrogen. - Recombination Lines. - Interstellar Molecules and Their Line Radiation. - Appendices A–E. - List of Symbols. - References. - Subject Index.

Springer-Verlag
Berlin Heidelberg New York
London Paris Tokyo
Hong Kong